

**Exploring Design Concepts for
Siderophore-Fluoroquinolone
Trojan Horse Antimicrobials**

Thomas James Sanderson

Doctor of Philosophy

University of York

Chemistry

September 2016

Abstract

Urgent action is required to combat the ongoing threat of antimicrobial resistance. Trojan horse conjugates, where antimicrobials are linked to a nutrient carrier, can evade permeability-related resistance through active transport of drugs into bacterial cells. The work presented herein explores modification of the linker moiety between a citrate siderophore and ciprofloxacin, as well as the addition of glycosyl groups to catecholate siderophore moieties to mimic the salmochelins; stealth siderophores which can evade the mammalian defence protein siderocalin.

Two linkers were investigated, one containing a carbamate and the other a disulfide bond neighbouring a carbamate group. These were chosen to give intracellular release of the antimicrobial, either by the action of carboxylesterases or through reduction of the disulfide bond by thiolate anions in the cytoplasm, respectively. A carbamate-linked conjugate was synthesised and screened against wild type *E. coli*, and demonstrated lower antimicrobial activity than that for the parent drug. Screening against a bacterial strain lacking the outer membrane ferric citrate receptor FecA demonstrated that FecA is not essential for uptake of the synthesised conjugate. The synthesis of a disulfide linked conjugate was unsuccessful, due to release of free ciprofloxacin during the final deprotection step.

A salmochelin-inspired conjugate was synthesised. Whilst it demonstrated reduced antimicrobial activity against wild type *E. coli* in iron rich media, compared to the parent drug, higher antimicrobial activity was observed in iron-limited media, suggesting active uptake. A DNA gyrase assay showed that the inhibitory activity of this conjugate was lower than the free drug, suggesting that the antimicrobial activity observed under iron deficiency may be due extracellular iron sequestration by the siderophore.

Table of Contents

Abstract.....	2
Table of Figures	8
Table of Schemes.....	18
Table of Tables	22
Accompanying Material	23
Acknowledgements.....	24
Declaration.....	26
Chapter 1: Introduction.....	27
1.1 Overview	28
1.2 Antibiotics.....	28
Fluoroquinolone antimicrobials.....	29
1.3 Bacterial Resistance to Antibiotics	35
Mechanisms of resistance	36
Combating antimicrobial resistance	39
1.4 Siderophores	40
Iron bioavailability.....	40
Types of siderophores.....	40
Ferric-siderophore uptake mechanisms	42
Mammalian response to siderophores and the fight-back by bacteria	45
1.5 Trojan Horse Strategy	47
Overview of the concept.....	47
Natural Trojan Horse Conjugates – The Sideromycins.....	49
Synthetic Trojan Horse Conjugates	50

1.6	Project Aims.....	65
Chapter 2: Synthesis and antimicrobial activity testing of a carbamate-linked citrate-ciprofloxacin conjugate		
67		
2.1	Aims and overview	68
2.2	Introduction.....	68
	Prodrugs: Carbamates	68
	Carbamates used as bio-labile linkers in Trojan Horse conjugates	77
	Conjugate Design.....	79
	Synthesis of carbamates.....	80
2.3	Synthesis	87
	Initial synthetic route targeting a 1,5-citrate-ciprofloxacin conjugate incorporating a carbamate linker	87
	Second synthetic route targeting a 1,5-citrate-ciprofloxacin conjugate incorporating a carbamate linker	98
	Determination of the mechanism of isomerisation of the citrate siderophore component.....	110
2.4	Antimicrobial Activity Testing of the 1,3-Citrate-Ciprofloxacin Conjugate, 2-12.....	115
	Stability Testing.....	115
	Bacterial Growth Assay.....	116
	DNA Gyrase Assay.....	122
2.5	Summary, conclusions and future work for Chapter 2	125
Chapter 3: Towards the synthesis of a disulfide-linked citrate-ciprofloxacin conjugate		
126		
3.1	Aims and overview	127
3.2	Introduction.....	127

Bio-labile linkers: Disulfides	128
Conjugate Design.....	134
Synthesis of unsymmetrical disulfides	137
3.3 Synthesis	140
Synthesis of the methyl ester protected disulfide conjugate 3-16	141
Attempted base-catalysed hydrolysis of the protected disulfide-linked conjugate 3-16 to target 3-8.....	146
Attempted acid-catalysed hydrolysis of the protected disulfide-linked conjugate 3-16 to target 3-8.....	160
3.4 Summary, conclusions and future work for Chapter 3	162
Chapter 4: Synthesis and antimicrobial activity testing of a salmochelin- inspired siderophore-ciprofloxacin conjugate.....	164
4.1 Aims and overview	165
4.2 Introduction.....	165
Salmochelin-inspired Trojan horse conjugate	166
Conjugate Design.....	168
Synthetic design of compound 4-3	173
Synthesis of aryl-C-glycosides	174
4.3 Synthesis	183
Synthesis of the lysine-linked ciprofloxacin component 4-12	184
Initial synthetic route targeting the glucosylated salmochelin-inspired siderophore component 4-19	190
Second synthetic route targeting the glucosylated salmochelin-inspired siderophore component 4-19	199
Completion of the synthesis of compound 4-3	206
4.4 Antimicrobial Testing of the Salmochelin Inspired Siderophore-Ciprofloxacin Conjugate 4-3	212

Growth Assay	212
DNA Gyrase Assay.....	216
4.5 Summary, conclusions and future work.....	219
Chapter 5: NMR characterisation of compounds 4-19 and 4-25	221
5.1 Introduction.....	222
5.2 NMR characterisation of Compound 4-19.....	223
Assignment of the glucosyl moiety of 4-19.....	223
Assignment of the catechol moiety of 4-19.....	233
Summary of the assignment for compound 4-19.....	241
5.3 NMR characterisation of Compound 4-25.....	243
Assignment of the ciprofloxacin moiety of 4-25.....	243
Assignment of the glucosyl moiety of 4-25.....	250
Assignment of the catechol moiety of 4-25.....	257
Assignment of the lysine linker moiety of 4-25	264
Summary of the assignment of 4-25.....	269
5.4 Summary of Chapter 5	270
Chapter 6: Summary, Conclusions and Future Work	271
6.1 Overall Summary, Conclusions and Future Work.....	272
Bio-labile linkers in Trojan horse conjugates (Chapters 2 and 3)	272
Synthesis and antimicrobial activity testing of a salmochelin-inspired Trojan horse conjugate (Chapter 4)	273
6.2 Concluding Remarks.....	274
Chapter 7: Experimental	276
7.1 General Chemistry Procedures	277

Mass Spectrometry	277
NMR	277
IR	278
HPLC	278
Melting Points.....	280
Elemental Analysis	280
X-Ray Crystallography	280
Solvents	280
Chemical Reagents	281
Moisture Sensitive Reactions	281
Chromatography	281
7.2 Chemical Synthesis	282
7.3 ¹ H NMR study into the base hydrolysis of 3-16	336
7.4 Biological Studies	337
Bacterial Strains.....	337
Media	337
Growth Assays.....	337
DNA Gyrase Assay.....	339
Appendix I. Crystal Data for Compound 2-39	341
Appendix II. Individual Growth Assay Plots for Compound 2-12...	343
Appendix III. Individual Growth Assay Plots for Compound 4-3 ...	356
Appendix IV. Supporting spectra for compound 4-19	365
Appendix V. Supporting spectra for compound 4-25.....	374
Abbreviations.....	396
References.....	399

Table of Figures

Figure 1 - Development of nalidixic acid (1-3) from impurity 1-2 discovered during the synthesis of chloroquine (1-1).....	29
Figure 2 - Ciprofloxacin co-crystallised with both DNA and DNA gyrase of <i>S. aureus</i> , where two fluoroquinolones stabilise the ternary complex by interchelating between the DNA base pairs.....	32
Figure 3 - Simplified representation of secondary binding mode for modified fluoroquinolones in DNA gyrase, proposed by Drlica <i>et al.</i> ²⁵	33
Figure 4 - Basic pharmacophore for fluoroquinolones with substitution positions numbered.....	35
Figure 5 - Horizontal transfer of antibiotic resistance genes between bacterial cells. ^{3, 36}	36
Figure 6 - Schematic diagram demonstrating the mechanisms of bacterial resistance. ^{4, 36-40}	37
Figure 7 – Enzymatic deactivation of ciprofloxacin 1-5 by <i>N</i> -acetylation. ⁴¹	38
Figure 8 - Common siderophore binding units, with representative examples enterobacin 1-9 , enterobactin linear dimer 1-10 , desferrioxamine B 1-11 and citric acid 1-12	41
Figure 9 - Schematic representation of ferric-siderophore complexes into a Gram-negative bacteria cell. Blue circle/half-circle = Siderophore / Red circle = Fe(III).	43
Figure 10 - Crystal structure of siderocalin bound to ferric-fluoribactin. PDB code: 4K19. ⁷³	46
Figure 11 - Simple representation of the Trojan horse strategy.	48
Figure 12 - Structure of ciprofloxacin demonstrating where conjugation is feasible.....	69
Figure 13 - Generic structure of a carbamate, and common carbamates used as protecting groups for amines, the Fmoc, Boc and CBz groups.	70
Figure 14 - Disconnection of compounds 2-11 and 2-12 to their key components.....	86
Figure 15 - ¹ H NMR spectrum of 2-29 in CD ₃ OD.	103

Figure 16 - ^1H NMR spectrum of 2-12 in CD_3OD	106
Figure 17 - ^1H NMR spectrum of the citrate moiety in 2-12 in $\text{d}_6\text{-DMSO}$	107
Figure 18 - ^{13}C NMR spectrum of 2-12 in $\text{d}_6\text{-DMSO}$	108
Figure 19 - HMBC spectrum of 2-12 in $\text{d}_6\text{-DMSO}$	109
Figure 20 - HSQC spectrum of 2-12 in $\text{d}_6\text{-DMSO}$	109
Figure 21 - ^{13}C NMR spectrum 2-12 in $\text{d}_6\text{-DMSO}$	110
Figure 22 - ^1H NMR spectrum of 2-39 in CDCl_3	112
Figure 23 - ORTEP diagram (50% probability ellipsoids) of 2-39 , shown as one chiral form of a racemate. Space group: P-1. Crystal contains both enantiomers that are related, with the <i>S</i> enantiomer shown and <i>R</i> omitted for clarity.	113
Figure 24 - ^1H NMR spectrum of 2-12 in D_2O with 0.042 M Na_2HPO_4 , 0.008 M NaCl and DCl (HCl in D_2O), at pD 7.01, as a mimic of M9 Minimal Media. The blue spectrum shows the sample at $t = 0$ h. The red spectrum shows the sample at $t = 74$ h.	116
Figure 25 - <i>E. coli</i> BW25113WT growth in LB media across concentrations at $t = 10$ h for both ciprofloxacin 1-5 (blue) and conjugate 2-12 (red).	118
Figure 26 - <i>E. coli</i> BW25113WT growth in M9 minimal media across concentrations at $t = 10$ h for both ciprofloxacin 1-5 (blue) and conjugate 2-12 (red).	119
Figure 27 - <i>E. coli</i> BW25113 FecA::kan growth in LB media across concentrations at $t = 10$ h for both ciprofloxacin 1-5 and conjugate 2-12	121
Figure 28 - <i>E. coli</i> BW25113 FecA::kan growth in M9 minimal media across concentrations at $t = 10$ h for both ciprofloxacin 1-5 and conjugate 2-12	121
Figure 29 - DNA gyrase assay of A) ciprofloxacin 1-5 and B) conjugate 2-12 at concentrations ranging from 20-0 μM . 0 μM = DMSO control. + = positive control, with DNA gyrase present without the antimicrobial. - = negative control, no DNA gyrase or antimicrobial.	123
Figure 30 - Schematic overview for monitoring a fluorescent probe released from 3-7 . ¹⁸⁰	134

Figure 31 - The key structural components of conjugate 3-8 .	136
Figure 32 - ¹ H NMR spectrum of 3-16 in CDCl ₃ .	145
Figure 33 - A) ¹ H NMR spectrum of the aromatic region of compound 3-16 in CD ₃ OD + 0.01% NaOD (40% in D ₂ O). B) Plot of the % ratio of species present in solution based on the relative integration of the resonances highlighted in the ¹ H NMR spectrum over time.	148
Figure 34 - Flow chart depicting the base hydrolysis reaction of 3-16 .	151
Figure 35 - ¹ H NMR spectrum of the aromatic region of the organic residue in CDCl ₃ . Four ciprofloxacin species are observed 1 , 2 , 3 and 4 .	152
Figure 36 - HPLC trace of the organic residue at 285 nm detection.	153
Figure 37 - Overlay of HPLC trace of the starting compound 3-16 (red) and the organic residue (blue), showing a possible impurity carried through into the organic residue at 7.7 minutes.	154
Figure 38 - ¹ H NMR spectrum of the aqueous residue in D ₂ O.	156
Figure 39 - HPLC trace of the aqueous residue at 285 nm detection.	157
Figure 40 - HPLC Trace of the isolated precipitate at 285 nm detection.	158
Figure 41 - HPLC Trace of the isolated precipitate at 285 nm detection.	158
Figure 42 - Conjugate 4-3 and salmochelin S4 1-16 .	169
Figure 43 - Early model for the uptake of salmochelin S4 and its hydrolysis products proposed by Hantke <i>et al.</i> in 2005. ⁷⁹	171
Figure 44 - Simplified schematic representation for salmochelin S4 1-16 uptake, according to Fang <i>et al.</i> ²⁰⁵ The updated proposed uptake mechanism by Hantke <i>et al.</i> for salmochelin S1 1-17 is also shown. ²⁰⁶	172
Figure 45 - The three key components of conjugate 4-3 .	174
Figure 46 - Difference in pK _a values for the catechol moieties. ^{45, 247}	192
Figure 47 - Simplified illustration of the resonance effects that favour an electrophilic addition in position C-5 (red).	193
Figure 48 - HPLC trace of 4-3 product at 285 nm after preparative HPLC purification.	211
Figure 49 - <i>E. coli</i> BW25113WT growth in LB media across concentrations at <i>t</i> = 10 h for both ciprofloxacin 1-5 (blue) and conjugate 4-3 (red).	213

Figure 50 - <i>E. coli</i> BW25113WT growth in M9 minimal media across concentrations at $t = 10$ h for both ciprofloxacin 1-5 (blue) and conjugate 4-3 (red).....	214
Figure 51 - <i>E. coli</i> BW25113WT growth in 0.2 μM [Fe(III)] M9 media, across concentrations at $t = 10$ h for both ciprofloxacin 1-5 (blue) and conjugate 4-3 (red).....	215
Figure 52 - DNA gyrase assay of A) ciprofloxacin 1-5 and B) conjugate 4-3 at concentrations ranging from 20-0 μM . 0 μM = DMSO control. + = positive control, with DNA gyrase present without the antimicrobial. - = negative control, no DNA gyrase or antimicrobial.....	217
Figure 53 - DNA gyrase assay of conjugate 4-3 at concentrations ranging from 100-20 μM . + = positive control, with DNA gyrase present without the antimicrobial. - = negative control, no DNA gyrase or antimicrobial.	218
Figure 54 - Full structure of compound 4-19	224
Figure 55 - ^1H NMR spectrum (CDCl_3) of 4-19	224
Figure 56 - COSY spectrum (CDCl_3) of 4-19	225
Figure 57 - HMQC spectrum (CDCl_3) of 4-19	227
Figure 58 - HMBC spectrum (CDCl_3) of 4-19	228
Figure 59 - HMQC spectrum (CDCl_3) of 4-19	229
Figure 60 - HMBC spectrum (CDCl_3) of 4-19	229
Figure 61 - ^1H NMR spectrum (CDCl_3) of 4-19	232
Figure 62 - HMBC spectrum (CDCl_3) of 4-19	233
Figure 63 - HMBC spectrum (CDCl_3) of 4-19	234
Figure 64 - ^1H NMR spectrum (CDCl_3) of 4-19	234
Figure 65 - COSY spectrum (CDCl_3) of 4-19	235
Figure 66 - HMBC spectrum (CDCl_3) of 4-19	236
Figure 67 - HMQC spectrum (CDCl_3) of 4-19	237
Figure 68 - HMBC spectrum (CDCl_3) of 4-19	238
Figure 69 - HMBC spectrum (CDCl_3) of 4-19	239
Figure 70 - HMQC spectrum (CDCl_3) of 4-19	240
Figure 71 - HMBC spectrum (CDCl_3) of 4-19	241
Figure 72 - Full structure of compound 4-25	244

Figure 73 - HMBC spectrum (CDCl ₃) of 4-25	245
Figure 74 - HMBC spectrum (CDCl ₃) of 4-25	246
Figure 75 - HMQC spectrum (CDCl ₃) of 4-25	246
Figure 76 - HMQC spectrum (CDCl ₃) of 4-25	247
Figure 77 - ¹ H NMR spectrum of 4-9 (Chapter 4) (CDCl ₃) showing the symmetry of the piperazinyl protons.	248
Figure 78 - ¹ H NMR spectrum (CDCl ₃) of 4-25	250
Figure 79 - Expansion of one benzyl protected glucosylated catechol unit of compound 4-25 for ease of reference visualisation.	251
Figure 80 - HMBC spectrum (CDCl ₃) of 4-25	253
Figure 81 - HMQC spectrum (CDCl ₃) of 4-25	254
Figure 82 - ¹ H NMR spectrum 3.72-3.86 ppm of 4-25	256
Figure 83 - ¹ H NMR spectrum (CDCl ₃) of 4-25	258
Figure 84 - HMBC spectrum (CDCl ₃) of 4-25	258
Figure 85 - HMBC spectrum (CDCl ₃) of 4-25	260
Figure 86 - HMBC spectrum (CDCl ₃) of 4-25	261
Figure 87 - HMBC spectrum (CDCl ₃) of 4-25	262
Figure 88 - HMQC spectrum (CDCl ₃) of 4-25	262
Figure 89 - HMBC spectrum (CDCl ₃) of 4-25	265
Figure 90 - ¹ H NMR (CDCl ₃) of 4-25	265
Figure 91 - HMQC spectrum (CDCl ₃) of 4-25	266
Figure 92 - COSY spectrum (CDCl ₃) of 4-25	267
Figure 93 - HMBC spectrum (CDCl ₃) of 4-25	268
Figure 94 - HMQC spectrum (CDCl ₃) of 4-25	268
Figure 95 - ¹ H NMR spectrum of the aromatic region of compound 3-16 in CD ₃ OD, prior to the addition of NaOD.	336
Figure 96 - 96 well plate layout.	338
Figure 97 - <i>E. coli</i> BW25113WT growth in LB media with drug concentrations of 0 μM for both ciprofloxacin 1-5 and conjugate 2-12 ...	343
Figure 98 - <i>E. coli</i> BW25113WT growth in LB media with drug concentrations of 0.01 μM for both ciprofloxacin 1-5 and conjugate 2-12	343

Figure 99 - <i>E. coli</i> BW25113WT growth in LB media with drug concentrations of 0.1 μ M for both ciprofloxacin 1-5 and conjugate 2-12	344
Figure 100 - <i>E. coli</i> BW25113WT growth in LB media with drug concentrations of 0.5 μ M for both ciprofloxacin 1-5 and conjugate 2-12	344
Figure 101 - <i>E. coli</i> BW25113WT growth in LB media with drug concentrations of 1 μ M for both ciprofloxacin 1-5 and conjugate 2-12 ...	345
Figure 102 - <i>E. coli</i> BW25113WT growth in LB media with drug concentrations of 10 μ M for both ciprofloxacin 1-5 and conjugate 2-12 .	345
Figure 103 - <i>E. coli</i> BW25113WT growth in M9 minimal media with drug concentrations of 0 μ M for both ciprofloxacin 1-5 and conjugate 2-12 ...	346
Figure 104 - <i>E. coli</i> BW25113WT growth in M9 minimal media with drug concentrations of 0.01 μ M for both ciprofloxacin 1-5 and conjugate 2-12	346
Figure 105 - <i>E. coli</i> BW25113WT growth in M9 minimal media with drug concentrations of 0.1 μ M for both ciprofloxacin 1-5 and conjugate 2-12	347
Figure 106 - <i>E. coli</i> BW25113WT growth in M9 minimal media with drug concentrations of 0.5 μ M for both ciprofloxacin 1-5 and conjugate 2-12	347
Figure 107 - <i>E. coli</i> BW25113WT growth in M9 minimal media with drug concentrations of 1 μ M for both ciprofloxacin 1-5 and conjugate 2-12 ...	348
Figure 108 - <i>E. coli</i> BW25113WT growth in M9 minimal media with drug concentrations of 10 μ M for both ciprofloxacin 1-5 and conjugate 2-12 .	348
Figure 109 - <i>E. coli</i> BW25113 FecA::kan growth in LB media with drug concentrations of 0 μ M for both ciprofloxacin 1-5 and conjugate 2-12 ...	349
Figure 110 - <i>E. coli</i> BW25113 FecA::kan growth in LB media with drug concentrations of 0.01 μ M for both ciprofloxacin 1-5 and conjugate 2-12	349
Figure 111 - <i>E. coli</i> BW25113 FecA::kan growth in LB media with drug concentrations of 0.1 μ M for both ciprofloxacin 1-5 and conjugate 2-12	350

Figure 112 - <i>E. coli</i> BW25113 FecA::kan growth in LB media with drug concentrations of 0.5 μ M for both ciprofloxacin 1-5 and conjugate 2-12	350
Figure 113 - <i>E. coli</i> BW25113 FecA::kan growth in LB media with drug concentrations of 1 μ M for both ciprofloxacin 1-5 and conjugate 2-12 ...	351
Figure 114 - <i>E. coli</i> BW25113 FecA::kan growth in LB media with drug concentrations of 10 μ M for both ciprofloxacin 1-5 and conjugate 2-12 .	351
Figure 115 - <i>E. coli</i> BW25113 FecA::kan growth in M9 minimal media with drug concentrations of 0 μ M for both ciprofloxacin 1-5 and conjugate 2-12	352
Figure 116 - <i>E. coli</i> BW25113 FecA::kan growth in M9 minimal media with drug concentrations of 0.01 μ M for both ciprofloxacin 1-5 and conjugate 2-12	352
Figure 117 - <i>E. coli</i> BW25113 FecA::kan growth in M9 minimal media with drug concentrations of 0.1 μ M for both ciprofloxacin 1-5 and conjugate 2-12	353
Figure 118 - <i>E. coli</i> BW25113 FecA::kan growth in M9 minimal media with drug concentrations of 0.5 μ M for both ciprofloxacin 1-5 and conjugate 2-12	353
Figure 119 - <i>E. coli</i> BW25113 FecA::kan growth in M9 minimal media with drug concentrations of 1 μ M for both ciprofloxacin 1-5 and conjugate 2-12	354
Figure 120 - <i>E. coli</i> BW25113 FecA::kan growth in M9 minimal media with drug concentrations of 10 μ M for both ciprofloxacin 1-5 and conjugate 2-12	354
Figure 121 - <i>E. coli</i> BW25113WT growth in LB media with drug concentrations of 0 μ M for both ciprofloxacin 1-5 and conjugate 4-3	356
Figure 122 - <i>E. coli</i> BW25113WT growth in LB media with drug concentrations of 0.01 μ M for both ciprofloxacin 1-5 and conjugate 4-3	356
Figure 123 - <i>E. coli</i> BW25113WT growth in LB media with drug concentrations of 0.1 μ M for both ciprofloxacin 1-5 and conjugate 4-3 ..	357
Figure 124 - <i>E. coli</i> BW25113WT growth in LB media with drug concentrations of 0.5 μ M for both ciprofloxacin 1-5 and conjugate 4-3 ..	357

Figure 125 - <i>E. coli</i> BW25113WT growth in LB media with drug concentrations of 1 μ M for both ciprofloxacin 1-5 and conjugate 4-3	358
Figure 126 - <i>E. coli</i> BW25113WT growth in LB media with drug concentrations of 10 μ M for both ciprofloxacin 1-5 and conjugate 4-3 ...	358
Figure 127 - <i>E. coli</i> BW25113WT growth in M9 minimal media with drug concentrations of 0 μ M for both ciprofloxacin 1-5 and conjugate 4-3	359
Figure 128 - <i>E. coli</i> BW25113WT growth in M9 minimal media with drug concentrations of 0.01 μ M for both ciprofloxacin 1-5 and conjugate 4-3	359
Figure 129 - <i>E. coli</i> BW25113WT growth in M9 minimal media with drug concentrations of 0.1 μ M for both ciprofloxacin 1-5 and conjugate 4-3 ..	360
Figure 130 - <i>E. coli</i> BW25113WT growth in M9 minimal media with drug concentrations of 0.5 μ M for both ciprofloxacin 1-5 and conjugate 4-3 ..	360
Figure 131 - <i>E. coli</i> BW25113WT growth in M9 minimal media with drug concentrations of 1 μ M for both ciprofloxacin 1-5 and conjugate 4-3	361
Figure 132 - <i>E. coli</i> BW25113WT growth in M9 minimal media with drug concentrations of 10 μ M for both ciprofloxacin 1-5 and conjugate 4-3 ...	361
Figure 133 - <i>E. coli</i> BW25113WT growth in 0.2 μ M [Fe(III)] M9 media with drug concentrations of 0 μ M for both ciprofloxacin 1-5 and conjugate 4-3	362
Figure 134 - <i>E. coli</i> BW25113WT growth in 0.2 μ M [Fe(III)] M9 minimal media with drug concentrations of 0.01 μ M for both ciprofloxacin 1-5 and conjugate 4-3	362
Figure 135 - <i>E. coli</i> BW25113WT growth in 0.2 μ M [Fe(III)] M9 minimal media with drug concentrations of 0.1 μ M for both ciprofloxacin 1-5 and conjugate 4-3	363
Figure 136 - <i>E. coli</i> BW25113WT growth in 0.2 μ M [Fe(III)] M9 minimal media with drug concentrations of 0.5 μ M for both ciprofloxacin 1-5 and conjugate 4-3	363
Figure 137 - <i>E. coli</i> BW25113WT growth in 0.2 μ M [Fe(III)] M9 minimal media with drug concentrations of 1 μ M for both ciprofloxacin 1-5 and conjugate 4-3	364

Figure 138 - <i>E. coli</i> BW25113WT growth in 0.2 μM [Fe(III)] M9 minimal media with drug concentrations of 10 μM for both ciprofloxacin 1-5 and conjugate 4-3	364
Figure 139 - Full ^{13}C spectrum (CDCl_3) of 4-19	366
Figure 140 - Full ^1H spectrum (CDCl_3) of 4-19	367
Figure 141 - Full HMBC spectrum (CDCl_3) of 4-19	368
Figure 142 - Full HMQC spectrum (CDCl_3) of 4-19	369
Figure 143 - Full COSY spectrum (CDCl_3) of 4-19	370
Figure 144 - Full DEPT spectrum (CDCl_3) of 4-19	371
Figure 145 - HMBC spectrum (CDCl_3) of 4-19	372
Figure 146 - HMQC spectrum (CDCl_3) of 4-19	372
Figure 147 - HMBC spectrum (CDCl_3) of 4-19	373
Figure 148 - Full ^1H spectrum (CDCl_3) of 4-25	375
Figure 149 - Full ^{13}C spectrum (CDCl_3) of 4-25	376
Figure 150 - Full HMBC spectrum (CDCl_3) of 4-25	377
Figure 151 - Full HMQC spectrum (CDCl_3) of 4-25	378
Figure 152 - Full COSY spectrum (CDCl_3) of 4-25	379
Figure 153 - Full DEPT spectrum (CDCl_3) of 4-25	380
Figure 154 - HMBC spectrum (CDCl_3) of 4-25	381
Figure 155 - HMQC spectrum (CDCl_3) of 4-25	381
Figure 156 - HMBC spectrum (CDCl_3) of 4-25	382
Figure 157 - HMBC spectrum (CDCl_3) of 4-25	382
Figure 158 - HMBC spectrum (CDCl_3) of 4-25	383
Figure 159 - HMBC spectrum (CDCl_3) of 4-25	383
Figure 160 - HMQC spectrum (CDCl_3) of 4-25	384
Figure 161 - HMQC spectrum (CDCl_3) of 4-25	384
Figure 162 - HMBC spectrum (CDCl_3) of 4-25	385
Figure 163 - HMQC spectrum (CDCl_3) of 4-25	385
Figure 164 - COSY spectrum (CDCl_3) of 4-25	386
Figure 165 - HMQC spectrum (CDCl_3) of 4-25	386
Figure 166 - COSY spectrum (CDCl_3) of 4-25	387
Figure 167 - COSY spectrum (CDCl_3) of 4-25	387
Figure 168 - HMQC spectrum (CDCl_3) of 4-25	388

Figure 169 - HMQC spectrum (CDCl ₃) of 4-25	388
Figure 170 - HMBC spectrum (CDCl ₃) of 4-25	389
Figure 171 - COSY spectrum (CDCl ₃) of 4-25	389
Figure 172 - HMQC spectrum (CDCl ₃) of 4-25	390
Figure 173 - HMBC spectrum (CDCl ₃) of 4-25	390
Figure 174 - HMQC spectrum (CDCl ₃) of 4-25	391
Figure 175 - HMBC spectrum (CDCl ₃) of 4-25	391
Figure 176 - HMQC spectrum (CDCl ₃) of 4-25	392
Figure 177 - HMQC spectrum (CDCl ₃) of 4-25	392
Figure 178 - HMBC spectrum (CDCl ₃) of 4-25	393
Figure 179 - HMQC spectrum (CDCl ₃) of 4-25	393
Figure 180 - HMQC spectrum (CDCl ₃) of 4-25	394
Figure 181 - HMBC spectrum (CDCl ₃) of 4-25	394
Figure 182 - COSY spectrum (CDCl ₃) of 4-25	395
Figure 183 - HMQC spectrum (CDCl ₃) of 4-25	395

Table of Schemes

Scheme 1 - Proposed mechanism of drug release from the trimethyl lock derived conjugates. ^{118, 119}	61
Scheme 2 - Carbamate cleavage <i>via</i> nucleophilic substitution.	71
Scheme 3 - Carbamate cleavage <i>via</i> an E1cB mechanism.	71
Scheme 4 - Acid based cleavage of carbamates.	72
Scheme 5 - β -galactosidase enzymatic cleavage of a linker incorporating a carbamate demonstrated by Devarakonda <i>et al.</i> as a prodrug for doxorubicin ¹⁴³ and by Tòth <i>et al.</i> for an imaging agent. ¹⁴⁴	74
Scheme 6 - Irinotecan is hydrolysed by carboxylesterases to its active form SN-38, 2-4 . ^{146, 147}	75
Scheme 7 - Cleavage of (acyloxy)alkyl carbamates following esterase cleavage of the ester group. ¹⁴⁹	76
Scheme 8 - Synthesis of carbamates using phosgene, with a chloroformate as the intermediate.	81
Scheme 9 - General scheme for the synthesis of carbamates using BTBC. ¹⁵⁴	82
Scheme 10 - General scheme for the synthesis of carbamates using <i>N,N'</i> -disuccinimidyl carbonate. ^{156, 157}	83
Scheme 11 - Formation of ureas using <i>N,N'</i> -disuccinimidyl carbonate to produce a carbamate intermediate. ¹⁵⁹	83
Scheme 12 - Use of metal carbonates in the synthesis of a carbamate and alkylated side product. ¹⁶⁰	84
Scheme 13 - Reported synthesis of carbamates by Jung <i>et al.</i> using carbon dioxide. ¹⁶²	84
Scheme 14 - Example Hoffmann rearrangement to synthesise methyl carbamates. ¹⁶³	85
Scheme 15 - Initial synthetic route towards compound 2-11	88
Scheme 16 - Planned synthesis of 2-12 from intermediate compound 2-20	89
Scheme 17 - Esterification of ciprofloxacin 1-5 to produce 2-15	90

Scheme 18 - Synthesis of 1,5-dimethyl citrate 2-21 from citric acid 1-12 , with 1,3,5-trimethyl citrate 2-25 as a by-product.	91
Scheme 19 - Synthesis of 1,3-dimethyl citrate 2-23 from 1,3,5-trimethyl citrate 2-25	93
Scheme 20 - Formation of the Fmoc protected carbamate target 2-18	94
Scheme 21 - Formation of the CBz protected carbamate target 2-19	96
Scheme 22 - Activation of <i>N</i> -CBz-ethanolamine 2-28 using <i>N,N'</i> -disuccinimidyl carbonate to form the required carbamate bond.	97
Scheme 23 - Second synthetic route towards compound 2-11	99
Scheme 24 - Attempted synthesis of 2-29	101
Scheme 25 - Synthesis of 2-29	102
Scheme 26 - Reaction utilising <i>N,N'</i> -disuccinimidyl carbonate to form the required carbamate bond to produce compound 2-22	104
Scheme 27 - Isomerisation of compound 2-22 on base hydrolysis, giving the regioisomeric target, 2-12	105
Scheme 28 - Base hydrolysis of succinimide 2-39 to give either 2-11 or 2-12 , or a mixture of both, through either Route 1 (Green) or Route 2 (Red).	114
Scheme 29 - Summary of the formation of 2-12 from 2-22	115
Scheme 30 - Proposed mechanism of drug release from a disulfide containing conjugate <i>via</i> two potential pathways as a result of attack from a thiolate species (A - blue / B - red). ¹⁷⁵	128
Scheme 31 - Proposed mechanism of ciprofloxacin 1-5 release from compound 3-8 <i>via</i> two potential pathways as a result of attack from a thiolate species (A - blue / B - red).	135
Scheme 32 - Synthesis of disulfides using sodium tellurite, reported by Suzuki <i>et al.</i> ¹⁹¹	137
Scheme 33 - Synthesis of disulfides using dichlorodicyanoquinone, reported by Wang <i>et al.</i> ¹⁹²	138
Scheme 34 - General scheme for the synthesis of unsymmetrical disulfides by thiol-disulfide exchange with a 2-pyridyl disulfanyl species. ^{193, 194}	139
Scheme 35 - Synthesis of disulfides using 2,2'-dithiobis(benzothiazole) as reported by Brzezinska and Ternay. ¹⁹⁵	139

Scheme 36 - Synthesis of compound 3-13 by thiol-disulfide exchange. ¹⁷⁸	140
Scheme 37 - Synthetic route towards compound 3-8	141
Scheme 38 - Synthesis of 3-13 by thiol-disulfide exchange. ¹⁷⁸	142
Scheme 39 - Synthesis of compound 3-15	143
Scheme 40 - Carbamate formation using <i>N,N'</i> -disuccinimidyl carbonate to produce compound 3-16	144
Scheme 41 - Attempted base hydrolysis of 3-16 to target 3-8	146
Scheme 42 - Proposed mechanisms of ester hydrolysis using potassium trimethylsilanolate. ¹⁹⁸	160
Scheme 43 - Attempted acid hydrolysis of 3-16 to target 3-8	161
Scheme 44 - Proposed future work synthesis of 3-8 <i>via</i> the use of <i>tert</i> -butyl ester protecting groups.....	162
Scheme 45 - Friedel-Crafts approach utilised by Hurd and Bonner to form an aryl- <i>C</i> -glucoside. ²¹³	175
Scheme 46 - Grignard reaction by Junge <i>et al.</i> , forming the α -anomer. ²¹⁶	176
Scheme 47 - Heck reaction employed by Lee and Kool to synthesise analogues of DNA bases. ²²⁸	177
Scheme 48 - Oxidative Heck coupling of glycols and aryl hydrazines by Liu <i>et al.</i> ²³⁰	177
Scheme 49 - Suzuki cross coupling to give 2-arylglycols as intermediates in the synthesis of aryl- <i>C</i> -glycosides. ²³¹	178
Scheme 50 - The first reported Negishi coupling. ²³⁴	178
Scheme 51 - Negishi coupling of a glycol with an iodoarene using a palladium catalyst, by Ousmer <i>et al.</i> ²³⁹	179
Scheme 52 - Direct Negishi cross-coupling reported by Gagné <i>et al.</i> for aryl- <i>C</i> -glycoside synthesis. ^{207, 208}	180
Scheme 53 - Rationalising the high β -selectivity of the Negishi reaction by neighbouring group participation of an acetate group. ²⁴⁰	180
Scheme 54 - Proposed Negishi mechanism of alkyl-alkyl couplings by Vicic <i>et al.</i> ²⁴¹	181
Scheme 55 - Proposed Negishi mechanism of alkyl-alkyl couplings by Cárdenas <i>et al.</i> ²⁴²	182

Scheme 56 - Summary of the proposed synthesis of 4-3 from three commercially available starting materials.	184
Scheme 57 - Synthesis of the lysine-linked, benzyl-protected ciprofloxacin component.....	185
Scheme 58 - Synthesis of 4-8 . ²⁴⁵	186
Scheme 59 - Synthesis of compound 4-9 . ^{126, 246}	188
Scheme 60 - Synthesis of compound 4-10 . ^{126, 246}	188
Scheme 61 - Synthesis of 4-11	189
Scheme 62 - Synthesis of 4-12	189
Scheme 63 - Synthesis of the Bn-protected glucosylated salmochelin-inspired siderophore component 4-19 as reported by Gagné <i>et al.</i> ^{207, 208} .	190
Scheme 64 - Synthesis of 4-14 . ²⁰⁷	191
Scheme 65 - Synthesis of 4-15 as reported by Gagné <i>et al.</i> ^{207, 208}	193
Scheme 66 - Iodination of 4-15 to produce 4-16	196
Scheme 67 - The iodination reaction to produce 4-22	197
Scheme 68 - Newly developed synthetic route to compound 4-5 . The remaining synthesis of the glucosylated salmochelin inspired siderophore component 4-19 was adapted from Gagné <i>et al.</i> ^{207, 208}	200
Scheme 69 - Methyl ether removal and re-esterification to produce 4-23	201
Scheme 70 - Synthesis of 4-5	202
Scheme 71 - Negishi coupling reaction of 4-5 to produce 4-7 , first reported by Gagné <i>et al.</i> ²⁰⁷	203
Scheme 72 - Protecting group manipulation to produce 4-17 and 4-18 . ²⁰⁷	205
Scheme 73 - Ester hydrolysis to furnish 4-19 . ²⁰⁷	206
Scheme 74 - Coupling of 4-12 and 4-19 to furnish the benzyl protected conjugate 4-25 , followed by hydrogenolysis to yield the target conjugate 4-3	207
Scheme 75 - Synthesis of 4-25	209
Scheme 76 - Hydrogenolysis to produce target 4-3	211

Table of Tables

Table 1 - Conditions used for the synthesis of 4-15	194
Table 2 - Test reaction conditions for the iodination of 4-21 to produce 4-22	198
Table 3 - ¹ H assignments of the glucosyl moiety 4-19 based on COSY coupling in Figure 56	226
Table 4 - ¹ H and ¹³ C assignment of the glucosyl moiety of 4-19 based on HMQC coupling in Figure 57	227
Table 5 - ¹ H and ¹³ C assignment of the benzyl groups associated with the glucosyl moiety based on HMQC and HMBC coupling.	231
Table 6 - Summary of the assignment of compound 4-19	242
Table 7 - Summary of the assignment of the protected ciprofloxacin moiety of 4-25 , compared to 4-9	249
Table 8 - ¹ H and ¹³ C assignment of the glucosyl moiety of 4-25	252
Table 9 - Likely ¹ H and ¹³ C assignment of the remaining benzyl groups associated with the glucosyl moiety for compound 4-25 , inferred from the previous assignment of 4-19	255
Table 10 - Summary of the assignment of the protect glucosyl and catechol moieties of 4-25 , compared to 4-19	264
Table 11 - Summary of the assignment of the lysine linker moiety of 4-25 , compared to 4-8 (Chapter 4).	269
Table 12 - Ciprofloxacin containing species (%). As a reference to determine the % ratios between the species in the spectrum by their relative integration, the NMR solvent was spiked with EtOH as a standard.	336
Table 13 - Volumes of solutions added to each sample for the DNA gyrase assay.	340

Accompanying Material

A compact disk with an electronic copy of this thesis, the growth assay data and the X-ray crystallography data is attached at the back of this thesis.

Acknowledgements

Both my thesis and PhD studies would not have been possible without the help and support of a number of people. Firstly, I wish to thank my supervisors Prof. Anne-Kathrin Duhme-Klair and Dr. Anne Routledge for the opportunity to undertake my research with them and also for their support and encouragement throughout my PhD. Their suggestions, ideas and patience have guided me through my research and for that I am very much grateful. Furthermore, I would like to thank my IPM Dr. Victor Chechik for his advice and discussion. Additionally, I thank the University of York and the EPSRC for funding this research.

A number of academics and technicians have assisted this research and I would like to thank: Heather, Pedro and Ben for their assistance with NMR, Karl and Helen for performing mass spectrometry experiments, Graeme for CHN analysis, Natalie for X-ray crystallography, our lab technician Emma, and Amanda for training me on the HPLC instruments. I wish to also thank our collaborator Dr. Gavin Thomas, and also members of his group Sophie and Rosanna, for their training and assistance with microbiology experiments. I have mentored a number of students during my time and I would like to thank them for their efforts, company and willingness to learn/allowing me to develop as a mentor; Katherine, Belina, Reece, Dan, Raymond, James, Katie, Hannah, Paulius, Abigail and Claire.

I have been fortunate to have made many great friends throughout my time here in York, and I wish to thank them for their help and enjoyable company. Including past and present group members I would like to thank: Abeda, Chris C, Aurélien, the E002/E014 lab, those upstairs in the Fairlamb and Lynam groups, George, Sarah, Matt, Mary and Ryan. In particular I am very much grateful to Chris U for his humour, Lucy for being Lucy, Andy for his advice (it was a privilege to be an usher for you

and Luisa), Luisa for her much needed coffee/always listening, Ellis for her humorous support/baking/keeping me fed/medal collecting, and Dan for his knowledge and never-ending support/advice. Additionally I wish to thank a many number of friends who have tolerated my general absence throughout the final months of this PhD.

I must thank the people most important in my life; my family on both sides of the Atlantic for their unconditional support and love. Without the support of my parents Isobel and Malcolm I would not have been able to embark on the challenges and goals I set myself in undertaking my PhD, thank you. Finally, I cannot begin to put into words how important my wife Alexandra has been to me throughout this process. You are amazing and I could not have managed this without your love, nor without you being there with me throughout.

Declaration

I declare that the work presented in this thesis is my own and to the best of my knowledge, original. This work was undertaken at The University of York under the supervision of Prof. Anne-Kathrin Duhme-Klair and Dr. Anne Routledge between October 2012 and August 2016. The work presented within this thesis has not been submitted for any other qualification or publication, unless declared below. The following work was carried out by or with the assistance of other researchers:

- All mass spectrometry and LC-MS experiments were performed by either Mr Karl Heaton or Miss Helen Robinson
- Elemental analyses were performed by Dr. Graeme McAllister
- X-Ray crystallography was collected, processed and solved by Dr. Natalie Pridmore
- NMR spectra recorded on the 700 MHz spectrometer were collected by Dr. Pedro Aguiar
- NMR spectra recorded on the 500 MHz spectrometer were collected by Mr. Ben Coulson
- Attempts to synthesise compound **4-15** were aided by Miss Ellis Wilde

Citation for a jointly authored book chapter related to the introduction:

- Raines D.J., Sanderson T.J., Wilde E.J. and Duhme-Klair A.-K. (2014) Siderophores. In: Reedijk, J. (Ed.) Elsevier Reference Module in Chemistry, Molecular Sciences and Chemical Engineering. Waltham, MA: Elsevier. 23-Jan-15 doi: 10.1016/B978-0-12-409547-2.11040-6.

Thomas James Sanderson

Chapter 1: Introduction

1.1 Overview

With the ever growing emergence of antibiotic resistance, new strategies are required to overcome the crisis. This thesis details one strategy in the development against the threat of resistance, the Trojan horse strategy. This strategy employs siderophore-antimicrobial conjugates which are designed to exploit bacterial iron uptake mechanisms to aid drug effectiveness. In turn this thesis discusses the synthesis, characterisation and investigation of siderophore-fluoroquinolone Trojan horse antimicrobial conjugates, with a view to provide further insight into the design features required. Therefore this introduction provides an overview of the literature to set the context for the work presented in this thesis. Most examples discussed herein relate predominantly to the fluoroquinolone class of antimicrobial agents, the focus of the work presented. However, it should be highlighted that many examples relate to other classes of antibiotics, which are highlighted where relevant.

1.2 Antibiotics

The discovery of antibiotics proved a turning point in modern medicine, allowing the treatment of a number of infectious diseases.^{1,2} The first class of antibiotics discovered were the sulfonamides in 1935, and were quickly followed by the β -lactams in 1941.^{1,2} A quick succession of other new antimicrobial classes were produced until 1968, though this age of antibiotic discovery was eventually succeeded by a development void.^{1,2} Subsequently, the next two classes of antibiotics were only discovered in 2000 and 2003, respectively.^{1,2} With the continued rise in bacterial resistance, novel antibiotics and strategies are required.³⁻⁸

Fluoroquinolone antimicrobials

During the synthesis of the antimalarial agent chloroquine (**1-1**) it was discovered in 1962 that an impurity (**1-2**) demonstrated activity against Gram-negative bacteria, which subsequently led to the development of synthetic nalidixic acid (**1-3**) as the first commercial quinolone (**Figure 1**).⁹⁻¹¹ However, nalidixic acid **1-3** demonstrates activity primarily against the *Enterobacteriaceae* family of bacterial species, which coupled with poor pharmacokinetics, limited clinical use.^{9, 12}

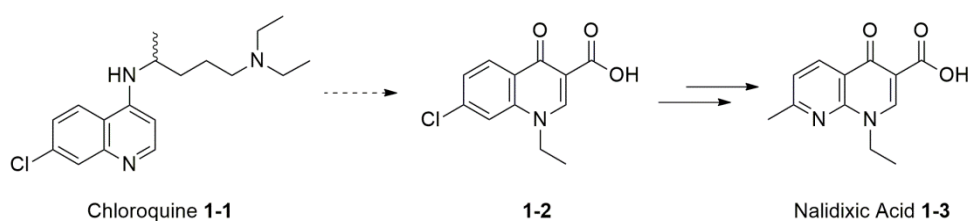
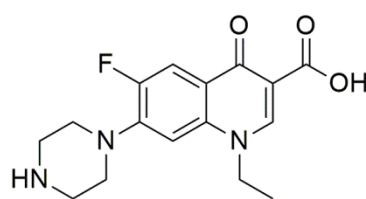
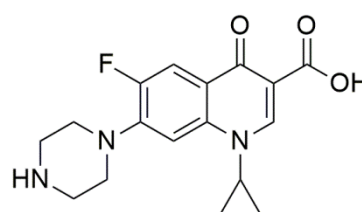
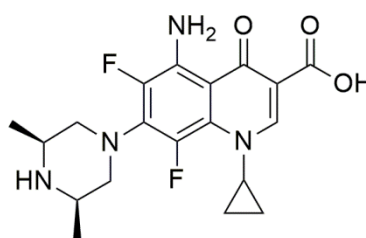
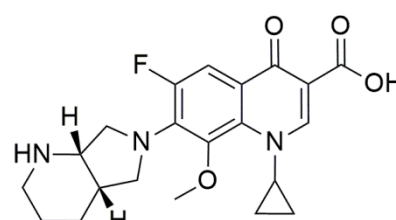
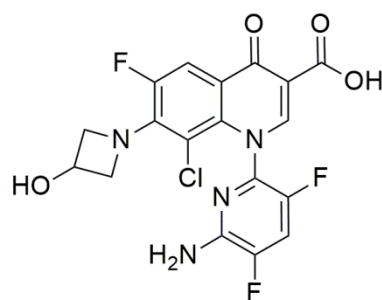


Figure 1 - Development of nalidixic acid (**1-3**) from impurity **1-2** discovered during the synthesis of chloroquine (**1-1**).

Later developments of the quinolone class saw the introduction of the fluoroquinolones in the early 1980s. Norfloxacin **1-4** (1980) and ciprofloxacin **1-5** (1983) are fully synthetic second-generation antimicrobials belonging to this class.^{13, 14} The enhancement of their activity and their broader spectrum against both Gram-negative and Gram-positive bacteria, compared to the original quinolones, led to their widespread use.^{10, 15} Indeed, ciprofloxacin **1-5** remains one of the most commonly prescribed antimicrobials worldwide.^{10, 16, 17} More recent developments include the introduction of the third and fourth generation fluoroquinolones, characterised as such due to their improved activity against Gram-positive strains and general enhancement in their spectrum of activity, with examples such as sparfloxacin **1-6** and moxifloxacin **1-7**.^{16, 18}

Currently, a new fluoroquinolone, delafloxacin **1-8**, is in phase III clinical trials, with its anionic charge contrasting with the typical zwitterionic character of other fluoroquinolones.¹⁹⁻²² Using moxifloxacin **1-7** as a comparison, delafloxacin **1-8** was shown to have enhanced uptake in bacteria under acidic conditions (pH 5.4), with increased activity against *Staphylococcus aureus*.²⁰ This enhancement in activity for delafloxacin **1-8** over moxifloxacin **1-7** under acidic conditions was proposed to be due to the transmembrane diffusion model.²⁰ Accounting for this, the authors suggest that under neutral conditions inside the bacterial cell, delafloxacin **1-8** will be deprotonated and thus will be less likely to diffuse from the cell than moxifloxacin **1-7**, thus explaining the increased accumulation of delafloxacin observed.²⁰

Norfloxacin **1-4**Ciprofloxacin **1-5**Sparfloxacin **1-6**Moxifloxacin **1-7**Delafloxacin **1-8**

Mechanism of fluoroquinolone action

The antimicrobial activity of the fluoroquinolones arises from their ability to disrupt two enzymes within bacterial species that are part of the deoxyribonucleic acid (DNA) replication pathway: DNA gyrase (Gram-negative strains) and topoisomerase IV (Gram-positive strains).²³⁻²⁶ These two enzymes are critical as they stabilise supercoiled bacterial DNA by creating negative supercoils to relieve topological stress during DNA replication.^{26, 27} Both DNA gyrase and topoisomerase IV comprise four subunits, though they differ in how DNA is allowed to pass through, with DNA gyrase wrapping DNA around itself while topoisomerase IV does not.^{26, 27} However, both use a double-strand passage mode of action and thus the mechanism of action of fluoroquinolones is similar for each enzyme.^{26, 27}

One early proposed mechanism of fluoroquinolone activity suggested that four fluoroquinolones were required to inhibit the enzymes by stacking into a binding pocket.²⁸ However, Laponogov *et al.* later co-crystallised moxifloxacin **1-7** with DNA and topoisomerase IV from *Streptococcus pneumoniae*, showing only two fluoroquinolones are required.²³ In addition, Bax *et al.* co-crystallised ciprofloxacin **1-5** with DNA and DNA gyrase from *S. aureus*, agreeing with Laponogov *et al.* that two fluoroquinolones interchelate DNA between the DNA base pairs, stabilising a ternary complex in the GyrB/ParC subunits of the enzyme (**Figure 2**).²⁴ As can be seen in **A**, **B** and **C** of **Figure 2**, the three viewpoints of the structure demonstrate where DNA sits within the subunits of DNA gyrase, as well as where ciprofloxacin interchelates (highlighted in **A**). View **D** in turn shows the specific binding of ciprofloxacin within the DNA base pairs (**Figure 2**). Whilst Bax *et al.* used MnCl₂ as part of their crystallisation conditions,²⁴ the presence of Mn²⁺ in their structure agrees with previous work demonstrating metal ions must be present for cleavage of the DNA backbone, though this was shown

in human topoisomerase II α .²⁹ It had been previously suggested that magnesium ions play a role in stabilising the ternary complex by encouraging tighter binding.³⁰ As such, the presence of metal ions in the structure reported by Bax *et al.* lends support to the role of metal ions in fluoroquinolone action.

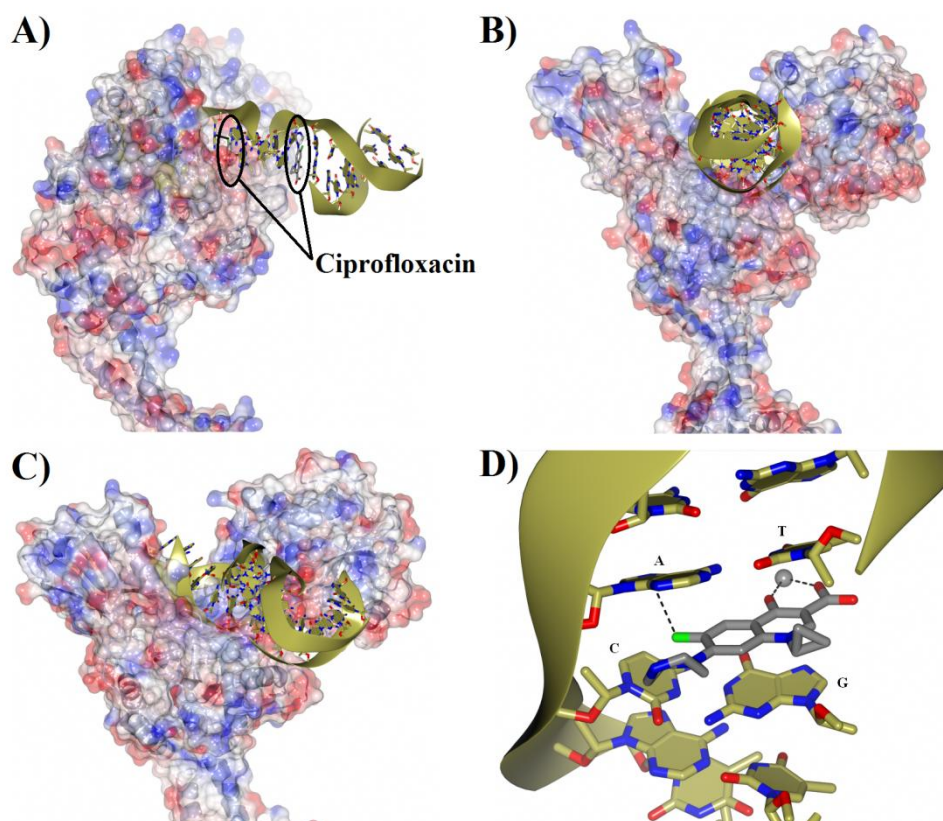


Figure 2 - Ciprofloxacin co-crystallised with both DNA and DNA gyrase of *S. aureus*, where two fluoroquinolones stabilise the ternary complex by interchelating between the DNA base pairs: **A** - side view; **B** - front view; **C** - angled view; **D** - zoom of one binding site. PDB code: 2xct.²⁴ Gold = DNA backbone/carbon; grey = carbon; blue = nitrogen; red = oxygen; green = fluorine; Mn = grey sphere. Translucent surface - negative charge shown in red and positive charge shown in blue.

More recently, Osheroff *et al.* demonstrated that topoisomerase IV-fluoroquinolone interactions are mediated through a water-metal ion bridge

through serine and glutamic acid residues, furthering support for the role of metal ions in fluoroquinolone binding.³¹ However, Drlica *et al.* have also recently proposed that there are two modes of drug binding for modified fluoroquinolones in gyrase-DNA complexes.²⁵ Drlica *et al.* found that attachment of a chloroacetyl moiety to the piperazinyl moiety of ciprofloxacin **1-5** can lead to an interaction with a different subunit of both DNA gyrase and topoisomerase IV. This new interaction occurred through nucleophilic attack of a cysteine unit at the chloroacetyl moiety of the modified drug, which resulted in the GyrA and GyrB subunits being cross-linked, despite being 17Å apart (**Figure 3**).²⁵ Furthermore Drlica *et al.* also reportedly identified a second potential binding pocket bridging the GyrA-GyrA interface.²⁵ However, it should be highlighted that the addition of a chloroacetyl moiety is not suitable within drug design given that it would be too reactive within untargeted cells. As such, the concept of a second mode of action must be considered with caution given that Drlica *et al.* did not use a standard fluoroquinolone, instead adding a reactive species which allowed for this observed interaction.

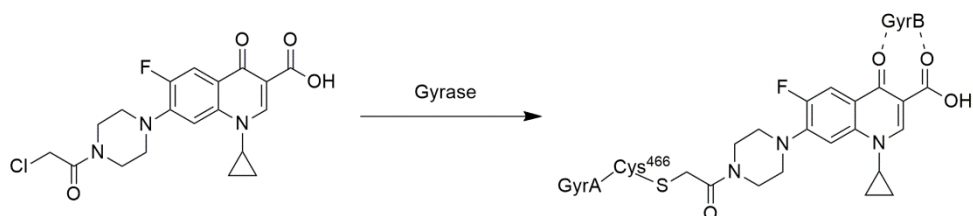


Figure 3 - Simplified representation of secondary binding mode for modified fluoroquinolones in DNA gyrase, proposed by Drlica *et al.*²⁵

Given that fluoroquinolone activity results in the inhibition of both DNA gyrase and topoisomerase IV, these antimicrobials ultimately lead to bacterial apoptosis. Furthermore, with ongoing discussion regarding the mechanism of fluoroquinolone activity, it is still important that this antimicrobial class continues to be developed, as alluded to earlier with delafloxacin **1-8**.

Understanding the fluoroquinolone pharmacophore

With the continued development of fluoroquinolones, it is important to consider the pharmacophore of fluoroquinolones to understand what functional groups are tolerated, and those which are essential for their activity (**Figure 4**).^{12, 32} As **Figure 4** shows, there are a number of positions where substitutions can be made on the fluoroquinolones. The β -keto acid, labelled 3, is essential for target site binding (purple - **Figure 4**),²⁶ and thus no changes should be made.^{12, 32} The R group at point 1 (gold - **Figure 4**) has been shown to control potency, with some effect on the pharmacokinetics, with small non polar groups the best tolerated.^{12, 32} Modification at point 2 (orange - **Figure 4**) is possible, with small rings tolerated, but given it is close to the gyrase binding unit, small hydrophobic groups are best, and this position is often left unfunctionalised. Addition of small polar groups at point 4 (pink - **Figure 4**), such as amino or hydroxyl groups, can aid potency, as well as improve Gram-positive activity.^{12, 32} The addition of the fluoride group at point 5 (green - **Figure 4**) to the original quinolones helped improve gyrase and antimicrobial potency by up to 100-fold more than other groups in the same position, and thus was the most important addition into the pharmacophore.^{12, 32} Perhaps the next most important substitution point on the pharmacophore is the R group at point 6 (blue - **Figure 4**), controlling pharmacokinetics, potency and spectrum activity. Generally, 5- and 6- membered rings are the most active, with an incorporated secondary or tertiary amino group being the most effective for oral efficacy.^{12, 32} Finally, the X group at point 7 (red - **Figure 4**) also helps control the pharmacokinetics as well as anaerobic activity, with small polar groups best tolerated.^{12, 32}

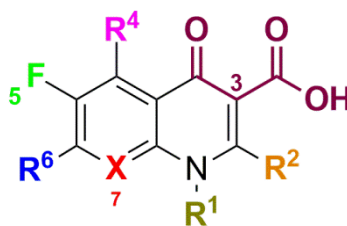


Figure 4 - Basic pharmacophore for fluoroquinolones with substitution positions numbered.

Despite the success of the fluoroquinolones, they, like most classes of antimicrobials, face the growing problem of antibiotic resistance. Bacterial resistance to fluoroquinolones results from a number of mechanisms, which are outlined below.

1.3 Bacterial Resistance to Antibiotics

The emergence of antibiotic resistance was reported almost as quickly as the introduction of the first antibiotics. In 1940 an enzyme able to decompose penicillin (later known as a β -lactamase) was discovered,³³ before even the widespread use of the drug. With an ever increasing number of drug resistant bacterial strains discovered, the problem has become a global threat, with the World Health Organisation concluding in their 2014 report that bacterial resistance is a “major public health concern”.³⁴ As such, there are warnings that unless the problem is tackled, the concept of returning to a pre-antibiotic era, where common infections cannot be effectively treated, will become a reality.³⁵

The increasing pace of resistance has been attributed to a number of factors, primarily through the misuse and overuse of antibiotics in both human and veterinary medicine.^{4, 36} Furthermore, some species of fungi and bacteria produce their own antibiotics in order to compete with other

organisms, and these, in turn, carry genes encoding resistance to the antibiotic they produced.³⁶ Coupled with the intrinsic resistance of some bacterial species to certain antimicrobial agents, these forms of resistance can lead to acquired resistance through the ability of microorganisms to trade DNA through horizontal transfer (**Figure 5**).^{3, 36} The rise in multi-drug resistant (MDR) strains of bacteria has therefore occurred through the ability of organisms to share resistance genes, with resistance arising through several mechanisms.

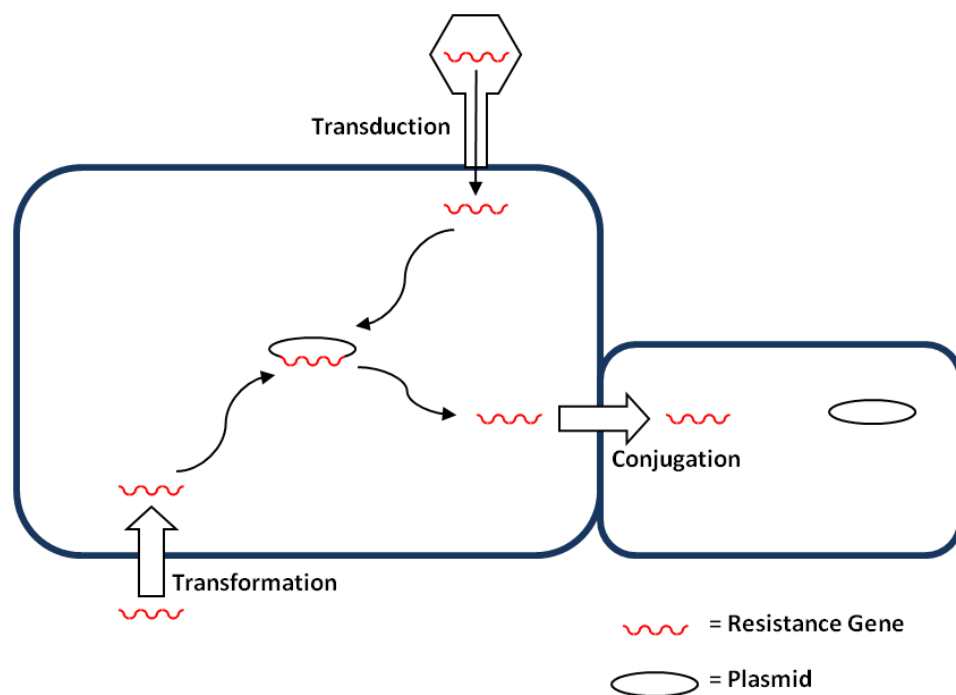


Figure 5 - Horizontal transfer of antibiotic resistance genes between bacterial cells.^{3, 36} Transduction = Viral transfer / Transformation = Foreign absorption / Conjugation = Intra- or Interspecies transfer.

Mechanisms of resistance

There are a number mechanisms by which bacteria exhibit antimicrobial resistance, with some combining several of these mechanisms, leading to MDR bacterial strains.^{4, 36-40} Such mechanisms include reduced

permeability (**A - Figure 6**), upregulation of efflux pumps (**B - Figure 6**), alterations or mutations to the intracellular drug binding sites (**C - Figure 6**), enzymes that inactivate the antibiotic through modification (**D - Figure 6**) and enzymes which can degrade the drug (**E - Figure 6**).^{4, 36-40}

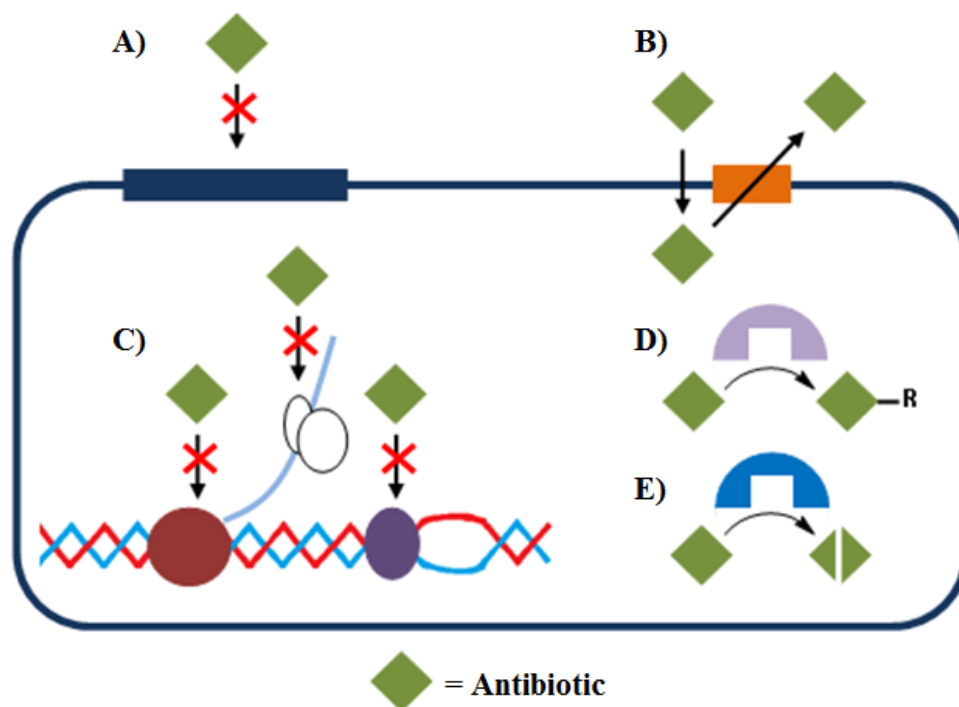


Figure 6 - Schematic diagram demonstrating the mechanisms of bacterial resistance.^{4, 36-40} **A** - Reduced permeability; **B** - Efflux pumps (orange rectangle); **C** - Alterations of binding sites, e.g. gyrase (purple), RNA polymerase subunits (maroon) or other target proteins (white); **D** - Modification by enzymes (light purple); **E** - Degradation by enzymes (light blue).

With regards to the fluoroquinolones, resistance has been shown to occur through each of the mechanisms highlighted above (**Figure 6**).^{16, 38-40} For example, it has been shown that a variant of an aminoglycoside acetyl transferase could modify fluoroquinolones through *N*-acetylation of the piperazinyl moiety of norfloxacin **1-4** and ciprofloxacin **1-5** (**Figure 7**), resulting in reduction of the antimicrobial activity.⁴¹

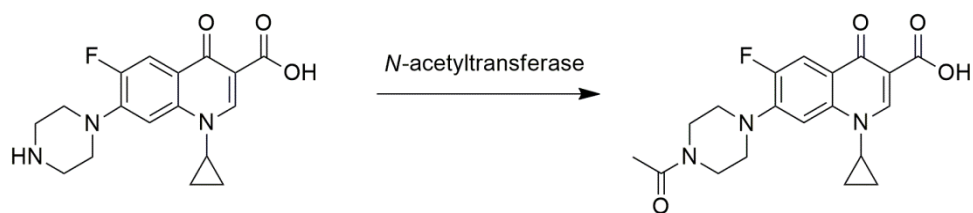


Figure 7 – Enzymatic deactivation of ciprofloxacin **1-5** by *N*-acetylation.⁴¹

As mentioned previously, Osheroff *et al.* have demonstrated that a water-metal ion bridge facilitates fluoroquinolone-topoisomerase IV binding through a serine and glutamic acid residue.³¹ Interestingly, this observation provides a likely mechanism for a previously known form of fluoroquinolone resistance resulting from mutations of these residues.^{31, 40} Indeed, mutations and alterations to binding sites are common forms of fluoroquinolone resistance and include proteins known as quinolone resistance proteins (Qnr), which shield the DNA-gyrase complex, preventing drug access.⁴⁰

In order to reduce intracellular drug concentration, expression of efflux pumps can cause resistance to fluoroquinolones by removing the antimicrobial agent from the bacterial cell.³⁷ Furthermore, a reduction in cell permeability can also result in a decrease in intracellular drug concentration. One form of reduced permeability results from the formation of bacterial biofilms, making it difficult for the antibiotic to penetrate the polymer matrix formed, ensuing resistance.⁴² In addition, the routes by which fluoroquinolones enter bacterial cells are through either passive diffusion or through non-specific porin channels, such as OmpF and OmpC, in the outer cell membrane.^{40, 43} As such, downregulation of these outer membrane porins can lead to a reduction in the intracellular concentration of the drug through reduced uptake into the cell.⁴⁰ It is resistance associated to a reduction in cell permeability that the Trojan

horse strategy aims to overcome, by increasing the intracellular concentration of the drug, discussed in greater detail later in this Chapter.⁵⁻⁸

Combating antimicrobial resistance

With the prevalence of antibiotic resistance, a number of strategies have been developed to counter the growing problem. However, as a recent study found, spending in the United Kingdom on antibiotic resistance research amounted to just £102 million between 1997 and 2010, accounting for only 3.9% of the total spend on infectious diseases,⁴⁴ presenting a significant hurdle in the development of new strategies against resistance.

Typical strategies employed against bacterial resistance include the development of new antibiotics, discovery of natural products with antibacterial activity, combination therapy, development of analogues of existing drugs, and new methodologies of drug delivery.³⁻⁸ All these strategies are important in the struggle against antimicrobial resistance. This thesis is concerned with the development of siderophore-antimicrobial conjugates, the so called ‘Trojan horse’ strategy, introduced as a means to overcome permeability-related resistance through the delivery of the drug *via* the iron uptake systems.^{5-8, 45} As such, the remainder of this Chapter focuses on this strategy as one approach against antimicrobial resistance.

1.4 Siderophores

Iron bioavailability

Iron is an essential nutrient for cells, being a cofactor in a number of enzymes as a result of its redox chemistry.⁴⁶ As a result almost all bacteria, like most other living organisms, require iron as a nutrient for survival.⁴⁶ Despite the abundance of iron in the environment, its bioavailability is severely limited as it exists mainly as insoluble ferric iron (Fe(III)), due to the aerobic conditions of our atmosphere limiting the presence of soluble ferrous iron (Fe(II)).⁴⁷ Consequently, the concentration of free Fe(III) is limited to $\sim 10^{-18}$ - 10^{-24} M under physiological conditions (for Fe(OH)₃).^{47, 48} With the scarce availability of Fe(II) in aerobic environments, bacteria have had to evolve mechanisms for the sequestration of Fe(III), producing chelating ligands known as siderophores. These chelators can solubilise Fe(III) and mediate its uptake into the cell, allowing bacteria to maintain adequate cellular iron concentrations for their survival within the mammalian host.^{45, 49-51}

Types of siderophores

The first siderophores were identified in the early 1950s and recognised as growth factors for the organisms from which they were acquired.⁵² Since then over 500 unique siderophores have been discovered, obtained from bacterial, fungal and plant species.^{45, 49-51}

Siderophores are generally grouped by their chelating units, with the most common siderophore classes being catecholate (e.g. enterobactin **1-9**), hydroxamate (e.g. desferrioxamine B **1-11**) or α -hydroxycarboxylate (e.g.

citric acid **1-12**) (**Figure 8**). As **Figure 8** shows, these iron binding units contain oxygen moieties as hard Lewis base donors, which can meet the binding requirements of the hard Lewis acid Fe(III), given its d^5 high-spin electronic configuration.^{45, 50} However, it is also possible for nitrogen and sulfur donating moieties to bind iron, though they have a lower affinity for iron(III). Enterobactin **1-9**, produced by a number of species including *Escherichia coli*, is one of the strongest iron chelators known, given that it is a hexadentate ligand capable of forming an octahedral 1:1 complex with Fe(III).⁵³ However, a number of hydrolysis products of enterobactin exist, such as the tetradentate linear dimer **1-10**, which are known to support bacterial growth.⁵⁴ Furthermore, citric acid **1-12** acts an exogenous siderophore, not produced by bacteria but uptaken due to its abundance in nature and iron binding capability.^{55, 56}

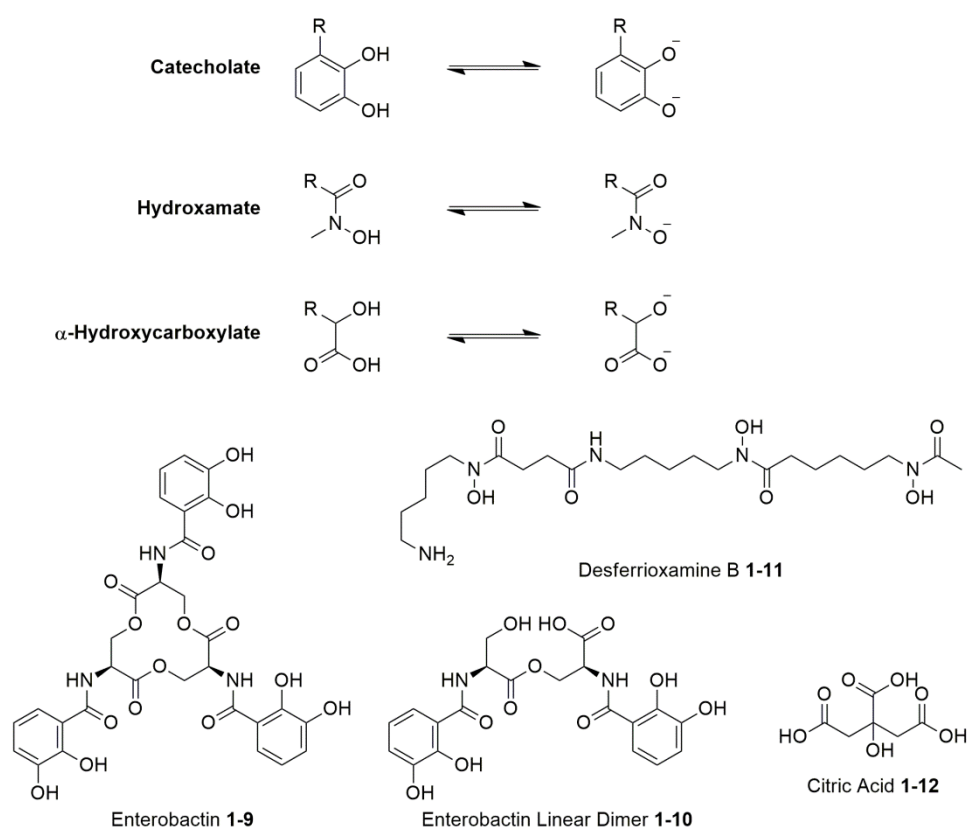


Figure 8 - Common siderophore binding units, with representative examples enterobactin **1-9**, enterobactin linear dimer **1-10**, desferrioxamine B **1-11** and citric acid **1-12**.

As mentioned above, the ability of siderophores to scavenge Fe(III) from the environment allows them to provide the required nutrient to the bacterial cell. Thus it is important to understand the iron-binding strength of siderophores, generally reported as a pFe(III) value, which is defined as the negative logarithm of free [Fe(III)] under fixed conditions ([siderophore] = 10 μ M and [Fe(III)] = 1 μ M at pH 7.4). Based on this, the pFe(III) values of enterobactin **1-9** have been determined as 35.5, desferrioxamine B **1-11** as 26.5 and citric acid **1-12** as 17.7.⁵⁷ As such, these pFe(III) values help demonstrate that hexadentate ligands are the strongest at Fe(III) binding, given their capacity to form octahedral complexes and thus complete the coordination sphere of Fe(III). However, a range of tetradentate, tridentate and bidentate siderophores have been shown to support bacterial growth, such as the aforementioned citric acid **1-12**.^{45, 50, 55, 56} Considering the abundance of siderophores available, and their variations in ligand geometry and structure, the siderophore uptake mechanisms are relatively general.^{45, 50}

Ferric-siderophore uptake mechanisms

Gram-negative bacteria have two membranes, with a periplasm in between. Whilst the outer membrane is freely permeable towards small hydrophobic molecules, due to the lipid bilayer which contains porins such as OmpF,^{40, 43} most ferric-siderophore complexes are too large for these porins and thus require specific uptake mechanisms.⁵⁸ These uptake mechanisms have developed so the ferric-siderophore complex can be transported through both cell membranes into the cytoplasm (**Figure 9**).

Ferric-siderophore uptake occurs whereby the complex is transported through an outer membrane receptor, generally specific to each ferric-

siderophore complex, into the periplasm (**Figure 9**).⁵⁸ Examples of these specific outer receptors include FecA for the uptake of ferric-citrate,⁵⁹⁻⁶² and FepA for the uptake of ferric-enterobactin.^{58, 63} Reported crystal structures of these two proteins, and those solved for other outer membrane receptors, demonstrate barrel structures spanning the membrane through which the complex is transported.^{62, 63} The process of transport through the outer membrane receptor is dependent on the TonB complex, consisting of three inner membrane proteins: TonB, ExbB and ExbD. The TonB complex is an energy transducer, aiding in the transfer of energy between the cytoplasmic membrane to the outer membrane.^{64, 65}

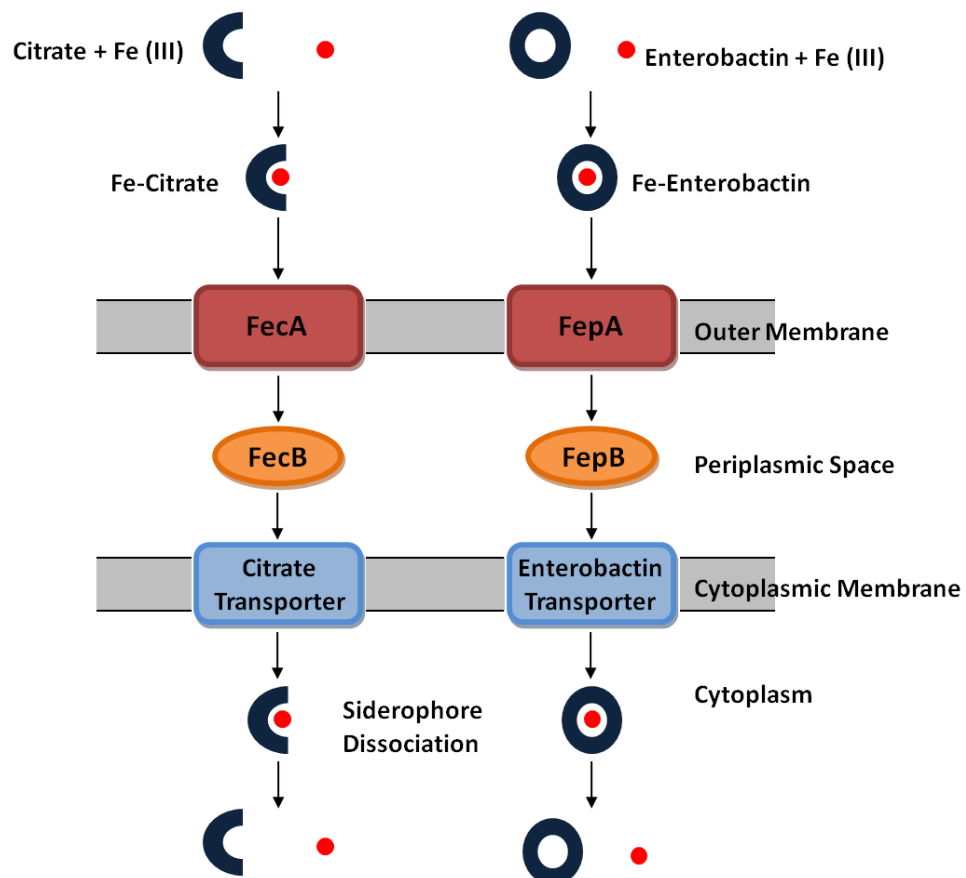


Figure 9 - Schematic representation of ferric-siderophore complexes into a Gram-negative bacterial cell. Blue circle/half-circle = Siderophore / Red circle = Fe(III).

Once inside the periplasm, the complexes are shuttled through to the ABC transporters by periplasmic-binding proteins (**Figure 9**).⁵⁸ Like the outer membrane receptors, there are generally specific periplasmic binding proteins for each ferric-siderophore complexes, such as FecB for citrate and FepB for catecholate siderophores, though they are accommodating for other related structures.⁵⁸ Finally, access into the cytoplasm occurs through ABC transporters, which consist of four structural domains: two transmembrane domains forming a channel and two ATP binding domains (**Figure 9**).⁵⁸ On entry into the cytoplasm, release of the iron from the complex can occur *via* two routes, either through reduction of Fe(III) to Fe(II), or through degradation of the siderophore itself.⁴⁵

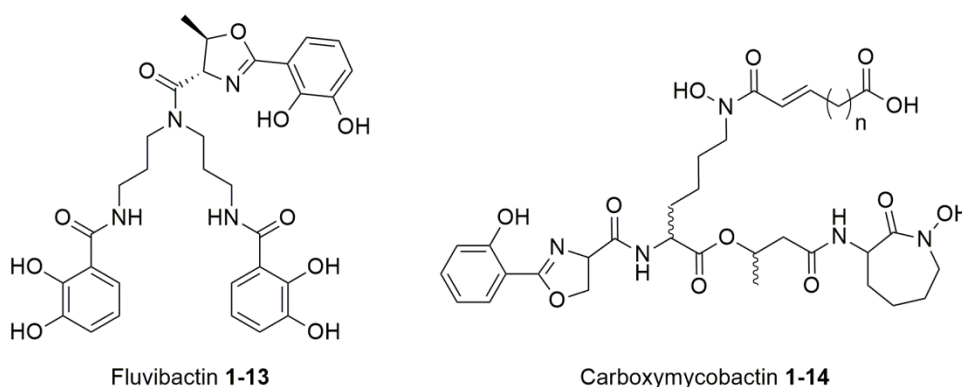
Compared to Gram-negative bacteria, less is known about the Fe(III) uptake mechanisms into Gram-positive bacteria, with research centered on *Bacillus subtilis* and *S. aureus*.^{45, 66} Given that Gram-positive bacteria do not have an outer membrane, the uptake mechanism is analogous to the inner membrane transport system of Gram-negative bacteria. Instead of a periplasmic-binding protein, there is a lipoprotein anchored to the membrane, which is assumed to interact with an ABC transporter to shuttle the complex into the cell.⁶⁶

Fortunately, the binding units of the siderophore are the only components essential for recognition for the uptake proteins, which allows for attachment of other moieties to the siderophore backbone without disrupting siderophore uptake.⁵ Such a feature can be exploited to deliver antimicrobials *via* the Trojan horse strategy through the uptake mechanisms, as a means to by-pass permeability-related resistance pathways,⁵⁻⁸ discussed later in this Chapter.

Mammalian response to siderophores and the fight-back by bacteria

Given the success of bacteria in scavenging iron within their host to survive, mammals have evolved several defence mechanisms to limit free iron concentration. Whilst not produced directly as a defence against pathogens, mammalian hosts do generate iron storage and transport proteins, ferritin and transferrin.^{67, 68} These proteins are produced predominantly to protect the host from free iron, which can otherwise be involved in Fenton chemistry that leads to cell damage, though these proteins are capable of competing for free iron.^{67, 68}

Further to production of iron storage and transport proteins, many mammalian hosts generate proteins known as siderocalins, a subset of the lipocalin family.⁶⁹⁻⁷³ These proteins are able to bind ferric-catecholate siderophores using three positively charged residues at the top of a hydrophobic pocket, which interact with the negative charge of the ferric-catecholate complexes.⁶⁹⁻⁷³ This was demonstrated by the crystal structure of siderocalin bound to fluvibactin (**1-13**), produced by *Vibrio fluvialis* (**Figure 10**).⁷³ A combination of cation- π and ionic interactions stabilise the protein-siderophore complex.⁶⁹⁻⁷³ Furthermore, a number of catecholate siderophores have been found to bind to siderocalin, including enterobactin **1-9**,⁷⁰ and the mixed ligand catecholate siderophore carboxymycobactin **1-14** (from *Mycobacterium*).⁷⁴



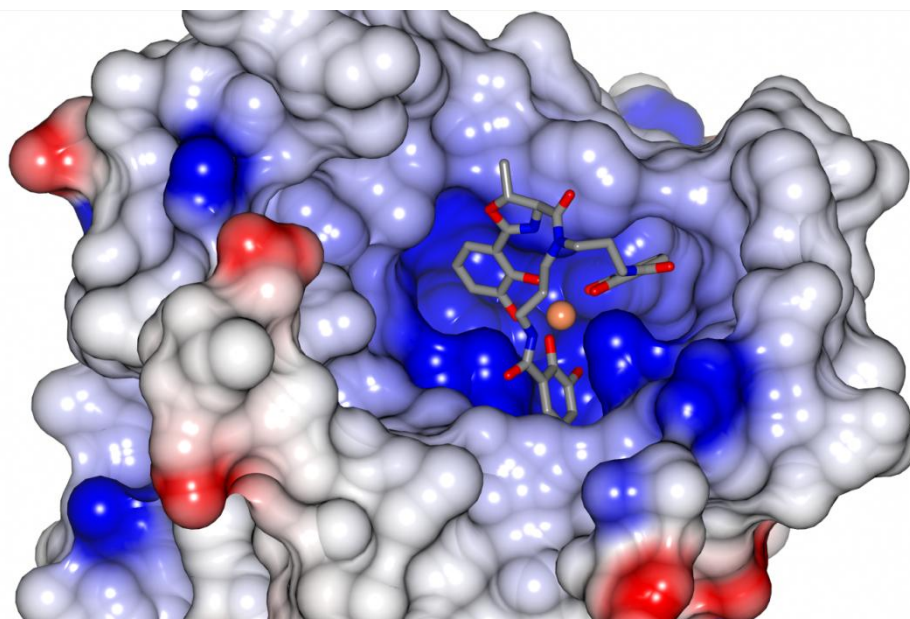
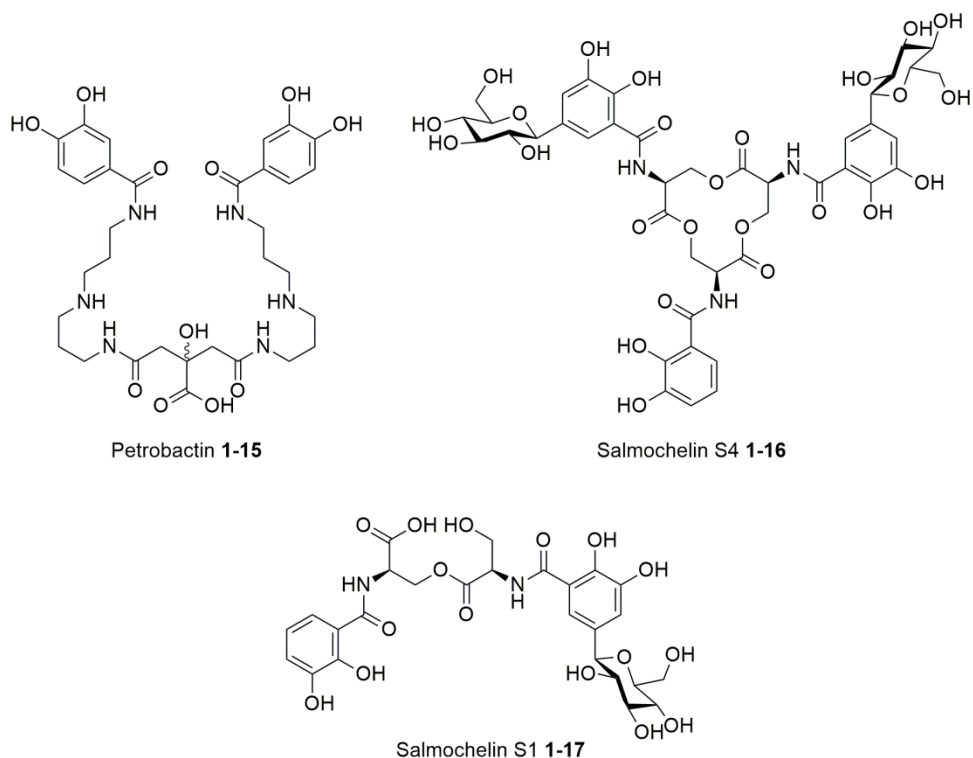


Figure 10 - Crystal structure of siderocalin bound to ferric-fluoribactin. PDB code: 4K19.⁷³ Grey = carbon; blue = nitrogen; red = oxygen; Fe = coral sphere. Surface - negative charge shown in red and positive charge shown in blue.

However, with the continuous struggle between the mammalian host and microorganisms in the competition for iron, bacteria have evolved to evade the siderocalin protein. By taking advantage of the strict binding requirements of siderocalin, some bacterial species now produce and secrete so called ‘stealth siderophores’. Petrobactin **1-15**, produced by both *Bacillus anthracis* and *Bacillus cereus*, contains an unusual 3,4-catecholate arrangement, and is thus able to avoid siderocalin binding by virtue of this change in configuration.^{75, 76} In addition, the bacterial species *E. coli*, *Salmonella* sp. and *Klebsiella* sp. have each been found to produce a glucosylated analogue of enterobactin known as salmochelin S4 **1-16**.^{77, 78} Furthermore, hydrolysis products of salmochelin S4, such as salmochelin S1 **1-17**, are known to support bacterial growth, though less is currently known about the production and uptake of these salmochelins.⁷⁷⁻⁷⁹ The glucosyl moieties introduce sufficient steric hindrance to disrupt the ability of siderocalin to scavenge the salmochelins.⁷⁰



With the knowledge that siderocalin can sequester catecholate siderophores, it is important to consider the siderocalin protein when designing siderophore-antimicrobial Trojan horse conjugates, as a means to avoid potential catecholate-antimicrobial conjugates also being scavenged by this protein. Such an approach is targeted with a salmochelin-inspired conjugate, discussed in detail in Chapter 4.

1.5 Trojan Horse Strategy

Overview of the concept

Inspired by Greek mythology, the concept of the Trojan horse strategy involves disguising an antimicrobial as an essential nutrient to a bacterial

species. The strategy aims to exploit bacterial iron uptake so as to actively transport a siderophore-antimicrobial conjugate into the cell, as a means to evade resistance associated with a reduction of cell membrane permeability or efflux pumps.^{5-8, 80} The requirement for iron enables these conjugates to be uptaken into microbial cells to avoid iron starvation, where the conjugate as a whole, or the released drug, can lead to antimicrobial activity (**Figure 11**).⁸⁰ The use of this strategy is of particular interest to the work presented in this thesis, with the approach having been widely studied previously. Moreover, it should be noted that the strategy was first developed in nature, with naturally occurring Trojan horse conjugates, known as the sideromycins.

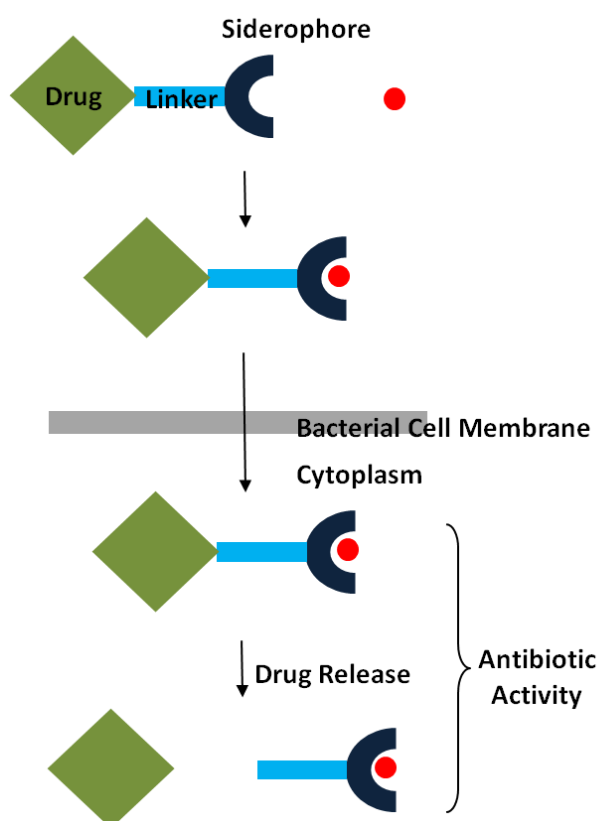
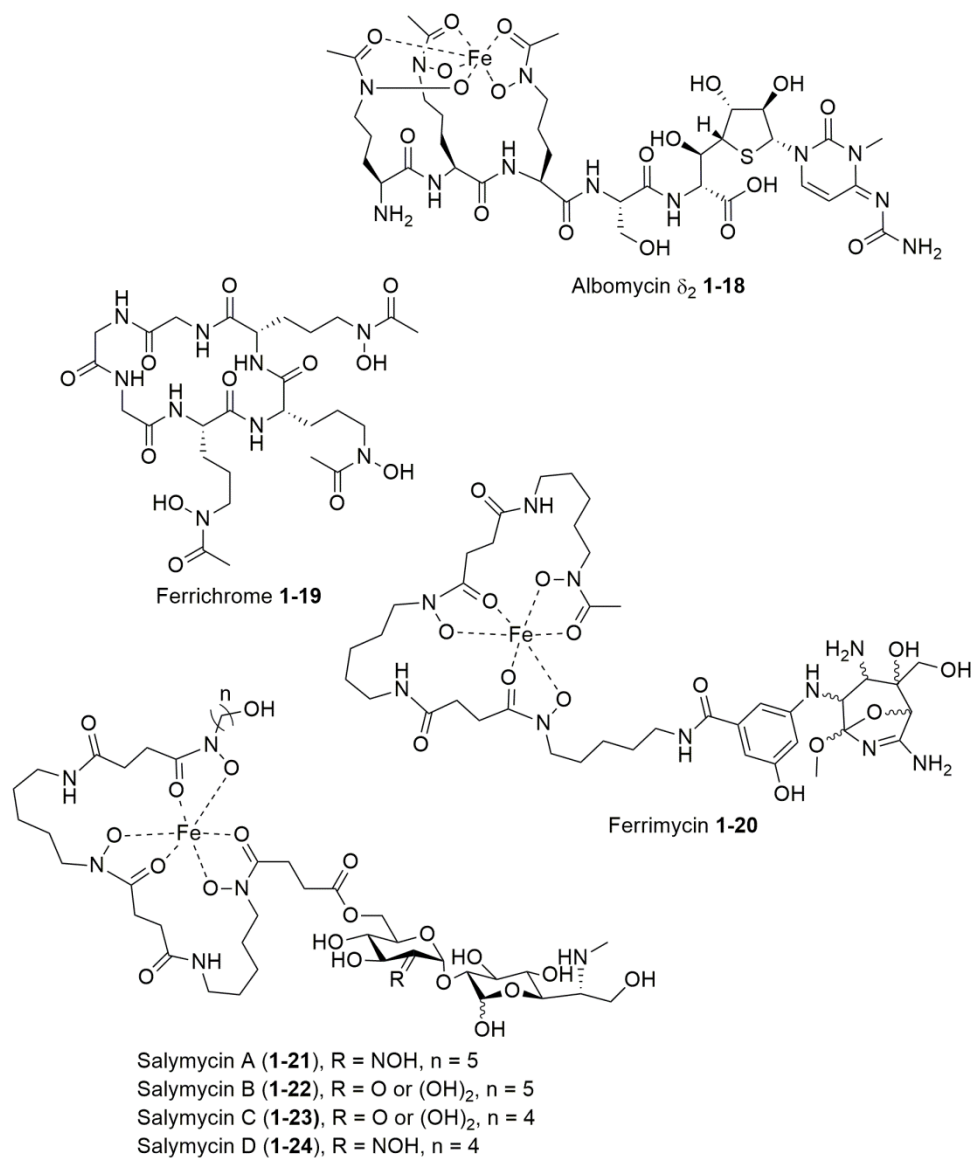


Figure 11 - Simple representation of the Trojan horse strategy. Green diamond = antibiotic drug; blue rectangle = linker; dark blue half circle = siderophore; red = Fe(III).

Natural Trojan Horse Conjugates – The Sideromycins

In the competition for iron between bacterial species, some bacterial strains have evolved to produce their own natural Trojan horse conjugates, the sideromycins, as a means to gain a survival advantage. For example *Actinomyces subtropicus* produces the albomycins (e.g. albomycin δ_2 **1-18**) which consists of a hydroxamate siderophore, analogous to ferrichrome **1-19**, linked through a serine spacer to a thioribosyl-pyrimidine antibiotic.^{80, 81} It was shown that albomycin is taken up through the ferrichrome outer membrane receptor protein FhuA. Once inside the cell the antibiotic is released by enzymatic action, leading to cell death.^{80, 82} Further examples include ferrimycin (**1-20**) and the salmycins (**1-21** - **1-24**), each containing the siderophore desferrioxamine B **1-11** linked to antimicrobial moieties which can act against a variety of bacterial species.^{6, 80}

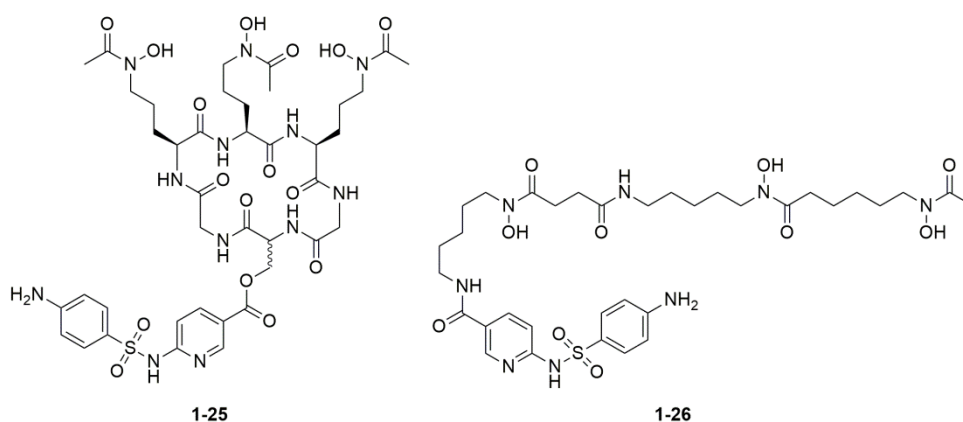


Unsurprisingly, the discovery of the sideromycins has inspired the targeted approach of developing synthetic Trojan horse conjugates, with extensive research in the design of these compounds.^{5-7, 80}

Synthetic Trojan Horse Conjugates

Among the first synthetic Trojan horse conjugates, Zähler *et al.* reported in 1977 two conjugates based on ferrichrome **1-19** and desferrioxamine B **1-11**, conjugated to a sulfonamide antimicrobial agent, compounds **1-25** and

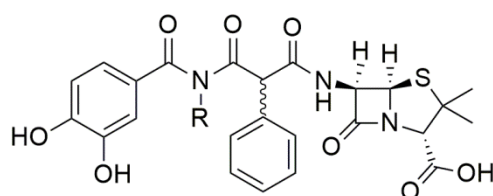
1-26 respectively.⁸³ Impressively, they found that compound **1-25** was active against *S. aureus*, at similar levels to the parent drug, though compound **1-26** had no activity.⁸³ Not only did this early study demonstrate the viability of the Trojan horse approach, but it was also the first to pose the questions of siderophore and linker choice, and whether drug release was required to retain antibiotic activity.⁸³ Further to the use of sulfonamides, conjugates have been designed using other antibiotics such as vancomycin, β -lactams and fluoroquinolones.^{5-8, 84}



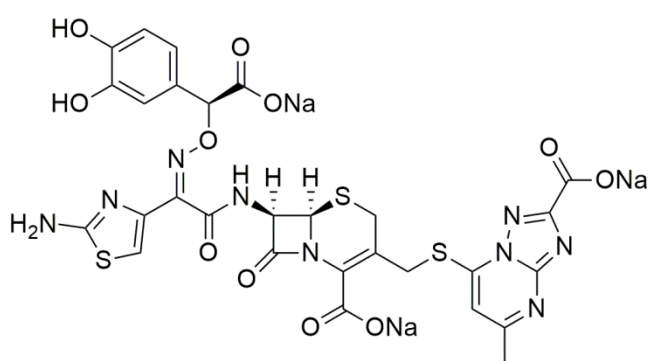
Siderophore- β -lactam Trojan horse conjugates

Since the original work of Zähler *et al.* a significant proportion of reported examples have focused on the use of β -lactam antibiotics in Trojan horse conjugates.⁵⁻⁸ The advantage of such an approach is that this antibiotic class targets proteins involved in the cell wall synthesis, which are located in the bacterial periplasm. As such, the siderophore- β -lactam conjugates only have to pass through the outer cell membrane to reach their target.⁸⁵ As a result, siderophore- β -lactam conjugates have generally had the most success.

Early studies of siderophore- β -lactam conjugates established the approach can lead to a significant improvement in antibiotic activity.⁸⁶⁻⁹¹ Two such early examples, reported by Ohi *et al.* in 1986, demonstrated that a single catechol moiety attached to ureidopenicillins, could lead to a 60-fold increase in activity against *Pseudomonas aeruginosa* strains compared to the parent drug (**1-27** and **1-28**).^{86, 87} Furthermore the authors postulated that the siderophore component was aiding conjugate uptake.^{86, 87} Soon after, Mochizuki *et al.* demonstrated the activity of their mono-catechol conjugate of cephalosporin (**1-29**) was significantly enhanced in low-iron environments in *E. coli*, by up to 20000-fold compared to when iron was not limited, suggesting their compound utilised the iron uptake systems.⁸⁸ As Miller later discussed, the fact these conjugates did not possess traditional hexadentate ligands suggests that a ligand:iron stoichiometry of 1:1 is not crucial for transport.⁹²



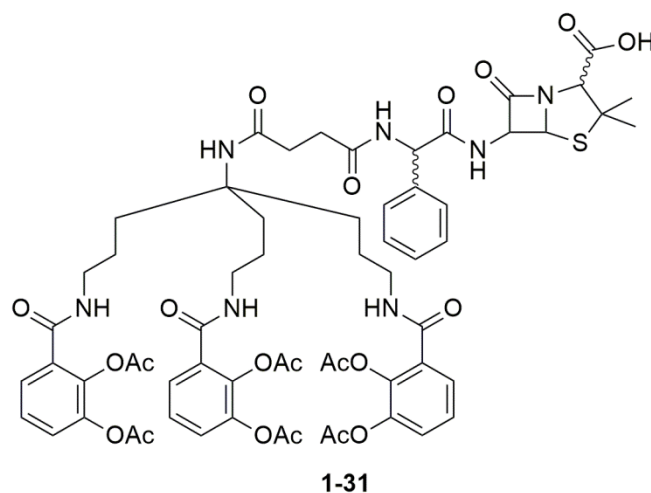
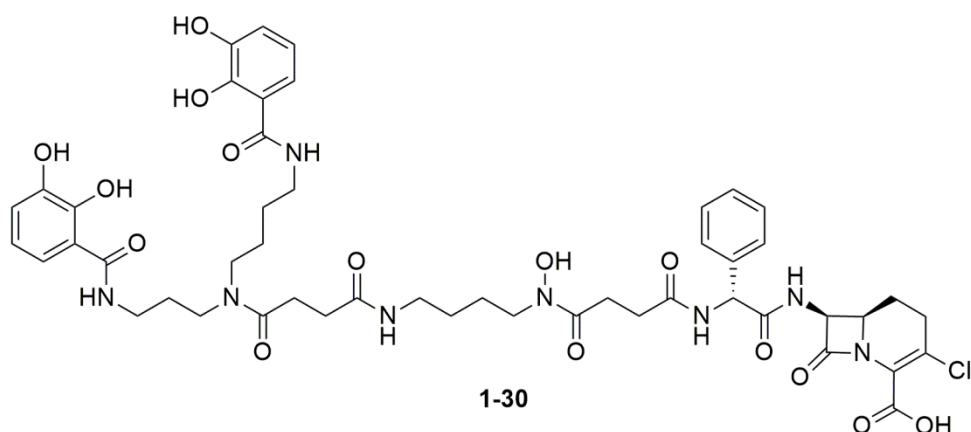
1-27 (R = -CH₃)
1-28 (R = -(CH₂)OH)



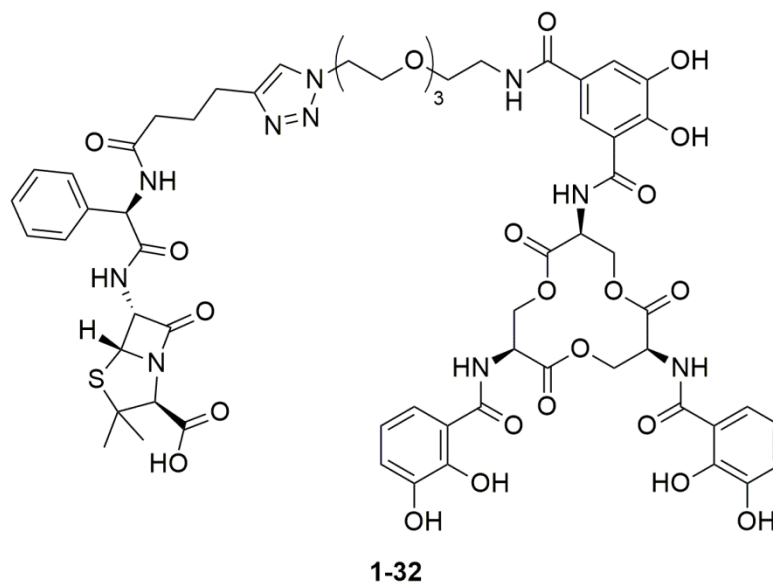
1-29

Subsequent studies of siderophore- β -lactam Trojan horse conjugates have investigated mixed ligand siderophores, such as that by Miller *et al.*⁹³ A conjugate containing both catechol and hydroxamate moieties, linked to the

antimicrobial Lorabid, conjugate **1-30**, showed a 2000-fold increase in activity against a strain of *Acinetobacter* compared to the parent drug.⁹³ Other promising siderophore- β -lactam conjugates followed,^{94, 95} including **1-31**, an acylated triscatecholate siderophore- β -lactam conjugate.⁹⁶ As a simple mimic of enterobactin **1-9**, conjugate **1-31** was designed to maintain the hexadentate ligand geometry without incorporating the synthetic challenge of the triserine backbone of enterobactin.⁹⁶ The use of acylated catechol moieties proved an interesting addition, designed to act as a prodrug to releasing the required iron binding hydroxylate moieties whilst allowing the conjugate to avoid potential methylation by catechol *O*-methyl transferase (COMT), which would prevent iron binding.⁹⁶ Such an approach was based on an earlier study by Ohi *et al.* who demonstrated improved stability of an acylated conjugate against COMT.^{96, 97} Further to this, conjugate **1-31** showed an eightfold increase in antimicrobial activity against *E. coli*, compared to ampicillin.⁹⁶



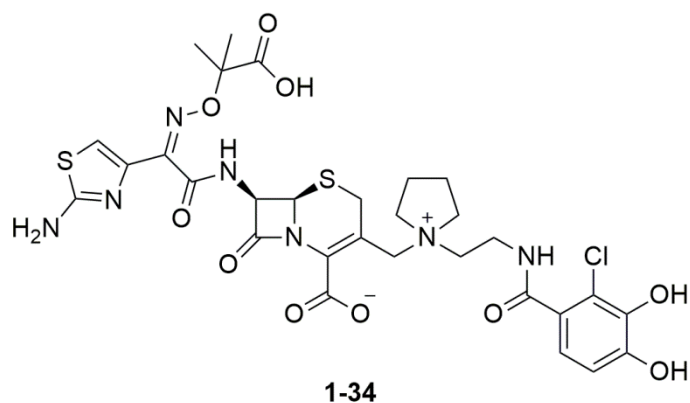
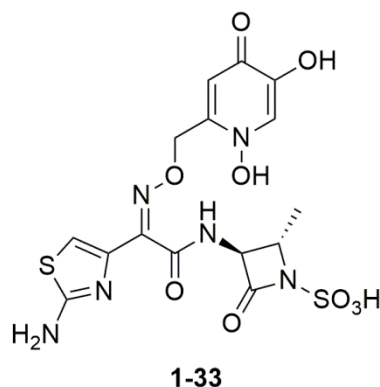
More recently, Nolan *et al.* employed enterobactin as the choice of siderophore in a β -lactam conjugate of ampicillin (**1-32**).⁹⁸ It was found that that antimicrobial activity was enhanced by up to 1000-fold compared to the parent drug against certain *E. coli* strains.⁹⁸ It was also demonstrated that attachment at the C-5 position of one of the catechol moieties did not disrupt conjugate uptake, assumed to be as a result of the long and flexible linker used between the antimicrobial and enterobactin siderophore.⁹⁸ However, as discussed earlier, the conjugate was scavenged by the mammalian response protein siderocalin, preventing its activity.⁹⁸ To avoid this unwanted outcome, Nolan *et al.* subsequently produced salmochelin-inspired conjugates, which were shown to avoid siderocalin binding and are discussed in greater detail in Chapter 4.⁹⁹



With the successes demonstrated by improved activity of siderophore- β -lactam conjugates compared to their parent drugs, it is important to highlight that comparative results have been achieved with monosulfactam and monocarbam siderophore-antimicrobial conjugates,¹⁰⁰⁻¹⁰³ including recent interest and development by AstraZeneca.¹⁰⁴⁻¹⁰⁶

Siderophore- β -lactam conjugates undergoing clinical trials

Of significance, it should be highlighted that two siderophore-antibiotic conjugates are currently undergoing clinical trials, demonstrating the progress in the Trojan horse strategy. Of these two conjugates one contains a monosulfactam antimicrobial **1-33**,¹⁰⁷⁻¹⁰⁹ and the other a β -lactam **1-34**.¹¹⁰⁻¹¹²



Conjugate **1-33**, known as BAL30072, is currently being developed by Basilea Pharmaceutica. The conjugate utilises a dihydropyridone moiety as the chelating unit,¹⁰⁷⁻¹⁰⁹ analogous in structure to the hydroxypridinone group of siderophores.¹¹³ This group of siderophores have a higher binding interaction with metal ions than hydroxamates.¹¹³ Moreover, conjugate **1-33** is undergoing phase I trials, having shown potent activity against numerous Gram-negative species, including MDR *Acinetobacter* spp. and MDR *P. aeruginosa*, with MIC₉₀ (MIC where 90% inhibition occurs) values of 4 and 8 µg/mL for each strain respectively.¹⁰⁷⁻¹⁰⁹

Making better progress, conjugate **1-34** (S-649266), in development through Shionogi & Co., is actively recruiting for phase III trials at the time of writing.^{110-112, 114} S-649266 **1-34** was shown to demonstrate activity against a number of MDR *Enterobacteriaceae*, and additionally it was

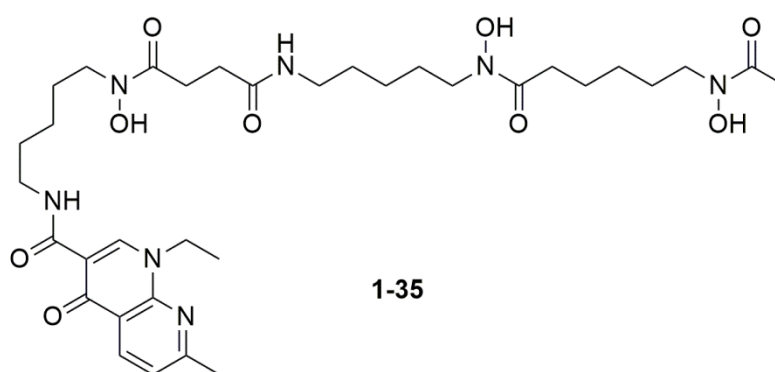
established that it maintains high stability against hydrolysis and degradation by β -lactamases.¹¹⁰⁻¹¹²

It should be noted that both conjugates **1-33** and **1-34** share a similar design feature, with the iron chelating moieties being in the 3,4-arrangement. This arrangement within these conjugates are similar in nature to the stealth siderophore petrobactin **1-15**, and therefore provides an attractive consideration for the future of conjugate design. Therefore, with these two compounds in clinical trials, it will be interesting to see their continued development, as well as their influence on the design of future siderophore- β -lactam Trojan horse conjugates.

Siderophore-fluoroquinolone Trojan horse conjugates

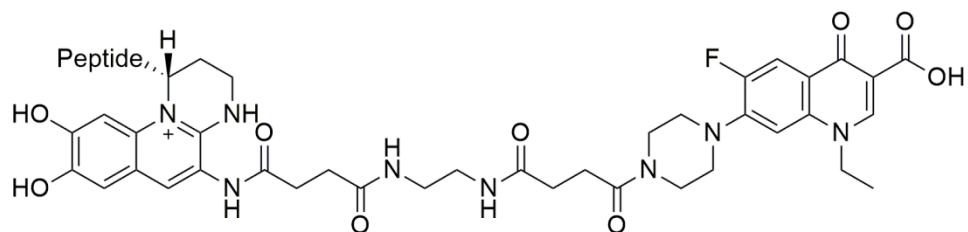
With the success demonstrated by siderophore- β -lactam conjugates, a number of studies have targeted siderophore-fluoroquinolone Trojan horse conjugates, given the widespread use of fluoroquinolone antimicrobials. However, the drug target within Gram-negative bacteria for the fluoroquinolones is located in the cytoplasm, providing an added challenge to conjugate design as they are required to cross both the outer and inner cell membranes. As such, there are fewer reported examples of fluoroquinolone conjugates. Whilst evidence has been demonstrated that siderophore-fluoroquinolone conjugates are taken up through the iron uptake mechanisms, it should be noted that no current siderophore-fluoroquinolone conjugates have demonstrated increased antimicrobial activity against either Gram-positive or Gram-negative bacteria.¹¹⁵⁻¹²⁸ Indeed, these studies have led to concerns that the siderophore/linker moieties of the conjugates may be reducing antimicrobial binding through steric hindrance within the target site. Nevertheless, these investigations provide understanding towards the key features required in siderophore-fluoroquinolone conjugate design.

One early example was a siderophore-quinolone conjugate, reported by Miller *et al.* producing a conjugate between nalidixic acid **1-3** and desferrioxamine B **1-11**, to give compound **1-35**.¹²⁹ Interestingly, the conjugate was connected through an amide bond at the β -keto acid, which, as highlighted earlier, is essential for gyrase binding. However, Miller *et al.* accounted for this as part of their design, hoping for the nalidixic acid moiety to intercalate into DNA, allowing the iron-siderophore complex to induce redox damage to the DNA through the Fenton reaction.¹²⁹ However, despite being found that the conjugate could perform DNA cleavage *in vitro*, it was only when Fe(II), hydrogen peroxide and ascorbate were present.¹²⁹

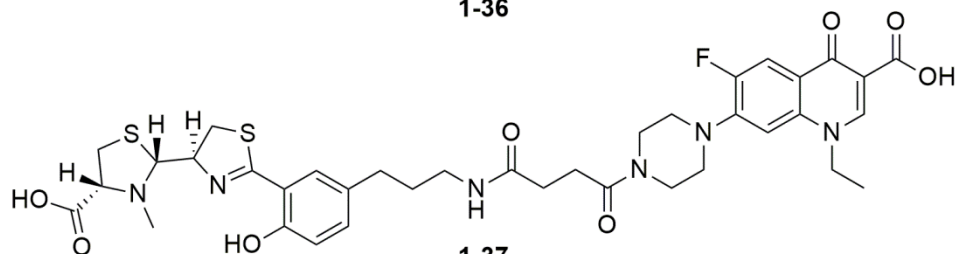


Later studies using fluoroquinolone antimicrobials investigated not only the choice of siderophore, but also linker design. For example, Hennard *et al.* reported a conjugate of norfloxacin **1-4** to the siderophore pyoverdinin (1-36), finding it to be approximately 50 times less active against DNA gyrase, with a corresponding reduction in antimicrobial activity, postulating this reduction in activity was due to steric hindrance.¹¹⁵ However, of importance in the Trojan horse strategy, Hennard *et al.* demonstrated that the conjugate was transported into the cells of *P. aeruginosa*, passing through FpvA, the outer membrane receptor for pyoverdinin.¹¹⁵ To investigate linker design, Hennard *et al.* also designed a

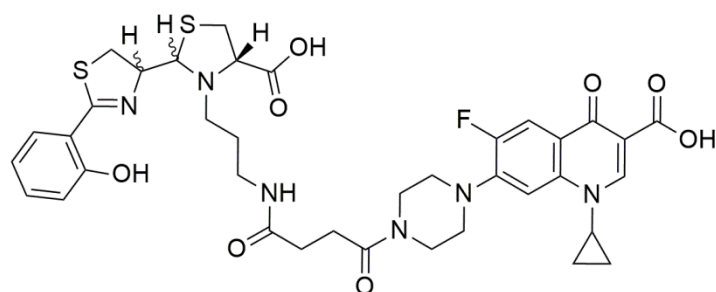
comparative siderophore-norfloxacin conjugate incorporating an (acyloxy)alkyl carbamate based linker, (discussed later in Chapter 2, **2-7**), designed to allow for intracellular release of the drug.¹¹⁵ It should be highlighted that Hennard *et al.* were among the first to discuss using a bio-labile linker as an essential requirement in siderophore-fluoroquinolone conjugates. Subsequent investigations also explored the differences between non-labile linkers and (acyloxy)alkyl carbamate based linkers, such as those by Rivault *et al.* (**1-37/2-8**),¹¹⁶ Noël *et al.* (**1-38/2-9**),¹¹⁷ and Nolan *et al.* (**1-39/2-10**),^{120, 123} with each showing that their non-labile linked siderophore-fluoroquinolone conjugates had reduced antimicrobial activity compared to the parent drug. With regards to these studies, it should be noted that Rivault *et al.* linked norfloxacin to pyochelin (**1-37**), a siderophore of *P. aeruginosa*.¹¹⁶ The authors reasoned that the reduced activity of **1-37** compared to the parent drug resulted from either a lack of active transport or from steric hindrance of the DNA gyrase site by the siderophore moiety.¹¹⁶ Similarly Noël *et al.* built on the work of Rivault *et al.* by also producing pyochelin based conjugates, such as **1-38**, though functionalised through the N3'' position.¹¹⁷ Like the investigation before theirs, Noël *et al.* found that the stable linker between the siderophore and antimicrobial led to reduced antimicrobial activity. However, Noël *et al.* did demonstrate active transport of **1-38**,¹¹⁷ once again showing the viability of using siderophores for active transport of fluoroquinolones *via* the iron uptake mechanisms. Furthermore, Nolan *et al.* also demonstrated that **1-39**, a conjugate between enterobactin and ciprofloxacin, was actively transported into *P. aeruginosa*.¹²³ It should be highlighted that each of these studies indicates the importance of linker choice. The use of (acyloxy)alkyl carbamates as bio-labile linkers will be discussed later in Chapter 2.



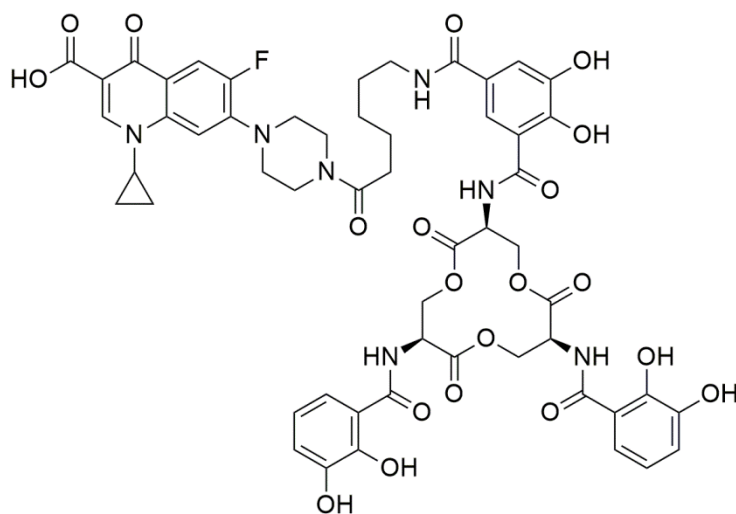
1-36



1-37



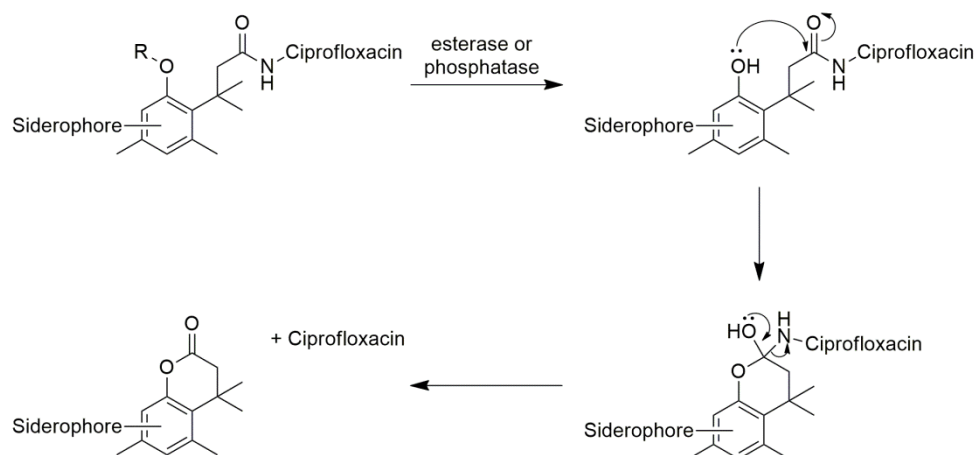
1-38



1-39

With the indication that linker choice is a key factor in the design of siderophore-fluoroquinolone conjugates, Ji and Miller have also explored the use of bio-labile linkers.^{118, 119} Based on the concept of a trimethyl lock as the linker moiety, they envisaged that drug release would occur through

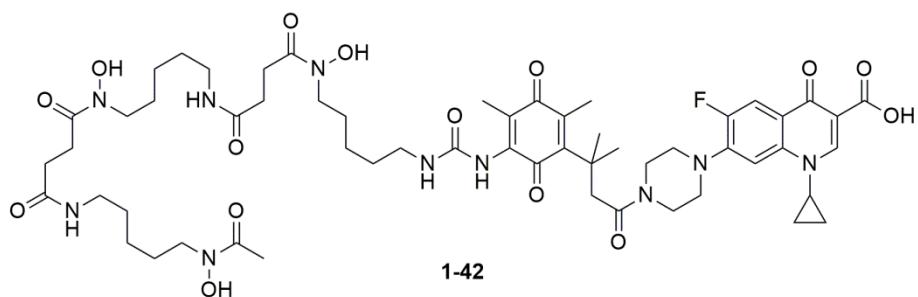
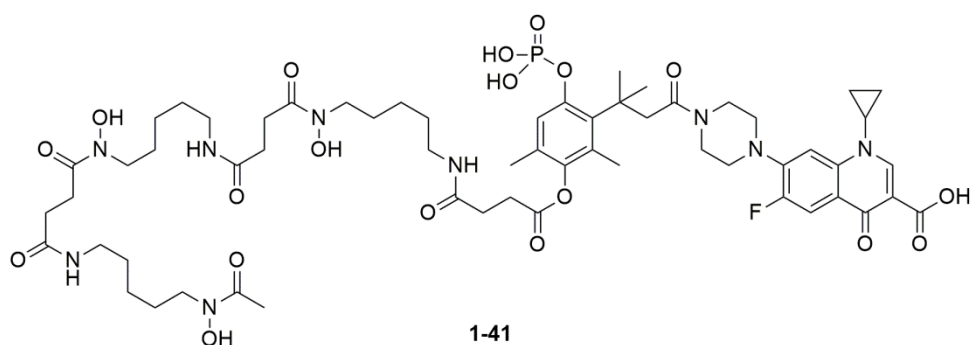
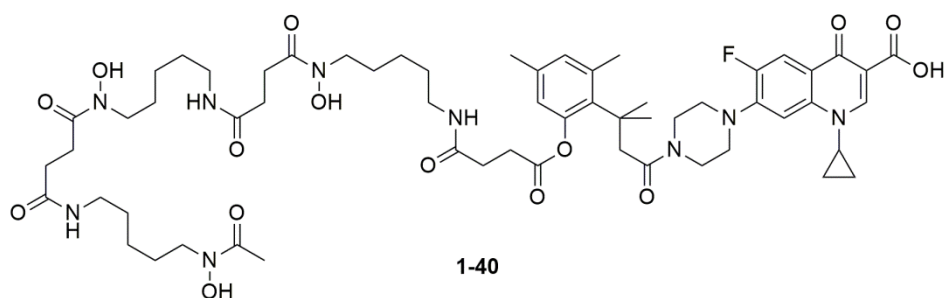
the route outlined in **Scheme 1**.^{118, 119} The notion of a trimethyl lock arises from three interlocking methyl groups with unfavourable steric interactions.¹³⁰ In turn, the steric clash between these methyl groups encourage lactonization on action by an enzyme, to give a hydrocoumarin.¹³⁰



Scheme 1- Proposed mechanism of drug release from the trimethyl lock derived conjugates.^{118, 119}

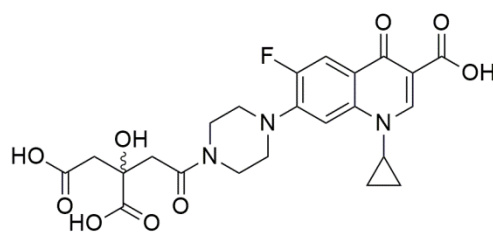
Ji and Miller designed conjugates **1-40** and **1-41** using desferrioxamine B **1-11** and ciprofloxacin **1-5** as the siderophore and antimicrobial moieties, respectively.¹¹⁸ Both conjugates incorporated a trimethyl lock-based linker, with **1-40** designed to undergo esterase cleavage of the linker, whilst **1-41** was expected to respond to phosphatase. It was found that the antimicrobial activity of **1-40** was lower than that for free ciprofloxacin **1-5**, and the authors postulated that either extracellular esterases could have led to early release of the drug or that the conjugate was a poor substrate for these esterases.¹¹⁸ In addition, it was found that conjugate **1-41** was inactive, suggesting that the linker did not cleave as planned or that it did not go through the active uptake systems.¹¹⁸ Subsequently, Ji and Miller produced conjugate **1-42**, designed to undergo drug release as a result of ferric reductases, allowing for release *via* an analogous mechanism to that outlined in **Scheme 1**.¹¹⁹ This alteration to the linker design was to exploit

the fact that ferric reductases, responsible for release of iron from ferric-siderophore complexes, are found inside the bacterial cell.^{119, 131} Unfortunately, Ji and Miller found that the activity of **1-42** was lower than that of free ciprofloxacin, with the authors suggesting that both the siderophore choice/recognition, as well as the linker activation efficiency require optimisation to allow for drug release.¹¹⁹

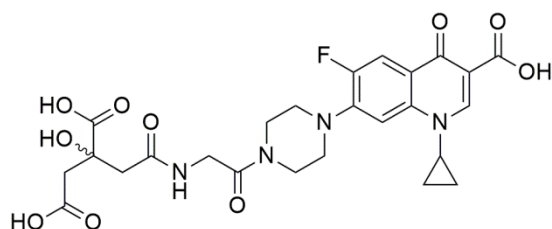


As a means to understand further the effects of linker choice, the Duhme-Klair/Routledge research group investigated citric acid **1-12** based siderophore-ciprofloxacin conjugates, performing DNA gyrase inhibition assays to determine the correlation between linker design and antimicrobial activity.^{121, 124, 128} The linker length was systematically increased through

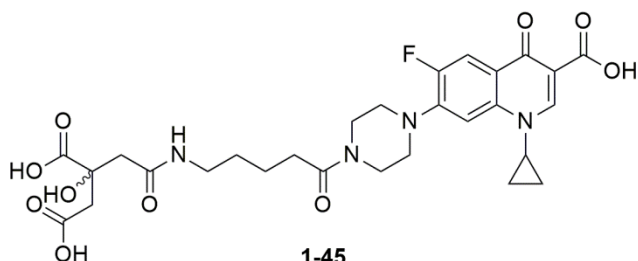
conjugates **1-43**, **1-44** and **1-45**. Furthermore, conjugate **1-46** was produced, using staphyloferrin A (secreted by *S. aureus*) as the siderophore, to increase the number of iron binding moieties. Interestingly, a correlation was established between an increase in the linker length/siderophore size and a decrease in DNA gyrase inhibition, which also matched a decrease in antimicrobial activity compared to the free antimicrobial ciprofloxacin **1-5**.^{121, 124, 128} These results indicate that choosing a suitable linker is fundamental in allowing for optimum activity of the fluoroquinolones inside the bacterial cell, and go to highlight further the requirement for bio-labile linkers.



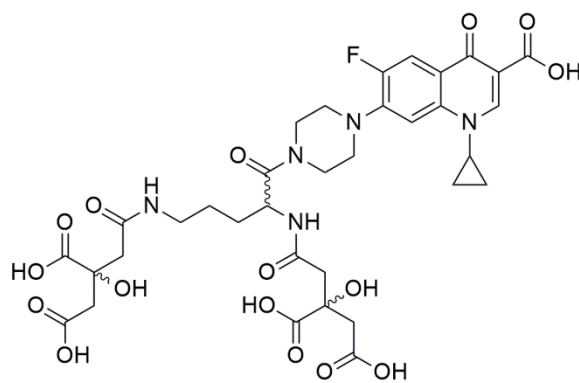
1-43



1-44



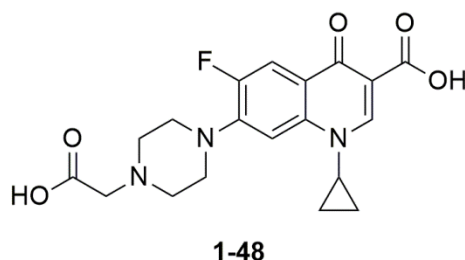
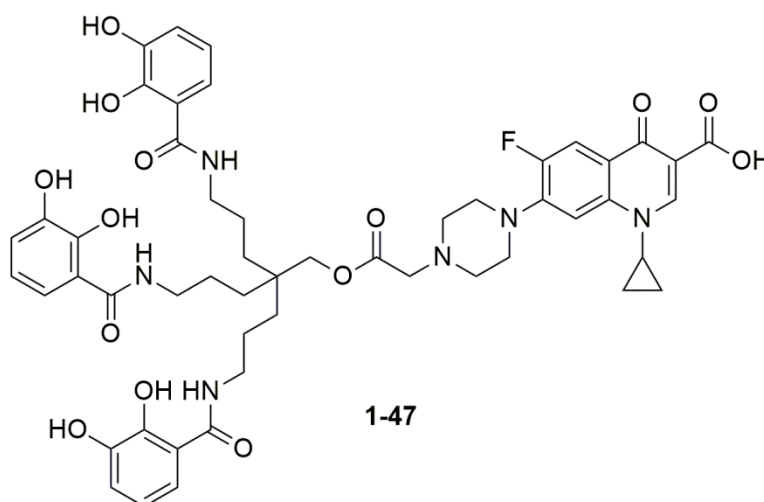
1-45



1-46

Fardeau *et al.* recently introduced an ester linkage, designed to allow release of the antimicrobial from conjugate **1-47**.¹²⁷ Whilst **1-47** demonstrated reduced activity against *P. aeruginosa* (DSM 1117), it was found that the hydrolysis product **1-48** matched the activity of free ciprofloxacin.¹²⁷ This indication that small functional groups can remain attached to the fluoroquinolones without an apparent loss of activity is encouraging, and can influence the design of future conjugates. However, as highlighted earlier, one form of resistance to fluoroquinolones results from *N*-acetylation,⁴¹ and so it should be noted that in some bacterial

species small groups attached to fluoroquinolones will be less tolerated than in others. The ultimate goal still remains to design siderophore-fluoroquinolone conjugates which incorporate a bio-labile linker which only allows for intracellular drug release after uptake.



1.6 Project Aims

The work presented in this thesis outlines the development of novel siderophore-fluoroquinolone Trojan horse conjugates, focusing on ciprofloxacin **1-5** as the antimicrobial. Two avenues of conjugate design were explored. The first involves the concept of linker design as a means of potentially allowing for intracellular drug release, with the synthesis and characterisation of a carbamate-linked citrate-ciprofloxacin conjugate (Chapter 2), and attempted synthesis of a disulfide-linked citrate-ciprofloxacin conjugate (Chapter 3). The second design concept involved

investigating the next generation of siderophore choice for Trojan horse conjugates, with the synthesis and characterisation of a salmochelin-inspired ciprofloxacin conjugate (Chapter 4). The isolated conjugates were evaluated for their antimicrobial activity and compared to the parent antimicrobial. Given that the aim of the Trojan horse strategy is to overcome resistance due to a reduction in intracellular drug concentration, resulting from reduced permeability and the expression of efflux pumps, it was anticipated that these conjugates will bypass these resistance mechanisms by their active uptake. It is thus aimed that the conjugates presented in this thesis will provide further understanding to the design concepts required in siderophore-fluoroquinolone conjugates.

**Chapter 2: Synthesis and
antimicrobial activity
testing of a carbamate-
linked citrate-
ciprofloxacin conjugate**

2.1 Aims and overview

In siderophore-fluoroquinolone Trojan horse conjugates, the linker is a key component in conjugate design, with it now understood that the linker requires bio-labile groups for drug release. This Chapter discusses the incorporation of a carbamate linker between a citrate siderophore and ciprofloxacin as the drug. The aim of the research presented in this Chapter was to investigate the function of a carbamate group as a bio-labile linker to release free ciprofloxacin after delivery of the conjugate into the cell.

2.2 Introduction

Prodrugs: Carbamates

Prodrugs have become an ever more important strategy in drug development.¹³² Most prodrugs are designed to include minor alterations to the physical properties of an existing drug, with the ability to undergo chemical or enzymatic transformation *in vivo*, releasing the active pharmacophore component as a means to improve properties, such as poor solubility.¹³² Further to this, the prodrug approach can also be applied to newly designed siderophore-fluoroquinolone conjugates, as a means of releasing the antimicrobial *in vivo* upon uptake.

As discussed in Chapter 1, a number of studies have investigated siderophore-fluoroquinolone conjugates.¹¹⁵⁻¹²⁸ However, at the time of writing, every reported siderophore-fluoroquinolone conjugate has seen a reduction of activity compared to the parent antimicrobial.¹¹⁵⁻¹²⁸ It is therefore necessary to consider bio-labile linker design as a means to

release the antimicrobial, following a prodrug approach. A number of studies have investigated using potentially bio-labile carbamate linkers between the siderophore and fluoroquinolone in prodrug Trojan horse conjugates.¹¹⁵⁻¹²⁰ Whilst these studies incorporated carbamate linkers into their conjugates, they all unfortunately found that their conjugates had reduced activity compared to the parent drug, as discussed later in this Chapter.¹¹⁵⁻¹²⁰ It is however clear that optimisation is required to find a suitable carbamate linker between the siderophore and fluoroquinolone moieties to allow for adequate drug release *in vivo*.

The importance of the quinolone moiety for target binding of the fluoroquinolones (discussed in Chapter 1) has thus far limited the diversity of possible Trojan horse conjugation (Red - **Figure 12**). The only siderophore-fluoroquinolone conjugates documented in the literature are bonded through the secondary amine of the piperazinyl moiety (Green - **Figure 12**).¹¹⁵⁻¹²⁸

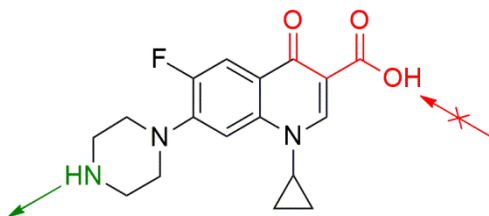


Figure 12 - Structure of ciprofloxacin demonstrating where conjugation is feasible.

For a prodrug approach in siderophore-fluoroquinolone Trojan horse conjugates, there are a number of bio-labile functionalisations available for the amino group, such as enamines, N-Mannich bases and carbamates, which can allow drug release *via* pH or enzymatic action, depending on which cleavage mechanism is used.^{132, 133} The carbamate functional group (**Figure 13**), utilised as a potential bio-labile group in siderophore-

fluoroquinolone conjugates,¹¹⁵⁻¹²⁰ is derived from an amine and carboxylic acid. The carbamate group has been of interest as it is often more enzymatically stable than its corresponding ester, yet more prone to hydrolysis than amides.¹³² As such, the bioconversion of carbamates requires esterases, classes of which are present in bacteria, to release the parent drug.^{134, 135}

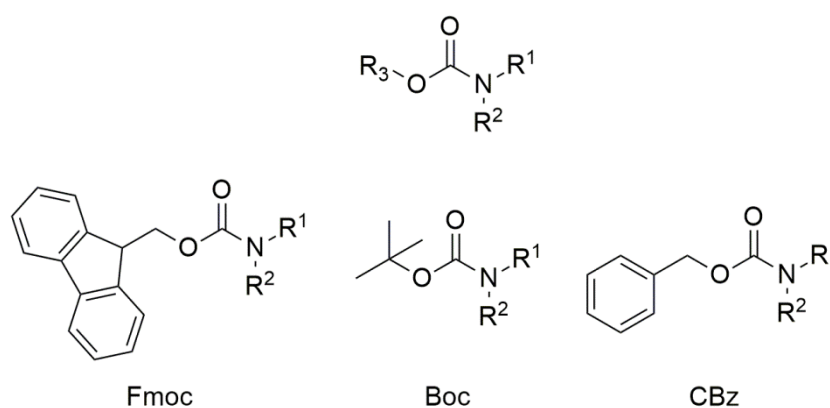
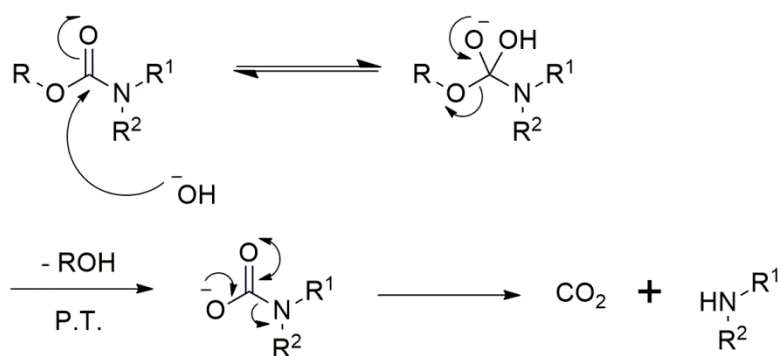


Figure 13 - Generic structure of a carbamate, and common carbamates used as protecting groups for amines, the Fmoc, Boc and CBz groups.

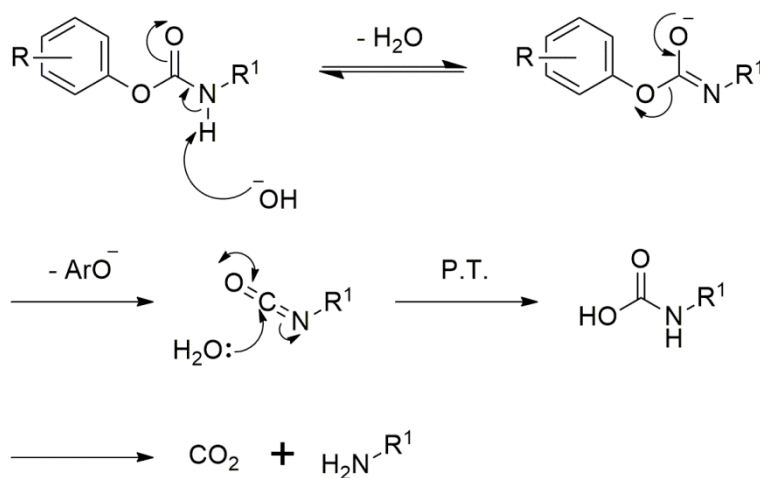
Chemical stability of carbamates

The ability to tune the stability of the carbamates can allow for the selective removal of individual carbamate moieties. Such a strategy can be exploited in the design of Trojan horse conjugates by incorporating a carbamate. The chemical stability of the carbamate group is influenced by its neighbouring groups, with there being two proposed mechanisms for carbamate decomposition by the hydroxide ion.¹³⁶⁻¹³⁸ The first results from nucleophilic substitution, with hydroxide attack at the carbonyl, followed by the loss of the alcohol from the ester end (**Scheme 2**).¹³⁶⁻¹³⁸ This in turn leaves the carbamic acid, which readily decomposes to the amine and carbon dioxide (**Scheme 2**).¹³⁶⁻¹³⁸ The second follows an E1cB mechanism, whereby deprotonation of a proton from the amide component

of the carbamate group allows for a cascade through to an isocyanate intermediate (**Scheme 3**).¹³⁶⁻¹³⁸ Addition of water to the quaternary carbon reforms carbamic acid, which can decompose to give the amine and carbon dioxide (**Scheme 3**).¹³⁶⁻¹³⁸



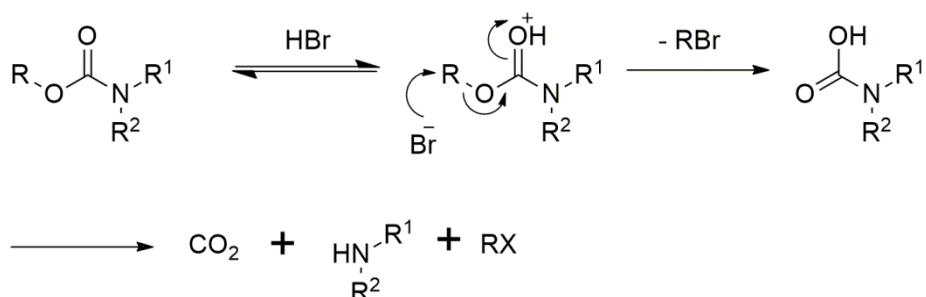
Scheme 2 - Carbamate cleavage *via* nucleophilic substitution.



Scheme 3 - Carbamate cleavage *via* an E1cB mechanism.

The differences between the two mechanisms relates to the availability of an amide proton, though the E1cB mechanism (**Scheme 3**) has only been demonstrated with a phenolic moiety, and is related to the pK_a of the phenol.¹³⁶⁻¹³⁸ On the other hand, nucleophilic substitution can occur with either aromatic or aliphatic based alcohols (**Scheme 2**), as well as in cases where there are two functional groups on the amide moiety. Steric effects

of the -OR group and the -NR₁R₂ groups were shown to have an effect on carbamates by slowing or even preventing hydroxide attack at the carbonyl, and thus improving their stability against hydroxides.¹³⁷ With regard to carbamate stability in acids, it has been shown that carbamates can be first protonated by strong acids such as hydrogen bromide, with the bromide ion next acting as a nucleophile to attack the methylene group in a S_N2-type manner to give carbon dioxide, the amine and an alkyl halide (**Scheme 4**),¹³⁹ though in general carbamates are otherwise considered stable in acids.¹³⁸



Scheme 4 - Acid based cleavage of carbamates.

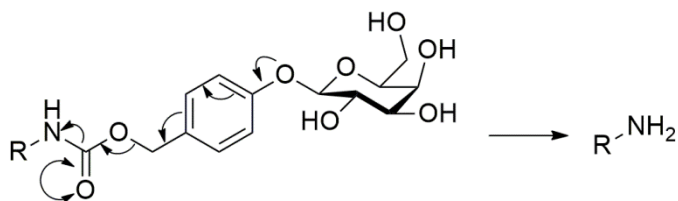
Depending on their relative stabilities, carbamates are frequently used as protecting groups for amines, such as the *tert*-butyloxycarbonyl (Boc), fluorenylmethoxycarbonyl (Fmoc) and carboxybenzyl (CBz) groups (**Figure 13**), as they can be tuned to be acid or base labile. Conditions for the removal of the Boc group, for example, require acidic conditions, such as hydrochloric or trifluoroacetic acid, due to the formation of isobutylene.¹⁴⁰ Additionally, the Boc group is stable under basic conditions, as a result of the steric hindrance of the -^tBu group preventing hydroxide attack. On the other hand, the CBz group is stable under dilute acidic, basic and neutral conditions, with cleavage carried out predominantly by hydrogenolysis.¹⁴⁰ However, the CBz group can be removed with strong acids such as hydrogen bromide, through the mechanism shown in **Scheme 4**. In contrast, the Fmoc group cannot be cleaved by acids or hydrogenolysis, as neither S_N1 or S_N2 mechanisms can work at the methylene group due to

steric hindrance. However, the Fmoc group can be cleaved using mild bases, such as piperidine, as the presence of the electron withdrawing fluorene ring system makes the proton on the β -carbon mildly acidic, with a pK_a of ~ 25 , compared to other alkyl groups. Deprotonation with a base in turn gives an aromatic anion intermediate, which obeys Hückel's rule of $4n+2$ π -electrons, before the elimination of dibenzofulvene, carbon dioxide and an amine.^{140, 141}

Whilst the chemical stability of carbamates can allow for the introduction of carbamates that are stable to a range of conditions used during synthesis, their enzymatic cleavage through carboxylesterases is determined generally by the access of the substrate to the active site.^{134, 142} As such, it can be hypothesised that the use of a carbamate linker in the Trojan horse strategy should allow for intracellular release of an antimicrobial, given that carboxylesterases are present in bacteria,^{134, 135} and that carbamates have been used as prodrugs in a range of substrates, demonstrating the versatility of such enzymes.

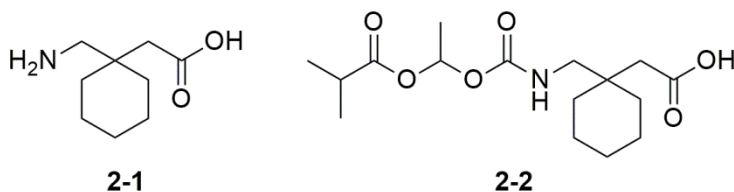
Carbamate containing prodrugs

Several examples are reported in the literature where carbamates are used as prodrugs in medicinal chemistry. One interesting approach, developed by Devarakonda *et al.*, saw a carbamate prodrug of doxorubicin which cleaved using an electron cascade that resulted from enzymatic attack on a β -galactoside.¹⁴³ The activity of β -galactosidase causes the self-immolative destruction of the spacer, releasing the drug (**Scheme 5**). Furthermore, this approach was later applied by Tóth *et al.* to allow for the enzymatic release of an imaging agent for PARACEST MRI.¹⁴⁴

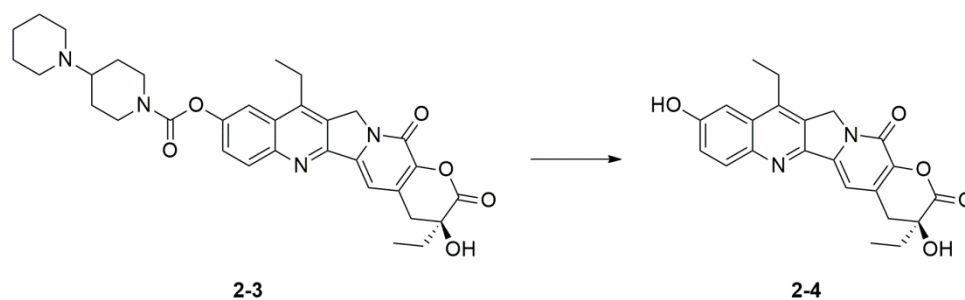


Scheme 5 - β -galactosidase enzymatic cleavage of a linker incorporating a carbamate demonstrated by Devarakonda *et al.* as a prodrug for doxorubicin¹⁴³ and by Tòth *et al.* for an imaging agent.¹⁴⁴

Other examples of carbamate prodrugs have been developed, such as a carbamate derivative of gabapentin, used for the treatment of epilepsy.¹⁴⁵ Gabapentin, **2-1**, has a limited ability to pass through cellular membranes by passive diffusion, as a result of its zwitterionic form at physiological pH. The carbamate prodrug XP13512, **2-2**, was therefore designed to overcome the pharmacokinetic limitations of gabapentin by removing the zwitterionic character, allowing for better passive absorption. Significantly, XP13512 **2-2** was found to be chemically stable at physiological pH yet was rapidly hydrolysed to gabapentin **2-1** by nonspecific carboxylesterases.¹⁴⁵

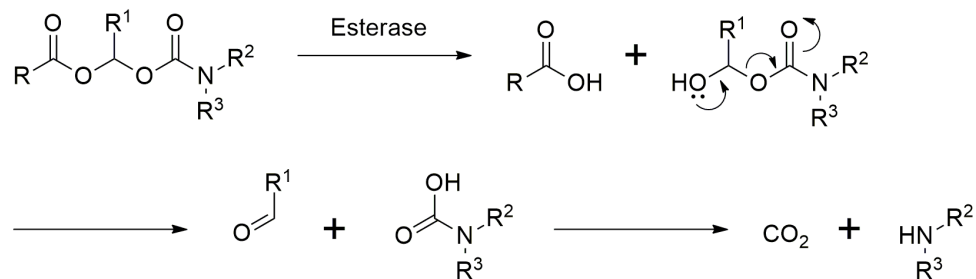
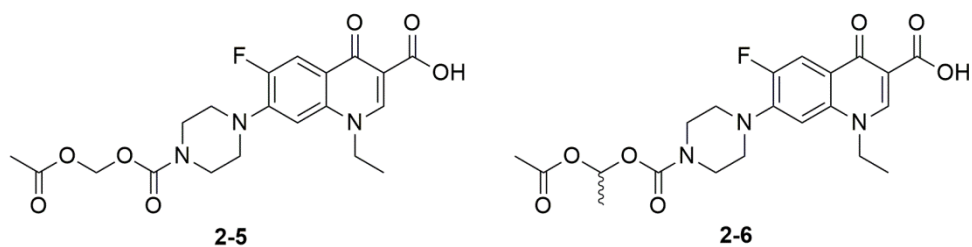


The carbamate prodrug approach has also been applied to colon cancer therapy, with the design of irinotecan **2-3**. Irinotecan acts as a prodrug, with the carbamate cleaved by carboxylesterases to release its active form, SN-38 **2-4** (**Scheme 6**), which can then inhibit topoisomerase I inside the cancer cell to prevent DNA replication and transcription.^{146, 147}



Scheme 6 - Irinotecan is hydrolysed by carboxylesterases to its active form SN-38, **2-4**.^{146, 147}

The use of carbamates as bio-labile linkers for fluoroquinolone antimicrobials was first introduced by Alexander *et al.*, who designed carbamate prodrugs of norfloxacin **1-4**.¹⁴⁸ They designed prodrugs **2-5** and **2-6**, using (acyloxy)alkyl carbamates as the bio-labile attachment on the antimicrobial, designed to undergo esterase-catalysed hydrolysis. These prodrugs were not designed to improve their uptake into bacteria, as per the Trojan horse strategy, but were instead designed to improve the oral absorption of the parent drug, by removing its zwitterionic character.¹⁴⁸ Nevertheless, their use of a carbamate group as the attachment provided an early insight into the potential of this functionalisation as a bio-labile linker. As Alexander *et al.* highlight, the success of using a carbamate is based on its ability to hydrolyse to a carbamic acid and an alcohol.¹⁴⁸ Their choice of using (acyloxy)alkyl carbamates was based on their earlier work, where they demonstrated esterase induced cleavage of the ester, producing a carboxylic acid and an intermediate that triggered spontaneous cleavage to give an aldehyde and the unstable carbamic acid (**Scheme 7**).¹⁴⁹ In turn the carbamic acid would breakdown to release the free amine and carbon dioxide.



Scheme 7 - Cleavage of (acyloxy)alkyl carbamates following esterase cleavage of the ester group.¹⁴⁹

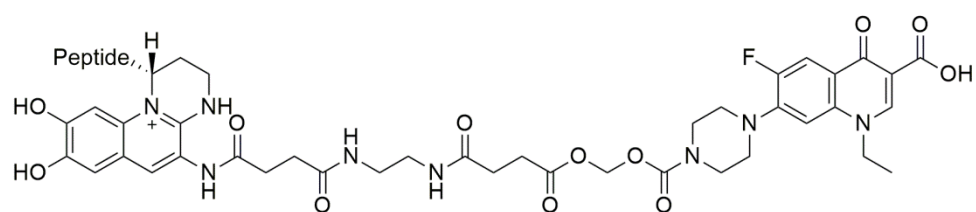
While Alexander *et al.* found that carbamate prodrugs **2-5** and **2-6** had good chemical stability at physiological pH, the prodrugs had lower solubility than norfloxacin in aqueous media.¹⁴⁸ However, while they found that **2-6** was active against *S. aureus*, the compound was not active in Gram-negative species, suggesting that the linker was either not hydrolysed, or was slow to hydrolyse.¹⁴⁸ Furthermore, by administering compound **2-6** to rhesus monkeys, they found that their compound was not efficiently absorbed and/or hydrolysed, indicating their compound had a lower bioavailability than the parent drug.¹⁴⁸ As such, Alexander *et al.* discussed that improving the aqueous solubility would improve the absorption rate, which in turn could potentially increase the rate of linker hydrolysis.¹⁴⁸ Despite the reduction in aqueous solubility, and subsequent reduction in antimicrobial activity of these compounds, their choice of carbamate linker, demonstrating its cleavage, inspired a number of other investigations into the use of (acyloxy)alkyl carbamates within the Trojan horse strategy.

Carbamates used as bio-labile linkers in Trojan Horse conjugates

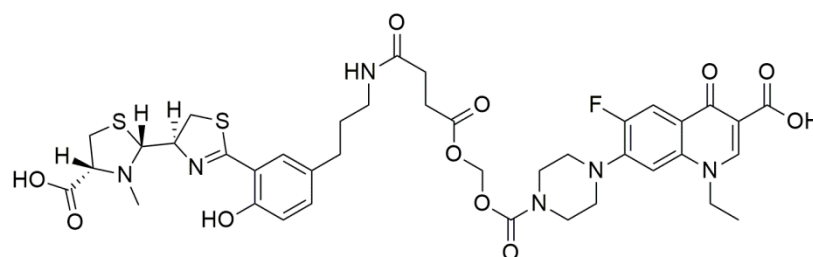
Following the work by Alexander *et al.*, later developments saw a number of attempts to introduce (acyloxy)alkyl carbamate based linkers in siderophore-fluoroquinolone conjugates.^{115-117, 120}

In 2001, Hennard *et al.* developed a conjugate of norfloxacin to the siderophore pyoverdine, with a methylenedioxy group, linked to the drug through a carbamate (compound **2-7**).¹¹⁵ The activity of **2-7** was higher than that of a comparable non-labile linked conjugate, yet was lower than that for the free drug norfloxacin. The authors also postulated premature hydrolysis by esterase of **2-7** prior to uptake, analogous to that demonstrated in **Scheme 7**, contributed to the lowered activity of their conjugate.¹¹⁵

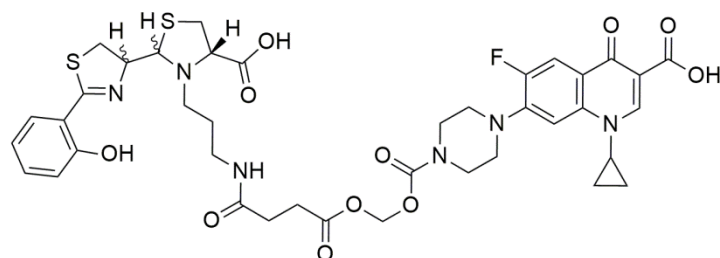
Similar studies reported in 2007 by Rivault *et al.* (**2-8**),¹¹⁶ in 2011 by Noël *et al.* (**2-9**),¹¹⁷ and in 2015 by Zheng and Nolan (**2-10**),¹²⁰ each also using methylenedioxy linkers through a carbamate between the siderophore and fluoroquinolone in Trojan horse conjugates, showed similar limitations, with premature release of the antimicrobials from the linkers, and a reduction in activity of the conjugates compared to the parent drug. Furthermore, highlighting the premature cleavage of their conjugate, Noël *et al.* demonstrated their conjugate was active against *P. aeruginosa* PAD14, a TonB deficient strain.^{7, 117} Expecting their conjugate to display no activity against this strain, and having anticipated it would require the iron uptake systems, they proposed that extracellular hydrolases secreted by the bacteria into the media had led to the premature cleavage of their linker.^{7, 117} With premature cleavage, leading to the release of the free drug from their conjugates,^{115-117, 120} the reduction in antimicrobial activity is therefore likely due to incomplete cleavage of the drug from the conjugate, though none of the investigations report such findings.



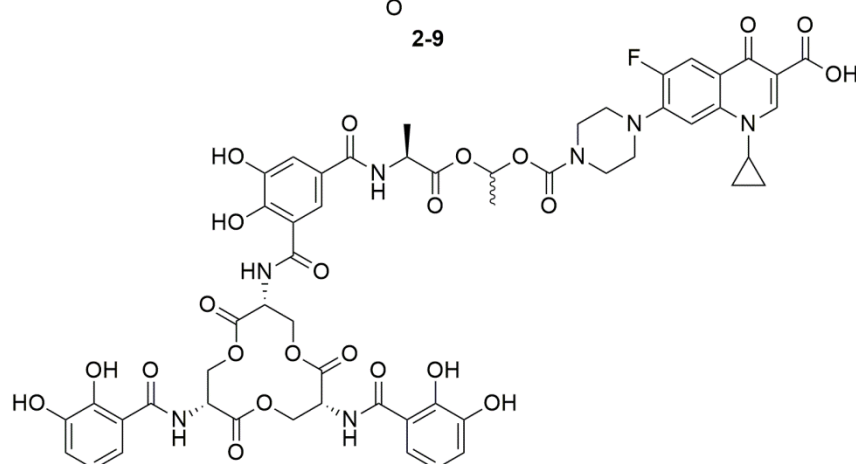
2-7



2-8



2-9

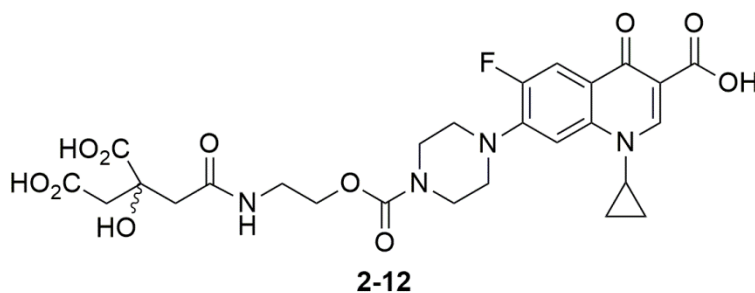
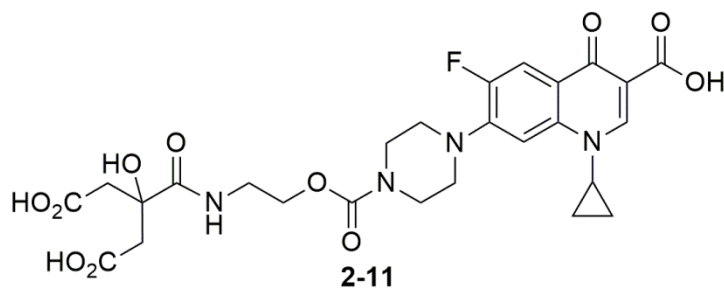


2-10

With the use of (acyloxy)alkyl carbamate based linkers having demonstrated premature cleavage, likely through the mechanism outlined in **Scheme 7**, it is clear the carbamate linkage between fluoroquinolones and the siderophore requires further optimisation, to allow controlled release of the parent drug.

Conjugate Design

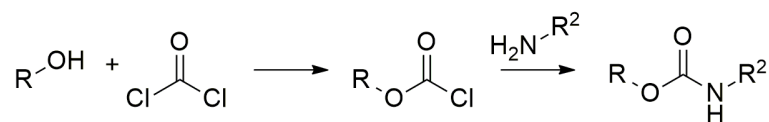
As previous investigations have demonstrated that stable, permanent linkers between the siderophore and fluoroquinolone antimicrobial components lead to reduced activity, and that those who introduced bio-labile linkers encountered premature drug release,¹¹⁵⁻¹²⁸ it is necessary to design new Trojan horse conjugates with bio-labile linkers that will release the drug inside the cell. Taking inspiration from other carbamate prodrugs and linkers, and knowing that a number of bacterial species produce carboxylesterases,¹³⁵ two regioisomeric conjugates, **2-11** and **2-12** were designed by incorporating citrate as the siderophore moiety and ciprofloxacin **1-5** as the antimicrobial component, linked through a carbamate. As can be seen, the carbamate linker does not incorporate a neighbouring methylenedioxy group like that used for conjugates with a (acyloxy)alkyl carbamate linker.^{115-117, 120} This potential design improvement was made to increase the stability of the carbamate group, by removing one cleavable site (the ester) that leads to the breakdown of the carbamate (**Scheme 7**). However, determination of the conjugates increased stability would only be confirmed on their isolation. Furthermore, these two designed conjugates **2-11** and **2-12** would allow for direct comparison to previous citrate based siderophore-fluoroquinolone conjugates, compounds **1-43**, **1-44** and **1-45** (Chapter 1), which had incorporated stable, permanent linkers.^{121, 128} Such a comparison could therefore help indicate the stability of the carbamate linker.



Synthesis of carbamates

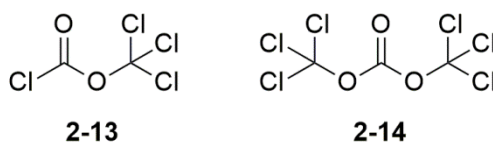
A number of syntheses are available to introduce carbamates.^{150, 151} For example, the common amino protecting carbamates, such as the Fmoc, and CBz groups, are introduced by reaction of their corresponding chloroformates or anhydrides with the necessary amine.¹⁴⁰ On the other hand, the Boc group is traditionally added using di-*tert*-butyl dicarbonate.¹⁴⁰

However, the use of a chloroformate or an anhydride may not always be optimal. The synthesis of a chloroformate generally requires the use of phosgene (**Scheme 8**).^{150, 151} Similarly, anhydrides can also require the use of phosgene for their synthesis. However, alkyl carbonates are common by-products, resulting from reaction of alcohols with the chloroformate, which can reduce the yields of carbamate formation.¹⁵²



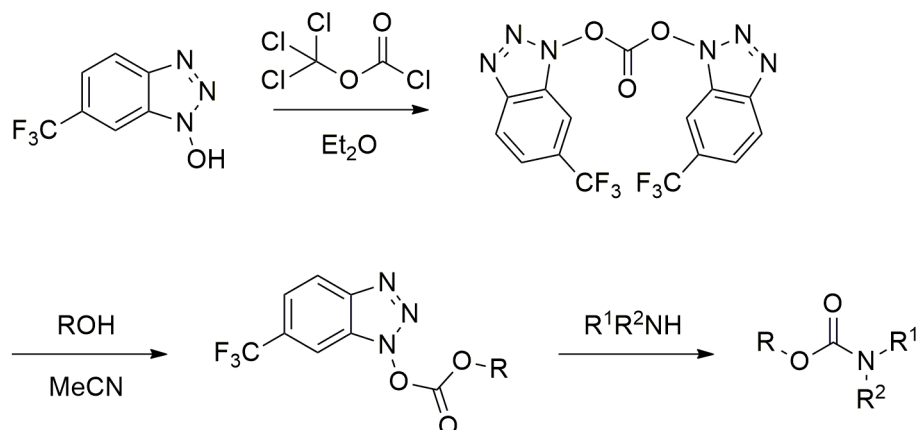
Scheme 8 - Synthesis of carbamates using phosgene, with a chloroformate as the intermediate.

Despite the ability of phosgene to form chloroformates and anhydrides, phosgene is an extremely toxic gas, proving a significant hazard in its handling and use.¹⁵⁰⁻¹⁵² As such, structurally related substitutes for phosgene were developed, diphosgene and triphosgene (**2-13** and **2-14** respectively), which are safer and easier to handle.^{150, 151, 153} Demonstrating this, Pasquato *et al.* reacted both triphosgene and diphosgene separately with methanol, finding that phosgene is produced as an intermediate in each reaction.¹⁵³ Furthermore, they were also able to show that reactivity of phosgene is two orders of magnitude faster than triphosgene, and therefore does not accumulate during the reaction, meaning the concentration of phosgene was always very low.¹⁵³ In turn, they concluded that triphosgene is a safer alternative to phosgene.



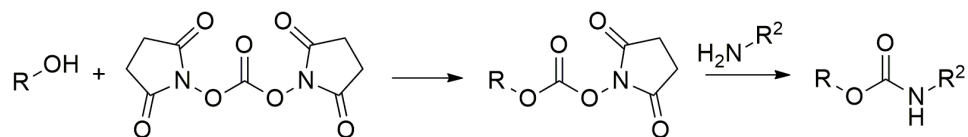
Given the risks associated with phosgene related agents, despite the development of the comparatively safer triphosgene reagent, alternative activating agents have been investigated. Analogous to the use of phosgene type reagents to activate alcohols are examples such as the use of benzotriazole carbonates,¹⁵⁴ carbonyldiimidazole,¹⁵⁵ and *N,N'*-disuccinimidyl carbonate,^{156, 157} as well as a number of other carbonate activating agents.^{150, 151, 158} The use of a benzotriazole carbonate first required the synthesis of 1,1-bis[6-(trifluoro-

methyl)benzotriazolyl]carbonate (though through the use of diphosgene), which in turn could be used to activate an alcohol before the addition of an amine to form the required carbamate (**Scheme 9**).¹⁵⁴ As indicated above, dimethyl or diphenyl carbonates,¹⁵⁸ and carbonyldiimidazole can activate alcohols in a similar manner.¹⁵⁵

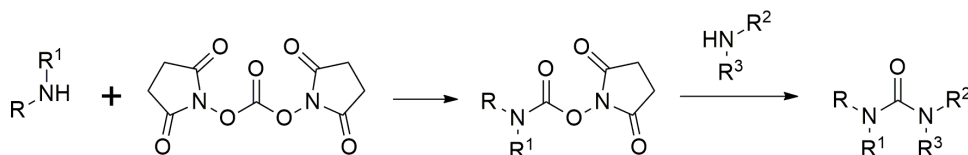


Scheme 9 - General scheme for the synthesis of carbamates using BTBC.¹⁵⁴

Analogous to the use of the examples described above is the use of *N,N'*-disuccinimidyl carbonate, also requiring the activation of an alcohol, followed by the addition of an amine (**Scheme 10**).^{156, 157} Interestingly, *N,N'*-disuccinimidyl carbonate had been previously used to activate an amine to form a carbamate intermediate, for the synthesis of ureas (**Scheme 11**).¹⁵⁹ However, the route outlined in **Scheme 11**, where the amine is activated, has not been applied in the synthesis of carbamates, presumably as a result of subsequent studies where the alcohol is activated first.

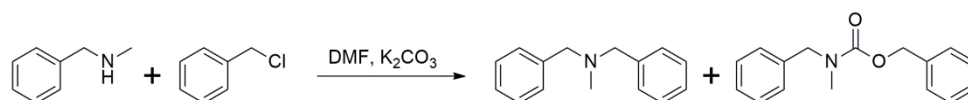


Scheme 10 - General scheme for the synthesis of carbamates using N,N' -disuccinimidyl carbonate.^{156, 157}



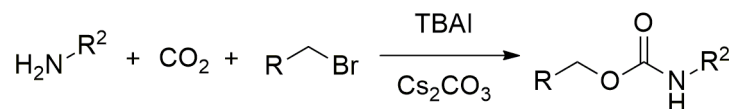
Scheme 11 - Formation of ureas using N,N' -disuccinimidyl carbonate to produce a carbamate intermediate.¹⁵⁹

Further to the use of activating agents, carbamates have also been accessed through other means that introduce the necessary carbonyl.^{150, 151} Early examples used carbon monoxide and oxygen in the presence of metal catalysts.^{150, 151} However, later studies moved away from using carbon monoxide in favour of safer alternatives, such as the use of metal carbonates and hydrogen carbonates.¹⁶⁰ Butcher investigated the use of potassium carbonate and its ability to synthesise carbamates obtaining them in 40% yield, though also observing an alkylated side product (**Scheme 12**).¹⁶⁰ It was hypothesised that carbon dioxide was generated *in situ*, limiting the potential yield of the carbamate to 50%. Therefore Butcher bubbled carbon dioxide gas into the reaction mixture, increasing the yield of carbamate to 60%.¹⁶⁰ Subsequent consideration of the metal carbonate lead to the use of caesium carbonate, giving a significant improvement in the carbamate yield at 96%.¹⁶⁰



Scheme 12 - Use of metal carbonates in the synthesis of a carbamate and alkylated side product.¹⁶⁰

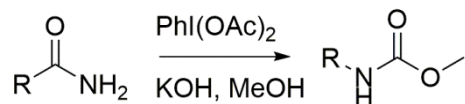
Subsequent studies based on Butcher's work saw different uses of carbon dioxide gas to aid in carbamate formation. For example, Rossi *et al.* used carbon dioxide with tetraethylammonium hydroxide to give tetraethylammonium hydrogen carbonate.¹⁶¹ Subsequent reaction of the tetraethylammonium hydrogen carbonate with an amine and alkylating agent gave a carbamate product.¹⁶¹ Later, Jung *et al.* reported the use of a three-component coupling of an amine with an alkyl halide and carbon dioxide gas in the presence of caesium carbonate and tetrabutylammonium iodide, producing carbamates in good yields (**Scheme 13**).¹⁶² In addition, they found that tetrabutylammonium iodide prevented direct *N*-alkylation by undergoing halide exchange to yield the more reactive iodide species.¹⁶²



Scheme 13 - Reported synthesis of carbamates by Jung *et al.* using carbon dioxide.¹⁶²

Beyond using activating agents, or introducing the carbonyl functionality through the use of gaseous carbon dioxide/monoxide, a number of rearrangement reactions also exist for the synthesis of carbamates.^{150, 151} For example the Hoffmann (**Scheme 14**),¹⁶³ and Curtius rearrangements.^{150, 151} However, the Hoffmann rearrangement requires a primary carboxamide, whilst the Curtius rearrangement requires the pyrolysis of an acyl azide to produce an isocyanate, which can then react with an alcohol to produce a carbamate.^{150, 151} As such these rearrangements are not

always suitable in circumstances where the precursor functionality is either not available, or not possible to synthesise.



Scheme 14 - Example Hoffmann rearrangement to synthesise methyl carbamates.¹⁶³

Synthetic considerations for the target compounds 2-11 and 2-12

With a number of synthetic methodologies available to produce carbamates, it is important to consider the target compounds of this Chapter, compounds **2-11** and **2-12**. The disconnection of compound **2-11** provides insight into the options available to introduce the carbamate group, by identifying the individual components (**Figure 14**). As can be seen, the target compound **2-11** consists of four key components that can be obtained as four individual starting materials: citric acid **1-12**, 2-bromoethylamine or ethanolamine, carbon dioxide and ciprofloxacin **1-5**. The disconnection of **2-12** provides the same individual components (**Figure 14**).

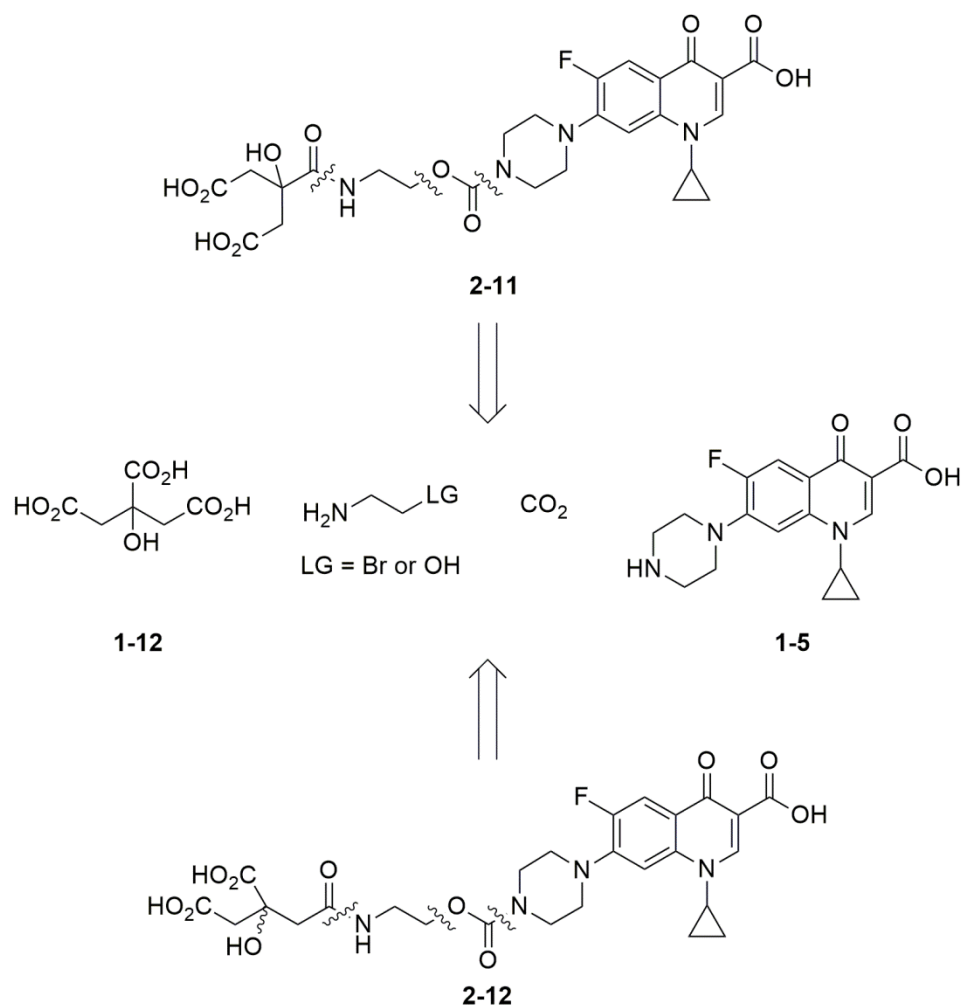


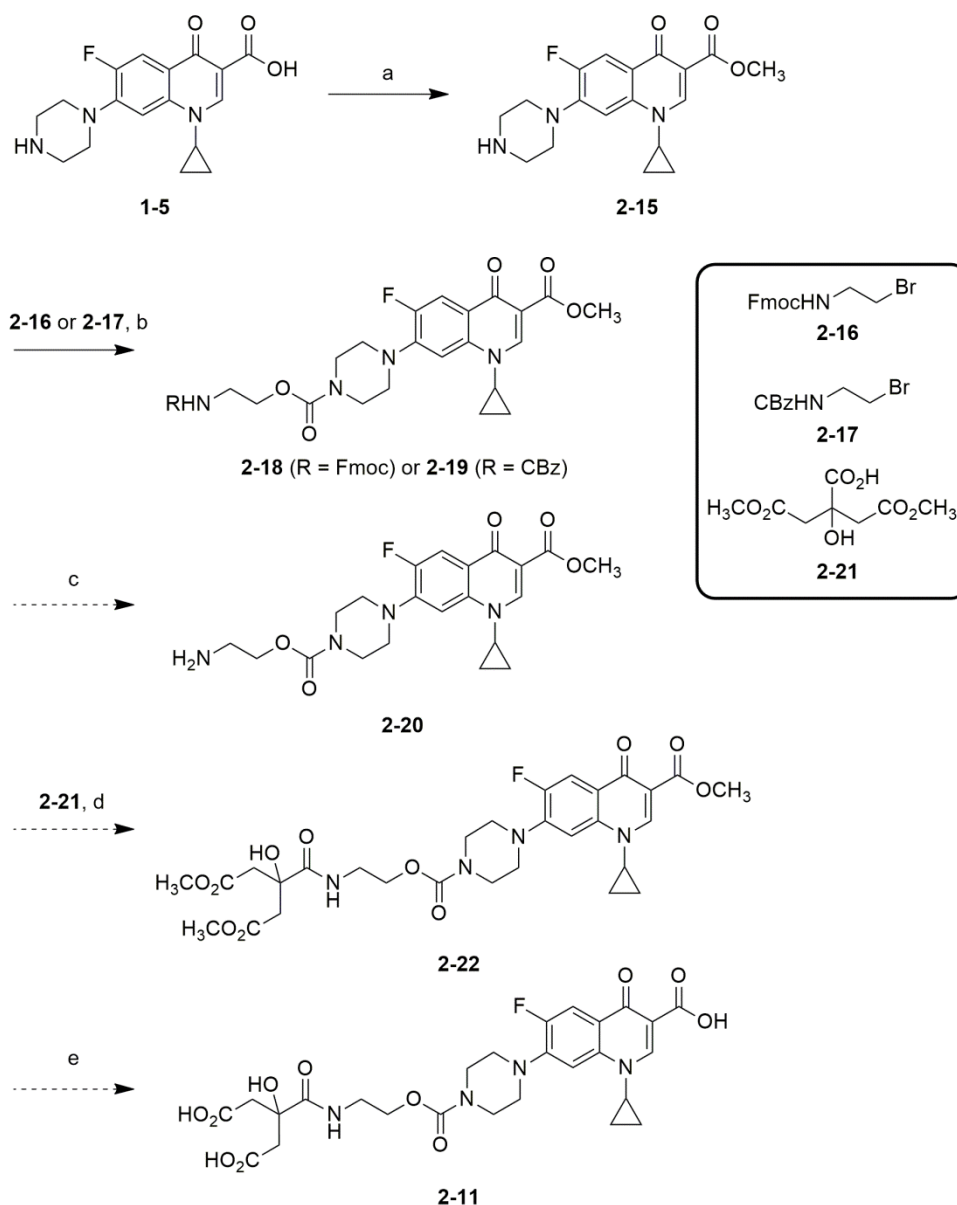
Figure 14 - Disconnection of compounds **2-11** and **2-12** to their key components.

As such the individual components of compound **2-11** suggest that suitable methodologies to introduce the carbonyl functionality would be *via* reaction with carbon dioxide gas, or by direct activation of an alcohol group. This Chapter discusses the introduction of a carbamate group into a Trojan horse conjugate by using these methodologies.

2.3 Synthesis

Initial synthetic route targeting a 1,5-citrate-ciprofloxacin conjugate incorporating a carbamate linker

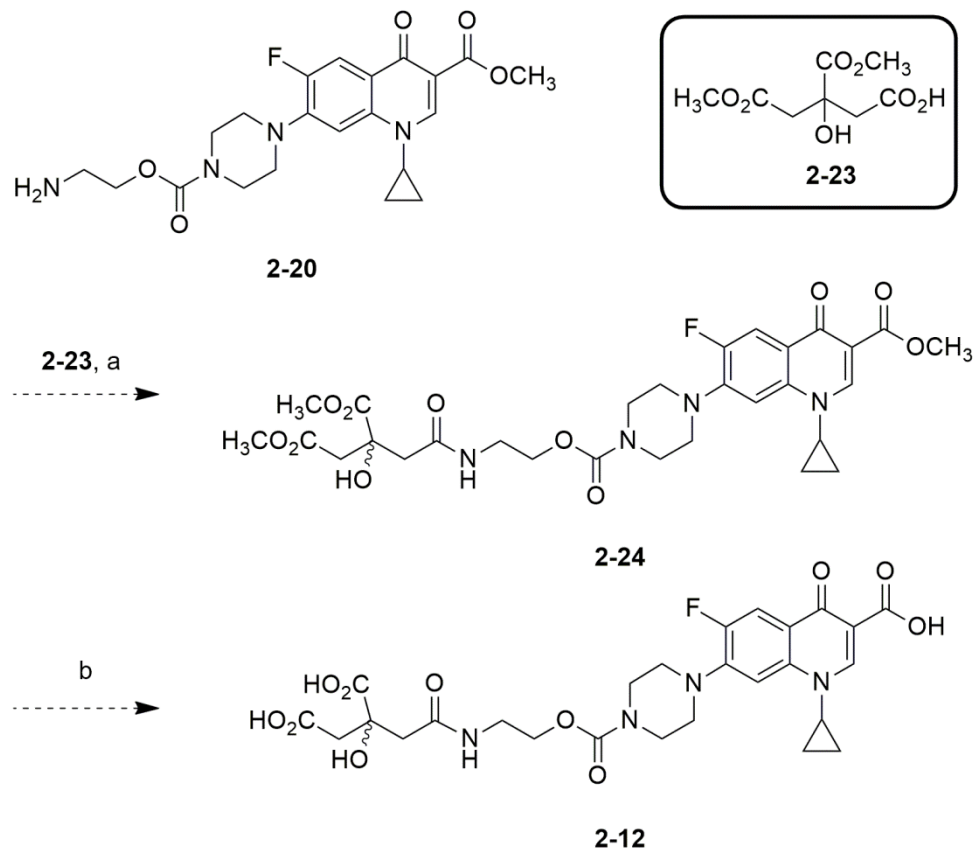
The first carbamate-linked conjugate targeted for synthesis was compound **2-11**. Having previously considered the synthesis and disconnection of the carbamate group in compound **2-11** (**Figure 14**), it was decided to introduce the carbamate group using carbon dioxide.¹⁶² As such the synthetic route for compound **2-11** was initially planned as shown in **Scheme 15**.



Scheme 15 - Initial synthetic route towards compound **2-11**. (a) MeOH, SOCl₂, reflux, 65%; (b) CO₂, Cs₂CO₃, TBAI, DMF, **2-18** = 9% / **2-19** = 22%; (c) Deprotection; (d) DCC, 1,4-dioxane; (e) (i) 0.1 M TBAH, (ii) 0.1 M HCl.

In addition, the isolation of compound **2-20** would allow for the synthesis of the other regioisomer target, compound **2-12**, through the use of a different dimethylcitrate moiety. Thus the planned synthesis of compound **2-12**, from **2-20**, is shown in **Scheme 16**. The syntheses to obtain two

regioisomeric dimethylcitrate moieties, which were planned for use in the synthesis of both **2-11** and **2-12**, are discussed later.



Scheme 16 - Planned synthesis of **2-12** from intermediate compound **2-20**.

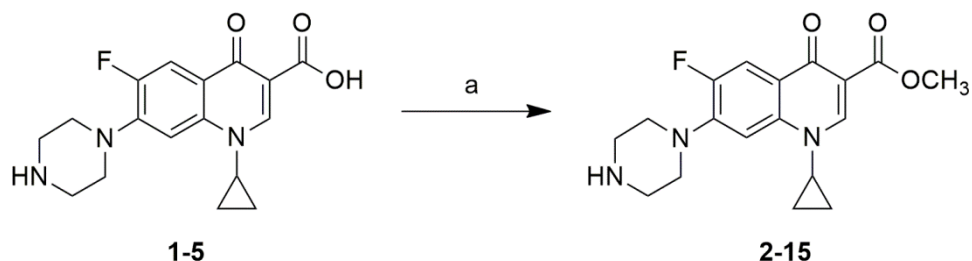
(a) DCC, 1,4-dioxane; (b) (i) 0.1 M TBAH, (ii) 0.1 M HCl.

Protection of ciprofloxacin 1-5 by methyl esterification

The first step in the synthesis was the protection of the carboxylic acid moiety of ciprofloxacin **1-5**. This protection was necessary to prevent unwanted side reactions later in the synthetic route, such as potential amide coupling to the β -keto acid, which is essential for antimicrobial activity (Chapter 1).^{10, 26} Furthermore, protection of the acid would remove the zwitterionic character of ciprofloxacin at neutral pH, which limits its solubility in both aqueous and organic solvents. This would allow easier

handling of the drug component during subsequent synthetic steps. It was decided to protect ciprofloxacin **1-5** with the methyl ester group to produce **2-15** in order to allow for global deprotection of the methyl ester groups of **2-22** later in the synthetic route.¹²¹

To protect the carboxylic acid, ciprofloxacin **1-5** was heated under reflux in methanol with thionyl chloride (**Scheme 17**).¹²¹ Compound **2-15** was isolated in 65% yield after work up and characterised using ¹H and ¹³C NMR spectroscopy, infra-red spectroscopy and ESI mass spectrometry. The formation of **2-15** was supported by ¹H NMR spectroscopy, with the appearance of a singlet resonance at 3.89 ppm of relative integration three, corresponding to the methyl ester group. The ¹³C NMR spectrum also showed a new resonance at 51.9 ppm, also corresponding to the methyl ester group. In addition, ESI-MS analysis gave a molecular ion peak [M+H]⁺ for **2-15** at *m/z* 346.1557, consistent with a compound of formula C₁₈H₂₀FN₃O₃.

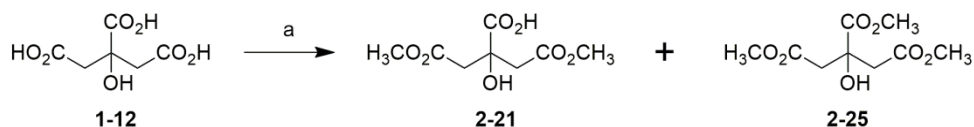


Scheme 17 - Esterification of ciprofloxacin **1-5** to produce **2-15**. (a) MeOH, SOCl₂, reflux, 65%.

Protection of citric acid 1-12

Citric acid **1-12** has three carboxylic acid groups, yet in the target compound **2-11** only the central acid moiety is required for the amide connection to the remainder of the molecule. It was therefore necessary to

protect the primary carboxylic acid groups, yet leave the central tertiary carboxylic acid unprotected, to give 1,5-dimethyl citrate **2-21**. To achieve this, citric acid **1-12** was heated under reflux in methanol with concentrated sulfuric acid for one hour to produce **2-21** in 16% yield (**Scheme 18**).^{121, 164, 165}



Scheme 18 - Synthesis of 1,5-dimethyl citrate **2-21** from citric acid **1-12**, with 1,3,5-trimethyl citrate **2-25** as a by-product. (a) MeOH, H₂SO₄, reflux 1 h, 16% (**2-21**) / 3% (**2-25**).

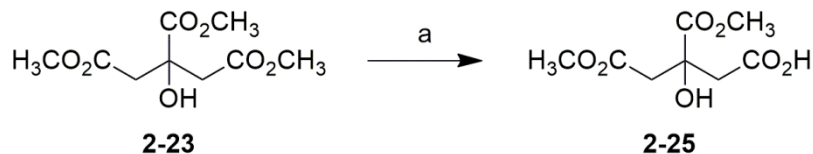
However, during the synthesis of 1,5-dimethyl citrate **2-21** the esterification process is non-specific, and so the by-product 1,3,5-trimethyl citrate **2-25** is also produced. The purification processes of two published procedures were combined to isolate each product separately. Firstly, the method of Hirota *et al.* was employed, whereby the reaction solution was neutralised using calcium hydroxide, the precipitate filtered, and the filtrate concentrated *in vacuo*.¹⁶⁴ Next the purification process followed that of Guo *et al.*¹⁶⁵ The resulting solid was sonicated in water and the insoluble material filtered off. The filtrate was acidified using concentrated hydrochloric acid, resulting in a precipitate that was then isolated by filtration. This precipitate was dissolved in aqueous sodium hydrogen carbonate and washed with chloroform. The aqueous phase was reacidified with concentrated hydrochloric acid to yield 1,5-dimethyl citrate **2-21** in 16% yield, characterised using ¹H and ¹³C NMR spectroscopy, infra-red spectroscopy and ESI mass spectrometry. The formation of 1,5-dimethyl citrate **2-21** was supported by ¹H NMR spectroscopy, with the appearance of a singlet resonance at 3.56 ppm of relative integration six, corresponding to the two methyl ester groups. Furthermore, ESI-MS analysis gave a

molecular ion peak $[M+Na]^+$ for **2-21** at m/z 243.0475, consistent with a molecule of formula $C_8H_{12}NaO_7$.

To isolate the by-product, the chloroform washes were concentrated *in vacuo*, affording 1,3,5-trimethyl citrate **2-25** in 3% yield, characterised using 1H and ^{13}C NMR spectroscopy, infra-red spectroscopy and ESI mass spectrometry. The formation of 1,3,5-trimethyl citrate **2-25** was supported by 1H NMR spectroscopy, with the appearance of a singlet resonance at 3.56 ppm of relative integration six, corresponding to two methyl ester groups. In addition, a singlet at 3.65 ppm of relative integration three, corresponding to the central methyl ester group, was also evident in the spectra. ESI-MS analysis showed a molecular ion peak $[M+Na]^+$ for **2-25** at m/z 257.0632, consistent with a molecule of formula $C_9H_{14}NaO_7$. The isolation of 1,3,5-trimethyl citrate **2-25** therefore allows for the synthesis of 1,3-dimethyl citrate **2-23** (**Scheme 19**). Whilst **2-23** was not required in the synthesis of **2-11**, it is useful for the synthesis of the other regioisomer target, **2-12**, demonstrated by the planned synthesis outlined earlier in **Scheme 16**.

Therefore, 1,3-dimethyl citrate **2-23** was synthesised from 1,3,5-trimethyl citrate **2-25** *via* reaction with 0.1 M sodium hydroxide solution in a 1:1 mixture of methanol and water for 2 hours (**Scheme 19**). The reaction mixture was extracted with ethyl acetate to recover unreacted 1,3,5-trimethyl citrate **2-25**. The aqueous fraction was then acidified with 1 M hydrochloric acid, followed by extraction with ethyl acetate to afford 1,3-dimethyl citrate **2-23**. Recrystallisation from toluene gave **2-23** in 27% yield, based on conversion from 1,3,5-trimethyl citrate **2-25**, and characterised using 1H and ^{13}C NMR spectroscopy, infra-red spectroscopy and ESI mass spectrometry. Successful formation of **2-23** was supported by 1H NMR spectroscopy, with the observation of two singlets, both of relative integration of three, at 3.76 ppm and 3.66 ppm, corresponding to the α -methyl and β -methyl esters respectively. In addition, ESI-MS

analysis gave a molecular ion peak $[M-H]^-$ for **2-23** at m/z 219.0514, consistent with a molecule of formula $C_8H_{11}O_7$.



Scheme 19 - Synthesis of 1,3-dimethyl citrate **2-23** from 1,3,5-trimethyl citrate **2-25**. (a) 0.1 M NaOH, MeOH:H₂O 1:1, 2 h, 27%.

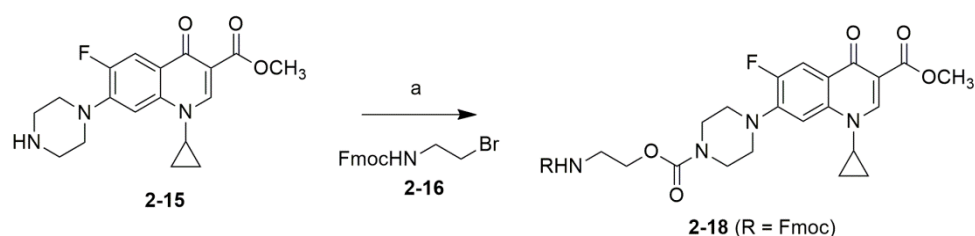
Formation of the carbamate utilising carbon dioxide

As highlighted in **Scheme 15**, the proposed synthesis of the carbamate group involved the use of carbon dioxide. This involved the use of the ciprofloxacin amine, carbon dioxide, an alkyl halide, caesium carbonate and tetrabutylammonium iodide, following the methodology of Jung *et al.* (**Scheme 13**).¹⁶²

It was decided to employ *N*-Fmoc-2-bromoethylamine **2-16** in order to synthesise **2-18**, as the Fmoc protecting group requires mild basic conditions for deprotection. Such deprotection conditions would be unlikely to cleave the required carbamate linker in **2-5**.

Compound **2-18** was synthesised using commercially available *N*-Fmoc-2-bromoethylamine **2-16**, and ciprofloxacin methyl ester **2-15** (**Scheme 20**). Firstly, ciprofloxacin methyl ester **2-15** was mixed with caesium carbonate and tetrabutylammonium iodide in anhydrous *N,N*-dimethylformamide, and then bubbled with carbon dioxide gas for 2 hours. *N*-Fmoc-2-bromoethylamine **2-16** was dissolved in anhydrous *N,N*-dimethylformamide and added dropwise with continued gas bubbling.

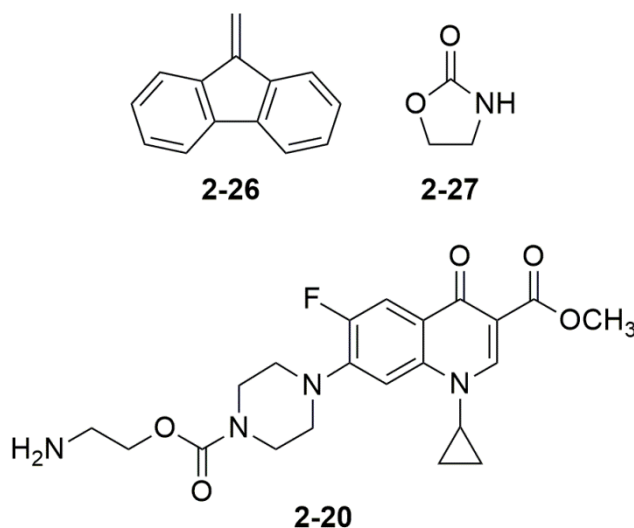
After work-up and purification compound **2-18** was isolated in 9% yield. Successful formation of **2-18** was supported by ESI-MS analysis, which gave a molecular ion peak $[M+H]^+$ for **2-18** at m/z 655.2566, consistent with a compound of formula $C_{36}H_{36}FN_4O_7$.



Scheme 20 - Formation of the Fmoc protected carbamate target **2-18**. (a) CO_2 , CS_2CO_3 , TBAI, DMF, 9%.

Despite repetitions, the best yield obtained for compound **2-18** remained at 9%. In each attempt, Fmoc deprotection occurred, with dibenzofulvene (**2-26**) formation observed, identified by a singlet resonance at 6.10 ppm in the 1H NMR spectrum, of relative integration two, characteristic of the two alkene protons. Furthermore, no evidence was found for the formation of **2-20** as a by-product, suggesting that Fmoc deprotection occurred from the starting material **2-16** prior to its reaction with ciprofloxacin methyl ester **2-15**. The potential cause for Fmoc deprotection could be due to either the piperazinyl moiety of the antimicrobial acting as a base, or due to the caesium carbonate base in the reaction mixture. However, the piperazinyl nitrogen of ciprofloxacin ($pK_a = 8.74$) is less basic than that of caesium carbonate ($pK_a = 10.25$ for carbonic acid), and also less than that of piperidine ($pK_a = 11.22$), which is generally used for Fmoc deprotection.¹⁶⁶⁻¹⁶⁸ Given the pK_a of the acidic proton in the Fmoc group is ~ 25 ,^{140, 141} it is likely that caesium carbonate is the reason for the Fmoc deprotection, given it is the stronger base. However, as reported pK_a values are based on aqueous media, these values can only indicate their reactivity in organic solvents, especially when a number of amines have been shown to have increased pK_a values in solvents such as acetonitrile

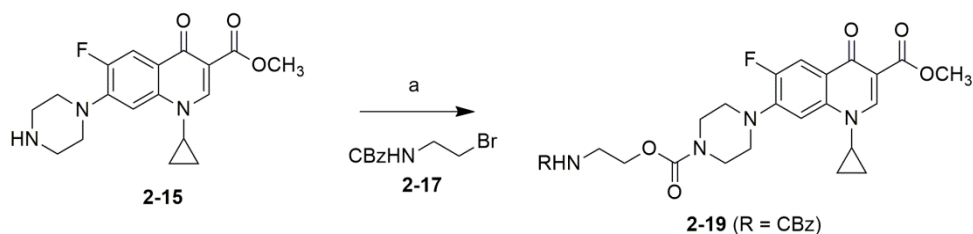
and tetrahydrofuran.¹⁶⁹ Based on this, the exact cause of Fmoc deprotection is not clear. Despite not knowing the cause of the deprotection, any early deprotection of the starting material **2-16** could lead to the formation of **2-27**, from the reaction of the released free amine to form the cyclic carbamate, though it should be noted that no evidence of **2-27** was observed. Given the low yields obtained for **2-18**, it was therefore decided to change the protecting group of the amine on the starting alkyl bromide, as a means to overcome the observed deprotection of the Fmoc group.



It was decided that the CBz protecting group was to be utilised as an alternative protecting group. As such, an analogous carbamate, **2-19**, was targeted (**Scheme 15** and **Scheme 21**).

Benzyl (2-bromoethyl)carbamate **2-17** was synthesised from 2-bromoethylamine and benzyl chloroformate, according to a literature procedure,¹⁷⁰ in 90% yield, and was characterised using ¹H and ¹³C NMR spectroscopy, infra-red spectroscopy and ESI mass spectrometry. The successful formation of **2-17** was supported by identical data to the literature, including a characteristic resonance at 156.5 ppm for the

carbamate functional group in the ^{13}C NMR spectrum. Furthermore, ESI-MS analysis gave a molecular ion peak $[\text{M}+\text{H}]^+$ for **2-17** at m/z 258.0127, consistent with a molecule of formula $\text{C}_{10}\text{H}_{13}\text{BrNO}_2$. On reacting **2-17** with ciprofloxacin methyl ester **2-15**, under the previously described conditions, **2-19** was isolated in 22% yield (**Scheme 21**). Successful formation of **2-19** was supported by ^{13}C NMR spectroscopy, with a characteristic resonance at 155.4 ppm for the carbamate functional group. ESI-MS analysis gave a molecular ion peak $[\text{M}+\text{H}]^+$ for **2-19** at m/z 567.2241, consistent with a molecule of formula $\text{C}_{29}\text{H}_{32}\text{FN}_4\text{O}_7$.



Scheme 21 - Formation of the CBz protected carbamate target **2-19**. (a) CO_2 , Cs_2CO_3 , TBAI, DMF, 22%.

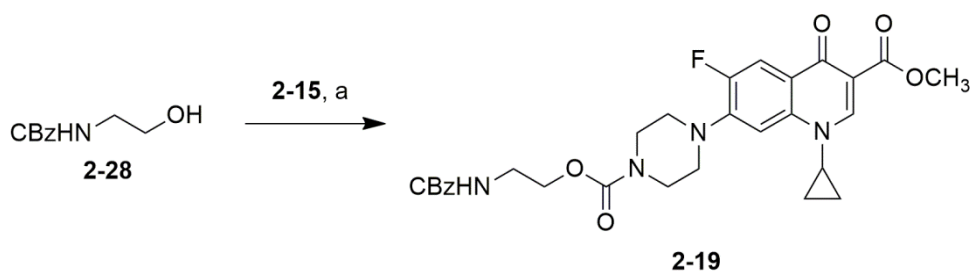
Despite the successful synthesis of compound **2-19** and the improvement in the yield of the carbamate formation, it was apparent that the use of gaseous carbon dioxide as a reagent was not as effective as desired. Thus it was determined that an alternative methodology be explored for the introduction of the carbamate group, so as to obtain higher yields.

Activation of N-CBz-ethanolamine 2-28 using N,N'-disuccinimidyl carbonate

It was decided to investigate the application of *N,N'*-disuccinimidyl carbonate to activate an alcohol, before the addition of ciprofloxacin methyl ester **2-15**, to produce the required carbamate.^{156, 157} Ethanolamine

was protected using benzyl chloroformate, according to a literature procedure,¹⁷¹ to afford **2-28** (**Scheme 22**) in 87% yield, characterised by ¹H and ¹³C NMR spectroscopy, infra-red spectroscopy and ESI mass spectrometry. The successful formation of **2-28** was supported by identical data to the literature, including a characteristic resonance at 157.5 ppm in the ¹³C NMR spectrum for the carbamate functional group. Furthermore, ESI-MS analysis gave a molecular ion peak [M+H]⁺ for **2-28** at *m/z* 196.0965, consistent with a compound of formula C₁₀H₁₄NO₃.

In order to form the carbamate bond, the alcohol of **2-28** was activated using *N,N'*-disuccinimidyl carbonate, in the presence of pyridine and potassium phosphate tribasic, followed by the addition of ciprofloxacin methyl ester **2-15**. After work up and purification, compound **2-19** was obtained in 65% yield (**Scheme 22**). Successful formation of the product was confirmed by comparative spectroscopic data from the previous reaction using carbon dioxide (**Scheme 15**), with the same characteristic resonance at 155.4 ppm for the carbamate functional group in the ¹³C NMR spectrum, as well as a matching ESI-MS peak.



Scheme 22 - Activation of *N*-CBz-ethanolamine **2-28** using *N,N'*-disuccinimidyl carbonate to form the required carbamate bond. (a) DSC, pyridine, DMF, K₃PO₄, 65%.

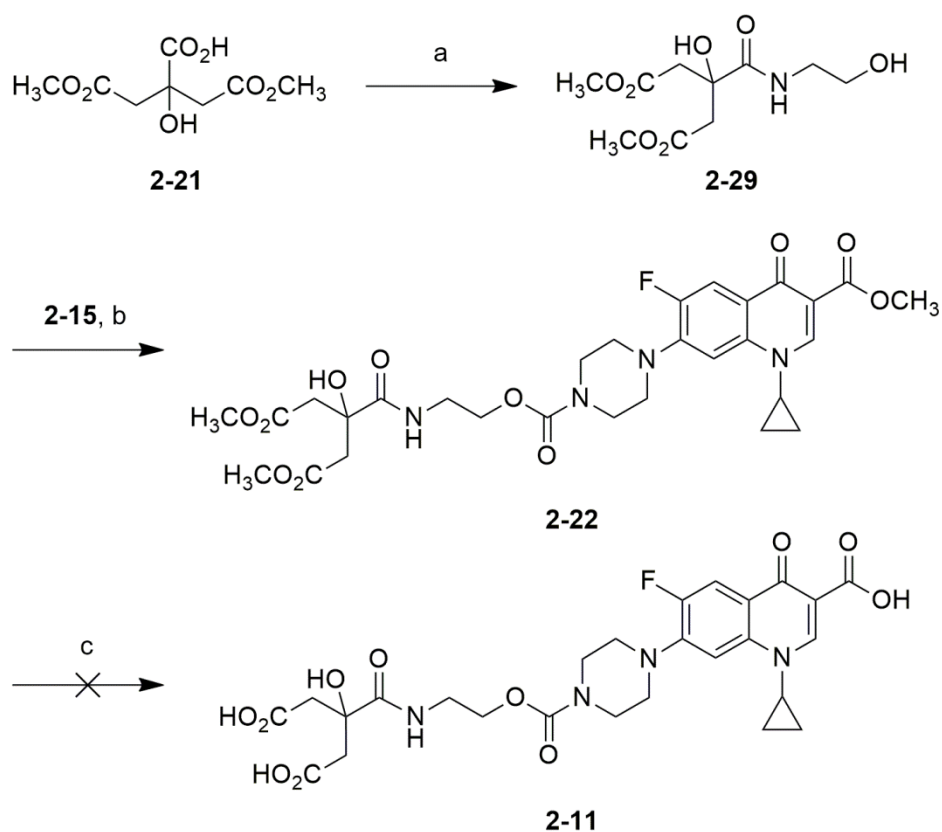
The successful synthesis of **2-19** would have allowed the continuation of the initial synthetic route outline in **Scheme 15**. Nevertheless a new

shorter synthetic route was planned as outlined in **Scheme 23**. This new route was aimed to provide a more efficient route to the target compound **2-11** as it is shorter, and could therefore potentially have a greater overall yield.

Second synthetic route targeting a 1,5-citrate-ciprofloxacin conjugate incorporating a carbamate linker

With the initial synthetic route determined to be unviable in terms of the low yields obtained at an early stage in the synthesis (**Scheme 15**), and the subsequent successful application of *N,N'*-disuccinimidyl carbonate to activate an alcohol and give a carbamate, a shorter route was considered.

Thus a new synthetic route was designed (**Scheme 23**), first involving the coupling of 1,5-dimethyl citrate **2-21** and ethanolamine to produce the intermediate **2-29**. Subsequent activation of **2-29**, using *N,N'*-disuccinimidyl carbonate, followed by the addition of ciprofloxacin methyl ester **2-15**, would introduce the carbamate group to give **2-22**.¹⁵⁷ Finally, it was planned that base hydrolysis would furnish the required target **2-11** (**Scheme 23**).



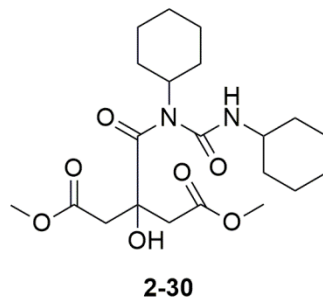
Scheme 23 - Second synthetic route towards compound **2-11**. (a) ethanolamine, coupling reagent; (b) DSC, DMF, DIPEA, 45%; (c) (i) 0.1 M TBAH, (ii) 0.1 M HCl.

*Coupling 1,5-dimethyl citrate **2-21** and ethanolamine*

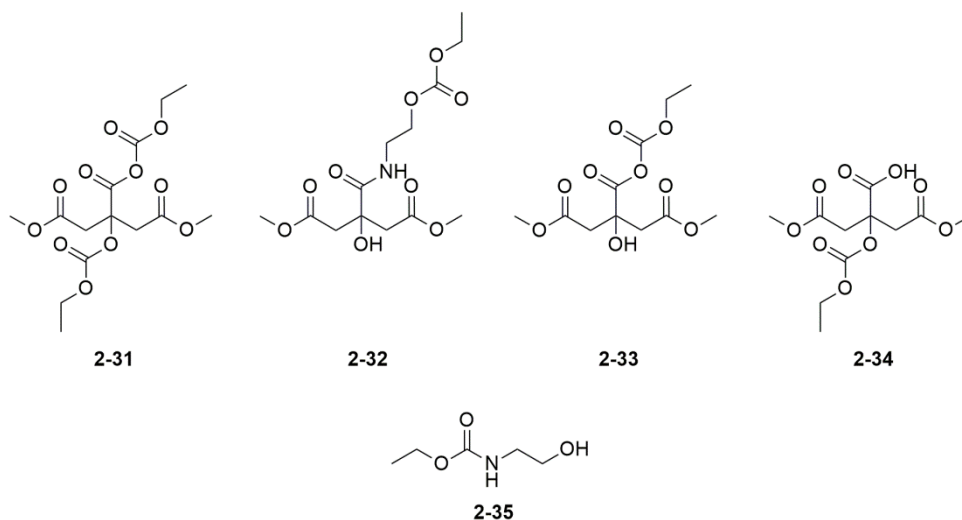
In order to proceed with the second synthetic route (**Scheme 23**), various reaction conditions were investigated in order to couple 1,5-dimethyl citrate **2-21** and ethanolamine utilising a range of coupling agents to produce **2-29** (**Scheme 24** and **Scheme 25**). The coupling agents investigated for the amide coupling were DCC, DCC/DMAP, ethyl chloroformate, CDI and HATU.

The use of DCC proved unsuccessful (**Scheme 24**), with a complex mixture observed in the ^1H NMR spectrum. Furthermore a $[\text{M}-\text{H}_2\text{O}]^+$ peak

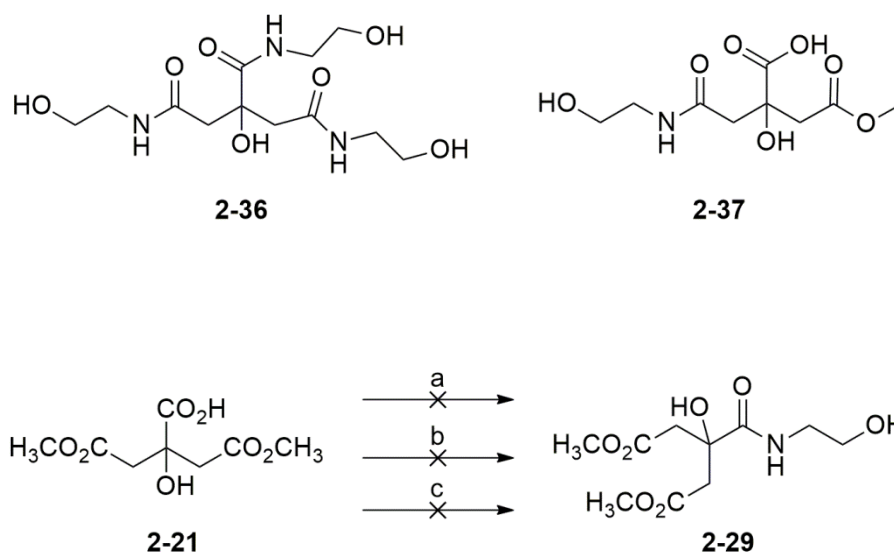
was observed in the ESI-MS spectrum at 409.2327, suggesting the reaction stopped at the *N*-acyl urea by-product, compound **2-30**.



The use of ethyl chloroformate also proved unsuccessful (**Scheme 24**), with side reactions occurring that indicated issues with chemoselectivity of the reaction. The crude ^1H NMR once again proved complex, and the ESI-MS spectrum indicated a number of intermediates which suggested the reaction did not proceed as desired, such as compounds **2-31**, **2-32**, and **2-33** either/or **2-34**, with $[\text{M}+\text{Na}]^+$ peaks for each intermediate compound at 387.0898, 358.1113 and 315.0687 respectively. Furthermore the by-product **2-35** was isolated, supported by ESI-MS analysis, with a $[\text{M}+\text{Na}]^+$ peak at 156.0632, consistent with a molecule of formula $\text{C}_5\text{H}_{11}\text{NNaO}_3$.



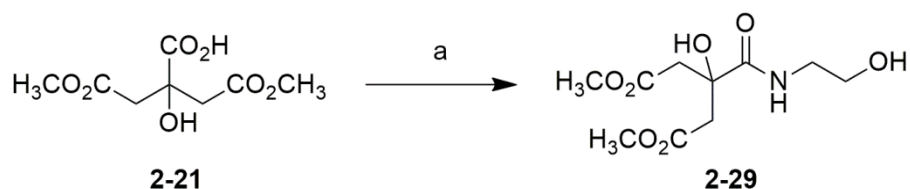
On using CDI, amide coupling was observed, yet not as desired, instead giving by-products (**Scheme 24**). On the first attempt, whereby CDI was used in 1.3-fold excess, and ethanolamine in 15-fold excess, compound **2-36** was isolated in 69% yield, supported by ESI-MS analysis, with a $[M+Na]^+$ peak at 344.1412, consistent with a molecule of formula $C_{12}H_{23}N_3NaO_7$. Dropping the excess amount of ethanolamine to 1.3-fold resulted in the formation of **2-37** in 24% yield, supported by ESI-MS analysis, with a $[M-H]^-$ peak at 248.0781, consistent with a molecule of formula $C_9H_{14}NO_7$. Furthermore, the citrate region in the 1H NMR indicated an unsymmetrical set of methylene CH_2 protons, with four sets of roofed doublets at 2.68, 2.93, 3.02 and 3.06 ppm, indicative of two pairs of diastereotopic protons for **2-37**.



Scheme 24 - Attempted synthesis of **2-29**. (a) ethanolamine, DCC, 1,4-dioxane. (b) ethanolamine, ethyl chloroformate, THF, *N*-methylmorpholine. (c) ethanolamine, CDI, THF.

It was thus found that HATU mediated coupling proved successful in giving **2-29**, in 92% yield (**Scheme 25**). The successful formation of **2-29** was supported by ^{13}C NMR spectroscopy, with a characteristic resonance at 176.3 ppm for the amide functional group. In addition, ESI-MS analysis

gave a molecular ion peak $[M+Na]^+$ for **2-29** at m/z 286.0904, consistent with a compound of formula $C_{10}H_{17}NNaO_7$. Additionally, a pair of roofed doublets, characteristic of a symmetrical citrate moiety, was present in the 1H NMR spectrum (**Figure 15**). These resonances can be assigned to the diastereotopic methylene protons (H_a , H_b), and hence couple to each other, arising as the pair of doublets with a coupling constant of 15.2 Hz, characteristic of geminal 2J coupling between protons on an sp^3 carbon.¹⁷² Their close chemical shifts mean they exhibit a roof effect, seen in their signal profile.



Scheme 25 - Synthesis of **2-29**. (a) HATU, DMF, DIPEA, ethanolamine, 92%.

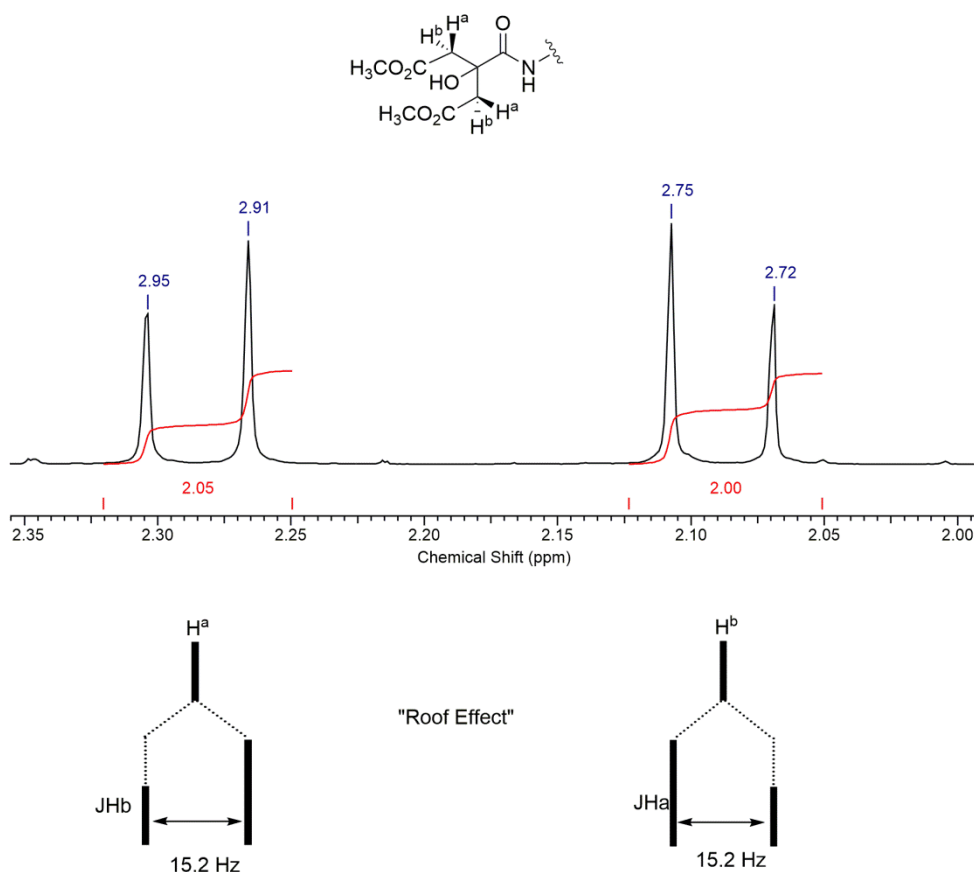
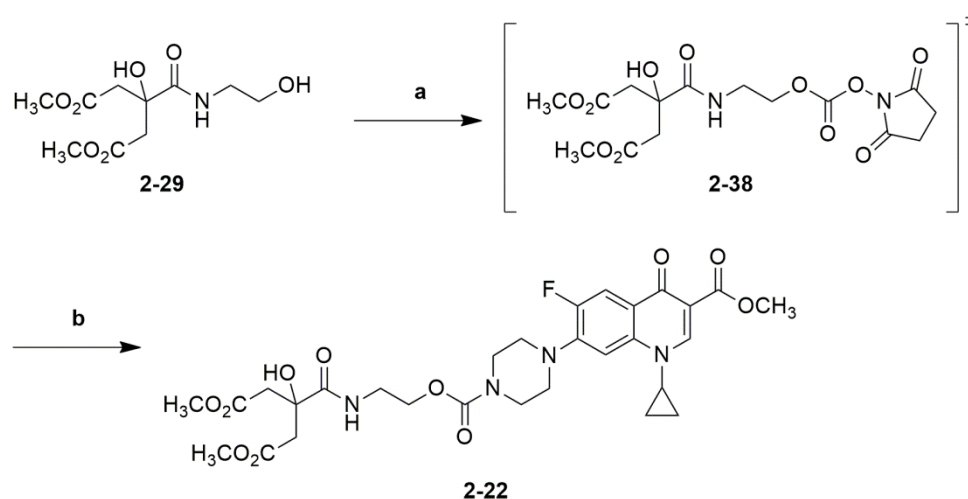


Figure 15 - ^1H NMR spectrum of **2-29** in CD_3OD , shown in the region between 2.00-2.35 ppm. The J-coupling splitting pattern is shown below, explaining the splitting for each of the resonances. *The assignment of H^a and H^b can be interchanged.

Formation of the carbamate functional group via N,N' -disuccinimidyl carbonate activation

The conditions used for the formation of **2-19** (**Scheme 22**) were employed towards the synthesis of **2-22**, from **2-29** and ciprofloxacin methyl ester **2-15**. However, on the first attempt using N,N' -disuccinimidyl carbonate, pyridine and potassium phosphate tribasic in DMF, **2-22** was not formed. The reaction conditions were therefore altered, substituting potassium phosphate and pyridine with DIPEA (**Scheme 26**). The crude reaction mixture was monitored by ESI-MS analysis, giving a molecular ion peak for **2-38** (**Scheme 26**). It was on confirmation of the presence of the

activated intermediate that the ciprofloxacin methyl ester **2-15** was added. After workup and purification, **2-22** was isolated in 45% yield, characterised using ^1H and ^{13}C NMR spectroscopy, infra-red spectroscopy and ESI mass spectrometry. The successful formation of **2-22** was supported by ^{13}C NMR spectroscopy, with a characteristic resonance at 155.5 ppm for the carbamate functional group. Furthermore, ESI-MS analysis gave a molecular ion peak $[\text{M}+\text{Na}]^+$ for **2-22** at m/z 657.2194, consistent with a molecule of formula $\text{C}_{29}\text{H}_{35}\text{FN}_4\text{NaO}_{11}$. Additionally, there was a pair of roofed doublets present in the ^1H NMR spectrum, characteristic of a symmetrical citrate moiety, similar to those already described for **2-29**, highlighting the retained symmetry of the methylene protons.

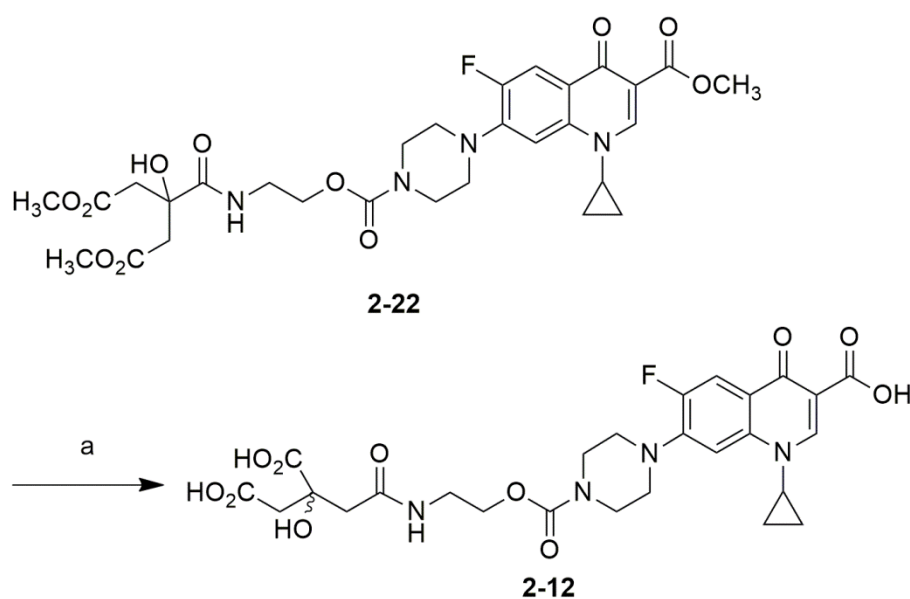


Scheme 26 - Reaction utilising N,N' -disuccinimidyl carbonate to form the required carbamate bond to produce compound **2-22**. (a) DSC, DMF, DIPEA; (b) **2-15**, DMF, 45%.

Base hydrolysis of compound 2-22 to target compound 2-11

With compound **2-22** synthesised, deprotection to give **2-11** was explored (**Scheme 23**). Compound **2-22** was treated with 0.1 M

tetrabutylammonium hydroxide in methanol, followed by the addition of 0.1 M hydrochloric acid until the solution was at pH 1.4 and precipitate had formed (**Scheme 23**). The chemical structure of the isolated precipitate was investigated. The loss of the characteristic methyl ester signals in the ^1H NMR spectrum was observed, and also ESI-MS gave a molecular ion peak $[\text{M-H}]^-$ at m/z 591.1749, consistent with a molecule of formula $\text{C}_{26}\text{H}_{28}\text{FN}_4\text{O}_{11}$. However, it was not compound **2-11** that was isolated, but instead it was the regioisomer **2-12**, in 64% yield (**Scheme 27**).



Scheme 27 - Isomerisation of compound **2-22** on base hydrolysis, giving the regioisomeric target, **2-12**. (a) (i) 0.1 M TBAH, (ii) 0.1 M HCl, 64%.

The characterisation data that supported the formation of **2-12** rather than the expected **2-11** was investigated. The ^1H NMR spectrum was recorded in both CD_3OD (**Figure 16**) and in d_6 -DMSO (**Figure 17**). The resonances due to the citrate moiety consist of two sets of roofed doublets, which are assigned to the methylene protons (H_a , H_b , H_c and H_d - **Figure 16**). As each pair of these methylene protons, H_a / H_b and H_c / H_d , respectively, are diastereotopic, they demonstrate geminal coupling, with two sets of doublets observed. Given the close chemical shifts for these signals, they

also exhibit a roof effect, seen in their signal profiles. The citrate region of the ^1H NMR spectrum in d_6 -DMSO (**Figure 17**) shows a similar signal profile, with one of the resonance peaks overlapping with the residual d_5 -DMSO solvent peak.

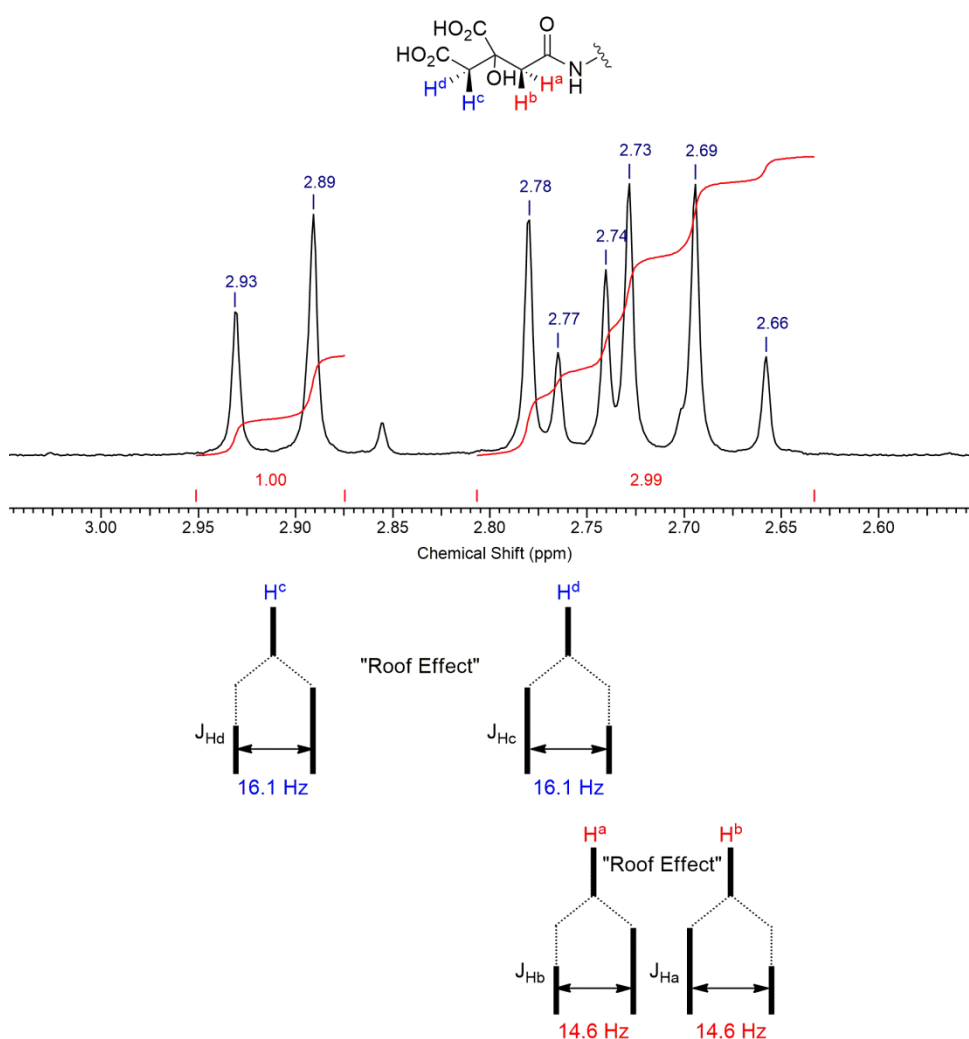


Figure 16 - ^1H NMR spectrum of **2-12** in CD_3OD , shown in the region between 2.55-3.05 ppm. The J -coupling splitting pattern is shown below, explaining the splitting for each of the resonances. *The assignment of H^a and H^b can be interchanged. **The assignment of H^c and H^d can be interchanged.

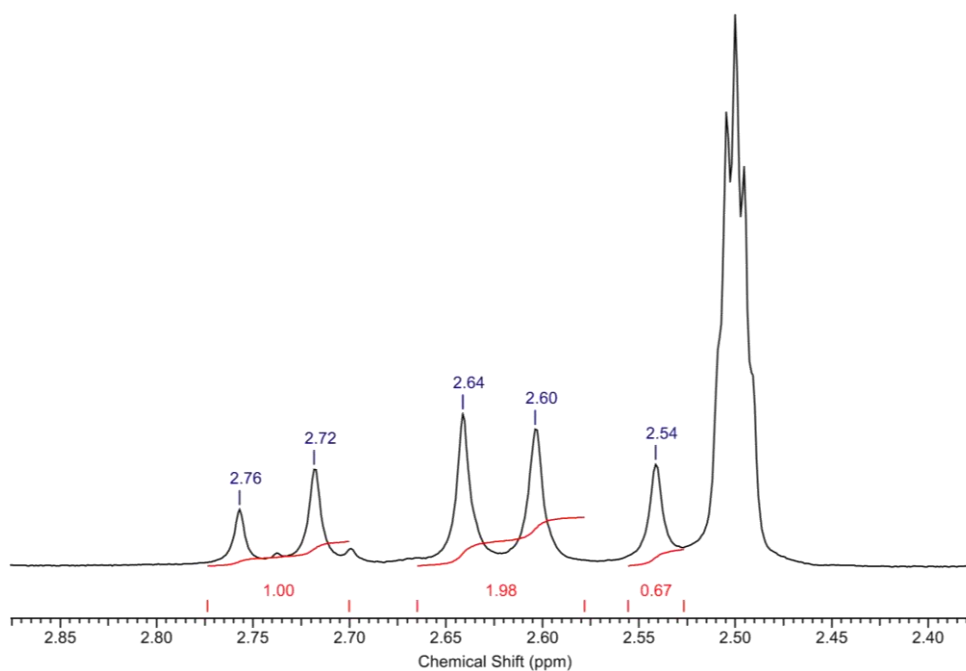


Figure 17 - ^1H NMR spectrum of the citrate moiety in **2-12** in d_6 -DMSO, shown in the region between 2.40-2.85 ppm.

While the ^1H NMR spectrum supported the formation of an unsymmetrical citrate, indicative of the citrate moiety of compound **2-12**, further supporting data was required. Firstly, the citrate region of the ^{13}C NMR spectrum showed two resonances corresponding to the methylene carbons, at 43.3 and 42.9 ppm, respectively, as opposed to one that would be expected for the symmetrical compound **2-11** (**Figure 18**).

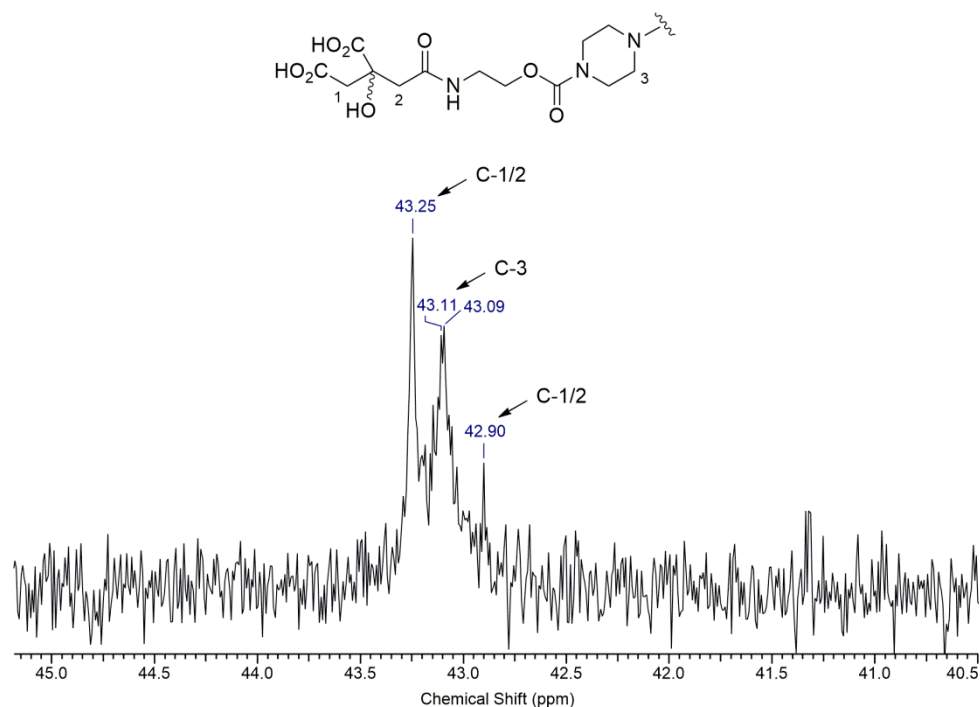


Figure 18 - ^{13}C NMR spectrum of **2-12** in d_6 -DMSO, shown in the region between 40.5-45.0 ppm.

The Heteronuclear Multiple Bond Correlation (HMBC) NMR spectrum was investigated, with a focus on the citrate region in the ^1H NMR spectrum (**Figure 19**). As the HMBC NMR spectrum shows, there are three carbonyl resonance signals at 175.7, 172.1 and 170.5 ppm around the two methylene proton environments 1 and 2. This is indicative of an unsymmetrical citrate moiety, supporting the formation of **2-12**. The Heteronuclear Single Quantum Correlation (HSQC) NMR spectrum was also investigated (**Figure 20**). With a focus on the citrate region in the ^1H NMR spectrum, the HSQC NMR spectrum also suggests the formation of **2-12**, with two carbon environments corresponding to the citrate protons. This supports the ^{13}C NMR spectrum (**Figure 18**), and was reinforced further by negative signals in the DEPT spectrum.

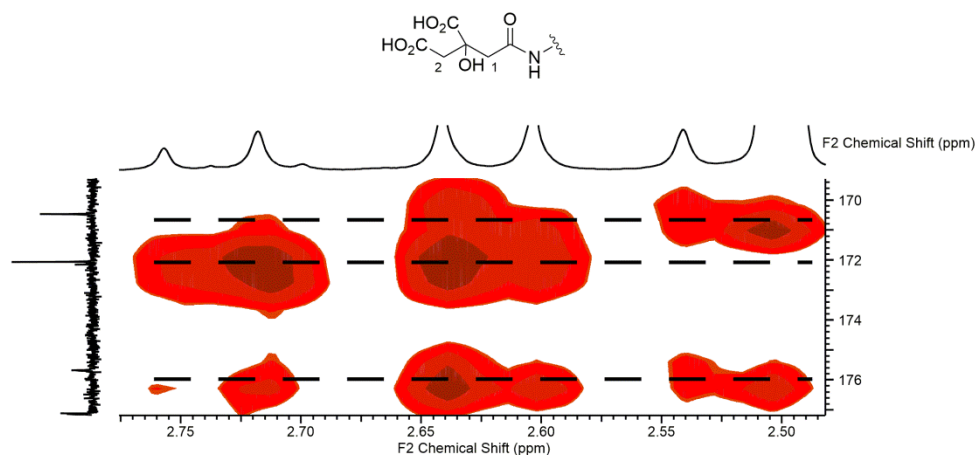


Figure 19 - HMBC spectrum of **2-12** in d_6 -DMSO, shown in the region between 169.5-175.5 ppm in the ^{13}C NMR and 2.45-2.80 ppm in the ^1H NMR spectrum. The resonance signals at 175.7, 172.1 and 170.5 ppm in the ^{13}C NMR spectrum show there are three different carbonyl environments around the two methylene proton environments (labelled 1 and 2).

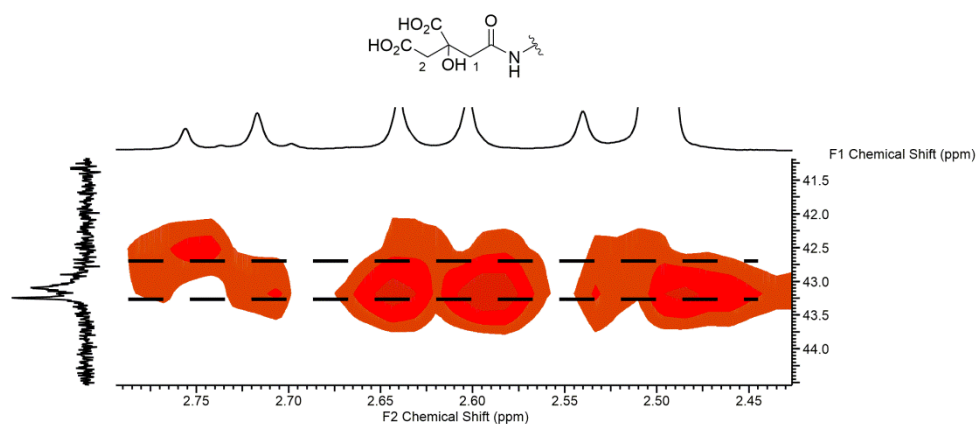


Figure 20 - HSQC spectrum of **2-12** in d_6 -DMSO, shown in the region between 41.45-44.5 ppm in the ^{13}C NMR and 2.45-2.85 ppm in the ^1H NMR spectrum. There are two resonance signals in the ^{13}C NMR spectrum, at 43.3 and 42.9 ppm corresponding to the methylene carbons of the citrate moiety (labelled 1 and 2).

The resonances observed in the ^{13}C NMR spectrum are essential for assignment of the carbonyl moieties (**Figure 21**). There are six carbonyl

environments for **2-12**, including a doublet with a coupling constant of 2.3 Hz at 177.1 ppm, characteristic of a $^4J_{C-F}$ coupling,¹⁷³ corresponding to the carbonyl in the fluoroquinolone moiety (C-2). The carbonyl environments of **2-12** were thus fully assigned (**Figure 21**). In a ^{13}C spectrum of compound **2-11** only five carbonyl environments would have been observed. The extra signal observed for the isolated product confirms that it was compound **2-12**.

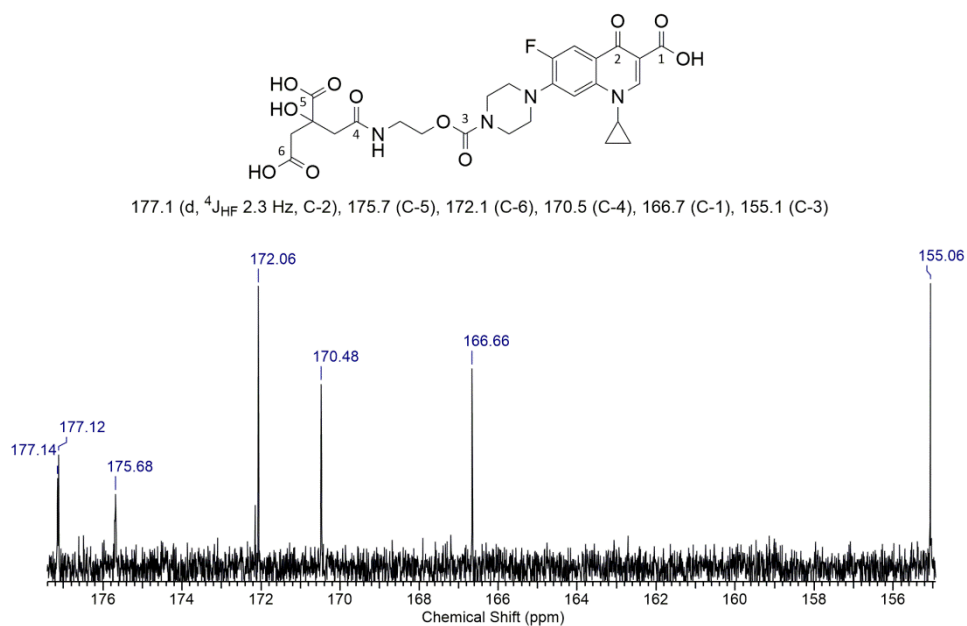
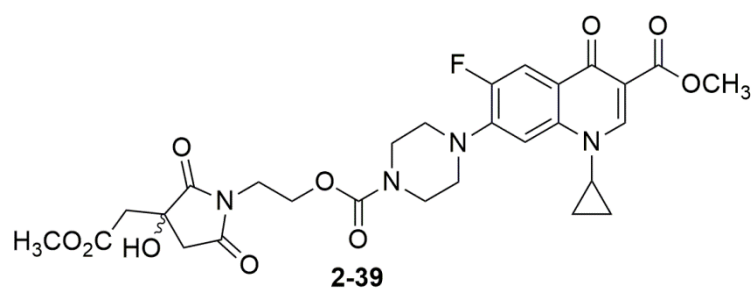


Figure 21 - ^{13}C NMR spectrum **2-12** in d_6 -DMSO, shown in the region between 177.2-155.0 ppm. The full assignment of the carbonyl environments of **2-12** was made using all the available NMR data.

Determination of the mechanism of isomerisation of the citrate siderophore component

As base hydrolysis of compound **2-2** led to the formation of **2-12**, rather than the expected product **2-11**, it was important to understand the mechanism by which isomerisation occurred. It was found during the purification of **2-22**, by silica gel column chromatography, that succinimide

2-39 was also isolated. Formation of succinimide **2-39** was supported by the loss of the signal for one methyl group in the ^1H NMR spectrum and also by ESI-MS analysis, with a molecular ion peak $[\text{M}+\text{H}]^+$ at m/z 603.2112, consistent with a molecule of formula $\text{C}_{28}\text{H}_{32}\text{FN}_4\text{O}_{10}$. Furthermore, the citrate region between 2.75-3.10 ppm of the ^1H NMR displayed a profile different to that of **2-22** (**Figure 22**).



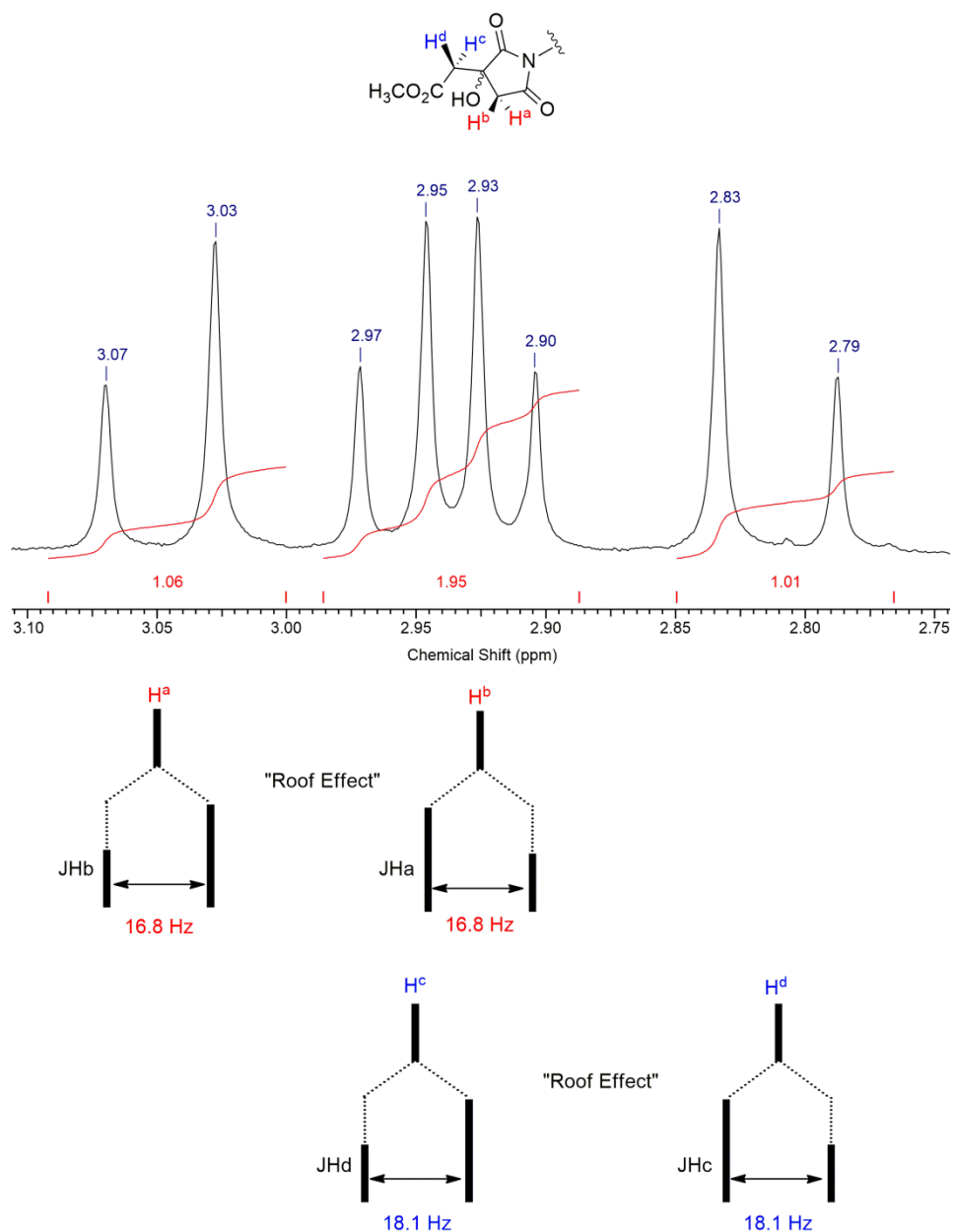


Figure 22 - ^1H NMR spectrum of **2-39** in CDCl_3 , shown in the region between 2.75-3.10 ppm. The J-coupling splitting pattern is shown below, explaining the splitting for each of the resonances. *The assignment of H^a and H^b can be interchanged. **The assignment of H^c and H^d can be interchanged.

As can be seen in **Figure 22**, the resonances due to the succinimide moiety consist of two sets of doublets, which are assigned to the methylene protons as before. Furthermore, Correlation Spectroscopy (COSY) NMR and HSQC NMR supported the formation of **2-39**. Final confirmation of

the formation of **2-39** was by single crystal X-ray diffraction analysis (**Figure 23**). The single crystals of **2-39** grew from a methanolic solution of **2-22**, suggesting that **2-39** could be an intermediate in the isolation of **2-12** from **2-22**, discussed later (**Scheme 29**).

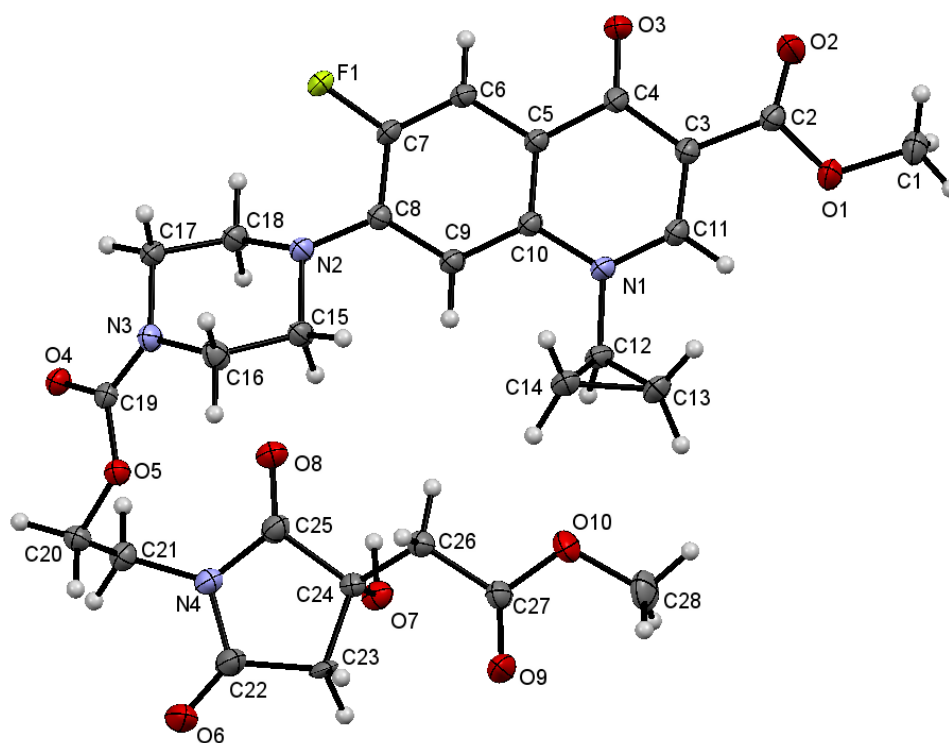
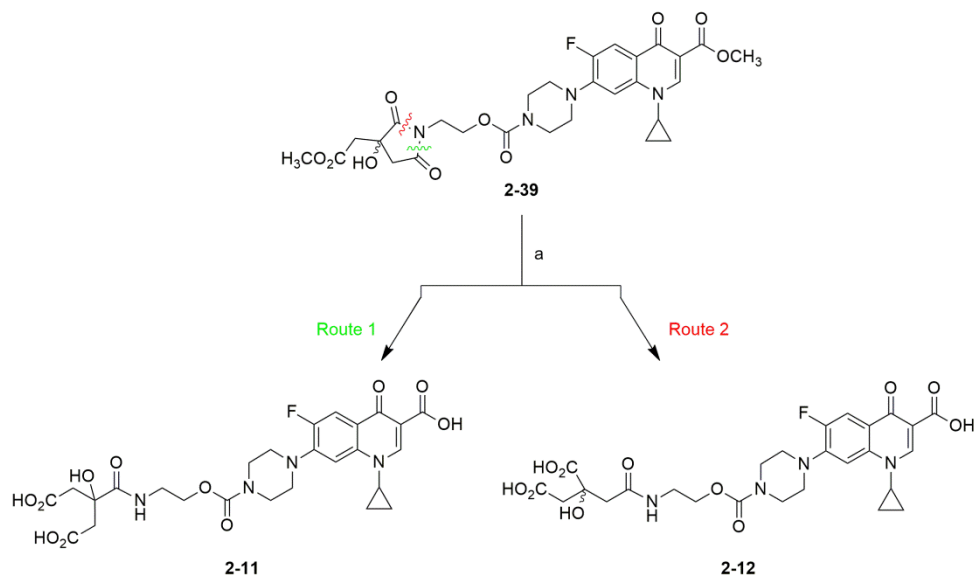


Figure 23 - ORTEP diagram (50% probability ellipsoids) of **2-39**, shown as one chiral form of a racemate. Space group: P-1. Crystal contains both enantiomers that are related, with the *S* enantiomer shown and *R* omitted for clarity.

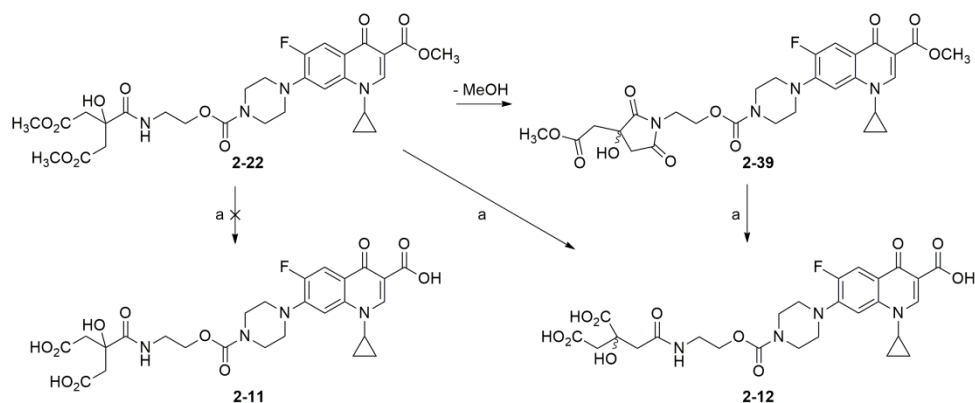
The isolation of compound **2-39** allowed for the investigation of the route of succinimide cleavage. The cleavage of **2-39** can proceed *via* two possible routes, giving either compound **2-11** or **2-12**. Compound **2-11** would require the succinimide to cleave *via* route 1 (Green - **Scheme 28**), whereas compound **2-12** would see cleavage *via* route 2 (Red - **Scheme 28**). On treating **2-39** with 0.1 M tetrabutylammonium hydroxide in methanol, followed by the addition of 0.1 M HCl to acidify the solution, it

was found that the only product was **2-12** (**Scheme 28**), with the characterisation data identical to that already discussed.



Scheme 28 - Base hydrolysis of succinimide **2-39** to give either **2-11** or **2-12**, or a mixture of both, through either Route 1 (Green) or Route 2 (Red).
(a) (i) 0.1 M TBAH, (ii) 0.1 M HCl.

It can therefore be summarised that the formation of **2-12** proceeded through the intermediate **2-39** with the loss of methanol, before ring opening of the succinimide to give the target compound (**Scheme 29**). As such it was also concluded that isolating compound **2-11** was not possible *via* the synthetic route carried out. The isolation of **2-12** did however allow for antimicrobial screening to determine the viability of the carbamate group as a bio-labile linker.



Scheme 29 - Summary of the formation of **2-12** from **2-22**. (a) (i) 0.1 M TBAH, (ii) 0.1 M HCl.

2.4 Antimicrobial Activity Testing of the 1,3-Citrate-Ciprofloxacin Conjugate, 2-12

Stability Testing

With compound **2-12** isolated, it was essential to determine its stability prior to biological screening. It was observed during the synthesis that the carbamate group was chemically stable between pH 1.4-12 in aqueous solution. However, it was still important to determine the stability of **2-12** over time at biologically relevant pH in aqueous media. The stability of **2-12** was monitored by ^1H NMR in D_2O with 0.042 M Na_2HPO_4 , 0.008 M NaCl and DCl (HCl in D_2O), at pD 7.01 as a mimic of the M9 minimal media to be used during the biological screening. As can be seen in **Figure 24** there was no change in the ^1H NMR spectrum after 74 h. It was therefore determined that **2-12** was stable for a suitable period of time for biological screening.

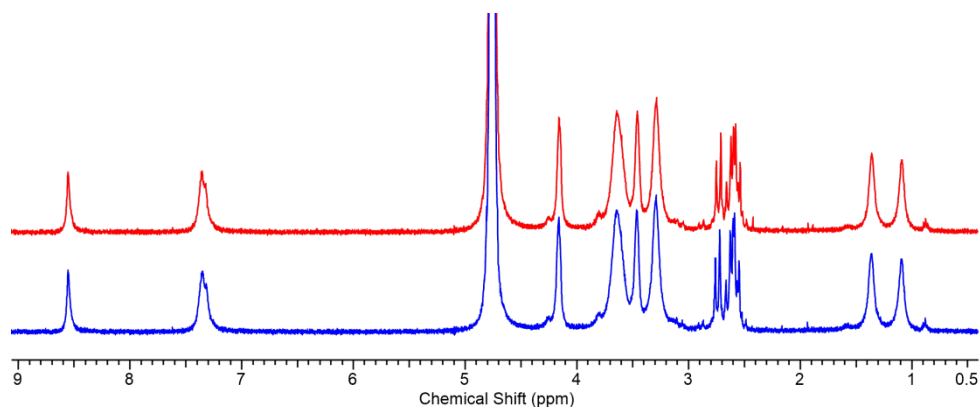


Figure 24 - ^1H NMR spectrum of **2-12** in D_2O with 0.042 M Na_2HPO_4 , 0.008 M NaCl and DCl (HCl in D_2O), at pD 7.01, as a mimic of M9 Minimal Media. The blue spectrum shows the sample at $t = 0$ h. The red spectrum shows the sample at $t = 74$ h.

Bacterial Growth Assay

Having isolated and determined the stability of the 1,3-citrate-carbamate ciprofloxacin conjugate **2-12**, it was necessary to test for its antimicrobial activity, with ciprofloxacin **1-5** as a positive control. The antimicrobial activity of **2-12** was first assessed by carrying out a growth assay of the bacterial strain *E. coli* BW25113 wild type in two media, Lysogeny broth (LB) nutrient and M9 minimal. LB media is a nutritionally rich medium containing tryptone and yeast, providing amino acids, organic compounds and Fe(III) essential for bacterial growth. With nutrient deficient conditions, M9 minimal media allows the nutrient composition to be controlled for a more direct comparison to *in vivo* conditions, where Fe(III) concentrations are extremely low. It is known that under iron deficiency, siderophore production and uptake would be upregulated in bacterial cells, and so screening a Trojan horse conjugate under such conditions should facilitate its uptake. Therefore screening in both media will allow for the direct comparison of the ability of the conjugate to compete for uptake under nutrient rich conditions, as well as under iron deficiency.

Using a plate reader the growth of the wild type *E. coli* cells was determined by the optical density (OD₆₅₀) values at drug concentrations of 0.01 μ M, 0.1 μ M, 0.5 μ M, 1 μ M and 10 μ M, with a negative control of 0 μ M (DMSO). The OD₆₅₀ values correspond to the absorbance of a sample against the length of the cuvette at 650 nm. This in turn allows for the quantification of the bacterial cell concentration. Readings were taken every 30 minutes over 16 hours, with the plate shaken at 37 °C in between each reading (Chapter 7). Although time points were taken over 16 hours, the data presented is at the time point at 10 hours, where bacterial growth has plateaued (**Figure 25** - **Figure 28** - see Appendix II for individual graphs).

The assay indicates that conjugate **2-12** is active against wild type *E. coli*, with growth suppressed at 10 μ M of the drug in both media (**Figure 25** and **Figure 26**). The assay carried out in LB demonstrates that at lower drug concentrations of 0.01 μ M, 0.1 μ M and 0.5 μ M for **2-12**, cell growth is relatively unaffected, comparable to when no drug is present (**Figure 25**). This is likely to be due to the readily available nutrients within the media. Activity was observed at a lower concentration of 0.1 μ M for free ciprofloxacin. However, at a much higher concentration of 10 μ M (**Figure 25**) there is near complete suppression of growth for the free ciprofloxacin drug, yet unfortunately some growth was still seen for the conjugate **2-12**. Therefore the growth assay in LB indicates that **2-12** is less active than the parent drug.

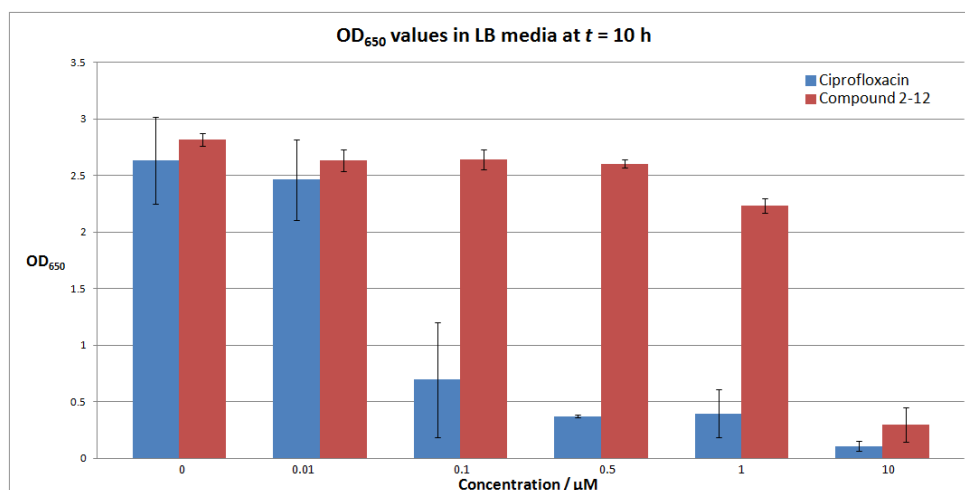


Figure 25 - *E. coli* BW25113WT growth in LB media across concentrations at $t = 10$ h for both ciprofloxacin **1-5** (blue) and conjugate **2-12** (red). The experiment was run in quadruplicate and the error bars show one standard deviation from the mean.

The trend of activity for the growth assay of wild type *E. coli* in M9 minimal media is comparable to that in LB media (**Figure 26**). Under these conditions *E. coli* growth was clearly diminished, with lower OD₆₅₀ values compared to when using LB media, due to the lower nutrient availability. From both assays the difference in activity between ciprofloxacin and conjugate **2-12** can be clearly seen at lower drug concentrations of 0.1 μM. Furthermore, an estimate of a minimum inhibitory concentration (MIC) value can be made. For ciprofloxacin **1-5**, the assays suggest an estimate of the MIC of between 0.01 μM and 0.1 μM (**Figure 26**), whereas for conjugate **2-12** an estimate of the MIC would be between 0.5 μM and 1 μM, suggesting the conjugate is approximately 50-100 times less active than the parent drug. Across all concentrations, the ciprofloxacin assay had less wild type *E. coli* growth in M9 minimal media than that observed for conjugate **2-12**, demonstrating again that the conjugate is less active than ciprofloxacin.

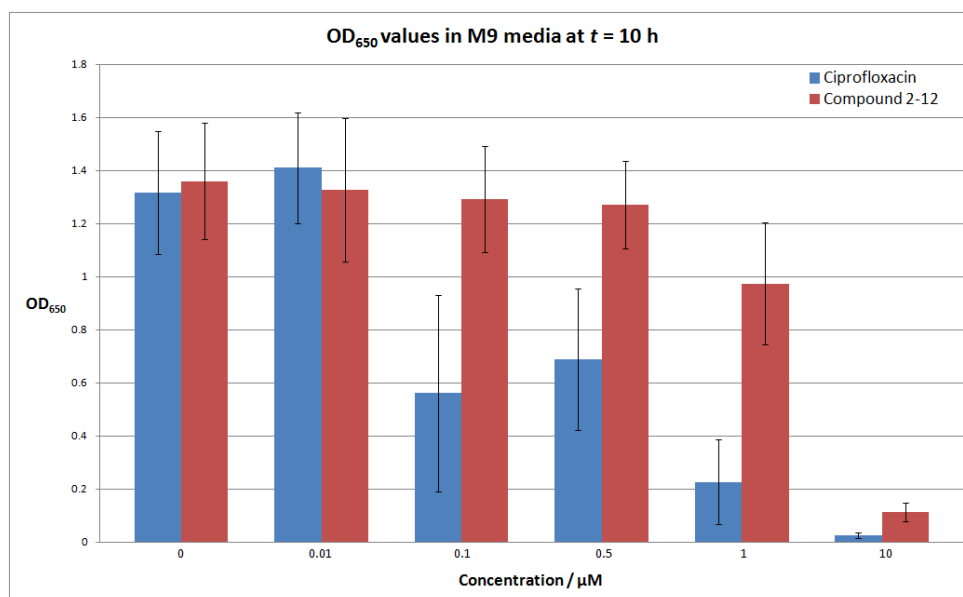


Figure 26 - *E. coli* BW25113WT growth in M9 minimal media across concentrations at $t = 10$ h for both ciprofloxacin **1-5** (blue) and conjugate **2-12** (red). The experiment was run in quadruplicate and the error bars show one standard deviation from the mean. For 0.01 μM ciprofloxacin the experiment was run in triplicate.

With the wild type *E. coli* strain demonstrating that conjugate **2-12** had antimicrobial activity, it was decided to investigate how the conjugate enters the bacterial cell. The Trojan horse strategy aims to exploit the iron uptake system, to actively uptake, and thus increase the intracellular concentration of the antimicrobial. Therefore, to test this hypothesis, conjugate **2-12** was next screened against *E. coli* BW25113 FecA::kan, a strain whereby the outer membrane receptor FecA is knocked-out.⁶⁰ As discussed in Chapter 1, FecA is the outer membrane receptor which recognises and transports citrate siderophores across the outer membrane.⁶⁰ Given that conjugate **2-12** incorporates citrate as its siderophore moiety, it would be advantageous to determine if it utilises the iron uptake mechanism to transport the antimicrobial into the cell.

Using the same methodology as that used for the growth assays against *E. coli* BW25113WT, conjugate **2-12** was screened against *E. coli* BW25113

FecA::kan in both LB and M9 minimal media (**Figure 27** and **Figure 28** - see Appendix II for individual graphs). As can be seen, both assays demonstrate that conjugate **2-12** retains activity at the highest concentration of 10 μM , and that this activity is reduced compared to the parent ciprofloxacin antimicrobial. As such, it was determined that the outer membrane receptor FecA is not essential for the uptake of conjugate **2-12**. However, it can be seen that at 1 μM , the approximate concentration at which conjugate **2-12** has an MIC value in wild type *E. coli* (**Figure 25** and **Figure 26**), the rate of growth for *E. coli* BW25113 FecA::kan matches that for lower concentrations of the drug, and even the growth control of 0 μM (**Figure 27** and **Figure 28**). Speculatively, this could indicate that whilst FecA is not essential for the uptake of conjugate **2-12** into *E. coli*, it may still have a role in aiding the active uptake of the conjugate at higher concentrations. It must be stated that this data does not allow for the potential role of FecA as an active transporter to be confirmed, and as such more assays are needed at intermittent concentrations between 1 μM and 10 μM to see if there is a more obvious correlation. Furthermore, with the highest concentration at 10 μM indicating activity of conjugate **2-12** in *E. coli* BW25113 FecA::kan, confirming that FecA is not essential, it would therefore suggest that conjugate **2-12** enters the bacterial cell *via* another mechanism, likely to be through passive diffusion.

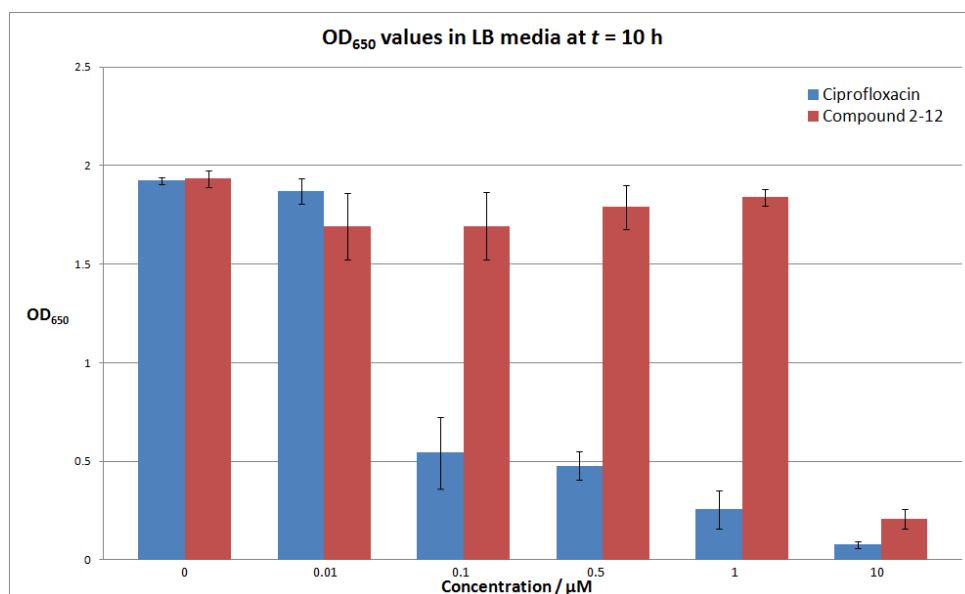


Figure 27 - *E. coli* BW25113 FecA::kan growth in LB media across concentrations at $t = 10$ h for both ciprofloxacin **1-5** and conjugate **2-12**. The experiment was run in quadruplicate and the error bars show one standard deviation from the mean.

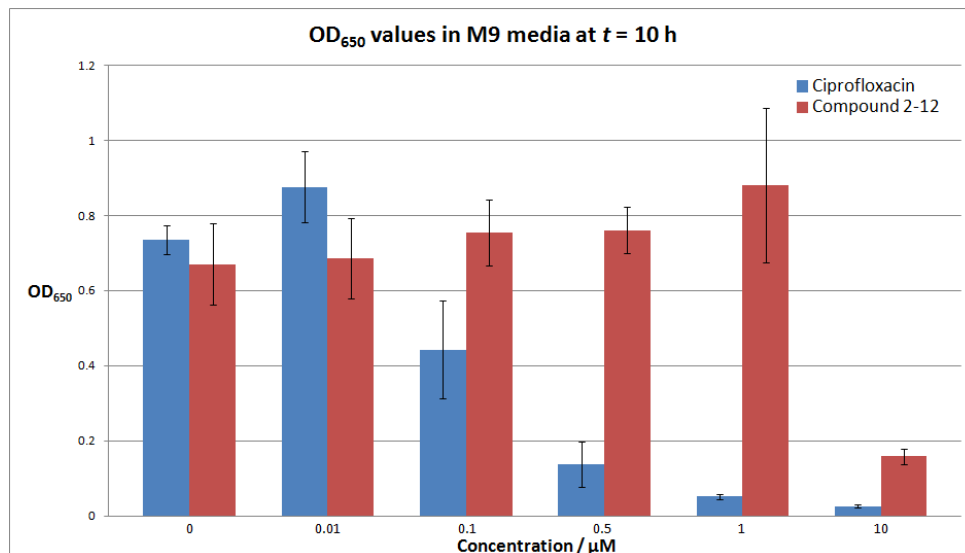


Figure 28 - *E. coli* BW25113 FecA::kan growth in M9 minimal media across concentrations at $t = 10$ h for both ciprofloxacin **1-5** and conjugate **2-12**. The experiment was run in quadruplicate and the error bars show one standard deviation from the mean. For 0 μM ciprofloxacin the experiment was run in triplicate.

The growth assays for both wild type and and BW25113 FecA::kan strains indicate that conjugate **2-12** is active against *E. coli*, yet also that its ability to prevent bacterial growth was less than that for ciprofloxacin **1-5**. These results are consistent with other reported fluoroquinolone-siderophore conjugates, which show reduced activity of the drug.¹¹⁵⁻¹²⁸ It has been proposed that non-labile substituent groups conjugated *via* the piperazinyl ring of ciprofloxacin **1-5** prevent the conjugates from forming the dimer in the DNA replication complex.¹²⁸ To test this theory a DNA gyrase assay was performed to test the activity of **2-12** in its ability to inhibit DNA replication.

DNA Gyrase Assay

To establish if the ciprofloxacin moiety of conjugate **2-12** inhibited the supercoiling of DNA by the gyrase protein (Chapter 1), a DNA gyrase assay was performed. Relaxed and supercoiled DNA run at different rates on an agarose gel, allowing for the two forms to be separated and then visualised. Compounds that inhibit DNA gyrase will show higher levels of relaxed DNA, with limited supercoiling, especially at higher drug concentrations. Alternatively, compounds with lower or no activity will still demonstrate higher levels of supercoiled DNA at higher drug concentrations.

The assay consisted of the conjugate **2-12** being mixed with the DNA and gyrase over a range of concentrations from 0 μM to 20 μM . Negative and positive controls were used whereby either the drug or gyrase were omitted from the mixtures, respectively. The DNA gyrase assay was also performed using ciprofloxacin **1-5** to allow for comparison. Relaxed DNA with gyrase was incubated with the drugs at 37 °C for 30 minutes and then separated using electrophoresis on an agarose gel (Chapter 7). After electrophoresis, the stained gel showed an increase in the inhibition of

DNA gyrase with an increase in drug concentration for both compounds, shown by the increased amounts of relaxed DNA. However, it was clear that **2-12** has lower inhibitory activity at higher concentrations with the presence of some supercoiled DNA at 20 μM , whereas the band assigned to the supercoiled form is not apparent at 5 μM for ciprofloxacin **1-5** (**Figure 29**). This indicates that ciprofloxacin **1-5** is more effective than conjugate **2-12** at inhibiting DNA gyrase, as a lower concentration is required for full inhibition.

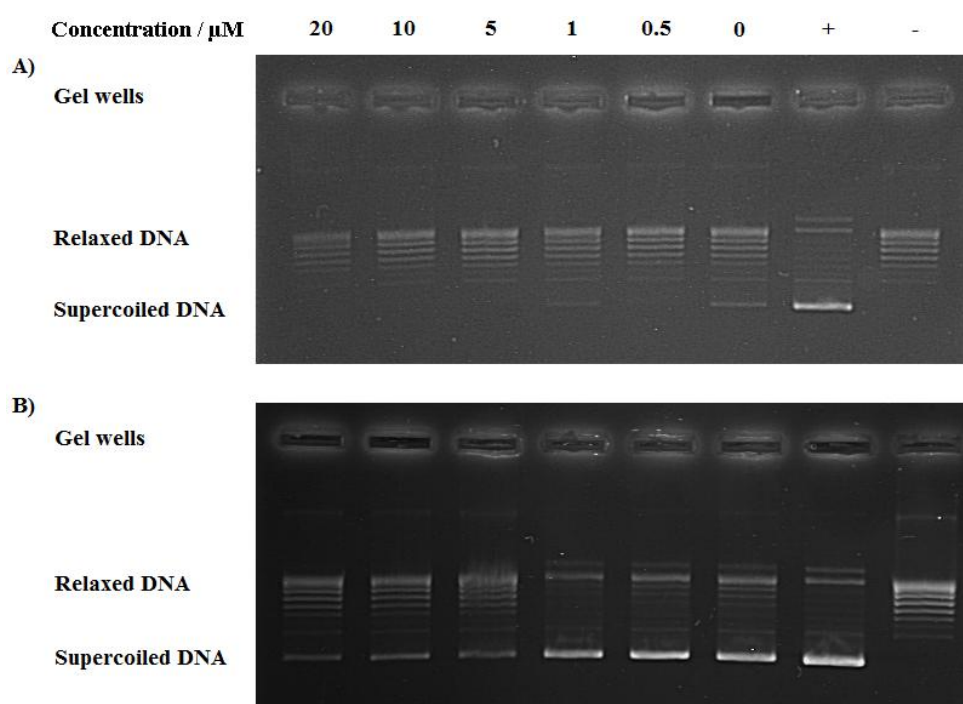


Figure 29 - DNA gyrase assay of **A)** ciprofloxacin **1-5** and **B)** conjugate **2-12** at concentrations ranging from 20-0 μM . 0 μM = DMSO control. + = positive control, with DNA gyrase present without the antimicrobial. - = negative control, no DNA gyrase or antimicrobial.

Interestingly, the DNA gyrase assay showed the presence of supercoiled DNA at both 10 μM and 20 μM for conjugate **2-12** (**Figure 29**). This in turn supports the fact there was growth at 10 μM , albeit limited, in both wild type and BW25113 *fecA::kan* *E. coli* strains in the presence of **2-12** (**Figure 25** - **Figure 28**). Given that it has been determined that FecA is

not essential for the uptake of **2-12**, the presence of supercoiled DNA at 20 μM in the gyrase assay can help support the suggestion that FecA may play some role in the active transport of conjugate **2-12** at higher concentrations. This is because at 10 μM concentration of **2-12** in the growth assays (**Figure 25 - Figure 28**), there is still near complete suppression of the growth of the *E. coli* strains. As the DNA gyrase assay directly delivers the compound to the gyrase target *in vitro*, the assay only gives an indication of the efficacy of the conjugate. However, the *in vivo* growth assays can potentially involve the active transport of conjugate **2-12** through the FecA system, and so potentially increase the intracellular concentration of the conjugate drug, leading to an observed improvement in activity at 10 μM concentration, compared to the DNA gyrase assay. Despite this speculative suggestion, more growth assay data is required to support this hypothesis, as stated previously. It should also be noted that for the *in vivo* growth assays, the conjugate has to pass through both the outer and cytoplasmic membranes to reach the target site.

Both the growth and gyrase assays indicated that conjugate **2-12** is an active antimicrobial, yet that its activity is reduced compared to the parent antimicrobial ciprofloxacin **1-5**. Whilst there is some suggestion that FecA is involved in the uptake of **2-12**, more data is required to confirm this, though it has been determined that FecA is not essential for the uptake and activity of the conjugate. Furthermore, it is unclear whether the lower activity of conjugate **2-12** is due to a lack of cleavage of the carbamate group to release the parent antimicrobial, or due to a lack of active transport, or a combination of both. Further growth assays at concentrations between 1 μM and 10 μM against *E. coli* BW25113 FecA::kan would allow for a greater understanding of the role of FecA, if any, in the uptake of conjugate **2-12**.

2.5 Summary, conclusions and future work for Chapter 2

The target compound **2-12**, a conjugate incorporating citrate as the siderophore, a carbamate as a potentially bio-labile linker, and ciprofloxacin as the antimicrobial, was synthesised and characterised. In addition, the isolation of **2-12** indicates that isomerisation occurred during base hydrolysis. Therefore, the synthetic route followed to obtain **2-12** only allows for the isolation of the one regioisomer. To target **2-11**, a new synthetic route would have to be established involving different protecting groups on both the antimicrobial and siderophore moieties, to avoid the base hydrolysis step where isomerisation occurred.

Furthermore, the antimicrobial screening of **2-12** was conducted, in both wild type and BW25113 *fecA::kan E. coli* strains. Additionally, a DNA gyrase assay was performed. These biological assays determined that conjugate **2-12** is an active antimicrobial, though less so than the parent ciprofloxacin. It was determined that the conjugate does not require the outer membrane receptor FecA for uptake into the cell, though it remains unclear whether FecA plays a role in aiding the uptake of the citrate containing conjugate **2-12**. Thus future work would require more assays to be undertaken at intermittent concentrations to determine any potential role of FecA. Furthermore, it is also unclear if there is a lack of cleavage the carbamate linker to release the parent drug. As such determination of whether the linker can cleave inside the cell must be examined. In addition to this, other potential bio-labile linkers must continue to be explored, to further the understanding of the requirements of linker design in siderophore-fluoroquinolone Trojan horse conjugates. The synthesis towards another such conjugate is discussed in Chapter 3.

**Chapter 3: Towards the
synthesis of a disulfide-
linked citrate-
ciprofloxacin conjugate**

3.1 Aims and overview

Having confirmed the importance of bio-labile linkers in siderophore-fluoroquinolone conjugate design, it was necessary to consider other available linkers which can allow intracellular drug release, building upon the previous investigation of a carbamate linker discussed in Chapter 2. This Chapter therefore discusses the design and synthesis towards a Trojan horse conjugate incorporating a disulfide linker at the β -position to a carbamate between the siderophore and fluoroquinolone moieties. The aim of the research presented in this Chapter was to examine whether the combination of a disulfide and carbamate group is suitable for intracellular release of free ciprofloxacin in the cytoplasm.

3.2 Introduction

In order to identify a suitable bio-labile linker for use in siderophore-fluoroquinolone Trojan horse conjugates, it was necessary to consider other functional groups that can allow for intracellular release of the antimicrobial. As Chapter 2 highlighted, the requirement for bio-labile linkers between the siderophore and fluoroquinolone antimicrobial components is essential, given the reduction in antimicrobial activity for all reported siderophore-fluoroquinolone Trojan horse conjugates.¹¹⁵⁻¹²⁸

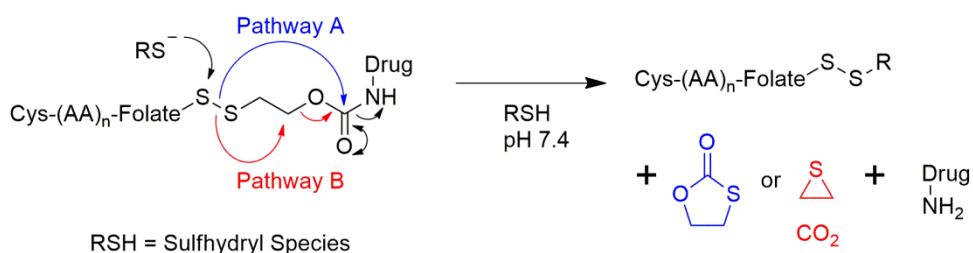
A potentially bio-labile linker incorporating a carbamate group with compound **2-12** was investigated in Chapter 2. One hypothesis for the reduction in activity for **2-12** is a lack of cleavage of the carbamate group. It was therefore necessary to consider alternative functional groups which can facilitate cleavage of a carbamate, to release the free drug, under conditions present in the cytoplasm of a bacterial cell. As studies into (acyloxy)alkyl carbamate based linkers of Trojan horse conjugates have

demonstrated premature cleavage, attributed to esterase action (Chapter 2),^{115-117, 120} other functional groups that can induce intramolecular cleavage of carbamates were considered.

Bio-labile linkers: Disulfides

Stability of disulfides under physiologically relevant conditions

It was recently highlighted that a disulfide-containing linker can lead to intramolecular cleavage of a carbamate group, to release a drug or probe within a range of cell types.¹⁷⁴ Indeed, two mechanisms for drug release from such linkers have been proposed (**Scheme 30**).¹⁷⁵ Pathway A (blue - **Scheme 30**) occurs through cleavage of the disulfide linker by a thiolate anion. The resulting linker-derived thiolate group in turn undergoes intramolecular attack at the carbamate carbonyl, releasing the free drug and cyclopentyl thiocarbonate.¹⁷⁵ Conversely, Pathway B (red - **Scheme 30**) occurs where the free thiolate can attack the carbon adjacent to the carbamate in an S_N2 reaction, leading to intramolecular decomposition, releasing carbon dioxide, thioepoxide and the free drug.¹⁷⁵



Scheme 30 - Proposed mechanism of drug release from a disulfide containing conjugate *via* two potential pathways as a result of attack from a thiolate species (A - blue / B - red).¹⁷⁵

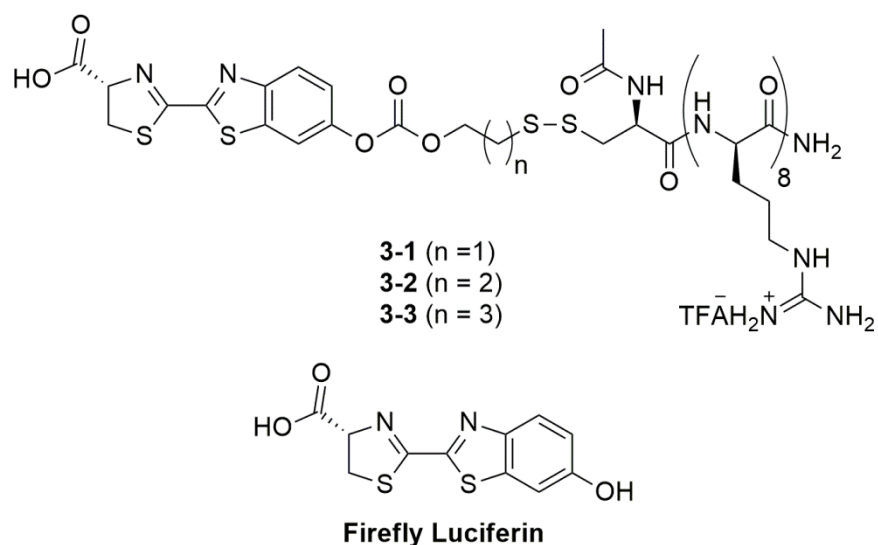
These mechanisms rely on the basis that most cell types contain free thiols which can reduce disulfide bonds, especially given that thioredoxin, an enzyme catalyst for thiol-disulfide exchange reactions, is ubiquitous in all organisms.¹⁷⁵⁻¹⁸² The ability of a thiol to attack the disulfide linker depends on its ability to deprotonate at physiological pH to give the reactive species, the thiolate anion.^{181, 183} This is clearly dependent on the pK_a of the thiol group. For example, if the pK_a was 6.4, there would be 90% of the thiolate anion present at a physiological pH of 7.4. Conversely, with a pK_a of 8.4 there would be only 10% thiolate.¹⁸³ Given that the pK_a values of the thiol groups of the common disulfide reducing agents dithiothreitol, glutathione and dithioerythritol are 9.20, 9.42 and 9.50, respectively, the presence of their respective thiolate anions at pH 7.4 are low.¹⁸⁴⁻¹⁸⁶ Despite this, thiolate anions are the reactive species required to reduce disulfide bonds, even if they are only present as a small fraction.¹⁸⁴

The fact that thioredoxin is present within bacterial species would indicate that use of a disulfide linker can be exploited for siderophore-fluoroquinolone Trojan horse conjugates. Furthermore, it should also be noted that in a number of Gram-negative bacteria species, the cytoplasm is kept under reducing conditions, due to the presence of free thiols such as glutathione and thioredoxin, whilst the periplasm is maintained under oxidising conditions by the disulfide-forming enzyme DsbA.^{181, 187} As such, cleavage of a disulfide bond would occur selectively in the cytoplasm. Additionally, it should also be highlighted that the redox environment in human blood is oxidative, ensuring that future developed disulfide containing drugs would be stable in transport to their intended targets.¹⁷⁴

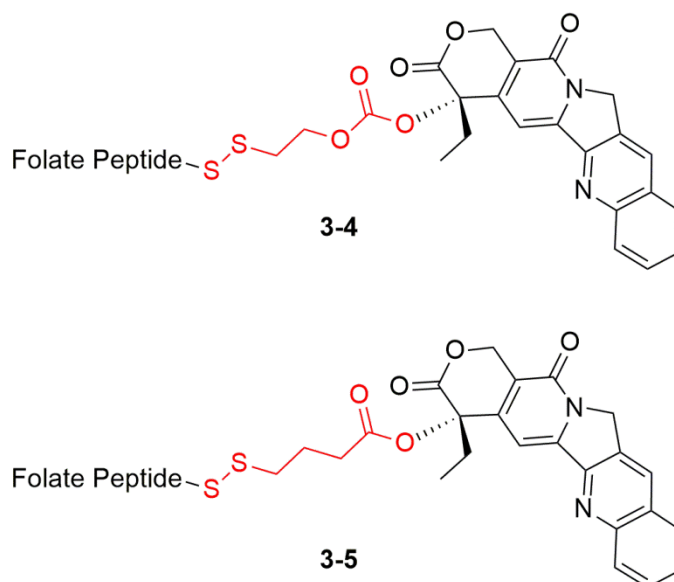
By considering the mechanisms of drug release (**Scheme 30**) it is possible to take advantage of the reducing conditions of the bacterial cell cytoplasm to target bio-labile linkers containing a disulfide bond in siderophore-fluoroquinolone Trojan horse conjugates.

Disulfides used in prodrugs and fluorescent probes

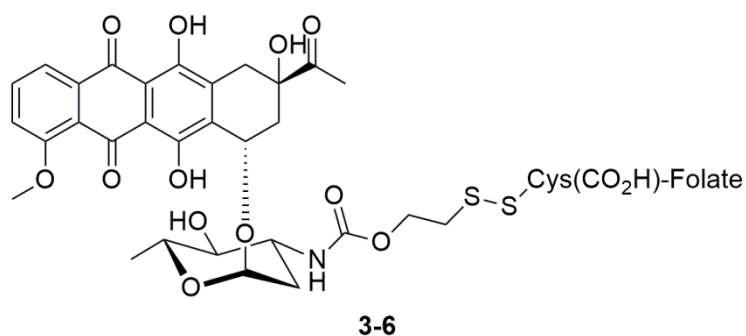
To exploit the ability of cells to reduce disulfide bonds, a number of studies have demonstrated the use of a disulfide at the β -position relative to a carbamate or carbonate.¹⁷⁵⁻¹⁸⁰ In turn, these studies planned for the disulfide to cleave the carbamate or carbonate groups, releasing either a drug or a probe, through the mechanisms outlined in **Scheme 30**.¹⁷⁵⁻¹⁸⁰ Wender *et al.* first introduced such a disulfide-based linker in 2006, designing a luciferin-transporter conjugate **3-1**, for the monitoring of uptake and release of luciferin within prostate cancer cells.¹⁷⁶ Luciferin is a general term used for light-emitting compounds,¹⁸⁸ which can be used as luminescent probes for studying cellular uptake.¹⁷⁶ Interestingly, Wender *et al.* also designed conjugates **3-2** and **3-3**, demonstrating increased stability of the conjugate as the neighbouring alkyl linker length increased.¹⁷⁶ On incubation of the conjugates in HEPES buffered saline (pH 7.4) at 37 °C they found the conjugates had half-lives of 3 hours, 11 hours and 33 hours for **3-1** to **3-2** to **3-3** respectively.¹⁷⁶ However, on addition of 10 mM dithiothreitol all three conjugates were cleaved within minutes, releasing luciferin, demonstrating that the bio-labile linker cleaves and releases the probe as planned.¹⁷⁶



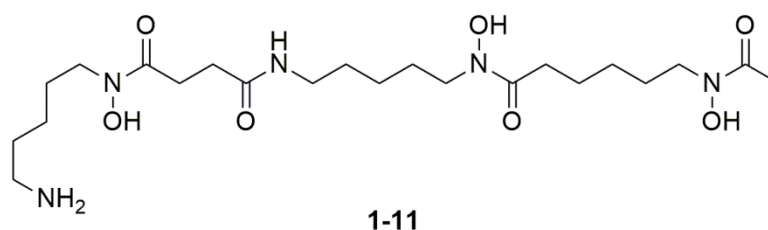
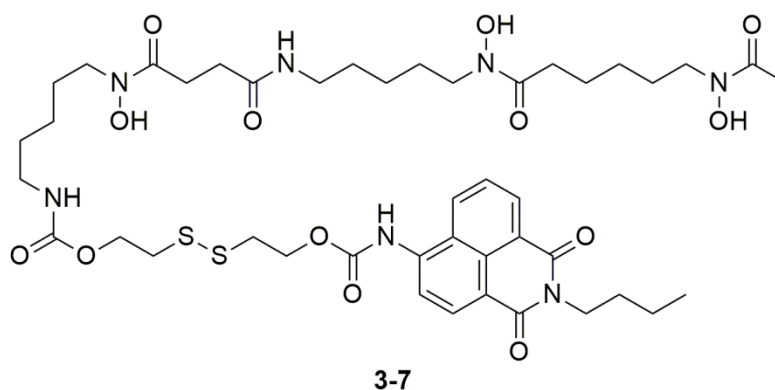
Later, Low *et al.* introduced prodrugs of camptothecin, conjugated through a disulfide to a folate peptide, using both a carbonate and a comparative ester linkage (**3-4** and **3-5**).¹⁷⁷ Interestingly, Low *et al.* found that drug release for the ester linker (**3-5**) was much lower than that of the carbonate (**3-4**),¹⁷⁷ indicating the necessity of a carbonate for drug release.



The use of carbamates with neighbouring disulfide linkages was later developed by Satyam, who developed folate-drug conjugates.¹⁷⁵ The conjugates, using anti-cancer drugs such as daunomycin (conjugate **3-6**) and paclitaxel, were linked through a carbamate with a disulfide linker at the β -position.¹⁷⁵ In turn, Satyam also demonstrated that these conjugates released the free drugs in the presence of sulfhydryl species such as dithiothreitol, dithioerythritol and glutathione at pH 7.4, proposing the mechanism discussed in **Scheme 30**.¹⁷⁵ Subsequent studies by Satyam *et al.* applied the use of the same linker in a range of other prodrugs.^{178, 179}



Significantly, Kim *et al.* recently demonstrated a fluorescent probe which gained cytoplasmic entry into bacterial cells through the use of the siderophore desferrioxamine B **1-11**, before cleavage of a disulfide bond to release the probe.¹⁸⁰ The conjugate, compound **3-7**, has a disulfide linkage at the β -position to two carbamates, one attached to a fluorescent probe, and another to the siderophore.¹⁸⁰ This study was reported whilst the work conducted and presented herein was already underway.



The linker of Kim *et al.* was designed to be reactive on entry into the cytoplasm, given the reducing capability of the cytoplasm, whereby cleavage of the disulfide bond releases the free amine of the fluorophore, which in turn altered the photochemical property of the probe (**Figure 30**). To assess **3-7**, *Pseudomonas putida* ATCC and *E. coli* BW25113 were selected as the bacterial strains, as neither produce desferrioxamine B, yet both are able to use it as a xenosiderophore.¹⁸⁰ Kim *et al.* were thus able to follow the conjugate into the cell, monitoring a range of fluorescent states that allowed the determination of the siderophore-fluorophore conjugate uptake and fluorophore release (**Figure 30**).¹⁸⁰ However, it was found that while conjugate **3-7** was able to access the cytoplasm of *P. putida*, it was not able to enter into *E. coli*, though it should be noted that this strain of *E. coli* lacks a high affinity outer membrane receptor for desferrioxamine B.¹⁸⁰ In turn, it could be hypothesised that a specific choice of siderophore would allow for improved uptake into various bacterial strains.

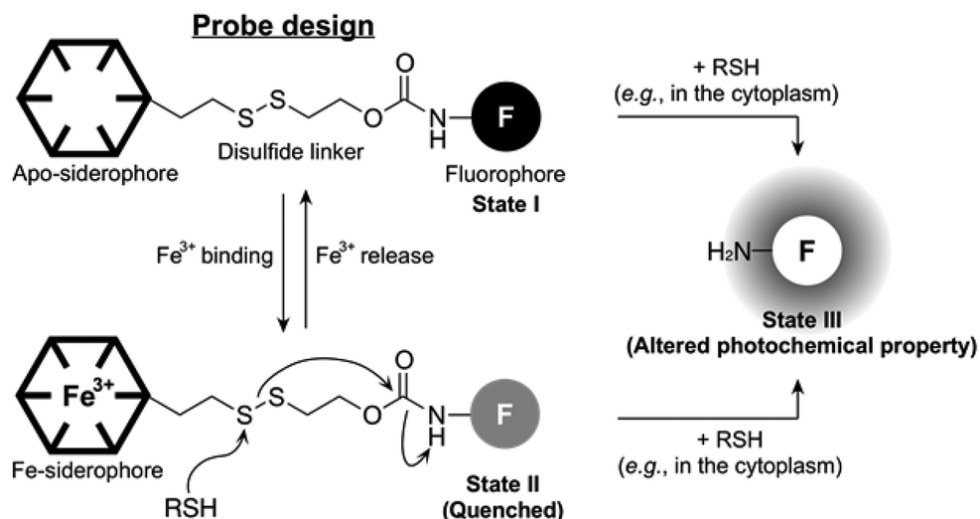


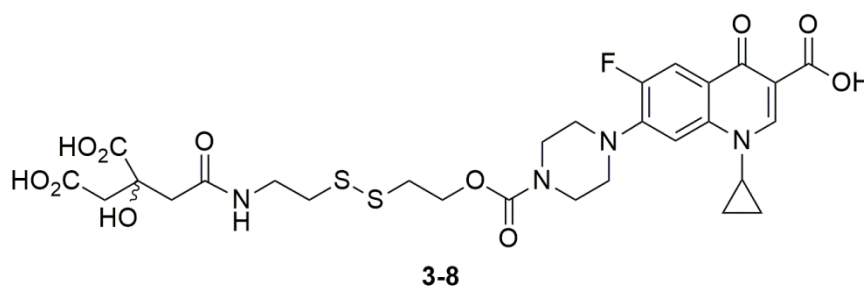
Figure 30 - Schematic overview for monitoring a fluorescent probe released from **3-7**.¹⁸⁰ Taken from H. S. Kim, W. Y. Song and H. K. Kim, *Org. Biomol. Chem.*, 2015, **37**, 73-76, with permission from The Royal Society of Chemistry.

Given the demonstration of siderophore uptake and subsequent cytoplasmic cleavage of a disulfide linkage by Kim *et al.*,¹⁸⁰ a rationale of the approach outlined within this Chapter for choosing a disulfide-linked carbamate linker for siderophore-fluoroquinolone Trojan horse conjugates was provided.

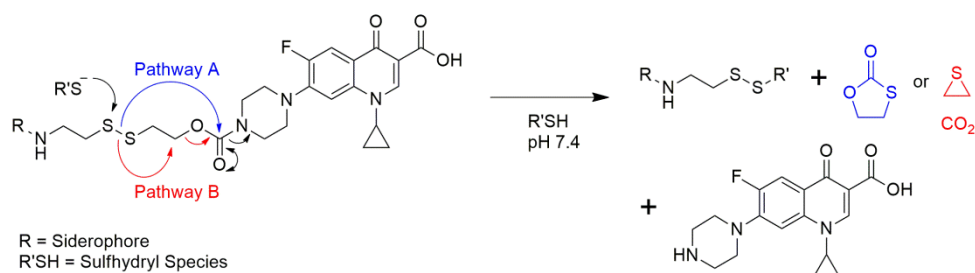
Conjugate Design

To further develop the carbamate-linked conjugate **2-12** (Chapter 2), it was decided to incorporate a disulfide linkage at the β -position to the carbamate. This approach, which was inspired by the previous investigations described above, was also chosen by Kim *et al.* whose work was reported in parallel to the study presented herein.¹⁷⁵⁻¹⁸⁰ The conjugate presented in this Chapter, compound **3-8**, was based on **2-12**, with a focus on decreasing the stability of the carbamate linker within the cytoplasm of bacterial cells, through the use of a neighbouring disulfide. Conjugate **3-8**

allowed a direct comparison with conjugate **2-12** (Chapter 2), with the disulfide linkage expected to allow for selective cleavage within the cytoplasm. In addition, based upon the observed isomerisation of the citrate moiety on treatment with hydroxide, discussed in Chapter 2, a single regioisomer of the citrate moiety was incorporated in the design of compound **3-8**.



In targeting compound **3-8**, it was planned to exploit the reducing conditions in the cytoplasm to allow for release of ciprofloxacin,¹⁸⁰ via the mechanism proposed by Satyam (**Scheme 31**).¹⁷⁵



Scheme 31 - Proposed mechanism of ciprofloxacin **1-5** release from compound **3-8** via two potential pathways as a result of attack from a thiolate species (A - blue / B - red).

Designing the synthesis of compound 3-8

In order to plan the synthetic route to compound **3-8**, its disconnection was considered to give the key components (**Figure 31**). Given the similarities between compound **3-8** and compound **2-12**, the two compounds have the same four key components: citric acid **1-12**, a linker unit consisting of a free alcohol and amine, carbon dioxide and ciprofloxacin **1-5**.

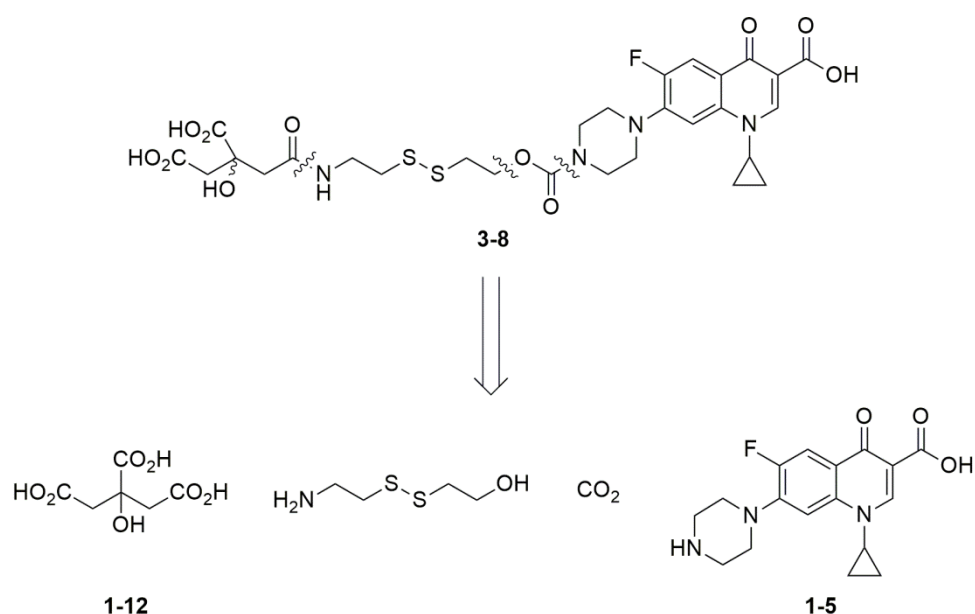


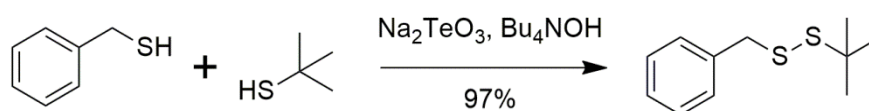
Figure 31 - The key structural components of conjugate **3-8**.

The individual components of compound **3-8** indicate that as for compound **2-12** previously, the carbonyl functionality of the carbamate can be introduced *via* activation of an alcohol. However, it was the introduction of the disulfide linker which required further consideration.

Synthesis of unsymmetrical disulfides

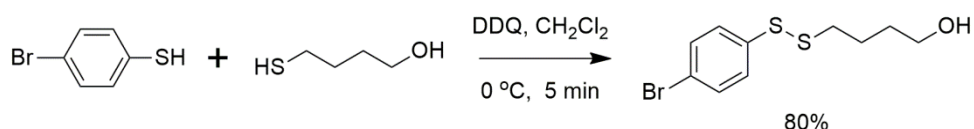
A number of synthetic routes are available to form disulfide bonds, such as oxidation of thiols and exchange reactions.^{189, 190} However, whilst many examples exist for the synthesis of symmetrical disulfides, most are not suitable for the synthesis of unsymmetrical disulfides due to the possibility of side reactions. Side reactions can include thiol-disulfide exchange resulting in symmetrical disulfides, or competitive formation of symmetrical disulfides, each reducing the yield of the desired unsymmetrical product.¹⁹⁰

One of the most common methods for the synthesis of disulfides involves oxidation of thiols, typically using oxidizing agents such as iodine, hydrogen peroxide and dichlorodicyanoquinone.^{189, 190} Unsymmetrical disulfides can be prepared through the oxidation route, though mixtures of three disulfides are often formed.^{189, 190} Nevertheless, examples have been reported with high yields of unsymmetrical disulfide products obtained through oxidation reactions.^{191, 192} For example, Suzuki *et al.* mixed two thiols in a 9:10 ratio with sodium tellurite to produce unsymmetrical disulfides in high yields (**Scheme 32**).¹⁹¹ However the authors proposed that the coupling of the two different thiols proceeds through the initial conversion of the more reactive thiol to form a symmetrical disulfide, followed by gradual thiol-disulfide exchange with the less reactive thiol.¹⁹¹



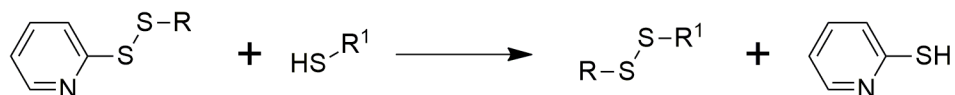
Scheme 32 - Synthesis of disulfides using sodium tellurite, reported by Suzuki *et al.*¹⁹¹

Another such example was more recently reported by Wang *et al.*, who employed dichlorodicyanoquinone (DDQ) to selectively form unsymmetrical disulfides from equimolar ratios of two different thiols (**Scheme 33**).¹⁹² It was found the reaction proceeds quickly as a ‘one pot’ method, using a range of different thiols, in high yields.¹⁹² However, Wang *et al.* found that whilst secondary thiols could also successfully form the required products, tertiary thiols could not, reasoning this was due to steric hindrance.¹⁹² In addition it was also found that the reactions were not successful when free amino groups were present on one thiol moiety.¹⁹² Given that one component required towards the synthesis of compound **3-8** incorporates a free amine (**Figure 31**), such a limitation of the methodology of Wang *et al.* would prove problematic.



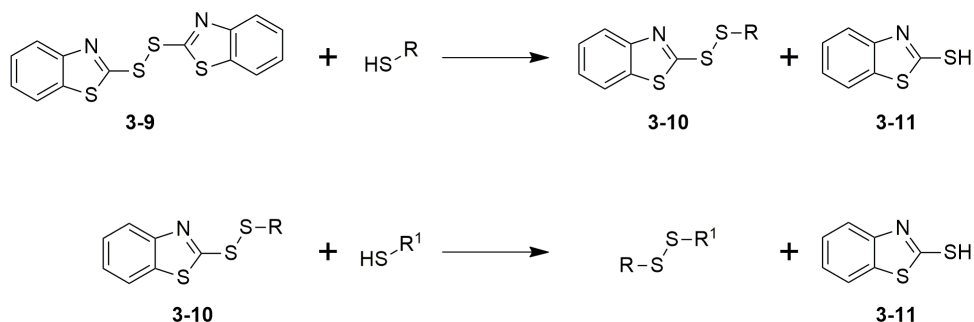
Scheme 33 - Synthesis of disulfides using dichlorodicyanoquinone, reported by Wang *et al.*¹⁹²

The use of thiol-disulfide exchange reactions can lead to a mixture of disulfide products, though this can be controlled by using an excess of the symmetrical disulfide.^{189, 190} However, this method of unsymmetrical disulfide preparation typically requires purification of the required product from the mixture, usually by column chromatography. Furthermore, whilst the exchange method is generally less efficient, it does allow for a potentially greater scope of use, as a wide range of functional groups are tolerated under the mild conditions used.¹⁹⁰ Perhaps the most widely applied thiol-disulfide exchange reactions involve exchanges with a 2-pyridyl disulfanyl species, prepared from reaction of a thiol with 2,2'-dipyridyl disulfide (**Scheme 34**).^{193, 194}



Scheme 34 - General scheme for the synthesis of unsymmetrical disulfides by thiol-disulfide exchange with a 2-pyridyl disulfanyl species.^{193, 194}

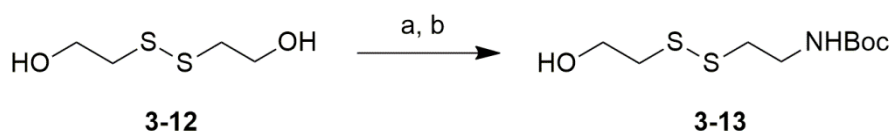
Brzezinska and Ternay developed an efficient method to produce unsymmetrical disulfides, containing a benzothiazole fragment, on mixing 2,2'-dithiobis(benzothiazole) (**3-9**) with a number of thiols (**Scheme 35**).¹⁹⁵ The by-product, 2-mercaptobenzothiazole (**3-11**), could be removed *via* aqueous extraction, allowing the isolation of product **3-10** in high yield, without the requirement for column chromatography.¹⁹⁵ In addition, it was then possible to mix the product **3-10** with other thiols, producing an unsymmetrical disulfide in high yield and another 2-mercaptobenzothiazole (**3-11**).¹⁹⁵



Scheme 35 - Synthesis of disulfides using 2,2'-dithiobis(benzothiazole) as reported by Brzezinska and Ternay.¹⁹⁵

However, whilst both viable approaches, the use of either a 2-pyridyl disulfanyl species or 2,2'-dithiobis(benzothiazole) each require the initial formation of an unsymmetrical disulfide bond, before subsequent exchange. Fortunately, the intermediate component required for the synthesis of compound **3-8** (**Figure 31**), has been reported in the literature (**Scheme 36**).¹⁷⁸ An advantage of this approach is that while non-selective

exchange can occur, producing a mixture of disulfides, the use of the *tert*-butyloxycarbonyl protecting group allows simple purification by column chromatography. A combination of easy purification, inexpensive starting materials, and avoiding precursor disulfide formation from 2-mercaptoethanol, makes this approach highly attractive to apply towards the synthesis of **3-8**. The use of the symmetrical 2-hydroxyethyl disulfide **3-12** demonstrates the versatility of thiol-disulfide exchange reactions, as it does not require the use of a sacrificial component like those when using a 2-pyridyl disulfanyl species or 2,2'-dithiobis(benzothiazole).

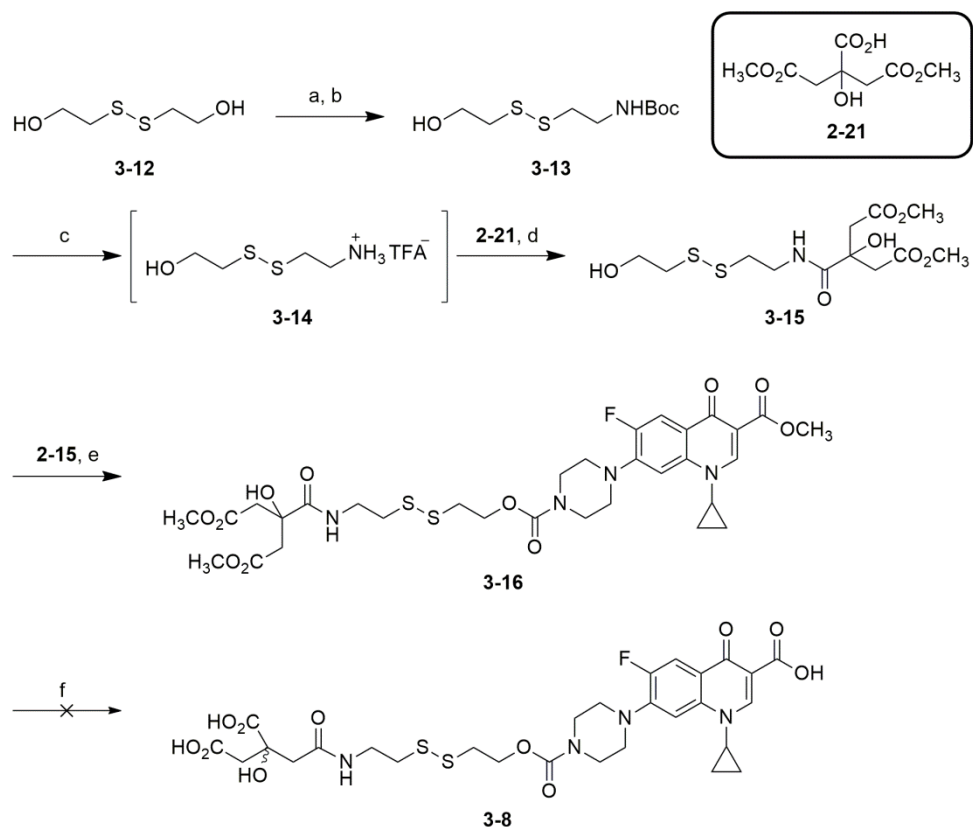


Scheme 36 - Synthesis of compound **3-13** by thiol-disulfide exchange.¹⁷⁸
 (a) Cysteamine.HCl, MeOH, Et₃N; (b) Boc₂O, MeOH.

3.3 Synthesis

Taking inspiration from the synthesis of compound **2-12**, and having considered the disconnection of compound **3-8** (**Figure 31**), the synthesis of compound **3-8** was attempted *via* the route planned in **Scheme 37**. Following a literature procedure, compound **3-13** was targeted through a thiol-disulfide exchange with cysteamine from 2-hydroxyethyl disulfide **3-12** (**Scheme 37**), followed by immediate Boc protection for ease of purification.¹⁷⁸ Deprotection of the Boc group to give **3-14**, also based on the literature,¹⁷⁸ followed by amide coupling with 1,5-dimethyl citrate **2-21** would provide intermediate **3-15**. Next the carbamate group would be introduced in the same manner as discussed in Chapter 2, *via* activation of a free alcohol utilising *N,N'*-disuccinimidyl carbonate, to produce compound **3-16**. Finally, it was planned that base hydrolysis of the ester

groups would isomerise the citrate moiety to give **3-8**, as established in Chapter 2 (**Scheme 37**). However, the attempts to produce compound **3-8** were not successful, as discussed in greater detail later.



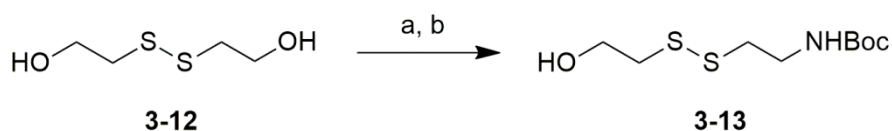
Scheme 37 - Synthetic route towards compound **3-8**. (a) Cysteamine.HCl, MeOH, Et₃N; (b) Boc₂O, MeOH, 48%; (c) TFA, CH₂Cl₂; (d) HATU, DMF, DIPEA, 46%; (e) DSC, DIPEA, DMF, 37%; (f) (i) 0.1 M NaOH, H₂O, (ii) HCl.

Synthesis of the methyl ester protected disulfide conjugate 3-16

Thiol-disulfide exchange of 2-hydroxyethyl disulfide 3-12 to produce 3-13

The first step in the synthesis was a thiol-disulfide exchange of 2-hydroxyethyl disulfide **3-12** with cysteamine hydrochloride in the presence

of triethylamine (**Scheme 38**), in line with a literature procedure.¹⁷⁸ This was followed by the addition of di-*tert*-butyl dicarbonate, to allow easier purification and isolation of compound **3-13**.¹⁷⁸ Compound **3-13** was isolated in 48% yield, and characterised using ¹H and ¹³C NMR spectroscopy, infra-red spectroscopy and ESI mass spectrometry. Formation of **3-13** was supported by a characteristic resonance at 156.0 ppm for the carbamate group in the ¹³C NMR spectrum, as well as a singlet in the ¹H NMR spectrum at 1.44 ppm, of relative integration nine, for the *tert*-butyl group. In addition, ESI-MS analysis gave a molecular ion peak [M+Na]⁺ for **3-13** at *m/z* 276.0700, consistent with a molecular formula of C₉H₁₉NNaO₃S₂, with all the spectroscopic data collected matching the literature.¹⁷⁸

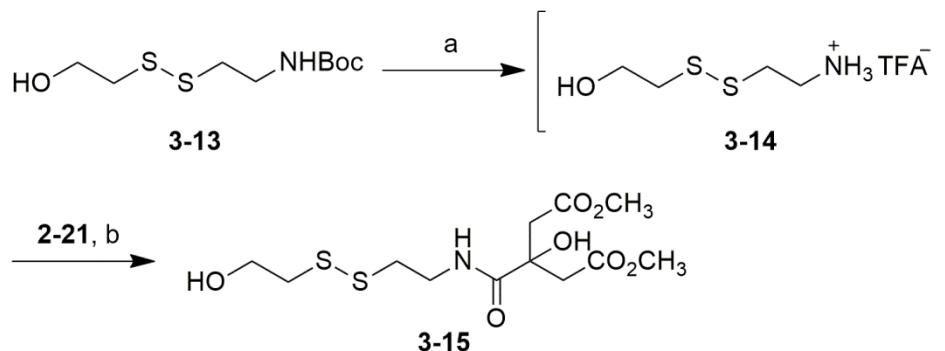


Scheme 38 - Synthesis of **3-13** by thiol-disulfide exchange.¹⁷⁸ (a) Cysteamine.HCl, MeOH, Et₃N; (b) Boc₂O, MeOH, 48%.

Boc deprotection of 3-13 and subsequent coupling with 1,5-dimethyl citrate 2-21 to produce 3-15

Having isolated compound **3-13**, it was possible to continue the synthesis towards intermediate **3-15**. First, the Boc protecting group was cleaved with trifluoroacetic acid to produce **3-14**.¹⁷⁸ Without further purification, **3-14** was coupled to 1,5-dimethyl citrate **2-21** using HATU and DIPEA in DMF to produce **3-15** in 46% yield (**Scheme 39**). Compound **3-15** was characterised using ¹H and ¹³C NMR spectroscopy, infra-red spectroscopy and ESI mass spectrometry. Formation of **3-15** was supported by ¹³C NMR spectroscopy, with a characteristic resonance at 171.7 ppm for the amide functional group present in the spectrum. Furthermore, ESI-MS

analysis gave a molecular ion peak $[M+Na]^+$ for **3-15** at m/z 378.0647, consistent with a molecular formula of $C_{12}H_{21}NNaO_7S_2$.

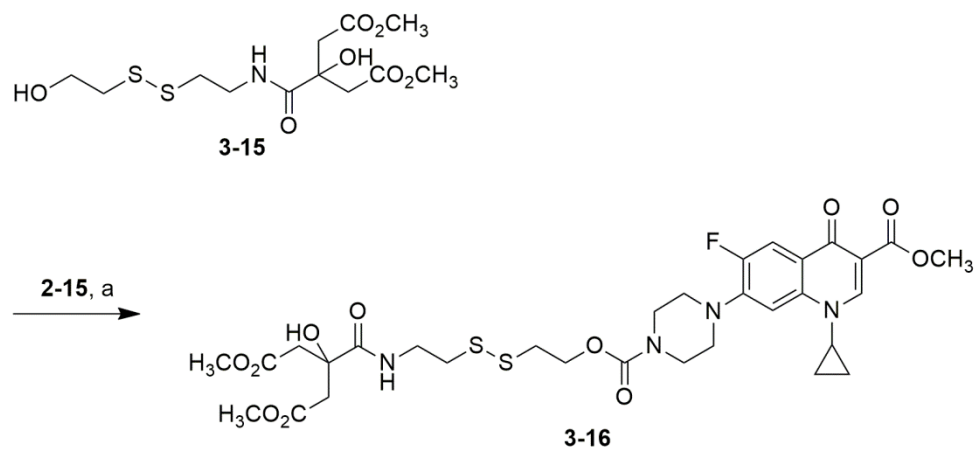


Scheme 39 - Synthesis of compound **3-15**. (a) TFA, CH_2Cl_2 ; (b) HATU, DMF, DIPEA, 46%

Formation of the carbamate functional group to produce compound 3-16

The conditions used for the formation of **2-22** (Chapter 2) were employed towards the synthesis of **3-16**, from **3-15** and ciprofloxacin methyl ester **2-15**. Compound **3-15** was treated with *N,N'*-disuccinimidyl carbonate and DIPEA in DMF, followed by the addition of ciprofloxacin methyl ester **2-15** (**Scheme 40**). Under these conditions, compound **3-16** was isolated in 37% yield. The formation of **3-16** was supported by ^{13}C NMR spectroscopy, with a characteristic resonance at 154.8 ppm for the carbamate group. Furthermore, ESI-MS analysis gave a molecular ion peak $[M+Na]^+$ for **2-22** at m/z 749.1921, consistent with a molecular formula of $C_{31}H_{39}FN_4NaO_{11}S_2$. Additionally the 1H NMR spectrum shows two triplets, representing the two methylene groups at 2.80 and 2.96 ppm in α -position to the disulfide linkage. The triplet at 2.96 ppm is part of a multiplet which also contains one of the roofed doublets (2.78 and 2.93 ppm), corresponding to the diastereotopic protons of the citrate moiety (**Figure 32**). The observation of the roofed doublets demonstrates the

retention of symmetry in the citrate moiety, supporting the assignment of **3-16**.



Scheme 40 - Carbamate formation using *N,N'*-disuccinimidyl carbonate to produce compound **3-16**. (a) DSC, DIPEA, DMF, 37%.

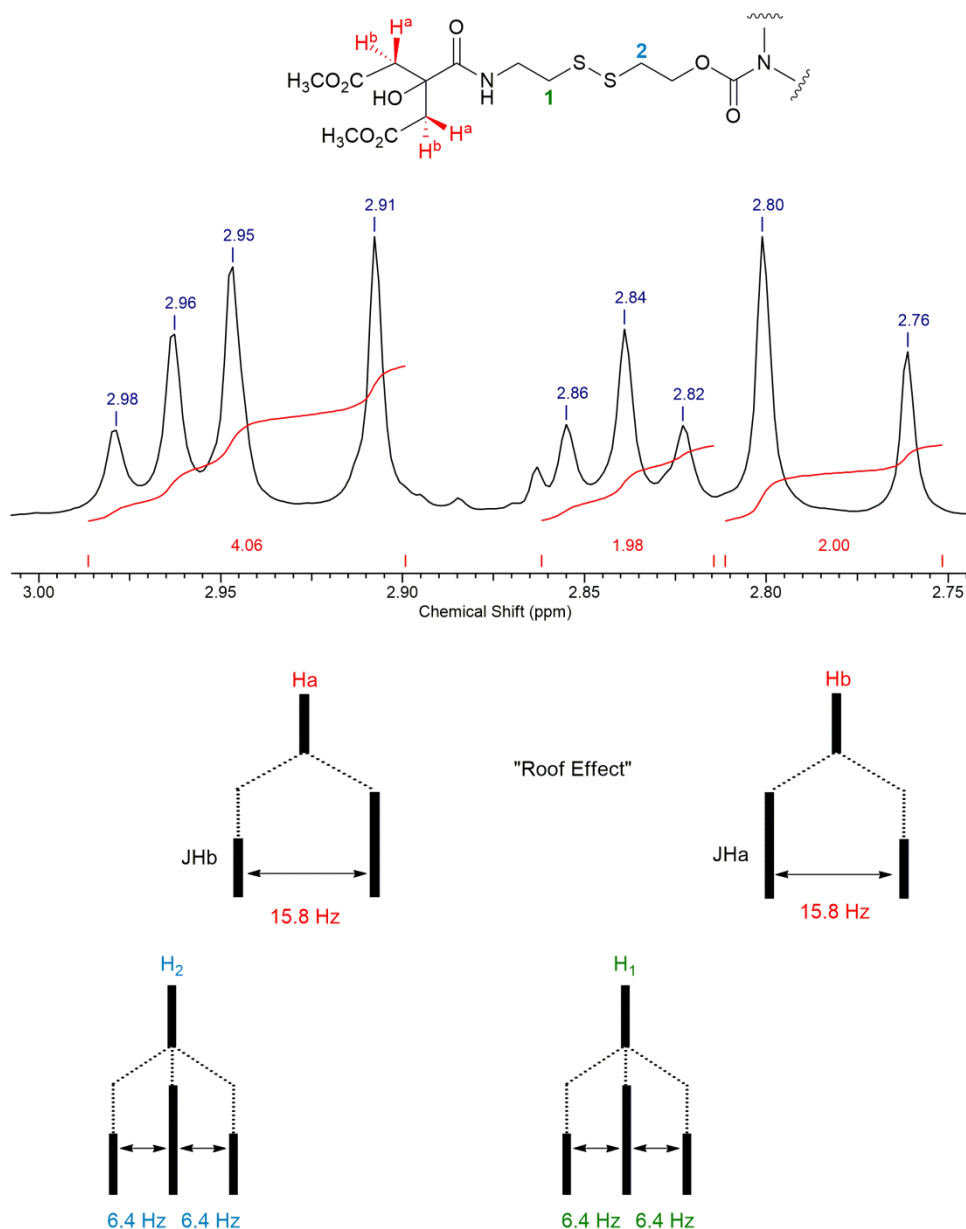
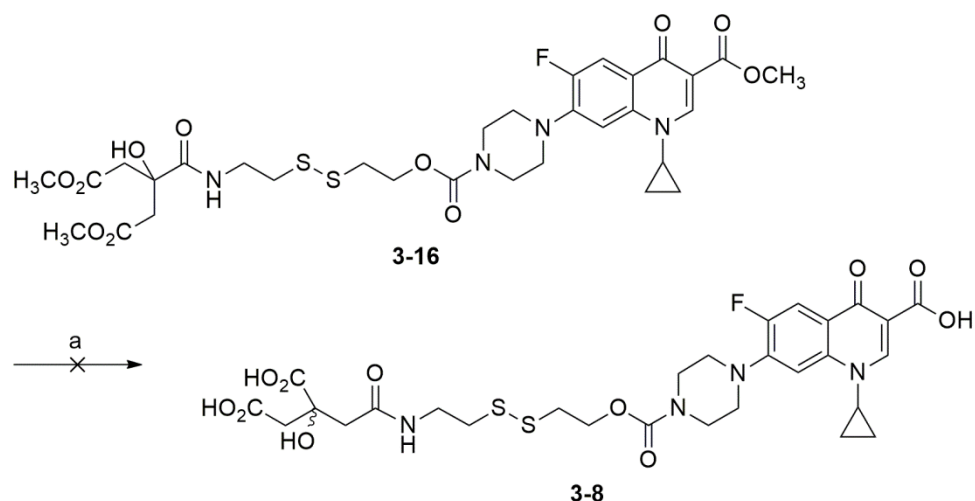


Figure 32 - ^1H NMR spectrum of **3-16** in CDCl_3 . The J-coupling splitting pattern is shown below. The assignment for H-2 overlaps partially with the doublet for the diastereotopic protons of the citrate moiety. *The assignment of H^a and H^b can be interchanged.

Attempted base-catalysed hydrolysis of the protected disulfide-linked conjugate **3-16** to target **3-8**

Having isolated compound **3-16**, the next step was to remove the methyl ester protecting groups (**Scheme 41**). It was expected that the citrate moiety would isomerise in a manner analogous to that discussed in Chapter 2. However, target compound **3-8** was never isolated under the reaction conditions investigated.



Scheme 41 - Attempted base hydrolysis of **3-16** to target **3-8**. (a) (i) 0.1 M NaOH, H₂O, (ii) HCl.

*Investigation of the base-catalysed hydrolysis reaction of **3-16** by ¹H NMR spectroscopy*

It was first decided to examine the hydrolysis reaction of **3-16** by ¹H NMR spectroscopy (400 MHz spectrometer). Compound **3-16** was dissolved in CD₃OD, followed by the addition of 0.01% NaOD (40% in D₂O). The reaction was monitored over time, observing a decrease in signal intensity of the resonances attributed to the starting compound **3-16**, and an increase

in intensity for free ciprofloxacin **1-5** (**Figure 33**), with three other ciprofloxacin containing species also observed (**1**, **2** and **3**), none of which were attributed to ciprofloxacin methyl ester **2-15**. As **Figure 33** shows, the hydrolysis of **3-16** proceeded slowly, with the presence of **3-16** still observed after 92 hours. Furthermore, free ciprofloxacin **1-5** appeared within the first hour of the reaction (**Figure 33**), accounting for 6% of the reaction mixture.

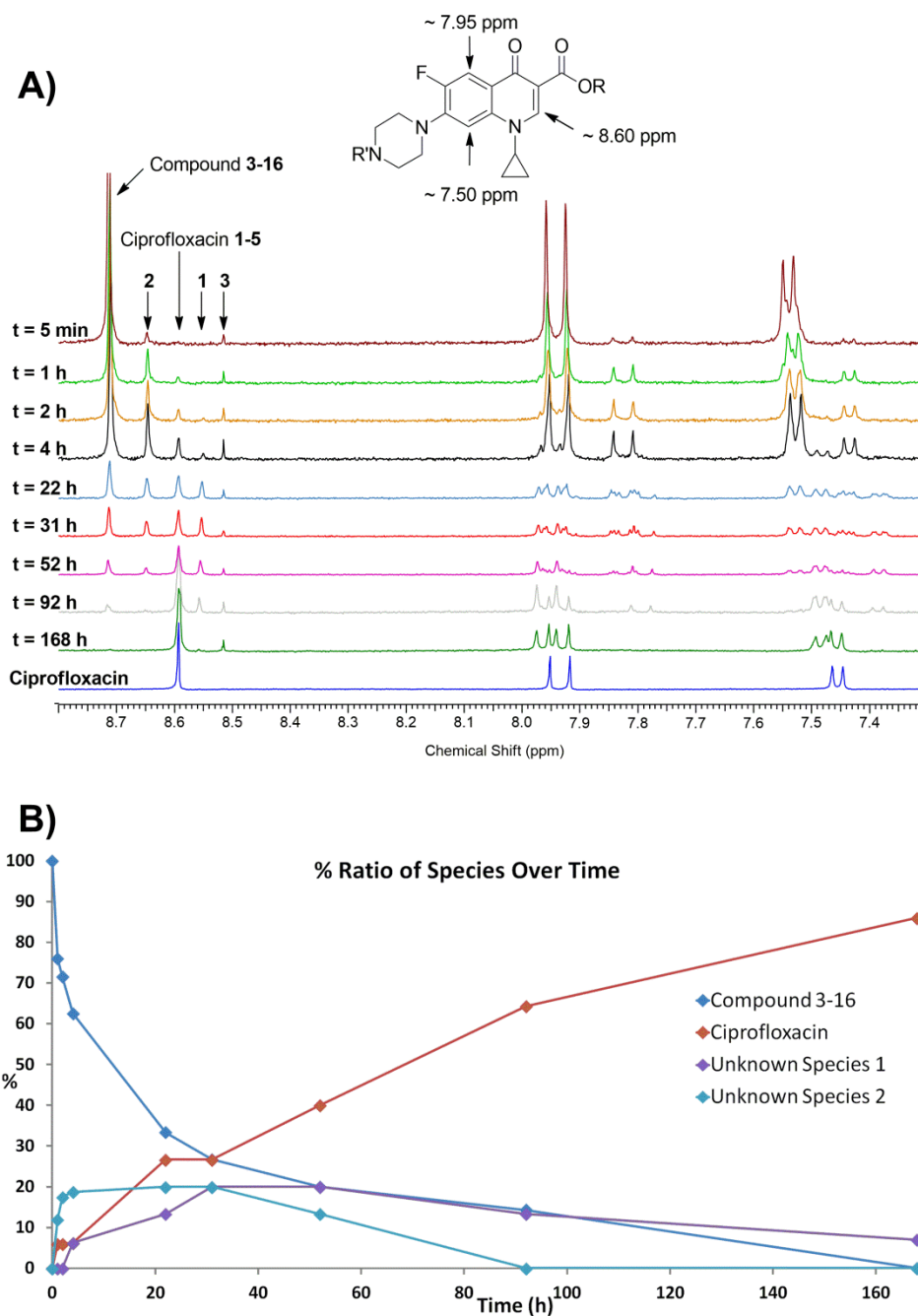


Figure 33 - A) ^1H NMR spectrum of the aromatic region of compound **3-16** in $\text{CD}_3\text{OD} + 0.01\%$ NaOD (40% in D_2O). The two extra resonances at 8.54 (**3**) and 8.67 (**2**) ppm at $t = 5$ min are attributed to an indeterminate fast reaction that occurred in the time (~ 5 minutes) between the addition of NaOD and collecting the ^1H NMR spectrum, as they were not present in the spectrum prior to the addition of NaOD. **B)** Plot of the % ratio of species present in solution based on the relative integration of the resonances highlighted in the ^1H NMR spectrum over time. Species **3** was omitted for clarity as it remained at a ratio of 6-7% throughout.

The ratio of the ciprofloxacin-containing species was plotted as a function of time, showing a trend between the decrease in compound **3-16** and an increase in released free ciprofloxacin (**B - Figure 33**). Two ciprofloxacin-containing species, **1** and **2**, were observed to gradually increase in % ratio over the first 31 hours, before decreasing as the reaction progressed (**B - Figure 33**). This suggests that both **1** and **2** eventually decomposed to give free ciprofloxacin **1-5**. In addition, species **3** was observed after the first hour at a ratio of 6%, which did not change over the course of the reaction. Whilst it was not possible to identify species **1**, **2** and **3** from the NMR data, it is conceivable that they were formed by the loss of the methyl ester groups from **3-16**, with one of the species expected to be the required product **3-8**. However, the observation of the concurrent release of free ciprofloxacin **1-5** during the reaction indicated that the disulfide linker cleaved on treatment with sodium hydroxide.

With the ^1H NMR study indicating that hydrolysis of **3-16** proceeded slowly in methanol, reasoned in part to be due to the partial solubility of **3-16** in the solvent, leading to dilute solutions in order to fully dissolve the compound. It was therefore necessary to find conditions that would improve the rate of reaction. Additionally, with the release of free ciprofloxacin **1-5** observed over time, it was also hoped that by increasing the rate of the deprotection reaction it would be possible to isolate the required target compound **3-8** prior to decomposition of the disulfide linkage. The caveat of this would be the risk that the rate of the release of ciprofloxacin could also be increased.

Treating 3-16 with sodium hydroxide in 1,4-dioxane and water

It was found through both TLC analysis and solubility screening that a mixture of 45 weight % 1,4-dioxane in water greatly improved both the solubility of **3-16** and the rate of reaction, with a complete reaction observed by TLC analysis within an hour, determined by the absence of **3-16**. Therefore, compound **3-16** was mixed with 3.6 equivalents of sodium hydroxide in 45 % 1,4-dioxane and water (w/w). TLC analysis showed that the reaction was complete after 15 minutes, as no starting compound **3-16** remained. When the pH was reduced to 2.15, a precipitate formed, which was filtered and washed with both water and chloroform (**Figure 34**). The precipitate, the aqueous residue, and the organic residue were analysed individually by HPLC, ESI-MS and ¹H NMR spectroscopy. These three samples equated to a total of 96% mass recovery based on the starting compound **3-16**.

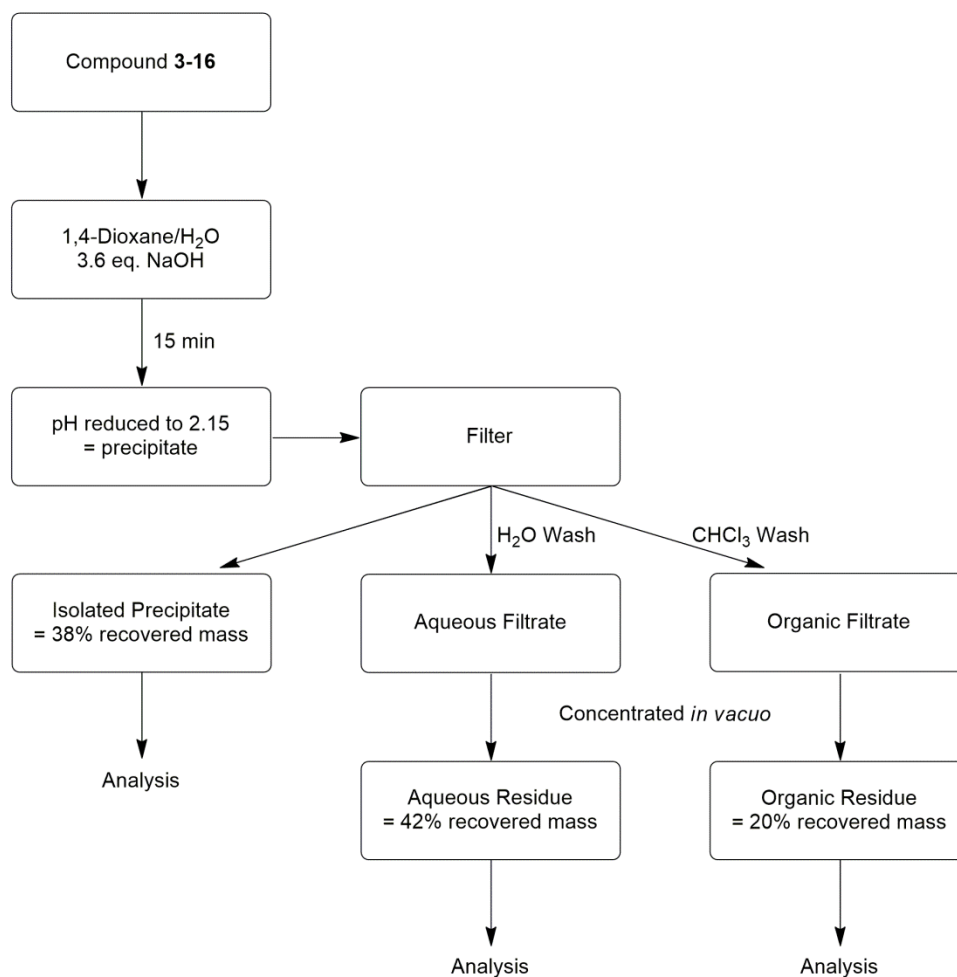


Figure 34 - Flow chart depicting the base hydrolysis reaction of **3-16**.

Analysis of the organic residue

The ^1H NMR spectrum of the organic residue was complex with at least four ciprofloxacin-containing compounds present (**Figure 35**). In addition, there were no resonances observed for the diastereotopic protons of the citrate moiety. However, the ESI mass spectrum suggested the presence of the starting compound **3-16**. Furthermore, the ESI mass spectrum of the organic filtrate indicated that another ciprofloxacin-related species was present, the homodisulfide compound **3-17**, with a peak observed at m/z 919.2574, corresponding to the sodiated molecular ion $[\text{M}+\text{Na}]^+$. This indicated that disulfide scrambling had occurred, suggesting cleavage of the disulfide bond.

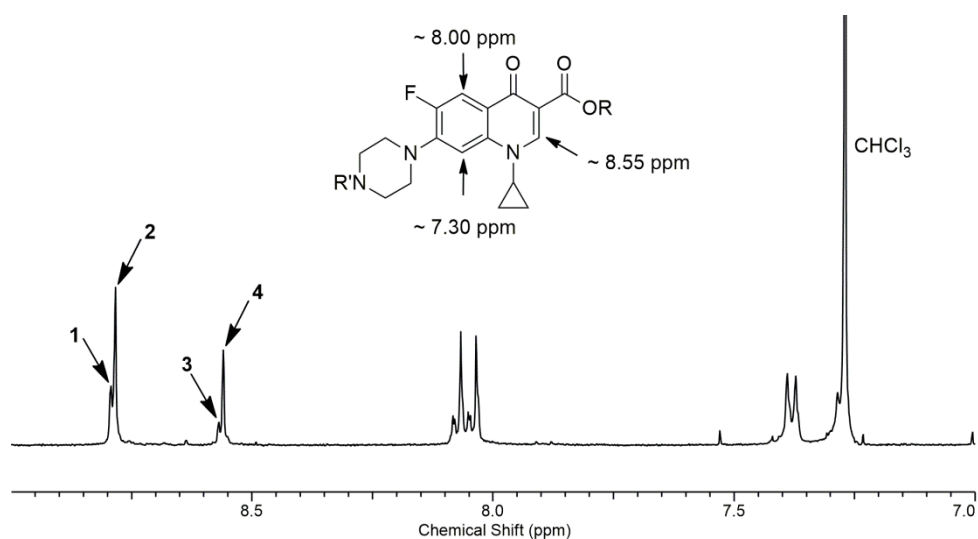
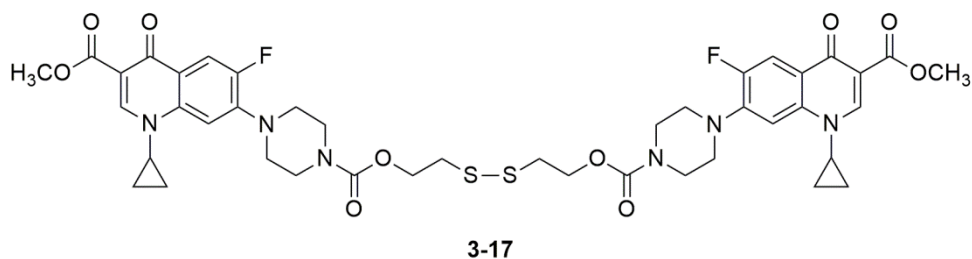


Figure 35 - ^1H NMR spectrum of the aromatic region of the organic residue in CDCl_3 . Four ciprofloxacin species are observed **1**, **2**, **3** and **4**. The four highlighted peaks correspond to an aromatic proton (pointed out as ~ 8.55 ppm) on a ciprofloxacin-containing species.



HPLC analysis was conducted on the organic residue, confirming that there were four major ciprofloxacin-containing species present in the residue (**Figure 36**). Compounds were observed to elute at 7.7, 10.4, 11.5 and 12.5 minutes. These were determined to be ciprofloxacin-containing species based on their similar UV/Vis absorption spectra, which were obtained by diode array detection, each with a λ_{max} of approximately 285 nm, comparable to free ciprofloxacin. It can also be seen that, in addition, there are several minor species present (**Figure 36**).

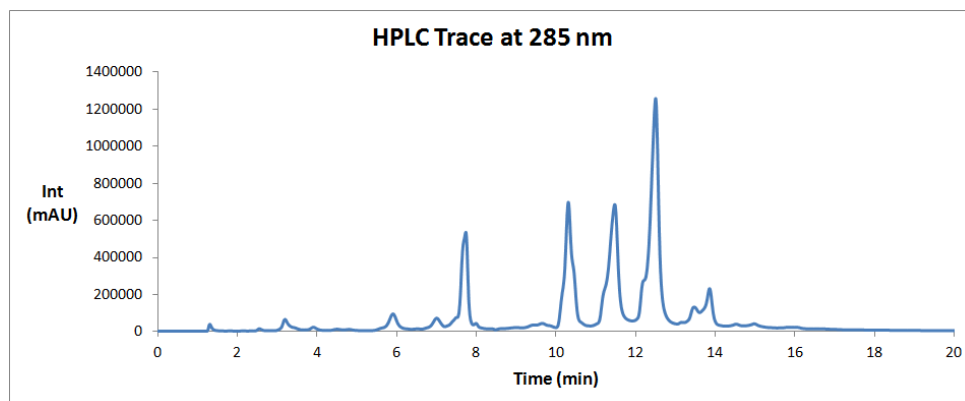
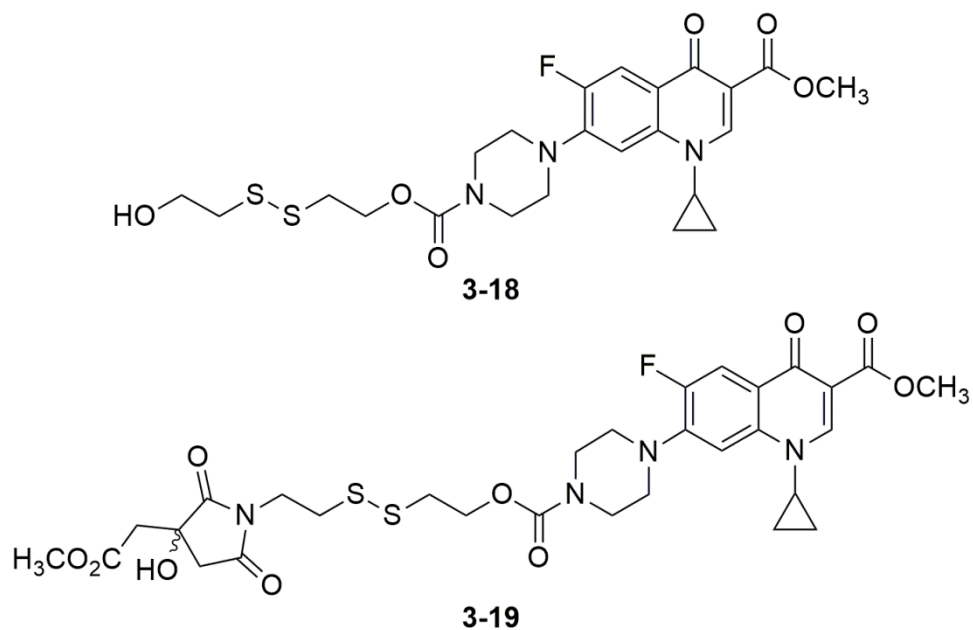


Figure 36 - HPLC trace of the organic residue at 285 nm detection. Nothing eluted after 20 minutes (total run time = 35 min). Conditions: Analytical HPLC Method A (Chapter 7).

None of the species evident in the HPLC trace, either major or minor, corresponded to ciprofloxacin methyl ester **2-15**, which elutes at 1.32 minutes under these conditions. It is also important to note that the starting compound **3-16** was not present, as it elutes at 7.2 minutes. To identify the species present in the organic residue LC-MS was performed (by Karl Heaton). From the LC-MS trace the first species to elute showed a molecular ion peak $[M+H]^+$ at m/z 526.1469, consistent with a molecular formula of $C_{23}H_{29}FN_3O_6S_2$, which is consistent with the formula of compound **3-18**. The second species to elute showed a molecular ion peak $[M+H]^+$ at m/z 695.1828, consistent with a molecular formula of $C_{30}H_{36}FN_4O_{10}S_2$, which is consistent with the molecular formula of compound **3-19**. The presence of the succinimide **3-19** indicated that cyclisation could have occurred in a manner analogous to that discussed in Chapter 2. The third compound to elute was the homodisulfide **3-17**, with a sodiated peak analogous to that stated above. The fourth compound to elute on the LC-MS had a mass of 568.1385, the structure for which could not be identified.



Finally, it should be noted that an impurity had carried through the reaction, with the corresponding species eluting at 7.7 minutes (**Figure 37**).

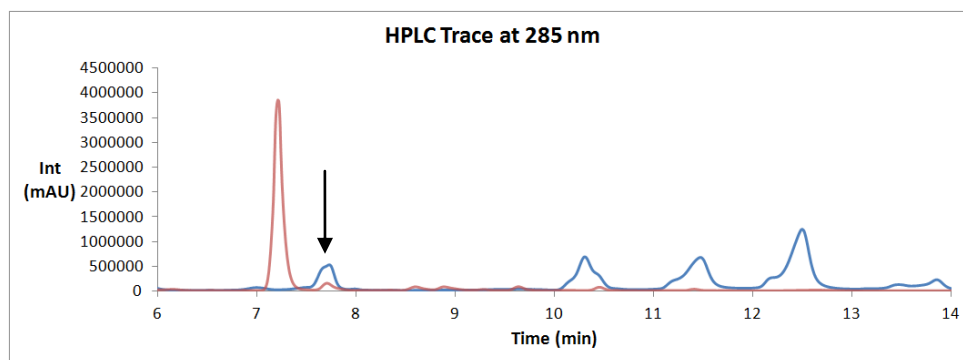


Figure 37 - Overlay of HPLC trace of the starting compound **3-16** (red) and the organic residue (blue), showing a possible impurity carried through into the organic residue at 7.7 minutes. The window is focused for clarity. Conditions: Analytical HPLC Method A (Chapter 7).

In conclusion, the analysis of the organic residue indicated that a mixture of species was present. Some of these species could have been produced through disulfide scrambling. In addition, the citrate moiety has undergone

cyclisation to form a succinimide, analogous to that previously discussed in Chapter 2. These observations confirm that the rate of deprotection is similar to those of the side reactions, therefore giving rise to a mixture of products, none of which are the cleanly deprotected target compound **3-8**. The next stage of the analysis was to investigate the compounds present in the aqueous residue to find out if **3-8** had partitioned into the aqueous phase due to its higher hydrophilicity.

Analysis of the aqueous residue

The ^1H NMR spectrum of the aqueous residue indicated that the isolated sample contained only one ciprofloxacin-containing species, free ciprofloxacin **1-5** itself, in agreement with the only observed product in the ESI mass spectrum. Interestingly, the ^1H NMR spectrum of the aqueous residue also demonstrated the presence of diastereotopic protons that indicated the presence of several citrate-related species through numerous roofed doublets (**Figure 38**). Furthermore, the relative integrations for these diastereotopic protons were above what would be expected if a citrate was still conjugated through a linker to the ciprofloxacin moiety, suggesting that decomposition products of the conjugate are present in the aqueous residue. Indeed, the HPLC trace of the aqueous residue indicated only one ciprofloxacin-containing species at 9.8 minutes (**Figure 39**), consistent with free ciprofloxacin **1-5**. On spiking the sample with ciprofloxacin **1-5**, there was no change in the observed trace. By combining these observations, it was clear that the residue isolated from the aqueous filtrate consisted of the decomposition products of compound **3-16**.

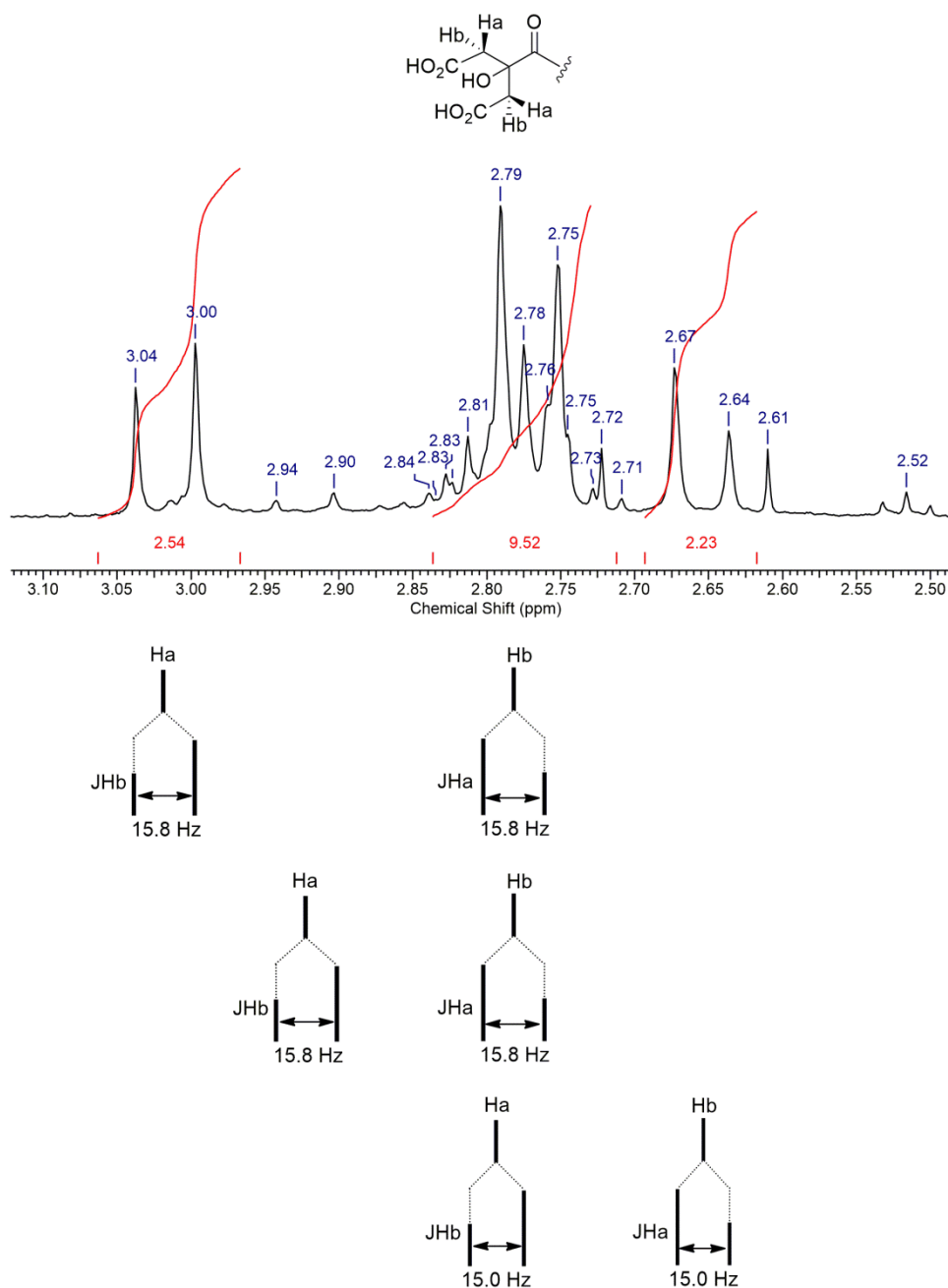


Figure 38 - ^1H NMR spectrum of the aqueous residue in D_2O , shown in the citrate region. The relative integrations are compared to a known integration of one for an aromatic ciprofloxacin proton at 8.62 ppm. Several species are present, with three examples of diastereotopic coupling highlighted below, though it can be seen that the multiplet between 2.72-2.83 ppm contains several more overlapping doublets.

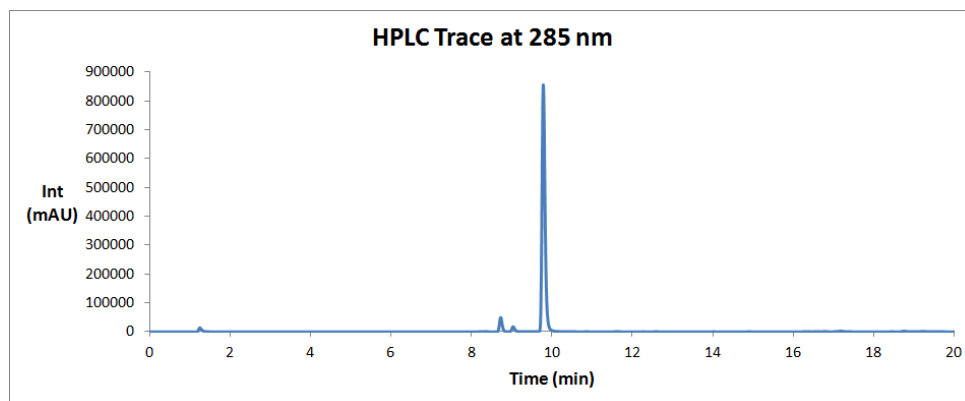


Figure 39 - HPLC trace of the aqueous residue at 285 nm detection. Nothing eluted after 20 minutes (total run time = 35 min). Conditions: Analytical HPLC Method B (Chapter 7).

Analysis of the isolated precipitate

Despite evidence indicating that both scrambling and decomposition of the disulfide linker had occurred, it was necessary to determine the composition of the isolated precipitate. The ESI mass spectrum indicated the presence of the desired product **3-8** in the precipitate, with a $[M+Na]^+$ peak at m/z 683.1512, which is consistent with a molecular formula of $C_{28}H_{32}FN_4O_{11}S_2$. However, the ESI mass spectrum also indicated the presence of free ciprofloxacin **1-5**. The 1H NMR spectrum was complex, and no resonances were observed for the diastereotopic protons of the citrate moiety. On analysis by HPLC, it was evident that there were a number of different species (**Figure 40**). Among the compounds observed in the HPLC trace of the precipitate was un-reacted starting compound **3-16** (7.2 minutes) and species also observed within the organic residue at 10.4, 11.5 and 12.5 minutes. Furthermore, on employing the same gradient used to analyse the aqueous filtrate, it was observed that one major species in the isolated precipitate was free ciprofloxacin **1-5**, with a peak at 9.8 minutes (**Figure 41**). In light of the observation that the precipitate also contained free ciprofloxacin **1-5**, it was deemed unlikely that the precipitate

contained the desired product **3-8** in sufficiently high quantities to merit isolation.

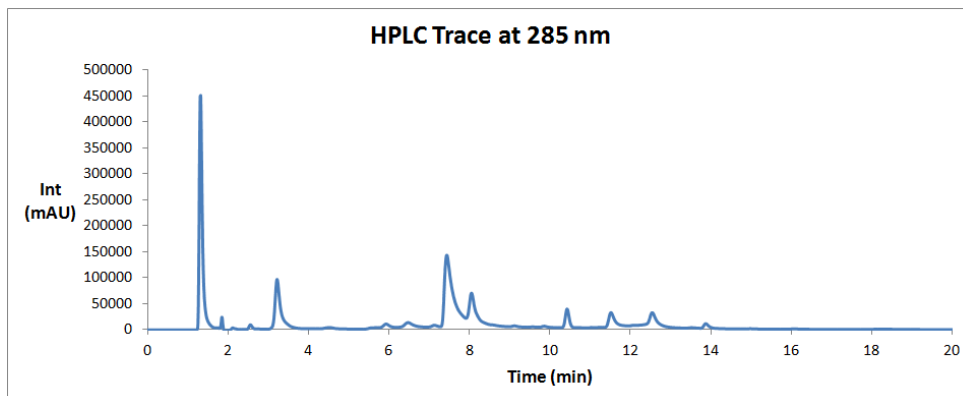


Figure 40 - HPLC Trace of the isolated precipitate at 285 nm detection. Nothing eluted after 20 minutes (total run time = 35 min). Conditions: Analytical HPLC Method A (Chapter 7).

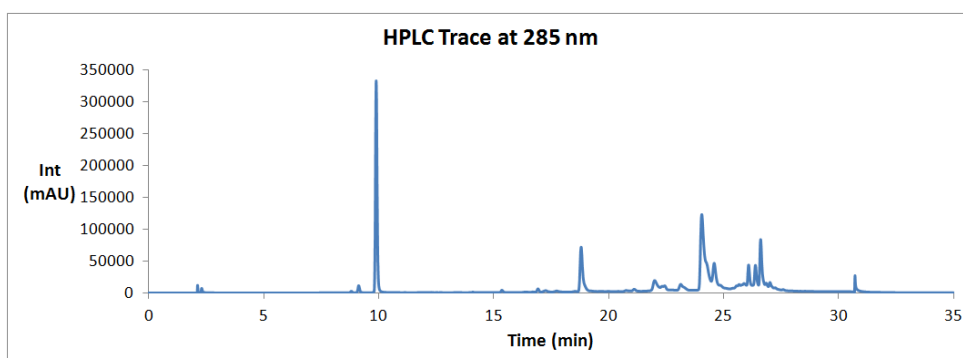


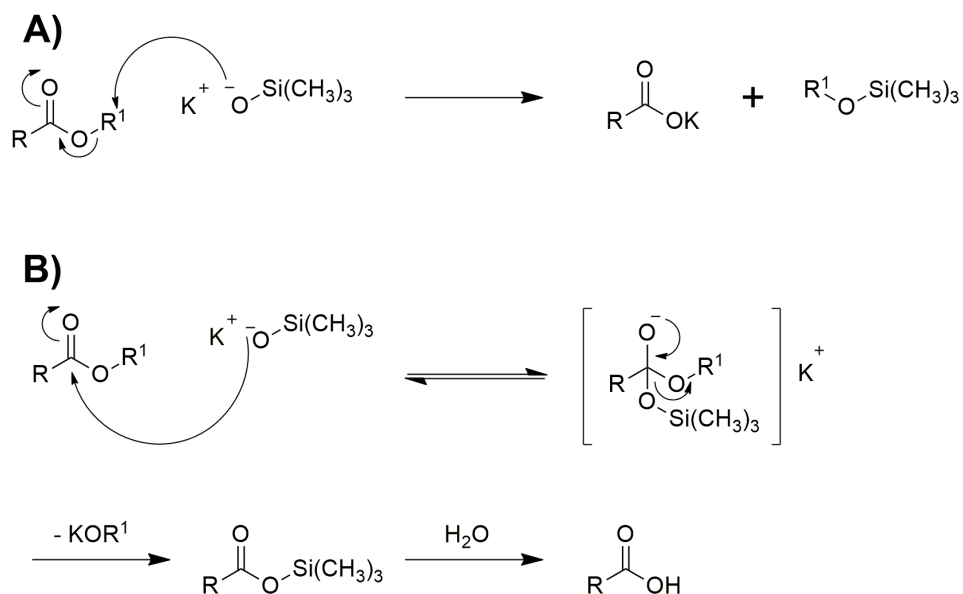
Figure 41 - HPLC Trace of the isolated precipitate at 285 nm detection.. Conditions: Analytical HPLC Method B (Chapter 7).

In summary, the treatment of **3-16** with sodium hydroxide for 15 minutes led to the decomposition of the conjugate, releasing free ciprofloxacin **1-5**. Whilst studies have reported the use of sodium hydroxide to cleave esters in the presence of disulfides, such as that by Schofield *et al.*,¹⁹⁶ it has been suggested by others that disulfide bonds are unstable above pH 11, with the addition of hydroxide across the disulfide bond, eliminating a free thiol, thereby resulting in cleavage of the disulfide bridge.^{186, 197} With these

conflicting studies, it is nevertheless important to note that a high pH used in this study, resulting from the use of 0.1 M sodium hydroxide, resulted in the decomposition and scrambling of the disulfide bond, despite using a maximum of 1.2 equivalents of base per ester group. As such, alternative methods of ester cleavage were necessary.

Attempted hydrolysis of 3-16 with potassium trimethylsilanolate

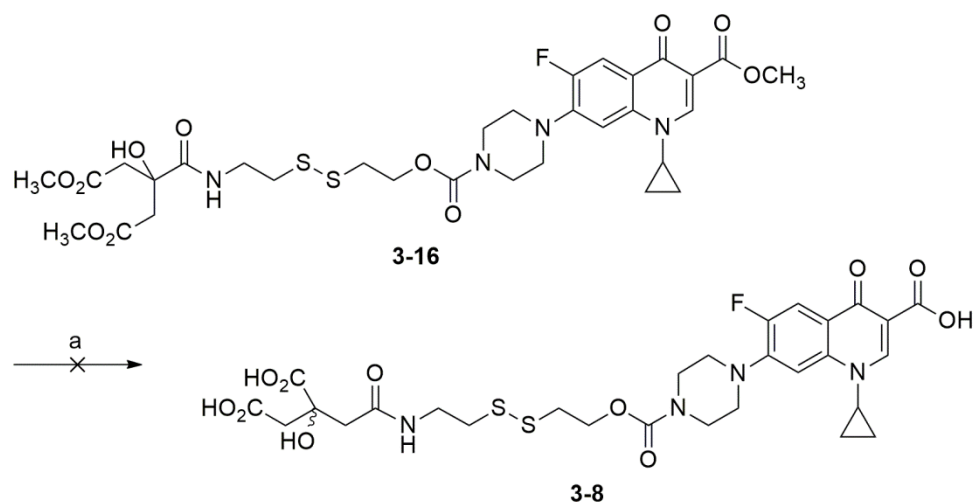
Potassium trimethylsilanolate could avoid any potential hydroxide-based decomposition of the disulfide linkage. There are two possible mechanisms for the action of the nucleophilic trimethylsilanolate ion, one following an S_N2 attack of the alkyl group (**A - Scheme 42**) and the second involving nucleophilic attack at the ester carbonyl (**B - Scheme 42**).¹⁹⁸ It has been suggested that the most likely mechanism is *via* the S_N2 route.¹⁹⁸ In turn, this would suggest that potassium trimethylsilanolate is less likely to attack the disulfide bond. Therefore compound **3-16** was dissolved in tetrahydrofuran and a solution of potassium trimethylsilanolate (2M in THF, 38 equivalents) was added. However, on work-up and characterisation of the reaction after one hour, a mixture of at least three species was observed in the 1H NMR spectrum. ESI-MS analysis of the mixture indicated that starting material **3-16** was present, with a molecular ion peak for $[M+Na]^+$ at m/z 749.1931, consistent with a molecular formula of $C_{31}H_{39}FN_4NaO_{11}S_2$. In addition, another $[M+Na]^+$ peak was observed, at m/z 721.1650, which was attributed to the loss of two methyl ester groups from compound **3-16**, as the peak was consistent with a molecular formula of $C_{29}H_{35}FN_4NaO_{11}S_2$. On treating the crude mixture with a greater amount of potassium trimethylsilanolate for several days, it was found that the reaction would not proceed any further and so it was concluded that this reagent was also not suitable for a continued investigation.



Scheme 42 - Proposed mechanisms of ester hydrolysis using potassium trimethylsilylanolate.¹⁹⁸

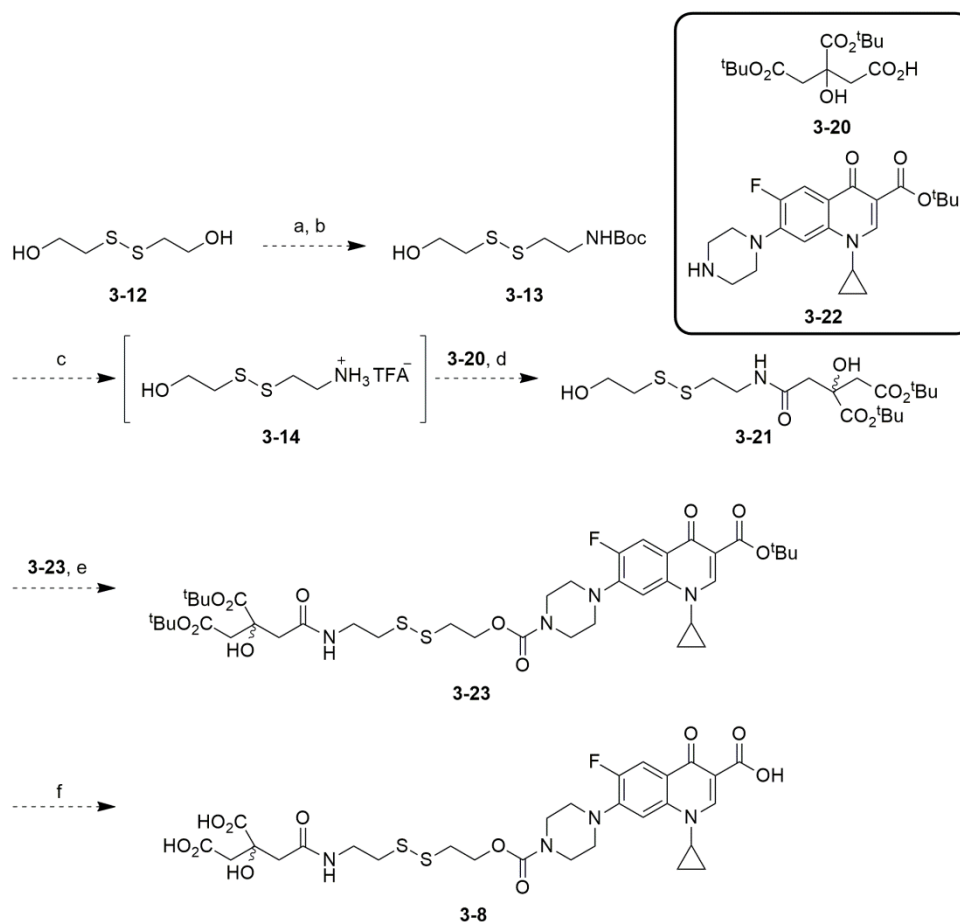
Attempted acid-catalysed hydrolysis of the protected disulfide-linked conjugate **3-16** to target **3-8**

It has been shown that methyl esters can be cleaved using acid-mediated hydrolysis, such as through the use of concentrated sulfuric acid.¹⁴⁰ However, under these conditions equilibrium between hydrolysis and formation occurs, which, when combined with the fact that such conditions are harsh for other functional groups in the molecule, meant that the use of sulfuric acid was deemed unsuitable. Instead, compound **3-16** was treated with a large excess of trifluoroacetic acid (295 equivalents) (**Scheme 43**). After the mixture was stirred for 24 hours the solvent was removed *in vacuo*. Unfortunately, the methyl esters were not removed. However, perhaps more importantly, no decomposition of the compound was observed, with the isolated product being unchanged **3-16**.



Scheme 43 - Attempted acid hydrolysis of **3-16** to target **3-8**. (a) TFA, CH_2Cl_2 .

Despite the unsuccessful acid-catalysed hydrolysis of **3-16**, trifluoroacetic acid could be used for future deprotection reactions, where an alternative protecting group strategy would be targeted towards the synthesis of **3-8**. Such a change of protecting group could see the use of *tert*-butyl ester protecting groups, for both the fluoroquinolone and citrate moieties, targeting a synthetic route proposed in **Scheme 44**. The synthesis of a fluoroquinolone *tert*-butyl ester has been reported using norfloxacin **1-4**,¹⁹⁹ which could be employed in the synthesis of **3-23**, though the synthesis of *tert*-butyl ester citrates (**3-20**) would have to be developed.



Scheme 44 - Proposed future work synthesis of **3-8** via the use of *tert*-butyl ester protecting groups. (a) Cysteamine.HCl, MeOH, Et₃N; (b) Boc₂O, MeOH; (c) TFA, CH₂Cl₂; (d) HATU, DMF, DIPEA; (e) DSC, DIPEA, DMF; (f) TFA, CH₂Cl₂.

3.4 Summary, conclusions and future work for Chapter 3

Compound **3-16** was synthesised as a methyl-protected precursor to the target conjugate **3-8**. The synthesis of **3-16** has provided procedures for the synthesis of a number of intermediates. However, attempts to deprotect conjugate **3-16** to yield **3-8** proved unsuccessful, with an apparent instability of the disulfide linkage in the presence of hydroxide. The mechanism by which compound **3-16** cleaves was not determined, though it is likely to be *via* cleavage of the disulfide linkage. Furthermore, the release of free ciprofloxacin **1-5** during base hydrolysis can tentatively be

said to act as a ‘proof of concept’ for the release of the drug from the conjugate through the disulfide linkage. However, only the isolation of **3-8**, and subsequent studies into the stability of the disulfide bond, can fully justify this argument.

Having established that the protected conjugate **3-16** is stable in the presence of trifluoroacetic acid, future work could involve the development of an alternative protecting group strategy to allow the synthesis of **3-8** (**Scheme 44**). Based on the potential success of such a strategy to obtain **3-8**, future work could therefore involve *ex vivo* stability studies of **3-8** against sulfhydryl species, such as glutathione, to determine the ability of **3-8** to cleave under reducing conditions analogous to within the cytoplasm. Furthermore, future work could also include the biological evaluation of the Trojan horse conjugate to determine the efficacy of **3-8** against bacterial strains. Such evaluation would involve growth assays and DNA gyrase assays analogous to Chapter 2.

In addition to the development of bio-labile linkers, and the need to complete the synthesis of compound **3-8** as future work for this Chapter, linker design is just one aspect of the Trojan horse strategy. Thus the understanding of design features required for siderophore-fluoroquinolone conjugates also needs to take into consideration the choice of siderophore, discussed in greater detail in Chapter 4.

**Chapter 4: Synthesis and
antimicrobial activity
testing of a salmochelin-
inspired siderophore-
ciprofloxacin conjugate**

4.1 Aims and overview

In Trojan horse conjugates, the siderophore is a key component to be considered. This Chapter discusses the use of a glucosylated-catecholate siderophore in the Trojan horse strategy, inspired by the stealth siderophores, the salmochelins. As the salmochelins have only recently been discovered, the development of salmochelin-inspired conjugates is a new field of research. The aim of the research presented in this Chapter is to explore the application of a salmochelin analogue as the siderophore component in a Trojan horse conjugate that incorporates ciprofloxacin as the drug.

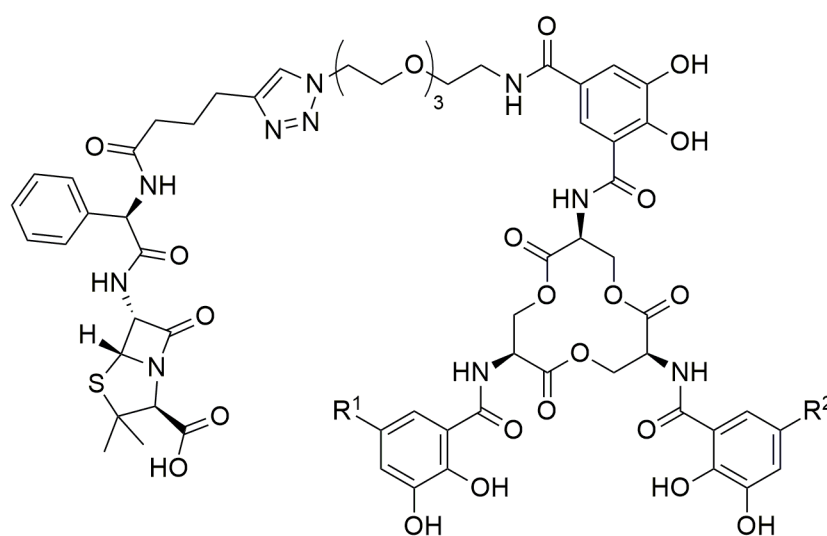
4.2 Introduction

In the continued development of siderophore-fluoroquinolone conjugates, it is important to consider the role of the siderophore moiety. The ability of many mammalian hosts to produce siderocalins to prevent the uptake and use of catecholate siderophores (Chapter 1),^{71, 200} suggests that siderocalins could also scavenge catecholate-antimicrobial conjugates, thereby preventing their uptake into the bacterial cell.

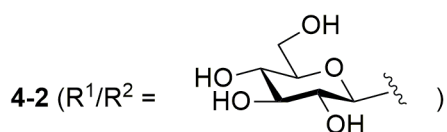
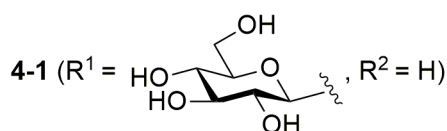
Given that some bacterial species respond to the host's production of siderocalin by producing stealth siderophores, such as the salmochelins (Chapter 1),^{77, 78} they provide interesting options for Trojan horse conjugates. Producing Trojan horse conjugates inspired by stealth siderophores is a strategy that may allow the conjugate to evade the host's immune response, whilst maintaining the iron-binding ability of the siderophore component.

Salmochelin-inspired Trojan horse conjugate

The salmochelins were discovered in 2003,⁷⁷ with the structures elucidated in 2004.⁷⁸ Only one example of their incorporation into a Trojan horse conjugate has been documented to date. This was published in 2015 by Nolan *et al.* who investigated a salmochelin-inspired β -lactam Trojan horse conjugate.⁹⁹ This study was reported whilst the work conducted and presented herein was in progress. Nolan *et al.* introduced glucosyl moieties onto the enterobactin scaffold of their conjugates *via* a chemoenzymatic approach, using two different *C*-glucosyltransferases, MceC and IroB to catalyse *C*-glucosylation, producing **4-1** and **4-2** respectively,⁹⁹ with conjugate **4-1** based on salmochelin S4 **1-16**.



1-32 ($R^1 = H$, $R^2 = H$)



Nolan *et al.* tested their conjugates against *E. coli* strains that expressed IroN, the outer membrane receptor for salmochelin S4 **1-16**, and those that do not. It was found that conjugates **4-1** and **4-2** were active against *E. coli* UTI89 and *E. coli* CFT073, which both express IroN, with 100- and 1000-fold enhanced activity against these two strains, respectively, compared to the parent drug.⁹⁹ This enhancement in activity matched the activity of a comparative non-glucosylated conjugate **1-32** (Chapter 1).⁹⁸ Additionally, conjugates **4-1** and **4-2** demonstrated negligible antibacterial activity against three *E. coli* strains which lacked IroN.⁹⁹ Significantly, Nolan *et al.* also demonstrated that conjugates **4-1** and **4-2** evaded the siderocalin protein, with the conjugates still able to kill *E. coli* in the presence of a 10-fold excess of siderocalin.⁹⁹ Indeed the activity of their non-glucosylated conjugate **1-32** was reduced in the presence of siderocalin,⁹⁸ suggesting the siderocalin protein scavenged and de-activated this conjugate.

As Nolan *et al.* successfully demonstrated that the β -lactam conjugates **4-1** and **4-2** were able to evade siderocalin binding,⁹⁹ the use of glucosylated siderophores for Trojan horse conjugates, the approach outlined in this Chapter, has been demonstrated as viable for designing a salmochelin-inspired siderophore-fluoroquinolone Trojan horse conjugate. Our work was conducted in parallel to the study reported by Nolan *et al.*

The chemoenzymatic glycosylation approach employed by Nolan *et al.*, using MceC and IroB to recognise and perform glycosylation of the enterobactin motif of conjugates, potentially limits the development of future conjugates to those with an enterobactin scaffold. Even though studies have found the residues involved in substrate binding of enterobactin, there is insufficient evidence to determine the exact specificity of substrate recognition for these enzymes.²⁰¹⁻²⁰³ Conversely, the chemical synthesis of a glucosylated siderophore component is likely to be more versatile for the future development of salmochelin-inspired Trojan horse conjugates, as it circumvents the likely requirement of

substrate recognition in an enzymatic approach. As such, the approach outlined in this Chapter is the chemical synthesis of a glucosylated siderophore mimic, which also provides a key intermediate that can be used towards future salmochelin-inspired Trojan horse conjugates. Furthermore, with no salmochelin-inspired Trojan horse conjugates incorporating fluoroquinolones reported at the time of writing, it is therefore important to explore such an approach.

Conjugate Design

A number of previous investigations have incorporated catecholate siderophore components into siderophore-fluoroquinolone conjugates.^{115, 119, 120, 123, 125, 127} However, these conjugates do not incorporate features which prevent scavenging by siderocalin.^{115, 119, 120, 123, 125, 127} As Nolan *et al.* have demonstrated that a non-glycosylated catecholate- β -lactam conjugate (**1-32**) was scavenged by siderocalin,⁹⁸ it can be hypothesised that that siderocalin could scavenge other catecholate siderophore-antimicrobial Trojan horse conjugates.

Taking inspiration from the salmochelin class of stealth siderophores, conjugate **4-3** was designed. Two glycosylated catecholate siderophore components were incorporated, with a lysine linker to connect to ciprofloxacin **1-5** (**Figure 42**). Conjugate **4-3** utilises a tetradentate siderophore in its design. It was therefore important to consider the uptake of tetradentate siderophores, as well as the uptake mechanisms of salmochelin-type siderophores.

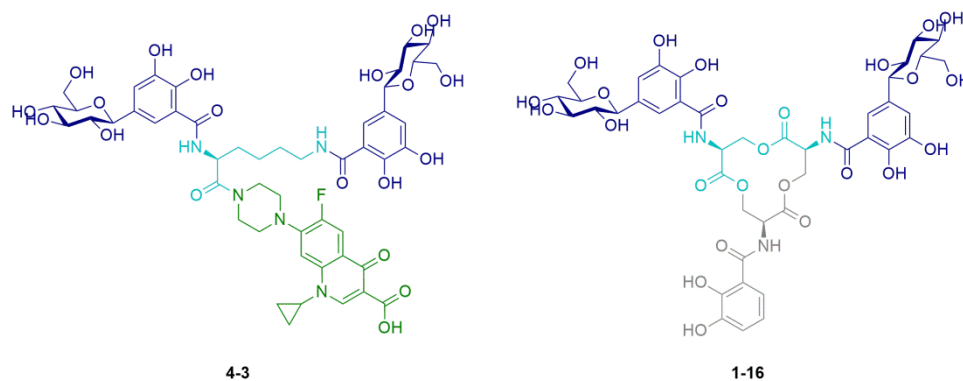
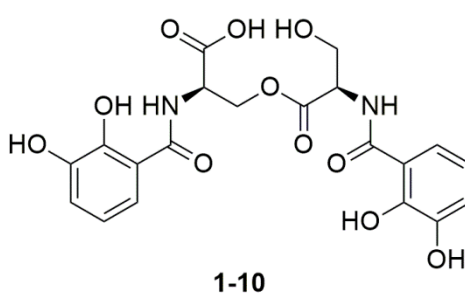
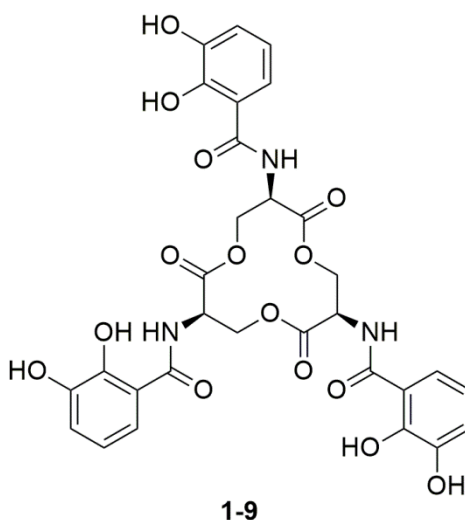


Figure 42 - Conjugate **4-3** and salmochelin S4 **1-16**. Dark blue = glucosylated catechol units; Light blue = backbone/linker; Green = ciprofloxacin antimicrobial; Grey = remainder of salmochelin S4 structure.

Uptake of tetradentate and salmochelin-type siderophores

With regards to the choice of a tetradentate siderophore in target **4-3**, it is worth noting that the bacterial uptake of Fe(III) bound tetradentate siderophores has been demonstrated in *E. coli*, with the uptake of the linear dimer enterobactin hydrolysis product **1-10**.⁵⁴ Indeed for *Campylobacter jejuni* preferential binding of the tetradentate enterobactin linear dimer **1-10** over hexadentate enterobactin **1-9** to a periplasmic binding protein was observed, indicating that this scavenger bacterium may have developed this strategy to compete with other pathogens.²⁰⁴



The uptake pathways for the salmochelins should also be highlighted. Since the discovery of the salmochelins, the proposed uptake mechanisms of salmochelin S4 **1-16** in *E. coli* has evolved from that first suggested by Hantke *et al.* in 2005 (**Figure 43**).⁷⁹ As can be seen, salmochelin S4 **1-16** was proposed to first pass through the outer membrane receptor IroN, followed by cleavage in the periplasm by the esterase IroE to give the linear trimer salmochelin S2, which would be subsequently taken into the cytoplasm through IroC (**Figure 43**).⁷⁹ In the cytoplasm, action by the esterase IroD cleaves the siderophore backbone to release the iron from the complex.

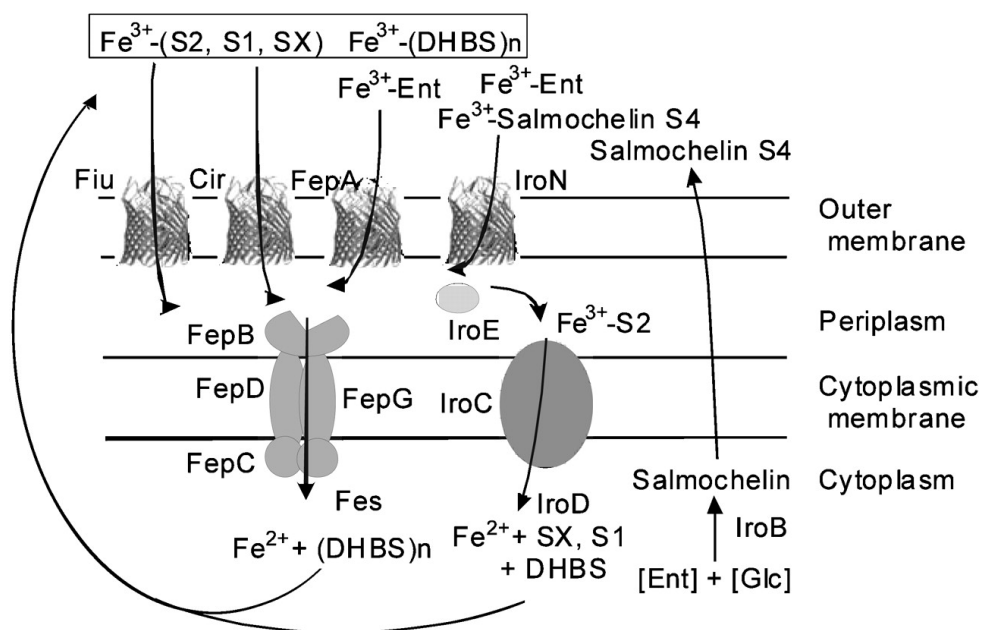


Figure 43 - Early model for the uptake of salmochelin S4 and its hydrolysis products proposed by Hantke *et al.* in 2005.⁷⁹ Ent = Enterobactin; DHBS = 2,3-dihydroxybenzoylserine; Glu = glucose. Taken from M., Zhu, M. Valdebenito, G. Winkelmann and K. Hantke, *Microbiology*, 2005, **151**, 2363-2372, with permission from the Microbiology Society.

Later studies by Fang *et al.* in 2008 established that on entering the cell through IroN, the esterase IroE is not required for the uptake of salmochelin S4 **1-16**, as an *entC iroE* mutant was able to transport this siderophore.²⁰⁵ It was determined that salmochelin S4 did not enter the cytoplasm through IroC, through the use of an IroC negative strain, but in fact was chaperoned by the periplasmic binding protein FepB to pass into the cytoplasm *via* FepCDG, the same ABC transporters utilised by enterobactin **1-9** (**Figure 44**).²⁰⁵ Indeed, IroC was in fact found to export salmochelin S4 from the cell.^{205, 206} However, whilst the understanding of the uptake mechanisms for salmochelin S4 **1-16** has developed, the study of the salmochelin hydrolysis products, such as the tetradentate salmochelin S1 **1-17**, remains less well investigated.

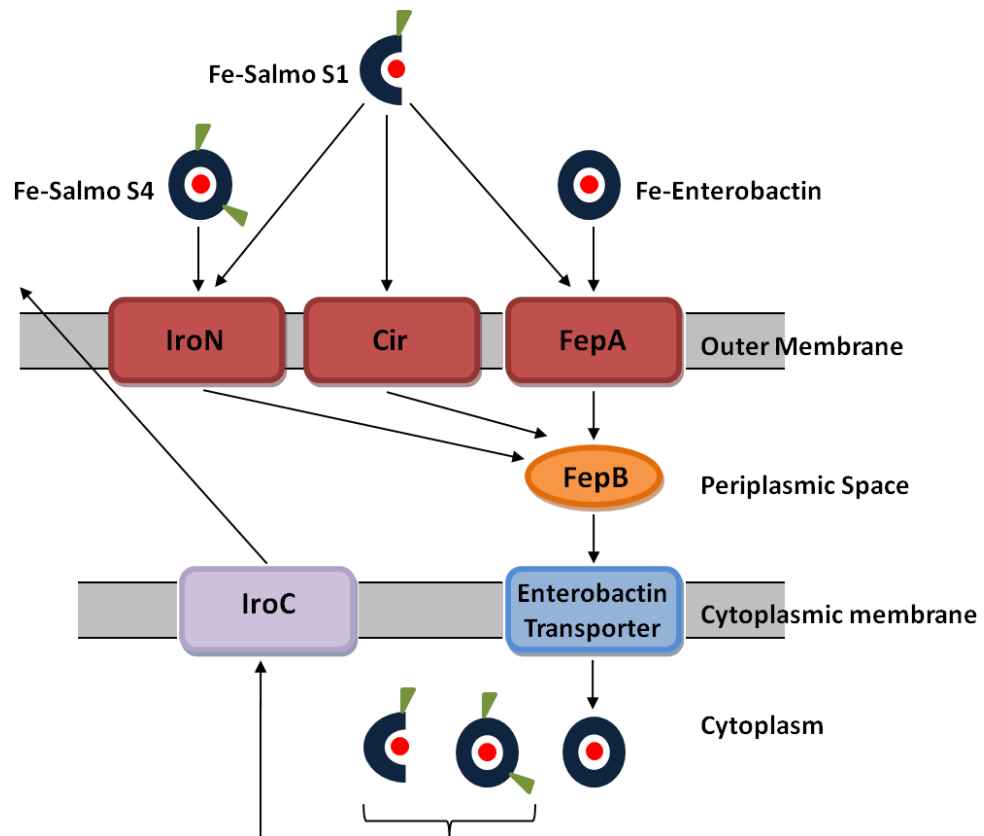
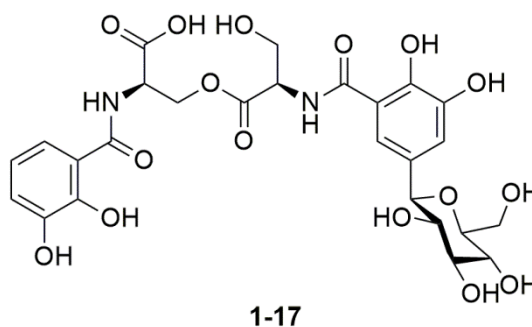


Figure 44 - Simplified schematic representation for salmochelin S4 **1-16** uptake, according to Fang *et al.*²⁰⁵ The updated proposed uptake mechanism by Hantke *et al.* for salmochelin S1 **1-17** is also shown.²⁰⁶ Blue circle/half-circle = Siderophore / Green triangle = Glucosyl Moiety / Red circle = Fe(III).

The uptake pathways of the hydrolysis products of salmochelin S4, such as tetradentate salmochelin S1 **1-17**, are still hypothetical (**Figure 44**).⁷⁹ In fact, the most recent proposed mechanism, also by Hantke *et al.* (2009), suggests that salmochelin S1 **1-17** enters into the periplasm through the outer membrane receptors Cir, IroN and FepA (**Figure 44**),²⁰⁶ analogous to their first proposed mechanism for salmochelin S1 uptake (**Figure 43**).⁷⁹ The only difference is that Hantke *et al.* instead propose that the remainder of salmochelin S1 **1-17** uptake proceeds through the Fep system,²⁰⁶ accounting for the mechanism outlined by Fang *et al.*²⁰⁵



With the lack of complete understanding in the uptake mechanisms of the salmochelin hydrolysis products, it is important to highlight that salmochelin S1 **1-17** supports bacterial growth.^{79, 205, 206} Despite the uptake mechanism of tetradentate salmochelin S1 **1-17** being less well understood, it is still expected that **4-3** would allow for the uptake of the conjugate as a whole *via* the Fep system. Therefore it should be highlighted that the design of a tetradentate siderophore in **4-3** allows for a shorter synthetic route than if the full tri-serine scaffold of salmochelin S4 **1-16** was used. Incorporating a hydrolytically stable lysine linker provides a simpler synthetic route to the target molecule. The carboxylic acid group of the lysine moiety provides an attachment point for the antimicrobial. This strategy differs from work presented by Nolan *et al.* where extra functionality must be introduced on one catechol moiety to attach the antimicrobial directly, demonstrated in conjugates **4-1** and **4-2**.⁹⁹

Synthetic design of compound **4-3**

In order to establish a synthetic route to compound **4-3**, a disconnection approach was applied to give the individual components (**Figure 45**), which could then be coupled *via* sequential amide bond formation. The target compound **4-3** consisted of three key components: a β-D-glucosylated dihydroxybenzoic acid **4-4**, L-lysine and ciprofloxacin **1-5**. The synthetic route was envisaged as shown in **Scheme 56**, discussed in greater detail later in the Chapter.

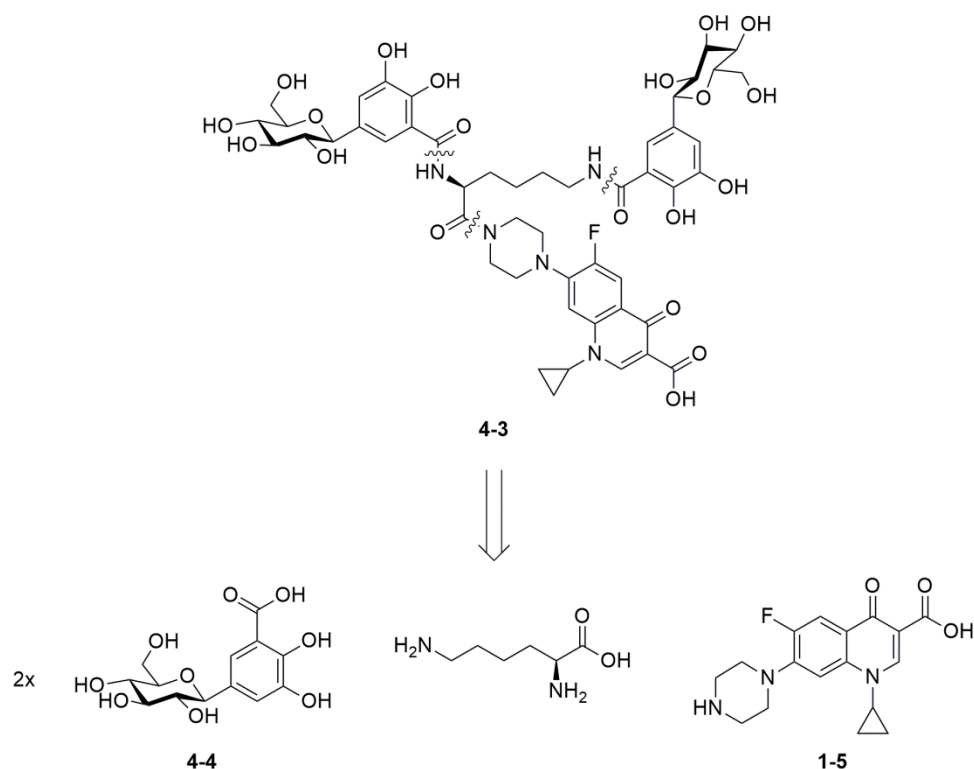


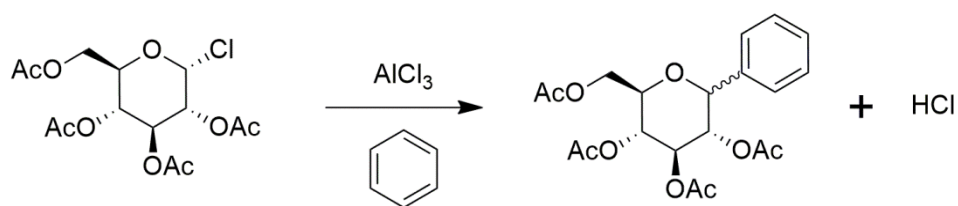
Figure 45 - The three key components of conjugate **4-3**.

Synthesis of aryl-*C*-glycosides

As **Figure 45** highlights, conjugate **4-3** required an aryl-β-*C*-glycoside (**4-4**) as the siderophore moiety. The synthesis of an acetyl-protected form of **4-4**, compound **4-7** has been reported, discussed in detail later.^{207, 208} It should however be highlighted that a number of approaches to aryl-*C*-glycoside formation are available, including direct C-C cross coupling, arylation and alkylation reactions.²⁰⁹⁻²¹² These approaches typically involve an electrophilic anomeric centre with a nucleophilic aryl ring (e.g. **Scheme 46**).

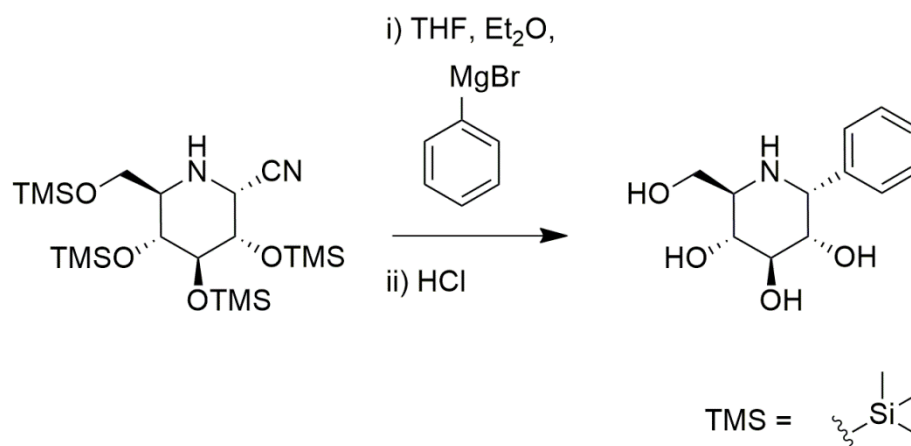
Aryl-C-glycoside synthesis via Lewis acid promoters and arylation

The first example of the synthesis of an aryl-*C*-glycoside was reported by Hurd and Bonner in 1945, who employed a Friedel-Crafts reaction using aluminium chloride with tetraacetyl- α -D-glucosyl chloride and benzene (**Scheme 45**).²¹³ However, the lack of stereo control makes this approach unsuitable towards the synthesis of **4-3**.



Scheme 45 - Friedel-Crafts approach utilised by Hurd and Bonner to form an aryl-*C*-glucoside.²¹³

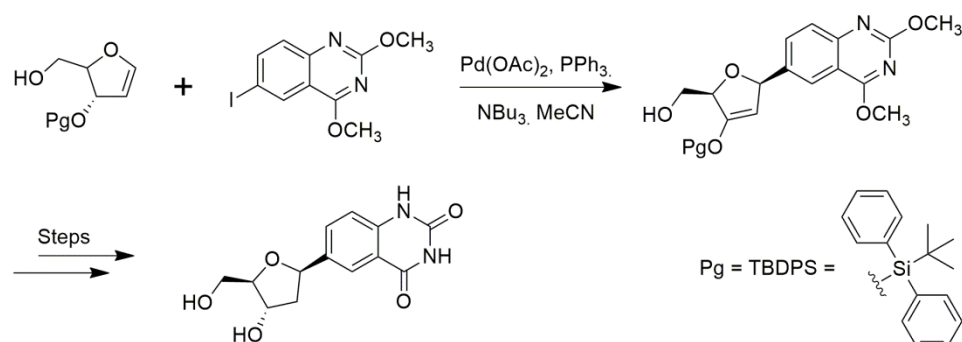
Arylation reactions utilising organometallic aromatics have proven as effective methods for the synthesis of aryl-*C*-glycosides.^{209, 211, 214} Grignard reagents were first reported for aryl-*C*-glycoside synthesis by Hurd and Bonner in 1945, at the same time as their investigation into the Friedel-Crafts approach, producing the same product as in **Scheme 45**.²¹⁵ Subsequent studies into stereoselective control saw a change of protecting group strategy for the hydroxyl moieties and changes in leaving groups, such as that by Junge *et al.* who produced only the α -anomer (**Scheme 46**).^{216, 217} In contrast, others have solely obtained the β -anomer through the use of benzyl protecting groups,²¹⁸ or through a combination of using a Grignard reagent on a lactone, followed by a hydride reaction with a Lewis acid.²¹⁹ Beyond the use of Grignard reagents, numerous studies have synthesised aryl-*C*-glycosides through other organometallic reagents for arylation reactions,^{209, 211, 214} including the use of aryllithium reagents,^{220, 221} and aryl cuprates.²²²



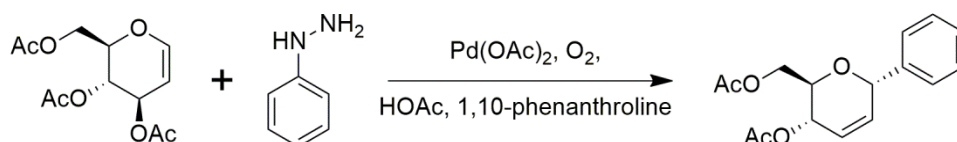
Scheme 46 - Grignard reaction by Junge *et al.*, forming the α -anomer.²¹⁶

Aryl-C-glycoside synthesis via metal catalysed C-C cross coupling

More recent syntheses of aryl-*C*-glycoside have involved the use of metal catalysts to perform C-C cross coupling reactions. Such couplings have predominantly involved the Heck, Suzuki, Stille and Negishi reactions,^{210, 223-225} though iron and cobalt catalysts were recently employed for the synthesis of α -anomer aryl-*C*-glycosides.²²⁶ In particular, the Heck reaction has been used extensively as a means to synthesise *C*-nucleosides, particularly as many natural *C*-nucleosides are antibiotics.^{223, 227} Based on this, Lee and Kool also employed Heck coupling to synthesise novel benzopyrimidines to act as analogues of DNA bases (**Scheme 47**).²²⁸ Furthermore, Lee and Kool found the β -anomer was formed exclusively, and attributed this to the large *tert*-butyldiphenylsilyl ether protecting group at the 3-position, directing the reaction to occur on the least sterically hindered face of the glycal.^{228, 229} This finding supported many other similar examples of Heck coupling for aryl-*C*-glycosides synthesis.^{228, 229} More recently, Liu *et al.* were able to selectively produce α -anomer products using oxidative Heck coupling of (3*R*)-glycals with aryl hydrazines (**Scheme 48**).²³⁰

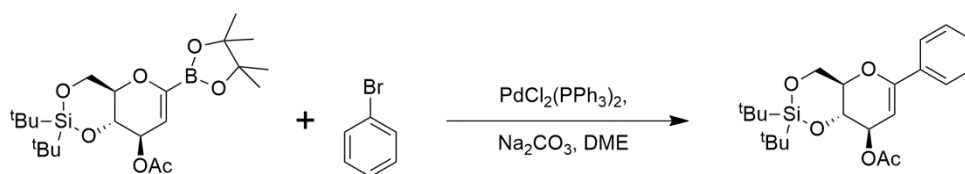


Scheme 47 - Heck reaction employed by Lee and Kool to synthesise analogues of DNA bases.²²⁸



Scheme 48 - Oxidative Heck coupling of glycols and aryl hydrazines by Liu *et al.*²³⁰

Suzuki and Stille cross coupling reactions for the synthesis of aryl-*C*-glycosides typically involve the reaction of an activated glycal with an aryl halide.^{210, 223-225} Among examples, Sakamaki recently employed Suzuki coupling to react a glycal boronate with aryl bromides, producing 2-arylglycals (**Scheme 49**).²³¹ In turn, subsequent steps led to the isolation of β -anomer aryl-*C*-glycosides.²³¹ Similarly, Stille cross couplings, using stannylated glycals with palladium catalysts and aryl halides have also been previously employed for the synthesis of 2-arylglycals.^{232, 233}

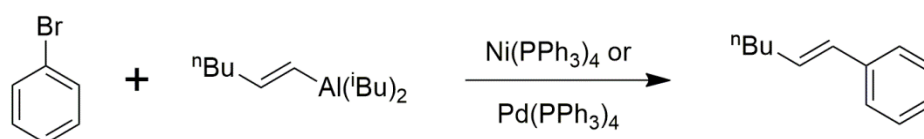


Scheme 49 - Suzuki cross coupling to give 2-arylglycals as intermediates in the synthesis of aryl-C-glycosides.²³¹

With the advances in aryl-C-glycoside synthesis to produce stereoselective products as either the α - or β - anomer as required, the synthesis of a key intermediate of interest in this Chapter (compound **4-7**) has been reported, involving a Negishi C-C cross coupling reaction.^{207, 208}

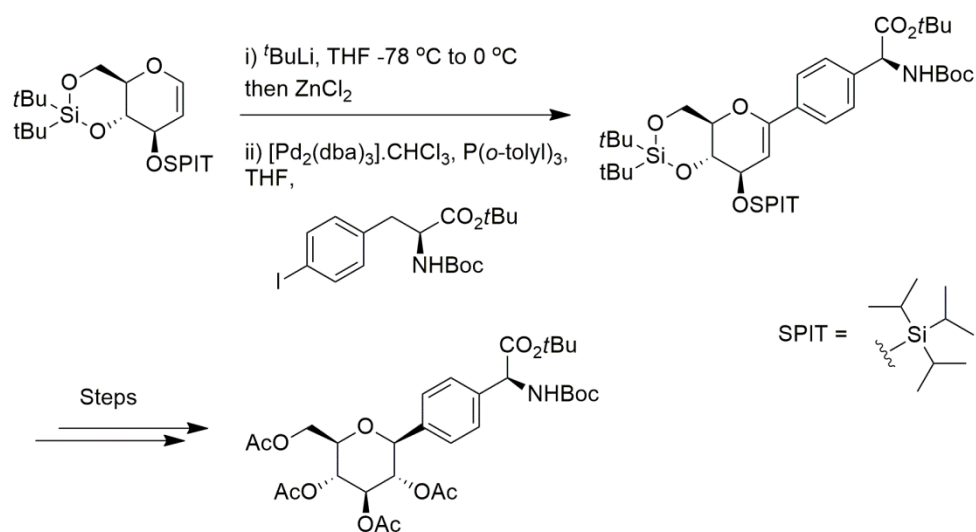
Aryl-C-glycoside synthesis via Negishi C-C cross-coupling

The Negishi coupling reaction first involved the coupling of an organohalide with an alkenylaluminium intermediate to produce C-C bonds using a palladium or nickel catalyst.²³⁴ Developed in 1976, Negishi was jointly awarded the 2010 Nobel Prize in Chemistry for this reaction (**Scheme 50**). Subsequent studies have developed a range of nickel and palladium catalysts, as well as the use of other organometallic intermediates containing Zn and Zr.²³⁵⁻²³⁷ There are disadvantages however, with organozinc compounds being extremely sensitive to both water and oxygen, and also it being difficult to couple large or sterically hindered organohalides.^{237, 238}



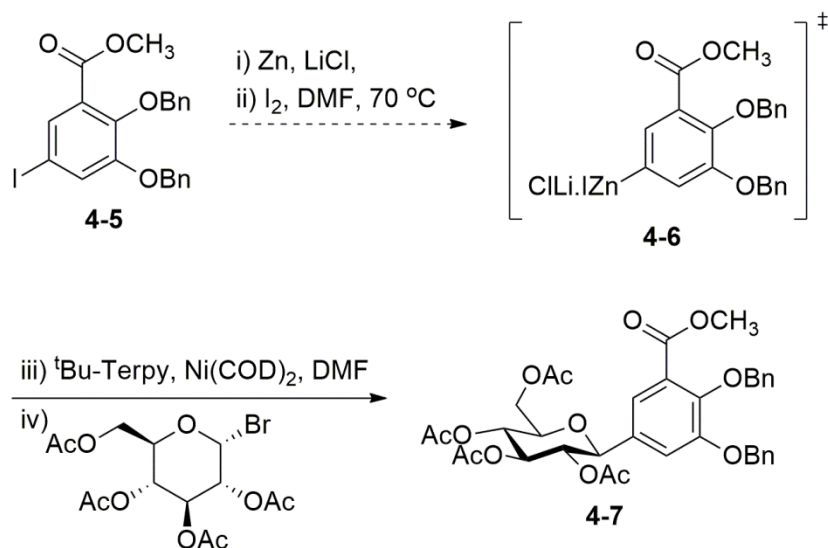
Scheme 50 - The first reported Negishi coupling.²³⁴

There are two reported examples using Negishi coupling for the synthesis of aryl-*C*-glycosides, with the first being by Ousmer *et al.* in 2006.²³⁹ They first formed an organozinc glycal, through deprotonation, followed by the addition of zinc dichloride. Following this *in situ* reaction, the palladium catalyst and an iodoarene were added to give the coupled product in 90% yield (**Scheme 51**).²³⁹ Subsequent steps afforded the acetyl protected aryl-*C*-glucoside as the β -anomer.²³⁹



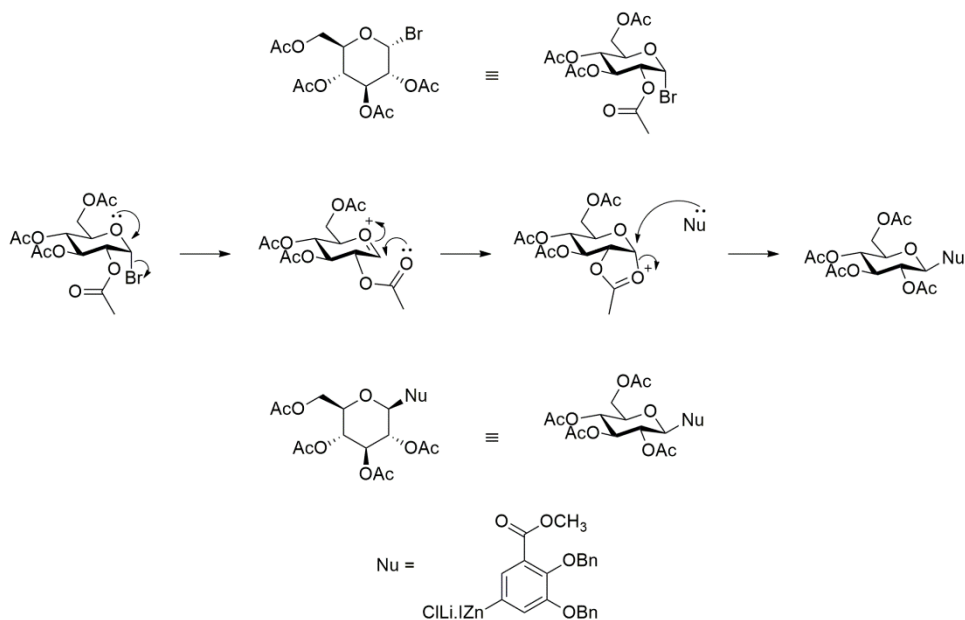
Scheme 51 - Negishi coupling of a glycal with an iodoarene using a palladium catalyst, by Ousmer *et al.*²³⁹

Later, Gagné *et al.* reported a direct Negishi cross-coupling to synthesise aryl- β -*C*-glycosides with high stereoselectivity (20:1 β : α).^{207, 208} Unlike the approach of Ousmer *et al.*, they formed an arylzinc compound (**4-6**) *in situ* by activating a benzylated-iodoarene (**4-5**) with zinc, lithium chloride and iodine in DMF at $70\text{ }^\circ\text{C}$ (**Scheme 52**).^{207, 208} On adding the organozinc to acetobromo- α -D-glucose in the presence of a nickel catalyst, the aryl-*C*-glucoside **4-7** was produced in high β -selectivity, due to nucleophilic substitution at the anomeric centre (**Scheme 52**).^{207, 208}



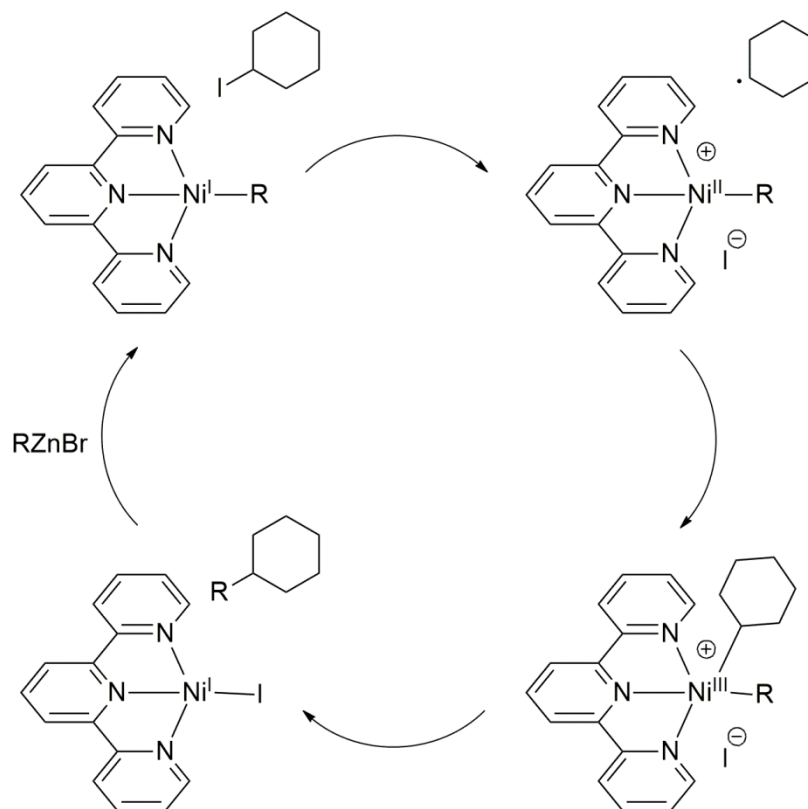
Scheme 52 - Direct Negishi cross-coupling reported by Gagné *et al.* for aryl-C-glycoside synthesis.^{207, 208}

The choice of the acetyl protecting groups by Gagné *et al.* can help direct stereoselectivity of the product to the β -anomer,^{207, 208} due to neighbouring group participation (**Scheme 53**).²⁴⁰



Scheme 53 - Rationalising the high β -selectivity of the Negishi reaction by neighbouring group participation of an acetate group.²⁴⁰

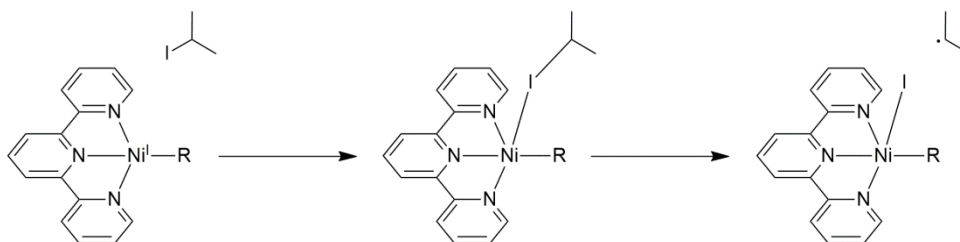
Gagné *et al.* also discuss two proposed variants on the mechanism of alkyl-alkyl Negishi cross-couplings, to hypothesise the role of the nickel catalyst in their reaction.^{207, 241, 242} The first, by Vicic *et al.*, proposes a reaction between the nickel-ligand complex and the alkyl halide to give an alkyl radical and intermediate complex (**Scheme 54**).²⁴¹ Next, Vicic *et al.* speculated that oxidative radical addition affords a nickel(III)-dialkyl species, followed by fast reductive elimination to produce the cross-coupled dialkyl species and an iodo-nickel complex, which in turn can undergo alkylation to restart the catalytic cycle (**Scheme 54**).²⁴¹



Scheme 54 - Proposed Negishi mechanism of alkyl-alkyl couplings by Vicic *et al.*²⁴¹

The second proposed mechanism, by Cárdenas *et al.*, differs from that suggested by Vicic *et al.*, proposing abstraction of the halide to leave an

alkyl radical (**Scheme 55**), which in turn can react in a similar manner to that already described.²⁴² As Gagné *et al.* highlight, these mechanisms differ slightly in how the alkyl radical is produced (single electron transfer versus halide abstraction), though they both proceed *via* a one-electron process.²⁰⁷



Scheme 55 - Proposed Negishi mechanism of alkyl-alkyl couplings by Cárdenas *et al.*²⁴²

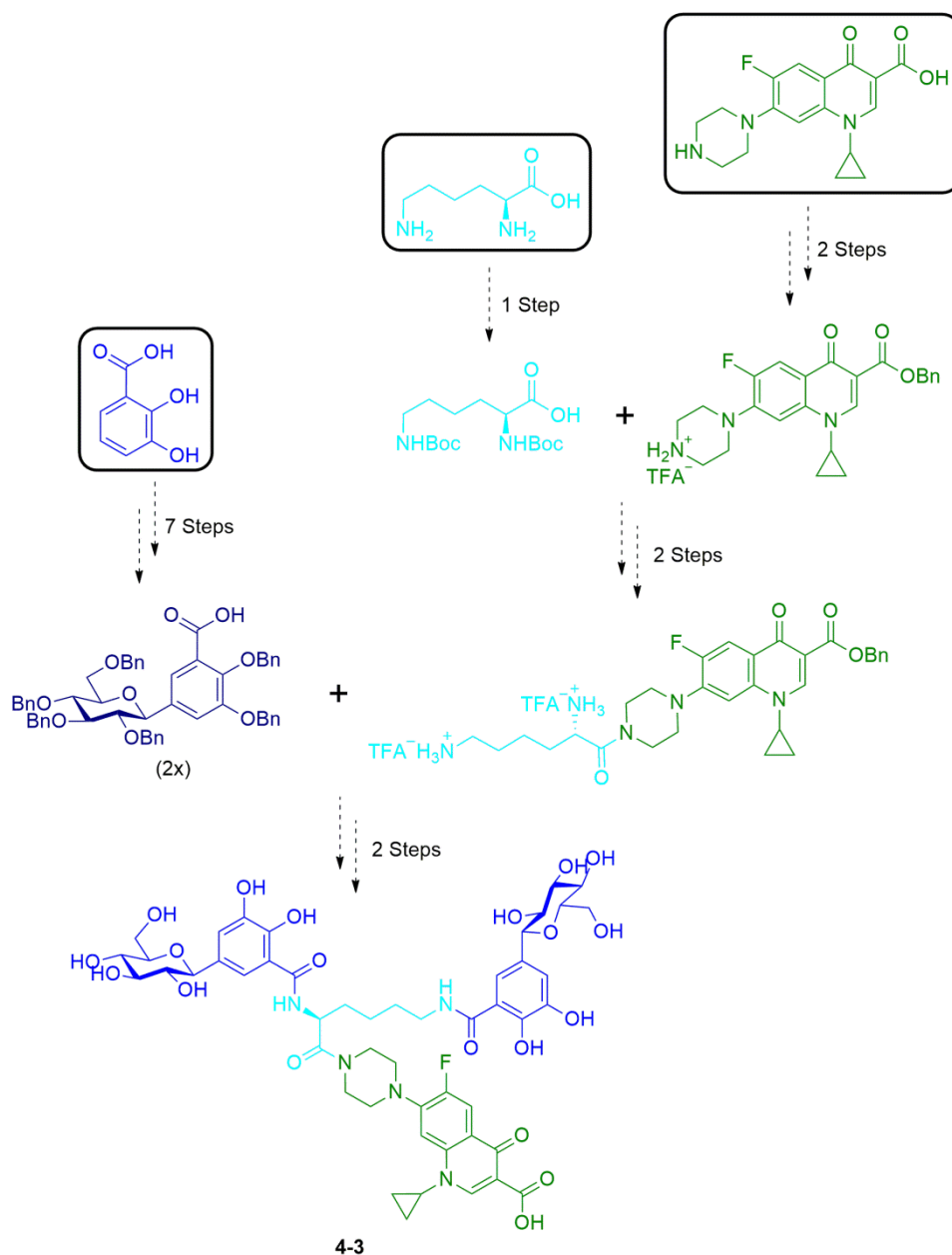
Gagné *et al.* continue their discussion on the potential mechanism of their reaction by highlighting the fact that radicals of their glucosyl unit would be subject to the anomeric effect.^{207, 243} In turn they point out that these radicals would likely form the α -organometallic intermediate, and by extension the α -products, assuming the transmetalation and reductive elimination steps remain the same as that by Vicic *et al.*²⁴¹ As Gagné *et al.* point out, the fact that they obtain high β -selectivity (20:1 β : α) for their synthesis of aryl-*C*-glucosides indicates there is likely another dominating effect.²⁰⁷ Finally, Gagné *et al.* discuss the complexity of radical-metal addition reactions, suggesting that more sterically encumbered metals, resulting from the choice of ligand, choose the β -face of the glucosyl radical, thus resulting in the β -anomeric product.²⁰⁷ To help understand this, Gagné *et al.* investigated other carbohydrate moieties to determine the scope of their reaction.²⁰⁷ In turn they found that on using acetobromo- α -D-mannose they obtained a ratio of β : α anomers of 1:2.9, whereas with acetobromo- α -D-galactoside the ratio of β : α was 10:1.²⁰⁷ Interestingly, they found that on changing the ligand from 4,4',4''-tri-*tert*-butyl-2,2':6',2''-terpyridine (*t*Bu-Terpy) to 2,6-bis(oxazolin-2-yl)-(15)N2-pyridine (PyBox),

the stereoselectivity of the mannosyl product increased significantly to 1:20 β : α .²⁰⁷ Given that neighbouring group participation of the acetyl protecting group of a mannosyl moiety would be expected to selectively direct the α -anomer, the significant difference in stereoselectivity on changing the ligand helps suggest that ligand choice is also key.

With the mechanism of the Negishi coupling for aryl-*C*-glucoside synthesis not fully understood, it is nevertheless encouraging that high stereoselectivity can be achieved. More recently, Lemaire *et al.* built upon the work of Gagné *et al.* by employing arylzinc reagents without the need for transition metal catalysts to selectively produce β -anomers in good yields.²⁴⁴ However, despite the avoidance of using transition metal catalysts, the methodology of Lemaire *et al.* has not been applied with the functionality required for compound **4-3**. As Gagné *et al.* have reported the synthesis of a key intermediate (compound **4-7**),^{207, 208} required towards the synthesis of compound **4-3**, it was thus decided to employ their methodology.

4.3 Synthesis

The full proposed synthesis of **4-3** is summarised in **Scheme 56**. As **Scheme 56** shows, the linker, the antimicrobial and the glucosylated siderophore, would be individually protected and coupled together by amide bond formation, before final global deprotection to reveal conjugate **4-3**.

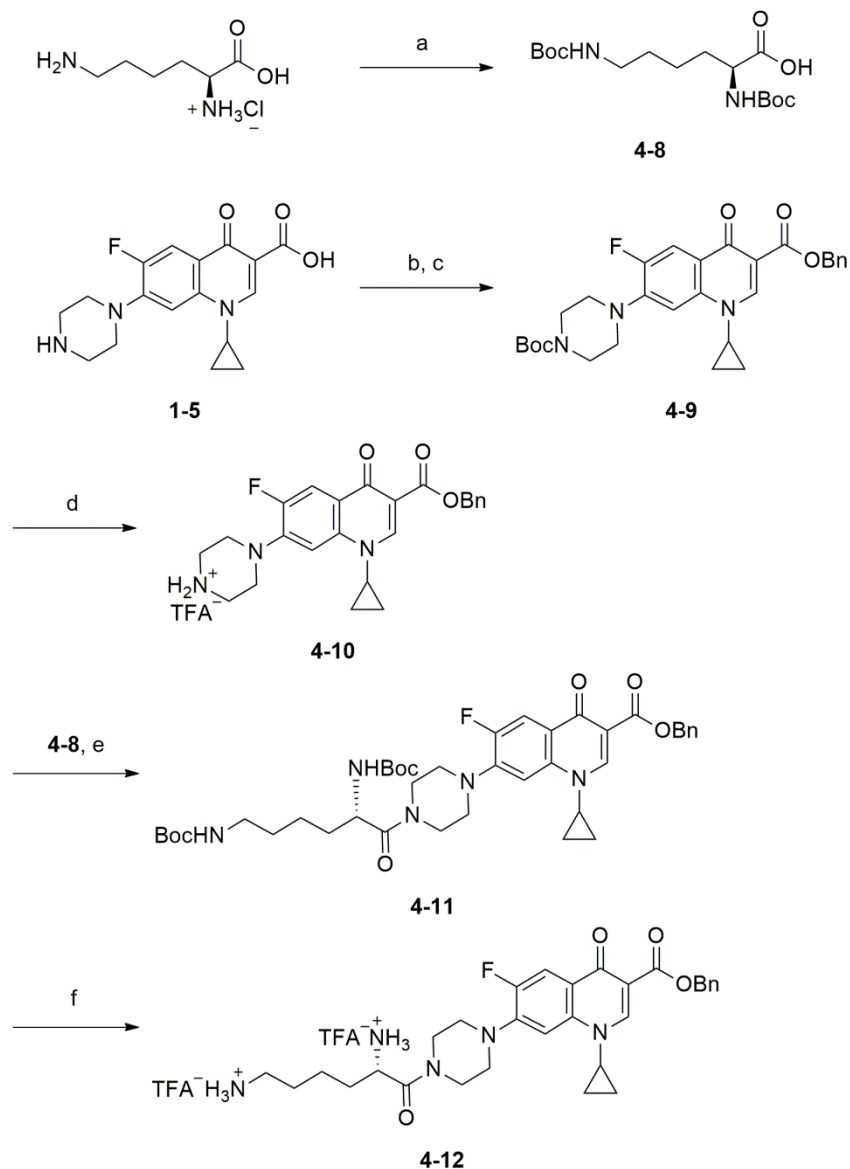


Scheme 56 - Summary of the proposed synthesis of **4-3** from three commercially available starting materials.

Synthesis of the lysine-linked ciprofloxacin component **4-12**

As **Scheme 56** demonstrates, the synthesis of conjugate **4-3** involves four convergent synthetic routes. Two of these routes provide access to a lysine-linked, benzyl-protected ciprofloxacin component, compound **4-12** (**Scheme 57**), which allows for coupling to the siderophore component. In

this case the ciprofloxacin antimicrobial requires protection with a benzyl ester, as opposed to the methyl ester utilised in other targets discussed in Chapters 2 and 3. The benzyl ester protecting group was chosen to allow for the final global deprotection by palladium catalysed hydrogenolysis to yield compound **4-3**.

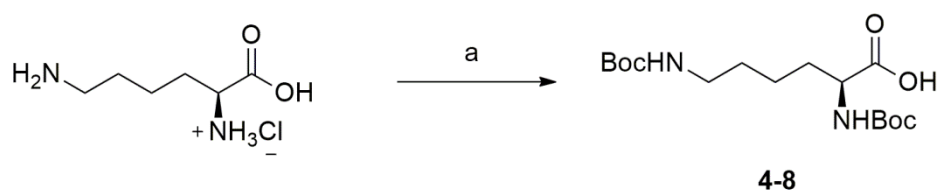


Scheme 57 - Synthesis of the lysine-linked, benzyl-protected ciprofloxacin component. (a) NaOH , Boc_2O , 1,4-dioxane, 50°C , 89%; (b) Boc_2O , NaOH , 1,4-dioxane, H_2O ; (c) BnBr , Cs_2CO_3 , DMF, 51%; (d) TFA, CH_2Cl_2 , quantitative; (e) EDC.HCl, $\text{HOBT} \cdot \text{H}_2\text{O}$, DMF, 55%, (f) TFA, CH_2Cl_2 , quantitative.

tert-Butyloxycarbonyl (Boc) protection of *L*-lysine

The first step required was protection of the α - and ϵ - amino groups of lysine.²⁴⁵ This protection was necessary as the amino groups were required to couple later to the glucosylated-catechol moieties. Given that the reaction to attach the lysine linker to the antimicrobial involves amide coupling, the amino groups would be free to participate in amide coupling if not protected.

L-lysine monohydrochloride was dissolved in water with sodium hydroxide, followed by the slow addition of di-*tert*-butyl dicarbonate (**Scheme 58**), according to a literature procedure.²⁴⁵ After work-up, **4-8** was isolated in 89% yield, with data consistent to the literature.²⁴⁵ The formation of **4-8** was supported by ¹H NMR spectroscopic analysis, with the appearance of a resonance at 1.44 ppm of relative integration eighteen, corresponding to the two Boc groups, evident in the spectra. Furthermore, ESI-MS analysis gave a molecular ion peak [M+H]⁺ for **4-8** at *m/z* 347.2117, consistent with a molecular formula of C₁₆H₃₁N₂O₆.

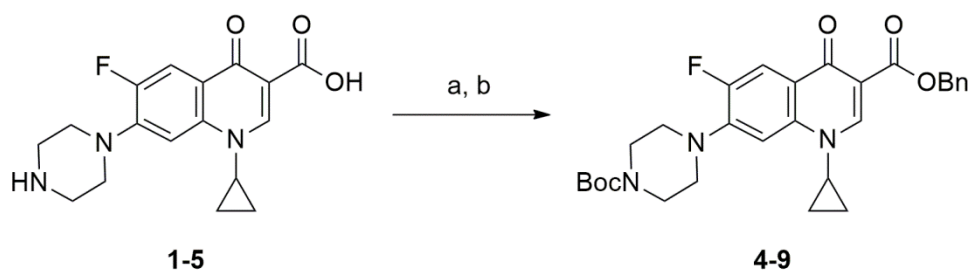


Scheme 58 - Synthesis of **4-8**.²⁴⁵ (a) NaOH, Boc₂O, 1,4-dioxane, 50°C, 89%.

Benzyl ester protection of ciprofloxacin 1-5 to produce 4-10

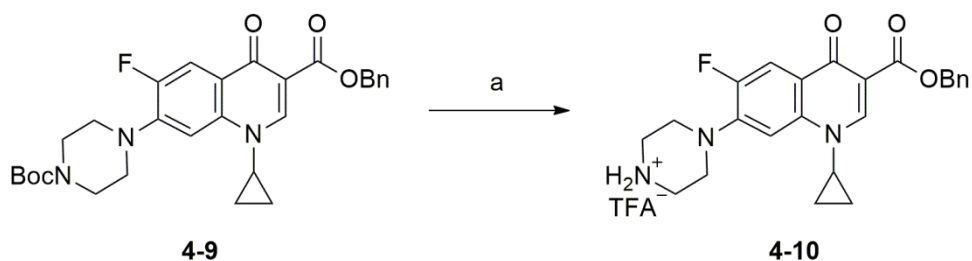
As previously stated, it was necessary to protect the carboxylic acid of ciprofloxacin **1-5** to prevent unwanted side reactions and therefore retain the β -keto acid moiety essential for antimicrobial activity. It was decided to protect ciprofloxacin **1-5** with a benzyl ester group to allow for the later global deprotection of all the benzyl groups of **4-25** by hydrogenolysis, discussed in detail later. However, in order to protect the carboxylic acid, it was first necessary to protect the nucleophilic secondary amine of the piperazine moiety. This amine protection was essential, to prevent reaction with benzyl bromide during the following protection of the carboxylic acid. If the amine was benzyl protected, selective deprotection would not be possible. As such Boc protection was chosen for the piperazinyl amine as it cleaves under orthogonal conditions to the benzyl ester group, allowing for selective removal.

Combining the methodologies of Lippur *et al.* and Miller *et al.*, ciprofloxacin **1-5** was first treated with di-*tert*-butyl dicarbonate and sodium hydroxide in a 1:1 1,4-dioxane:water mixture.^{126, 246} The intermediate was then treated with benzyl bromide and caesium carbonate in DMF.^{126, 246} After work-up and purification by column chromatography, compound **4-9** was isolated in 51% yield (**Scheme 59**), with data consistent with the literature.^{126, 246} Formation of **4-9** was supported by singlet resonances at 5.40 ppm and 1.50 ppm evident in the ¹H NMR spectrum, corresponding to the methylene and Boc protons respectively. Furthermore, ESI-MS analysis gave a molecular ion peak [M+H]⁺ for **4-9** at *m/z* 522.2423, consistent with a molecular formula of C₂₉H₃₃FN₃O₅.



Scheme 59 - Synthesis of compound **4-9**.^{126, 246} (a) Boc_2O , NaOH, 1,4-dioxane, H_2O ; (b) BnBr, Cs_2CO_3 , DMF, 51%.

Compound **4-9** was treated with trifluoroacetic acid in dichloromethane to reveal the piperazine ammonium salt (**Scheme 60**).^{126, 246} On removing the solvent, **4-10** was isolated in quantitative yield, supported by the absence of the resonance due to the Boc group protons in the ^1H NMR spectrum, and ESI-MS analysis showing a $[\text{M}+\text{H}]^+$ peak at 422.1878, consistent with a molecular formula of $\text{C}_{24}\text{H}_{25}\text{FN}_3\text{O}_3$.

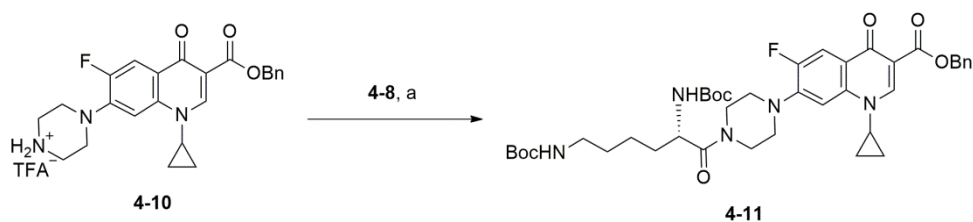


Scheme 60 - Synthesis of compound **4-10**.^{126, 246} (a) TFA, CH_2Cl_2 , quantitative.

Amide coupling of the protected lysine and antimicrobial moieties

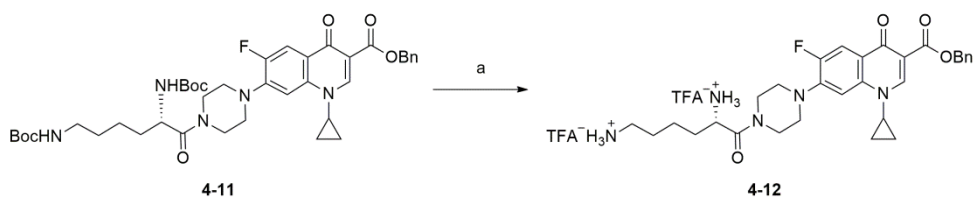
Next it was necessary to couple **4-8** and **4-10** via an amide link. It was decided to use the methodology reported by Milner *et al.* for a structurally related molecule.¹²⁴ Therefore **4-8** and **4-10** were mixed with EDC.HCl, HOBT. H_2O and DIPEA in DMF (**Scheme 61**). After work up and

purification by column chromatography, compound **4-11** was isolated in 55% yield. Formation of **4-11** was supported by the presence of a peak at 170.8 ppm in the ^{13}C NMR spectrum, corresponding to the amide carbonyl, and ESI-MS analysis showing a $[\text{M}+\text{H}]^+$ peak at 750.3873, consistent with a molecular formula of $\text{C}_{40}\text{H}_{53}\text{FN}_5\text{O}_8$.



Scheme 61 - Synthesis of **4-11**. (a) EDC.HCl, HOBt.H₂O, DMF, 55%.

Compound **4-11** was then treated with trifluoroacetic acid in dichloromethane to remove the lysine-associated Boc protecting groups (**Scheme 62**). On removing the solvent, **4-12** was isolated in quantitative yield, supported by the loss of the resonances in both the ^1H and ^{13}C NMR spectrum for the Boc groups, and also the ESI-MS analysis showing a $[\text{M}+\text{H}]^+$ peak at 550.2819, consistent with a molecular formula of $\text{C}_{30}\text{H}_{37}\text{FN}_5\text{O}_4$. The isolation of **4-12** provided the lysine linked antimicrobial component that formed the first key part of target **4-3**.

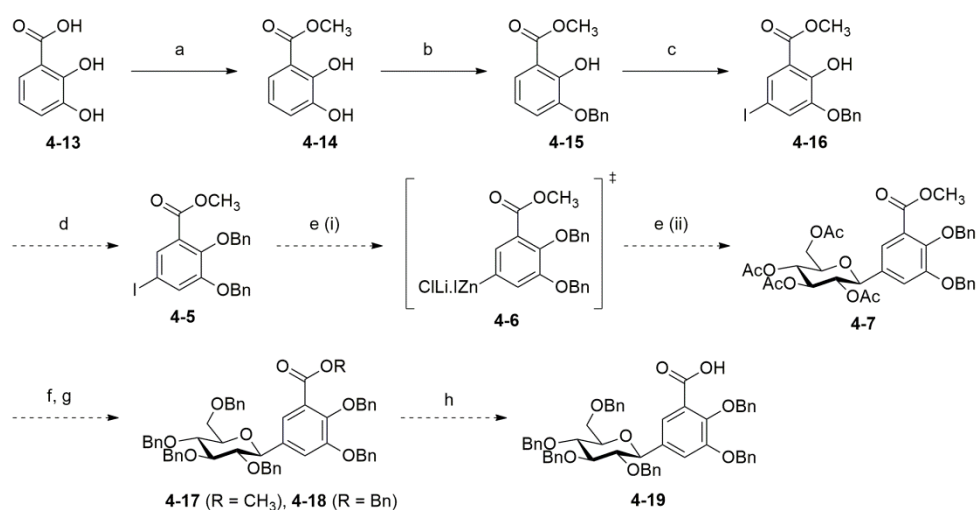


Scheme 62 - Synthesis of **4-12**. (a) TFA, CH_2Cl_2 , quantitative.

Initial synthetic route targeting the glucosylated salmochelin-inspired siderophore component 4-19

The work in this section was completed with the assistance of Ellis Wilde, a PhD student. Ellis worked in collaboration with me to synthesise compound **4-15** to target **4-19** for her research.

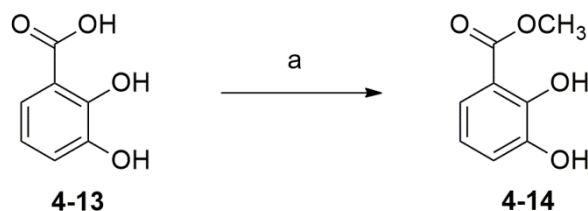
As highlighted in **Scheme 56**, a key intermediate in the synthesis of conjugate **4-3** required the benzyl-protected glucosylated siderophore component **4-19**, which has been reported by Gagné *et al.*^{207, 208} It was decided to follow the published method to synthesise this key intermediate. The synthesis of **4-19** would allow for its later coupling to **4-12**, forming **4-25** in the synthesis towards compound **4-3**, discussed in detail later.



Scheme 63 - Synthesis of the Bn-protected glucosylated salmochelin-inspired siderophore component **4-19** as reported by Gagné *et al.*^{207, 208} (a) MeOH, H₂SO₄, reflux, 90%; (b) K₂CO₃, BnBr, MeOH, 32%; (c) NaClO, NaOH, NaI, MeOH, 14%; (d) BnBr, NaI, K₂CO₃, acetone; (e) (i) Zn, LiCl, I₂, DMF, 70°C, (ii) ^tBu-Terpy, Ni(COD)₂, DMF, acetobromo- α -D-glucose; (f) Na₂CO₃, MeOH; (g) BnBr, Bu₄NI, NaH, DMF; (h) NaOH, THF, MeOH.

Protection of 2,3-dihydroxybenzoic acid 4-13 by esterification to produce 4-14

In order to avoid the unwanted formation of a benzyl ester during the synthetic step to produce **4-15**, it was planned to protect the carboxylic acid with a methyl ester. Commercial 2,3-dihydroxybenzoic acid **4-13** was heated under reflux in methanol with sulfuric acid to give the methyl ester protected catechol **4-14** in 90% yield (**Scheme 64**), following the procedure by Gagné *et al.*²⁰⁷ Formation of **4-14** was supported by ¹H NMR spectroscopy, with the appearance, in the spectrum, of a singlet resonance at 3.96 ppm of relative integration three corresponding to the methyl ester group. ESI-MS analysis also gave a molecular ion peak [M+Na]⁺ for **4-14** at *m/z* 191.0313, consistent with a molecular formula of C₈H₈NaO₄.



Scheme 64 - Synthesis of **4-14**.²⁰⁷ (a) MeOH, H₂SO₄, reflux, 90%.

Mono-benzyl ether protection of 4-14 to produce 4-15

Next it was necessary to selectively protect the hydroxyl group in 3-position of the catechol ring. When mixed with one equivalent of benzyl bromide, selective protection should occur at the 3-position due to its lower *pK_a* value (red - **Figure 46**).^{45, 247} Despite expecting the lower *pK_a* value to be at the 2-position, resulting from increased resonance stabilisation of the hydroxyl anion with the ester functionality, the 3-position in fact has the

lower pK_a value.²⁴⁷ A strong intramolecular hydrogen bond formed between the ester and the *ortho* hydroxyl proton is reasoned to stabilise this proton, increasing the pK_a value for the 2-position (**Figure 46**).²⁴⁷ This observation has been supported by other studies investigating the pK_a values of the hydroxyl protons for both 2,3-dihydroxybenzoic acid and 2,3-dihydroxybenzaldehyde.²⁴⁸⁻²⁵⁰ In each case, the authors also reason that a strong hydrogen bond forms with the hydroxyl proton at the 2-position leading to a higher pK_a value for this proton in each compound.²⁴⁸⁻²⁵⁰ The reason for the selective protection of one catechol moiety to produce **4-15** is to help direct selective iodination at the C-5 position in the later synthesis of **4-16** (**Figure 47**).

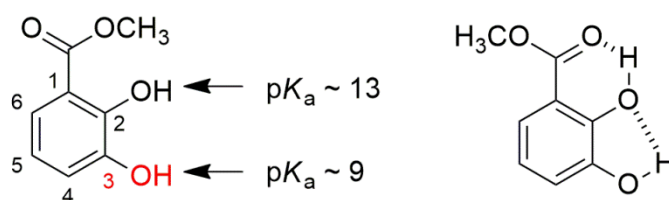


Figure 46 - Difference in pK_a values for the catechol moieties.^{45, 247}

The importance of the free hydroxyl group in **4-15** should be noted. The hydroxyl group is both *ortho* and *para* directing on the aryl ring, relative to itself, due to its electron donating ability (**Figure 47**). Given that each *ortho* position is occupied, the free hydroxyl will therefore direct addition exclusively to the position *para* to itself. While the benzyl ether also directs addition to both the *ortho* and *para* position, again due to its electron donating ability, it has a weaker effect than the free hydroxyl group. Furthermore, the electron-withdrawing ester group is *meta* directing with respect to addition. Combining these resonance effects of the free hydroxyl and ester groups allows selective electrophilic addition at the C-5 position required in compound **4-16** (**Figure 47**).

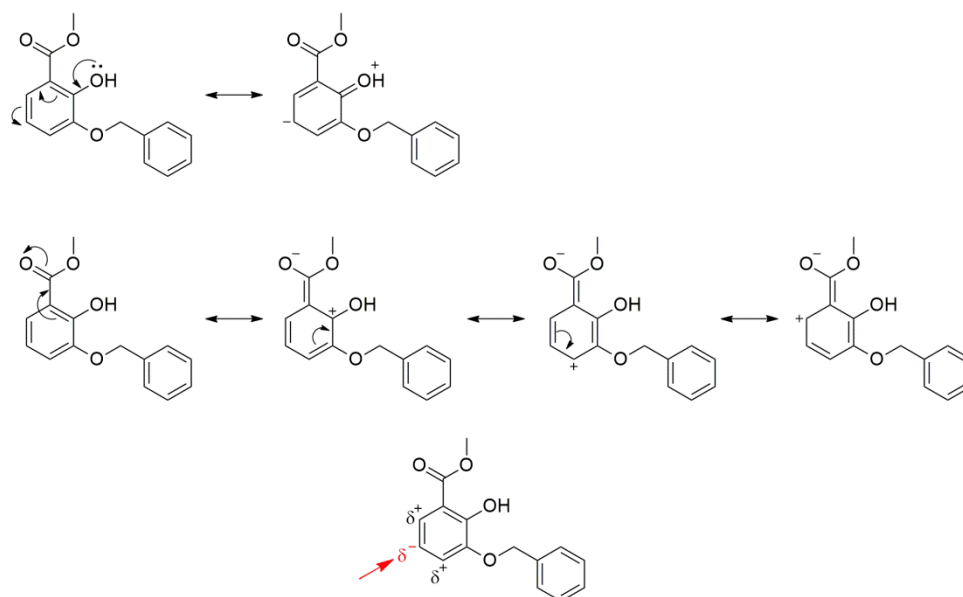
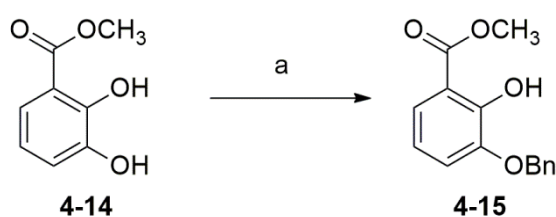


Figure 47 - Simplified illustration of the resonance effects that favour an electrophilic addition in position C-5 (red).

The method of Gagné *et al.* was used. Compound **4-14** was mixed with sodium hydride, followed by the addition of benzyl bromide in a 1:1:1 ratio of reagents, under an inert atmosphere (**Scheme 65/Run 1 - Table 1**).^{207, 208} However, the crude mixture was difficult to separate, and attempts at purification twice by column chromatography gave a mixture of products with an apparent yield of **4-15** of ~31%, against residual starting material.



Scheme 65 - Synthesis of **4-15** as reported by Gagné *et al.*^{207, 208} (a) NaH, BnBr, THF, ~31%.

Run	Electrophile	Base	Anhydrous Solvent	Yield of 4-8 (%)
1	BnBr	NaH	THF	~31 ^a
2	BnBr	NaH	THF	10 ^c
3 ^d	BnCl	K ₂ CO ₃	EtOH	<3 ^b
4 ^d	BnCl	K ₂ CO ₃	MeOH	27 ^c
5 ^d	BnBr	K ₂ CO ₃	MeOH	19 ^c
6	BnBr	K ₂ CO ₃	MeOH	32 ^c
7 ^d	BnBr	DIPEA	MeOH	12 ^c

Table 1 - Conditions used for the synthesis of **4-15**. ^a = Approximate yield determined by the relative integration of the product against residual starting material observed in the ¹H NMR spectrum. ^b = Approximate yield of the product within in the crude ¹H NMR spectrum. ^c = Isolated yield. ^d = Reaction undertaken by Ellis Wilde.

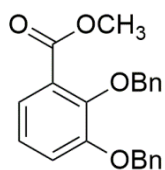
It was decided to apply more rigorous anhydrous conditions, utilising a Schlenk apparatus (Run 2 - **Table 1**), whilst maintaining a 1:1:1 ratio. However, despite the previous run indicating a yield of ~31%, the isolated yield was 10% (**Scheme 65**). The formation of **4-15** was supported by ¹H NMR spectroscopy, with the appearance of a singlet resonance at 5.19 ppm of relative integration two due to the methylene protons of the benzyl moiety. ESI-MS analysis gave a molecular ion peak [M+H]⁺ at *m/z* 259.0964, consistent with molecular formula of C₁₅H₁₅O₄.

It was clear that a 10% yield was too low to continue with the synthetic route to compound **4-19**. As such it was decided to systematically vary the reaction conditions and reagents in order to improve the yield of **4-15**. Variations in the method included the use of potassium carbonate as the base, the change of electrophile to benzyl chloride and the use of ethanol as the solvent in a nitrogen-purged vessel (Run 3 - **Table 1**), conditions successfully utilised for the formation of benzyl ethers,²⁵¹ maintaining a 1:1:1 ratio of reagents. However, there was clear evidence of a partial *trans*-esterification of the methyl ester to the ethyl ester, and an apparent

very low yield of **4-8** of <3% by ^1H NMR spectroscopy. The solvent was changed to methanol (Run 4 - **Table 1**), to avoid *trans*-esterification, leading to an improved isolated yield of 27%.

It was decided to return to the use of the more reactive electrophilic benzyl bromide, although this reagent is more prone to hydrolysis. Unfortunately, the yield dropped to 19% (Run 5 - **Table 1**). Under more rigorously anhydrous conditions, utilising a Schlenk apparatus, the yield was improved to 32% (Run 6 - **Table 1**). The final run saw the use of DIPEA as the base, maintaining the 1:1:1 ratio of reagents. Utilising the Schlenk apparatus, the yield was only 12% (Run 7 - **Table 1**). It was clear the method still required optimisation.

It should be noted that in each attempt, an undesired side product was also isolated, indicated by the presence of two methylene groups in the ^1H NMR spectrum at 5.13 and 5.16 ppm, each of relative integration two. Furthermore, ESI-MS analysis showed a $[\text{M}+\text{H}]^+$ at 349.1431, consistent with a molecular formula of $\text{C}_{22}\text{H}_{21}\text{O}_5$. This data matches that for a dibenzylated product, **4-20**.¹²⁶

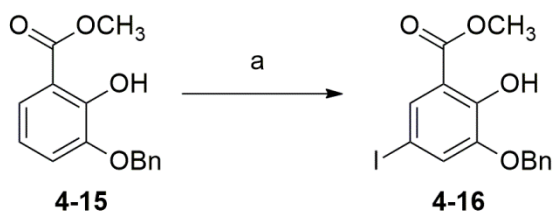


4-20

Electrophilic addition of an iodonium cation to the catechol moiety

Despite the low yields obtained for compound **4-15**, it was possible to investigate the next step of the synthetic route, the iodination of **4-15** to generate **4-16** (**Scheme 63**). The conditions used were originally reported by Gerdes *et al.*, employing reagents for a disproportionation reaction, and were applied by Gagné *et al.* for the specific target.^{207, 208, 252} The iodinated product, **4-16**, would provide the required aryl halide for the later Negishi coupling.

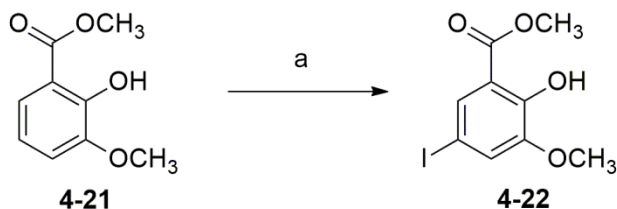
Compound **4-15** was treated with sodium iodide and sodium hydroxide in methanol and the solution cooled to 0 °C, followed by dropwise addition of 10-15% sodium hypochlorite solution (**Scheme 66**). After work-up and purification by column chromatography, compound **4-16** was isolated in 14% yield. Formation of **4-16** was supported by the loss of an aromatic proton in the ¹H NMR spectrum, as well as ESI-MS analysis indicating a [M+H]⁺ at 384.9932, consistent with a molecular formula of C₁₅H₁₄IO₄.



Scheme 66 - Iodination of **4-15** to produce **4-16**. (a) NaClO, NaOH, NaI, MeOH, 14%.

Clearly the yield from the reaction was too low to scale up in the full synthetic route, and consequently an alternative procedure had to be developed. Since compound **4-21** is commercially available, attempts were made to use it as an alternative starting material. Initially a number of test reactions were performed in order to iodinate **4-21** (**Scheme 67**).

Iodination selectively occurs at the C-5 position for the same reasoning as with compound **4-15** (Figure 47).



Scheme 67 - The iodination reaction to produce **4-22**. (a) Sources of 'I⁺'.

The iodination of **4-21** was first attempted using the conditions described by Gagné *et al.*, using 1.5 equivalents of both sodium iodide and sodium hydroxide in methanol, followed by the addition of two equivalents of 10-15% sodium hypochlorite solution.^{207, 208} Formation of **4-22** was supported by the loss of an aromatic proton in the ¹H NMR spectrum, with the remaining two protons observed as doublets, each with a *J* value of 2.1 Hz, indicative of a ⁴*J*_{H-H} split. In addition, formation of **4-22** was supported by a molecular ion peak in the ESI mass spectrum for [M+Na]⁺ at *m/z* 330.9426, consistent for a molecular formula of C₉H₉INaO₄. Unfortunately, the isolated yield of **4-22** was only 4%, indicating that the reaction conditions required further optimisation.

A series of test reactions were designed to determine suitable reaction conditions for the iodination of **4-21**, all using one equivalent of **4-21** (Scheme 67/Table 2). These test reactions included modification of the original conditions previously explored, with changes to the relative ratios of the reagents (entries 1-4, Table 2). Conditions were also explored for iodination using iodine and potassium hydroxide in methanol (entries 5-7, Table 2).²⁵³ Finally, entry 8 (Table 2) saw the use of triethylamine as a base, as a means of avoiding any potential hydrolysis of the ester by the use of sodium hydroxide.

The test reactions showed a marginal improvement in the conversion, by TLC and ^1H NMR of the crude mixture, of **4-21** to **4-22** for entries 5-8. There was no improvement using triethylamine (entry 8 - **Table 2**) and so it was not considered further. The most promising conditions appeared to be for entry 6, yet its isolated yield for **4-22** was only 17%. It was decided not to purify the remaining entries given the potentially very low yields.

Entry	Reagent 1	Equiv. Reagent 1	Reagent 2	Equiv. Reagent 2	Base	Equiv. Base
1	NaI	1	NaClO	1	NaOH	1
2	NaI	2	NaClO	2	NaOH	2
3	NaI	5	NaClO	5	NaOH	5
4 ^a	NaI	2	NaClO	2	NaOH	2
5	I ₂	1	KI	1	NaOH	1
6	I ₂	1.5	KI	1.5	NaOH	2
7	I ₂	3	KI	3	NaOH	4
8	I ₂	1.5	KI	1.5	Et ₃ N	2

Table 2 - Test reaction conditions for the iodination of **4-21** to produce **4-22**. All entries used MeOH as the solvent, except entry 4 where ^a = DMF.

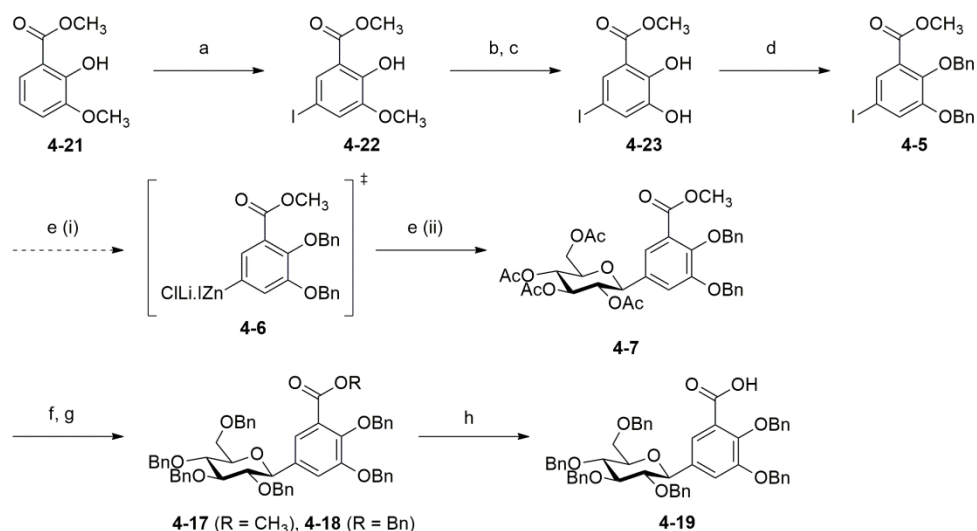
The use of iodine monochloride, with pyridine and silver nitrate in chloroform can result in selective iodination (**Scheme 67/Scheme 68**).²⁵⁴ When these conditions were applied, **4-22** was isolated in 40% yield. Repetition of the reaction saw an improvement in the yield to 68%, with spectroscopic data of **4-22** consistent with that described earlier.

With an improvement in the yield for the iodination of **4-21** to produce **4-22** and the difficulty in obtaining higher yields for the mono-benzyl

protection of **4-14** to produce **4-15**, it was decided to continue the synthesis towards **4-19** *via* compound **4-22**.

Second synthetic route targeting the glucosylated salmochelin-inspired siderophore component 4-19

As shown in **Scheme 68**, the second synthetic route adapts the early steps of **Scheme 63**, with one less synthetic step than that reported by Gagné *et al.*,^{207, 208} giving six synthetic steps rather than seven to obtain **4-19**. Following the iodination of **4-21** to produce **4-22**, described above, it was planned to deprotect the methyl ether using boron tribromide to give **4-23**,²⁵⁵ followed by benzyl ether protection of the hydroxyl groups to yield compound **4-5**. This change in protecting group from the methyl ether to benzyl ethers was decided upon to allow for the final deprotection of **4-25** *via* global hydrogenolysis, conditions known to be high yielding and simple to purify.¹⁴⁰ Therefore, on producing **4-5**, it was planned to continue the synthesis as reported by Gagné *et al.*^{207, 208}

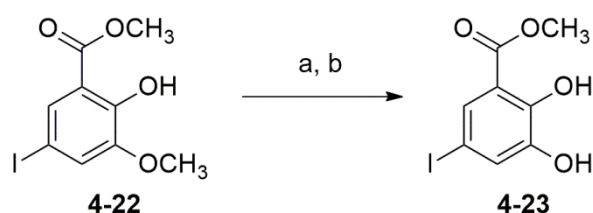


Scheme 68 - Newly developed synthetic route to compound **4-5**. The remaining synthesis of the glucosylated salmochelin inspired siderophore component **4-19** was adapted from Gagné *et al.*^{207, 208} (a) AgNO_3 , ICl , pyridine, CHCl_3 , 68%, (b) BBr_3 , CH_2Cl_2 , (c) MeOH , H_2SO_4 , reflux, 91%, (d) BnBr , NaI , K_2CO_3 , DMF , 72%, (e) (i) Zn , LiCl , I_2 , DMF , 70 °C, (ii) $t\text{Bu-Terpy}$, $\text{Ni}(\text{COD})_2$, DMF , acetobromo- $\alpha\text{-D}$ -glucose, 63% (f) Na_2CO_3 , MeOH , reflux, (g) BnBr , Bu_4NI , NaH , DMF , 74% combined (h) NaOH , THF , MeOH , 87%.

Methyl ether deprotection utilising boron tribromide

Deprotection of the methoxy group of **4-22** was carried out using boron tribromide in dichloromethane,²⁵⁵ to produce **4-23** in 13% yield after recrystallisation. Formation of **4-23** was supported by the loss of a singlet with relative integration of three at 3.86 ppm in the ^1H NMR spectrum, equating to the loss of the methoxy group. In addition, a new singlet resonance at 5.67 ppm with a relative integration of one was observed, corresponding to the new hydroxyl proton. ESI-MS analysis gave a molecular ion peak $[\text{M}+\text{Na}]^+$ at m/z 316.9274, consistent with molecular formula of $\text{C}_9\text{H}_7\text{INaO}_4$. However, repetition did not allow for an improvement in yield from 13% and therefore the crude reaction mixture was analysed.

After quenching the reaction mixture with water, it was observed that there was a mixture of the required product **4-23**, and the free carboxylic acid, which were difficult to separate. As a result, the reaction was developed into a two-stage process, with the boron tribromide reaction first, followed by the immediate re-esterification of the crude mixture using sulfuric acid in methanol (**Scheme 69**). Following work-up, the yield of **4-23** improved to 91%.

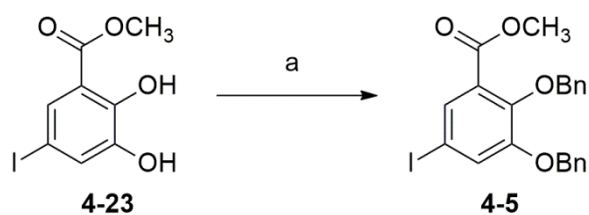


Scheme 69 - Methyl ether removal and re-esterification to produce **4-23**.

(a) BBr_3 , CH_2Cl_2 , (b) MeOH , H_2SO_4 , reflux, 91%.

Benzyl ether protection of 4-23 to produce 4-5

The next stage in the synthesis was the protection of the free hydroxyl groups of **4-23** to give **4-5** (**Scheme 70**). Using benzyl bromide, with sodium iodide as a Williamson's catalyst in DMF, and using potassium carbonate as a base, compound **4-5** was isolated in 72% yield after purification, with data consistent to the literature.^{207, 208} Formation of **4-5** was supported by the presence of two singlets at 5.11 and 5.07 ppm in the ^1H NMR spectrum, both with a relative integration of two, corresponding to the methylene protons of the two benzyl groups. In addition, a multiplet corresponding to the benzyl protons was observed between 7.30 and 7.46 ppm. The formation of **4-5** was also supported by the observation of a molecular ion peak at $[\text{M}+\text{Na}]^+$ at m/z 497.0230 in the ESI mass spectrum, consistent with a molecular formula of $\text{C}_{22}\text{H}_{19}\text{INaO}_4$.

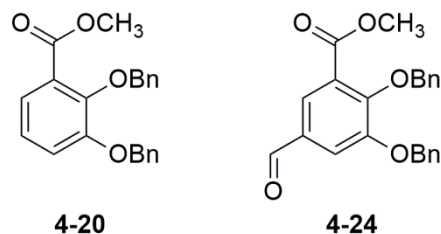


Scheme 70 - Synthesis of **4-5**. (a) BnBr, NaI, K₂CO₃, DMF, 72%.

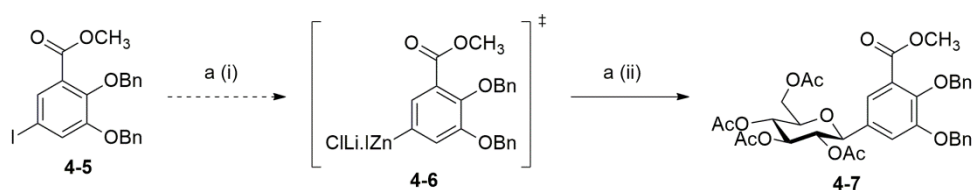
Negishi coupling of acetobromo- α -D-glucose and 4-5 to produce the C-aryl glucoside 4-7

On isolating **4-5**, Negishi coupling with acetobromo- α -D-glucose to produce **4-7** was explored (**Scheme 68** and **Scheme 71**). Given the success of Gagné's approach, their conditions were applied in an attempt to synthesise **4-7**.^{207, 208} In a glove box, zinc and lithium chloride were mixed together and then dried further *in vacuo* on a Schlenk line. To this, a solution of iodine and **4-5** in DMF were added, and then heated overnight at 70 °C, to produce **4-6** (**Scheme 71**). Separately in the glove box, 4,4',4''-*tert*-butyl-2,2':6',2''-terpyridine and bis(1,5-cyclooctadiene)nickel(0) were mixed together in DMF to activate the nickel catalyst, giving a deep blue colour, followed by the addition of acetobromo- α -D-glucose. Once outside of the glove box, the solution of **4-6** was added to the catalyst mixture. However, on purification by column chromatography no product was isolated. It was found that the products formed were the reduced arene **4-20**, and the aldehyde **4-24**, possibly as a result of reaction with the DMF solvent. Formation of the reduced arene product **4-20** was supported by the gain of an aromatic proton in the ¹H NMR spectrum, as well as the loss of the clear ⁴J_{H-H} coupling between the two protons either side of the original iodide. In the case of the aldehyde **4-24**, a 2.0 Hz ⁴J_{H-H} coupling between the two protons either side of the aldehyde group was present, as well as a singlet resonance peak at 9.92 ppm of relative integration one, characteristic of an aldehyde proton. A

new peak at 190.4 ppm was present in the ^{13}C NMR spectrum, characteristic of an aldehyde carbonyl.



For the next attempt it was decided to modify the reaction by reducing the time activating **4-5** to produce **4-6**. Activation was carried out for one hour, followed by addition to the catalyst mixture. After purification the aryl-C-glucoside **4-7** was isolated in 50% yield, with the side products of **4-20** and **4-24** isolated as minor impurities. Repetition saw the yield of **4-7** improve to 63%, a moderate improvement on the reported literature yield of 56%.²⁰⁷ The formation of **4-7** was supported by ESI-MS analysis, with a $[\text{M}+\text{Na}]^+$ peak at 701.2195, consistent with a molecular formula of $\text{C}_{36}\text{H}_{38}\text{NaO}_{13}$. The data was consistent with that reported in the literature.²⁰⁷



Scheme 71 - Negishi coupling reaction of **4-5** to produce **4-7**, first reported by Gagné *et al.*²⁰⁷ (a) (i) Zn, LiCl, I_2 , DMF, 70°C , (ii) $^t\text{Bu-Terpy}$, $\text{Ni}(\text{COD})_2$, DMF, acetobromo- α -D-glucose, 63%.

It was also necessary to confirm the β -stereoselectivity in **4-12**. This could be achieved by analysis of the signal for the anomeric proton at 4.39 ppm

in the ^1H NMR spectrum. Typically, $^3J_{\text{H-H}}$ coupling constants between diaxial protons in a β -configuration have values of 7-9 Hz, whereas coupling between equatorial-axial protons in the α -anomer have coupling constant values of 2-4 Hz.²⁵⁶ In compound **4-12**, the coupling constant for the anomeric proton was 10.1 Hz, thereby confirming that the isolated product was the β -anomer, with no α -anomer isolated or observed.

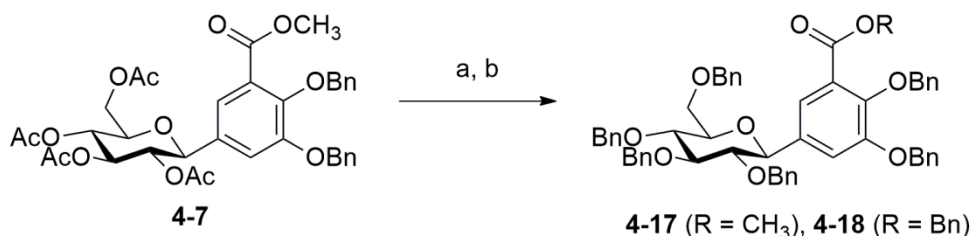
Protecting group manipulation – deacetylation and subsequent benzylation of the glucosyl hydroxyl groups

The next stage of the synthetic route required protecting group manipulation on the glucosyl moiety of **4-7**. While necessary for aiding β -selectivity for the Negishi reaction (**Scheme 53**), the acetate protecting group is base labile,¹⁴⁰ and would cleave under the hydrolysis conditions used to deprotect the ester to produce the carboxylic acid. As such, the change in protecting groups first required the removal of the acetate groups then formation of benzyl ethers to give **4-17** (**Scheme 72**).^{207, 208}

The methodology reported by Gagné *et al.* was followed, first treating **4-7** with sodium carbonate in methanol.^{207, 208} Once the acetate groups were removed, as determined by TLC analysis, the filtered mixture was concentrated *in vacuo*. The residue was dissolved in DMF, and subsequently added to sodium hydride in DMF. A solution of benzyl bromide and tetrabutylammonium iodide in DMF was added (**Scheme 72**). After work-up and purification by column chromatography compounds **4-17** and **4-18** were isolated with a combined yield of 40%. The formation of **4-17** was supported by the presence of multiple methylene groups in both the ^1H and ^{13}C NMR spectra. ESI-MS analysis showing a $[\text{M}+\text{Na}]^+$ peak at 893.3676 consistent with a molecular formula of $\text{C}_{56}\text{H}_{54}\text{NaO}_9$. This data was consistent with the literature.²⁰⁷ In addition, successful formation of **4-**

18 was supported by the ESI spectrum showing a $[M+Na]^+$ peak at 969.3977 for a molecule of formula $C_{62}H_{58}NaO_9$.

The yield of 40% was lower than required, and lower than those of the combined 73% of **4-17** and **4-18** reported by Gagné *et al.*^{207, 208} It was found that the first stage acetate deprotection of **4-7** proceeded poorly, with **4-7** being sparingly soluble in methanol. This was overcome by heating the reaction mixture under reflux, increasing the solubility of the starting material. It was also found that the de-protected intermediate was sparingly soluble in DMF, and therefore transfer of the residue to the sodium hydride solution was problematic. The sodium hydride reagent was added directly to the intermediate and the molar ratio of sodium hydride and benzyl bromide were both increased. This was to ensure the complete deprotonation of the free hydroxyl moieties, and that there was sufficient benzyl bromide available. With these modifications the yield was improved to a combined 74%.

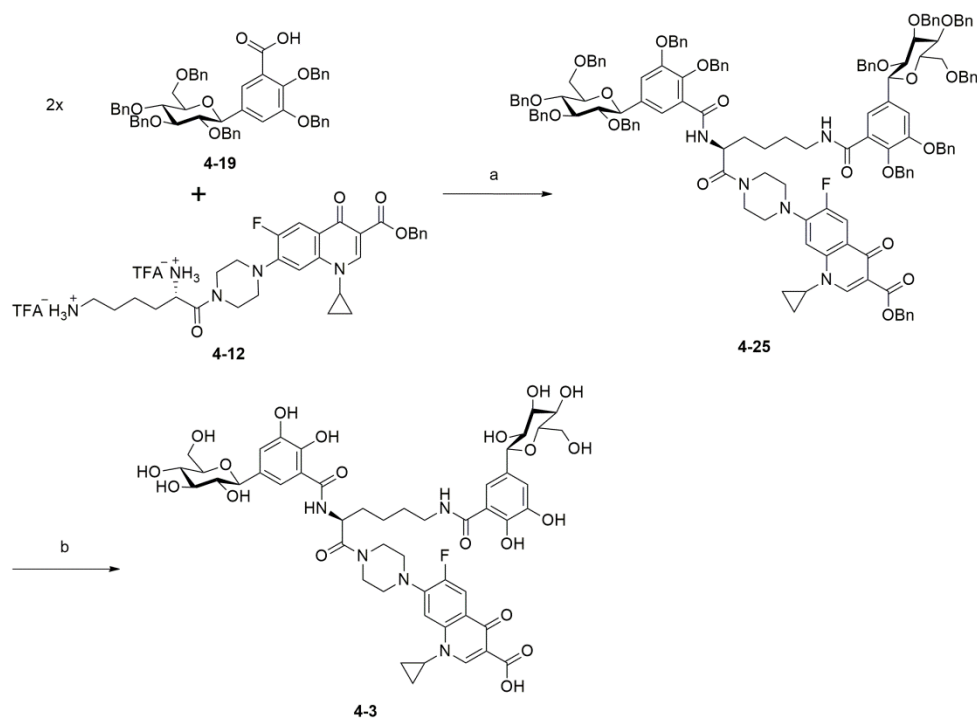


Scheme 72 - Protecting group manipulation to produce **4-17** and **4-18**.²⁰⁷

(a) Na_2CO_3 , MeOH, reflux, (b) BnBr, Bu_4NI , NaH, DMF, 74% combined.

Ester hydrolysis to produce compound 4-15

The isolation of both esters **4-17** and **4-18** allowed for the completion of the synthesis of the glucosylated catechol intermediate **4-19**. A mixture of **4-17** and **4-18** was dissolved in tetrahydrofuran and methanol (3:1), and



Scheme 74 - Coupling of **4-12** and **4-19** to furnish the benzyl protected conjugate **4-25**, followed by hydrogenolysis to yield the target conjugate **4-3**. (a) coupling reagent, (b) Pd catalyst, H₂.

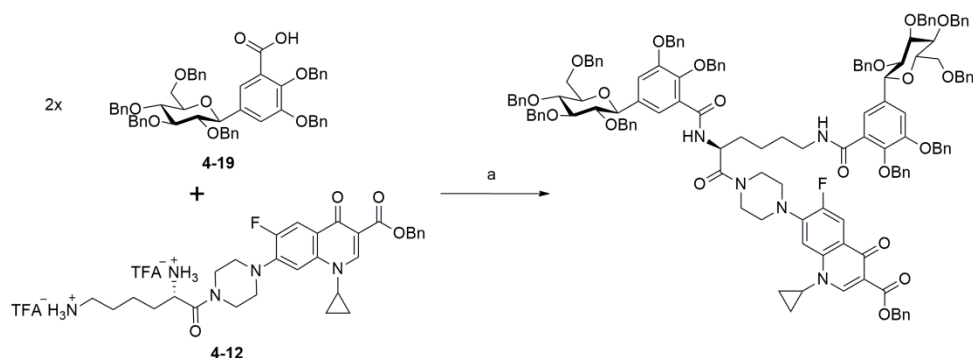
Coupling of 4-12 and 4-19 to give the fully benzylated conjugate 4-25

The first step towards the synthesis of **4-3** was an amide coupling reaction between **4-12** and **4-19** to produce the fully benzylated conjugate **4-25**. During the synthesis of the salmochelins, Gagné *et al.* utilised thionyl chloride to form the acid chloride with catalytic DMF, before the addition of the amine to form the amide bond.^{207, 208} These conditions were trialled, with **4-19** treated with thionyl chloride and DMF in dichloromethane for 3 hours. After isolating the acid chloride, by removing the solvent *in vacuo* on a Schlenk line, a solution of **4-12** in dichloromethane and triethylamine was added and the mixture stirred for 19 hours. Purification by column chromatography gave compound **4-25** in 19% yield. However, replication of these conditions proved problematic with low yields, and in some cases, as evidenced in the ¹H NMR spectrum, partial cleavage of benzyl protecting groups. This de-benzylation may have resulted from the acidic

conditions generated by the formation of hydrogen chloride as a by-product in the acid chloride formation.

Therefore, other amide coupling conditions were explored. The coupling reagent HATU was used due to its wide application in challenging coupling reactions.²⁵⁷ Compound **4-19** and HATU were dissolved in dichloromethane with DIPEA, before the addition of **4-12** in dichloromethane and DIPEA. Despite the use of column chromatography, giving compound **4-25** in 35% yield, there was still unreacted HATU present, with the observation of the PF_6^- counter ion in the ^{19}F NMR spectrum, with a doublet resonance at -73.3 ppm, and a $^1J_{\text{F-P}}$ coupling constant of 712.4 Hz. Whilst it was possible to remove the unreacted HATU *via* further purification, it was decided to find an alternative coupling reagent to avoid this impurity.

A coupling reaction was carried out between **4-12** and **4-19** using EDC.HCl, HOBt.H₂O and DIPEA in dichloromethane (**Scheme 75**). After work up and purification by column chromatography, compound **4-25** was isolated in 42% yield. The formation of **4-25** was supported by ESI-MS analysis, with a molecular ion peak for $[\text{M}+\text{Na}]^+$ at m/z 2249.9665, consistent with a molecular formula of $\text{C}_{140}\text{H}_{137}\text{FN}_5\text{NaO}_{20}$.



Scheme 75 - Synthesis of **4-25**. (a) EDC.HCl, HOBT.H₂O, DIPEA, CH₂Cl₂, 42%.

Furthermore, the ¹³C NMR spectrum supported the isolation of **4-25**, with characteristic carbonyl resonances observed at 164.5 and 164.7 ppm, corresponding to the two amides between the lysine and catechol moieties. A more detailed NMR assignment of **4-25** is discussed in Chapter 5. With the amide coupling reaction indicating that **4-25** was produced, the next synthetic step was to proceed to **4-3** by hydrogenolysis.

Hydrogenolysis of 4-25 to give the target conjugate 4-3

The final stage in the synthesis of **4-3** was to remove the benzyl ether protecting groups on **4-25** by global hydrogenolysis using a palladium catalyst (**Scheme 74**).

It had previously been demonstrated that ciprofloxacin **1-5** containing compounds gave low yields and poor mass recovery when deprotected by hydrogenolysis using palladium on charcoal.²⁵⁸ It was suggested that the poor mass recovery was due to adsorption of either the product or starting material on the catalyst surface.²⁵⁸ Indeed activated carbon has been shown to adsorb ciprofloxacin **1-5**.²⁵⁹ Therefore, compound **4-25** was dissolved in toluene and ethanol and a catalytic amount of palladium black

was added. The resultant suspension was stirred under H₂ at 34 atm. However, despite adding more catalyst and leaving the reaction over a number of days, the deprotection failed to proceed to completion. There was evidence of partial deprotection in the ¹H NMR spectrum of the crude product, yet the spectrum proved complex. An alternative catalyst Pd/C was used with **4-25** in toluene and ethanol, despite the risk that product adsorption to the charcoal support may reduce the yield of the product. These conditions were also not successful in completing the hydrogenolysis of **4-25**.

Other palladium catalysts were considered. It has been suggested that Pearlman's catalyst, Pd(OH)₂/C is particularly effective for the removal of sterically inaccessible and/or multiple benzyl ethers.²⁴⁰ Therefore unsupported Pd(OH)₂ was used with compound **4-25** in DMF under H₂, again resulting in an inconclusive and complex crude mixture, as indicated by the ¹H NMR spectrum.

Finally, 20% wt. Pd(OH)₂/C with **4-25** in a 1:1 mixture of methanol:ethyl acetate resulted in the successful isolation of **4-3** in a crude yield of 80%, with no obvious indication of significant product retention by the charcoal support. After purification by reverse-phase preparative HPLC (**Figure 48**), compound **4-3** was isolated in 45% yield (**Scheme 76**). The isolation of **4-3** was supported by the presence of seven aromatic protons in the ¹H NMR spectrum, with the loss of the benzyl protecting groups within the aromatic region and also the loss of the methylene signals between 4.50-5.50 ppm. Furthermore, ESI-MS analysis showed a [M-H]⁻ peak at 1054.3556, consistent with a molecular formula of C₄₉H₅₇FN₅O₂₀.

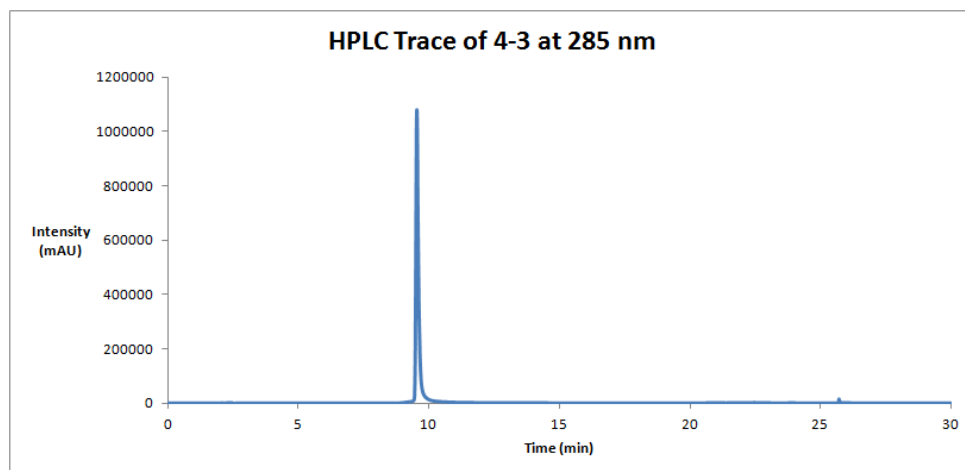
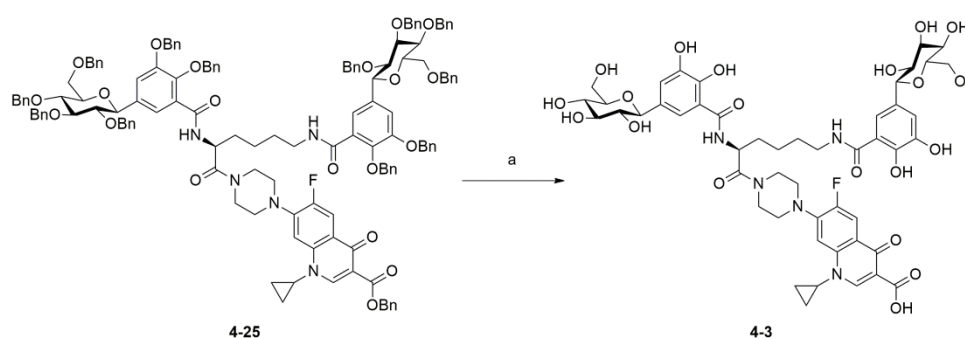


Figure 48 - HPLC trace of **4-3** product at 285 nm after preparative HPLC purification. Conditions: Analytical HPLC Method C (Chapter 7).



Scheme 76 - Hydrogenolysis to produce target **4-3**. (a) $\text{Pd}(\text{OH})_2/\text{C}$ (20% wt.), H_2 , 1:1 MeOH:EtOAc, 45%.

One possible rationale for why $\text{Pd}(\text{OH})_2$ failed yet $\text{Pd}(\text{OH})_2/\text{C}$ succeeded could be based on the function of the charcoal support. A number of investigations have demonstrated that sugar moieties coordinate palladium nanoparticles.²⁶⁰⁻²⁶⁵ Indeed, Sarkar *et al.* established that palladium(II) nanoparticles stabilised by glucose exhibited enhanced ferromagnetic properties under exposure to hydrogen.²⁶⁵ Given the complex nature of the ^1H NMR spectra obtained during the unsuccessful attempts at hydrogenolysis using unsupported $\text{Pd}(\text{OH})_2$, potential reasoning could be that the charcoal support is required to prevent the glucosyl moieties of the deprotected conjugate from coordinating to palladium. This explanation

could possibly be extended further to the failure in palladium black to complete the hydrogenolysis of **4-25**, though steric factors may also be a reason for incomplete removal of the benzyl groups.

In summary, **4-3** was synthesised, with key intermediates **4-10** and **4-19**, which can be used for future salmochelin-inspired Trojan horse conjugates, also produced. The finding that Pearlman's catalyst, Pd(OH)₂/C, can be utilised for complete global deprotection of the benzyl protecting groups on both the glucosyl and antimicrobial moieties allows for the conditions to be applied to future target compounds. The isolation of compound **4-3** allowed for an investigation into its antimicrobial activity.

4.4 Antimicrobial Testing of the Salmochelin Inspired Siderophore-Ciprofloxacin Conjugate 4-3

Growth Assay

The antimicrobial activity of **4-3** was assessed against *E. coli* BW25113 wild type in two media, LB nutrient and M9 minimal, mirroring the conditions used in Chapter 2. The OD₆₅₀ values were also taken every 30 minutes over 16 hours on a plate reader at drug concentrations of 0.01 μM, 0.1 μM, 0.5 μM, 1 μM and 10 μM, with a negative control of 0 μM (DMSO). As in Chapter 2, the data presented here is at the time point at 10 hours, where bacterial growth has plateaued (**Figure 49** - **Figure 51** - see Appendix III for individual graphs).

Unfortunately, the growth assay in iron-rich LB media indicates that conjugate **4-3** has no activity against wild type *E. coli* across all of the concentrations tested, with no suppression of growth observed (**Figure 49**).

However, suppression of wild type *E. coli* growth was observed for conjugate **4-3** in iron-poor M9 minimal media, even at the lowest drug concentration of 0.01 μM (**Figure 50**). The disparity between the bacterial growth in these two media can potentially be explained by the different availabilities of iron in these media. Under the iron rich conditions provided by the LB media, it may be that the outer membrane receptors required for the transport of conjugate **4-3** were not expressed, with outer membrane receptors generally not present when sufficient nutrient iron is available.²⁶⁶ In turn, under the iron deficient conditions in M9 minimal media, the expression of outer membrane receptors, such as *IroN*, may have allowed for the uptake of conjugate **4-3**, increasing the intracellular concentration of the drug resulting in antimicrobial activity and therefore reduced bacterial growth (**Figure 50**).

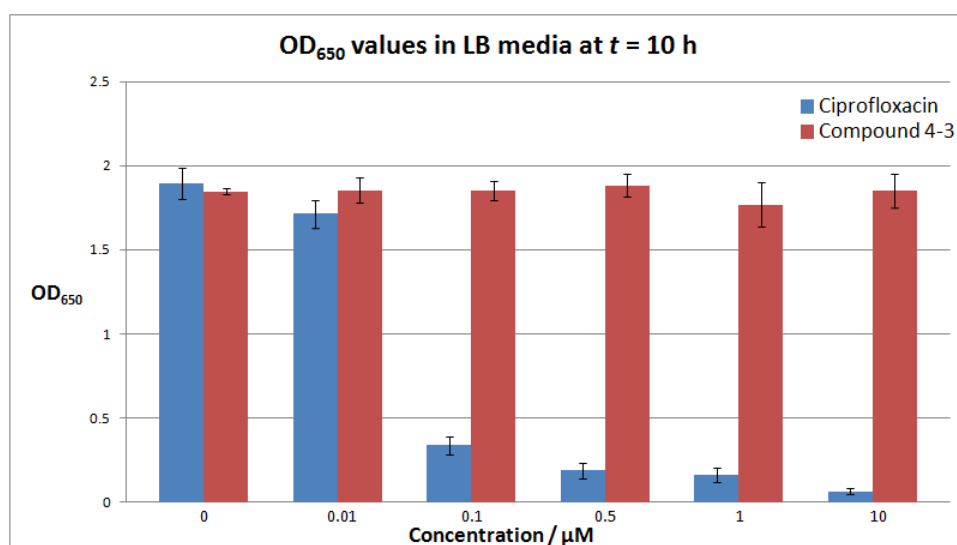


Figure 49 - *E. coli* BW25113WT growth in LB media across concentrations at $t = 10$ h for both ciprofloxacin **1-5** (blue) and conjugate **4-3** (red). The experiment was run in quadruplicate and the error bars show one standard deviation from the mean.

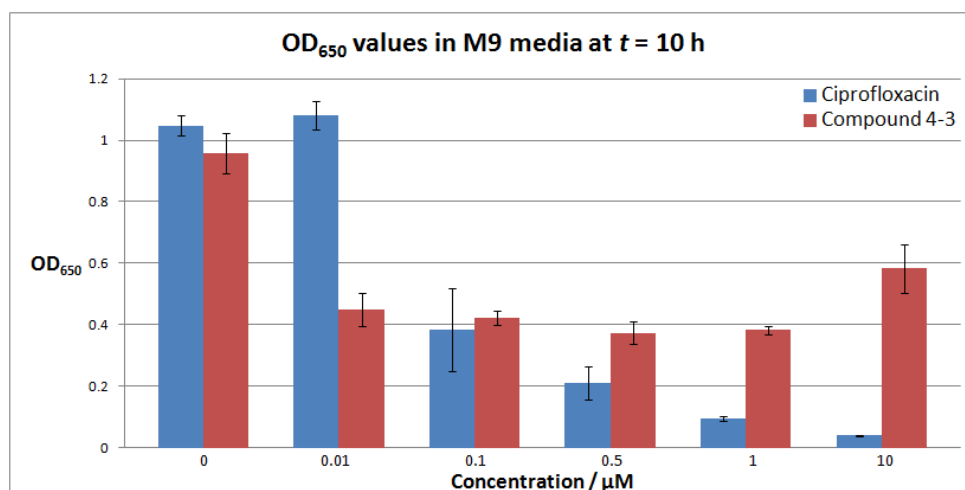


Figure 50 - *E. coli* BW25113WT growth in M9 minimal media across concentrations at $t = 10$ h for both ciprofloxacin **1-5** (blue) and conjugate **4-3** (red). The experiment was run in quadruplicate and the error bars show one standard deviation from the mean.

To test this hypothesis, a growth assay was performed in M9 media, with a controlled Fe(III) concentration. The addition of iron, using ferric chloride at a concentration of 0.2 μM, would provide nutrient iron for bacterial growth, which could in turn reduce expression of the outer membrane receptors required for the transport of conjugate **4-3**. As can be seen in **Figure 51**, the addition of iron resulted in no reduction in wild type *E. coli* growth across any of the concentrations, analogous to the results seen in LB media (**Figure 49**). Indeed the addition of iron to M9 media negated the reduction in growth observed when there was no added iron in M9 minimal media (**Figure 50**). Based on the lack of activity observed for conjugate **4-3** in iron sufficient media, it can again be suggested that under such conditions the uptake of **4-3** is reduced or nullified, resulting in the observed bacterial growth across all concentrations (**Figure 49** and **Figure 51**). However, as mentioned previously in Chapter 2, M9 minimal media best resembles the *in vivo* conditions of a host, where iron concentrations are very low. In turn, the lack of bacterial growth observed in M9 minimal media (**Figure 50**) could again suggest that there is active uptake of conjugate **4-3**.

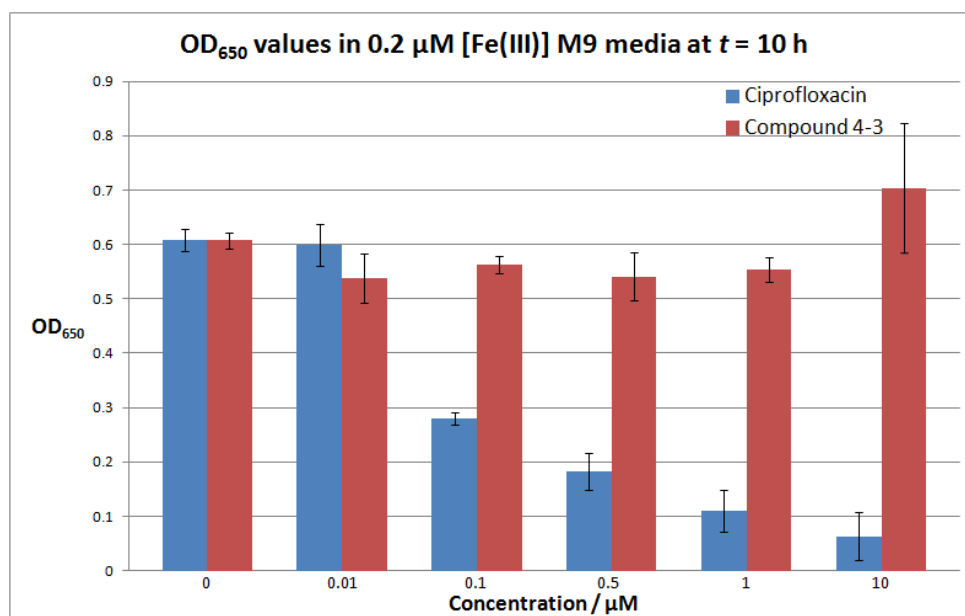


Figure 51 - *E. coli* BW25113WT growth in 0.2 μM [Fe(III)] M9 media, across concentrations at $t = 10$ h for both ciprofloxacin **1-5** (blue) and conjugate **4-3** (red). The experiment was run in quadruplicate and the error bars show one standard deviation from the mean.

However, it should be noted that these growth assays do not determine whether the lack of conjugate activity for **4-3** in iron-sufficient media results from an inability of **4-3** to utilise the active transport mechanisms into the cell, especially as the conjugate would have to pass through both the outer and cytoplasmic membranes to reach the gyrase target. The reduction in bacterial growth observed in M9 minimal media could suggest that conjugate **4-3** is utilising the active transport mechanisms, though this is not conclusive. If the conjugate does not enter the cell *via* active transport, the reduction of bacterial growth observed in M9 minimal media could be hypothesised to result from the extracellular binding of any residual iron in the media by the siderophore moiety of the conjugate, preventing the ability of bacteria to sequester this crucial nutrient. Indeed, Nolan *et al.* found that whilst conjugate **4-2** demonstrated no antibacterial activity against *E. coli* strains which did not express IronN (discussed earlier), it was able to reduce bacterial growth of these strains at a

concentration of 10 μM .⁹⁹ They reasoned that this reduction in bacterial growth resulted from **4-2** sequestering iron in the medium, causing iron deprivation for the bacterial cells.⁹⁹ This hypothesis is however difficult to confirm without further study, especially as it is known that wild type *E. coli* produces enterobactin,²⁶⁷ the tightest iron binding siderophore known, which would likely compete with the siderophore moiety of conjugate **4-3**.

In addition, it was important to determine if the conjugate is able to inhibit the drug target DNA gyrase. It could be argued that if conjugate **4-3** is not actively transported into the cell, then the lack of activity observed in iron rich media could be as a result of disrupted binding of the ciprofloxacin moiety in the gyrase target site, due to steric hindrance of the siderophore moiety.

DNA Gyrase Assay

With one suggested hypothesis that the siderophore moiety is disrupting binding at the DNA gyrase site, it was important to determine if the ciprofloxacin moiety of conjugate **4-3** inhibits the supercoiling of DNA gyrase (Chapter 1), by performing a DNA gyrase assay.

Using the same method as described in Chapter 2, it is apparent that conjugate **4-3** demonstrates no inhibition at concentrations up to 20 μM , (**Figure 52**). It can therefore be argued that the siderophore moiety could prevent the antimicrobial from binding within the active site of DNA gyrase, due to steric hindrance. This would agree with similar findings of siderophore hindrance of DNA gyrase binding for other siderophore-fluoroquinolone conjugates.^{121, 124, 128} However, as discussed earlier in Chapter 2, the DNA gyrase assay directly delivers the compound to the gyrase target *in vitro*, and so only gives a suggestion of conjugate

effectiveness. As the *in vivo* growth assays potentially involve the active transport of conjugate **4-3**, it could be explained that the reduction in growth observed in M9 minimal media results from the increase in intracellular concentration of the drug, especially as expression of the uptake proteins would be increased under iron limited conditions.²⁶⁶ The apparent activity observed at 0.01 μM in the M9 minimal media growth assay (**Figure 50**) is however in contrast to the lack of activity observed up to 20 μM in the DNA gyrase assay (**Figure 52**).

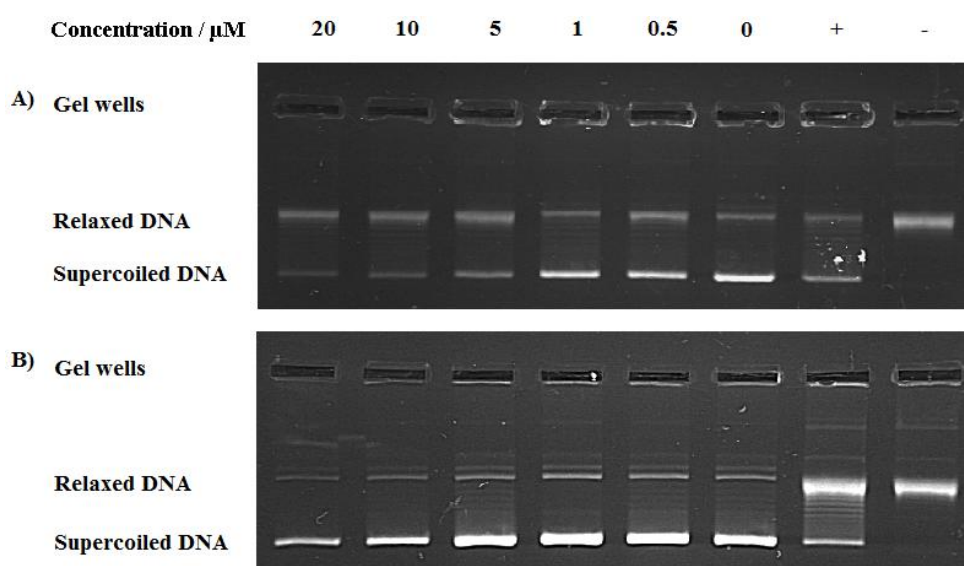


Figure 52 - DNA gyrase assay of **A)** ciprofloxacin **1-5** and **B)** conjugate **4-3** at concentrations ranging from 20-0 μM . 0 μM = DMSO control. + = positive control, with DNA gyrase present without the antimicrobial. - = negative control, no DNA gyrase or antimicrobial.

Despite the lack of DNA gyrase inhibition at concentrations up to 20 μM , it was prudent to determine if conjugate **4-3** retains any activity at higher concentrations. Thus another DNA gyrase assay was performed with concentrations up to 100 μM . As can be seen, the assay indicates that conjugate **4-3** does have inhibitory activity at these higher concentrations (**Figure 53**). The assay suggests that conjugate **4-3** has a MIC value of between 20 and 30 μM , with the observation of a portion of relaxed DNA

gyrase at 30 μM (**Figure 53**). However, complete inhibition is not observed until 75 μM , and thus the concentration required for 100% inhibition is between 50-75 μM (**Figure 53**). With the ability to bind DNA gyrase being key for the antimicrobial activity, it is clear that while conjugate **4-3** demonstrates some inhibitory activity, it is much lower than the free ciprofloxacin **1-5** drug.

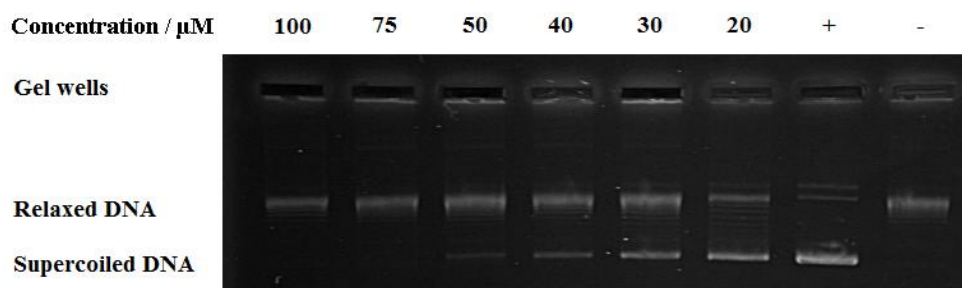


Figure 53 - DNA gyrase assay of conjugate **4-3** at concentrations ranging from 100-20 μM . + = positive control, with DNA gyrase present without the antimicrobial. - = negative control, no DNA gyrase or antimicrobial.

The disparity between the DNA gyrase assays and the bacterial growth assays should be highlighted. The immediate reduction in bacterial growth in M9 media at 0.01 μM (**Figure 50**) could be due to the active uptake of **4-3**, as discussed. However, as **Figure 50** also shows, there is no further reduction in bacterial growth as the concentration of **4-3** is increased. This could in turn suggest that the siderophore disrupts binding of the antimicrobial target site after uptake. On the other hand, the conjugate may not be actively transported at all, or it could be that the concentration of iron was so low that it was a growth limiting factor in the uptake of the conjugate beyond 0.01 μM . In this case adding higher concentrations of the conjugate would not lead to an increase in uptake, leading to the activity of the conjugate levelling off. To support this, it would be suitable to determine the concentration of Fe(III) within M9 minimal media. It could also be that the reduction in growth results from extracellular iron scavenging by the siderophore moiety of the conjugate, preventing the

sequestering of iron by the bacterial cells. This would be similar to findings suggested by Nolan *et al.*⁹⁹ As such, this could explain the reduction in antimicrobial activity observed for conjugate **4-3** in both LB and iron added media (**Figure 49/Figure 51**), as well as the DNA gyrase binding assays (**Figure 52/Figure 53**), compared to free ciprofloxacin **1-5**. However, more data is required to confirm this, including iron binding and uptake studies to determine the iron binding ability and uptake pathway of the conjugate.

4.5 Summary, conclusions and future work

The target compound **4-3**, a conjugate inspired by the salmochelin class of siderophores, was synthesised and characterised. In turn, the synthesis involved the isolation of a number of key intermediates, including compounds **4-10** and **4-19**, which can be used for future salmochelin-inspired conjugates. In addition, the NMR characterisation of these glucosylated compounds, discussed in detail in Chapter 5, allows for the understanding of the complexity of the NMR spectra to aid in the assignment of future glucosylated Trojan horse conjugates.

The activity of **4-3** is lower than that of the parent drug, as determined by the DNA gyrase assay. Furthermore, the gyrase assay indicates that the siderophore moiety disrupts conjugate **4-3** from binding at the target site, and so it is clear that the development of bio-labile linkers, targeted in Chapters 2 and 3, is important for the future development of salmochelin-inspired siderophore-fluoroquinolone conjugates. However, the synthesis of conjugate **4-3** was necessary as it can allow for comparison against future salmochelin-inspired siderophore-fluoroquinolone conjugates which would be designed to incorporate a bio-labile linker.

It is important to understand the function of the siderophore moiety further, and so studies must be conducted to investigate the iron uptake pathway of the conjugate, as well as iron binding studies to determine how well the siderophore moiety captures iron. In turn, the iron binding studies would help determine if the siderophore moiety of conjugate **4-3** is a factor in causing the reduction of wild type *E. coli* growth in M9 minimal media, by determining if the siderophore moiety can compete with the siderophores secreted by the bacteria itself. In addition, determination of transport protein expression for the salmochelins would be essential in establishing if conjugate **4-3** was actively transported. Finally, screening of conjugate **4-3** against siderocalin would determine if the glucosyl moieties prevent binding to the mammalian response protein, so allowing a greater understanding of the potential of salmochelin-inspired Trojan horse conjugates.

**Chapter 5: NMR
characterisation of
compounds 4-19 and 4-25**

5.1 Introduction

The complexity of the NMR spectra for the glucosylated compounds discussed in Chapter 4 needs to be considered. The resonances from the spectra obtained for compounds **4-17** and **4-19** generally match the characterisation data reported by Gagné *et al.*²⁰⁷ However, there are a number of resonances reported which did not agree with those obtained within the present work. For example, Gagné *et al.* report two singlets for two methylene CH₂ groups,²⁰⁷ which in the present work appeared as two pairs of doublets, indicating diastereotopic protons. Additionally, a number of other resonances did not match those reported, highlighted within this Chapter. Furthermore, Gagné *et al.* do not provide an assignment for compounds **4-17** or **4-19**, listing only the relevant resonances obtained for both the ¹H and ¹³C spectra. Whilst the provided data allowed for confirmation that the compounds were isolated in the present work, the assignment of these compounds was necessary to provide understanding towards the assignment of other glucosylated compounds. The assignments of the NMR resonances of these two glucosylated compounds, and those for **4-18** (for which Gagné *et al.* do not report any characterisation data), were therefore made using a combination of HMQC, HMBC and COSY NMR spectra to support the ¹H and ¹³C NMR spectra.

In addition, two novel compounds reported in this thesis, **4-25** and **4-3**, also require characterisation by NMR. This Chapter discusses the NMR characterisation of compound **4-19**, to clarify the reported NMR data by Gagné *et al.*,²⁰⁷ as well as to provide a basis of understanding towards the NMR assignment of **4-25**, also discussed within this Chapter.

5.2 NMR characterisation of Compound 4-19

The successful formation of compound **4-19** was supported by NMR spectroscopy (700 MHz spectrometer). Assignments were made using a combination of Heteronuclear Multiple-Quantum Correlation (HMQC), Heteronuclear Multiple-Bond Correlation (HMBC) and Correlation Spectroscopy (COSY) two-dimensional NMR experiments to confirm proton and carbon environments in the respective one-dimensional ^1H and ^{13}C NMR spectra. For easier visualisation of **4-19** a pullout is provided at the back of this thesis as a reference. Furthermore, the full ^1H , ^{13}C , HMQC, HMBC, COSY and DEPT spectra of compound **4-19** can be found in Appendix IV - **Figures 139-144**.

Assignment of the glucosyl moiety of 4-19

At the start of the assignment process of compound **4-19** it was observed that the anomeric proton, H_{18} (**Figure 54**), was within the expected region of the ^1H NMR spectrum,²⁵⁶ with a doublet at 4.24 ppm (**Figure 55**). Furthermore, the anomeric proton (H-18) demonstrated a coupling constant of 9.3 Hz, which is typical of a $^3J_{\text{H-H}}$ coupling between two diaxial protons for the β -configuration of a carbohydrate moiety.²⁵⁶ On investigating the COSY spectrum (**Figure 56**), the doublet at 4.24 ppm (H-18) was observed to couple with a pseudo triplet at 3.43 ppm, also with a coupling constant of 9.3 Hz. In turn, this pseudo triplet at 3.43 ppm was assigned as H-19, with the coupling constant of this resonance confirming the stereochemistry of the β -configuration.

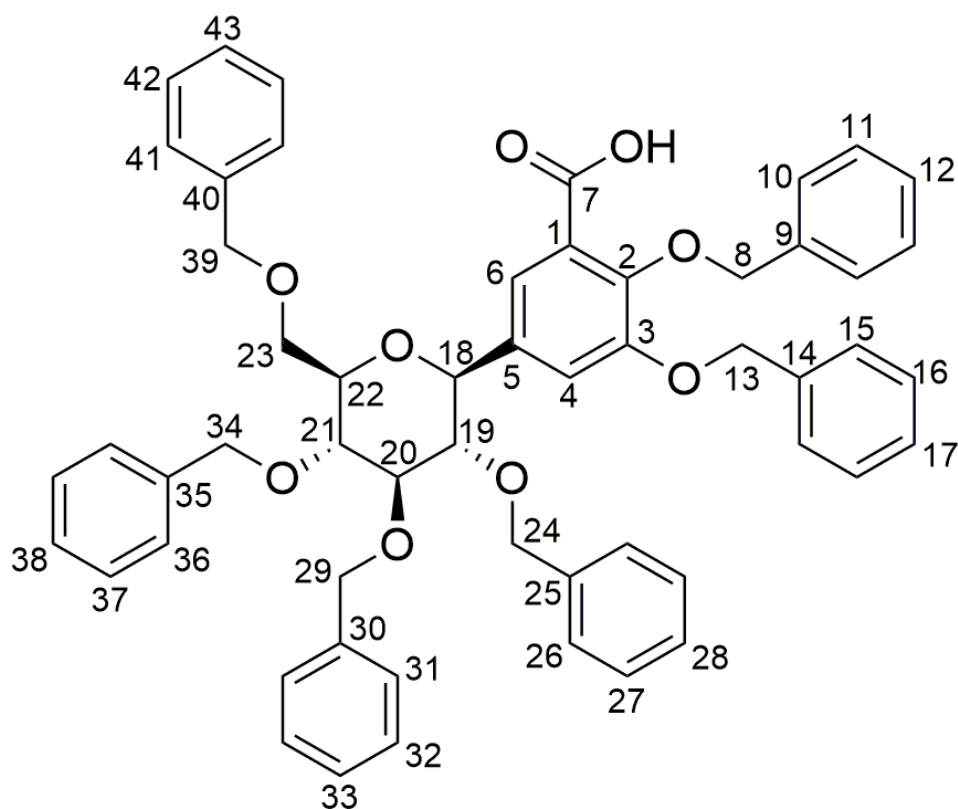


Figure 54 - Full structure of compound **4-19**.

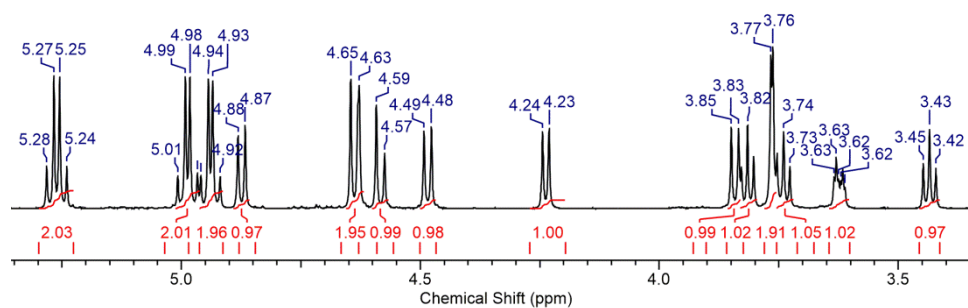


Figure 55 - ^1H NMR spectrum (CDCl_3) of **4-19**.

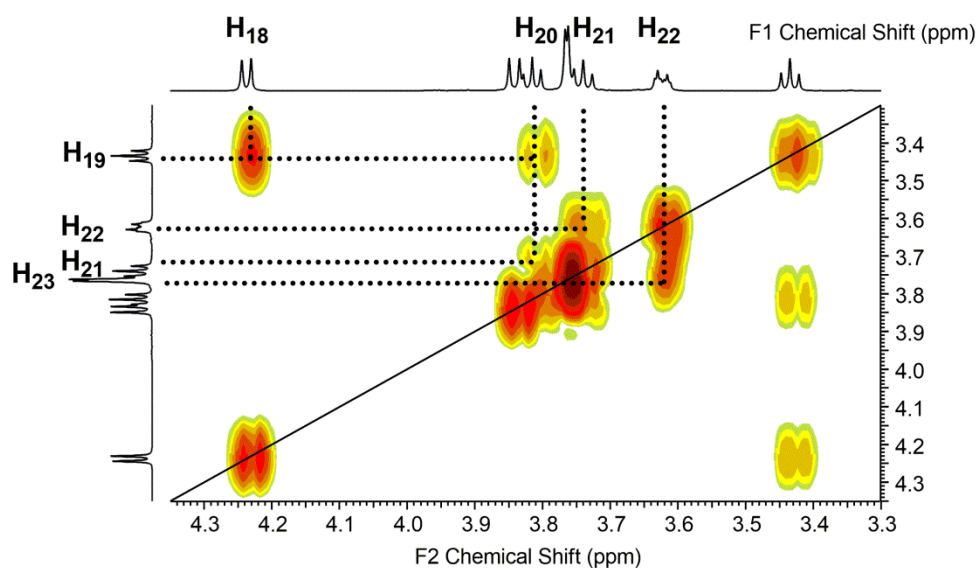


Figure 56 - COSY spectrum (CDCl_3) of **4-19**.

From the pseudo triplet at 3.43 ppm, the COSY spectrum allowed the assignments of the remaining glucosyl protons (**Figure 56**), summarised in **Table 3**. It should be noted that three of these protons appear as pseudo triplets, and there is also some overlap between resonances, demonstrated in both **Figure 55** and **Figure 56**. The doublet of triplets for H-22 at 3.63 ppm was expected, due to its coupling with two unique proton environments, H-21 (pseudo triplet at 3.74 ppm) and H-23 (doublet at 3.76 ppm). In turn, the assignment of H-22 confirms the previous assignments of the glucosyl protons, given the coupling observed between all the proton environments in the COSY spectrum (**Figure 56/Table 3**).

Assignment	¹ H Resonance (ppm)	Multiplicity	COSY Coupled ¹ H Resonance (ppm)	Reported ¹ H Resonance by Gagné <i>et al.</i> ²⁰⁷ (ppm)
18	4.24	d	3.43 (H-19)	4.25 (d)
19	3.43	Pseudo t	3.82 (H-20)/4.24 (H-18)	3.44 (t)
20	3.82	Pseudo t	3.43 (H-19)/3.74 (H-21)	3.70-3.86 (m)
21	3.74	Pseudo t	3.63 (H-22)/3.82 (H-20)	3.70-3.86 (m)
22	3.63	dt	3.74 (H-21)/3.76 (H-23)	3.51 (m)
23	3.76	Overlap d	3.63 (H-22)	3.70-3.86 (m)

Table 3 - ¹H assignments of the glucosyl moiety **4-19** based on COSY coupling in **Figure 56**.

Next the HMQC NMR spectrum was investigated to correlate the proton environments on the glucosyl moiety with their respective carbon environments (**Figure 57**). The carbon environments of the glucosyl moiety are assigned as shown in **Table 4**.

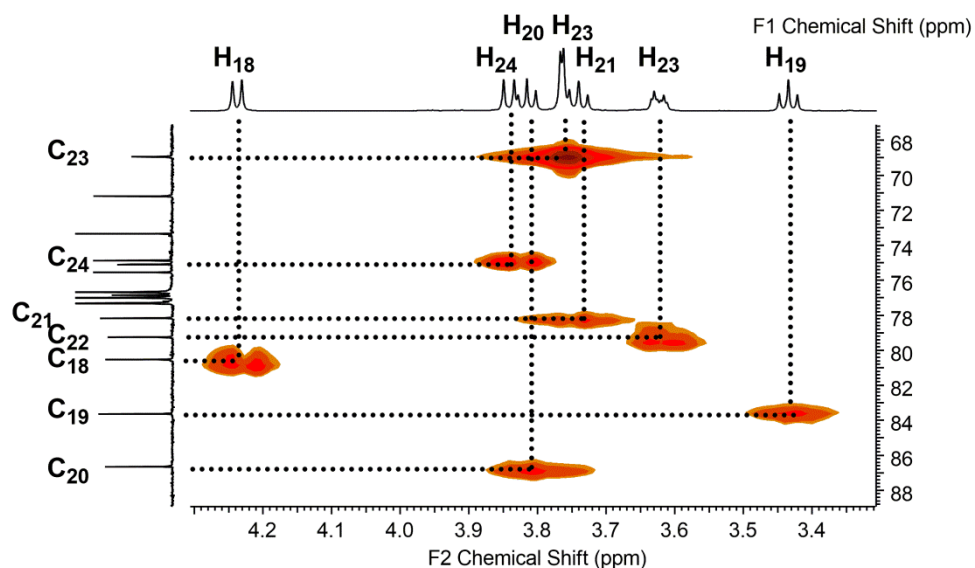


Figure 57 - HMBC spectrum (CDCl_3) of **4-19**.

Assignment	^1H Resonance (ppm)	HMBC Coupled ^{13}C Resonance (ppm)
18	4.24	80.5
19	3.43	83.6
20	3.82	86.7
21	3.74	78.2
22	3.63	79.3
23	3.76	69.0

Table 4 - ^1H and ^{13}C assignment of the glucosyl moiety of **4-19** based on HMBC coupling in **Figure 57**.

To determine the proton and carbon environments of the benzyl protecting groups on the glucosyl moiety, the HMBC spectrum was examined. From the HMBC spectrum, coupling is observed between the pseudo triplet at 3.43 ppm (H-19) with three resonances in the ^{13}C NMR spectrum; 74.9, 80.5 and 86.3 ppm (**Figure 58**). With the resonances at 80.5 and 86.7 ppm previously assigned as C-18 and C-20, respectively, it can be therefore reasoned that the resonance at 74.9 ppm corresponds to the methylene CH_2 group of C₂₄, supported by a negative signal in the DEPT spectrum.

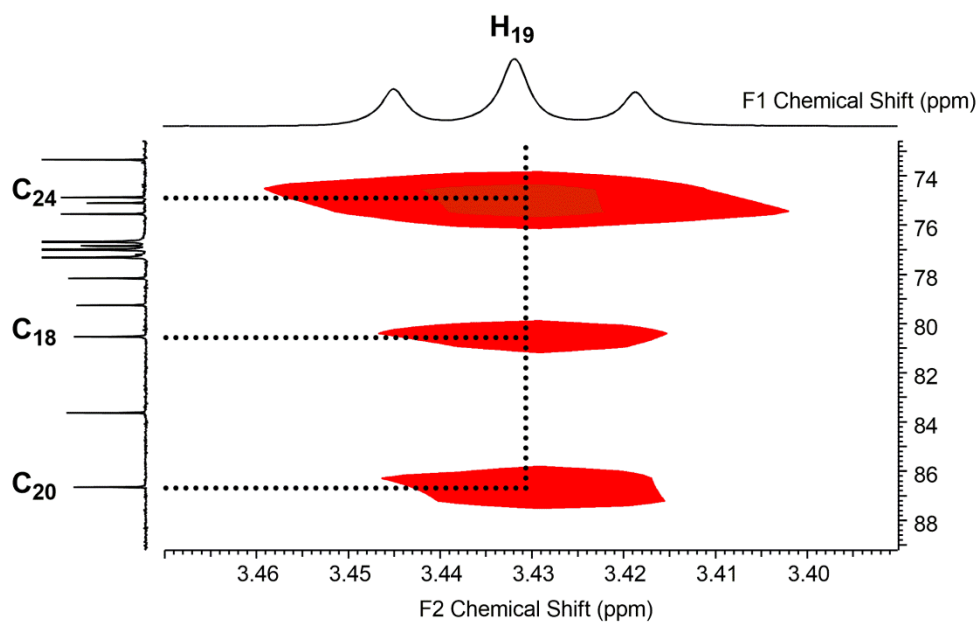


Figure 58 - HMBC spectrum (CDCl_3) of **4-19**.

Based on this assignment for C-24, the HMQC spectrum showed coupling between the resonance at 74.9 ppm in the ^{13}C spectrum and two doublets in the ^1H NMR, at 3.84 ppm and 4.48 ppm, each with a relative integration of one (**Figure 59**). The coupling constants for these doublets are 10.8 Hz, which are typical of geminal $^2J_{\text{H-H}}$ coupling.¹⁷² As such, these doublets were assigned as the two diastereotopic protons H-24^a and H-24^b, as part of an AB system.

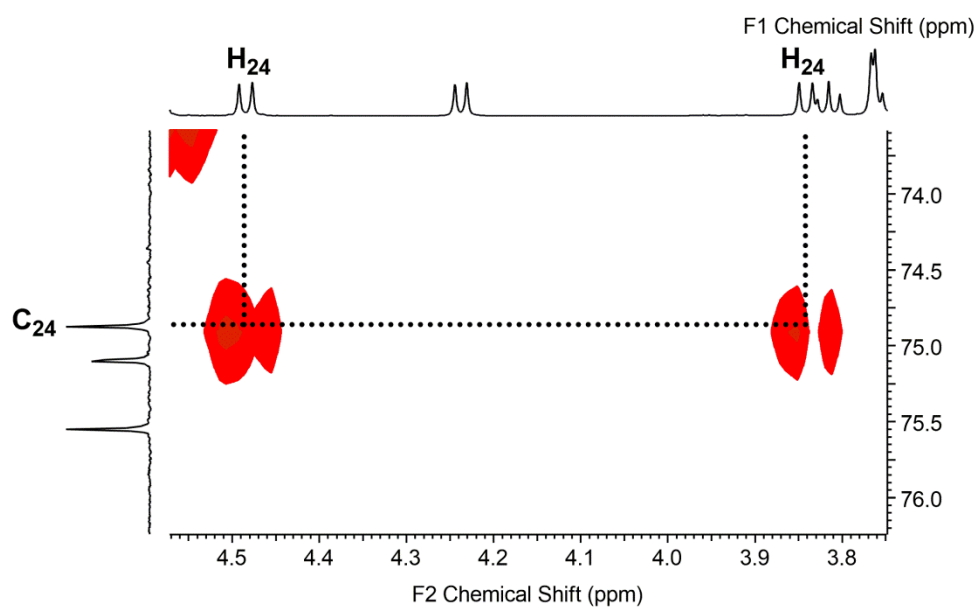


Figure 59 - HMQC spectrum (CDCl₃) of **4-19**.

From the assignment of H-24, coupling was observed in the HMBC spectrum between these diastereotopic protons and a carbon resonance at 137.4 ppm in the ¹³C NMR spectrum (**Figure 60**), which can thus be assigned as the quaternary carbon C-25.

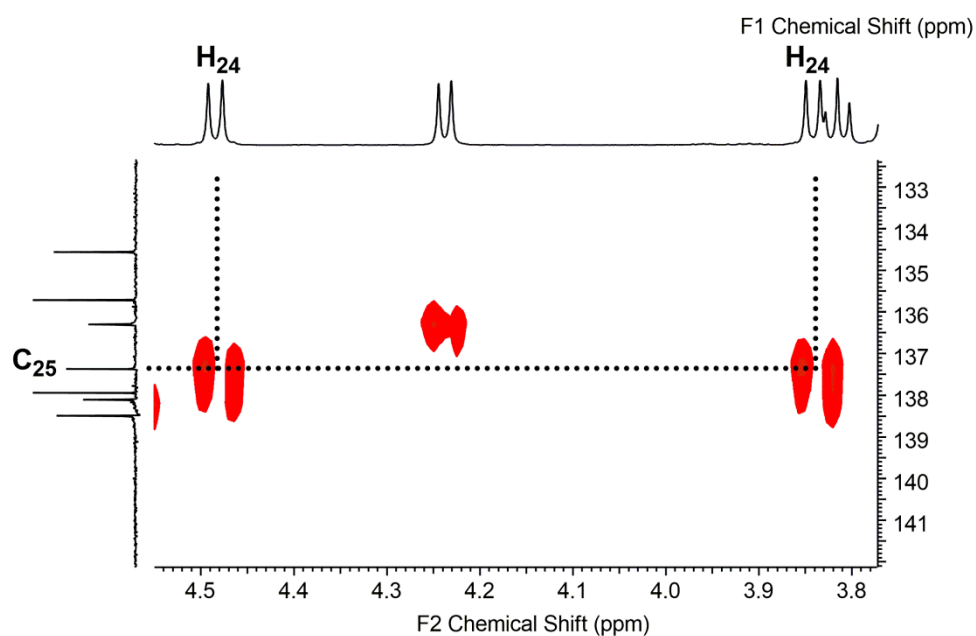


Figure 60 - HMBC spectrum (CDCl₃) of **4-19**.

The same approach described for the assignment of environments H/C-24 and C-25 was also applied to assign the remaining benzylic proton and carbon resonances associated with the glucosyl moiety, summarised in **Table 5**. Furthermore, the doublets assigned to H-29^{a/b}, H-34^{a/b} and H-39^{a/b} demonstrated a roofing effect, due to their diastereotopic nature, as shown in **Figure 61**. Also, it can be seen in **Figure 61** that two doublets overlap at 4.64 ppm, giving an apparent doublet. However, on closer inspection it is possible to see a shoulder on the resonance at 4.63 ppm, which in turn explains why two different carbon resonances couple to this apparent doublet in the HMBC spectrum. It should be noted that Gagné *et al.* report the resonance at 4.95 ppm in the ¹H NMR spectrum as a doublet with a *J* value of 3.3 Hz.²⁰⁷ As **Table 5** shows, this has been clarified in the present assignment as two doublets at 4.93 and 4.95 ppm, each with a *J* value of 11.1 Hz, and herein assigned as H-29^{a/b}.

Assignment	¹³ C Resonance (ppm)	HMQC Coupled ¹ H Resonance (ppm)	HMBC Coupled ¹ H Resonance (ppm)	Reported ¹ H Resonance by Gagné <i>et al.</i> ²⁰⁷ (ppm)
24	74.9	3.84 (d), 4.48 (d)	3.43 (H-19)	3.70-3.86 (m)/4.49 (d)
25	137.4	-	3.84/4.48 (H-24 ^{a/b})	-
29	75.6	4.93 (d), 4.95 (d)	3.82 (H-20)	4.95 (d, <i>J</i> = 3.3 Hz)
30	138.5	-	4.93/4.95 (H-29 ^{a/b})	-
34	75.1	4.64 (d), 4.87 (d)	3.74 (H-21)	4.56-4.67 (m)/4.80-4.90 (m)
35	138.0/138.1	-	4.64/4.87 (H-34 ^{a/b})	-
39	73.4	4.53 (d), 4.64 (d)	3.76 (H-23)	4.56-4.67 (m)
40	138.0/138.1	-	4.53/4.64 (H-39 ^{a/b})	-

Table 5 - ¹H and ¹³C assignment of the benzyl groups associated with the glucosyl moiety based on HMQC and HMBC coupling. Figures supporting these assignments can be found in Appendix IV - **Figures 145-147**. The resonances for the carbons of C-35 and C-40 are indistinguishable.

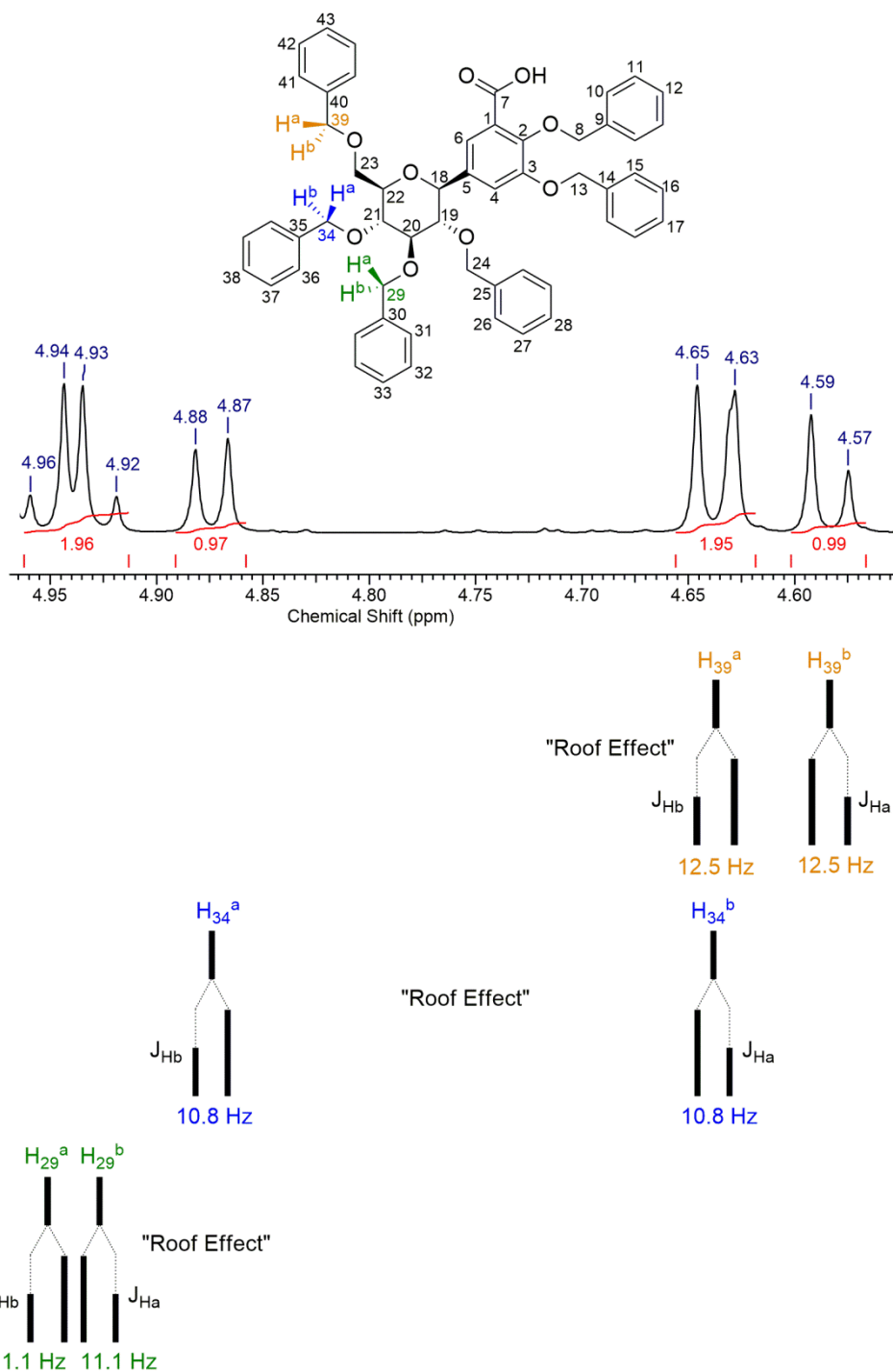


Figure 61 - ^1H NMR spectrum (CDCl_3) of **4-19**. The J-coupling splitting pattern is shown below, explaining the splitting for each of the resonances. *The assignment of H^a and H^b can be interchanged for each region.

It should be highlighted that there are a number of resonances for the aromatic carbons between 127.6 - 129.3 ppm in the ^{13}C spectrum.

Likewise there are a number of protons at 6.94-6.96 ppm and 7.28-7.43 ppm in the ^1H NMR spectrum which cannot be individually assigned to their respective aromatic protons due to the complexity of the HMQC, HMBC and COSY spectra within these regions.

Assignment of the catechol moiety of 4-19

The assignment continued onto the protected catechol acid moiety of **4-19**. Coupling was observed in the HMBC spectrum between the doublet at 4.24 ppm for the anomeric proton (H-18), and a resonance at 136.3 ppm in the ^{13}C spectrum (**Figure 62**), which was therefore assigned as C-5.

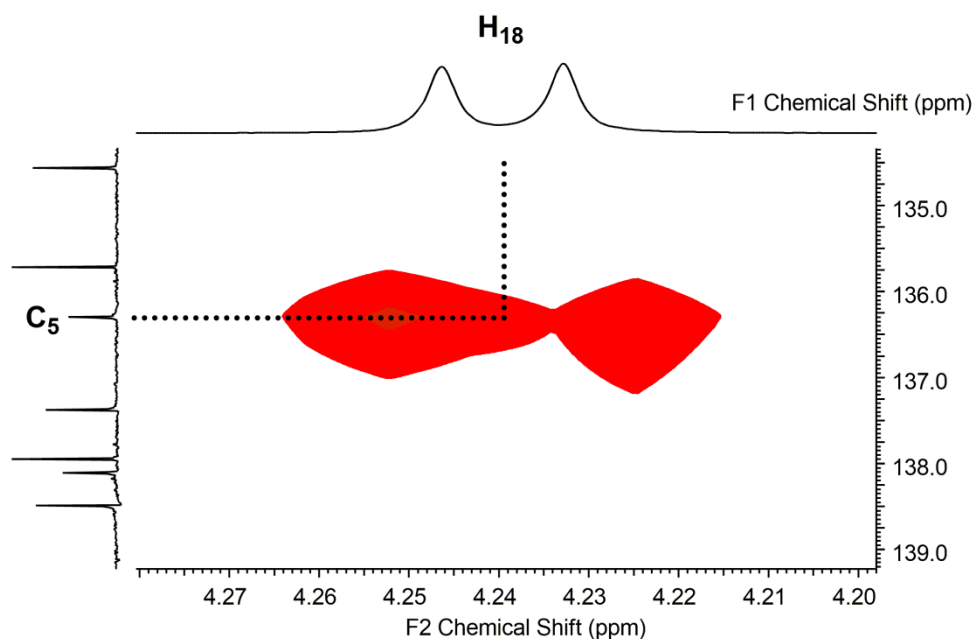


Figure 62 - HMBC spectrum (CDCl_3) of **4-19**.

Coupling was observed in the HMBC spectrum between the resonance at 136.3 ppm (C-5) and a doublet at 7.26 ppm in the ^1H NMR spectrum, for either aromatic protons H-4 or H-6 (**Figure 63**). This doublet at 7.26 ppm (**Figure 64**) has a coupling constant of 1.7 Hz, indicative of a $^4J_{\text{H-H}}$

coupling. Furthermore, the COSY spectrum indicates coupling between the doublet at 7.26 ppm and another doublet at 7.88 ppm, also with a coupling constant of 1.7 Hz (**Figure 65**). It should be noted that Gagné *et al.* report the resonance at 7.88 ppm as a singlet.²⁰⁷

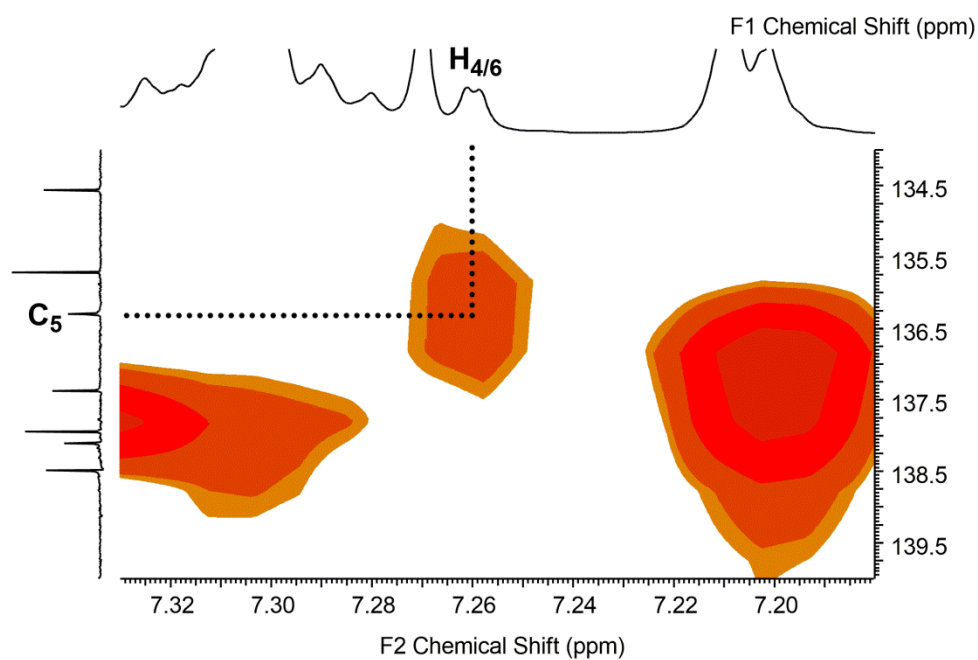


Figure 63 - HMBC spectrum (CDCl_3) of **4-19**.

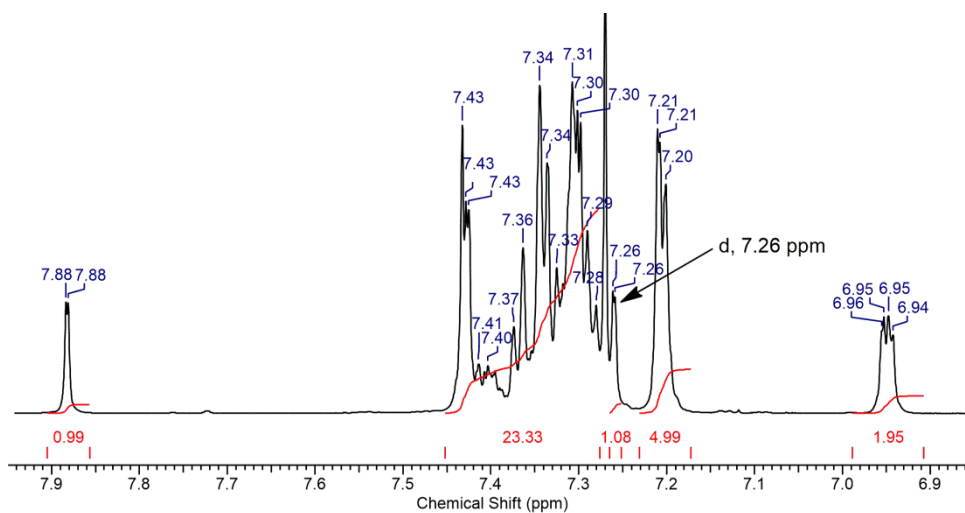


Figure 64 - ^1H NMR spectrum (CDCl_3) of **4-19**.

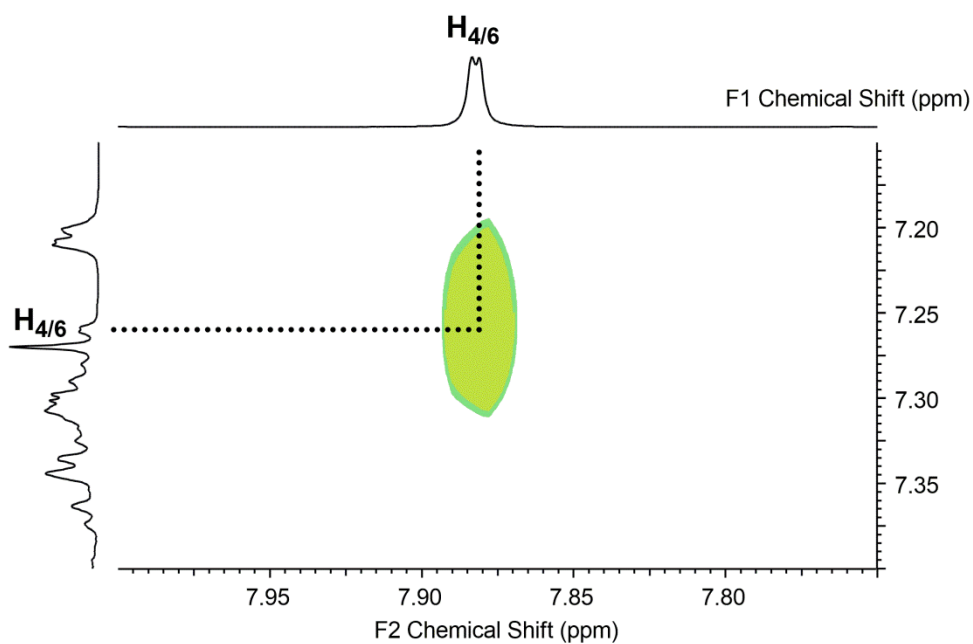


Figure 65 - COSY spectrum (CDCl_3) of **4-19**.

To confirm the assignment of the two doublets at 7.26 and 7.88 ppm as either H-4 or H-6, coupling was observed in the HMBC spectrum between the doublet at 7.88 ppm and a carbonyl resonance at 165.2 ppm, which corresponds to the carboxylic acid C_7 (**Figure 66**). Therefore it can be determined that proton H-6 is the doublet at 7.88 ppm, based on the $^3J_{\text{C-H}}$ coupling observed in the HMBC spectrum, which in turn indicates that H-4 corresponds to the doublet at 7.26 ppm.

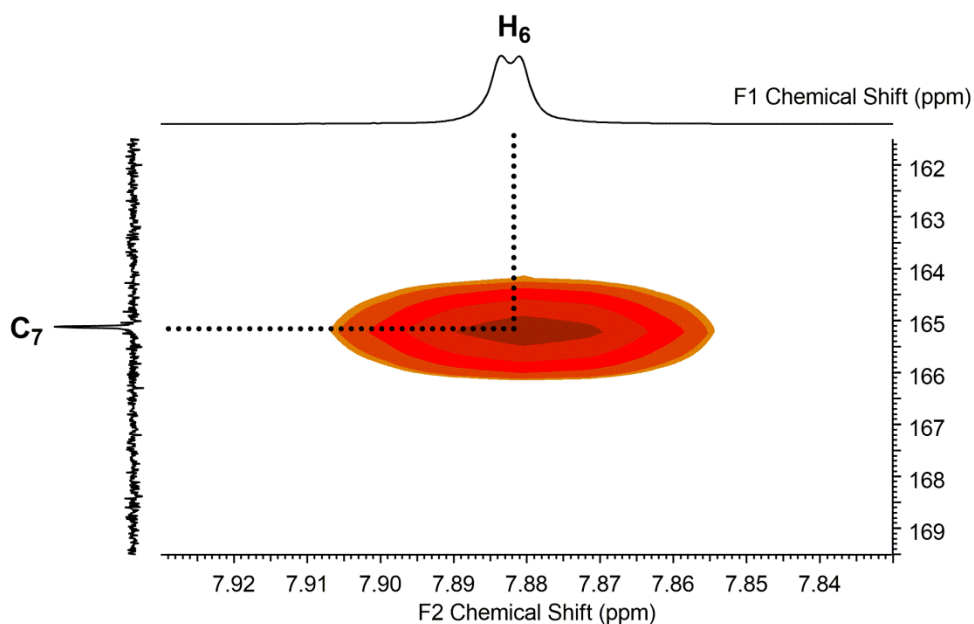


Figure 66 - HMBC spectrum (CDCl_3) of **4-19**.

Based on their proton assignments, the carbon resonances for C-4 and C-6 were assigned by inspection of the HMQC spectrum (**Figure 67**). Coupling was observed between, the doublet at 7.26 ppm (H-4) and a resonance at 117.7 ppm, whilst the doublet at 7.88 ppm (H-6) coupled with a peak at 123.1 ppm. Both these resonances were confirmed as tertiary CH carbons by positive signals in the DEPT spectrum and so C-4 was assigned as 117.7 ppm and C-6 as 123.1 ppm. It should be noted that the peak at 122.8 ppm shown in the HMQC spectrum (**Figure 67**) is not present in the DEPT spectrum, and thus is a quaternary carbon, which is assigned later.

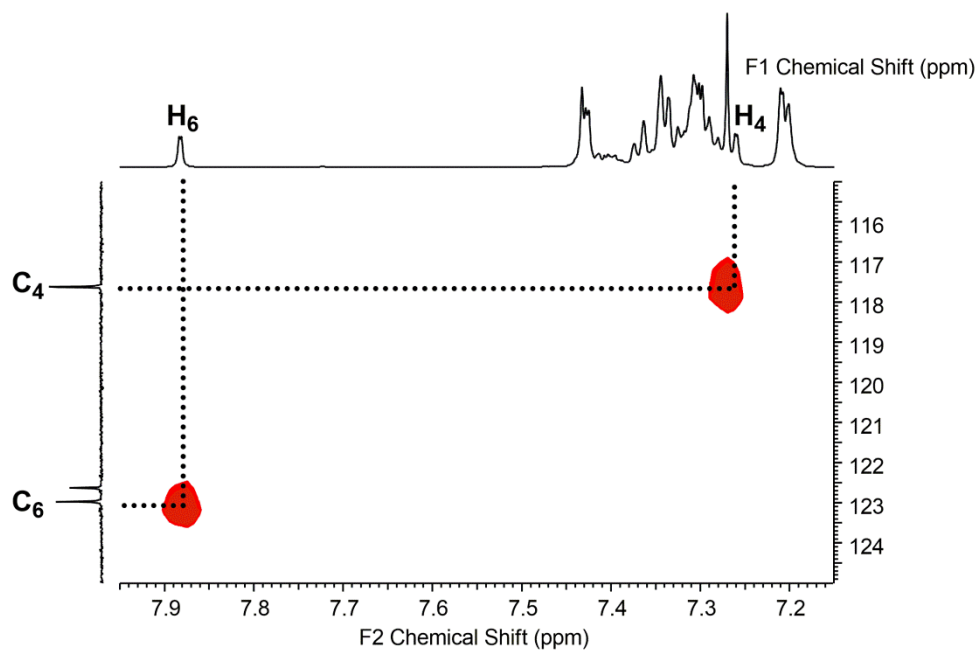


Figure 67 - HMQC spectrum (CDCl_3) of **4-19**.

To determine the quaternary carbons of C-2 and C-3, the HMBC spectrum was examined (**Figure 68**). The spectrum shows coupling between the doublet at 7.88 ppm (H-6) and a resonance at 146.5 ppm, whilst the doublet at 7.26 ppm (H-4) also couples with the resonance at 146.5 ppm, and another at 151.0 ppm. As such it can be determined that the resonance at 146.5 ppm corresponds to C-2, with $^3J_{\text{C-H}}$ coupling to both H-4 and H-6, whilst the resonance at 151.0 ppm relates to C-3, with $^2J_{\text{C-H}}$ coupling to H-4 observed.

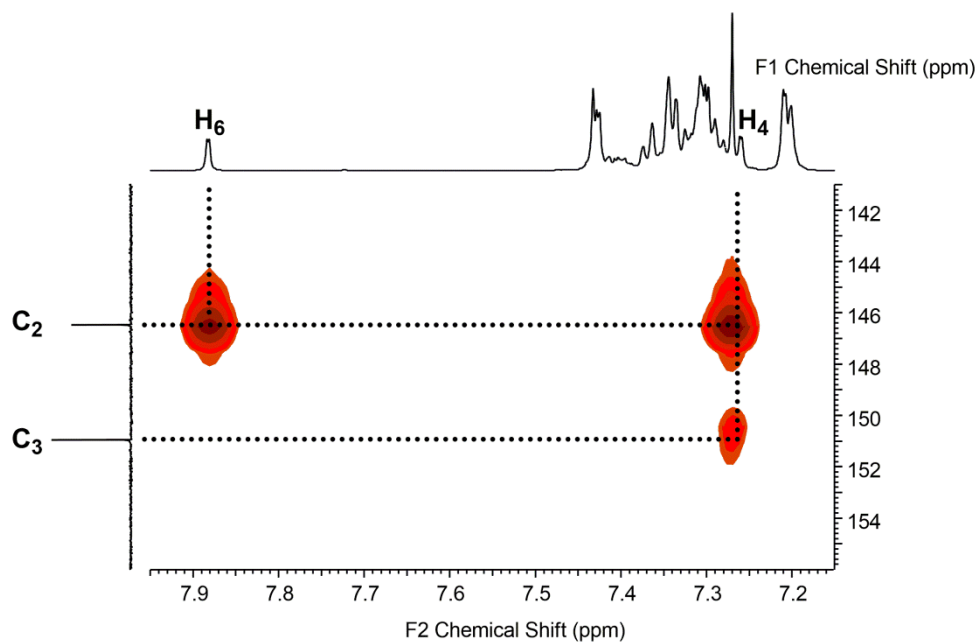


Figure 68 - HMBC spectrum (CDCl_3) of **4-19**.

From the assignments of C-2 and C-3, the assignments of both methylene benzyl CH_2 groups are also possible. From investigation of the HMBC spectrum, it is possible to see coupling between the quaternary carbons of C-2 and C-3 with two pairs of highly roofed doublets for each (**Figure 69**). The coupling observed between 146.5 ppm for C-2 and the two roofed doublets at 5.25 and 5.27 ppm indicates that these correlate to two diastereotopic protons, H-8^a and H-8^b. In turn, the coupling between C-3 at 151.0 ppm and the two roofed doublets at 4.97 and 5.00 ppm indicates that these doublets correspond to the diastereotopic protons H-13^a and H-13^b. It should be highlighted that both of these methylene CH_2 groups were reported by Gagné *et al.* as singlets, at 5.26 and 4.99 ppm respectively.²⁰⁷

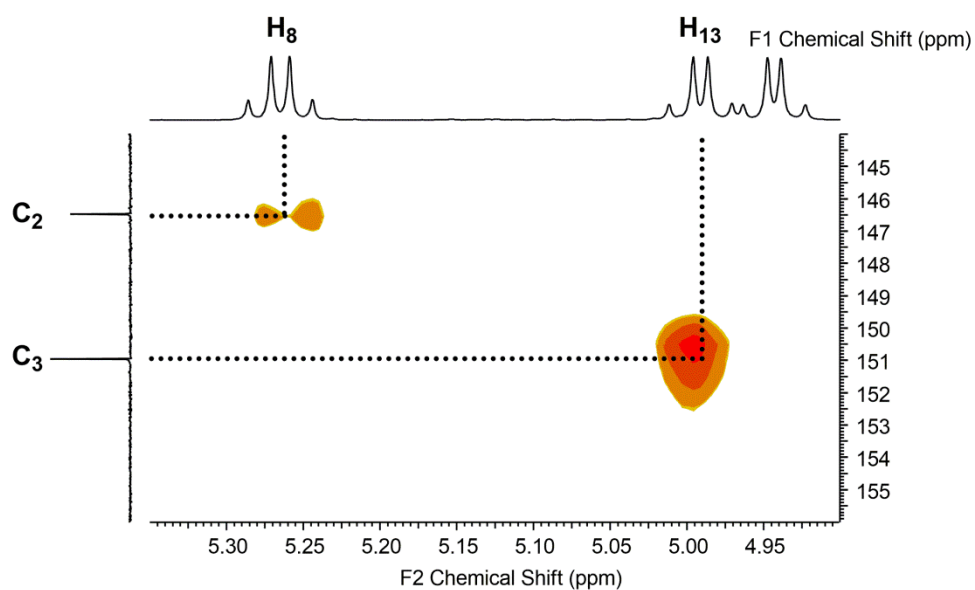


Figure 69 - HMBC spectrum (CDCl_3) of **4-19**.

As such, the HMQC spectrum allowed the assignment of the relevant CH_2 methylene carbons (**Figure 70**). Coupling was observed between the doublets at 4.97 and 5.00 ppm (H-13) with a resonance at 71.2 ppm, thereby allowing this resonance to be assigned as C-13. Subsequently, the resonance at 76.9 ppm (within the residual solvent peaks) can be assigned as C-8, with both resonances confirmed as methylene groups by their negative signals in the DEPT spectrum.

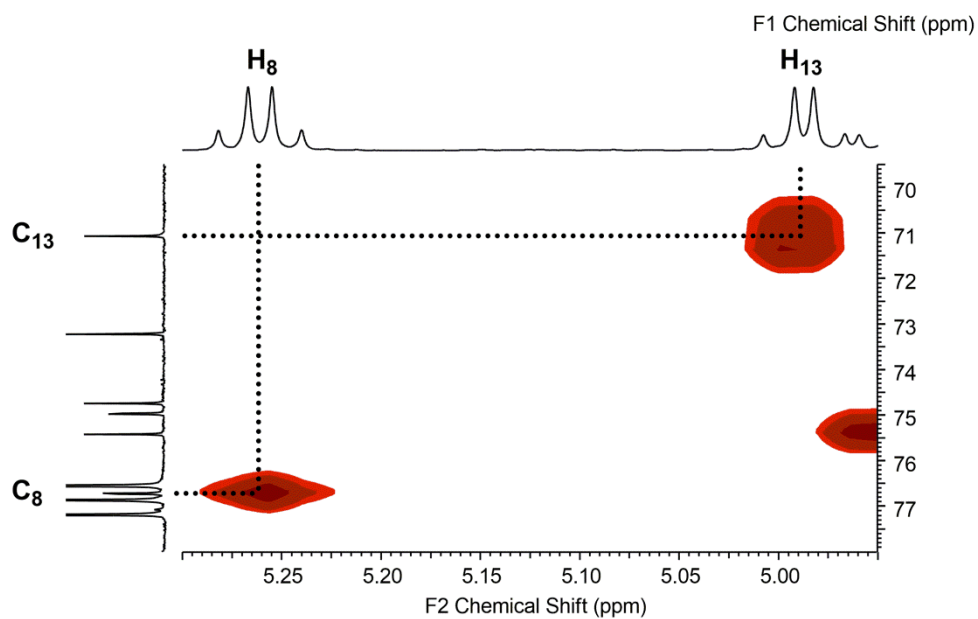


Figure 70 - HMBC spectrum (CDCl_3) of **4-19**.

Investigation of the HMBC spectrum also allowed for the assignment of the benzyl quaternary carbons. As **Figure 71** shows, the doublets at 4.97 and 5.00 ppm (H-13) couple with a resonance at 135.7 ppm, subsequently assigned as C-14, whilst the doublets at 5.25 and 5.27 ppm (H-8) couple with a resonance at 134.6 ppm, allowing its assignment as C-9.

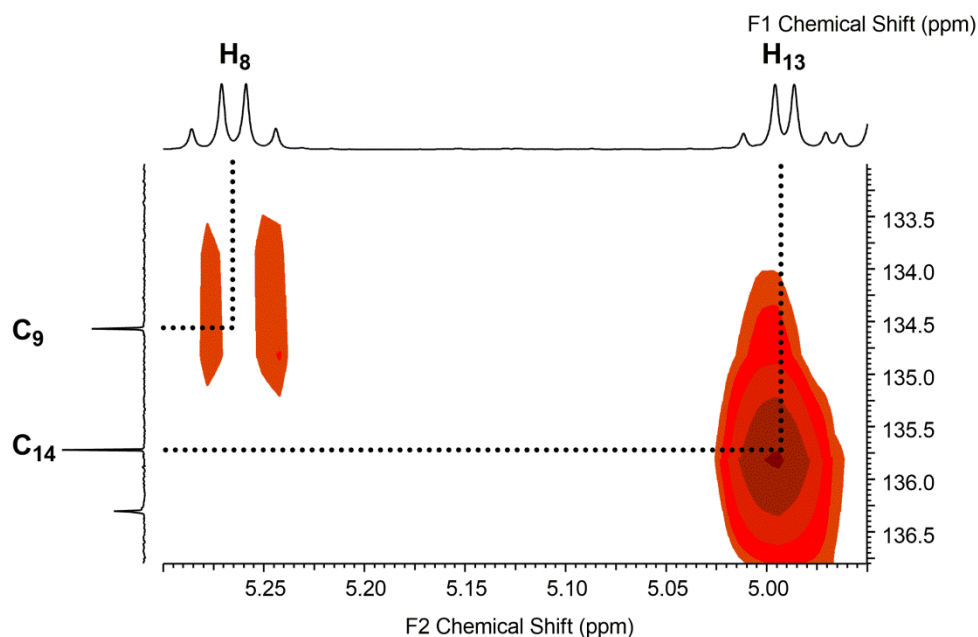


Figure 71 - HMBC spectrum (CDCl_3) of **4-19**.

Despite the successful assignment of nearly all the proton and carbon resonances for compound **4-19**, except some aromatic carbon and proton resonances of the benzyl groups as discussed previously, there remains one unassigned carbon resonance at 122.8 ppm. This resonance is not present in the DEPT spectrum, indicating that it is a quaternary carbon. While this resonance demonstrates no observed coupling in the HMBC spectrum, it can be assigned as the sole remaining unassigned quaternary carbon, C-1.

Summary of the assignment for compound 4-19

The assignment of compound **4-19** is outlined in **Table 6**. This assignment clarifies the ^1H NMR resonances reported by Gagné *et al.*,²⁰⁷ with regards to a number of multiplets and singlets, which are compared in **Table 6**. The assignment of **4-19** facilitated the assignment of **4-7**, **4-17** and **4-18** and also allowed assignment of compound **4-25**, discussed next in this Chapter.

Assignment	¹ H NMR (ppm) / (multiplicity)	¹³ C NMR (ppm)	Reported ¹ H Resonance by Gagné <i>et al.</i> ²⁰⁷ (ppm)
1	-	122.8	-
2	-	146.5	-
3	-	151.0	-
4	7.26 (d)	117.7	6.95-7.43 (m)
5	-	136.3	-
6	7.88 (d)	123.1	7.89 (s)
7	-	165.2	-
8	5.25 (d) / 5.27 (d)	76.9	5.26 (s)
9	-	135.7	-
13	4.97 (d) / 5.00 (d)	71.2	4.99 (s)
14	-	134.6	-
18	4.24 (d)	80.5	4.25 (d)
19	3.43 (pseudo t)	83.6	3.44 (t)
20	3.82 (pseudo t)	86.7	3.70-3.86 (m)
21	3.74 (pseudo t)	78.2	3.70-3.86 (m)
22	3.62 (dt)	79.3	3.51 (m)
23	3.76 (overlap d)	69.0	3.70-3.86 (m)
24	3.84 (d) / 4.48 (d)	74.9	3.70-3.86 (m) / 4.49 (d)
25	-	137.4	-
29	4.93 (d) / 4.95 (d)	75.6	4.95 (d, <i>J</i> = 3.3 Hz)
30	-	138.5	-
34	4.64 (d) / 4.87 (d)	75.1	4.56-4.67 (m) / 4.80-4.90 (m)
35	-	138.0 / 138.1	-
39	4.58 (d) / 4.64 (d)	73.4	4.56-4.67 (m)
40	-	138.0 / 138.1	-

Table 6 - Summary of the assignment of compound **4-19**.

5.3 NMR characterisation of Compound 4-25

The assignment of compound **4-25** was completed using NMR spectroscopy (400 MHz), also through the examination of a combination of COSY, HMBC and HMQC NMR spectra to support the ^1H and ^{13}C NMR spectra. For easier visualisation of **4-25** a pullout is also provided at the back of this thesis as a reference. Furthermore, the full ^1H , ^{13}C , HMQC, HMBC, COSY and DEPT spectra for compound **4-25** can be found in Appendix V - **Figures 148-153**.

Assignment of the ciprofloxacin moiety of 4-25

There are four main components of compound **4-25**, the protected ciprofloxacin antimicrobial, the lysine linker, the protected catechols and the protected glucosyl moieties (**Figure 72**). The starting point for the discussion on the assignment of **4-25** will be the protected antimicrobial (green - **Figure 72**).

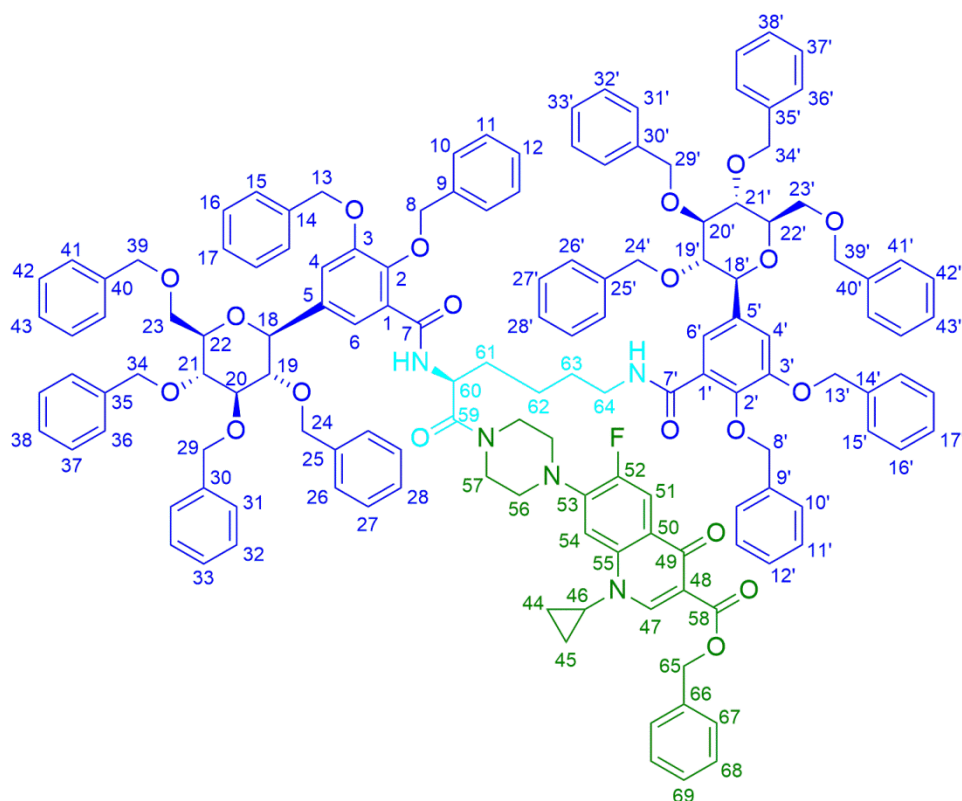


Figure 72 - Full structure of compound **4-25**. Dark blue = protected glucosylated siderophore moiety. Light blue = lysine linker moiety. Green = protected antimicrobial moiety.

The full NMR assignment of free ciprofloxacin in d_6 -DMSO is established,²⁶⁸ which in turn aided the full NMR assignment of compound **4-9** (Chapter 4) in $CDCl_3$ (not discussed). As such, the full assignment of the protected antimicrobial OF **4-25** will also not be discussed, with supporting figures for the assignments given in the appendices where highlighted. With the assignment of ciprofloxacin moieties well understood, the NMR assignment of the antimicrobial moiety of **4-25** is listed later in **Table 7**. However, a few key signals should be highlighted which differ from usual ciprofloxacin related resonances, as well as those which aid confirmation that the antimicrobial and lysine linker moieties are coupled together. Furthermore, it was also necessary to determine that the benzyl protecting group was present.

To start, investigation of the proton assigned as H-47 (8.51 ppm) demonstrated coupling in the HMBC spectrum with two carbonyl peaks in the ^{13}C NMR, 173.0 ppm (C-49) and 165.6 ppm (C-58) (**Figure 73**). In turn, the assignment of the methylene protons H₆₅ were possible due to observed coupling in the HMBC spectrum. Coupling was observed between a carbonyl at 165.5 ppm (C-58) with a singlet of relative integration two at 5.41 ppm in the ^1H NMR (**Figure 74**). Based on this assignment, C-65 was subsequently assigned as 66.3 ppm in the ^{13}C NMR, due to coupling observed in the HMQC spectrum (**Figure 75**), as well as being supported by a negative signal in the DEPT spectrum.

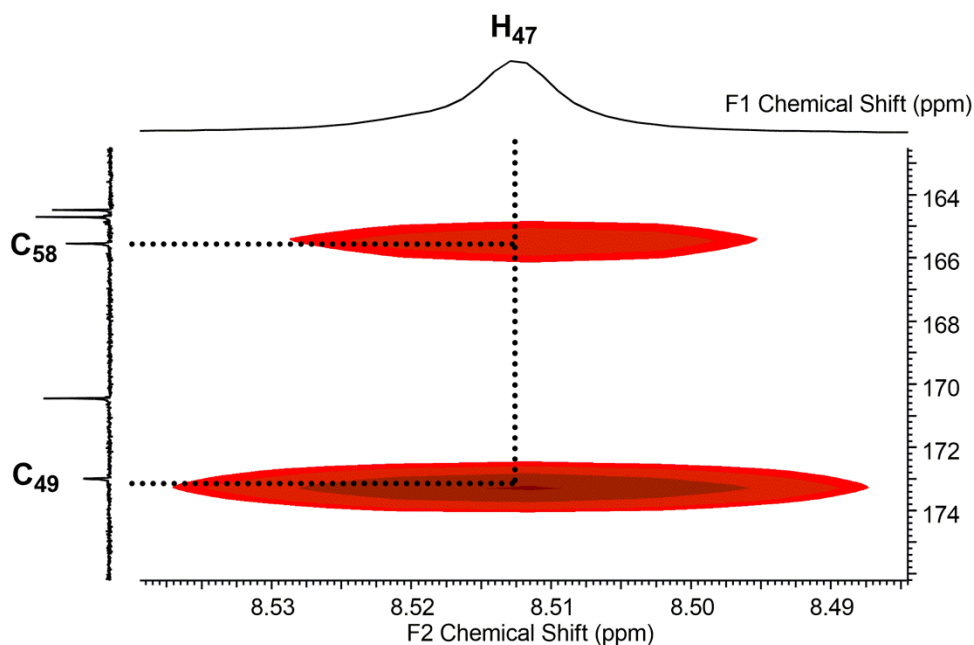


Figure 73 - HMBC spectrum (CDCl_3) of **4-25**.

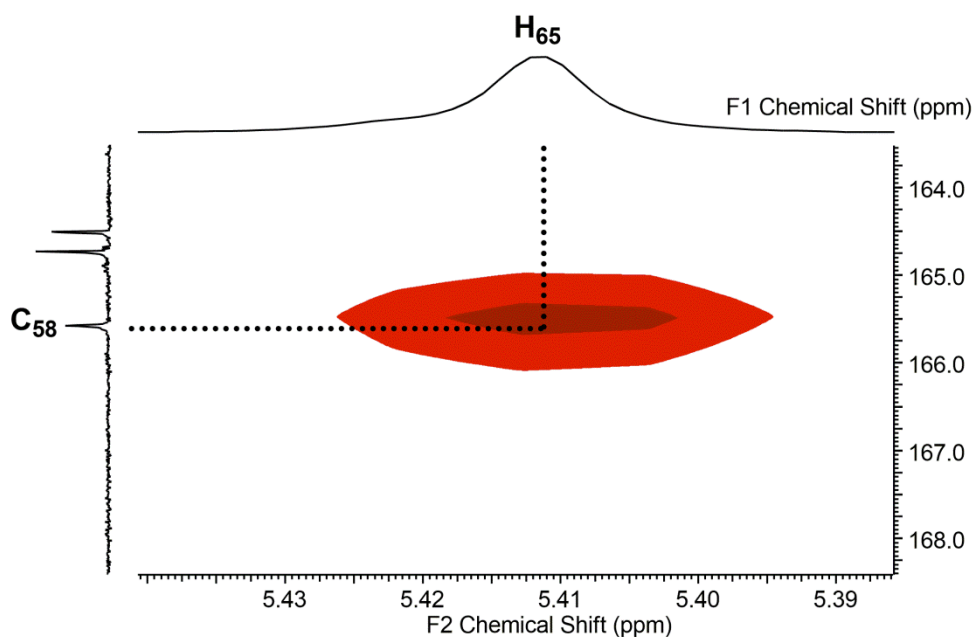


Figure 74 - HMBC spectrum (CDCl_3) of **4-25**.

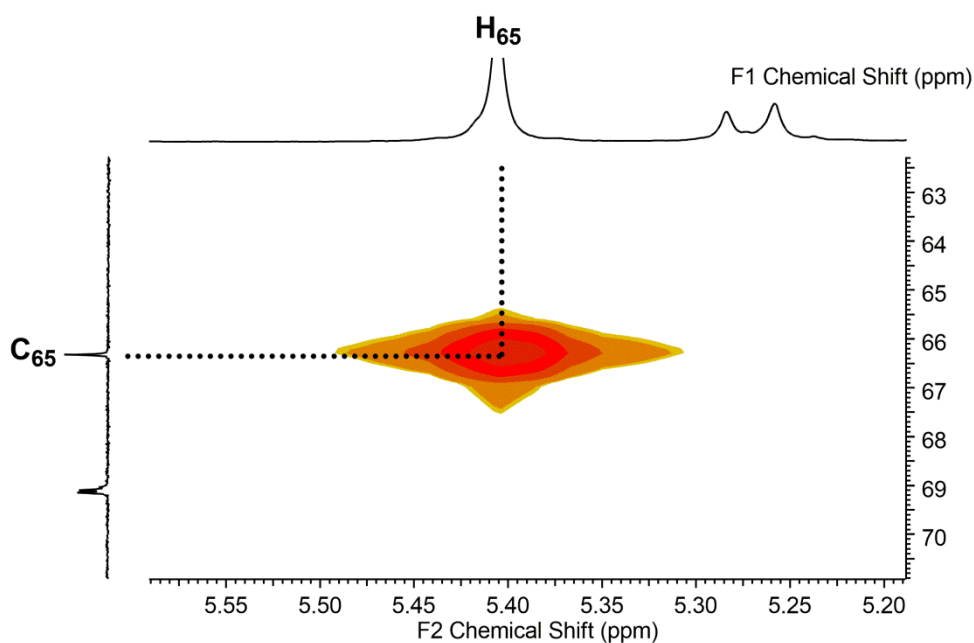


Figure 75 - HMQC spectrum (CDCl_3) of **4-25**.

The assignments of the piperazinyll CH_2 groups are based on their expected proton environments, and subsequent coupling within the HMQC spectrum (**Figure 76**). Interestingly, the protons and subsequent carbons are non-equivalent, likely as a result of the chirality of the lysine moiety. These

proton and carbon environments usually show symmetry, demonstrated in the ^1H spectrum for compound **4-9** (Chapter 4) (**Figure 77**), and so the spectra observed for **4-25**, where the protons and carbons are non-equivalent, indicates that the ciprofloxacin and lysine moieties are coupled together. However, without corresponding HMBC coupling observed from either C-59 (assigned later) or C-53 it is not possible to directly assign H/C-56 or H/C-57, and so they have to be considered as interchangeable. Thus H/C-56 and H/C-57 are assigned as the multiplets 3.22-3.35/3.72-4.01 ppm in the ^1H spectrum, and as 41.9/45.6/49.9/50.2 ppm in the ^{13}C spectrum.

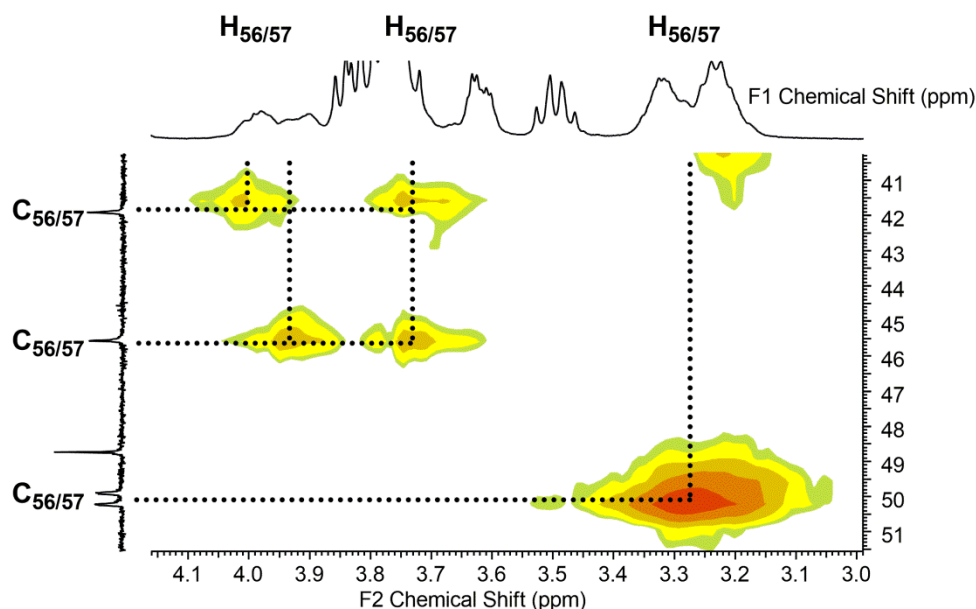


Figure 76 - HMQC spectrum (CDCl_3) of **4-25**.

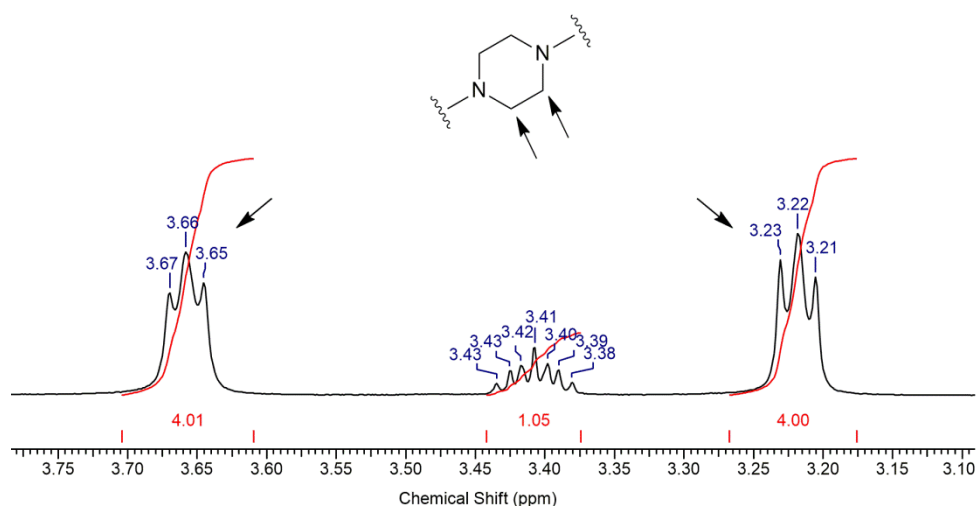


Figure 77 - ^1H NMR spectrum of **4-9** (Chapter 4) (CDCl_3) showing the symmetry of the piperazinyl protons.

It should be noted that there was no observed coupling within the spectra to allow the assignment of C-48. However, based on previous understanding and assignments for other ciprofloxacin based compounds, such as **4-9** (Chapter 4), C-48 was assigned as 110.1 ppm. As such, the full assignment of the antimicrobial moiety is listed in **Table 7**. This assignment of one component therefore supports the isolation of **4-25**, though for confirmation of the isolation of **4-25** the remainder of the assignment must be conducted.

Assign.	¹ H NMR (ppm) / (multi.)	¹³ C NMR (ppm) / (multi.)	Append. V - Figure No.	¹ H NMR Resonance of 4-9 (ppm)	¹³ C NMR Resonance of 4-9 (ppm)
44	1.03 (m) / 1.29 (m)	8.1	164/165	1.13 (m) / 1.31 (m)	8.1
45	1.03 (m) / 1.29 (m)	8.1	164/165	1.13 (m) / 1.31 (m)	8.1
46	3.33 (m)	34.5	162/163	3.42 (m)	34.5
47	8.51 (s)	148.3	161	8.54	148.3
48	-	110.1	-	-	110.1
49	-	173.0	157	-	172.9
50	-	123.5 (d)	156	-	123.3 (d)
51	8.12 (d)	113.5 (d)	154/155	8.09 (d)	113.4 (d)
52	-	153.4 (d)	-	-	153.3 (d)
53	-	144.0 (d)	158	-	144.4 (d)
54	7.17-7.21 (m)	105.3 (d)	159/160	7.53 (m)	105.0 (d)
56	3.22-3.33 (m) / 3.72-4.01 (m)	41.9 / 45.6 / 49.9 / 50.2	-	3.22 (m) / 3.66 (m)	50.0
57	3.22-3.33 (m) / 3.72-4.01 (m)	41.9 / 45.6 / 49.9 / 50.2	-	3.22 (m) / 3.66 (m)	50.0
58	-	165.6	-	-	165.5
65	5.41 (s)	66.3	-	5.40 (s)	66.3

Table 7 - Summary of the assignment of the protected ciprofloxacin moiety of **4-25**, compared to **4-9**. Figures supporting these assignments can be found in Appendix V - **Figures 154-165**.

Assignment of the glucosyl moiety of 4-25

Analogous to compound **4-19**, the assignment of the glucosyl moieties of **4-25** could be started with the anomeric protons. As before, it was known that the two doublets at 4.19 and 4.25 ppm in the ^1H NMR spectrum (**Figure 78**) correspond to anomeric protons on the glucosyl moieties, H-18/18' (**Figure 79**). This assignment is again supported by their typical $^3J_{\text{H-H}}$ coupling constants of the β -configuration, with 9.6 Hz and 9.2 Hz respectively.²⁵⁶

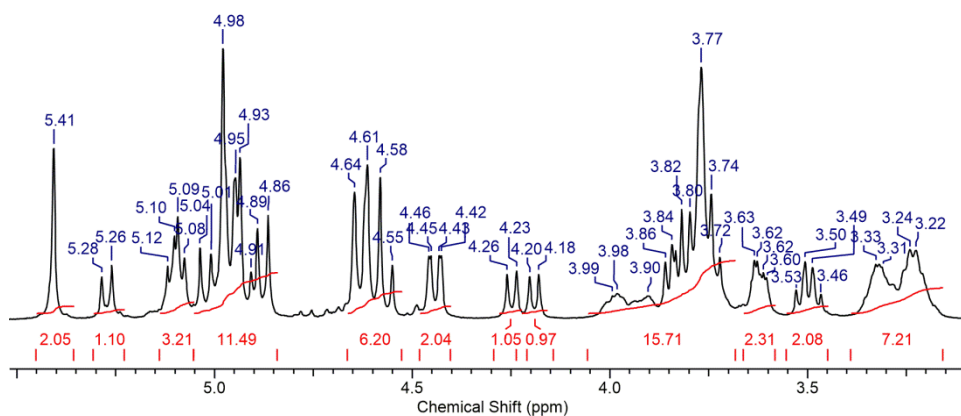


Figure 78 - ^1H NMR spectrum (CDCl_3) of **4-25**.

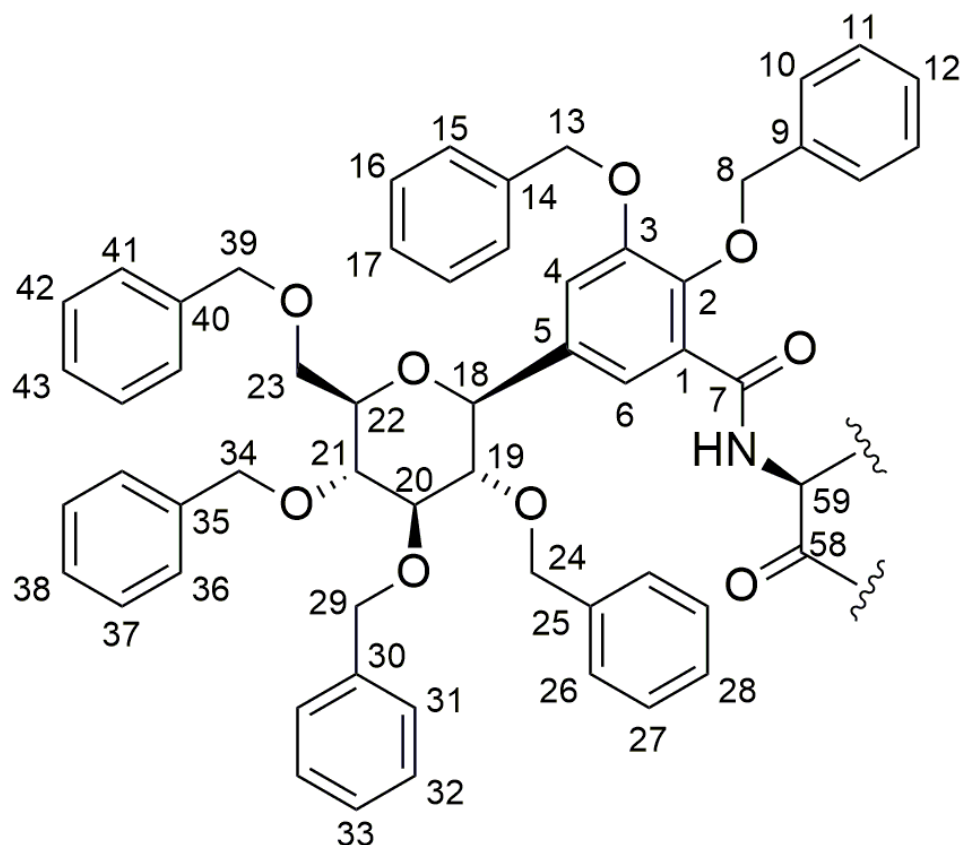


Figure 79 - Expansion of one benzyl protected glucosylated catechol unit of compound **4-25** for ease of reference visualisation.

The chemical shift of the anomeric protons allowed for the continued assignment of compound **4-25** in a manner similar to that employed for compound **4-19** (**Table 8**), and so these will not be discussed in detail. However, the assignments for H/C-20/20', H/C-21/21' and also for H/C-23/23' are much harder to confirm, given the complexity of a multiplet observed between 3.72-3.86 ppm in the ^1H NMR spectrum (**Figure 78**). It could be possible to infer the likely assignments of these resonances, based on the assignment of **4-19** described previously. However, the evidence for the exact confirmation of these resonances is insufficient, meaning the assignments of H/C-20/20'/21/21'/23/23' should therefore be considered as interchangeable (**Table 8**).

Assignment	¹ H Resonance (ppm)	¹³ C Resonance (ppm)
18/18'	4.19/4.25	81.0/81.1
19/19'	3.50	83.8/83.9
20/20'	3.72-3.86	78.3 / 86.6 / 86.7
21/21'	3.72-3.86	78.3 / 86.6 / 86.7
22/22'	3.62	79.3/79.3
23/23'	3.72-3.86	69.1 / 69.2

Table 8 - ¹H and ¹³C assignment of the glucosyl moiety of **4-25**. Figures supporting these assignments can be found in Appendix V - **Figures 166-169**.

Also similar to the assignment of **4-19**, it was possible to assign some of the proton and carbon environments of the benzyl protecting groups. It should be highlighted that in compound **4-25**, the protons H_{19/19'} appear as an apparent quartet, which differs to the pseudo triplet for the analogous proton in **4-19**. From the HMBC NMR spectrum (**Figure 80**), a coupling between the apparent quartet at 3.50 ppm (H-19/19') in the ¹H NMR and 74.8/74.8 and/or 75.1/75.1 ppm in the ¹³C NMR spectrum is seen. Therefore, the methylene CH₂ group of C-24/24' can be assigned as either/or 74.8/74.8/75.1/75.1 ppm in the ¹³C NMR spectrum, also reinforced by negative signals in the DEPT spectrum.

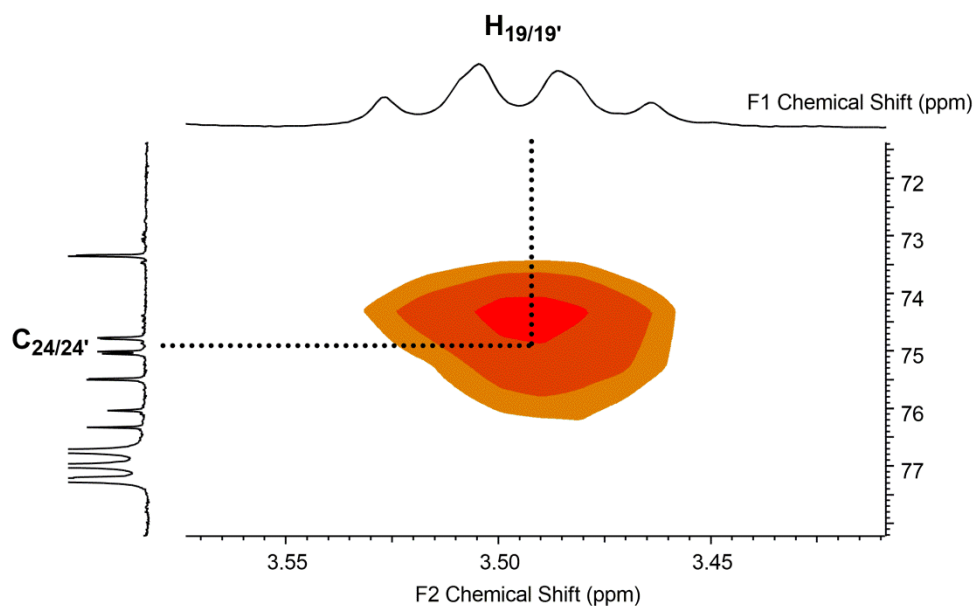


Figure 80 - HMBC spectrum (CDCl_3) of **4-25**.

Using the HMQC spectrum (**Figure 81**), coupling was observed between a multiplet at 3.82-3.86 ppm (within a greater multiplet at 3.72-3.86 ppm), and two overlapping doublets at 4.44 ppm, with the resonances 75.1/75.0/74.8/74.8 ppm (C-24/24') in the ^{13}C spectrum. From the assignment of **4-19**, it is likely that resonances at 3.82-3.86 ppm and 4.44 ppm correspond to the diastereotopic protons of the methylene CH_2 groups H-24^a/H-24^b/H-24^{'a}/H-24^{'b} (**Figure 82**). This assignment was supported by the COSY spectrum, where coupling was observed between the multiplet at 3.82-3.86 ppm and the two overlapping doublets at 4.44 ppm.

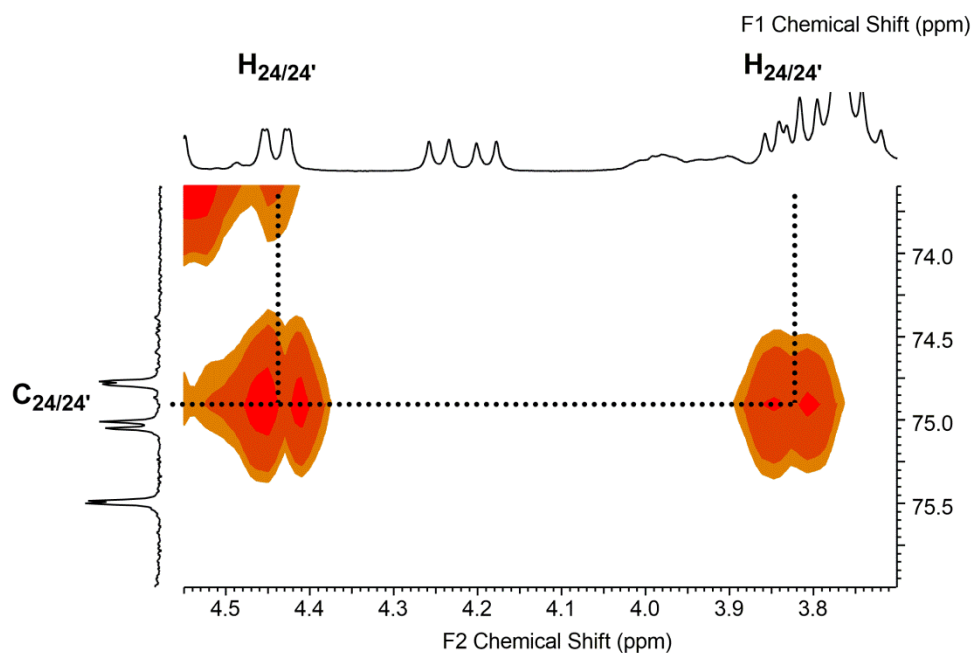


Figure 81 - HMBC spectrum (CDCl_3) of **4-25**.

The assignments of the remaining methylene CH_2 groups, 29/29'/34/34'/39/39', are more challenging, also due to the complexity of the multiplet between 3.72-3.86 ppm in the ^1H NMR spectrum, as well the inability to confirm the exact carbon assignments for C-20/20' and C-21/21'. With this multiplet at 3.72-3.86 ppm not allowing a confirmation of the assignment of the carbon resonances for C-20/20'/21/21', the assignments of both the ^1H and ^{13}C resonances for 29/29'/34/34'/39/39' can again only be indirect. The likely assignments for these regions are listed in **Table 9**, though they must be considered interchangeable. Despite the difficulty in confirming the exact assignments of the methylene CH_2 groups associated with the protected glucosyl moiety, the protons are all diastereotopic in nature, analogous to compound **4-19**, as demonstrated in **Figure 82**.

Assignment	¹ H Resonance (ppm)	HMQC Coupled ¹³ C Resonance (ppm)	HMBC Coupled ¹³ C Resonance (ppm)
29/29'	4.95	75.5 / 75.5	86.6/86.7
34/34'	4.63 / 4.88	74.8/74.8/75.1/75.1	78.3
39/39'	4.56 / 4.63	73.3 / 73.4	69.1/69.2 (C-23/23')

Table 9 - Likely ¹H and ¹³C assignment of the remaining benzyl groups associated with the glucosyl moiety for compound **4-25**, inferred from the previous assignment of **4-19**. Figures suggesting these assignments can be found in Appendix V - **Figures 170-176** though they must all be considered interchangeable.

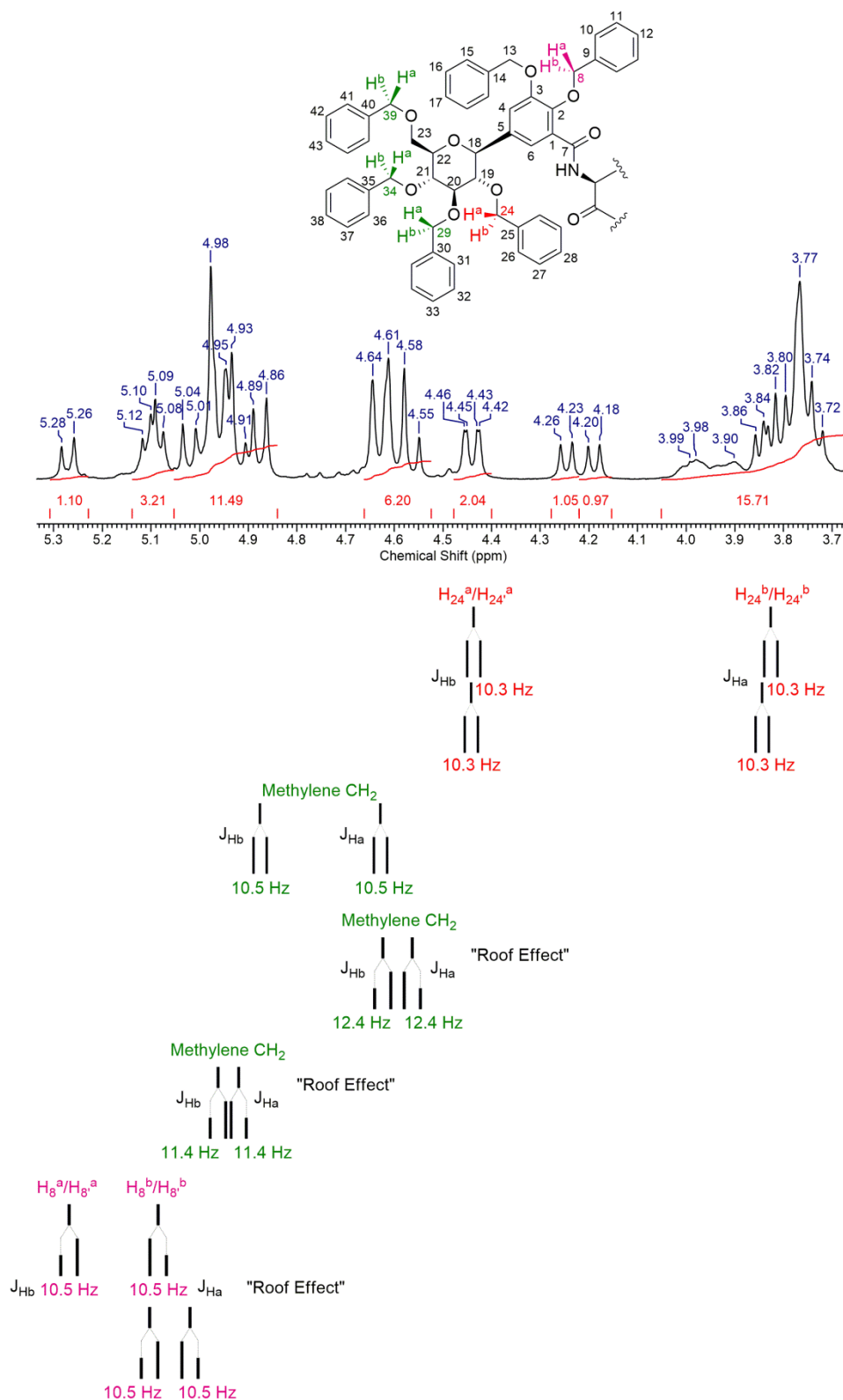


Figure 82 - ^1H NMR spectrum 3.72–3.86 ppm of **4-25**. The J-coupling splitting pattern is shown below, explaining the splitting for each of the resonances. *The assignment of H^a and H^b can be interchanged for each region. **The assignment of $\text{H}-8^a$ and $\text{H}-8^b$ is discussed later.

The assignment of the glucosyl moieties is listed later, in **Table 10**. However, the assignment of another component further supports the isolation of **4-25**, though for full confirmation the remainder of the assignment must be also discussed.

Assignment of the catechol moiety of 4-25

The assignment of the catechol moiety could also be completed in a similar fashion to that described for **4-19**. It was deemed that the multiplet at 7.88 ppm in the ^1H NMR spectrum (**Figure 83**) contains two doublets, each with a $^4J_{\text{H-H}}$ coupling constant of 1.8 Hz, corresponding to the aromatic protons H-6/6'. This would agree with the assignment for this proton environment in compound **4-19**, discussed earlier. Furthermore, this assignment also confirmed by the HMBC spectrum, with coupling observed to two carbonyl resonances at 164.5 and 164.7 ppm, which in turn correspond to the amides C-7/7' (**Figure 84**). It should be noted that within the multiplet at 7.88 ppm there is an amide proton, the assignment of which is discussed later.

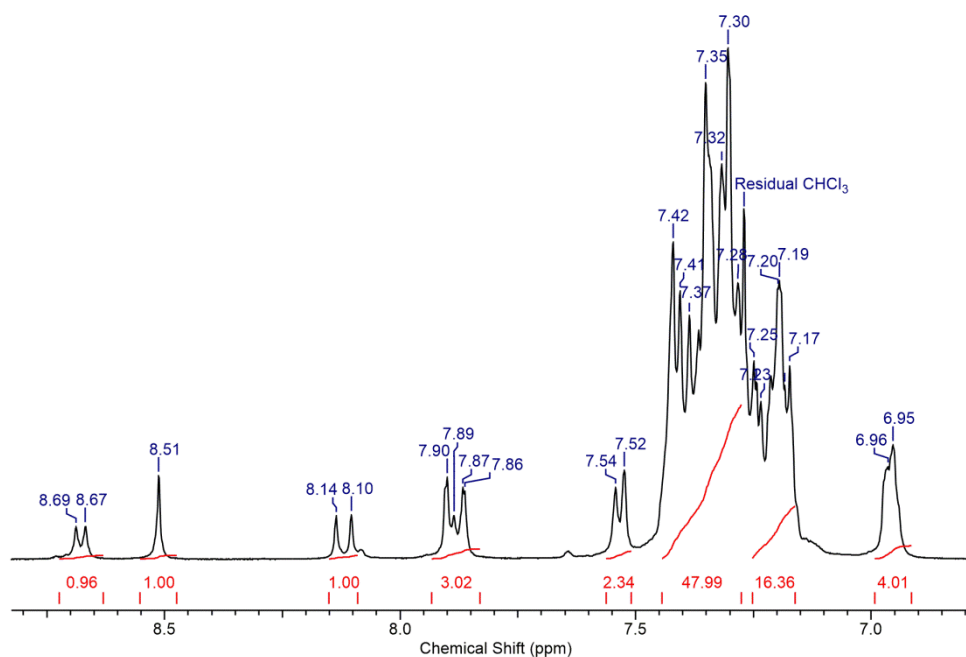


Figure 83 - ^1H NMR spectrum (CDCl_3) of **4-25**.

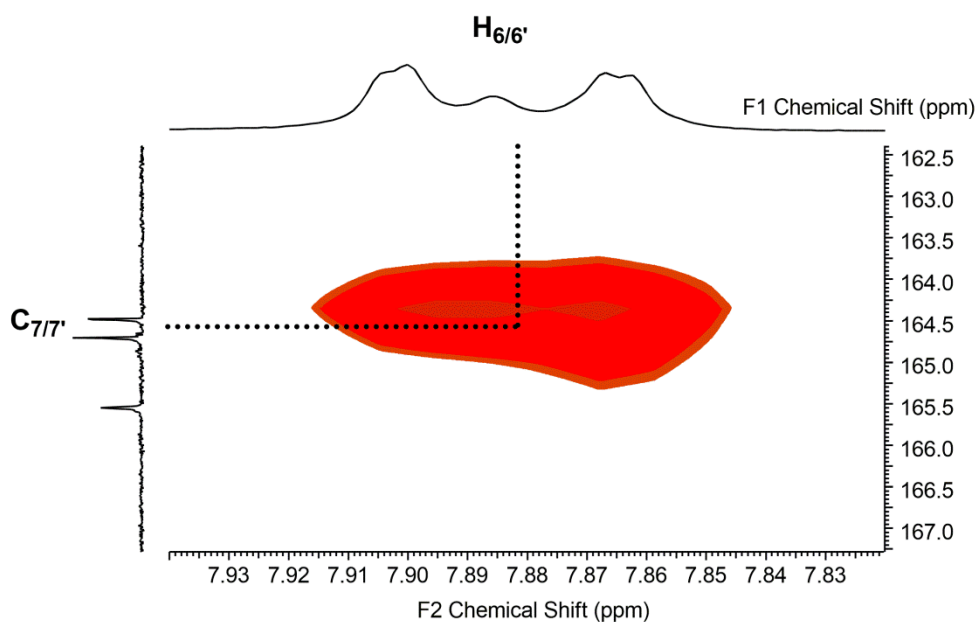


Figure 84 - HMBC spectrum (CDCl_3) of **4-25**.

Like compound **4-19**, coupling was observed within the HMQC and HMBC spectra with H-6/6', which allowed the assignments of C-6/6' (122.1/122.1 ppm), C-2/2' (146.2/146.5 ppm) and C-3/3' (115.8/116.3 ppm). In turn the assignment of H/C-8/8' could be made from the

assignments of C-2/2'. However, the resonances for the diastereotopic methylene CH₂ protons H-8/8' were observed to be more complex than those for **4-19**, with two sets of doublets in the ¹H NMR at 5.02, 5.09 and 5.27 ppm (**Figure 85**). The assignment for these protons were determined by coupling observed in the HMBC spectrum between the resonances at 146.2 and 146.5 ppm for C-2/2' and these doublets (**Figure 85**). It should be noted that underneath the multiplet of overlapping doublets at 5.09 ppm there is another proton, given this multiplet has a relative integration of three as opposed to two; the assignment of which is discussed later. In turn, the assignment of H-8/8' allowed for the assignment of their corresponding carbon resonances using the HMQC spectrum (C-8/8' = 76.0/76.3 ppm).

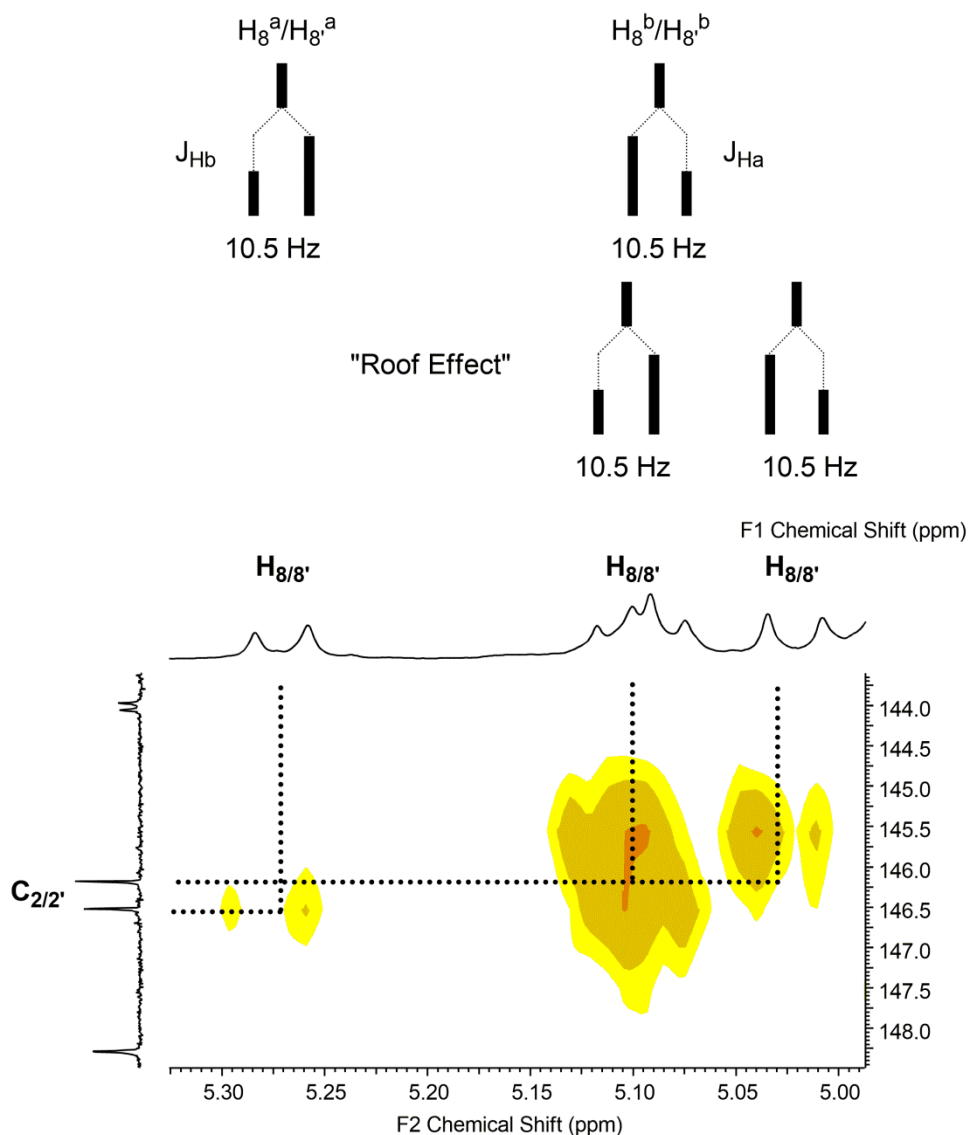


Figure 85 - HMBC spectrum (CDCl_3) of **4-25**. The J-coupling splitting pattern for $\text{H-8}^a/\text{H-8}^b$ is shown above, explaining the splitting for each of the resonances.

Furthermore, the assignment of $\text{C-3/3}'$ (115.8/116.3 ppm) allowed the assignment of $\text{H/C-13/13}'$ (4.98 ppm and 71.0/71.2 ppm) also using HMBC/HMQC spectra. However, unlike in compound **4-19**, where the protons of H-13 appeared as two doublets, corresponding to diastereotopic protons, the resonance observed for $\text{H-13/13}'$ in **4-25** instead appeared as an apparent singlet resonance at 4.98 ppm in the ^1H NMR (**Figure 86**), overlapping another resonance.

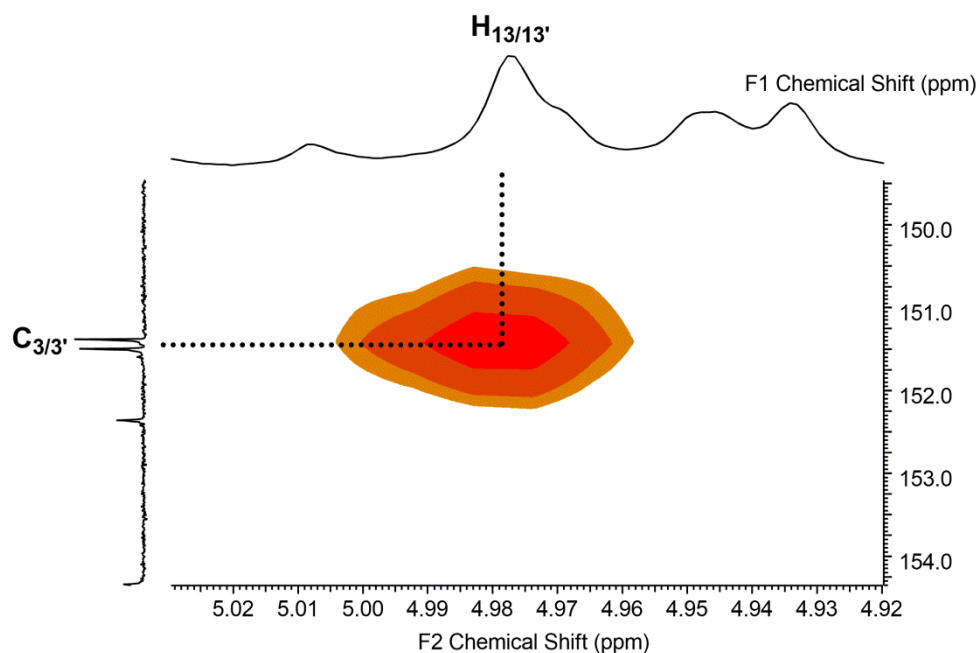


Figure 86 - HMBC spectrum (CDCl_3) of **4-25**.

To complete the assignment of the catechol units, it was observed in the HMBC spectrum (**Figure 87**) that there is coupling between the protons at 7.88 ppm (H-6/6') with two resonances at 115.8 and 116.3 ppm in the ^{13}C NMR spectrum. Based on the assignment for **4-19**, and the coupling observed in the HMQC spectrum (**Figure 88**), it can be inferred that the resonances at 115.8 and 116.3 ppm correlate to C-4/4' . In turn, the HMQC spectrum thereby indicates that protons H-4/4' lie within the multiplet between 7.17-7.25 ppm in the ^1H NMR. In this instance for compound **4-25** the resonances observed for H-4/4' are not as defined as in compound **4-19**, where a doublet was observed.

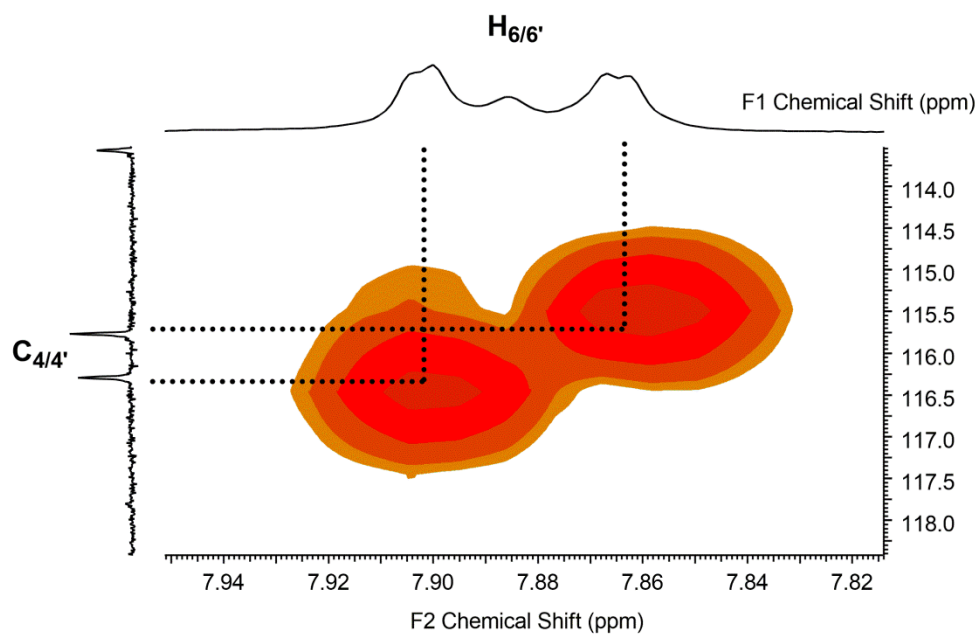


Figure 87 - HMBC spectrum (CDCl_3) of **4-25**.

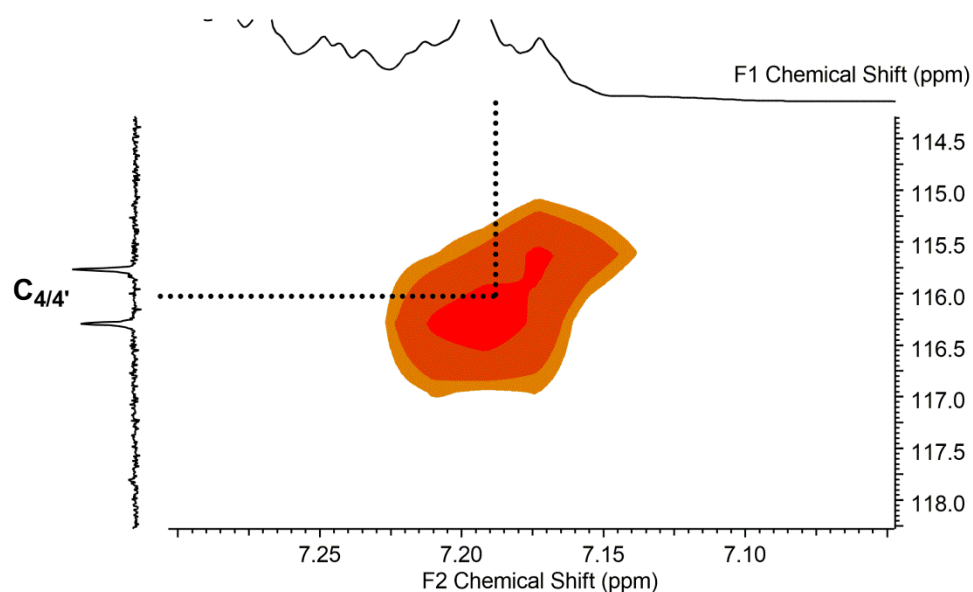


Figure 88 - HMQC spectrum (CDCl_3) of **4-25**.

The assignments of both the glucosyl and catechol moieties are listed in **Table 10**. Once again, the assignment of yet another component further supported the successful isolation of **4-25**. It was next required to assign the lysine moiety to complete the NMR characterisation of **4-25**.

Assign.	¹ H NMR (ppm) / (multiplicity)	¹³ C NMR (ppm)	Append. V - Figure No.	¹ H NMR of 4-19 (ppm)	¹³ C NMR of 4-19 (ppm)
7/7'	-	164.5 / 164.7	-	-	165.2
6/6'	7.88 (m)	122.1 / 122.1	177	7.88 (d)	123.1
4/4'	7.17-7.21 (m)	115.8 / 116.3	-	7.26 (d)	117.7
3/3'	-	151.4 / 151.5	178	-	151.0
2/2'	-	146.2 / 146.5	178	-	146.5
18/18'	4.19 (d) / 4.25 (d)	81.0 / 81.1	166/168	4.24 (d)	80.5
19/19'	3.50 (ap. q)	83.8 / 83.9	166/168	3.43 (ps t)	83.6
20/20'	3.72-3.86 (m)	78.3 / 86.6 / 86.7	167/168	3.82 (ps t)	86.7
21/21'	3.72-3.86 (m)	78.3 / 86.6 / 86.7	167/168	3.74 (ps t)	78.2
22/22'	3.63 (m)	79.3 / 79.3	167/168	3.62 (dt)	79.3
23/23'	3.72-3.86 (m)	69.1 / 69.2	167/168/169	3.76 (d)	69.0
8/8'	5.02 (d) / 5.09 (m) / 5.27 (d)	76.0 / 76.3	179	5.25 (d) / 5.27 (d)	76.9
13/13'	4.98 (ap. s)	71.0 / 71.2	180	4.97 (d) / 5.00 (d)	71.2
24/24'	3.72-3.86 (m)	74.8 / 74.8 / 75.0 / 75.1	167	3.84 (d) / 4.48 (d)	74.9
29/29'	4.56 (d) / 4.63 (d) / 4.63 (d) / 4.88 (d) / 4.93 (m)	73.3/ 73.4 / 75.0 / 75.1 / 75.5 / 75.5	170 /171 /172 / 174 / 175 / 176	4.93 (d) / 4.95 (d)	75.6
34/34'	4.56 (d) / 4.63 (d) / 4.63 (d) / 4.88 (d) / 4.93	73.3/ 73.4 / 75.0 / 75.1 / 75.5 / 75.5	170 / 171 / 172 / 174 / 176	4.64 (d) / 4.87 (d)	75.1

	(m)				
39/39'	4.56 (d) / 4.63 (d) / 4.63 (d) / 4.88 (d) / 4.93 (m)	73.3/ 73.4 / 75.0 / 75.1 / 75.5 / 75.5	170 /171 / 172 /173 / 174	4.58 (d) / 4.64 (d)	73.4

Table 10 - Summary of the assignment of the protect glucosyl and catechol moieties of **4-25**, compared to **4-19**. Figures supporting these assignments can be found in Appendix V - **Figures 166-180**.

Assignment of the lysine linker moiety of **4-25**

It was determined earlier that the amide carbonyls, C-7/7', corresponded to the resonances 164.5 and/or 164.7 ppm in the ^{13}C NMR spectrum (**Figure 84**). From these amide carbonyls, coupling was observed in the HMBC spectrum with a multiplet at 5.09 ppm (**Figure 89**). Therefore it was determined that the third proton in this multiplet at 5.09 ppm corresponded to H-60 (**Figure 90**). This assignment was supported by the HMQC spectrum (**Figure 91**). A coupling between the multiplet at 5.09 ppm and a resonance of 48.7 ppm in the ^{13}C NMR spectrum was observed. This resonance is positive in the DEPT spectrum and so is a tertiary carbon. As such, the resonance at 48.7 ppm was assigned as C-60. Furthermore, the proton H-60 coupled with a resonance at 170.5 ppm in the ^{13}C spectrum, which thus corresponded to the amide carbonyl C-59, observed in the HMBC spectrum (**Figure 89**).

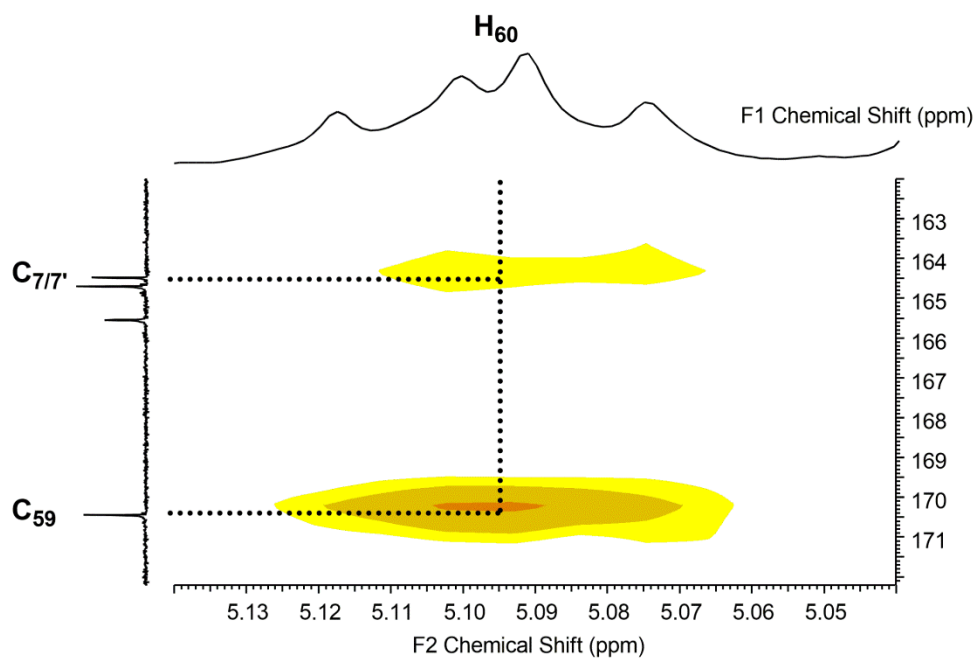


Figure 89 - HMBC spectrum (CDCl_3) of **4-25**.

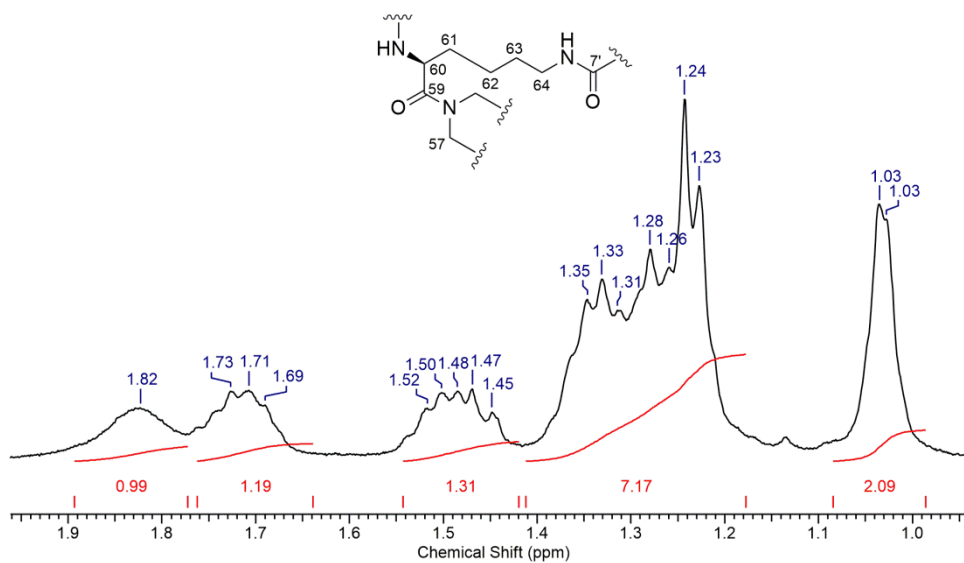


Figure 90 - ^1H NMR (CDCl_3) of **4-25**.

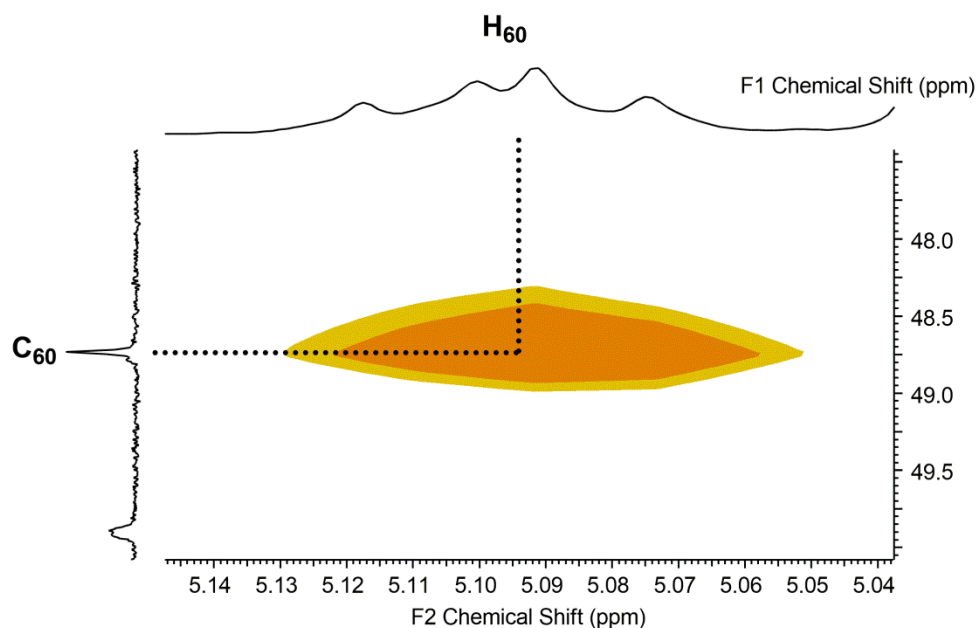


Figure 91 - HMBC spectrum (CDCl_3) of **4-25**.

To assign the amide proton nearest C_7 , coupling was inspected with H-60 in the COSY spectrum (**Figure 92**), and also within the HMBC spectrum with C-7 and C-60. It was observed that these resonances coupled with a doublet at 8.68 ppm in the ^1H NMR spectrum, which was therefore assigned as the amide. Furthermore, the assignment of the amide nearest C-7 also allowed for the subsequent assignment of the other amide (nearest C-7') as within the multiplet at 7.88 ppm.

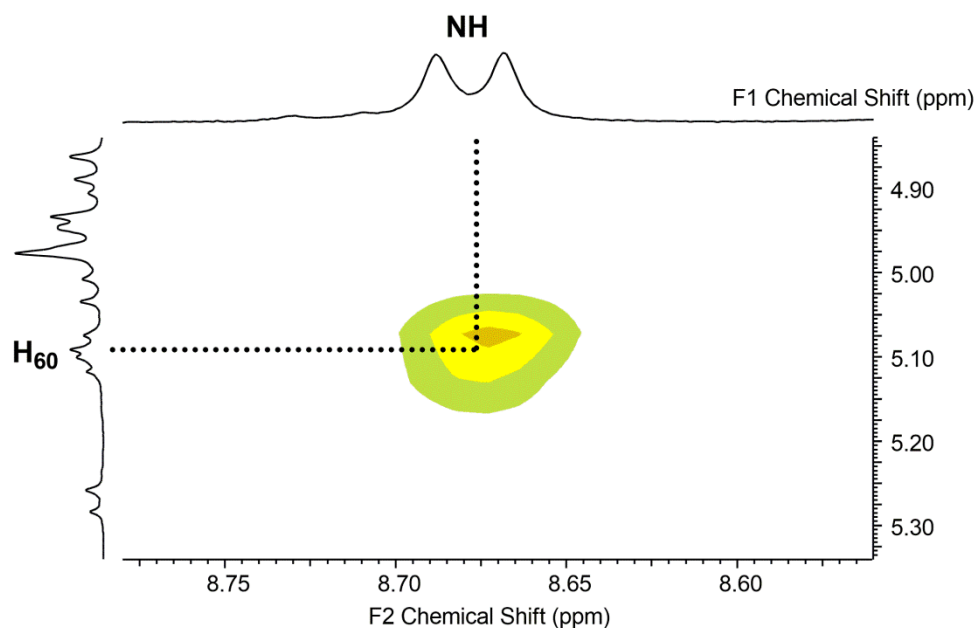


Figure 92 - COSY spectrum (CDCl_3) of **4-25**.

In order to assign the remainder of the lysine moiety (**Figure 90**), coupling of H-60 was examined. It was observed within the HMBC spectrum that there is coupling between the multiplet at 5.09 ppm and a singlet resonance at 32.4 ppm in the ^{13}C spectrum (**Figure 93**). It was determined that the resonance at 32.4 ppm relates to C-61, supported by a negative signal in the DEPT spectrum. Coupling in the HMQC spectrum between 32.4 ppm (C-61) in the ^{13}C spectrum and multiplets at 1.48 and 1.71 or 1.82 ppm in the ^1H spectrum (**Figure 94**) indicates that these multiplets, each with a relative integration of one, correlate to the two diastereotopic protons H-61^a/H-61^b, supported by coupling between these resonances in the COSY spectrum. The two multiplets for the protons of H-61 are likely due to their non-equivalence resulting from the chiral centre at C-60.

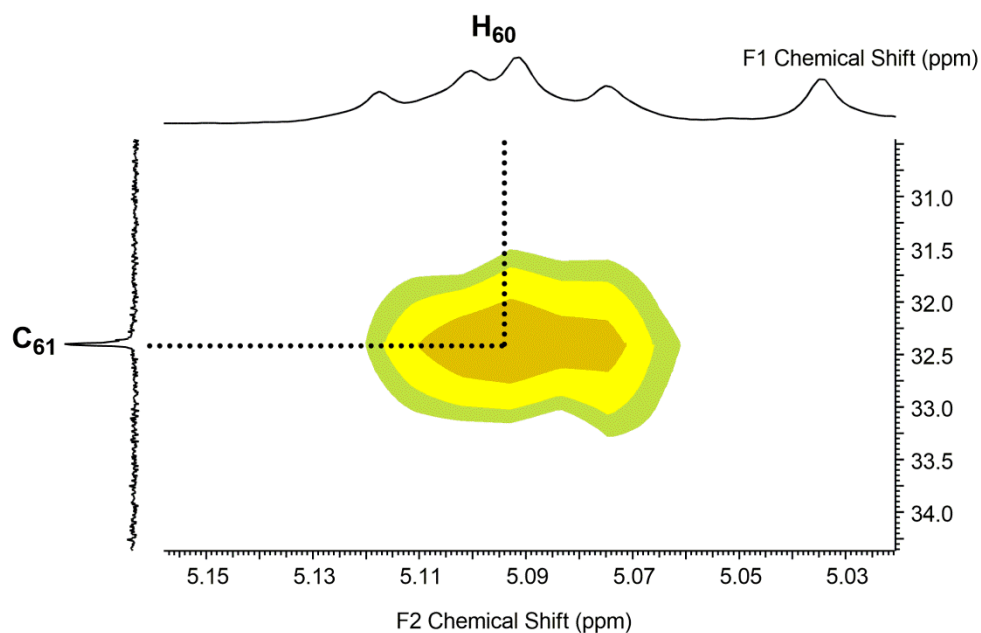


Figure 93 - HMBC spectrum (CDCl_3) of **4-25**.

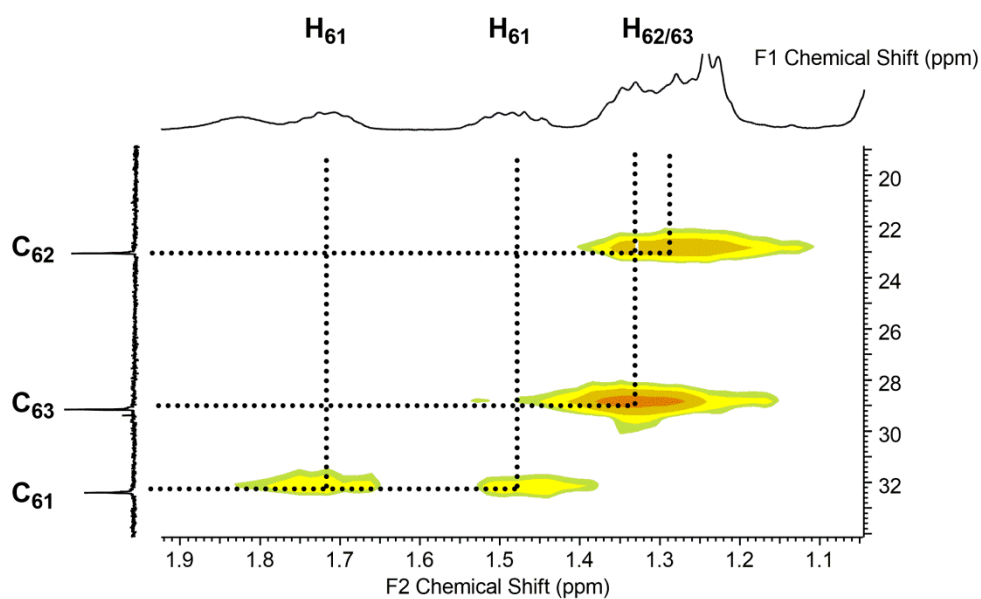


Figure 94 - HMQC spectrum (CDCl_3) of **4-25**.

Based on the above assignment for H-18, the remainder of the lysine chain for regions 62, 63 and 64 were possible. Again using a combination of COSY, HMQC and HMBC spectra, the assignments of the lysine chain were made as outlined in **Table 11**. Having assigned the final component, it was thus confirmed that **4-25** was the isolated product (Chapter 4).

Assignment	¹ H NMR (ppm) / (multiplicity)	¹³ C NMR (ppm)	¹ H NMR of 4-8 (ppm)	¹³ C NMR of 4-8 (ppm)
59	-	170.5	-	176.3
60	5.09 (m)	48.7	4.30 (m)	52.9
61	1.48 (m) / 1.71 (m) or 1.82 (m)	32.4	1.73 (m) / 1.85 (m)	31.7
62	1.23-1.35 (m)	23.1	1.49 (m)	22.0
63	1.23-1.35 (m)	29.2	1.49 (m)	29.0
64	3.24 (m)	39.3	3.11 (m)	39.8

Table 11 - Summary of the assignment of the lysine linker moiety of **4-25**, compared to **4-8** (Chapter 4). Figures supporting the assignments of H/C-62, H/C-63 and H/C-64 can be found in Appendix V - **Figures 181-183**.

Summary of the assignment of 4-25

The NMR assignment of compound **4-25** is outlined in **Table 7**, **Table 10** and **Table 11**. This assignment therefore confirmed the isolation of compound **4-25**. With the NMR assignment of **4-25**, it should be noted that the assignment for a number of the quaternary carbons, were not possible. These include C-1/C-1'/C-5/C-5'/C-55, and all those on the benzyl groups which are indistinguishable from one another, given the number of resonances between 135.5 and 138.7 ppm in the ¹³C spectrum corresponding to these carbon environments. Furthermore, the benzyl CH carbons are also interchangeable, with a number of resonances between 126.5 and 129.0 ppm present for these carbon environments. Likewise the aromatic protons for the benzyl CH protons are also not assigned due to their indistinguishable nature.

5.4 Summary of Chapter 5

The NMR assignments have been presented for the glucosylated compounds **4-19** and **4-25**, outlined in **Table 6**, **Table 7**, **Table 10** and **Table 11**. These assignments validate the synthesis and isolation of both **4-19** and **4-25**. Indeed the intermediate catechol acid **4-19** can be utilised to access future targets, building upon the work presented in Chapter 4. Therefore the characterisation of **4-19** can aid characterisation of future targets, in a manner analogous to that applied for the NMR characterisation of **4-25**.

Chapter 6: Summary, Conclusions and Future Work

6.1 Overall Summary, Conclusions and Future Work

Bio-labile linkers in Trojan horse conjugates (Chapters 2 and 3)

The synthesis and characterisation of conjugate **2-12**, incorporating a carbamate linker between a citrate siderophore and the antimicrobial ciprofloxacin, was achieved. During the synthesis towards conjugate **2-11**, isomerisation of the citrate moiety was observed on treatment of **2-22** with hydroxide. The mechanism was proposed, with the isolation of a succinimide intermediate **2-39** during the purification of **2-22**, which, on treatment with base, selectively ring-opened to produce the single regioisomer **2-12**. Antimicrobial activity of **2-12** was investigated against both BW25113 wild type and BW25113 *fecA::kan E. coli* strains. The conjugate is an active antimicrobial against these strains, though has lower activity than free ciprofloxacin. The limited growth observed for the FecA negative strain when subjected to 10 μ M of **2-12** indicates that FecA is not essential for active transport of this citrate-based conjugate. The mechanism by which conjugate **2-12** enters the cell was not determined, but it is likely to be passive diffusion given that activity was retained in the FecA negative strain. It also remains unclear if the carbamate group gives intracellular release of free ciprofloxacin. Future work is required to establish if FecA does actively transport citrate conjugates, despite FecA being non-essential. In addition, determining the stability of the carbamate group against a range of carboxylesterases would aid in understanding if the linker can cleave inside bacterial cells.

The synthesis of a disulfide-linked citrate-ciprofloxacin conjugate was unsuccessful as the methyl ester protected precursor decomposed on treatment with hydroxide, releasing free ciprofloxacin. Release of the free drug is a ‘proof of concept’ in the development of a bio-labile linker for siderophore-fluoroquinolone Trojan horse conjugates. However,

successful synthesis of compound **3-8** is required to allow investigation into the application of a bio-labile disulfide linker to Trojan horse conjugate synthesis. There is a balance to be established between developing an extracellular stable compound whilst retaining intracellular bio-lability. Future work would involve completing the synthesis of conjugate **3-8** via a revised protecting group strategy, such as the use of *tert*-butyl esters, which can be removed using an acid. Furthermore future work would also involve testing the *ex vivo* stability and *in vivo* antimicrobial activity of **3-8**.

Synthesis and antimicrobial activity testing of a salmochelin-inspired Trojan horse conjugate (Chapter 4)

The synthesis and characterisation of **4-3**, a salmochelin-inspired conjugate was completed. The synthesis involved thirteen synthetic steps over four convergent routes. Several synthetically versatile intermediates were produced which could be used in future salmochelin-inspired conjugate synthesis. The antimicrobial activity of **4-3** was tested against wild type *E. coli*, with higher antimicrobial activity observed in iron deficient media at low concentrations of the conjugate, compared to free ciprofloxacin. However, this reduction in growth did not correlate with the activity of the conjugate against DNA gyrase, which demonstrated reduced inhibitory activity compared to free ciprofloxacin. The gyrase assay suggests that the siderophore moiety is disrupting the ability of the antimicrobial to bind DNA gyrase. Future work should establish the function of the siderophore moiety of the conjugate, both in its iron binding ability and its role in mediating the active uptake of the conjugate. Additionally, the conjugate should be screened against siderocalin to determine if the glucosyl moieties prevent binding to this protein in an analogous manner to salmochelin S4. Finally, combining the choice of a salmochelin-based siderophore with a suitable bio-labile linker would tie together the two concepts explored in this thesis. A design containing both features could work towards a new

antimicrobial with the potential to combat permeability-associated resistance and evade host mammalian immune responses.

6.2 Concluding Remarks

The conclusion that FecA is not essential for transport of citrate-based conjugates suggests that siderophore choice is a key factor for the development of actively transported Trojan horse conjugates. Any development of new citrate-based conjugates, such as the production of the disulfide conjugate **3-8**, should consider this finding. Furthermore, the synthesis of a salmochelin-inspired conjugate **4-3** could also provide insight into the choice of siderophore in conjugate design, though further study is required to determine the role of the siderophore moiety in both iron binding and uptake. Such conjugates are a relatively new field of study and so their development is essential for understanding this new class of Trojan horse conjugates. The choice of a bio-labile linker between the siderophore and antimicrobial moieties is key for the development of future fluoroquinolone Trojan horse conjugates. The reduction in antimicrobial activity of the carbamate-linked conjugate **2-12**, compared to free ciprofloxacin, suggests that the linker is not sufficiently labile to allow for intracellular release of the drug, though this needs further investigation. Conversely, the premature decomposition of the disulfide-based linker during synthesis may suggest that such a linker could function as a bio-labile linker. As such, a disulfide-based linker should be explored further to determine if it is indeed suitable for the desired intracellular release of a fluoroquinolone following uptake.

In addition to the continued development and synthesis of novel siderophore-fluoroquinolone Trojan horse conjugates, the current conjugates in this thesis should also be screened against a range of other clinically relevant bacterial strains. This may unveil improved efficacy of

these conjugates for specific Gram-positive and Gram-negative bacteria species. Additionally, different bacterial species may allow for better release of the carbamate linker if more compatible carboxylesterases are present. Furthermore, screening against a larger range of bacterial strains would aid in the understanding of the scope for using salmochelin-based siderophores in Trojan horse conjugates.

Chapter 7: Experimental

7.1 General Chemistry Procedures

Mass Spectrometry

High resolution positive and negative ESI mass spectrometry was performed on a Thermo-Finnigan LCQ Spectrometer by Karl Heaton or Helen Robinson. LC-MS was performed by Karl Heaton on an Agilent Series 1200 LC with Bruker MicrOTOF using an analogous method to Analytical HPLC Method A described later.

NMR

^1H NMR (400 MHz), ^{13}C NMR (100.6 MHz) and ^{19}F NMR (376 MHz) spectra were acquired on a Jeol ECX400 or ECS400 spectrometer in the stated deuterated solvents. ^1H NMR (700 MHz) and ^{13}C NMR (175 MHz) were acquired on a Bruker AV700 NMR spectrometer by Pedro Aguiar. ^{13}C NMR (125 MHz) was acquired on a Bruker AV500 NMR spectrometer by Ben Coulson. Variable temperature NMR was performed on either a Jeol ECX400 or ECS400 spectrometer. All chemical shifts (δ) are reported in parts per million (ppm) using the residual solvent signal as a reference. All J values are reported in Hertz to one decimal place. All ^{13}C NMR spectra are proton de-coupled. Reference signals are as follows: 7.26 ppm and 77.16 ppm (CD_3Cl), 3.31 ppm and 49.00 ppm (CD_3OD), 2.50 ppm and 39.52 ppm ($\text{d}_6\text{-DMSO}$). Chemical shifts for multiplets are reported from the middle of the multiplet. Multiplicity abbreviations are as follows: br. = br; s = singlet; d = doublet; t = triplet; q = quartet; m = multiplet; dd = double doublet; dt = double triplet. All NMR assignments were aided by DEPT 135, HSQC, HMQC, COSY and HMBC experiments when required. All spectra were processed using ACD/NMR Processor Academic Edition software.

IR

IR were recorded on a Perkin Elmer FT-IR Spectrum Two spectrometer (ATIR) in the region 4000-400 cm^{-1} .

HPLC

Analytical HPLC was performed on a Shimadzu HPLC system (Prominence) with a LC-20AD pump, SIL-20A autosampler, DGU-20AS degasser, CTO-20AC column oven, CBM-20A communication bus module and SPD-M20A diode array detector, using a SunFire C₁₈ column (5 μm , 4.6 x 150 mm), with the specified eluent gradient. Preparative HPLC was performed on a Varian ProStar HPLC system with two 210 series pumps (25 mL), a 325 series UV detector, a model 701 fraction collector and model 410 autosampler, using a SunFire Prep C₁₈ column (10 μm , 19 x 550 mm), with the specified eluent gradient.

Analytical HPLC Method A:

Starting ratio is 2:3 MeCN + 0.1% Formic Acid (FA):H₂O + 0.1% FA. Gradient raised over 10 minutes to 4:1 MeCN + 0.1% FA:H₂O + 0.1% FA. Ratio maintained at 4:1 MeCN + 0.1% FA:H₂O + 0.1% FA for 5 minutes. At 15 minutes - ratio raised to 95:5 MeCN + 0.1% FA:H₂O + 0.1% FA. Ratio maintained at 95:5 MeCN + 0.1% FA:H₂O + 0.1% FA for 10 minutes. At 25 minutes - ratio reduced to 2:3 MeCN + 0.1% Formic Acid (FA):H₂O + 0.1% FA. Ratio maintained at 2:3 MeCN + 0.1% Formic Acid (FA):H₂O + 0.1% FA for 10 minutes. Total method = 35 minutes. Flow rate = 1 mL/min.

Analytical Method B:

Starting ratio is 5:95 MeCN + 0.1% FA:H₂O + 0.1% FA. Gradient raised over 20 minutes to 1:1 MeCN + 0.1% FA:H₂O + 0.1% FA. At 20 minutes - ratio raised to 95:5 MeCN + 0.1% FA:H₂O + 0.1% FA. Ratio maintained at 95:5 MeCN + 0.1% FA:H₂O + 0.1% FA for 5 minutes. At 25 minutes - ratio reduced to 5:95 MeCN + 0.1% FA:H₂O + 0.1% FA. Ratio maintained at 5:95 MeCN + 0.1% FA:H₂O + 0.1% FA for 10 minutes. Total method = 35 minutes. Flow rate = 1 mL/min.

Analytical Method C:

Starting ratio is 1:4 MeCN + 0.1% Formic Acid (FA):H₂O + 0.1% FA. Gradient raised over 10 minutes to 1:1 MeCN + 0.1% FA:H₂O + 0.1% FA. Ratio maintained at 1:1 MeCN + 0.1% FA:H₂O + 0.1% FA for 5 minutes. At 15 minutes - ratio raised to 95:5 MeCN + 0.1% FA:H₂O + 0.1% FA. Ratio maintained at 95:5 MeCN + 0.1% FA:H₂O + 0.1% FA for 5 minutes. At 20 minutes - ratio reduced to 1:4 MeCN + 0.1% Formic Acid (FA):H₂O + 0.1% FA. Ratio maintained at 1:4 MeCN + 0.1% Formic Acid (FA):H₂O + 0.1% FA for 10 minutes. Total method = 30 minutes. Flow rate = 1 mL/min.

Preparative HPLC Method A:

Starting ratio is 1:4 MeCN + 0.1% Formic Acid (FA):H₂O + 0.1% FA. Gradient raised over 15 minutes to 1:1 MeCN + 0.1% FA:H₂O + 0.1% FA. Ratio maintained at 1:1 MeCN + 0.1% FA:H₂O + 0.1% FA for 10 minutes. At 25 minutes - ratio raised to 95:5 MeCN + 0.1% FA:H₂O + 0.1% FA. Ratio maintained at 95:5 MeCN + 0.1% FA:H₂O + 0.1% FA for 5 minutes. At 20 minutes - ratio reduced to 1:4 MeCN + 0.1% Formic Acid (FA):H₂O + 0.1% FA. Ratio maintained at 1:4 MeCN + 0.1% Formic Acid (FA):H₂O + 0.1% FA for 10 minutes. Total method = 40 minutes. Flow rate = 20 mL/min.

Melting Points

Uncorrected melting points were recorded using a Stuart Scientific SMP3 instrument and are accurate to ± 0.05 °C.

Elemental Analysis

Elemental analysis was collected on an Exeter CE-440 elemental analyser by Graeme McAllister.

X-Ray Crystallography

Single crystal X-ray diffraction data was collected, processed and solved by Natalie Pridmore.

Solvents

Solvents were supplied by Aldrich, Fischer Scientific and VWR. Solvents were dried over 3 or 4 Å molecular sieves prior to use where appropriate. Deionised water was used for all synthetic procedures. Dry solvents were obtained from departmental solvent stills (Prosolv MD 7 solvent purification system where solvents are passed through two columns of molecular sieves). For the Negishi coupling reaction Acros Organics DMF AcroSeal[®] (99.8%, extra dry, over molecular sieves) was used.

Chemical Reagents

All chemical reagents were used as supplied unless otherwise stated and purchased from commercial suppliers: Acros, Alfa-Aesar, Fisher Scientific, Fluka, Fluorochem, Sigma Aldrich, TCI Chemicals. Chemicals were handled according to their toxicity. Acetobromo- α -D-glucose was passed through a short silica gel column (anhydrous EtOAc) and rigorously dried prior to use.

Moisture Sensitive Reactions

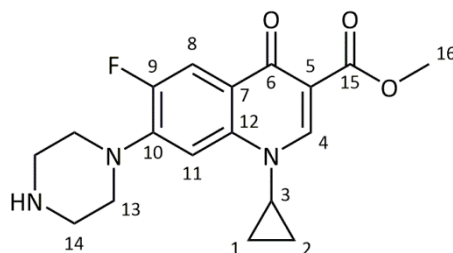
Moisture sensitive reactions were carried out under a N₂ or Ar atmosphere with flame-dried glassware when appropriate. Reactions were carried out on a Schlenk apparatus where appropriate as well as in a glove box for the Negishi coupling reaction.

Chromatography

Analytical TLC used Merck silica gel 60 F₂₅₄ aluminium-backed plates, with the specified eluent. All plates were visualised through UV light using Chromato-vue Model CC-10 at 254 nm or 365 nm, or stained with potassium permanganate. Column chromatography was performed with the specified eluent using Sigma-Aldrich high-purity grade silica gel, pore size 60 Å, 220-440 mesh particle size, 35-75 μ m.

7.2 Chemical Synthesis

Methyl-1-cyclopropyl-6-fluoro-4-oxo-7-(piperazin-1-yl)-1,4-dihydroquinoline-3-carboxylate, 2-15



Thionyl chloride (4.4 mL, 7.216 g, 60.7 mmol) was added dropwise to a stirred solution of 1-cyclopropyl-6-fluoro-4-oxo-7-(piperazin-1-yl)-1,4-dihydroquinoline-3-carboxylic acid (**1-5**) (1.017 g, 3.07 mmol) in anhydrous MeOH (35 mL). The reaction mixture was heated under reflux for 26 h. The reaction was cooled to room temperature and concentrated *in vacuo* to give a yellow oil. The oil was basified to pH 10 using 5% *w/v* aqueous K₂CO₃ (40 mL). The aqueous solution was extracted with CH₂Cl₂ (5 x 20 mL). The combined organic extracts were washed with H₂O (2 x 15 mL). The aqueous phase was then diluted with 5% *w/v* aqueous K₂CO₃ (40 mL) and re-extracted with CH₂Cl₂ (5 x 20 mL). The organic extracts were combined, dried over MgSO₄, filtered and the solvent removed *in vacuo* to give the title compound **2-15** as an off white solid.

Yield: 0.688 g, 1.99 mmol, 65%

m.p. 228.2 - 229.6 °C (dec.) (lit. 227 - 228 °C dec.¹²¹)

R_f 0.12 (3:1 CHCl₃:MeOH)

HRMS (ESI): *m/z* calculated for C₁₈H₂₁FN₃O₃ [M+H]⁺ 346.1561 found 346.1557 (1.3 ppm error), C₁₈H₂₀FN₃NaO₃ [M+Na]⁺ 368.1381 found 368.1387 (-1.8 ppm error)

^1H NMR (400 MHz, CDCl_3) δ (ppm): 8.53 (s, 1H, H-4), 8.00 (d, $^3J_{\text{H-F}}$ 13.2 Hz, 1H, H-8), 7.26 (d, $^4J_{\text{H-F}}$ 7.0 Hz, 1H, H-11), 3.90 (s, 3H, H-16), 3.46-3.41 (m, 1H, H-3), 3.26-3.24 (m, 4H, H-14), 3.12-3.10 (m, 4H, H-13), 2.28 (br s, 1H, NH), 1.34-1.29 (m, 2H, H-1^a/2^a), 1.15-1.11 (m, 2H, H-1^b/2^b)

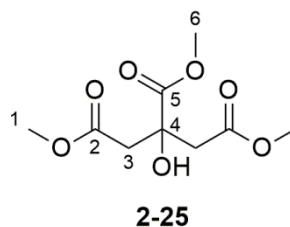
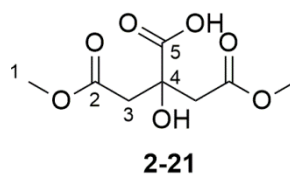
^{13}C NMR (100 MHz, CDCl_3) δ (ppm): 173.6 (d, $^4J_{\text{C-F}}$ 2.3 Hz, C-6), 166.8 (C-15), 153.8 (d, $^1J_{\text{C-F}}$ 248.6 Hz, C-9), 148.7 (C-4), 145.3 (d, $^2J_{\text{C-F}}$ 10.7 Hz, C-10), 138.3 (C-12), 123.1 (d, $^3J_{\text{C-F}}$ 6.9 Hz, C-7), 113.4 (d, $^2J_{\text{C-F}}$ 23.0 Hz, C-8), 110.1 (C-5), 104.9 (d, $^4J_{\text{C-F}}$ 3.1 Hz, C-11), 51.9 (C-16), 50.7 (d, $^4J_{\text{C-F}}$ 4.6 Hz, C-13), 45.7 (C-14), 34.3 (C-3), 7.7 (C-1/2)

^{19}F NMR (376 MHz, CDCl_3) δ (ppm): -123.4 (dd, $^3J_{\text{H-F}}$ 13.2 Hz, $^4J_{\text{H-F}}$ 7.0 Hz)

IR (ATIR) (cm^{-1}): 2950.5 *w* (C-H), 2832.4 *w* (C-H), 1720.8 *s* (C=O), 1616.7 *s* (C=C), 1255.7 *s* (C-N)

Characterisation data consistent with literature.¹²¹

2-hydroxy-4-methoxy-2-(2-methoxy-2-oxoethyl)-4-oxobutanoic acid, 2-21 and trimethyl 2-hydroxypropane-1,2,3-tricarboxylate, 2-25



Citric acid **1-12** (30.242 g, 0.16 mol) was dissolved in anhydrous MeOH (150 mL) and conc. H₂SO₄ (0.6 mL, 0.11 mol). The mixture was heated under reflux for 1 h. The mixture was neutralised to pH 7 with Ca(OH)₂ and the white precipitate was filtered. The filtrate was reduced *in vacuo* giving an oil which crystallised on standing. The white crystalline solid was ground to a powder and dried under vacuum. The powder was suspended in H₂O (60 mL) and sonicated for 20 min. The insoluble material was filtered and the filtrate acidified using conc. HCl (6 mL), giving a white precipitate. The precipitate was isolated by vacuum filtration and dissolved in sat. aq. NaHCO₃ (100 mL). The aqueous solution was washed with CHCl₃ (3 x 40 mL) and the aqueous layer acidified to pH 0 with conc. HCl (10 mL), giving a precipitate. The precipitate was filtered, washed with CHCl₃ (20 mL), and then dried to give the title compound **2-21**. The CHCl₃ extracts were combined, dried over MgSO₄, and the solvent removed *in vacuo* to give **2-25**.

Compound 2-21:

Yield: 5.708 g, 0.026 mol, 16%

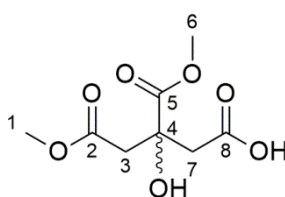
m.p. 123.1 - 125.3 °C (lit. 118 - 123 °C²⁶⁹)

HRMS (ESI): *m/z* calculated for C₈H₁₂NaO₇ [M+Na]⁺ 243.0474 found 243.0475 (0.4 ppm error)

¹H NMR (400 MHz, DMSO-d₆) δ (ppm): 3.56 (s, 6H, H-1), 2.84 (d, ²J_{H-H} 15.2 Hz, 2H, H-3^a), 2.73 (d, ²J_{H-H} 15.2 Hz, 2H, H-3^b)

¹³C NMR (100 MHz, DMSO-D₆) δ (ppm): 175.0 (C-5), 170.6 (C-2), 72.7 (C-4), 51.5 (C-1), 42.7 (C-3)

IR (ATIR) (cm⁻¹): 3406.7 *br m* (O-H), 2963.7 *w* (C-H), 1732.8 *s* (C=O), 1714.2 *s* (C=O), 1438.0 *m* (C-O)

Compound 2-25:**Yield:** 1.089 g, 0.005 mol, 3%**m.p.** 78.1 - 79.2 °C (lit. 74.5 - 75.0 °C ²⁶⁹)**HRMS** (ESI): m/z calculated for $C_9H_{14}NaO_7$ $[M+Na]^+$ 257.0630 found 257.0632 (0.7 ppm error)**¹H NMR** (400 MHz, DMSO-D₆) δ (ppm): 5.75 (s, 1H, -OH), 3.65 (s, 3H, H-6), 3.56 (s, 6H, H-1), 2.87 (d, ² J_{H-H} 15.2 Hz, 2H, H-3^a), 2.73 (d, ² J_{H-H} 15.2 Hz, 2H, H-3^b)**¹³C NMR** (100 MHz, DMSO-D₆) δ (ppm): 173.8 (C-5), 170.4 (C-2), 73.3 (C-4), 52.2 (C-6), 51.6 (C-1), 43.1 (C-3)**IR** (ATIR) (cm⁻¹): 3477.4 *m* (O-H), 2960.3 *w* (C-H), 1740.2 *s* (C=O), 1718.8 *s* (C=O), 1436.6 *m* (C-O)Characterisation data consistent with literature.^{164, 165}**3-hydroxy-5-methoxy-3-(methoxycarbonyl)-5-oxopentanoic acid, 2-23**

Trimethyl 2-hydroxypropane-1,2,3-tricarboxylate (**2-25**) (1.061 g, 4.50 mmol) was dissolved in MeOH:H₂O (1:1 50 mL). 0.1 M NaOH (21.5 mL) was added and the mixture stirred at room temperature for 2 h. The mixture was extracted with EtOAc (3 x 40 mL). The combined organic extracts were dried over MgSO₄, filtered and the solvent removed *in vacuo* to yield unreacted trimethyl 2-hydroxypropane-1,2,3-tricarboxylate (**2-25**)

(0.430 g, 1.83 mmol). The aqueous phase was concentrated *in vacuo* to ~15 mL, acidified to pH 0 with 1 M HCl (4.5 mL). The mixture was extracted with EtOAc (3 x 15 mL) and the combined organic extracts dried over MgSO₄, and the solvent removed *in vacuo* to yield an oil. The oil was crystallised from hot PhMe to give the title compound **2-23** as a colourless solid.

Yield: 0.160 g, 0.73 mmol, 27%

m.p. 73.4 - 75.8 °C (lit. 80 - 81 °C¹⁶⁴)

HRMS (ESI): *m/z* calculated for C₈H₁₂NaO₇ [M+Na]⁺ 243.0475 found 243.0468 (2.9 ppm error), C₈H₁₁O₇ [M-H]⁻ 219.0510 found 219.0514 (-1.6 ppm error)

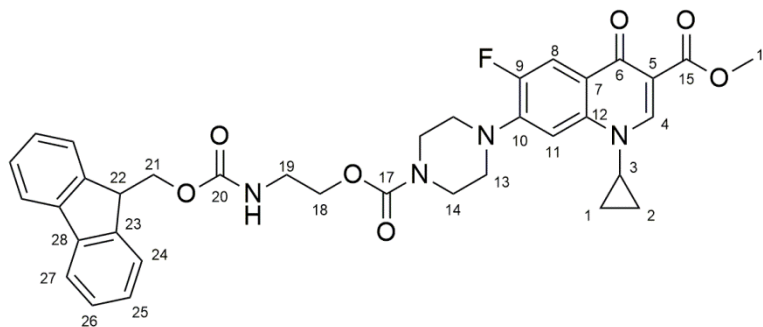
¹H NMR (400 MHz, DMSO-D₆) δ (ppm): 12.36 (br s, 1H, -COOH), 5.61 (br s, 1H, -OH), 3.63 (s, 3H, H-6), 3.56 (s, 3H, H-10), 2.85 (d, ²*J*_{H-H} 15.1 Hz, 1H, H-3^a/7^a), 2.80 (d, ²*J*_{H-H} 15.6 Hz, 1H, H-3^a/7^a), 2.72 (d, ²*J*_{H-H} 15.1 Hz, 1H, H-3^b/7^b), 2.65 (d, ²*J*_{H-H} 15.6 Hz, 1H, H-3^a/7^a)

¹³C NMR (100 MHz, DMSO-D₆) δ (ppm): 173.2 (C-8), 171.0 (C-5), 169.8 (C-2), 73.0 (C-4), 52.1 (C-1/6), 51.5 (C-1/6), 43.1 (C-3/7), 43.0 (C-3/7)

IR (ATIR) (cm⁻¹): 3404.1 *br m* (O-H), 3000.4 *w* (C-H), 2956.1 *w* (C-H), 2933.1 *w* (C-H), 1730.4 *s* (C=O), 1703.4 *s* (C=O), 1440.1 *m* (C-O)

Characterisation data consistent with literature.^{164, 165}

Methyl 7-(4-((2-(((9H-fluoren-9-yl)methoxycarbonyl)amino)ethoxy)carbonyl)piperazin-1-yl)-1-cyclopropyl-6-fluoro-4-oxo-1,4-dihydroquinoline-3-carboxylate, 2-18



To methyl-1-cyclopropyl-6-fluoro-4-oxo-7-(piperazin-1-yl)-1,4-dihydroquinoline-3-carboxylate (**2-15**) (0.206 g, 0.60 mmol) in anhydrous DMF (10 mL) were added Cs_2CO_3 (0.235 g, 0.72 mmol) and tetrabutylammonium iodide (0.270 g, 0.73 mmol). Carbon dioxide gas was bubbled through the reaction mixture for 1.5 h. *N*-Fmoc-2-bromoethylamine (**2-16**) (0.252 g, 0.73 mmol) was dissolved in anhydrous DMF (3 mL) and then added dropwise over 40 min with continued bubbling. The mixture was stirred for 23 h, with continuous carbon dioxide aspiration. The reaction mixture was poured into H_2O (30 mL) and extracted with EtOAc (3 x 30 mL). The organic extracts were washed with H_2O (2 x 30 mL) and brine (3 x 30 mL). The combined organic extracts were dried over MgSO_4 , filtered and the solvent removed *in vacuo* to give an oil (0.277 g). The oil was purified by column chromatography (9:1:0.5 CHCl_3 :EtOAc:MeOH) and the solvent removed *in vacuo* to give the title compound **2-18** as a pale brown crystalline solid.

Yield: 0.035 mg, 0.05 mmol, 9%

R_f 0.23 (9:1:0.5 CHCl_3 :EtOAc:MeOH)

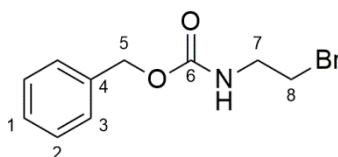
HRMS (ESI): m/z calculated for $C_{36}H_{36}FN_4O_7$ $[M+H]^+$ 655.2563 found 655.2553 (1.5 ppm error), $C_{36}H_{35}FN_4NaO_7$ $[M+Na]^+$ 677.2382 found 677.2406 (-3.5 ppm error)

1H NMR (400 MHz, $CDCl_3$) δ (ppm): 8.53 (s, 1H, H-4), 8.05 (d, $^3J_{H-F}$ 13.0 Hz, 1H, H-8), 7.73 (d, $^3J_{H-H}$ 7.2 Hz, 2H, H-27), 7.57 (d, $^3J_{H-H}$ 7.3 Hz, 2H, H-24), 7.38 (t, $^3J_{H-H}$ 7.3 Hz, 2H, H-26), 7.30 (t, $^3J_{H-H}$ 7.3 Hz, 2H, H-25), 7.19 (d, $^4J_{H-F}$ 6.6 Hz, 1H, H-11), 4.37 (d, $^3J_{H-H}$ 7.3 Hz, 2H, H-21) 4.26 - 4.20 (m, 3H, H-18/22), 3.92 (s, 3H, H-16), 3.68 (br s, 1H, H-14), 3.52 (m, 2H, H-19), 3.31 (m, 1H, H-3), 3.15 (br s, 4H, H-13), 1.25 (m, 2H, H-1^a/2^a), 1.06 (br s, 2H, H-1^b/2^b)

^{19}F NMR (376 MHz, $CDCl_3$) δ (ppm): -123.7 (dd, $^3J_{H-F}$ 13.0 Hz, $^4J_{H-F}$ 7.2 Hz)

IR (ATIR) (cm^{-1}): 3321.2 *w*, 2980.7 *m* (C-H), 1696.6 *s* (C=O), 1617.8 *s* (C=O), 1239.3 *s* (C=O)

Benzyl (2-bromoethyl)carbamate, 2-17



2-Bromoethylamine hydrobromide (3.005 g, 14.7 mmol) was dissolved in 1,4-dioxane (15 mL) and treated with 1 M NaOH (30 mL). The mixture was stirred and cooled in an ice bath for 15 min under an inert atmosphere. Benzyl chloroformate (2.1 mL, 2.498 g, 14.6 mmol) was added dropwise to the cooled mixture over 5 min. The reaction mixture was stirred for a further 10 min, then allowed to warm to room temperature and stirring was continued for 22 h. The reaction mixture was diluted with Et_2O (75 mL) and washed with H_2O (2 x 20 mL). The organic extracts were dried over

MgSO₄, filtered and the solvent removed *in vacuo* to give the title compound **2-17** as a colourless oil.

Yield: 3.390 g, 13.2 mmol, 90%

HRMS (ESI): *m/z* calculated for C₁₀H₁₃⁷⁹BrNO₂ [M+H]⁺ 258.0124 found 258.0117 (2.9 ppm error), C₁₀H₁₂⁷⁹BrNNaO₂ [M+Na]⁺ 279.9944 found 279.9930 (5.0 ppm error)

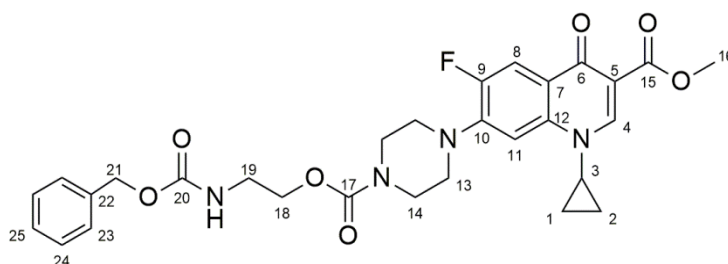
¹H NMR (400 MHz, CDCl₃) δ (ppm): 7.40 - 7.32 (m, 5H, H-1/2/3), 5.12 (s, 2H, H -5), 3.61 (q, ³J_{H-H} 5.9, 2H, H-7), 3.47 (t, ³J_{H-H} 5.9, 2H, H-8)

¹³C NMR (100 MHz, CDCl₃) δ (ppm): 156.5 (C-6), 136.5 (C-4), 128.8 (C-2), 128.5 (C-1), 128.4 (C-3), 66.9 (C-5), 42.5 (C-7), 32.2 (C-8)

IR (ATIR) (cm⁻¹): 3256.1 *m*, 2980.7 *m* (C-H), 2912.5 *m* (C-H), 1718.3 *s* (C=O)

Characterisation data consistent with literature.¹⁷⁰

Methyl **7-(4-((2-(((benzyloxy)carbonyl)amino)ethoxy)carbonyl)piperazin-1-yl)-1-cyclopropyl-6-fluoro-4-oxo-1,4-dihydroquinolne-3-carboxylate, 2-19**



Method A:

To methyl-1-cyclopropyl-6-fluoro-4-oxo-7-(piperazin-1-yl)-1,4-dihydroquinoline-3-carboxylate (**2-15**) (0.208 g, 0.60 mmol) in anhydrous

DMF (10 mL) were added Cs_2CO_3 (0.296 g, 0.91 mmol) and tetrabutylammonium iodide (0.336 g, 0.91 mmol). Carbon dioxide gas was bubbled through the reaction mixture for 1.17 h. (2-Bromo-ethyl)-carbamic acid benzyl ester (**2-17**) (0.234 g, 0.91 mmol) was dissolved in anhydrous DMF (5 mL) and then added dropwise over 20 min. The mixture was stirred at room temperature for 22 h, with continuous carbon dioxide aspiration. The reaction mixture was poured into H_2O (30 mL) and extracted with EtOAc (3 x 30 mL). The organic extracts were washed with H_2O (2 x 30 mL) and brine (4 x 30 mL). The combined organic extracts were dried over MgSO_4 , filtered and the solvent removed *in vacuo* to give an oil. The oil was purified by column chromatography (9:1:0.5 CHCl_3 :EtOAc:MeOH) and the solvent removed *in vacuo* to leave the title compound **2-19** as a colourless solid.

Yield: 0.074 g, 0.13 mmol, 22%

Method B:

Benzyl (2-hydroxyethyl)carbamate (**2-29**) (0.117 g, 0.60 mmol) was dissolved in anhydrous DMF (4 mL). DSC (0.185 g, 0.72 mmol) and pyridine (9.7 μL , 0.010 g, 0.12 mmol) were added. The reaction mixture was heated to 40 °C and stirred for 19 h, then the reaction mixture cooled to room temperature. A mixture of methyl-1-cyclopropyl-6-fluoro-4-oxo-7-(piperazin-1-yl)-1,4-dihydroquinoline-3-carboxylate (**2-15**) (0.208 g, 0.60 mmol) and potassium phosphate tribasic (0.256 g, 1.20 mmol) in anhydrous DMF (4 mL) was added. The reaction mixture was stirred at room temperature for 26 h. The reaction mixture was poured into H_2O (20 mL) and the aqueous phase extracted with EtOAc (5 x 15 mL). The combined organic extracts were washed with 1 M HCl (20 mL), H_2O (2 x 20 mL) and brine (20 mL). The organic phase was dried over MgSO_4 , filtered and the solvent removed *in vacuo* to leave a crude oil. The oil was purified by column chromatography (7:3 CHCl_3 :MeCN) and the solvent removed *in vacuo* to give the title compound **2-19** as a colourless solid.

Yield: 0.223 g, 0.39 mmol, 65%

m.p. 194.1 - 195.0 °C

R_f 0.18 (9:1:0.5 CHCl₃:EtOAc:MeOH) / 0.31 (7:3 CHCl₃:MeCN)

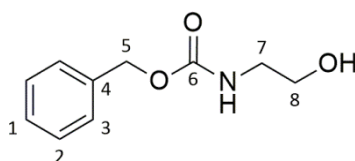
HRMS (ESI): *m/z* calculated for C₂₉H₃₂FN₄O₇ [M+H]⁺ 567.2250 found 567.2241 (1.4 ppm error), C₂₉H₃₁FN₄NaO₇ [M+Na]⁺ 589.2069 found 589.2059 (1.8 ppm error)

¹H NMR (400 MHz, CDCl₃) δ (ppm): 8.51 (s, 1H, H-4), 7.99 (d, ³J_{H-F} 13.1 Hz, 1H, H-8), 7.35 - 7.31 (m, 5H, H-22/23/24/25), 7.24 (d, ⁴J_{H-F} 7.1 Hz, 1H, H-11), 5.09 (s, 2H, H-21), 4.21 (d, ³J_{H-H} 5.1 Hz, 2H, H-18), 3.89 (s, 3H, H-16), 3.66 (br s, 1H, H-14), 3.49 (m, 2H, H-19), 3.40 (m, 1H, H-3), 3.18 (br s, 4H, H-13), 1.29 (m, 2H, H-1^a/2^a), 1.12 (br s, 2H, H-1^b/2^b)

¹³C NMR (100 MHz, CDCl₃) δ (ppm): 173.4 (d, ⁴J_{C-F} 1.5 Hz, C-6), 166.7 (s, C-15), 156.8 (s, C-20), 155.4 (s, C-17), 153.7 (d, ¹J_{C-F} 248.6 Hz, C-9), 148.7 (s, C-4), 144.5 (d, ²J_{C-F} 10.7 Hz, C-10), 138.2 (d, ⁴J_{C-F} 1.5 Hz, C-12), 136.6 (s, C-22), 128.8 (s, C-24), 128.4 (s, C-23), 128.3 (s, C-25), 123.6 (d, ³J_{C-F} 6.9 Hz, C-7), 113.5 (d, ²J_{C-F} 23.0 Hz, C-8), 110.2 (s, C-5), 105.2 (d, ⁴J_{C-F} 3.1 Hz, C-11), 66.7 (s, C-21), 64.5 (s, C-18), 51.9 (s, C-16), 49.6 (d, ⁴J_{C-F} 3.8 Hz, C-13), 43.4 (s, C-14), 40.4 (s, C-19), 34.2 (s, C-3), 7.7 (s, C-1/2)

¹⁹F NMR (376 MHz, CDCl₃) δ (ppm): -123.7 (dd, ³J_{H-F} 13.1 Hz, ⁴J_{H-F} 7.1 Hz)

IR (ATIR) (cm⁻¹): 2917.1 *w* (C-H), 1698.5 *s* (C=O), 1618.7 *s* (C=C), 1432.4 *m*, 1238.5 *s* (C=O)

Benzyl (2-hydroxyethyl)carbamate, 2-29

To a solution of ethanolamine (2.0 mL, 2.024 g, 33.1 mmol) in anhydrous CH_2Cl_2 (30 mL) at 0 °C was added a solution of benzyl chloroformate (3.7 mL, 4.422 g, 25.9 mmol) in anhydrous CH_2Cl_2 (20 mL) over 30 min. The reaction was stirred at 0 °C for 2 h then allowed to warm to room temperature and stirring continued for 18 h. The mixture was washed with sat. aq. NaHCO_3 (3 x 50 mL) and the aqueous phase extracted with CH_2Cl_2 (3 x 50 mL). The organic extracts were dried over MgSO_4 , filtered, and the solvent removed *in vacuo* to give the title compound **2-29** as a colourless oil.

Yield: 4.381 g, 22.5 mmol, 87%

HRMS (ESI): m/z calculated for $\text{C}_{10}\text{H}_{14}\text{NO}_3$ $[\text{M}+\text{H}]^+$ 196.0968 found 196.0965 (1.6 ppm error), $\text{C}_{10}\text{H}_{13}\text{NNaO}_3$ $[\text{M}+\text{Na}]^+$ 218.0788 found 218.0788 (0.0 ppm error)

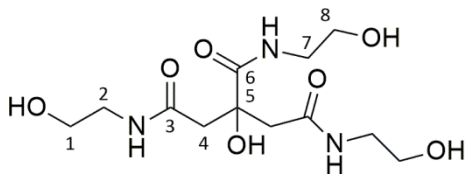
^1H NMR (400 MHz, CDCl_3) δ (ppm): 7.34 - 7.22 (m, 5H, H-1/2/3), 5.30 (br s, 1H, -NH), 5.02 (s, 2H, H-5), 3.59 (m, 2H, H-7), 3.24 (br s, 2H, H-8), 2.57 (br s, 1H, -OH)

^{13}C NMR (100 MHz, CDCl_3) δ (ppm): 157.5 (C-5), 136.6 (C-4), 128.7 (C-2), 128.4 (C-1), 128.3 (C-3), 66.8 (C-5), 61.9 (C-8), 43.2 (C-7)

IR (ATIR) (cm^{-1}): 3320.2 *br s* (O-H), 2941.0 *m* (C-H), 2885.4 *m* (C-H), 1692.0 *s* (C=O)

Characterisation data consistent with literature.¹⁷¹

2-hydroxy- N^1,N^2,N^3 -tris(2-hydroxyethyl)propane-1,2,3-tricarboxamide, 2-36



1,5-Dimethylcitrate (**2-21**) (0.110 g, 0.50 mmol) was dissolved in anhydrous THF (6 mL). CDI (0.103 g, 0.63 mmol) was added and the mixture was stirred for 1 h at room temperature under an inert atmosphere. Ethanolamine (0.452 mL, 0.458 g, 7.50 mmol) was added and the mixture stirred for 42 h. The solvent was removed *in vacuo* and the residue purified by column chromatography (3:1 CHCl₃:MeOH) to give the title compound as **2-36** a colourless oil.

Yield: 0.111 g, 0.34 mmol, 69%

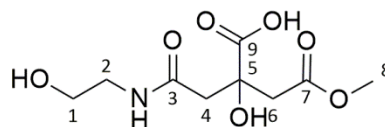
R_f 0.24 (3:1 CHCl₃:MeOH) (permanganate stain)

HRMS (ESI): *m/z* calculated for C₁₂H₂₃N₃NaO₇ [M+Na]⁺ 344.1428 found 344.1412 (4.6 ppm error)

¹H NMR (400 MHz, CD₃OD) δ (ppm): 3.60 (m, 6H, H-1/8), 3.33 (m, 2H, H-7), 3.29 - 3.23 (m, 4H, H-2), 2.73 (d, ²*J*_{H-H} 14.4, 2H, H-4), 2.57 (d, ²*J*_{H-H} 14.4, 2H, H-4)

¹³C NMR (100 MHz, CD₃OD) δ (ppm): 177.4 (C-6), 173.5 (C-3), 76.6 (C-5), 61.7 (C-1/8), 61.6 (C-1/8), 44.5 (C-2/4/7), 43.0 (C-2/4/7), 42.9 (C-2/4/7)

2-hydroxy-4-((2-hydroxyethyl)amino)-2-(2-methoxy-2-oxoethyl)-4-oxobutanoic acid, 2-37



1,5-Dimethylcitrate (**2-21**) (0.110 g, 0.50 mmol) was dissolved in anhydrous THF (7 mL). CDI (0.101 g, 0.63 mmol) was added and the mixture was stirred for 1.5 h at room temperature. Ethanolamine (0.038 mL, 0.038 g, 0.62 mmol) was added and the mixture stirred for 18 h. The solvent was removed *in vacuo* and the residue purified by column chromatography (3:1 CHCl₃:MeOH) to give the title compound **2-37** as a colourless oil.

Yield: 0.030 g, 0.12 mmol, 24%

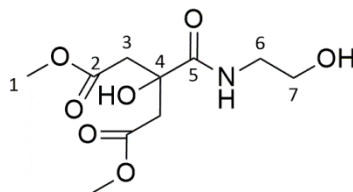
R_f 0.89 (3:1 CHCl₃:MeOH) (permanganate stain)

HRMS (ESI): *m/z* calculated for C₉H₁₄NO₇ [M-H]⁻ 248.0776 found 248.0781 (-2.1 ppm error)

¹H NMR (400 MHz, CD₃OD) δ (ppm): 3.69 - 3.62 (m, 7H, H-1/2/8), 3.08 - 2.91 (m, 3H, H-4/6^a), 2.68 (d, ²*J*_{H-H} 18.3, 1H, H-6^b)

¹³C NMR (100 MHz, CD₃OD) δ (ppm): 181.1 (C-9), 177.6 (C-3), 172.9 (C-7), 73.5 (C-5), 59.5 (C-1), 52.5 (C-8), 43.1 (C-2), 42.0 (C-4), 41.7 (C-6)

Dimethyl 3-hydroxy-3-((2-hydroxyethyl)carbamoyl)pentanedioate, 2-29



1,5-Dimethylcitrate (**2-21**) (0.441 g, 2.0 mmol) and HATU (0.912 g, 2.4 mmol) were dissolved in anhydrous DMF (40 mL) at 0 °C under an inert atmosphere. The mixture was stirred for 1.5 h. Ethanolamine (0.145 mL, 0.147 g, 2.4 mmol) and DIPEA (1.05 mL, 0.775 g, 6.0 mmol) were added. The mixture was allowed to warm to room temperature and stirring continued for 19 h. The solvent was removed *in vacuo* and the residue purified by column chromatography (18:1 CHCl₃:MeOH) to give the title compound **2-29** as a colourless oil.

Yield: 0.483 g, 1.8 mmol, 92%

R_f 0.41 (18:1 CHCl₃:MeOH) (permanganate stain)

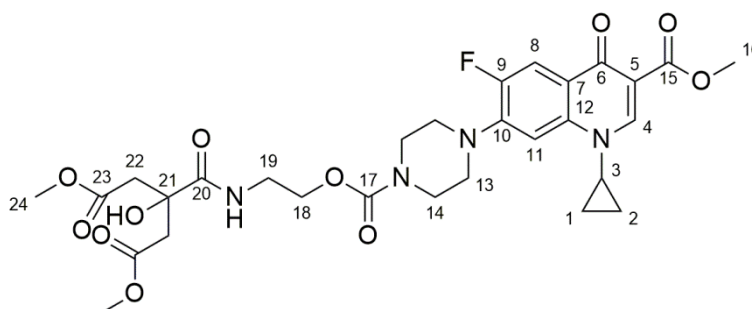
HRMS (ESI): *m/z* calculated for C₁₀H₁₈NO₇ [M+H]⁺ 264.1078 found 264.1079 (-0.6 ppm error), C₁₀H₁₇NNaO₇ [M+Na]⁺ 286.0897 found 286.0904 (-2.4 ppm error)

¹H NMR (400 MHz, CD₃OD) δ (ppm): 3.66 - 3.62 (m, 8H, H-1/7), 3.35 (m, 2H, H-6), 2.93 (d, ²J_{H-H} 15.2 Hz, 2H, H-3), 2.74 (d, ²J_{H-H} 15.2 Hz, 2H, H-3)

¹³C NMR (100 MHz, CD₃OD) δ (ppm): 177.0 (C-5), 172.8 (C-2), 75.5 (C-4), 61.7 (C-7), 52.4 (C-1), 44.3 (C-6), 42.9 (C-3)

IR (ATIR) (cm⁻¹): 3382.3 *br w* (O-H), 2954.8 *w* (C-H), 1726.4 *s* (C=O), 1651.8 *s* (C=O)

Dimethyl 3-((2-((4-(1-cyclopropyl-6-fluoro-3-(methoxycarbonyl)-4-oxo-1,4-dihydroquinolin-7-yl)piperazine-1-carbonyl)oxy)ethyl)carbamoyl)-3-hydroxypentanedioate, 2-22



Dimethyl 3-hydroxy-3-((2-hydroxyethyl)carbamoyl)pentanedioate (**2-29**) (0.154 g, 0.58 mmol) was dissolved in anhydrous DMF (4 mL). DSC (0.185 g, 0.72 mmol) and DIPEA (0.105 mL, 0.078 g, 0.60 mmol) were added. The reaction mixture was heated to 40 °C and stirred for 5.5 h. The reaction mixture was cooled to room temperature then methyl-1-cyclopropyl-6-fluoro-4-oxo-7-(piperazin-1-yl)-1,4-dihydroquinoline-3-carboxylate (**2-15**) (0.208 g, 0.60 mmol) in DMF (4 mL) was added. The reaction mixture was stirred at room temperature for 18.5 h. The solvent was removed *in vacuo* and the residue purified by column chromatography (9:1 CHCl₃:MeOH) to give the title compound **2-22** as a colourless solid.

Yield: 0.165 g, 0.26 mmol, 45%

m.p. 124.3 - 126.8 °C

R_f 0.29 (9:1 CHCl₃:MeOH)

HRMS (ESI): *m/z* calculated for C₂₉H₃₆FN₄O₁₁ [M+H]⁺ 635.2359 found 635.2372 (-2.0 ppm error), C₂₉H₃₅FN₄NaO₁₁ [M+Na]⁺ 657.2179 found 657.2194 (-2.4 ppm error)

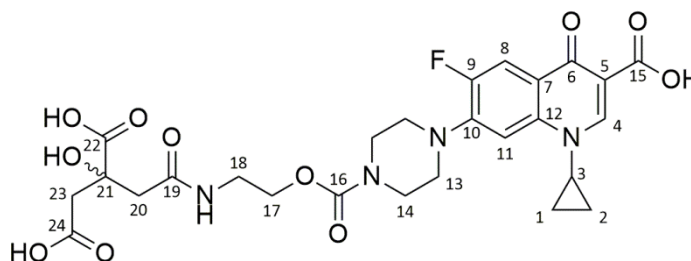
¹H NMR (400 MHz, CDCl₃) δ (ppm): 8.58 (s, 1H, H-4), 8.09 (d, ³J_{H-F} 13.1 Hz, 1H, H-8), 7.30 (d, ⁴J_{H-F} 7.1 Hz, 1H, H-11), 4.98 (br s, 1H, -NH), 4.25 (t, ³J_{H-H} 5.4 Hz, 2H, H-18), 3.92 (s, 3H, H-16), 3.72 – 3.70 (m, 10H, H-14/24), 3.58 (q, ³J_{H-H} 5.4 Hz, 2H, H-19), 3.44 (m, 1H, H-3), 2.91 (d, ²J_{H-H} 15.7 Hz, 2H, H-22), 2.81 (d, ²J_{H-H} 15.7 Hz, 2H, H-22), 1.34 (m, 2H, H-1^a/2^a), 1.15 (m, 2H, H-1^b/2^b)

¹³C NMR (100 MHz, CDCl₃) δ (ppm): 173.7 (C-23), 173.5 (d, ⁴J_{C-F} 2.3 Hz, C-6), 172.1 (C-20), 166.9 (C-15), 155.5 (C-17), 153.8 (d, ¹J_{C-F} 248.6 Hz, C-9), 148.8 (C-4), 144.7 (d, ²J_{C-F} 10.7 Hz, C-10), 138.3 (d, ⁴J_{C-F} 1.5 Hz, C-12), 123.7 (d, ³J_{C-F} 1.5 Hz, H-7), 113.7 (d, ²J_{C-F} 23.0 Hz, C-8), 110.3 (C-5), 105.2 (d, ³J_{C-F} 3.1 Hz, C-11), 74.3 (C-21), 64.1 (C-18), 52.0 (C-16), 51.9 (C-24), 49.7 (C-13), 43.5 (C-14), 41.3 (C-19), 38.8 (C-22), 34.3 (C-3), 7.8 (C-1/2)

¹⁹F NMR (376 MHz, CDCl₃) δ (ppm): -123.7 (dd, ³J_{H-F} 13.1 Hz, ⁴J_{H-F} 7.1 Hz)

IR (ATIR) (cm⁻¹): 3448.1 *w*, 3317.4 *w*, 2995.1 *w* (C-H), 2954.9 *w* (C-H), 2858.3 *w* (C-H), 1728.0 *s* (C=O), 1706.2 *s* (C=O), 1615.8 *s* (C=O), 1431.1 *s* (C-H bend), 1235.5 *s*, 1207.1 *s*

2-(2-((2-((4-(3-carboxy-1-cyclopropyl-6-fluoro-4-oxo-1,4-dihydroquinolin-7-yl)piperazine-1-carbonyl)oxy)ethyl)amino)-2-oxoethyl)-2-hydroxysuccinic acid, 2-12



Dimethyl 3-((2-((4-(1-cyclopropyl-6-fluoro-3-(methoxycarbonyl)-4-oxo-1,4-dihydroquinolin-7-yl)piperazine-1-carbonyl)oxy)ethyl)carbamoyl)-3-hydroxypentanedioate (**2-22**) (0.100 g, 0.16 mmol) was dissolved in 0.1 M tetrabutylammonium hydroxide (1 M in MeOH diluted with H₂O, 7 mL, 0.70 mmol) and stirred at room temperature for 19.5 h. The pH was adjusted to 1.38 by the addition of 1 M HCl (~0.6 mL). The resultant precipitate was filtered, washed with H₂O (30 mL) and CHCl₃ (50 mL), and dried to give the title compound **2-12** as a cream solid.

Yield: 0.059 g, 0.10 mmol, 64%

m.p. 176.2 - 178.3 °C

HRMS (ESI): *m/z* calculated for C₂₆H₂₈FN₄O₁₁ [M-H]⁻ 591.1744 found 591.1749 (-0.7 ppm error)

¹H NMR (400 MHz, DMSO-D₆) δ (ppm): 8.68 (s, 1H, H-4), 8.10 (br t, ³*J*_{H-H} 5.5 Hz, -NH), 7.94 (d, ³*J*_{H-F} 13.1 Hz, 1H, H-8), 7.60 (d, ⁴*J*_{H-F} 7.2 Hz, 1H, H-11), 4.01 (t, ³*J*_{H-H} 5.3 Hz, 2H, H-17), 3.82 (br s, 1H, H-3), 3.61 (br s, 4H, H-14), 2.76 - 3.54 (m, 4H, H-20/23), 1.32 (m, 2H, H-1^a/2^a), 1.18 (m, 2H, H-1^b/2^b)

¹³C NMR (100 MHz, DMSO-D₆) δ (ppm): 177.1 (d, ⁴*J*_{C-F} 7.7 Hz, C-6), 175.7 (C-22), 172.1 (C-24), 170.5 (C-19), 166.7 (C-15), 155.1 (C-16),

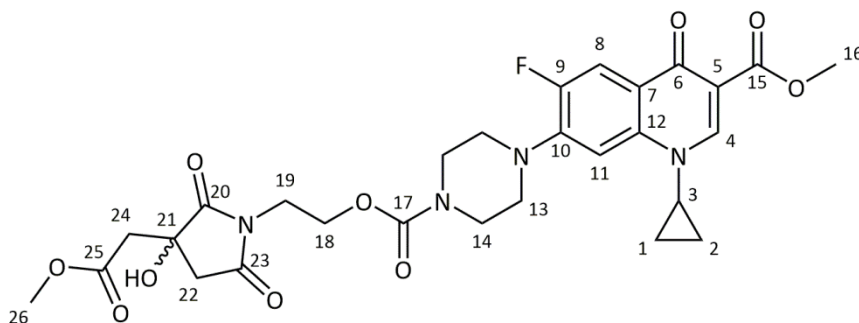
153.6 (d, $^1J_{C-F}$ 248.6 Hz, C-9), 148.7 (C-4), 145.7 (d, $^2J_{C-F}$ 10 Hz, C-10), 139.7 (C-7), 119.4 (C-5), 119.3 (d, $^4J_{C-F}$ 1.5 Hz, H-12), 111.4 (d, $^2J_{C-F}$ 23.8 Hz, C-8), 107.1 (C-11), 73.0 (C-21), 64.0 (C-17), 49.3 (C-14), 43.3 (C-20/23), 43.1 (C-13), 42.9 (C-20/23), 37.9 (C-18), 35.9 (C-3), 7.5 (C-1/2)

^{19}F NMR (376 MHz, DMSO- D_6) δ (ppm): -121.7 (dd, $^3J_{H-F}$ 13.1 Hz, $^4J_{H-F}$ 7.2 Hz)

IR (ATIR) (cm^{-1}): 3357.8 *br w* (O-H), 1712.9 *s* (C=O), 1675.8 *s* (C=O), 1628.3 *s* (C=O), 1467.9 *s* (C-H bend), 1440.3 *s* (C-H bend), 1247.3 *s* (C=O)

Elemental Analysis: Calculated for $[\text{C}_{26}\text{H}_{29}\text{FN}_4\text{O}_{11}\cdot 1.5\text{H}_2\text{O}]$ %C 50.40, %H 5.21, %N 9.04, Measured for $[\text{C}_{26}\text{H}_{29}\text{FN}_4\text{O}_{11}\cdot 1.5\text{H}_2\text{O}]$ %C 50.68, %H 4.93, %N 8.77

Methyl 1-cyclopropyl-6-fluoro-7-(4-((2-(3-hydroxy-3-(2-methoxy-2-oxoethyl)-2,5-dioxypyrrolidin-1-yl)ethoxy)carbonyl)piperazin-1-yl)-4-oxo-1,4-dihydroquinoline-3-carboxylate, 2-39



Isolated during the chromatographic purification of **2-22**.

R_f 0.31 (9:1 CHCl_3 :MeOH) / 0.10 (MeCN)

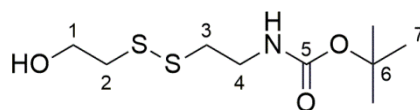
HRMS (ESI): m/z calculated for $C_{28}H_{32}FN_4O_{10}$ $[M+H]^+$ 603.2091 found 603.2112 (-3.5 ppm error), $C_{28}H_{31}FN_4NaO_{10}$ $[M+Na]^+$ 625.1916 found 625.1934 (-2.9 ppm error)

1H NMR (400 MHz, $CDCl_3$) δ (ppm): 8.52 (s, 1H, H-4), 7.94 (d, $^3J_{H-F}$ 12.8 Hz, 1H, H-8), 7.26 (d, $^4J_{H-F}$ 7.1 Hz, 1H, H-11), 4.30 (t, $^3J_{H-H}$ 5 Hz, 2H, H-18), 3.88 (s, 3H, H-16), 3.83 (q, $^3J_{H-H}$ 5 Hz, 2H, H-19), 3.66 - 3.63 (m, 7H, H-14/26), 3.44 (m, 1H, H-3), 3.19 (br s, 4H, H-13), 3.05 (d, $^2J_{H-H}$ 16.8 Hz, 1H, H-22), 2.95 (d, $^2J_{H-H}$ 18.1 Hz, 1H, H-24), 2.95 (d, $^2J_{H-H}$ 16.8 Hz, 1H, H-22), 2.81 (d, $^2J_{H-H}$ 18.1 Hz, 1H, H-24), 1.32 (m, 2H, H-1^a/2^a), 1.11 (m, 2H, H-1^b/2^b)

^{13}C NMR (100 MHz, $CDCl_3$) δ (ppm): 178.8 (C-25), 174.9 (C-23), 173.4 (C-6), 171.1 (C-20), 166.5 (C-15), 155.4 (C-17), 153.7 (d, $^1J_{C-F}$ 248.6 Hz, C-9), 148.8 (C-4), 144.8 (d, $^2J_{C-F}$ 10.7 Hz, C-10), 138.3 (d, $^4J_{C-F}$ 1.5 Hz, C-12), 123.4 (d, $^3J_{C-F}$ 1.5 Hz, C-7), 113.4 (d, $^2J_{C-F}$ 22.2 Hz, C-8), 110.0 (C-5), 105.3 (d, $^3J_{C-F}$ 3.1 Hz, C-11), 72.3 (C-21), 62.1 (C-18), 51.9 (C-16), 51.9 (C-26), 49.5 (C-13), 43.4 (C-14), 42.1 (C-19), 40.2 (C-22), 38.3 (C-24), 34.4 (C-3), 7.8 (C-1/2)

^{19}F NMR (376 MHz, $CDCl_3$) δ (ppm): -123.7 (dd, $^3J_{H-F}$ 12.9 Hz, $^4J_{H-F}$ 7.1 Hz)

IR (ATIR) (cm^{-1}): 3365.4 *br w* (O-H), 2912.6 *w* (C-H), 1722.0 *s* (C=O), 1702.1 *s* (C=O), 1699.6 *s* (C=O), 1667.3 *s* (C=O), 1515.6 *m* (C=C), 1247.1 *s* (C=O)

Tert-butyl (2-((2-hydroxyethyl)disulfanyl)ethyl)carbamate, 3-13

Cysteamine hydrochloride (10.067 g, 88.61 mmol) was dissolved in MeOH (70 mL) then cooled to 0 °C. A solution of 2-hydroxyethyl disulfide (**3-12**) (11 mL, 8.723 g, 56.55 mmol) and Et₃N (25 mL, 34.435 g, 340.30 mmol) in MeOH (50 mL) was added dropwise over 40 min. The reaction was stirred at 0 °C for 15 min and then warmed to room temperature and stirring continued for 19h. The mixture was cooled to 0 °C and di-*tert*-butyl carbonate (29.169 g, 133.65 mmol) in MeOH (30 mL) added dropwise over 15 min. The reaction mixture was stirred 0 °C for 30 min and then warmed to room temperature and stirring continued for 71h. The solvent was removed *in vacuo* and the residue dissolved in EtOAc (200 mL). The organic phase was washed with H₂O (2 x 100 mL) and brine (100 mL), then dried over MgSO₄, filtered and the solvent removed *in vacuo*. The residue was purified by column chromatography (1:1 EtOAc:Petroleum Ether 40-60) to give the title compound **3-13** as a colourless oil.

Yield: 6.842 g, 27.00 mmol, 48%

R_f 0.23 (1:1 EtOAc:Petroleum Ether 40-60) (permanganate stain)

HRMS (ESI): *m/z* calculated for C₉H₁₉NNaO₃S₂ [M+Na]⁺ 276.0699 found 276.0700 (-0.5 ppm error)

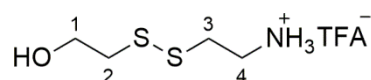
¹H NMR (400 MHz, CDCl₃) δ (ppm): 4.95 (br s, 1H, -OH), 3.88 (t, ³*J*_{H-H} 5.7 Hz, 2H, H-1), 3.46 (m, 2H, H-4), 2.88 (t, ³*J*_{H-H} 5.7 Hz, 2H, H-2), 2.80 (t, ³*J*_{H-H} 6.4 Hz, 2H, H-3), 1.44 (s, 9H, H-7)

¹³C NMR (100 MHz, CDCl₃) δ (ppm): 156.0 (C-5), 79.8 (C-6), 60.3 (C-1), 41.8 (C-2), 39.4 (C-4), 38.2 (C-3), 28.5 (C-7)

IR (ATIR) (cm^{-1}): 3323.5 *br w* (O-H), 2970.8 *w* (C-H), 2929.0 *w* (C-H), 2867.4 *w* (C-H), 1675.8 *s* (C=O)

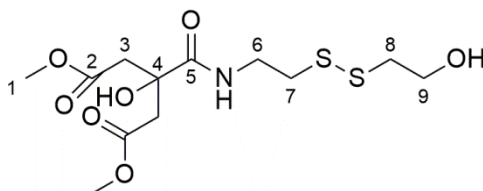
Characterisation data consistent with literature.¹⁷⁸

2-((2-aminoethyl)disulfanyl)ethanol trifluoroacetic acid salt, 3-14



Prepared using a literature preparation and used without purification.¹⁷⁸

Dimethyl 3-hydroxy-3-((2-((2-hydroxyethyl)disulfanyl)ethyl)carbamoyl)pentanedioate, 3-15



2-Hydroxy-4-methoxy-2-(2-methoxy-2-oxoethyl)-4-oxobutanoic acid (**2-21**) (0.910 g, 4.13 mmol) and HATU (2.034 g, 5.34 mmol) were dissolved in anhydrous DMF (30 mL) and stirred at 0 °C under an inert atmosphere for 30 min. A solution of 2-((2-aminoethyl)disulfanyl)ethanol trifluoroacetic acid salt (**3-14**) (2.243 g, 8.39 mmol) and DIPEA (3.2 mL, 4.313 g, 33.37 mmol) in anhydrous DMF (20 mL) was added. The mixture was warmed to room temperature and stirring continued for 68 h. The solvent was removed *in vacuo* and the residue purified by column

chromatography (1:1 MeCN:CHCl₃) to give the title compound **3-15** as a colourless oil.

Yield: 0.676 g, 1.90 mmol, 46%

R_f 0.31 (1:1 MeCN:CHCl₃) (permanganate stain)

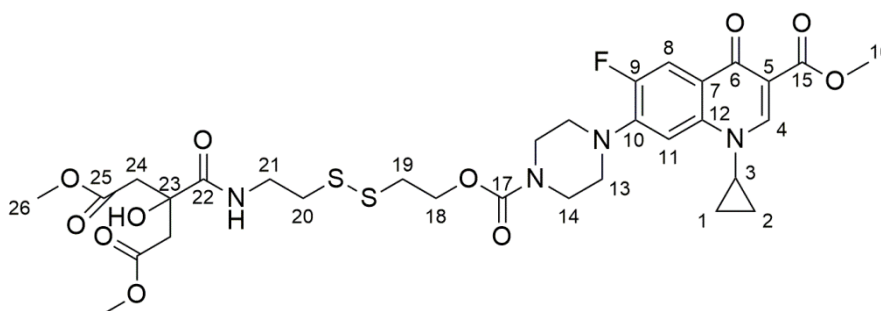
HRMS (ESI): *m/z* calculated for C₁₂H₂₁NNaO₇S₂ [M+Na]⁺ 378.0652
found 378.0647 (1.2 ppm error)

¹H NMR (400 MHz, CDCl₃) δ (ppm): 7.34 (br s, 1H, -NH), 4.94 (s, 1H, -OH), 3.93 (t, ³J_{H-H} 5.5 Hz, 1H, -OH), 3.89 (t, ³J_{H-H} 5.5 Hz, 2H, H-9), 3.72 (s, 6H, H-1), 3.65 (q, ³J_{H-H} 6.5 Hz, 2H, H-6), 2.96 (d, ²J_{H-H} 16.0 Hz, 2H, H-3^a), 2.90 (m, 2H, H-8), 2.85 (t, ³J_{H-H} 6.5 Hz, 2H, H-7), 2.80 (d, ²J_{H-H} 16.0 Hz, 2H, H-3^b)

¹³C NMR (100 MHz, CDCl₃) δ (ppm): 173.4 (C-2), 171.7 (C-5), 74.3 (C-4), 60.3 (C-9), 52.1 (C-1), 41.8 (C-8), 41.5 (C-3), 38.3 (C-6), 37.3 (C-7)

IR (ATIR) (cm⁻¹): 3380.2 *br m* (O-H), 2952.2 *m* (C-H), 1728.9 *s* (C=O), 1656.0 *s* (C=O)

Dimethyl 3-((2-((4-(1-cyclopropyl-6-fluoro-3-(methoxycarbonyl)-4-oxo-1,4-dihydroquinolin-7-yl)piperazine-1-carbonyloxy)ethyl)disulfanyl)ethyl)carbonyl)-3-hydroxypentanedioate, 3-16



Dimethyl 3-hydroxy-3-((2-((2-hydroxyethyl)disulfanyl)ethyl)carbonyl)pentanedioate (**3-15**) (0.246 g, 0.69 mmol), DSC (0.278 g, 1.09 mmol) and DIPEA (0.19 mL, 0.141 g, 1.09 mmol) were dissolved in anhydrous DMF (10 mL). The mixture was stirred for 17 h at 40 °C. The mixture was cooled to room temperature and a solution of methyl-1-cyclopropyl-6-fluoro-4-oxo-7-(piperazin-1-yl)-1,4-dihydroquinoline-3-carboxylate (**2-15**) (0.245 g, 0.71 mmol) in anhydrous DMF (10 mL) was added. The mixture was stirred at room temperature for 25 h. The solvent was removed *in vacuo* and the residue purified by column chromatography (15:1 CHCl₃:MeOH) to give the title compound **3-16** as a cream solid.

Yield: 0.184 g, 0.25 mmol, 37%

m.p. 136.2 - 139.4 °C

R_f 0.24 (15:1 CHCl₃:MeOH)

HRMS (ESI): *m/z* calculated for C₃₁H₄₀FN₄O₁₁S₂ [M+H]⁺ 727.2114 found 727.2098 (2.2 ppm error), C₃₁H₃₉FN₄NaO₁₁S₂ [M+Na]⁺ 749.1933 found 749.1921 (1.6 ppm error)

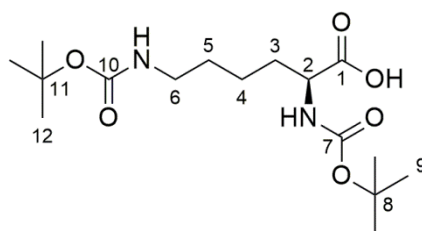
¹H NMR (400 MHz, CDCl₃) δ (ppm): 8.50 (s, 1H, H-4), 7.97 (d, ³J_{H-F} 13.1 Hz, 1H, H-8), 7.35 (m, 1H, -NH), 7.26 (d, ⁴J_{H-F} 7.3 Hz, 1H, H-11), 4.97 (br s, 1H, -OH), 4.38 (t, ³J_{H-H} 6.4 Hz, 2H, H-18), 3.89 (s, 3H, H-16), 3.72 (m, 10H, H-14/26), 3.61 (q, ³J_{H-H} 6.4 Hz, 2H, H-21), 3.44 (m, 1H, H-3), 3.22 (m, 4H, H-13), 2.96 (t, ³J_{H-H} 6.4 Hz, 2H, H-19), 2.93 (d, ²J_{H-H} 15.8 Hz, 2H, H-24^a), 2.84 (t, ³J_{H-H} 6.4 Hz, 2H, H-20), 2.78 (d, ²J_{H-H} 15.8 Hz, 2H, H-24^b), 1.32 (m, 2H, H-1^a/2^a), 1.14 (m, 2H, H-1^b/2^b)

¹³C NMR (100 MHz, CDCl₃) δ (ppm): 173.2 (C-25), 172.9 (C-6), 166.2 (C-15), 154.8 (C-17), 153.3 (d, ¹J_{C-F} 248.3 Hz, C-9), 148.4 (C-4), 144.2 (d, ²J_{C-F} 10.5 Hz, C-10), 138.9 (C-12), 123.3 (d, ³J_{C-F} 6.7 Hz, C-7), 109.9 (C-5), 105.1 (d, ³J_{C-F} 2.9 Hz, C-11), 74.2 (C-23), 63.4 (C-18), 52.0 (C-26), 52.0 (C-16), 49.8 (C-13), 43.6 (C-14), 41.6 (C-24), 38.1 (C-21), 37.6 (C-20), 37.4 (C-19), 34.5 (C-3), 8.1 (C-1/2)

¹⁹F NMR (376 MHz, CDCl₃) δ (ppm): -123.7 (dd, ³J_{H-F} 13.1 Hz, ⁴J_{H-F} 7.3 Hz)

IR (ATIR) (cm⁻¹): 3378.9 *br w* (O-H), 2951.0 *w* (C-H), 1720.0 *s* (C=O), 1703.7 *s* (C=O), 1617.8 *s* (C=C)

Elemental Analysis: Calculated for [C₃₁H₃₉FN₄O₁₁S₂] %C 51.23, %H 5.41, %N 7.71, Measured for [C₃₁H₃₉FN₄O₁₁S₂] %C 50.77, %H 5.37, %N 7.55

(S)-2,6-bis((tert-butoxycarbonyl)amino)hexanoic acid, 4-8

L-lysine monohydrochloride (1.253 g, 6.9 mmol) and NaOH (0.556 g, 13.9 mmol) were dissolved in H₂O (13 mL) and the mixture heated to 50 °C. A solution of di-*tert*-butyl dicarbonate (4 mL, 3.800 g, 17.4 mmol) in anhydrous 1,4-dioxane (25 mL) was added dropwise over 30 min and stirring was continued for 18 h. The reaction mixture was concentrated to ~6 mL *in vacuo*, diluted with H₂O (20 mL) and washed with cyclohexane (3 x 25 mL). The pH of the aqueous layer was reduced to ~3 through addition of 1 M HCl (6 mL). The resulting precipitate was dissolved in EtOAc (25 mL) and the aqueous layer extracted with EtOAc (3 x 25 mL) and the combined organic extracts dried over MgSO₄. The solvent was removed *in vacuo* to give the title compound **4-8** as a thick colourless gel.

Yield: 2.115 g, 6.1 mmol, 89%

HRMS (ESI): *m/z* calculated for C₁₆H₃₁N₂O₆ [M+H]⁺ 347.2186 found 347.2117 (-2.6 ppm error), C₁₆H₃₀FN₂NaO₆ [M+Na]⁺ 369.1987 found 369.1996 (2.4 ppm error)

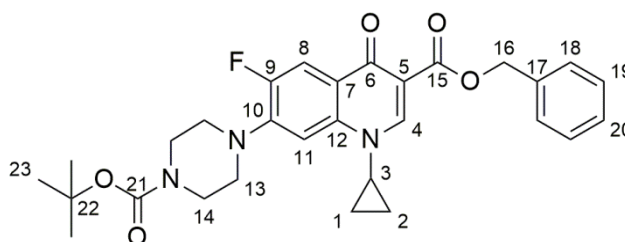
¹H NMR (400 MHz, CDCl₃) δ (ppm): 5.27 (d, ²J_{H-H} 7.0 Hz, 1H, H-14), 4.68 (br s, 1H, H-13), 4.31 (br s, 1H, H-2), 3.11 (br s, 2H, H-6), 1.85 (br s, 1H, H-3^a), 1.73 (br s, 1H, H-3^b), 1.51-1.47 (m, 4H, H-4/5), 1.44 (s, 18H, H-9/12)

¹³C NMR (100 MHz, CDCl₃) δ (ppm): 176.3 (C-1), 156.7 (C-7/10), 156.1 (C-7/10), 79.8 (C-8/11), 79.2 (C-8/11), 52.9 (C-2), 39.8 (C-6), 31.7 (C-3), 29.0 (C-5), 28.0 (C-9/12), 28.0 (C-9/12), 22.0 (C-4)

IR (ATIR) (cm^{-1}): 3334.4 *br m* (O-H), 2977.7 *m* (C-H), 2933.0 *m* (C-H), 1687.6 *s* (C=O)

Characterisation data consistent with literature.²⁴⁵

Benzyl 7-(4-(*tert*-butoxycarbonyl)piperazin-1-yl)-1-cyclopropyl-6-fluoro-4-oxo-1,4-dihydroquinoline-3-carboxylate, 4-9



1-Cyclopropyl-6-fluoro-4-oxo-7-(piperazin-1-yl)-1,4-dihydroquinoline-3-carboxylic acid (**1-5**) (2.008 g, 6.06 mmol) was suspended in 1,4-dioxane:H₂O (1:1, 40 mL) and 1 M NaOH (10 mL) was added. The mixture was stirred for 1 h. Di-*tert*-butyl dicarbonate (2.030 g, 9.30 mmol) was added and stirring continued for 19.5 h. The reaction mixture was concentrated *in vacuo* to ~¼ volume and acetone (50 mL) added to give a precipitate (2.308 g). The precipitate (2.010 g) and Cs₂CO₃ (2.429 g, 7.45 mmol) were suspended in DMF (50 mL) and stirred at room temperature for 1 h. BnBr (1.5 mL, 2.157 g, 12.61 mmol) was added and stirring continued for 23 h. The solvent was removed *in vacuo* and the residue dissolved in CHCl₃ (150 mL). The organic phase was washed with H₂O (2 x 100 mL) and brine (100 mL). The organic phase was dried over MgSO₄, and the solvent removed *in vacuo* to give a solid. The solid was suspended in Et₂O (100 mL), filtered and washed with Et₂O, and then purified by column chromatography (1:1 EtOAc:CHCl₃) to give the title compound **4-9** as a colourless solid.

Yield: 1.383 g, 2.65 mmol, 51%

m.p. 195.3 - 197.8 °C (lit. 191 - 193 °C ¹²⁶)

R_f 0.41 (1:1 EtOAc:CHCl₃)

HRMS (ESI): *m/z* calculated for C₂₉H₃₃FN₃O₅ [M+H]⁺ 522.2399 found 522.2423 (-4.7 ppm error), C₂₉H₃₂FN₃NaO₅ [M+Na]⁺ 544.2218 found 544.2232 (-2.4 ppm error)

¹H NMR (400 MHz, CDCl₃) δ (ppm): 8.54 (s, 1H, H-4), 8.09 (d, ³J_{H-F} 13.5 Hz, 1H, H-8), 7.53 (m, 2H, H-11/20), 7.26-7.40 (m, 4H, H-18/19), 5.40 (s, 2H, H-16), 3.66 (m, 4H, H-13), 3.41 (m, 1H, H-3), 3.22 (m, 4H, H-14), 1.50 (s, 9H, H-23), 1.31 (m, 2H, H-1^a/2^a), 1.13 (m, 2H, H-1^b/2^b)

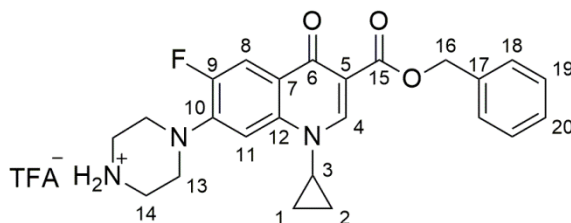
¹³C NMR (100 MHz, CDCl₃) δ (ppm): 172.9 (C-6), 165.5 (C-15), 154.6 (C-21), 153.3 (d, ¹J_{C-F} 248.3 Hz, C-9), 148.3 (C-4), 144.4 (d, ²J_{C-F} 10.5 Hz, C-10), 137.9 (C-12/17), 136.4 (C-12/17), 128.5 (C-18/19/20), 127.9 (C-18/19/20), 127.9 (C-18/19/20), 123.3 (d, ³J_{C-F} 6.7 Hz, C-7), 113.4 (d, ²J_{C-F} 23.0 Hz, C-8), 110.1 (C-5), 105.0 (d, ³J_{C-F} 2.9 Hz, C-11), 80.2 (C-22), 66.3 (C-16), 49.9 (C-13/14), 49.8 (C-13/14), 34.5 (C-3), 28.4 (C-23), 8.1 (C-1/2)

¹⁹F NMR (376 MHz, CDCl₃) δ (ppm): -123.6 (dd, ³J_{H-F} 13.5 Hz, ⁴J_{H-F} 6.5 Hz)

IR (ATIR) (cm⁻¹): 2979.9 *m* (C-H), 1698.4 *s* (C=O), 1623.0 *s* (C=O), 1588.9 *m* (C=C)

Characterisation data consistent with literature.¹²⁶

Benzyl 1-cyclopropyl-6-fluoro-4-oxo-7-(piperazin-1-yl)-1,4-dihydroquinoline-3-carboxylate trifluoroacetic acid salt, 4-10



Benzyl 7-(4-(*tert*-butoxycarbonyl)piperazin-1-yl)-1-cyclopropyl-6-fluoro-4-oxo-1,4-dihydroquinoline-3-carboxylate (**4-9**) (1.239 g, 2.38 mmol) was dissolved in CH₂Cl₂ (50 mL). Trifluoroacetic acid (5 mL) was added and the mixture stirred at room temperature for 17 h. The reaction was concentrated *in vacuo*. The residue was dissolved in EtOH (10 x 20 mL) and the solvent removed *in vacuo* to remove residual trifluoroacetic acid and give the title compound **4-10** as a cream solid.

Yield: 1.270 g, 2.38 mmol, 100%

m.p. 229.1 - 231.3 °C (lit. 250 -255 °C dec. for HCl salt ¹²⁶)

HRMS (ESI): *m/z* calculated for C₂₄H₂₅FN₃O₃ [M+H]⁺ 422.1874 found 422.1878 (-0.8 ppm error), C₂₄H₂₄FN₃NaO₃ [M+H]⁺ 444.1694 found 444.1713 (-4.2 ppm error)

¹H NMR (400 MHz, DMSO-d₆) δ (ppm): 9.20 (br s, 2H, -NH₂), 8.47 (s, 1H, H-4), 7.78 (d, ³J_{H-F} 13.5 Hz, 1H, H-8), 7.31-7.50 (m, 6H, H-11/18/19/20), 5.27 (s, 2H, H-16), 3.66 (m, 1H, H-3), 3.45 (m, 6H, H-13/14), 3.34 (m, 2H, H-13/14), 1.24 (m, 2H, H-1^a/2^a), 1.09 (m, 2H, H-1^b/2^b)

¹³C NMR (100 MHz, DMSO-d₆) δ (ppm): 171.6 (d, ⁴J_{C-F} 1.9 Hz, C-6), 164.6 (C-15), 152.5 (d, ¹J_{C-F} 246.3 Hz, C-9), 148.6 (C-4), 142.8 (d, ²J_{C-F} 10.5 Hz, C-10), 138.0 (C-12/17), 136.6 (C-12/17), 128.4 (C-18/19/20), 127.8 (C-18/19/20), 127.6 (C-18/19/20), 122.6 (d, ³J_{C-F} 6.7 Hz, C-7), 111.8

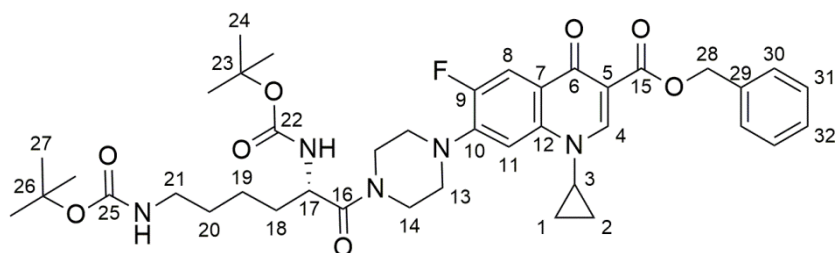
(d, $^2J_{C-F}$ 22.0 Hz, C-8), 108.9 (C-5), 106.8 (d, $^3J_{C-F}$ 2.9 Hz, C-11), 65.3 (C-16), 46.6 (d, $^4J_{C-F}$ 3.8 Hz, C-13), 42.7 (C-14), 34.9 (C-3), 7.6 (C-1/2)

^{19}F NMR (376 MHz, DMSO- d_6) δ (ppm): -73.6 (s), -124.5 (dd, $^3J_{H-F}$ 13.5 Hz, $^4J_{H-F}$ 7.9 Hz)

IR (ATIR) (cm^{-1}): 3488.6 *br w*, 2968.8 *m* (C-H), 2843.3 *m* (C-H), 2742.9 *m* (C-H), 2544.1 *m*, 1708.4 *s* (C=O), 1688.3 *s* (C=O), 1613.7 *s* (C=C)

Characterisation data consistent with literature.¹²⁶

(S)-benzyl **7-(4-(2,6-bis((*tert*-butoxycarbonyl)amino)hexanoyl)piperazin-1-yl)-1-cyclopropyl-6-fluoro-4-oxo-1,4-dihydroquinoline-3-carboxylate, 4-11**



Benzyl 1-cyclopropyl-6-fluoro-4-oxo-7-(piperazin-1-yl)-1,4-dihydroquinoline-3-carboxylate trifluoroacetic acid salt (**4-10**) (0.376 g, 0.70 mmol), (*S*)-2,6-bis((*tert*-butoxycarbonyl)amino)hexanoic acid (**4-8**) (0.246 g, 0.71 mmol), HOBT.H₂O (0.096 g, 0.71 mmol), EDC.HCl (0.138 g, 0.72 mmol) and DIPEA (0.185 mL, 0.138 g, 1.06 mmol) were dissolved in anhydrous DMF (25 mL). The mixture was stirred at room temperature for 18.5 h. The reaction mixture was concentrated *in vacuo*, the residue taken up in H₂O (80 mL) and extracted with CH₂Cl₂ (3 x 100 mL). The combined organic extracts were washed with H₂O (80 mL), 0.05 M HCl (80 mL), 0.05 M NaHCO₃ (80 mL), brine (80 mL) and H₂O (80 mL). The organic phase was dried over MgSO₄, and the solvent removed *in vacuo*

and the residue purified by column chromatography (20:1 CHCl₃:MeOH) to give the title compound **4-11** as a colourless solid.

Yield: 0.290 g, 0.386 mmol, 55%

m.p. 103.1 - 105.4 °C

R_f 0.19 (20:1 CHCl₃:MeOH)

HRMS (ESI): *m/z* calculated for C₄₀H₅₃FN₅O₈ [M+H]⁺ 750.3873 found 750.3873 (-0.0 ppm error), C₄₀H₅₂FN₅NaO₈ [M+H]⁺ 772.3692 found 752.3690 (0.2 ppm error)

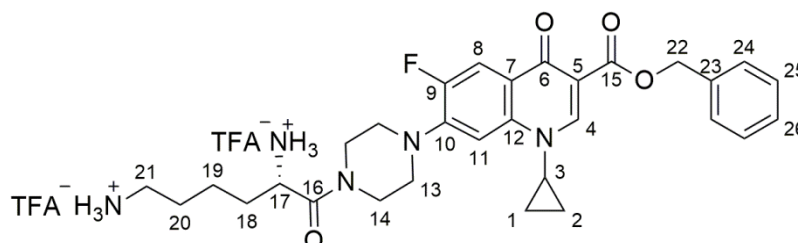
¹H NMR (400 MHz, CDCl₃) δ (ppm): 8.55 (s, 1H, H-4), 8.10 (d, ³J_{H-F} 12.9 Hz, 1H, H-8), 7.53 (m, 2H, H-11/32), 7.29-7.40 (m, 4H, H-30/31), 5.43 (d, ³J_{H-H} 9.2 Hz, -NH), 5.40 (s, 2H, H-28), 4.63 (m, 2H, H-17/-NH), 3.73 (m, 4H, H-13), 3.42 (m, 1H, H-3), 3.09-3.30 (m, 6H, H-14/21), 1.74 (m, 1H, H-18^a), 1.55 (m, 3H, H-18^b/20), 1.43 (m, 20H, H-19/24/27), 1.33 (m, 2H, H-1^a/2^a), 1.13 (m, 2H, H-1^b/2^b)

¹³C NMR (100 MHz, CDCl₃) δ (ppm): 172.9 (d, ⁴J_{C-F} 1.9 Hz, C-6), 170.8 (C-16), 165.5 (C-15), 156.0 (C-22/25), 155.6 (C-22/25), 153.3 (d, ¹J_{C-F} 248.3 Hz, C-9), 148.4 (C-4), 143.8 (d, ²J_{C-F} 10.5 Hz, C-10), 137.9 (C-12/29), 136.4 (C-12/29), 128.5 (C-30/31/32), 127.9 (C-30/31/32), 127.9 (C-30/31/32), 123.6 (d, ³J_{C-F} 6.7 Hz, C-7), 113.5 (d, ²J_{C-F} 23.0 Hz, C-8), 110.2 (C-5), 105.2 (d, ³J_{C-F} 2.9 Hz, C-11), 79.8 (C-22/25), 79.1 (C-22/25), 66.4 (C-28), 50.3 (C-13), 49.7 (C-17), 45.4 (C-14), 41.8 (C-19), 40.1 (C-21), 34.5 (C-3), 33.2 (C-18), 29.5 (C-20), 28.4 (C-24/27), 28.3 (C-24/27), 22.3 (C-18), 8.1 (C-1/2)

¹⁹F NMR (376 MHz, CDCl₃) δ (ppm): -123.8 (dd, ³J_{H-F} 12.9 Hz, ⁴J_{H-F} 7.2 Hz)

IR (ATIR) (cm⁻¹): 3321.1 *br w*, 2975.2 *m* (C-H), 1693.8 *s* (C=O), 1620.7 *s* (C=O)

(S)-benzyl 1-cyclopropyl-7-(4-(2,6-diaminohexanoyl)piperazin-1-yl)-6-fluoro-oxo-1,4-dihydroquinoline-3-carboxylate trifluoroacetic acid salt, 4-12



(S)-Benzyl 7-(4-(2,6-bis((*tert*-butoxycarbonyl)amino)hexanoyl)piperazin-1-yl)-1-cyclopropyl-6-fluoro-4-oxo-1,4-dihydroquinoline-3-carboxylate (**4-11**) (0.502 g, 0.67 mmol) was dissolved in CH₂Cl₂ (50 mL). Trifluoroacetic acid (2 mL) was added and the mixture stirred at room temperature for 16 h. The solvent was removed *in vacuo*. The residue was dissolved in EtOH (20 x 20 mL) and the solvent removed *in vacuo* to remove residual trifluoroacetic acid and give the title compound **4-12** as a cream solid.

Yield: 0.520 g, 0.67 mmol, 100%

m.p. 68.1 - 71.1 °C (dec.), 97.4 - 99.7 °C

HRMS (ESI): *m/z* calculated for C₃₀H₃₇FN₅O₄ [M+H]⁺ 550.2824 found 550.2819 (1.0 ppm error), C₃₀H₃₆FN₅NaO₄ [M+H]⁺ 572.2644 found 552.2632 (0.2 ppm error)

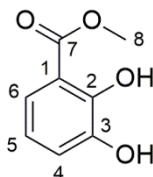
¹H NMR (400 MHz, CD₃OD) δ (ppm): 8.54 (s, 1H, H-4), 7.67 (d, ³J_{H-F} 12.8 Hz, 1H, H-8), 7.44 (m, 2H, H-11/29), 7.34 (m, 4H, H-24/25), 5.27 (s, 2H, H-22), 4.58 (m, 1H, H-17), 3.94 (m, 1H, H-14), 3.72 (m, 3H, H-14), 3.54 (m, 1H, H-13), 3.35 (m, 2H, H-13), 3.20 (m, 1H, H-13), 3.00 (m, 2H, H-21), 1.93 (m, 2H, H-18), 1.77 (m, 2H, H-19/20), 1.58 (m, 2H, H-19/20), 1.26 (m, 2H, H-1^a/2^a), 1.06 (m, 2H, H-1^b/2^b)

^{13}C NMR (100 MHz, CD_3OD) δ (ppm): 175.2 (C-6), 168.9 (C-16), 165.7 (C-15), 154.7 (d, $^1J_{\text{C-F}}$ 248.3 Hz, C-9), 150.2 (C-4), 145.7 (d, $^2J_{\text{C-F}}$ 10.5 Hz, C-10), 139.7 (d, $^4J_{\text{C-F}}$ 1.9 Hz, C-12), 137.9 (C-23), 129.8 (C-24/25/26), 129.4 (C-24/25/26), 129.4 (C-24/25/26), 121.1 (C-7), 113.2 (d, $^2J_{\text{C-F}}$ 24.0 Hz, C-8), 109.8 (C-5), 107.5 (d, $^3J_{\text{C-F}}$ 1.9 Hz, C-11), 67.3 (C-22), 51.6 (C-17), 51.2 (d, $^4J_{\text{C-F}}$ 3.8 Hz, C-13), 50.7 (d, $^4J_{\text{C-F}}$ 2.9 Hz, C-13), 46.6 (C-14), 43.4 (C-14), 40.4 (C-21), 36.5 (C-3), 31.6 (C-18), 28.3 (C-20), 22.7 (C-19), 8.7 (C-1/2)

^{19}F NMR (376 MHz, CD_3OD) δ (ppm): -76.7 (s), -124.4 (m)

IR (ATIR) (cm^{-1}): 3414.7 *w* (N-H), 2950.4 *m* (C-H), 1672.5 *s* (C=O), 1621.7 *s* (C=O), 1478.7 *s* (C-H bend)

Methyl 2,3-dihydroxybenzoate, 4-14



2,3-Dihydroxybenzoic acid (**4-13**) (2.008 g, 13.03 mmol) was dissolved in MeOH (17 mL) and conc. H_2SO_4 (0.7 mL) was added. The mixture was heated under reflux for 23 h, then cooled to room temperature and concentrated *in vacuo*. The residue was dissolved in EtOAc (70 mL) washed with sat. aq. NaHCO_3 (3 x 30 mL) and brine (2 x 30 mL). The organic phase was dried over MgSO_4 , filtered and the solvent removed *in vacuo* to give the title compound **4-14** a pale yellow solid.

Yield: 1.981 g, 11.78 mmol, 90%

m.p. 79.6 - 81.2 $^\circ\text{C}$ (lit. 77 - 80 $^\circ\text{C}$ ²⁷⁰)

R_f 0.19 (1:9 EtOAc:Petroleum Ether 40-60)

HRMS (ESI): m/z calculated for $C_8H_8NaO_4$ $[M+Na]^+$ 191.0315 found 191.0313 (1.0 ppm error)

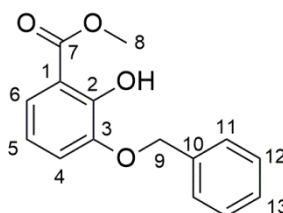
1H NMR (400 MHz, $CDCl_3$) δ (ppm): 10.92 (s, 1H, -OH), 7.37 (dd, $^3J_{H-H}$ 8.1 Hz, $^4J_{H-H}$ 1.5 Hz, 1H, H-6), 7.12 (m, 1H, H-4), 6.80 (t, $^3J_{H-H}$ 8.1 Hz, 1H, H-5), 5.74 (s, 1H, -OH), 3.96 (s, 3H, H-8)

^{13}C NMR (100 MHz, $CDCl_3$) δ (ppm): 171.2 (C-7), 149.2 (C-2), 145.3 (C-3), 120.8 (C-6), 120.0 (C-5), 119.4 (C-4), 112.5 (C-1), 52.3 (C-8)

IR (ATIR) (cm^{-1}): 3453.8 *br s* (O-H), 2956.5 *w* (C-H), 1668.3 *s* (C=O)

Characterisation data consistent with literature.^{207, 208, 270}

Methyl 3-(benzyloxy)-2-hydroxybenzoate, 4-15



Methyl 2,3-dihydroxybenzoate (**4-14**) (0.495 g, 2.94 mmol) was dissolved in MeOH (20 mL) with K_2CO_3 (0.407 g, 2.94 mmol). BnBr (0.35 mL, 0.503 g, 2.94 mmol) was added and the reaction mixture heated under reflux for 19.5 h under an inert atmosphere. The reaction mixture was cooled to room temperature and concentrated *in vacuo*. The residue was taken up in EtOAc (60 mL) and washed with H_2O (40 mL) and brine (2 x 40 mL). The organic layer was dried over $MgSO_4$, and the solvent removed *in vacuo* to give an oily residue. The residue was purified by column chromatography (1:9 EtOAc:Petroleum Ether 40-60) to give the title compound **4-15** as a colourless solid.

Yield: 0.245 g, 0.95 mmol, 32%

m.p. 63.3 - 65.1 °C (lit. 69.5 - 70.5 °C²⁷¹)

R_f 0.31 (1:9 EtOAc:Petroleum Ether 40-60)

HRMS (ESI): *m/z* calculated for C₁₅H₁₅O₄ [M+H]⁺ 259.0965 found 259.0964 (0.3 ppm error), C₁₅H₁₄NaO₄ [M+Na]⁺ 281.0784 found 281.0784 (0.1 ppm error)

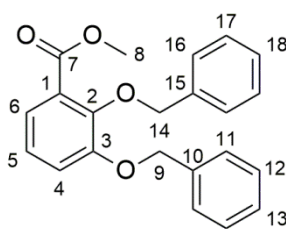
¹H NMR (400 MHz, CDCl₃) δ (ppm): 11.05 (s, 1H, -OH), 7.48 – 7.29 (m, 6H, H-4/11/12/13), 7.06 (dd, ³J_{H-H} 8.1 Hz, ⁴J_{H-H} 1.1 Hz, 1H, H-6), 6.76 (t, ³J_{H-H} 8.1 Hz, 1H, H-5), 5.18 (s, 2H, H-9), 3.96 (s, 3H, H-1)

¹³C NMR (100 MHz, CDCl₃) δ (ppm): 170.9 (C-2), 152.8 (C-8), 147.5 (C-7), 136.9 (C-10), 128.7 (C-12), 128.1 (C-13), 127.5 (C-11), 121.9 (C-4), 119.8 (C-5), 118.5 (C-6), 113.0 (C-3), 71.4 (C-9), 52.5 (C-1)

IR (ATIR) (cm⁻¹): 3057.8 *w* (C-H), 3028.5 *m* (C-H), 2948.8 *m* (C-H), 2873.9 *w* (C-H), 1728.0 *s* (C=O)

Characterisation data consistent with literature.^{207, 208}

Methyl 2,3-bis(benzyloxy)benzoate, 4-20



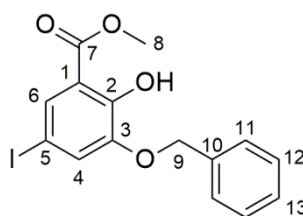
Isolated during the synthesis of **4-15**.

HRMS (ESI): *m/z* calculated for C₂₂H₂₁O₅ [M+H]⁺ 349.1434 found 349.1431 (1.0 ppm error), C₂₂H₂₀NaO₅ [M+Na]⁺ 371.1254 found 371.1250 (1.0 ppm error)

$^1\text{H NMR}$ (400 MHz, CDCl_3) δ (ppm): 7.33-7.48 (m, 11H, H-6/11/12/13/16/17/18), 7.16 (dd, $^3J_{\text{H-H}}$ 7.9 Hz, $^4J_{\text{H-H}}$ 1.1 Hz, 1H, H-6), 7.10 (t, $^3J_{\text{H-H}}$ 7.9 Hz, 1H, H-5), 5.16 (s, 2H, H-9/14), 5.13 (s, 2H, H-9/14), 3.86 (s, 3H, H-8)

Characterisation data consistent with literature.²⁷⁰

Methyl 3-(benzyloxy)-2-hydroxy-5-iodobenzoate, **4-16**



Methyl 3-benzyloxy)-2-hydroxybenzoate (**4-15**) (0.100 g, 0.39 mmol) was dissolved in MeOH (2 mL). NaI (0.087 g, 0.58 mmol) and NaOH (0.023 g, 0.58 mmol) were added and the solution cooled to 0 °C. NaClO (10-15%, 0.48 mL) was added dropwise and the reaction mixture allowed to warm to room temperature and stirred for 18 h. The mixture was quenched with $\text{Na}_2\text{S}_2\text{O}_3$ (10%, 3 mL) and adjusted to pH 7 with 1 M HCl. The aqueous phase was extracted with Et_2O (20 mL) and the combined organic phase dried over MgSO_4 , and concentrated *in vacuo*. The residue was purified by column chromatography (1:9 EtOAc:Petroleum Ether 40-60) to give the title compound **4-16** as a pale yellow solid.

Yield: 0.021 g, 0.05 mmol, 14%

m.p. 138.1 - 139.2 °C

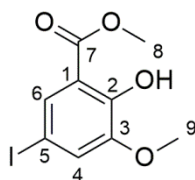
R_f 0.28 (1:9 EtOAc:Petroleum Ether 40-60)

HRMS (ESI): m/z calculated for $C_{15}H_{14}IO_4$ $[M+H]^+$ 384.9931 found 384.9932 (-0.3 ppm error), $C_{15}H_{13}INaO_4$ $[M+Na]^+$ 406.9751 found 406.9753 (-0.5 ppm error)

1H NMR (400 MHz, $CDCl_3$) δ (ppm): 11.01 (s, 1H, -OH), 7.79 (d, $^4J_{H-H}$ 1.8 Hz, 1H, H-6), 7.32-7.47 (m, 5H, H-4/11/12/13), 5.13 (s, 2H, H-9), 3.96 (s, 3H, H-8)

Characterisation data consistent with literature.²⁰⁸

Methyl 2-hydroxy-5-iodo-3-methoxybenzoate, 4-22



Iodine monochloride (0.825 mL, 2.673 g, 1.65 mmol) was dissolved in $CHCl_3$ (25 mL) then added dropwise over 30 min. to a solution of $AgNO_3$ (2.816 g, 1.66 mmol) in $CHCl_3$ (30 mL) and pyridine (20 mL). The mixture was stirred for 1 h at room temperature, then a solution of methyl-3-methoxysalicylate (**4-21**) (1.999 g, 1.10 mmol) in $CHCl_3$ (25 mL) was added dropwise over 30 min, and stirring was continued for 22 h. The mixture was diluted with Et_2O (100 mL), the insoluble material filtered off and washed with a mixture of $CHCl_3:Et_2O$ (1:1, 200 mL). The combined filtrates were concentrated *in vacuo*, giving a solid-residue which was dissolved in $CHCl_3$ (200 mL) and washed with 0.1 M hydrochloric acid (100 mL), sat. aq. $Na_2S_2O_3$ (2 x 100 mL) and H_2O (100 mL). The organic layer was dried over $MgSO_4$, and concentrated *in vacuo*. The residual solid was recrystallised with hot $EtOH$ and co-crystallised with a minimal amount of H_2O to induce precipitation. The resulting precipitate was

filtered and washed with cold H₂O to give the title compound **4-22** as a pale yellow solid.

Yield: 2.286 g, 0.74 mmol, 68%

m.p. 112.4 - 114.3 °C

R_f 0.20 (10% EtOAc in Petroleum Ether 40-60)

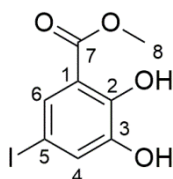
HRMS (ESI): *m/z* calculated for C₉H₁₀IO₄ [M+H]⁺ 308.9618 found 308.9619 (-0.1 ppm error), C₉H₉INaO₄ [M+Na]⁺ 330.9438 found 330.9426 (3.6 ppm error)

¹H NMR (400 MHz, CDCl₃) δ (ppm): 10.98 (s, 1H, -OH), 7.74 (d, ⁴J_{H-H} 2.1 Hz, 1H, H-4/6), 7.23 (d, ⁴J_{H-H} 2.1 Hz, 1H, H-4/6), 3.95 (s, 3H, H-8), 3.88 (s, 3H, H-9)

¹³C NMR (100 MHz, CDCl₃) δ (ppm): 169.5 (C-7), 152.0 (C-2/3), 149.3 (C-2/3), 129.5 (C-4/6), 124.9 (C-4/6), 114.1 (C-1), 79.2 (C-5), 56.4 (C-9), 52.6 (C-8)

IR (ATIR) (cm⁻¹): 3087.2 w (C-H), 2982.5 w (C-H), 2942.1 w (C-H), 1672.6 m (C=O)

Methyl 2,3-dihydroxy-5-iodobenzoate, **4-23**



Methyl 2-hydroxy-5-iodo-3-methoxybenzoate (**4-22**) (4.052 g, 13.15 mmol) was dissolved in CH₂Cl₂ (10 mL). BBr₃ (1 M in CH₂Cl₂, 22 mL, 22 mmol) was added and the mixture stirred at room temperature for 17.5 h. Ice cold H₂O (25 mL) was slowly added and the mixture stirred for a

further 1 h. The reaction was concentrated *in vacuo*. MeOH was added then removed *in vacuo* (3 x 100 mL). The residue was dissolved in MeOH (100 mL) and conc. H₂SO₄ (4 mL), and heated under reflux for 18.5 h. The reaction was concentrated *in vacuo*, the residue dissolved in EtOAc (300 mL) and washed with sat. aq. NaHCO₃ (3 x 150 mL) and brine (2 x 150 mL). The organic layer was dried over over MgSO₄, the solvent removed *in vacuo* to give the title compound **4-23** as a pale brown solid.

Yield: 3.512 g, 11.94 mmol, 91%

m.p. 136.1 - 137.6 °C

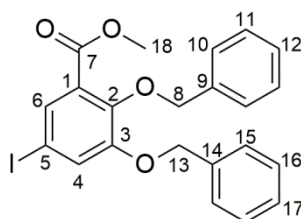
R_f 0.14 (1:9 EtOAc:Petroleum Ether 40-60)

HRMS (ESI): *m/z* calculated for C₈H₈IO₄ [M+H]⁺ 294.9462 found 294.9457 (1.7 ppm error), C₉H₇INaO₄ [M+Na]⁺ 316.9281 found 316.9274 (2.2 ppm error)

¹H NMR (400 MHz, CDCl₃) δ (ppm): 10.89 (s, 1H, -OH), 7.70 (d, ⁴J_{H-H} 2.3 Hz, 1H, H-4/6), 7.40 (d, ⁴J_{H-H} 2.3 Hz, 1H, H-4/6), 5.67 (br s, 1H, -OH), 3.97 (s, 3H, H-8)

¹³C NMR (100 MHz, CDCl₃) δ (ppm): 169.6 (C-7), 148.9 (C-2/3), 146.0 (C-2/3), 129.2 (C-4/6), 128.3 (C-4/6), 114.1 (C-1), 80.1 (C-5), 52.8 (C-8)

IR (ATIR) (cm⁻¹): 3448.7 *br s* (O-H), 3088.0 *m* (C-H), 2956.5 *m* (C-H), 1663.5 *s* (C=O)

Methyl 2,3-bis(benzyloxy)-5-iodobenzoate, 4-5

A mixture of methyl 2,3-dihydroxy-5-iodobenzoate (**4-23**) (1.499 g, 5.09 mmol), NaI (0.057 g, 0.38 mmol) and K_2CO_3 (3.110 g, 22.50 mmol) were suspended in anhydrous DMF (30 mL). BnBr (3.9 mL, 5.608 g, 32.79 mmol) was added and the mixture stirred at room temperature for 19 h. The reaction was concentrated *in vacuo* and the residue partitioned between EtOAc (100 mL) and H_2O (60 mL). The layers were separated and the aqueous phase extracted with EtOAc (2 x 100 mL). The combined organic extracts were dried over $MgSO_4$, filtered and the solvent removed *in vacuo* to give a solid residue which was purified by column chromatography (1:9 EtOAc:Petroleum Ether 40-60) to give the title compound **4-5** as a colourless solid.

Yield: 1.730 g, 3.65 mmol, 72%

m.p. 101.9 - 102.8 °C (lit. 105 - 106 °C²⁰⁷)

R_f 0.26 (1:9 EtOAc:Petroleum Ether 40-60)

HRMS (ESI): m/z calculated for $C_{22}H_{19}INaO_4$ $[M+Na]^+$ 497.0220 found 497.0230 (-2.0 ppm error)

¹H NMR (400 MHz, $CDCl_3$) δ (ppm): 7.70 (d, $^4J_{H-H}$ 1.8 Hz, 1H, H-4/6), 7.30-7.46 (m, 11H, H-4/6/10/11/12/15/16/17), 5.11 (s, 2H, H-8/13), 5.07 (s, 2H, H-8/13), 3.85 (s, 3H, H-18)

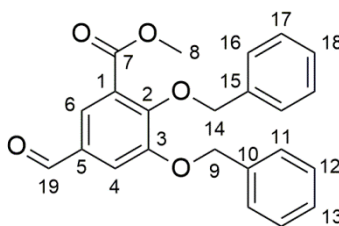
¹³C NMR (100 MHz, $CDCl_3$) δ (ppm): 165.2 (C-7), 153.5 (C-2/3), 148.2 (C-2/3), 137.0 (C-5/9/14), 135.8 (C-5/9/14), 131.5 (C-5/9/14), 128.7 (C-

4/6/10/11/12/15/16/17), 128.6 (C-4/6/10/11/12/15/16/17), 128.4 (C-4/6/10/11/12/15/16/17), 128.3 (C-4/6/10/11/12/15/16/17), 128.1 (C-4/6/10/11/12/15/16/17), 127.6 (C-4/6/10/11/12/15/16/17), 126.5 (C-1/4/6/10/11/12/15/16/17), 86.3 (C-5), 75.1 (C-8/13), 71.5 (C-8/13), 52.4 (C-18)

IR (ATIR) (cm^{-1}): 3027.9 *w* (C-H), 1716.7 *s* (C=O)

Characterisation data consistent with literature.²⁰⁷

Methyl 2,3-bis(benzyloxy)-5-formylbenzoate, 4-24



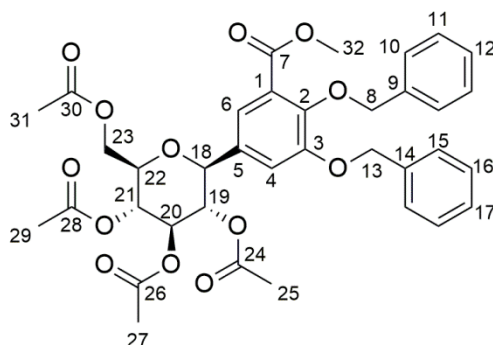
By-product isolated during the synthesis of **4-7**.

HRMS (ESI): *m/z* calculated for $\text{C}_{23}\text{H}_{20}\text{NaO}_5$ $[\text{M}+\text{Na}]^+$ 399.1203 found 399.1189 (3.5 ppm error)

^1H NMR (400 MHz, CDCl_3) δ (ppm): 9.92 (s, 1H, H-19), 7.89 (d, $^4J_{\text{H-H}}$ 2.0 Hz, 1H, H-4/6), 7.68 (d, $^4J_{\text{H-H}}$ 2.0 Hz, 1H, H-4/6), 7.31-7.48 (m, 10H, H-11/12/13/16/17/18), 5.22 (s, 2H, H-9/14), 5.20 (s, 2H, H-9/14), 3.89 (s, 3H, H-8)

^{13}C NMR (100 MHz, CDCl_3) δ (ppm): Crude spectrum indicated 190.4 (C-19)

(2*R*,3*R*,4*R*,5*S*,6*S*)-2-(acetoxymethyl)-6-(3,4-bis(benzyloxy)-5-(methoxycarbonyl)phenyl)tetrahydro-2*H*-3,4,5-triyl triacetate, 4-7



Part 1:

To a flame dried Schlenk flask in a glove box was added Zn (0.186 g, 2.84 mmol) and LiCl (0.077 g, 1.82 mmol). The flask was taken from the glove box and heated at 70 °C for 1.75 h *in vacuo*. A solution of I₂ (0.029 g, 0.11 mmol) and methyl 2,3-bis(benzyloxy)-5-iodobenzoate (**4-5**) (0.775 g, 1.63 mmol) in anhydrous DMF (3.3 mL) was added to the flask *via* syringe. The resultant mixture was stirred at 70 °C for 1 h under an inert atmosphere to give **4-6** (~0.5 M concentration in DMF).

Part 2:

To a flame dried Schlenk flask in a glove box was added 4,4',4''-tri-*tert*-butyl-2,2':6'2''-terpyridine (0.066 g, 0.17 mmol), bis(1,5-cyclooctadiene)nickel(0) (0.032 g, 0.12 mmol) and anhydrous DMF (2 mL). The mixture was stirred for 15 min and then acetobromo- α -D-glucose (0.402 g, 0.98 mmol) was added. The flask was taken from the glove box and the solution of **4-6** (~0.5 M in DMF, 3.2 mL) was added *via* syringe, and the mixture stirred at room temperature under an inert atmosphere for 19 h.

Work-Up/Purification:

The reaction mixture was concentrated *in vacuo* and the residue purified by silica gel chromatography (1:1 EtOAc:Petroleum Ether 40-60) to give the title compound **4-7** as a colourless solid.

Yield: 0.420 g, 0.62 mmol, 63%

m.p. 124.1 - 126.6 °C (lit. 128 - 129 °C²⁰⁷)

R_f 0.36 (1:1 EtOAc:Petroleum Ether 40-60)

HRMS (ESI): *m/z* calculated for C₃₆H₃₈NaO₁₃ [M+Na]⁺ 701.2205 found 701.2195 (1.4 ppm error)

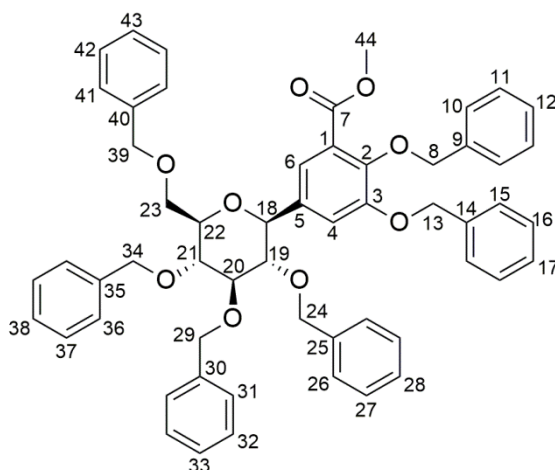
¹H NMR (400 MHz, CDCl₃) δ (ppm): 7.48-7.29 (m, 11H, H-4/10/11/12/15/16/17), 7.22 (d, ⁴J_{H-H} 2.3 Hz, 1H, H-6), 5.34 (t, ³J_{H-H} 9.6 Hz, 1H, H-20), 5.24 (t, ³J_{H-H} 9.6 Hz, 1H, H-21), 5.16-5.08 (m, 5H, H-8/13/19), 4.39 (d, ³J_{H-H} 10.1 Hz, 1H, H-18), 4.30 (dd, ²J_{H-H} 12.4 Hz, ³J_{H-H} 5.0 Hz, 1H, H-23^a), 4.18 (dd, ²J_{H-H} 12.4 Hz, ³J_{H-H} 2.3 Hz, 1H, H-23^b), 3.86 (m, 1H, H-22), 3.84 (s, 3H, H-32), 2.11 (s, 3H, H-25/27/29/31), 2.08 (s, 3H, H-25/27/29/31), 2.02 (s, 3H, H-25/27/29/31), 1.83 (s, 3H, H-25/27/29/31)

¹³C NMR (100 MHz, CDCl₃) δ (ppm): 170.6 (C-24/26/28/30), 170.2 (C-24/26/28/30), 169.5 (C-24/26/28/30), 168.9 (C-24/26/28/30), 166.2 (C-7), 153.1 (C-3), 148.5 (C-2), 137.1 (C-9/14), 136.2 (C-9/14), 132.0 (C-5), 128.5 (C-10/11/12/15/16/17), 128.2 (C-10/11/12/15/16/17), 128.1 (C-10/11/12/15/16/17), 127.9 (C-10/11/12/15/16/17), 127.6 (C-10/11/12/15/16/17), 126.2 (C-1), 122.1 (C-4), 115.7 (C-6), 79.4 (C-18), 76.2 (C-22), 75.5 (C-8/13), 74.0 (C-20), 72.2 (C-19), 71.3 (C-8/13), 68.5 (C-23), 62.3 (C-23), 52.1 (C-32), 20.7 (C-25/27/29/31), 20.6 (C-25/27/29/31), 20.3 (C-25/27/29/31)

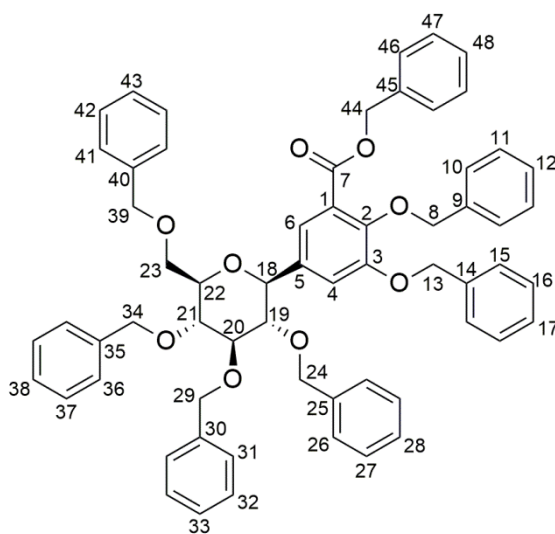
IR (ATIR) (cm⁻¹): 2950.3 *w* (C-H), 1739.6 *s* (C=O), 1713.9 *s* (C=O)

Characterisation data consistent with literature.²⁰⁷

Methyl 2,3-bis(benzyloxy)-5-((2*S*,3*S*,4*R*,5*R*,6*R*)-3,4,5-tris(benzyloxy)-6-((benzyloxy)methyl)tetrahydro-2*H*-pyran-2-yl)benzoate, 2-17 and benzyl 2,3-bis(benzyloxy)-5-((2*S*,3*S*,4*R*,5*R*,6*R*)-3,4,5-tris(benzyloxy)-6-((benzyloxy)methyl)tetrahydro-2*H*-pyran-2-yl)benzoate, 2-18



4-17



4-18

(2*R*,3*R*,4*R*,5*S*,6*S*)-2-(acetoxymethyl)-6-(3,4-bis(benzyloxy)-5-(methoxycarbonyl)phenyl)tetrahydro-2*H*-3,4,5-triyl triacetate (**4-7**) (0.777 g, 1.14 mmol) and Na₂CO₃ (0.607 g, 5.73 mmol) were suspended in anhydrous MeOH (50 mL). The mixture was heated under reflux for 18 h.

The cooled mixture was filtered and the residue washed with MeOH (3 x 20 mL). The reaction mixture was concentrated *in vacuo* to give a solid residue. To the solid was added NaH (60% dispersion in oil, 0.314 g, 7.85 mmol) and anhydrous DMF (15 mL). The mixture was stirred at 0 °C for 15 min. A solution of tetrabutylammonium iodide (0.047 g, 0.13 mmol) and BnBr (1.8 mL, 1.250 g, 7.3 mmol) in anhydrous DMF (5 mL) was added over 5 min. The reaction was stirred at 0 °C for 5 min then at room temperature for 19 h. To the reaction mixture was added H₂O (20 mL) and extracted with EtOAc (5 x 50 mL). The combined organic extracts were dried over MgSO₄, and the solvent removed *in vacuo* to give an oily residue which was purified by column chromatography (2:8 EtOAc:Petroleum Ether 40-60) to give the title compounds **4-17** and **4-18** as two colourless solids (combined yield 74%).

Compound 4-17:

Yield: 0.476 g, 0.55 mmol, 48%

R_f 0.16 (2:8 EtOAc:Petroleum Ether 40-60)

HRMS (ESI): *m/z* calculated for C₅₆H₅₄NaO₉ [M+Na]⁺ 893.3660 found 893.3676 (-1.8 ppm error)

¹H NMR (400 MHz, CDCl₃) δ (ppm): 7.51 (d, ⁴*J*_{H-H} 1.5 Hz, 1H, H-6), 7.31-7.46 (m, 24H, H-Ar), 7.21 (m, 5H, H-Ar), 6.95 (m, 2H, H-Ar), 5.12 (s, 2H, H-8), 5.00 (s, 2H, H-13), 4.87-4.97 (m, 3H, H-24/29/39), 4.58-4.68 (m, 3H, H-23/24/29), 4.46 (d, ³*J*_{H-H} 9.9 Hz, 1H, H-23), 4.22 (d, ³*J*_{H-H} 9.2 Hz, 1H, H-18), 3.86 (s, 3H, H-44), 3.76-3.82 (m, 5H, H-20/21/24/34), 3.61 (m, 1H, H-22), 3.44 (t, ³*J*_{H-H} 9.2 Hz, 1H, H-19)

¹³C NMR (100 MHz, CDCl₃) δ (ppm): 166.4 (C-7), 152.7 (C-3), 148.0 (C-2), 138.6 (C-5/9/14/25/30/35/40), 138.3 (C-5/9/14/25/30/35/40), 138.1 (C-5/9/14/25/30/35/40), 137.4 (C-5/9/14/25/30/35/40), 136.4 (C-5/9/14/25/30/35/40), 135.1 (C-5/9/14/25/30/35/40), 128.7 (C-Ar), 128.5 (C-Ar), 128.4 (C-Ar), 128.4 (C-Ar), 128.3 (C-Ar), 128.3 (C-Ar), 128.1

(C- Ar), 128.0 (C- Ar), 128.0 (C- Ar), 127.8 (C- Ar), 127.7 (C- Ar), 127.6 (C- Ar), 127.6 (C- Ar), 127.6 (C- Ar), 126.4 (C- Ar), 121.9 (C-6), 116.7 (C-4), 86.7 (C-20), 84.0 (C-19), 80.9 (C-18), 79.3 (C-22), 78.2 (C-21), 75.7 (C-8/13/23/24/29/34/39), 75.6 (C-8/13/23/24/29/34/39), 75.2 (C-8/13/23/24/29/34/39), 75.0 (C-8/13/23/24/29/34/39), 73.4 (C-8/13/23/24/29/34/39), 71.2 (C-8/13/23/24/29/34/39), 69.0 (C-8/13/23/24/29/34/39)

Ar = 10/11/12/15/16/17/26/27/28/31/32/33/36/37/38/41/42/43

Characterisation data consistent with literature.²⁰⁷

Compound 4-18:

Yield: 0.287 g, 0.30 mmol, 26%

R_f 0.20 (2:8 EtOAc:Petroleum Ether 40-60)

HRMS (ESI): *m/z* calculated for C₆₂H₅₈NaO₉ [M+Na]⁺ 969.3973 found 969.3977 (-0.4 ppm error)

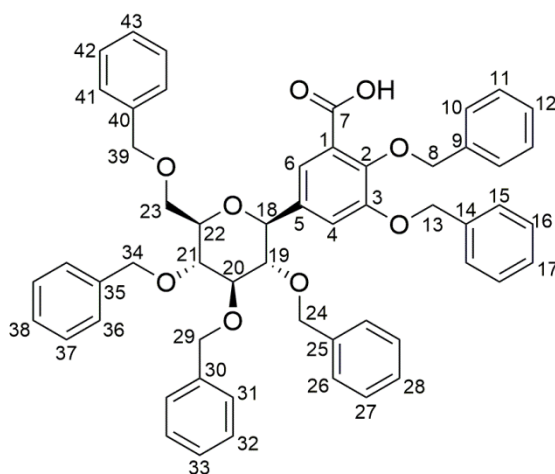
¹H NMR (400 MHz, CDCl₃) δ (ppm): 7.52 (d, ⁴*J*_{H-H} 1.7 Hz, 1H, H-6), 7.29-7.43 (m, 27H, H-Ar), 7.14-7.29 (m, 9H, H-4/Ar), 6.95 (m, 2H, H-Ar), 5.36 (d, ¹*J*_{H-H} 12.4 Hz, 1H, H-44^a), 5.32 (d, ¹*J*_{H-H} 12.4 Hz, 1H, H-44^b), 5.10 (d, ¹*J*_{H-H} 10.1 Hz, 1H, H-8^a), 5.08 (d, ¹*J*_{H-H} 10.1 Hz, 1H, H-8^b), 5.00 (s, 2H, H-13), 4.88-4.97 (m, 3H, H-24/29/39), 4.66 (d, ¹*J*_{H-H} 11.4 Hz, 2H, H-23/24/29), 4.59 (d, ¹*J*_{H-H} 12.4 Hz, 1H, H-23/24/29), 4.45 (¹*J*_{H-H} 10.5 Hz, 1H, H-23), 4.23 (d, ³*J*_{H-H} 9.2 Hz, 1H, H-18), 3.77-3.83 (m, 5H, H-20/21/24/34), 3.62 (m, 1H, H-22), 3.46 (t, ³*J*_{H-H} 9.4 Hz, H-19), 3.61 (m, 1H, H-22), 3.44 (t, ³*J*_{H-H} 9.2 Hz, 1H, H-19)

¹³C NMR (100 MHz, CDCl₃) δ (ppm): 165.9 (C-7), 152.5 (C-3), 148.0 (C-2), 138.6 (C-5/9/14/25/30/35/40/45), 138.2 (C-5/9/14/25/30/35/40/45), 138.1 (C-5/9/14/25/30/35/40/45), 137.4 (C-5/9/14/25/30/35/40/45), 137.2 (C-5/9/14/25/30/35/40/45), 136.3 (C-5/9/14/25/30/35/40/45), 135.9 (C-5/9/14/25/30/35/40/45), 135.1 (C-5/9/14/25/30/35/40/45), 128.7 (C-Ar),

128.5 (C-Ar), 128.4 (C- Ar), 128.4 (C- Ar), 128.4 (C- Ar), 128.3 (C- Ar), 128.2 (C- Ar), 128.2 (C- Ar), 128.1 (C- Ar), 128.1 (C- Ar), 128.0 (C- Ar), 127.9 (C- Ar), 127.8 (C- Ar), 127.8 (C- Ar), 127.7 (C- Ar), 127.6 (C- Ar), 127.6 (C- Ar), 126.4 (C- Ar), 122.0 (C-6), 116.5 (C-4), 86.6 (C-20), 83.9 (C-19), 80.9 (C-18), 79.3 (C-22), 78.2 (C-21), 75.6 (C-8/13/23/24/29/34/39/44), 75.6 (C-8/13/23/24/29/34/39/44), 75.1 (C-8/13/23/24/29/34/39/44), 75.0 (C-8/13/23/24/29/34/39/44), 73.4 (C-8/13/23/24/29/34/39/44), 71.0 (C-8/13/23/24/29/34/39/44), 68.9 (C-8/13/23/24/29/34/39/44), 67.0 (C-8/13/23/24/29/34/39/44)

Ar = 10/11/12/15/16/17/26/27/28/31/32/33/36/37/38/41/42/43/46/47/48

2,3-bis(benzyloxy)-5-((2*S*,3*S*,4*R*,5*R*,6*R*)-3,4,5-tris(benzyloxy)-6-((benzyloxy)methyl)tetrahydro-2*H*-pyran-2-yl)benzoic acid, 4-19



A mixture of methyl 2,3-bis(benzyloxy)-5-((2*S*,3*S*,4*R*,5*R*,6*R*)-3,4,5-tris(benzyloxy)-6-((benzyloxy)methyl)tetrahydro-2*H*-pyran-2-yl)benzoate, (**4-17**) and benzyl 2,3-bis(benzyloxy)-5-((2*S*,3*S*,4*R*,5*R*,6*R*)-3,4,5-tris(benzyloxy)-6-((benzyloxy)methyl)tetrahydro-2*H*-pyran-2-yl)benzoate, (**4-18**) (0.190 g) were dissolved in THF:MeOH (3:1, 20 mL). 5 M NaOH (5 mL) was added and the mixture stirred at room temperature for 14 h.

The mixture was acidified to pH 2.79 with 6 M HCl (~2 mL) and extracted with CH₂Cl₂ (5 x 30 mL). The combined organic extracts were dried over MgSO₄, and the solvent removed *in vacuo* to give an oily residue which was purified by column chromatography (30:1 CHCl₃:MeOH) to give the title compound **4-19** as a colourless solid.

Yield: 0.150 g, 0.17 mmol, 87%

m.p. 93.3 - 95.8 °C (lit. 94 - 96 °C²⁰⁷)

R_f 0.44 (30:1 CHCl₃:MeOH)

HRMS (ESI): *m/z* calculated for C₅₅H₅₂NaO₉ [M+Na]⁺ 879.3504 found 879.3516 (-1.4 ppm error)

¹H NMR (700 MHz, CDCl₃) δ (ppm): 11.27 (br s, 1H, -OH), 7.88 (d, ⁴J_{H-H} 1.7 Hz, 1H, H-6), 7.28-7.43 (m, 23H, H-Ar), 7.26 (d, ⁴J_{H-H} 1.7 Hz, 1H, H-4), 7.21 (m, 5H, H-Ar), 6.95 (m, 2H, H-Ar), 5.27 (d, ¹J_{H-H} 10.3 Hz, 1H, H-8^a), 5.25 (d, ¹J_{H-H} 10.3 Hz, 1H, H-8^b), 5.00 (d, ¹J_{H-H} 11.0 Hz, 1H, H-13^a), 4.97 (d, ¹J_{H-H} 11.0 Hz, 1H, H-13^b), 4.95 (d, ¹J_{H-H} 11.1 Hz, 1H, H-29^a), 4.93 (d, ¹J_{H-H} 11.1 Hz, 1H, H-29^b), 4.87 (d, ¹J_{H-H} 10.8 Hz, 1H, H-34^a), 4.64 (d, ¹J_{H-H} 10.8 Hz, 1H, H-34^b), 4.64 (d, ¹J_{H-H} 12.5 Hz, 1H, H-39^a), 4.58 (d, ¹J_{H-H} 12.5 Hz, 1H, H-39^b), 4.48 (d, ¹J_{H-H} 10.8 Hz, 1H, H-24^a), 4.24 (d, ³J_{H-H} 9.3 Hz, 1H, H-18), 3.84 (d, ¹J_{H-H} 10.8 Hz, 1H, H-24^b), 3.82 (t, ³J_{H-H} 9.2 Hz, 1H, H-20), 3.76 (d, ³J_{H-H} 3.2 Hz, 2H, H-23), 3.74 (t, ³J_{H-H} 9.3 Hz, 1H, H-21), 3.62 (dt, ³J_{H-H} 9.3, ³J_{H-H} 3.2 Hz, 1H, H-22), 3.43 (t, ³J_{H-H} 9.3 Hz, 1H, H-19)

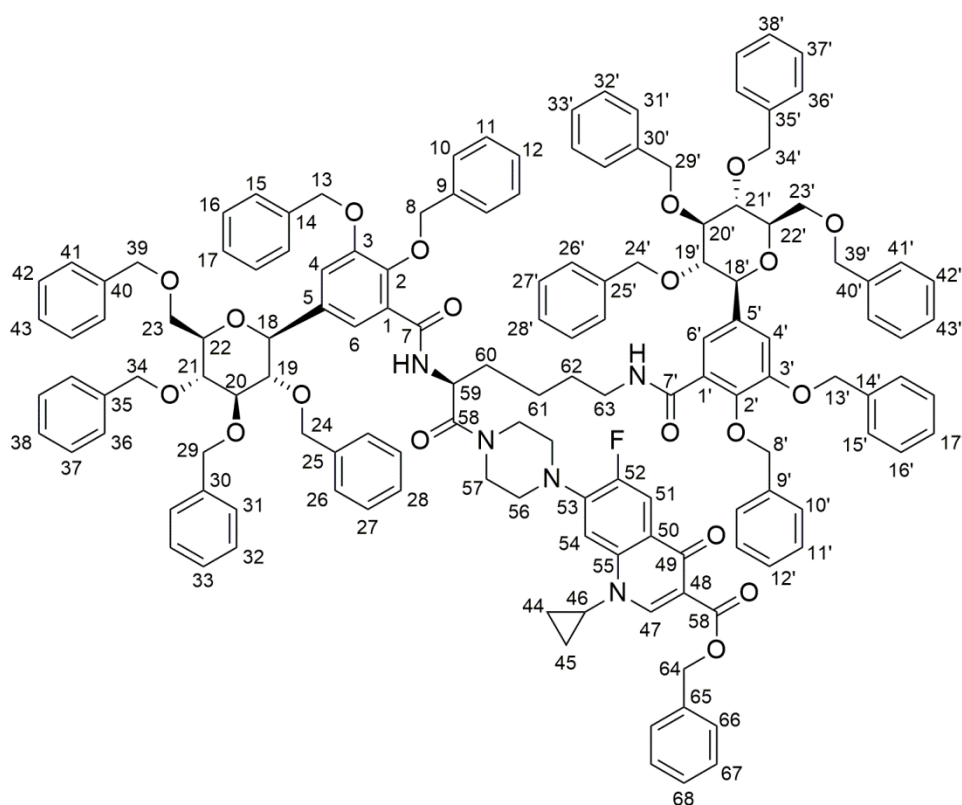
¹³C NMR (100 MHz, CDCl₃) δ (ppm): 165.2 (C-7), 151.0 (C-3), 146.5 (C-2), 138.5 (C-30), 138.1 (C-35/40), 138.0 (C-35/40), 137.7 (C-25), 136.3 (C-5), 135.7 (C-9), 134.6 (C-14), 129.3 (C-Ar), 129.2 (C-Ar), 128.7 (C-Ar), 128.7 (C-Ar), 128.5 (C-Ar), 128.4 (C-Ar), 128.4 (C-Ar), 128.2 (C-Ar), 128.1 (C-Ar), 128.0 (C-Ar), 127.8 (C-Ar), 127.7 (C-Ar), 127.7 (C-Ar), 127.6 (C-Ar), 127.6 (C-Ar), 127.6 (C-Ar), 123.1 (C-6), 122.8 (C-1), 117.7 (C-4), 86.7 (C-20), 83.6 (C-19), 80.5 (C-18), 79.3 (C-22), 78.2 (C-21), 76.9 (C-8), 75.6 (C-29), 75.1 (C-34), 74.9 (C-24), 73.4 (C-39), 71.2 (C-13), 69.0 (C-23)

IR (ATIR) (cm^{-1}): 3063.1 *w* (C-H), 3031.1 *w* (C-H), 2863.7 *w* (C-H), 1697.9 *m* (C=O), 1605.8 *w* (C=O)

Ar = 10/11/12/15/16/17/26/27/28/31/32/33/36/37/38/41/42/43

Characterisation data consistent with literature.²⁰⁷

Benzyl 7-(4-((*S*)-2,6-bis(2,3-bis(benzyloxy)-5-((*2S,3S,4R,5R,6R*)-3,4,5-tris(benzyloxy)-6-((benzyloxy)methyl)tetrahydro-2*H*-pyran-2-yl)benzamido)hexanoyl)piperazin-1-yl)-1-cyclopropyl-6-fluoro-4-oxo-1,4-dihydroquinoline-3-carboxylate, 4-25



Method A:

2,3-bis(benzyloxy)-5-((*2S,3S,4R,5R,6R*)-3,4,5-tris(benzyloxy)-6-((benzyloxy)methyl)tetrahydro-2*H*-pyran-2-yl)benzoic acid (**2-19**) (0.023

g, 0.03 mmol) was dissolved in anhydrous CH_2Cl_2 (2 mL) and anhydrous DMF (0.02 mL). Thionyl chloride (0.05 mL) was added and the mixture stirred at room temperature for 3 h. The mixture was concentrated *in vacuo* then dried for 2 h. The residue was dissolved in anhydrous CH_2Cl_2 (5 mL) a solution of (*S*)-benzyl 1-cyclopropyl-7-(4-(2,6-diaminohexanoyl)piperazin-1-yl)-6-fluoro-4-oxo-1,4-dihydroquinoline-3-carboxylate trifluoroacetic acid salt (**4-12**) (0.011 g, 0.01 mmol) and Et_3N (0.05 mL) in anhydrous CH_2Cl_2 (1 mL) was added at 0 °C. The mixture was warmed to room temperature and stirred for 19 h. The reaction was concentrated *in vacuo* to give an oily residue which was purified by column chromatography (3:2 CHCl_3 :EtOAc) to give the title compound **4-25** as a colourless solid.

Yield: 0.006 g, 0.003 mmol, 19%

Method B:

A mixture of (*S*)-benzyl 1-cyclopropyl-7-(4-(2,6-diaminohexanoyl)piperazin-1-yl)-6-fluoro-4-oxo-1,4-dihydroquinoline-3-carboxylate trifluoroacetic acid salt (**4-12**) (0.228 g, 0.29 mmol), 2,3-bis(benzyloxy)-5-((2*S*,3*S*,4*R*,5*R*,6*R*)-3,4,5-tris(benzyloxy)-6-((benzyloxy)methyl)tetrahydro-2*H*-pyran-2-yl)benzoic acid (**2-19**) (0.552 g, 0.64 mmol), HOBT. H_2O (0.122 g, 0.90 mmol), EDC.HCl (0.141 g, 0.73 mmol) and DIPEA (1.5 mL, 2.022 g, 15.6 mmol) were dissolved in anhydrous CH_2Cl_2 (40 mL). The mixture was stirred at room temperature for 19 h. The reaction was concentrated *in vacuo*. The residue was dissolved in EtOAc (200 mL) and washed with 0.1 M HCl (100 mL), 0.1 M NaHCO_3 (100 mL), brine (100 mL) and H_2O (100 mL). The organic layer was dried over MgSO_4 , and the solvent removed *in vacuo* to give a solid residue which was purified by column chromatography (4:1 to 3:2 CHCl_3 :MeCN) to give the title compound **4-25** as a colourless solid.

Yield: 0.275 g, 0.12 mmol, 42%

R_f 0.28 (3:2 CHCl_3 :MeCN)

HRMS (ESI): m/z calculated for $C_{140}H_{137}FN_5NaO_{20}$ $[M+Na]^+$ 2249.9733
found 2249.9665 (3.0 ppm error)

1H NMR (400 MHz, $CDCl_3$) δ (ppm): 8.68 (d, $^3J_{H-H}$ 7.8 Hz, 1H, -NH), 8.51 (s, 1H, H-47), 8.12 (d, $^3J_{H-F}$ 12.8 Hz, 1H, H-51), 7.88 (m, 3H, H-6/6'/-NH), 7.53 (m, 2H, H-51/Ar), 7.28-7.42 (m, 46H, H-51/Ar), 7.17-7.25 (m, 16H, H-Ar), 6.96 (m, 4H, H-Ar), 5.41 (s, 2H, H-64), 5.27 (d, $^1J_{H-H}$ 10.5 Hz, 1H, H-8/8'), 5.09 (m, 3H, H-8/8'/60), 5.02 (d, $^1J_{H-H}$ 10.5 Hz, 1H, H-8/8'), 4.98 (s, 4H, H-39/39'), 4.93 (m, 4H, H-29/29'/34/34'/39/39'), 4.88 (d, $^1J_{H-H}$ 10.5 Hz, 2H, H-29/29'/34/34'/39/39'), 4.63 (d, $^1J_{H-H}$ 10.5 Hz, 2H, H-29/29'/34/34'/39/39'), 4.63 (d, $^1J_{H-H}$ 12.6 Hz, 2H, H-29/29'/34/34'/39/39'), 4.56 (d, $^1J_{H-H}$ 12.6 Hz, 2H, H-29/29'/34/34'/39/39') 4.44 (d, $^1J_{H-H}$ 10.5 Hz, 1H, H-24/24'), 4.44 (d, $^1J_{H-H}$ 10.5 Hz, 1H, H-24/24'), 4.26 (d, $^3J_{H-H}$ 9.6 Hz, 1H, H-18/18'), 4.19 (d, $^3J_{H-H}$ 9.2 Hz, 1H, H-18/18'), 3.90-4.01 (m, 3H, H-56/57), 3.72-3.86 (m, 13H, H-20/20'/21/21'/24/24'/56/57), 3.62 (m, 2H, H-22/22'), 3.50 (m, 4H, H-19/19'), 3.31 (m, 3H, H-46/56/57), 3.24 (m, 4H, H-56/57/64), 1.82 (m, 1H, H-61), 1.71 (m, 1H, H-61), 1.48 (m, 1H, H-62), 1.23-1.35 (m, 7H, H-44/45/62/63), 1.03 (m, 2H, H-44/45)

Ar = 10/10'/11/11'/12/12'/15/15'/16/16'/17/17'/26/26'/27/27'/28/28'/31/31'/32/32'/33/33'/36/36'/37/37'/41/41'/42/42'/43/43'

^{13}C NMR (125 MHz, $CDCl_3$) δ (ppm): 173.0 (C-49), 170.5 (C-59), 165.6 (C-58), 164.7 (C-7/7'), 164.5 (C-7/7'), 153.4 (d, $^1J_{C-F}$ 249.3 Hz, C-52), 151.5 (C-3/3'), 151.4 (C-3/3'), 148.3 (C-47), 146.5 (C-2/2'), 146.2 (C-2/2'), 144.0 (d, $^2J_{C-F}$ 11.0 Hz, C-53), 138.7 (C-Ar_a), 138.6 (C-Ar_a), 138.2 (C-Ar_a), 138.2 (C-Ar_a), 138.1 (C-Ar_a), 138.1 (C-Ar_a), 137.9 (C-Ar_a), 137.7 (C-Ar_a), 137.6 (C-Ar_a), 136.4 (C-Ar_a), 136.2 (C-Ar_a), 136.2 (C-Ar_a), 136.1 (C-Ar_a), 136.1 (C-Ar_a), 135.6 (C-Ar_a), 135.5 (C-Ar_a), 129.0 (C-Ar_b), 128.8 (C-Ar_b), 128.7 (C-Ar_b), 128.6 (C-Ar_b), 128.4 (C-Ar_b), 128.4 (C-Ar_b), 128.4 (C-Ar_b), 128.4 (C-Ar_b), 128.3 (C-Ar_b), 128.2 (C-Ar_b), 128.2 (C-Ar_b), 128.2 (C-Ar_b), 128.1 (C-Ar_b), 128.1 (C-Ar_b), 128.1 (C-Ar_b), 127.9 (C-Ar_b), 127.9 (C-Ar_b), 127.9 (C-Ar_b), 127.8 (C-Ar_b), 127.8 (C-Ar_b), 127.7 (C-Ar_b), 127.7 (C-Ar_b), 127.6 (C-Ar_b), 127.6 (C-Ar_b), 127.6 (C-Ar_b), 127.5 (C-Ar_b), 127.5 (C-Ar_b), 127.1 (C-Ar_b), 126.5 (C-Ar_b), 123.5 (d, $^3J_{C-F}$ 6.4 Hz, C-50), 122.1

(C-6/6'), 122.1 (C-6/6'), 116.3 (C-4/4'), 115.8 (C-4/4'), 113.5 (d, $^3J_{C-F}$ 22.9 Hz, C-51), 110.1 (C-48), 105.3 (d, $^3J_{C-F}$ 1.8 Hz, C-54), 86.7 (C-20/20'/21/21'), 86.6 (C-20/20'/21/21'), 83.9 (C-19/19'), 83.8 (C-19/19'), 81.1 (C-18/18'), 81.0 (C-18/18'), 79.3 (C-22/22'), 79.3 (C-22/22'), 78.3 (C-20/20'/21/21'), 76.3 (C-8/8'), 76.0 (C-8/8'), 75.5 (C-29/29'/34/34'/39/39'), 75.5 (C-29/29'/34/34'/39/39'), 75.1 (C-29/29'/34/34'/39/39'), 75.0 (C-29/29'/34/34'/39/39'), 74.8 (C-24/24'), 74.8 (C-24/24'), 73.4 (C-29/29'/34/34'/39/39'), 73.3 (C-29/29'/34/34'/39/39'), 71.2 (C-13/13'), 71.0 (C-13/13'), 69.2 (C-23/23'), 69.1 (C-23/23'), 66.3 (C-48), 50.2 (C-56/57), 49.9 (C-56/57), 48.7 (C-60), 45.6 (C-56/57), 41.9 (C-56/57), 39.3 (C-64), 34.5 (C-46), 32.4 (C-61), 29.2 (C-62), 23.1 (C-62), 8.1 (C-44/45)

Ar_a = 1/1'/5/5'/9/9'/14/14'/25/25'/30/30'/35/35'/40/40'/66

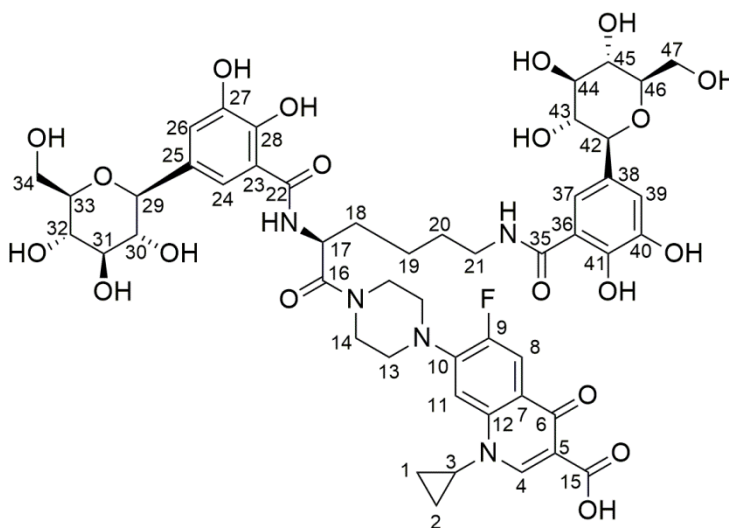
Ar_b = 10/10'/11/11'/12/12'/15/15'/16/16'/17/17'/26/26'/27/27'/28/28'/31/31/31'/32/32'/33/33'/36/36'/37/37'/38/38'/41/41'/42/42'/43/43'/67/68/69

^{19}F NMR (376 MHz, CDCl_3) δ (ppm): -123.6 (m)

IR (ATIR) (cm^{-1}): 3030.3 *w* (C-H), 2862.9 *w* (C-H), 1728.8 *m* (C=O), 1690.6 *m* (C=O), 1644.0 *s* (C=O), 1621.1 *s* (C=O)

Elemental Analysis: Calculated for $[\text{C}_{140}\text{H}_{136}\text{FN}_5\text{O}_{20}\cdot 0.35\text{CHCl}_3]$ %C 74.28, %H 6.06, %N 3.09, Measured for $[\text{C}_{140}\text{H}_{136}\text{FN}_5\text{O}_{20}\cdot 0.35\text{CHCl}_3]$ %C 74.28, %H 6.08, %N 3.07

7-(4-((*S*)-2,6-bis(2,3-dihydroxy-5-((2*S*,3*R*,4*R*,5*S*,6*R*)-3,4,5-trihydroxy-6-(hydroxymethyl)tetrahydro-2*H*-pyran-2-yl)benzamido)hexanoyl)piperazin-1-yl)-1-cyclopropyl-6-fluoro-4-oxo-1,4-dihydroquinoline-3-carboxylic acid, 4-3



Benzyl 7-(4-((*S*)-2,6-bis(2,3-bis(benzyloxy)-5-((2*S*,3*S*,4*R*,5*R*,6*R*)-3,4,5-tris(benzyloxy)-6-((benzyloxy)methyl)tetrahydro-2*H*-pyran-2-yl)benzamido)hexanoyl)piperazin-1-yl)-1-cyclopropyl-6-fluoro-4-oxo-1,4-dihydroquinoline-3-carboxylate (**4-25**) (0.125 g, 0.06 mmol) was dissolved in MeOH:EtOAc (1:1, 50 mL). Pd(OH)₂/C (20 wt. %, 0.192 g) was added and the mixture purged with N₂. The mixture was stirred under H₂ for 17 h, then filtered and washed with MeOH (50 mL). The filtrate was concentrated *in vacuo* to give a residue. The residue was taken up in MeOH (50 mL) and filtered again. The solvent was removed *in vacuo* to leave a solid residue which was purified by reverse phase preparative HPLC to give the title compound **4-3** as a white solid.

Preparative HPLC: Preparative HPLC Method A. Compound elutes at 9.24 minutes.

Analytical HPLC: Analytical HPLC Method C. Compound elutes at 9.53 minutes.

Yield: 0.027 g, 0.03 mmol 45%

m.p. 225.3 - 228.2 °C (dec.)

HRMS (ESI): m/z calculated for $C_{49}H_{58}FN_5NaO_{20}$ $[M+Na]^+$ 1078.3551 found 1078.3557 (-0.5 ppm error), $C_{49}H_{57}FN_5O_{20}$ $[M-H]^-$ 1054.3586 found 1054.3556 (2.8 ppm error)

1H NMR (700 MHz, DMSO- D_6) δ (ppm): 8.66 (s, 1H, H-4), 7.93 (d, $^3J_{H-F}$ 13.2 Hz, 1H, H-8), 7.56 (d, $^4J_{H-F}$ 6.6 Hz, 1H), 7.43 (br. s, 1H, H-24/26/37/39), 7.25 (br. s, 1H, H-24/26/37/39), 6.91 (br. s, 1H, H-24/26/37/39), 6.87 (br. s, 1H, H-24/26/37/39), 4.96-5.01 (m, 2H, H-13/14/17/29/30/31/32/33/34/42/43/44/45/46/47), 3.80-3.87 (m, 8H, H-13/14/17/29/30/31/32/33/34/42/43/44/45/46/47), 3.66-3.68 (m, 5H, H-13/14/17/29/30/31/32/33/34/42/43/44/45/46/47), 3.15-3.31 (m, 14H, H-13/14/17/29/30/31/32/33/34/42/43/44/45/46/47), 1.77-1.83 (m, 2H, H-18), 1.58 (m, 2H, H-20), 1.41 (m, 2H, H-19), 1.28 (m, 2H, H-1^a/2^a), 1.15 (m, 2H, H-1^b/2^b)

^{13}C NMR (175 MHz, DMSO- D_6) δ (ppm): 176.4 (C-6), 169.8 (C-16/22/35), 169.7 (C-16/22/35), 168.6 (C-16/22/35), 165.9 (C-15), 152.9 (d, $^1J_{C-F}$ 250.0 Hz, C-9), 149.2 (C-27/28/40/41), 148.1 (C-27/28/40/41), 145.6 (C-27/28/40/41), 144.8 (C-10), 139.2 (C-7), 118.9 (C-12/24/26/37/39), 118.4 (C-12/24/26/37/39), 116.9 (C-24/26/37/39), 114.7 (C-24/26/37/39), 114.0 (C-24/26/37/39), 111.0 (d, $^2J_{C-F}$ 24.1 Hz, H-8), 106.8 (C-11), 81.6 (C-29/30/31/32/33), 81.6 (C-29/30/31/32/33), 81.3 (C-29/30/31/32/33), 81.2 (C-29/30/31/32/33), 78.4 (C-29/30/31/32/33), 78.4 (C-29/30/31/32/33), 74.1 (C-29/30/31/32/33), 74.1 (C-29/30/31/32/33), 70.5 (C-29/30/31/32/33), 70.4 (C-29/30/31/32/33), 61.4 (C-34/47), 49.6 (C-13/14/17), 49.3 (C-13/14/17), 48.9 (C-13/14/17), 44.8 (C-13/14), 38.8 (C-21), 35.9 (C3), 31.0 (C-18), 28.8 (C-20), 22.9 (C-19), 7.6 (C-1/2), 7.6 (C-1/2)

^{19}F NMR (376 MHz, DMSO- D_6) δ (ppm): -121.6 (m)

IR (ATIR) (cm^{-1}): 3330.6 *br s* (O-H), 2951.8 *w* (C-H), 1704.9 *w* (C=O), 1625.5 *s* (C=O), 1445.8 *s*, 1332.0 *m*, 1257.9 *s* (C-O)

Elemental Analysis: Calculated for $[\text{C}_{49}\text{H}_{58}\text{FN}_5\text{O}_{20} \cdot 2.3\text{H}_2\text{O} \cdot 0.9.4\text{CH}_2\text{O}_2]$
%C 45.84, %H 5.36, %N 4.58, Measured for
 $[\text{C}_{49}\text{H}_{58}\text{FN}_5\text{O}_{20} \cdot 2.3\text{H}_2\text{O} \cdot 0.9.4\text{CH}_2\text{O}_2]$ %C 45.30, %H 4.80, %N 5.15

7.3 ^1H NMR study into the base hydrolysis of 3-16

Compound **3-16** (2.7 mg) was dissolved in CD_3OD (1 mL) and EtOH (0.1 mL). 0.7 mL of the solution was added to an NMR tube and a ^1H NMR spectrum collected (400MHz spectrometer - **Figure 95**). NaOD (40% in D_2O , 7 μL) was added and a spectrum ^1H NMR collected at time points: 1, 2, 4, 22, 31, 52, 92 and 168 h. The % ratio of species observed is listed in **Table 12** and plotted in Chapter 3.

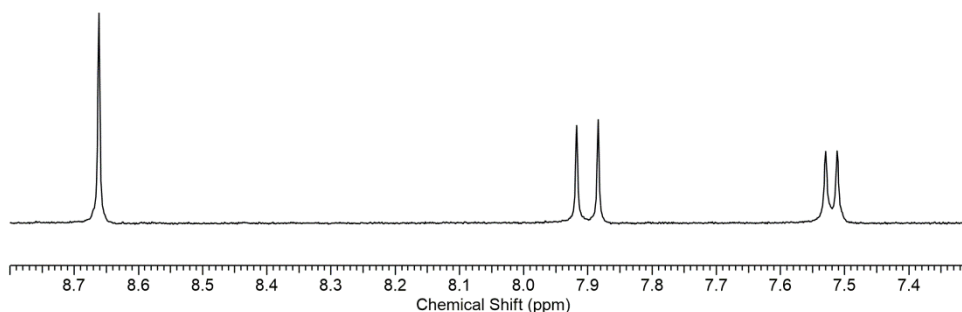


Figure 95 - ^1H NMR spectrum of the aromatic region of compound **3-16** in CD_3OD , prior to the addition of NaOD.

Time (h)	Compound 3-16	Ciprofloxacin 1-5	1 (8.55 ppm)	2 (8.65 ppm)	3 (8.52 ppm)
0	100	0	0	0	0
1	76	6	0	12	6
2	72	6	0	16	6
4	63	6	6	19	6
22	33	27	13	20	7
31	26	27	20	20	7
52	20	40	20	13	7
92	14	65	14	0	7
168	0	86	7	0	7

Table 12 - Ciprofloxacin containing species (%). As a reference to determine the % ratios between the species in the spectrum by their relative integration, the NMR solvent was spiked with EtOH as a standard.

7.4 Biological Studies

Bacterial Strains

Two bacterial strains were used: *E. coli* BW25113 Wild Type and BW25113 FecA::kan.^{60, 272}

Media

All solutions and media were prepared using MilliQ deionised H₂O and sterilised by autoclave prior to use. The antibiotic kanamycin was also added where required. LB media was prepared using 10 g tryptone, 5 g of yeast extract and 10 g NaCl per litre. M9 minimal media was prepared using 6 g Na₂HPO₄, 3 g KH₂PO₄, 1 g NH₄Cl and 0.5 g NaCl per litre and adjusted to pH 7. After autoclaving, the solution was supplemented with sterilised solutions of 20% w/v glucose, 1 M MgSO₄ and 1 M CaCl.

Growth Assays

*O/D*₆₅₀ measurements

Optical densities were recorded to 3 decimal places using a Jenway 6305 spectrophotometer in plastic cuvettes with a 1 cm path length, and are accurate to ± 0.0005 . These values were used to normalise the OD₆₅₀ of each culture prior to use in each growth assay.

Plate reader

The plate reader used was a BMG LabTech FLUOstar Omega plate reader. The OD₆₅₀ was measured every 30 minutes for 16 hours. The plate was shaken at 200 RPM between each measurement to maintain aerobic bacterial growth. Blank wells were measured for their optical densities and subtracted from the sample wells to normalise the OD₆₅₀ measurements used for data analysis.

Growth assay

Cultures of the selected strain were inoculated into 5 mL of media and shaken at 37 °C overnight. The OD₆₅₀ of each were normalised prior to use in the assay. To a 96 well plate was added (**Figure 96**): sterile H₂O (200 µL) in all perimeter wells; media (198 µL) in blank wells; media (193 µL) into remaining wells; specific concentrations of antimicrobial into each well (2 µL); normalised bacterial culture into each well (5 µL); DMSO into 0 µM row/DMSO row (2 µL); H₂O into blank wells (2 µL). The plate was placed into the plate reader and the experiment run as described above.

| H ₂ O |
|------------------|------------------|------------------|------------------|------------------|------------------|------------------|------------------|------------------|------------------|------------------|------------------|
| H ₂ O | Cip 1 | Cip 2 | Cip 3 | Cip 4 | DMSO | Conj 1 | Conj 2 | Conj 3 | Conj 4 | BLANK | H ₂ O |
| H ₂ O | Cip 1 | Cip 2 | Cip 3 | Cip 4 | DMSO | Conj 1 | Conj 2 | Conj 3 | Conj 4 | BLANK | H ₂ O |
| H ₂ O | Cip 1 | Cip 2 | Cip 3 | Cip 4 | DMSO | Conj 1 | Conj 2 | Conj 3 | Conj 4 | BLANK | H ₂ O |
| H ₂ O | Cip 1 | Cip 2 | Cip 3 | Cip 4 | DMSO | Conj 1 | Conj 2 | Conj 3 | Conj 4 | BLANK | H ₂ O |
| H ₂ O | Cip 1 | Cip 2 | Cip 3 | Cip 4 | DMSO | Conj 1 | Conj 2 | Conj 3 | Conj 4 | BLANK | H ₂ O |
| H ₂ O | Cip 1 | Cip 2 | Cip 3 | Cip 4 | DMSO | Conj 1 | Conj 2 | Conj 3 | Conj 4 | BLANK | H ₂ O |
| H ₂ O |
Drug Conc (µM)	Stock Conc (µM)										
0	0										
0.01	1										
0.1	10										
0.5	50										
1	100										
10	1000 (1 mM)										

Figure 96 - 96 well plate layout.

DNA Gyrase Assay

Agarose gel electrophoresis

TAE running buffer was prepared using 750 mL of H₂O, 48.4 g/L of Tris, 22.8 mL of glacial acetic acid, 200 mL of 29.2 g/L EDTA. The solution was made up to 1 L using H₂O. To produce a working concentration of TAE buffer the solution was diluted by 1 in 10 in H₂O. The agarose gels used were prepared using 1% w/v agarose in 1 x TAE buffer.

Stop buffer

To terminate the assay a combination of 24:1 solution of chloroform/isoamyl alcohol and stop buffer were used. The stop buffer was prepared using 40% w/v sucrose, 12.11 g/L Tris·HCl (pH 7.5), 0.29 g/L EDTA and 0.5 mg/mL of bromophenol blue.

DNA gyrase assay buffer

A pre-prepared kit from Inspiralis contained the DNA gyrase assay buffer. The buffer contained 3.92 g/L Tris·HCl (pH 7.5), 1.79 g/L KCl, 0.38 g/L MgCl₂, 0.3 g/L dithiothreitol, 0.26 g/L spermidine, 0.5 g/L ATP, 6.5% (w/v) glycerol and 0.1 mg/mL BSA.

DNA Gyrase Assay

Stock solutions of ciprofloxacin and the conjugates were prepared in 0.1 M acetic acid and DMSO, respectively. The antimicrobial compounds were combined with relaxed pBR322 DNA, DNA gyrase and assay buffer in H₂O at fixed proportions (**Table 13**). The solutions were incubated at 37 °C for 30 minutes. The assay was stopped with the addition of 30 µL of 24:1 CHCl₃:isoamyl alcohol and 30 µL stop buffer. A portion of 20 µL was loaded into a 1% agarose gel. The gel was subjected to electrophoresis for 80 minutes at 80 volts. The gel was then stained using ethidium bromide for 20 minutes and photographed using a gel doc.

Antimicrobial Concentration (µM) [Solution conc. Used]	Vol. of Anti. (µL)	Diluted Gyrase (µL)	Assay Buffer (µL)	pBR322 (µL)	H ₂ O (µL)
Positive Control	0	2	6	0.5	21.5
Negative Control	0	0	6	0.5	23.5
100 [300 µM]	10	2	6	0.5	11.5
75 [300 µM]	7.5	2	6	0.5	14
50 [300 µM]	5	2	6	0.5	16.5
40 [300 µM]	4	2	6	0.5	17.5
30 [300 µM]	3	2	6	0.5	18.5
20 [600 µM]	1	2	6	0.5	20.5
10 [300 µM]	1	2	6	0.5	20.5
5 [150 µM]	1	2	6	0.5	20.5
1 [30 µM]	1	2	6	0.5	20.5
0.5 [15 µM]	1	2	6	0.5	20.5
0 [0 µM]	1 (DMSO)	2	6	0.5	20.5

Table 13 - Volumes of solutions added to each sample for the DNA gyrase assay.

Appendix I. Crystal Data for Compound 2-39

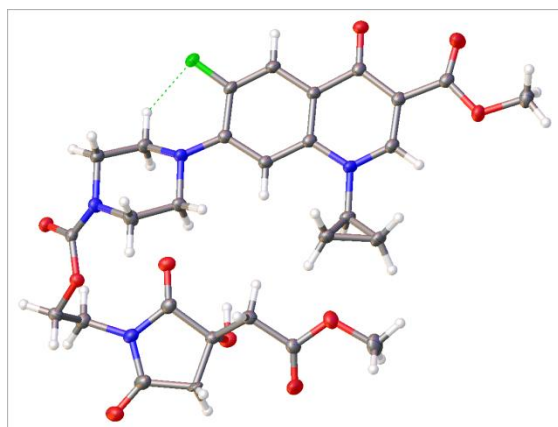


Table: Crystal data and structure refinement for akdk1401a (2-39).

Identification code	akdk1401a
Empirical formula	$C_{28}H_{31}FN_4O_{10}$
Formula weight	602.57
Temperature/K	110.05(10)
Crystal system	triclinic
Space group	P-1
$a/\text{\AA}$	10.3489(3)
$b/\text{\AA}$	11.1094(4)
$c/\text{\AA}$	12.6060(4)
$\alpha/^\circ$	76.067(3)
$\beta/^\circ$	73.907(3)
$\gamma/^\circ$	76.812(3)

Volume/Å ³	1331.14(9)
Z	2
ρ_{calc} mg/mm ³	1.503
m/mm ⁻¹	0.120
F(000)	632.0
Crystal size/mm ³	0.2282 × 0.1592 × 0.0624
Radiation	MoK α (λ = 0.71073)
2 Θ range for data collection	5.972 to 64.252°
Index ranges	-15 ≤ h ≤ 14, -15 ≤ k ≤ 15, -17 ≤ l ≤ 17
Reflections collected	12410
Independent reflections	8324 [R_{int} = 0.0195, R_{sigma} = 0.0431]
Data/restraints/parameters	8324/9/427
Goodness-of-fit on F ²	1.119
Final R indexes [$I \geq 2\sigma(I)$]	R_1 = 0.0631, wR_2 = 0.1478
Final R indexes [all data]	R_1 = 0.0849, wR_2 = 0.1597
Largest diff. peak/hole / e Å ⁻³	0.44/-0.41

Structure solved by Natalie Pridmore.

Appendix II. Individual Growth Assay Plots for Compound 2-12

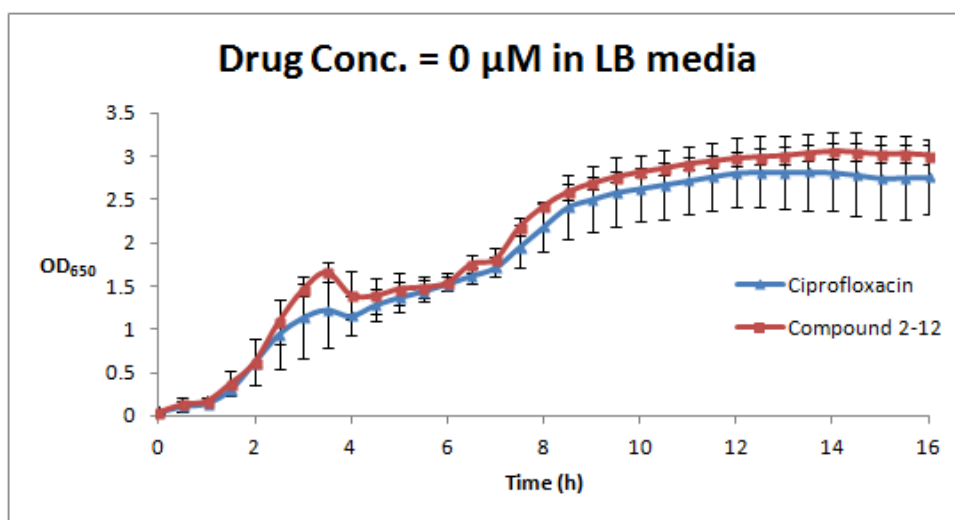


Figure 97 - *E. coli* BW25113WT growth in LB media with drug concentrations of 0 μ M for both ciprofloxacin **1-5** and conjugate **2-12**. The experiment was run in quadruplicate and the error bars show one standard deviation from the mean.

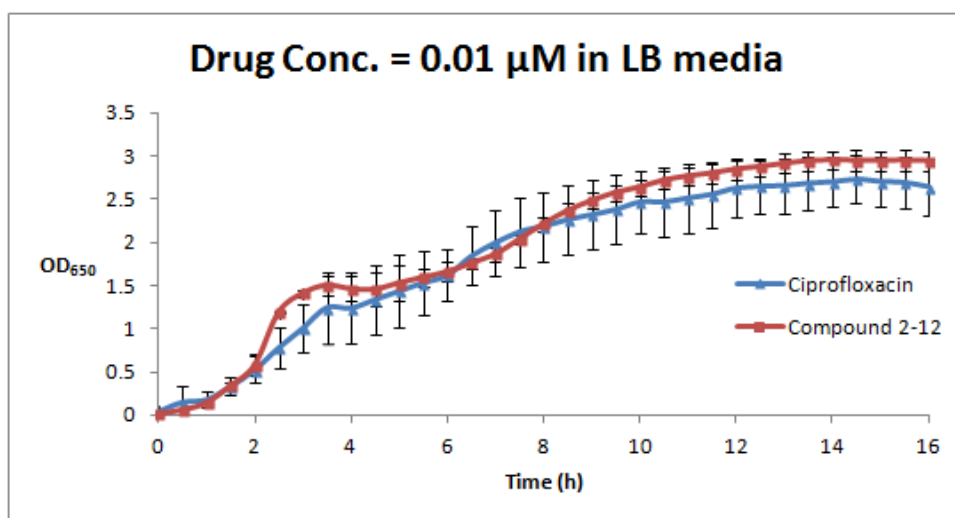


Figure 98 - *E. coli* BW25113WT growth in LB media with drug concentrations of 0.01 μ M for both ciprofloxacin **1-5** and conjugate **2-12**. The experiment was run in quadruplicate and the error bars show one standard deviation from the mean.

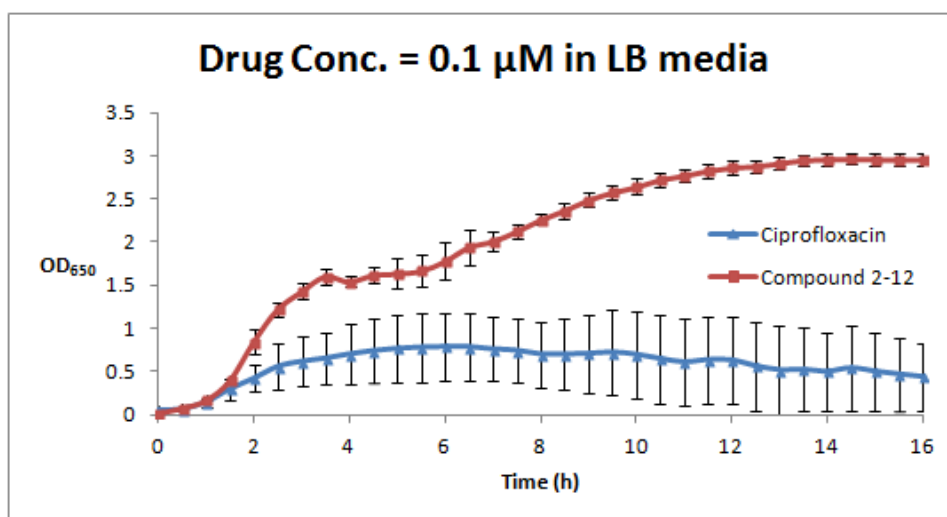


Figure 99 - *E. coli* BW25113WT growth in LB media with drug concentrations of 0.1 μM for both ciprofloxacin **1-5** and conjugate **2-12**. The experiment was run in quadruplicate and the error bars show one standard deviation from the mean.

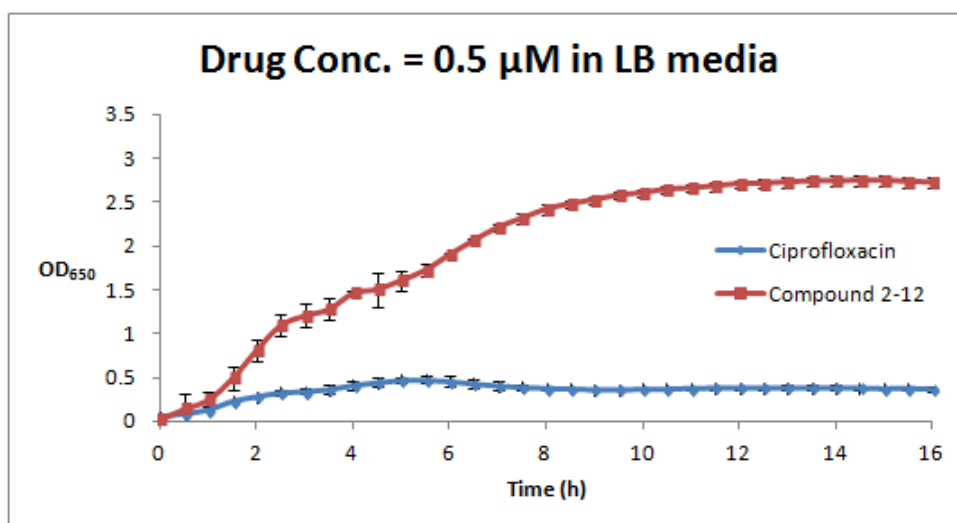


Figure 100 - *E. coli* BW25113WT growth in LB media with drug concentrations of 0.5 μM for both ciprofloxacin **1-5** and conjugate **2-12**. The experiment was run in quadruplicate and the error bars show one standard deviation from the mean.

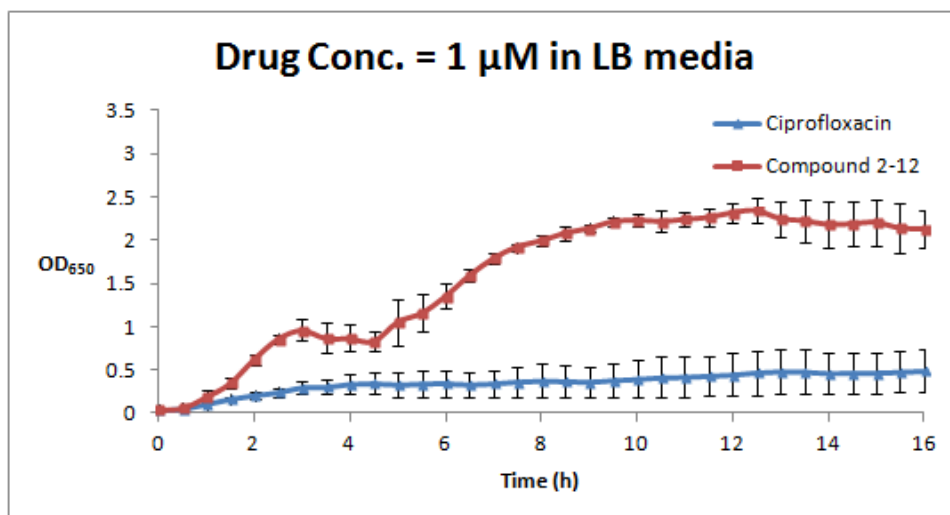


Figure 101 - *E. coli* BW25113WT growth in LB media with drug concentrations of 1 μM for both ciprofloxacin **1-5** and conjugate **2-12**. The experiment was run in quadruplicate and the error bars show one standard deviation from the mean.

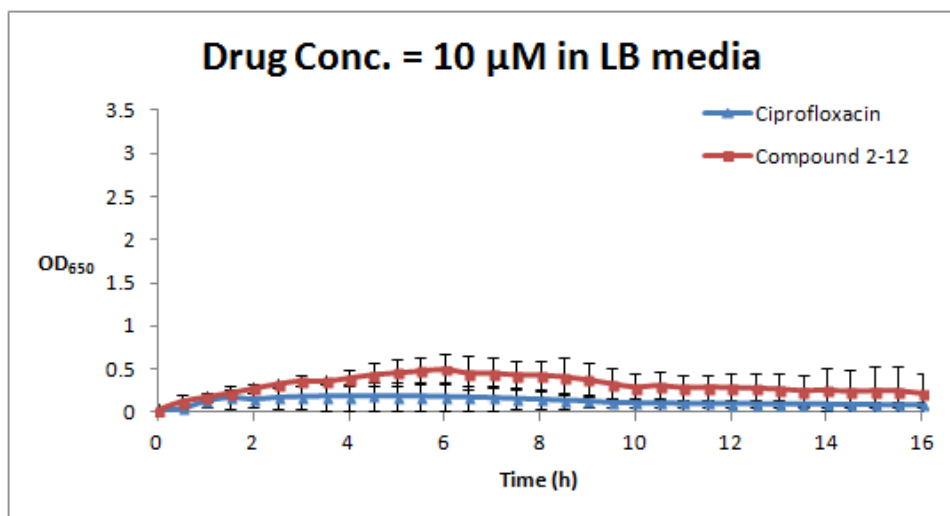


Figure 102 - *E. coli* BW25113WT growth in LB media with drug concentrations of 10 μM for both ciprofloxacin **1-5** and conjugate **2-12**. The experiment was run in quadruplicate and the error bars show one standard deviation from the mean.

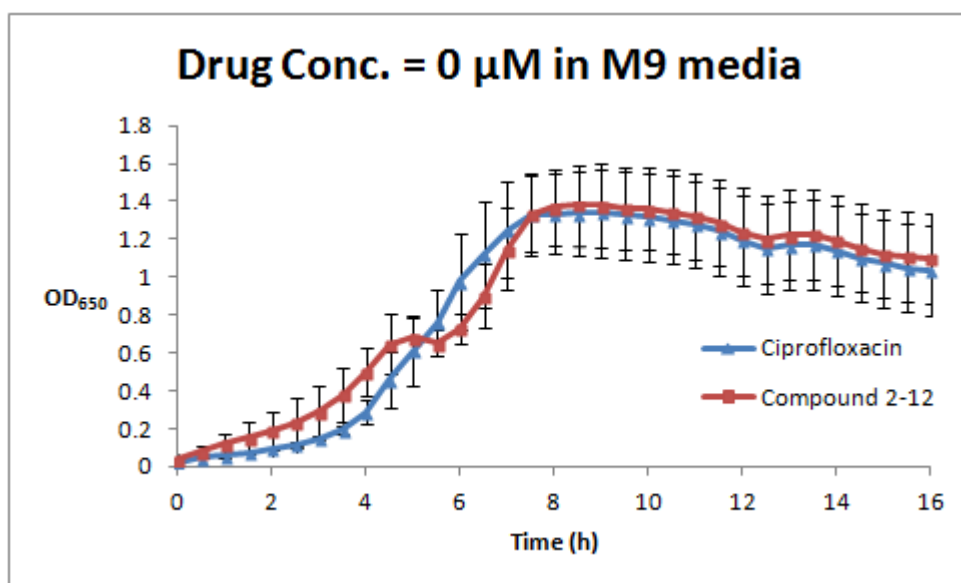


Figure 103 - *E. coli* BW25113WT growth in M9 minimal media with drug concentrations of 0 μM for both ciprofloxacin **1-5** and conjugate **2-12**. The experiment was run in quadruplicate and the error bars show one standard deviation from the mean.

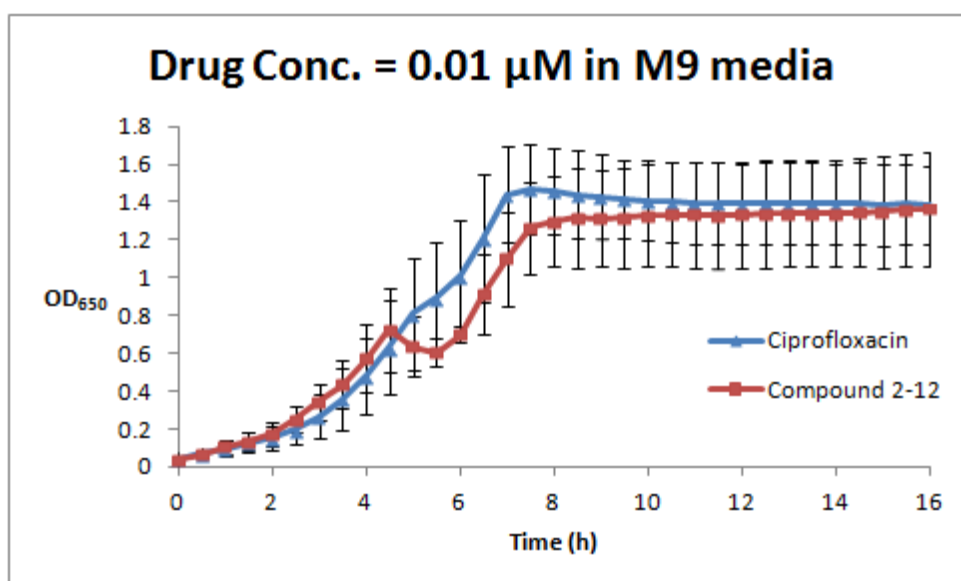


Figure 104 - *E. coli* BW25113WT growth in M9 minimal media with drug concentrations of 0.01 μM for both ciprofloxacin **1-5** and conjugate **2-12**. The experiment was run in quadruplicate for **2-12** and triplicate for ciprofloxacin, and the error bars show one standard deviation from the mean.

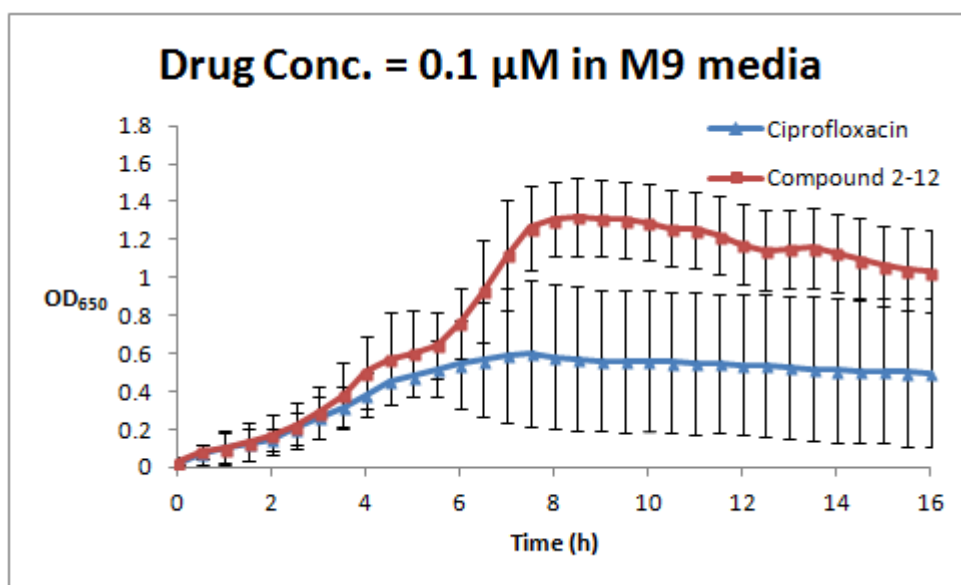


Figure 105 - *E. coli* BW25113WT growth in M9 minimal media with drug concentrations of 0.1 μM for both ciprofloxacin **1-5** and conjugate **2-12**. The experiment was run in quadruplicate and the error bars show one standard deviation from the mean.

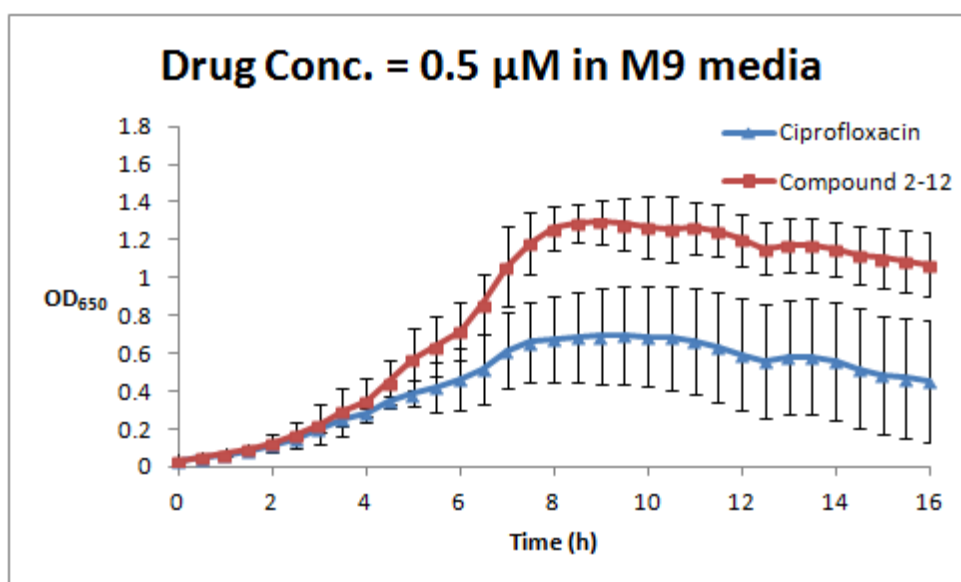


Figure 106 - *E. coli* BW25113WT growth in M9 minimal media with drug concentrations of 0.5 μM for both ciprofloxacin **1-5** and conjugate **2-12**. The experiment was run in quadruplicate and the error bars show one standard deviation from the mean.

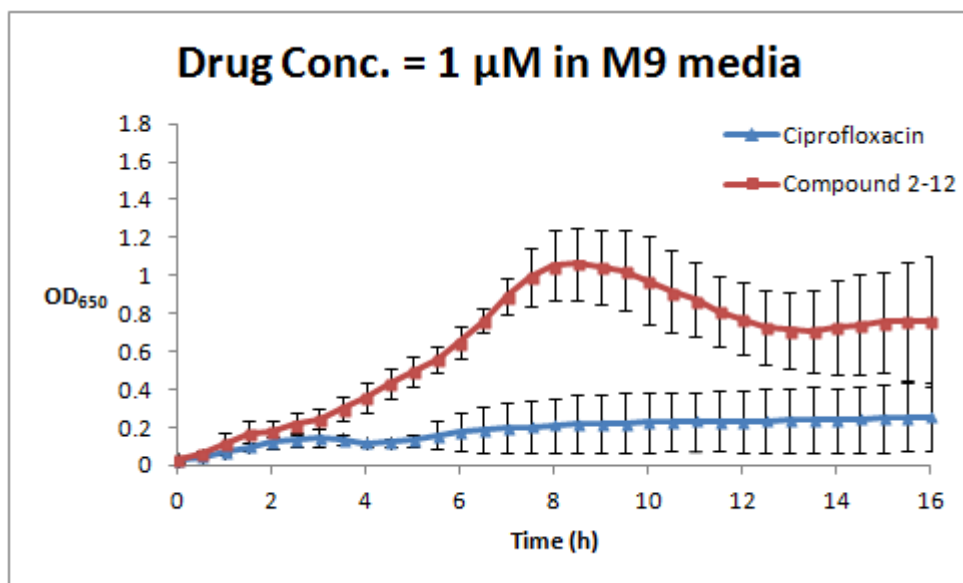


Figure 107 - *E. coli* BW25113WT growth in M9 minimal media with drug concentrations of 1 μ M for both ciprofloxacin **1-5** and conjugate **2-12**. The experiment was run in quadruplicate and the error bars show one standard deviation from the mean.

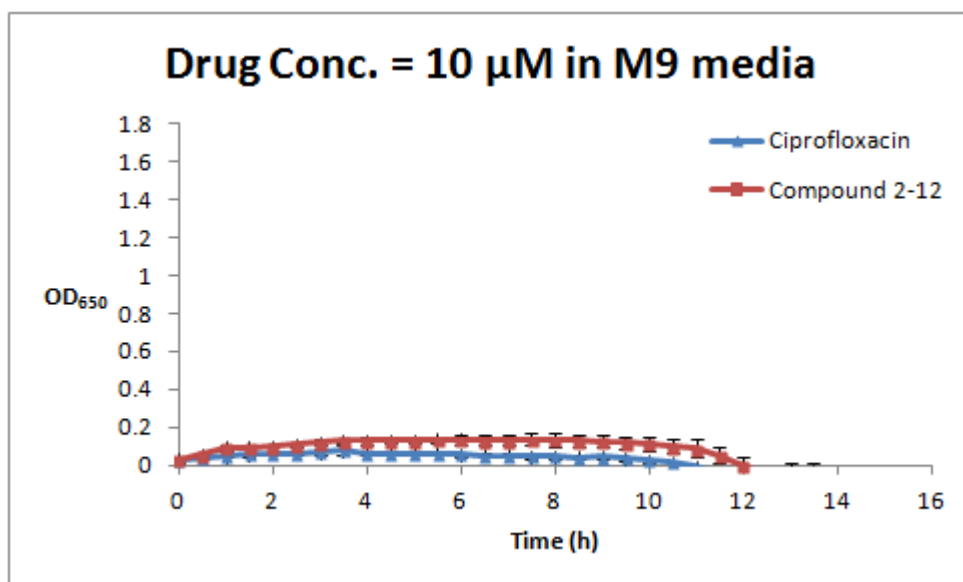


Figure 108 - *E. coli* BW25113WT growth in M9 minimal media with drug concentrations of 10 μ M for both ciprofloxacin **1-5** and conjugate **2-12**. The experiment was run in quadruplicate and the error bars show one standard deviation from the mean.

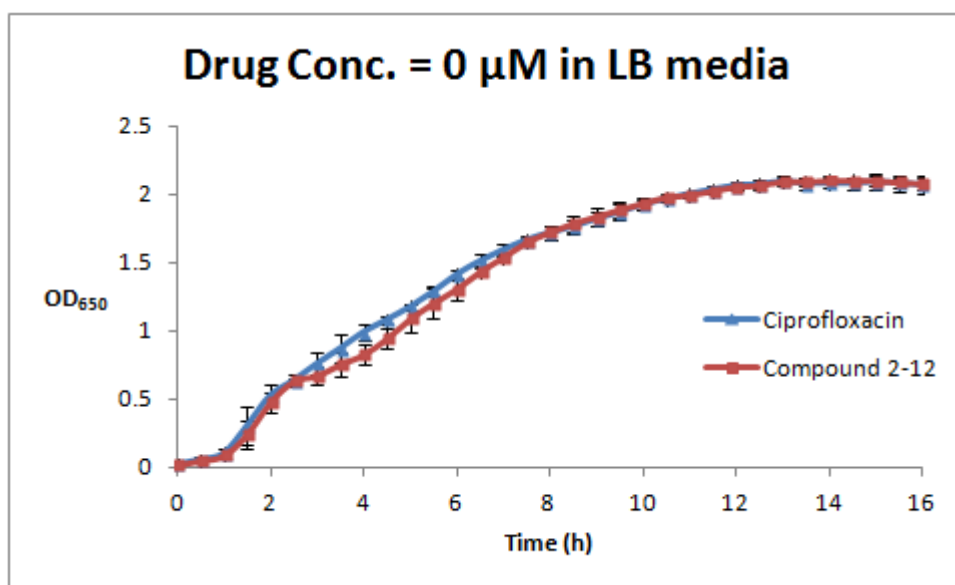


Figure 109 - *E. coli* BW25113 FecA::kan growth in LB media with drug concentrations of 0 μM for both ciprofloxacin **1-5** and conjugate **2-12**. The experiment was run in quadruplicate and the error bars show one standard deviation from the mean.

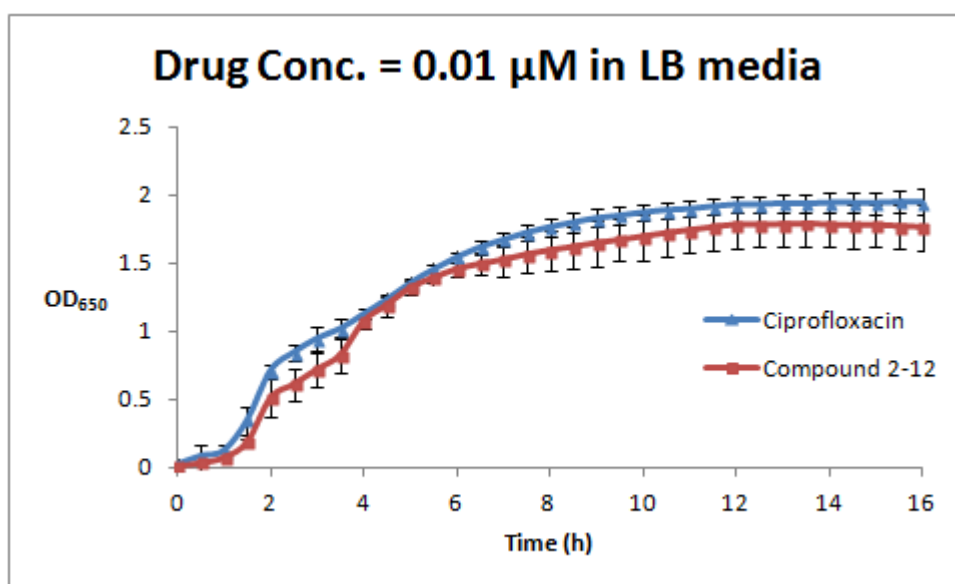


Figure 110 - *E. coli* BW25113 FecA::kan growth in LB media with drug concentrations of 0.01 μM for both ciprofloxacin **1-5** and conjugate **2-12**. The experiment was run in quadruplicate and the error bars show one standard deviation from the mean.

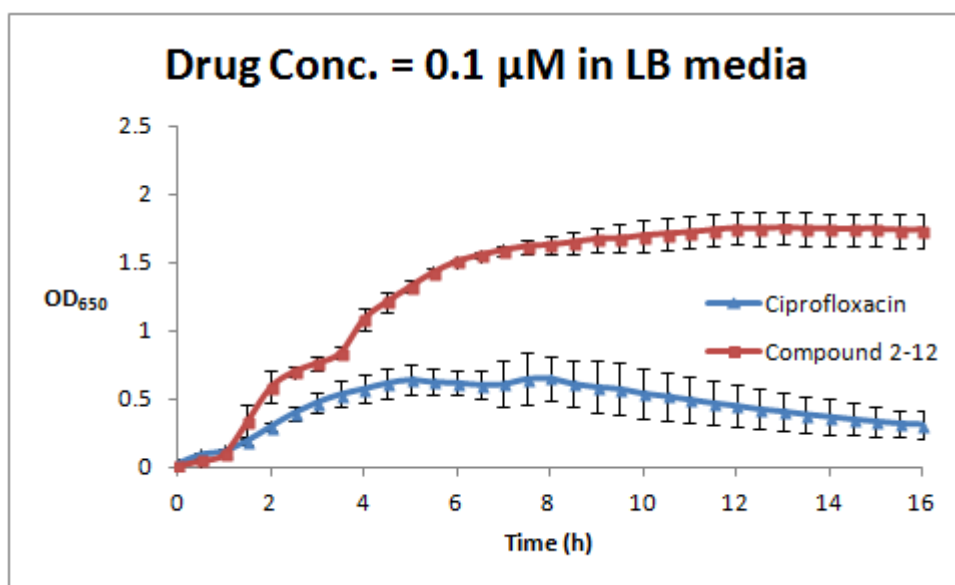


Figure 111 - *E. coli* BW25113 FecA::kan growth in LB media with drug concentrations of 0.1 μ M for both ciprofloxacin **1-5** and conjugate **2-12**. The experiment was run in quadruplicate and the error bars show one standard deviation from the mean.

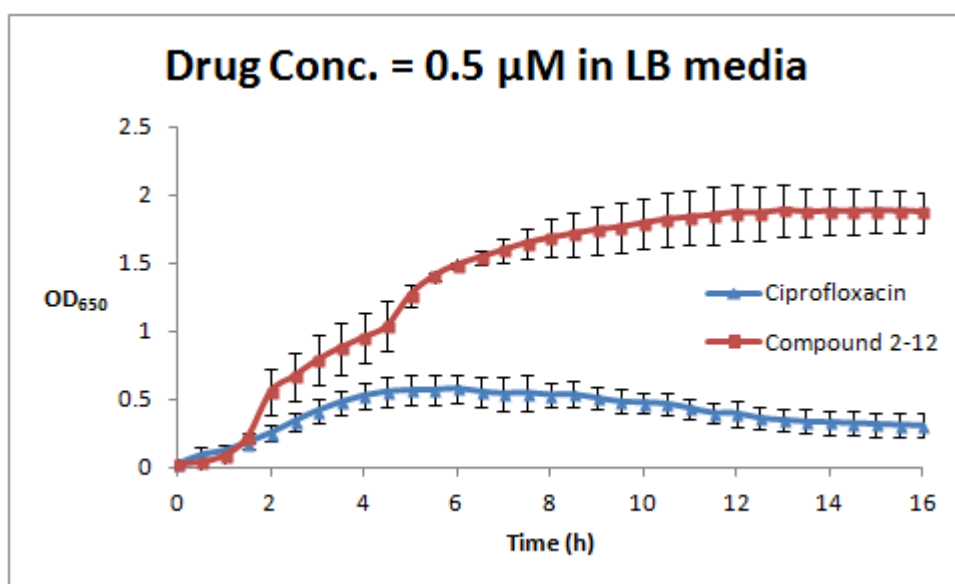


Figure 112 - *E. coli* BW25113 FecA::kan growth in LB media with drug concentrations of 0.5 μ M for both ciprofloxacin **1-5** and conjugate **2-12**. The experiment was run in quadruplicate and the error bars show one standard deviation from the mean.

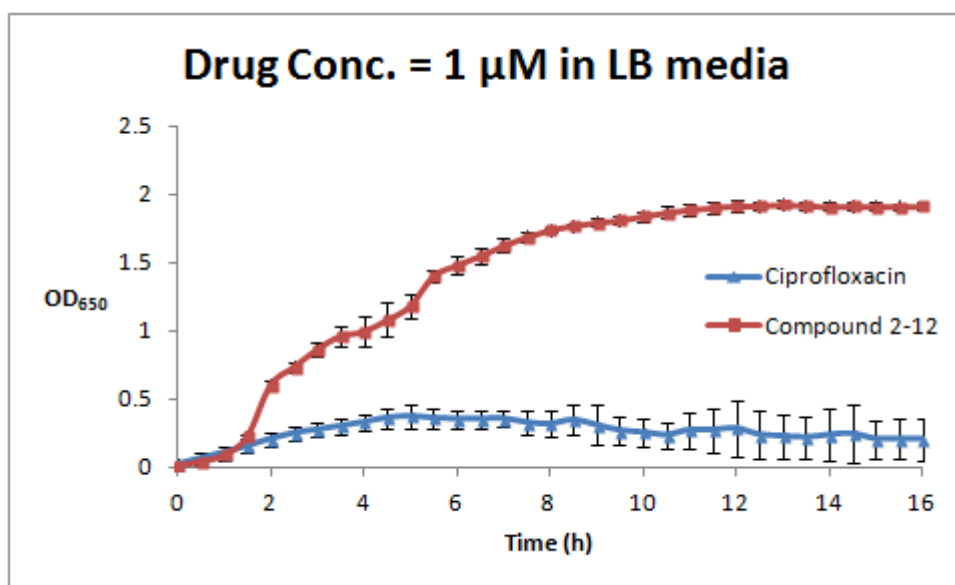


Figure 113 - *E. coli* BW25113 FecA::kan growth in LB media with drug concentrations of 1 μ M for both ciprofloxacin **1-5** and conjugate **2-12**. The experiment was run in quadruplicate and the error bars show one standard deviation from the mean.

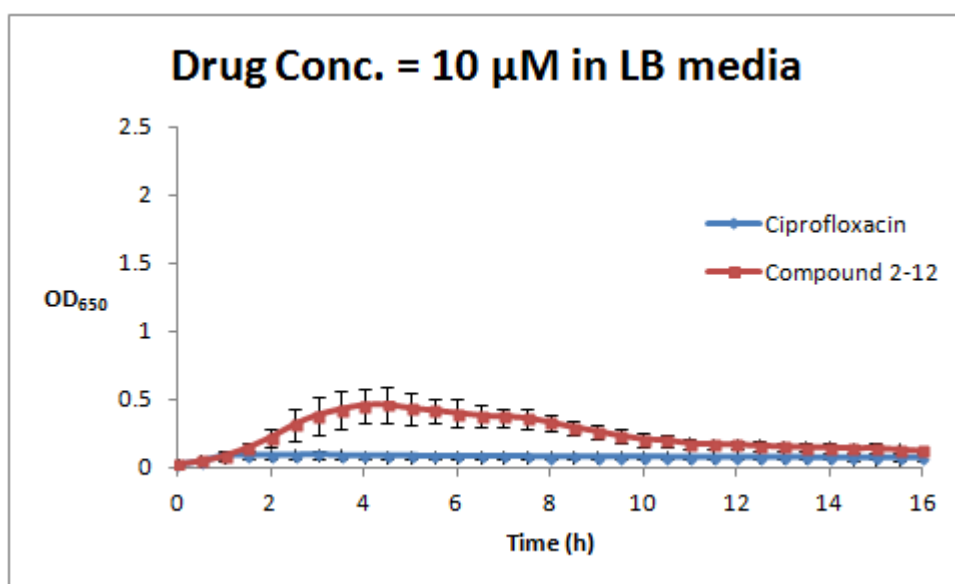


Figure 114 - *E. coli* BW25113 FecA::kan growth in LB media with drug concentrations of 10 μ M for both ciprofloxacin **1-5** and conjugate **2-12**. The experiment was run in quadruplicate and the error bars show one standard deviation from the mean.

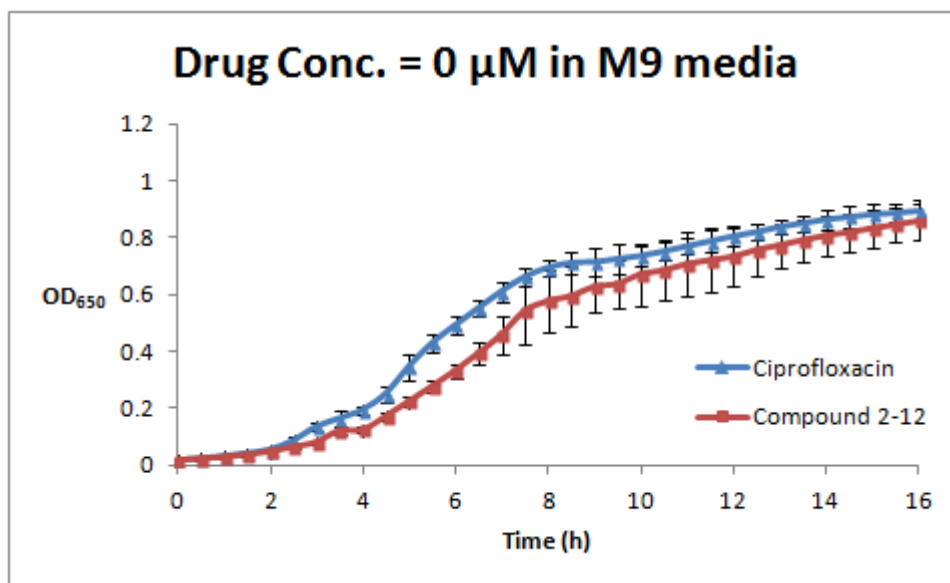


Figure 115 - *E. coli* BW25113 FecA::kan growth in M9 minimal media with drug concentrations of 0 μ M for both ciprofloxacin **1-5** and conjugate **2-12**. The experiment was run in quadruplicate for **2-12** and triplicate for ciprofloxacin, and the error bars show one standard deviation from the mean.

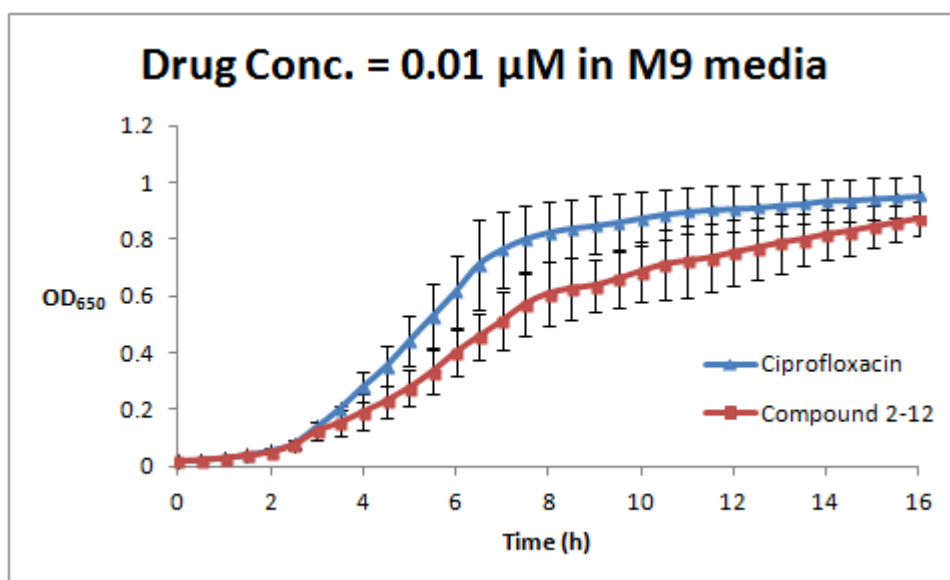


Figure 116 - *E. coli* BW25113 FecA::kan growth in M9 minimal media with drug concentrations of 0.01 μ M for both ciprofloxacin **1-5** and

conjugate **2-12**. The experiment was run in quadruplicate and the error bars show one standard deviation from the mean.

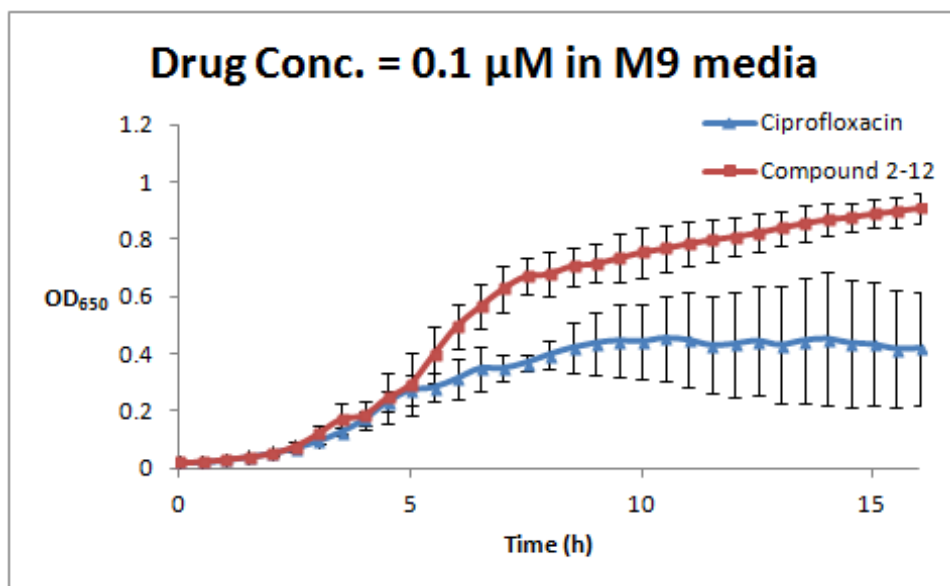


Figure 117 - *E. coli* BW25113 FecA::kan growth in M9 minimal media with drug concentrations of 0.1 μM for both ciprofloxacin **1-5** and conjugate **2-12**. The experiment was run in quadruplicate and the error bars show one standard deviation from the mean.

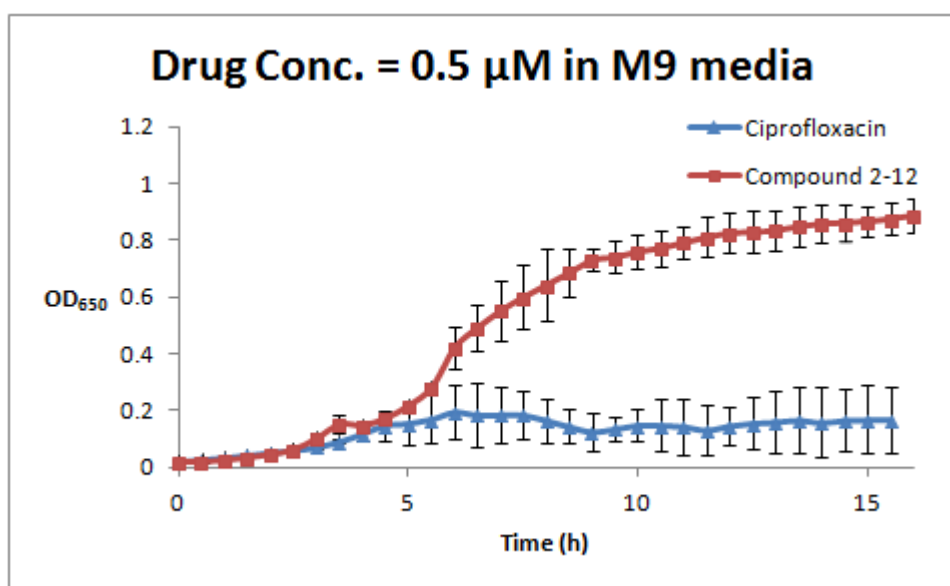


Figure 118 - *E. coli* BW25113 FecA::kan growth in M9 minimal media with drug concentrations of 0.5 μM for both ciprofloxacin **1-5** and

conjugate **2-12**. The experiment was run in quadruplicate and the error bars show one standard deviation from the mean.

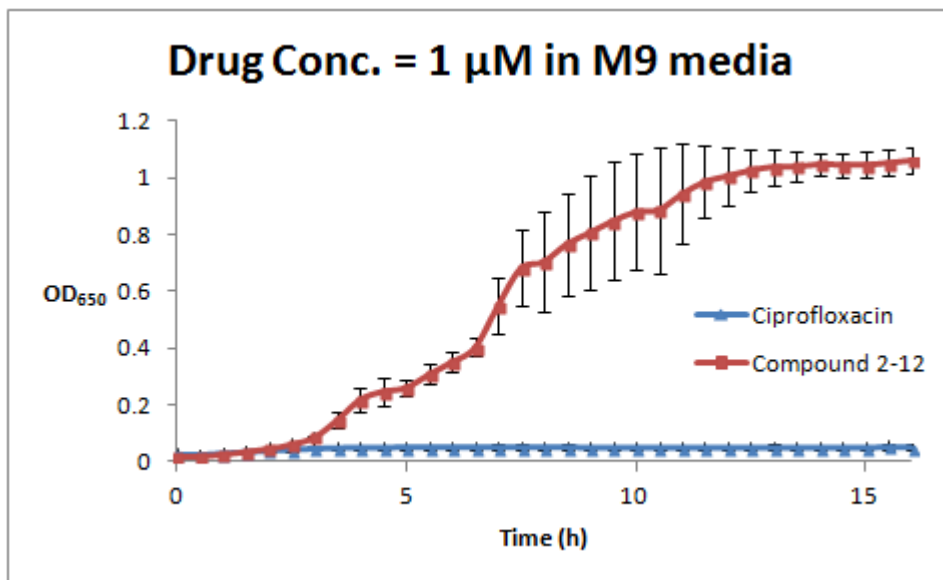


Figure 119 - *E. coli* BW25113 FecA::kan growth in M9 minimal media with drug concentrations of 1 μM for both ciprofloxacin **1-5** and conjugate **2-12**. The experiment was run in quadruplicate and the error bars show one standard deviation from the mean.

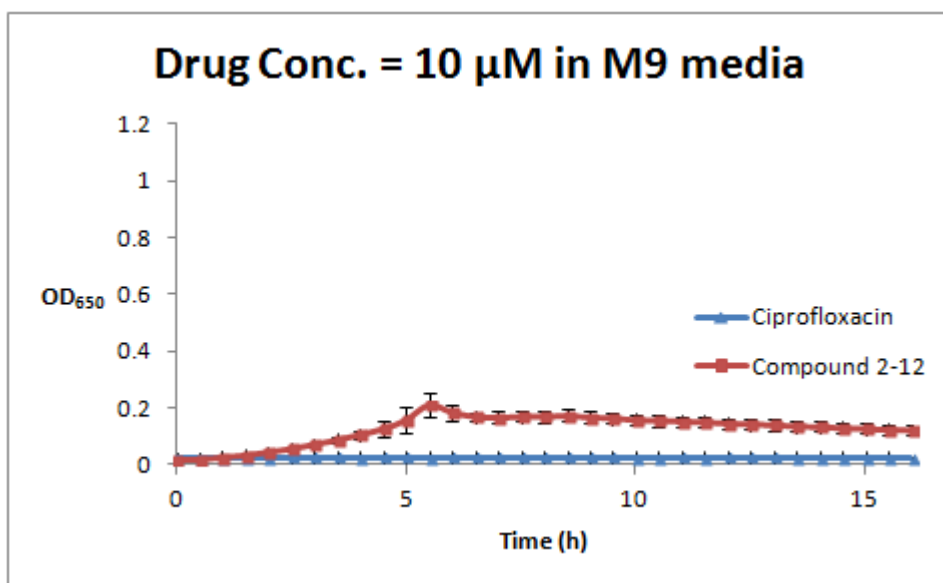


Figure 120 - *E. coli* BW25113 FecA::kan growth in M9 minimal media with drug concentrations of 10 μM for both ciprofloxacin **1-5** and

conjugate **2-12**. The experiment was run in quadruplicate and the error bars show one standard deviation from the mean.

Appendix III. Individual Growth Assay Plots for Compound 4-3

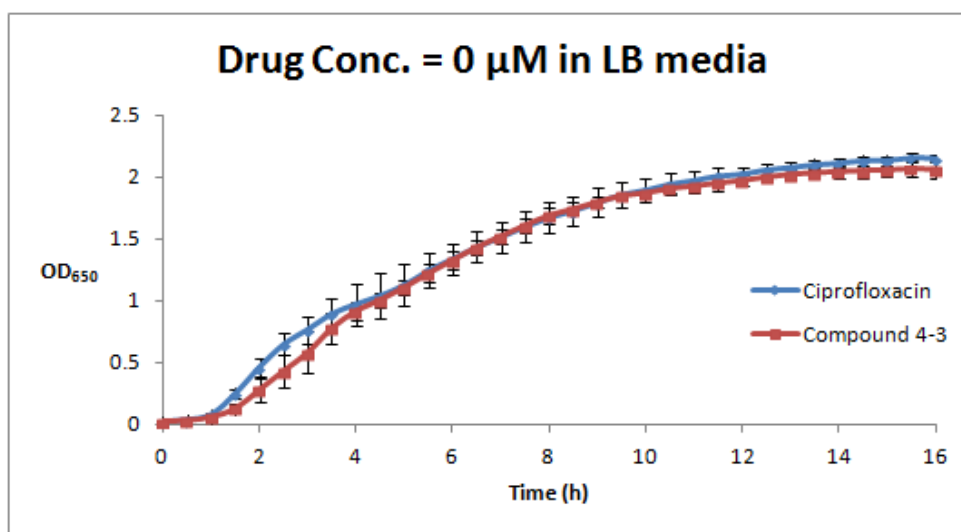


Figure 121 - *E. coli* BW25113WT growth in LB media with drug concentrations of 0 μM for both ciprofloxacin 1-5 and conjugate 4-3. The experiment was run in quadruplicate and the error bars show one standard deviation from the mean.

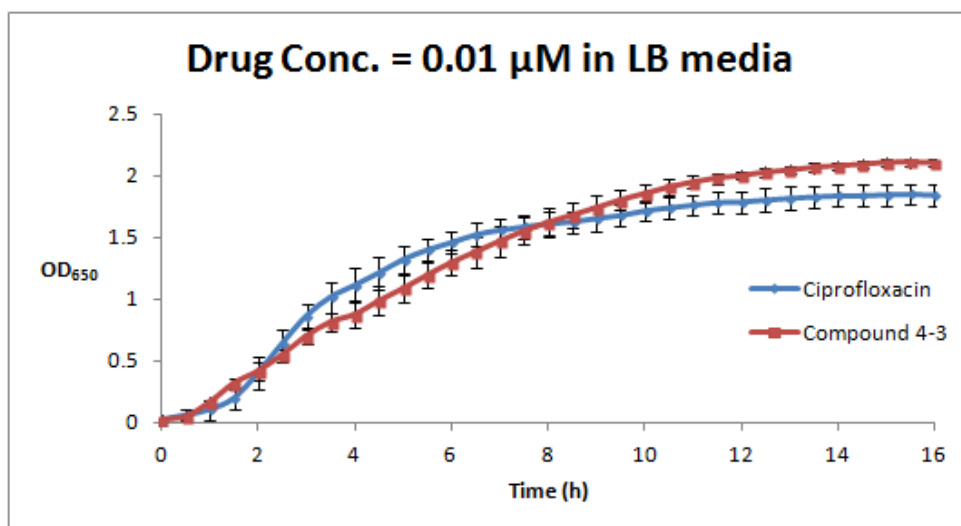


Figure 122 - *E. coli* BW25113WT growth in LB media with drug concentrations of 0.01 μM for both ciprofloxacin 1-5 and conjugate 4-3. The experiment was run in quadruplicate and the error bars show one standard deviation from the mean.

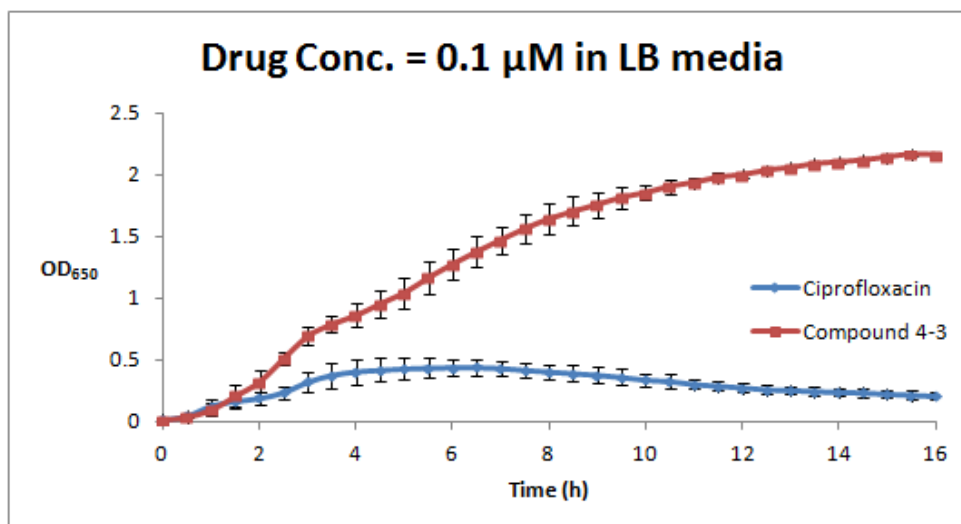


Figure 123 - *E. coli* BW25113WT growth in LB media with drug concentrations of 0.1 μM for both ciprofloxacin **1-5** and conjugate **4-3**. The experiment was run in quadruplicate and the error bars show one standard deviation from the mean.

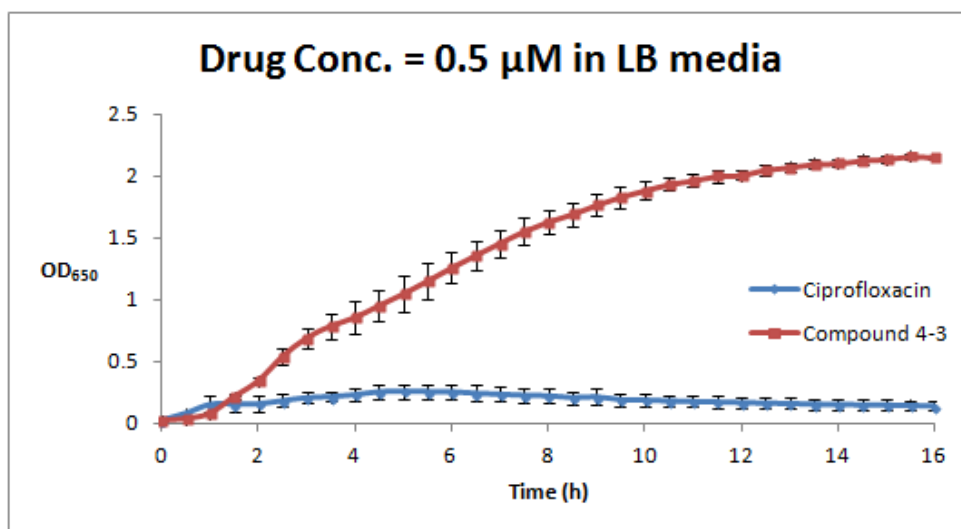


Figure 124 - *E. coli* BW25113WT growth in LB media with drug concentrations of 0.5 μM for both ciprofloxacin **1-5** and conjugate **4-3**. The experiment was run in quadruplicate and the error bars show one standard deviation from the mean.

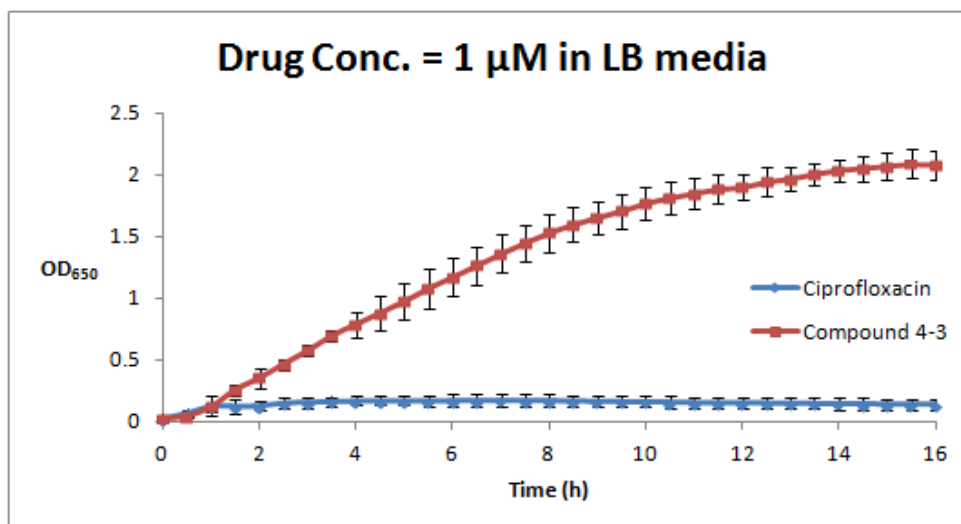


Figure 125 - *E. coli* BW25113WT growth in LB media with drug concentrations of 1 μM for both ciprofloxacin **1-5** and conjugate **4-3**. The experiment was run in quadruplicate and the error bars show one standard deviation from the mean.

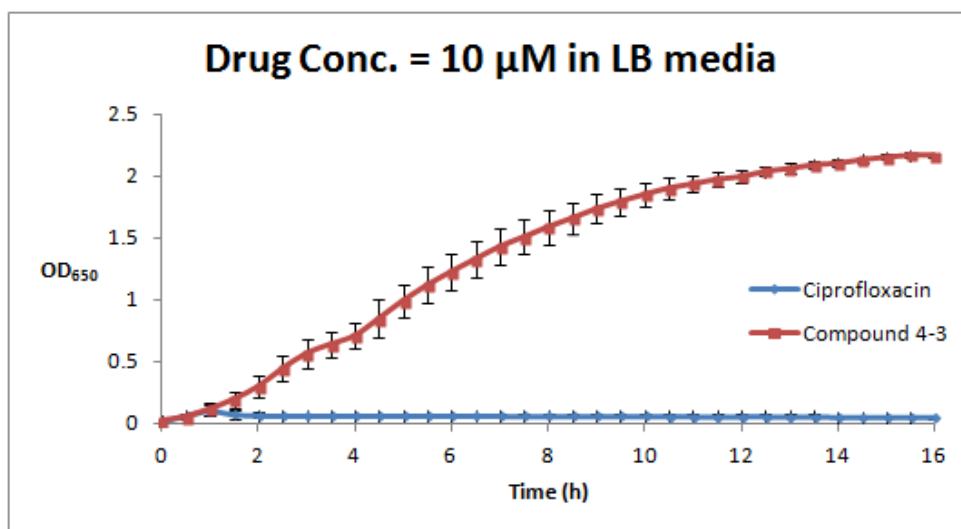


Figure 126 - *E. coli* BW25113WT growth in LB media with drug concentrations of 10 μM for both ciprofloxacin **1-5** and conjugate **4-3**. The experiment was run in quadruplicate and the error bars show one standard deviation from the mean.

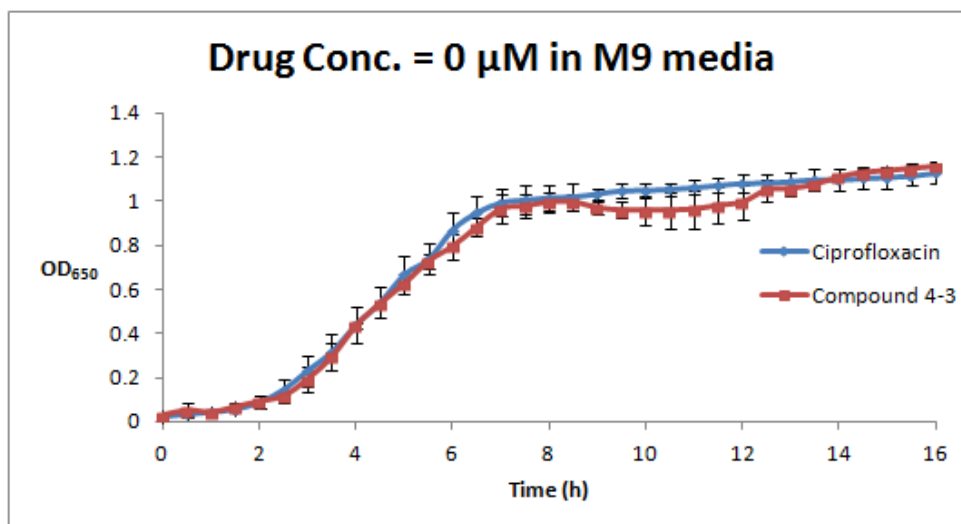


Figure 127 - *E. coli* BW25113WT growth in M9 minimal media with drug concentrations of 0 μM for both ciprofloxacin **1-5** and conjugate **4-3**. The experiment was run in quadruplicate and the error bars show one standard deviation from the mean.

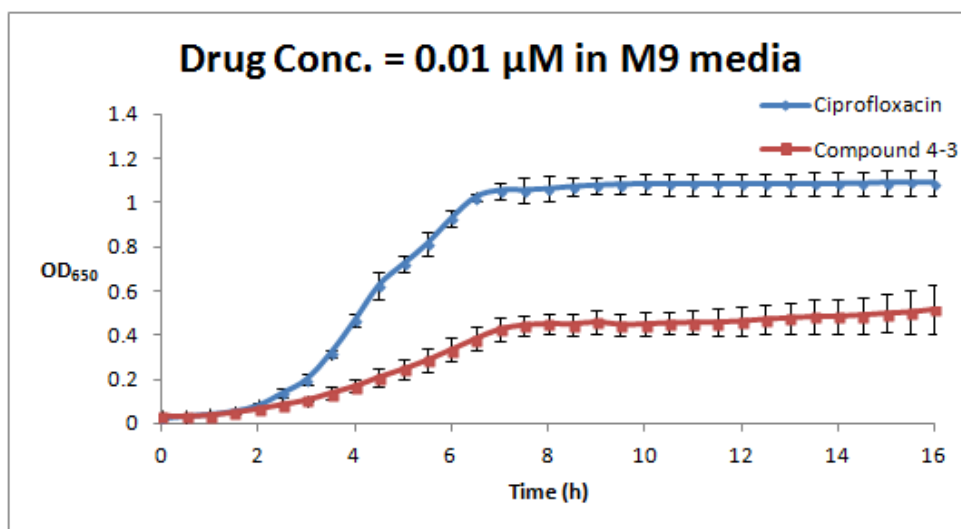


Figure 128 - *E. coli* BW25113WT growth in M9 minimal media with drug concentrations of 0.01 μM for both ciprofloxacin **1-5** and conjugate **4-3**. The experiment was run in quadruplicate and the error bars show one standard deviation from the mean.

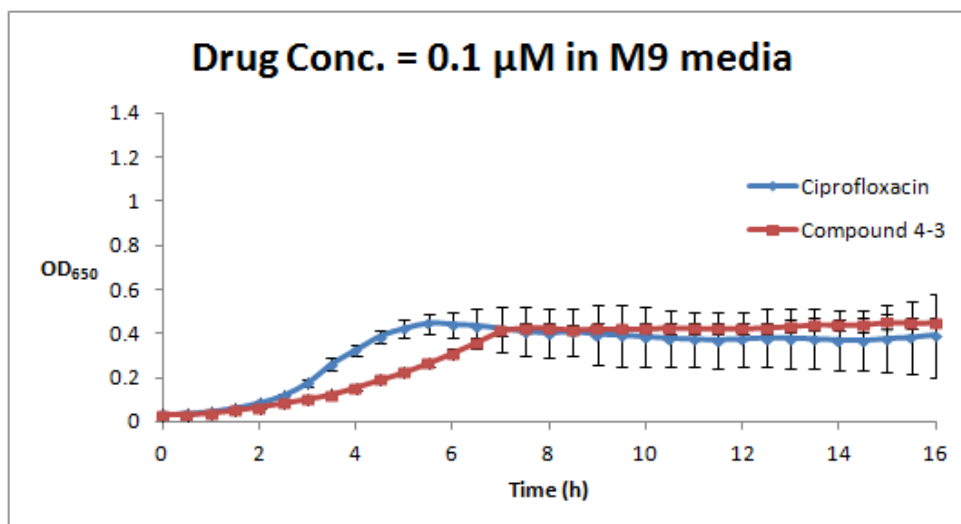


Figure 129 - *E. coli* BW25113WT growth in M9 minimal media with drug concentrations of 0.1 μM for both ciprofloxacin **1-5** and conjugate **4-3**. The experiment was run in quadruplicate and the error bars show one standard deviation from the mean.

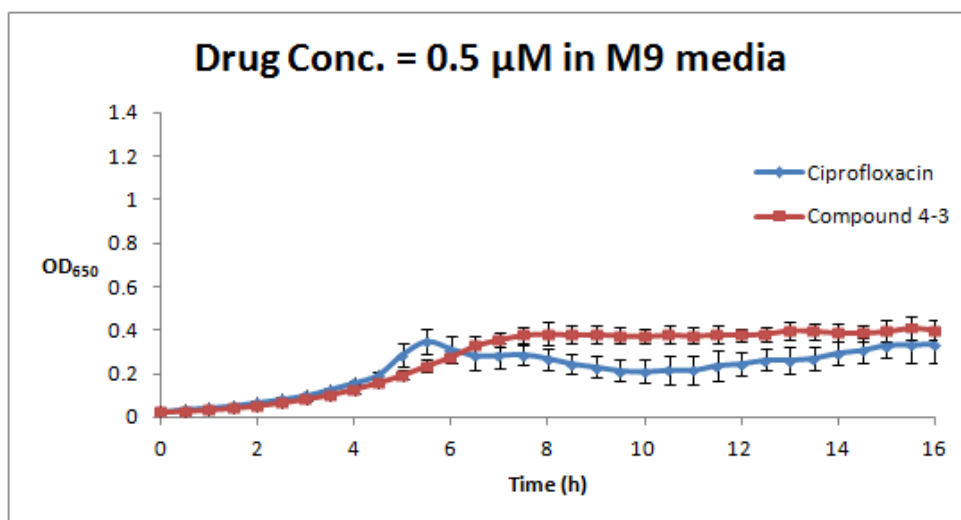


Figure 130 - *E. coli* BW25113WT growth in M9 minimal media with drug concentrations of 0.5 μM for both ciprofloxacin **1-5** and conjugate **4-3**. The experiment was run in quadruplicate and the error bars show one standard deviation from the mean.

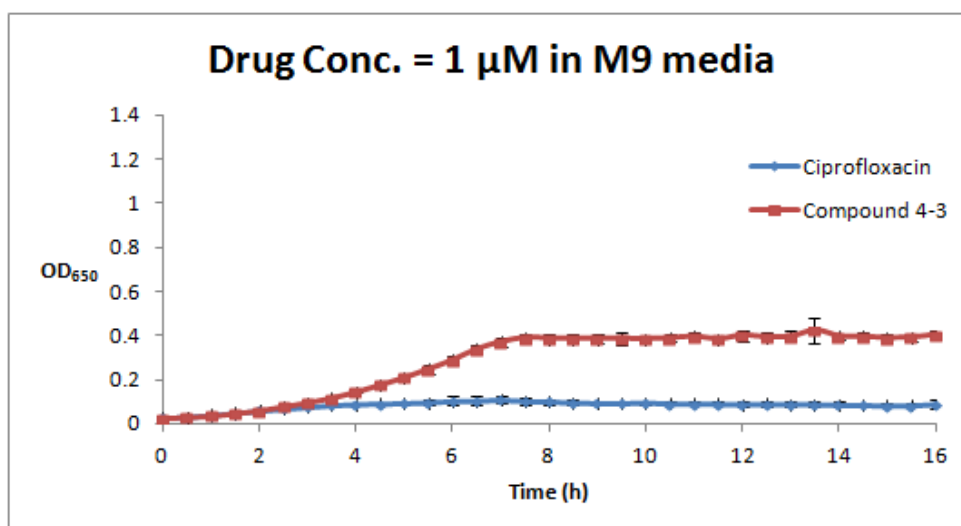


Figure 131 - *E. coli* BW25113WT growth in M9 minimal media with drug concentrations of 1 μ M for both ciprofloxacin **1-5** and conjugate **4-3**. The experiment was run in quadruplicate and the error bars show one standard deviation from the mean.

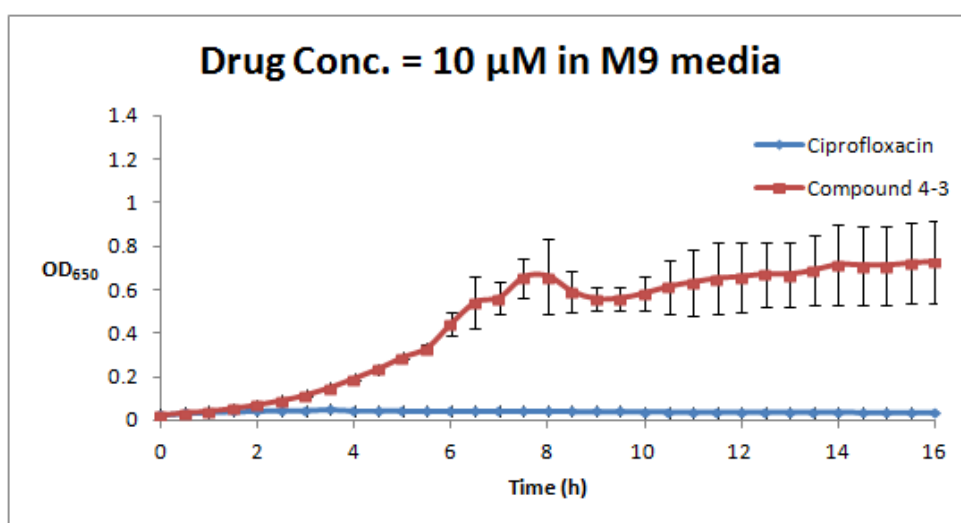


Figure 132 - *E. coli* BW25113WT growth in M9 minimal media with drug concentrations of 10 μ M for both ciprofloxacin **1-5** and conjugate **4-3**. The experiment was run in quadruplicate and the error bars show one standard deviation from the mean.

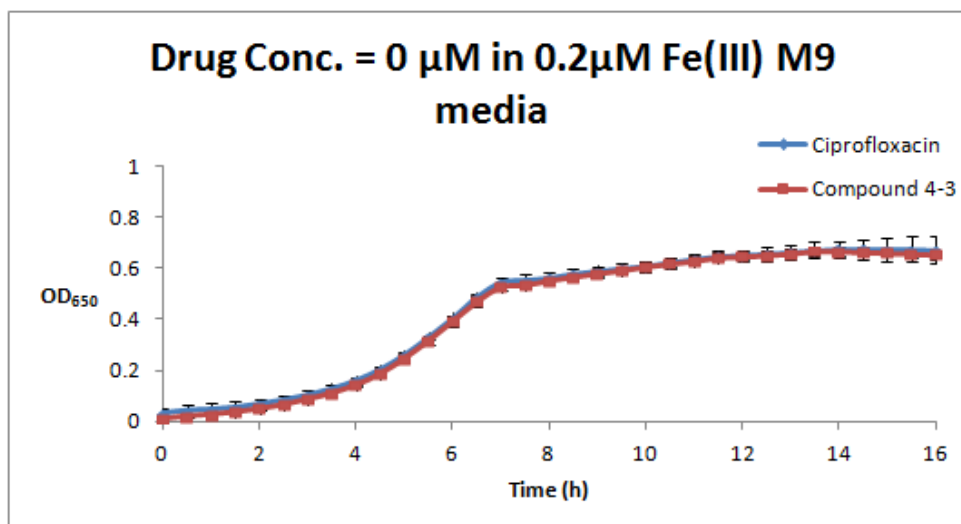


Figure 133 - *E. coli* BW25113WT growth in 0.2 μ M [Fe(III)] M9 media with drug concentrations of 0 μ M for both ciprofloxacin **1-5** and conjugate **4-3**. The experiment was run in quadruplicate and the error bars show one standard deviation from the mean.

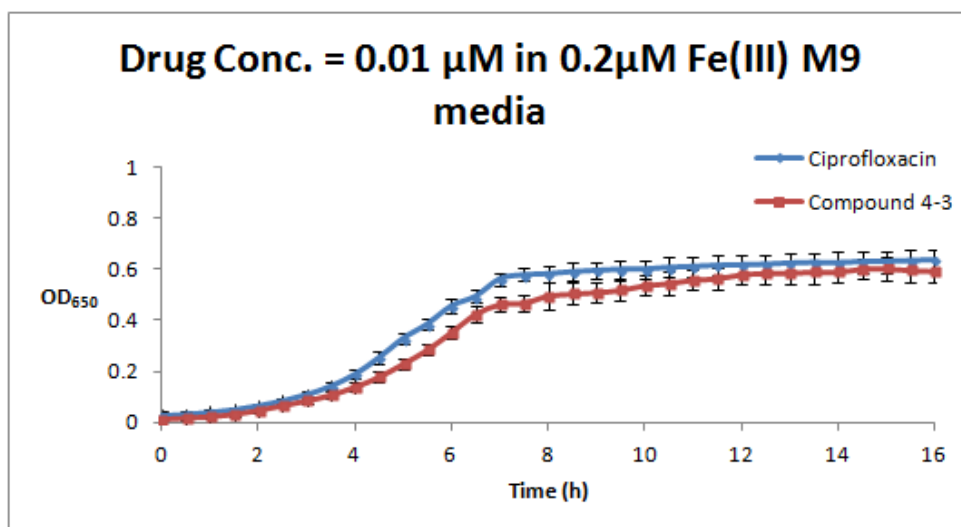


Figure 134 - *E. coli* BW25113WT growth in 0.2 μ M [Fe(III)] M9 minimal media with drug concentrations of 0.01 μ M for both ciprofloxacin **1-5** and conjugate **4-3**. The experiment was run in quadruplicate and the error bars show one standard deviation from the mean.

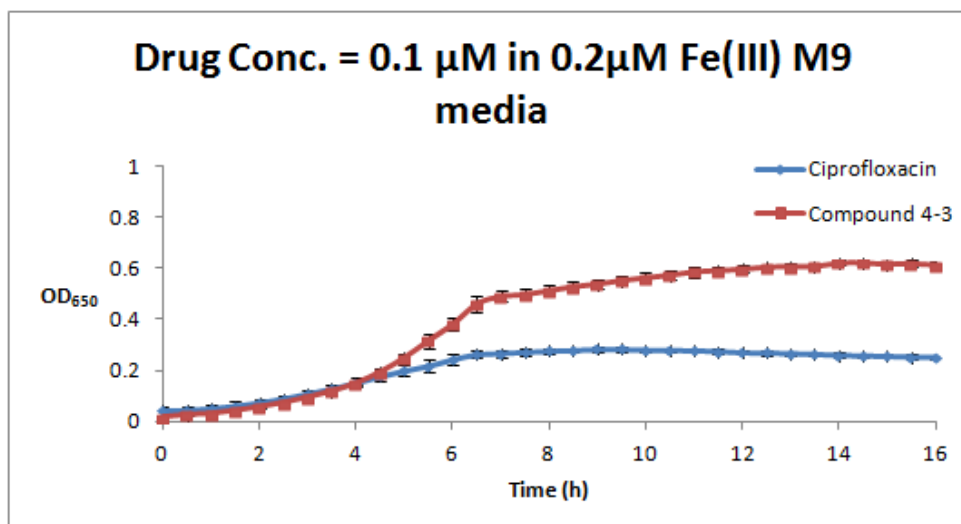


Figure 135 - *E. coli* BW25113WT growth in 0.2 μM [Fe(III)] M9 minimal media with drug concentrations of 0.1 μM for both ciprofloxacin **1-5** and conjugate **4-3**. The experiment was run in quadruplicate and the error bars show one standard deviation from the mean.

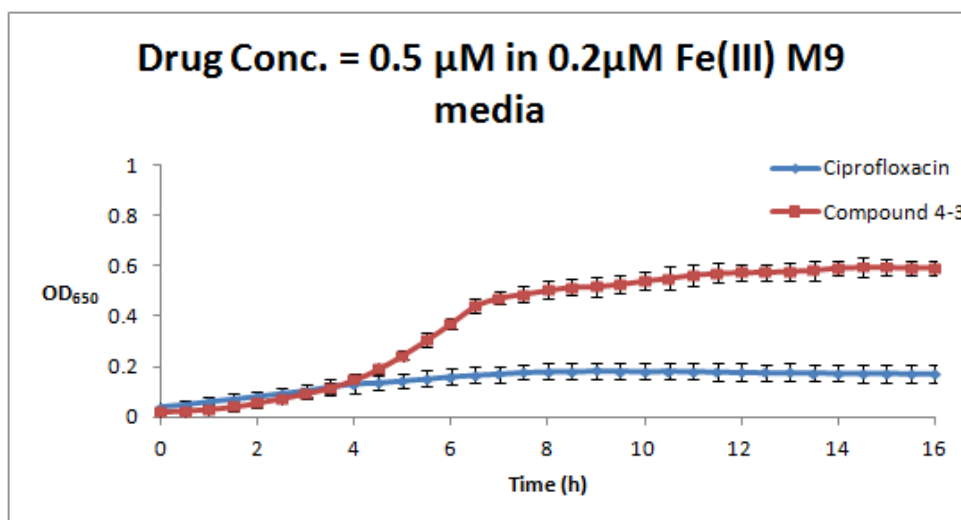


Figure 136 - *E. coli* BW25113WT growth in 0.2 μM [Fe(III)] M9 minimal media with drug concentrations of 0.5 μM for both ciprofloxacin **1-5** and conjugate **4-3**. The experiment was run in quadruplicate and the error bars show one standard deviation from the mean.

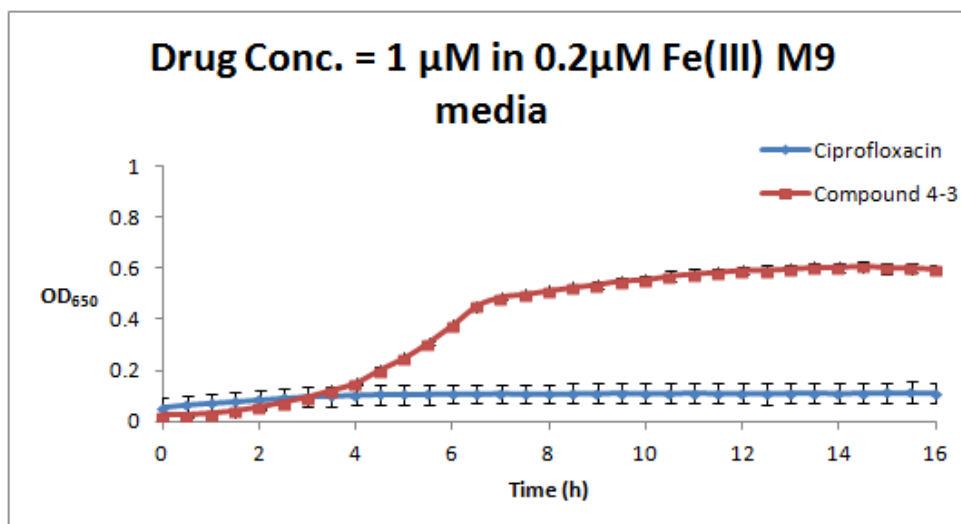


Figure 137 - *E. coli* BW25113WT growth in 0.2 μ M [Fe(III)] M9 minimal media with drug concentrations of 1 μ M for both ciprofloxacin **1-5** and conjugate **4-3**. The experiment was run in quadruplicate and the error bars show one standard deviation from the mean.

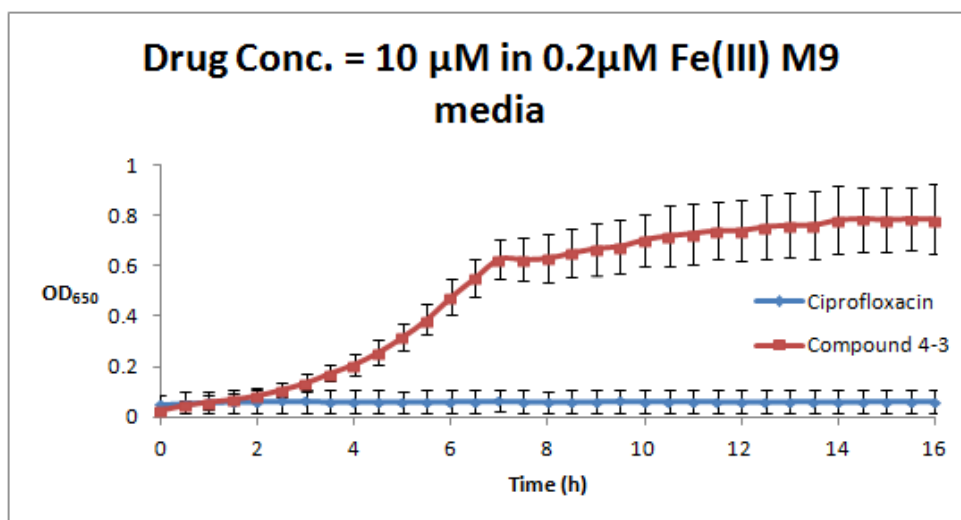


Figure 138 - *E. coli* BW25113WT growth in 0.2 μ M [Fe(III)] M9 minimal media with drug concentrations of 10 μ M for both ciprofloxacin **1-5** and conjugate **4-3**. The experiment was run in quadruplicate and the error bars show one standard deviation from the mean.

Appendix IV. Supporting spectra for compound 4-19

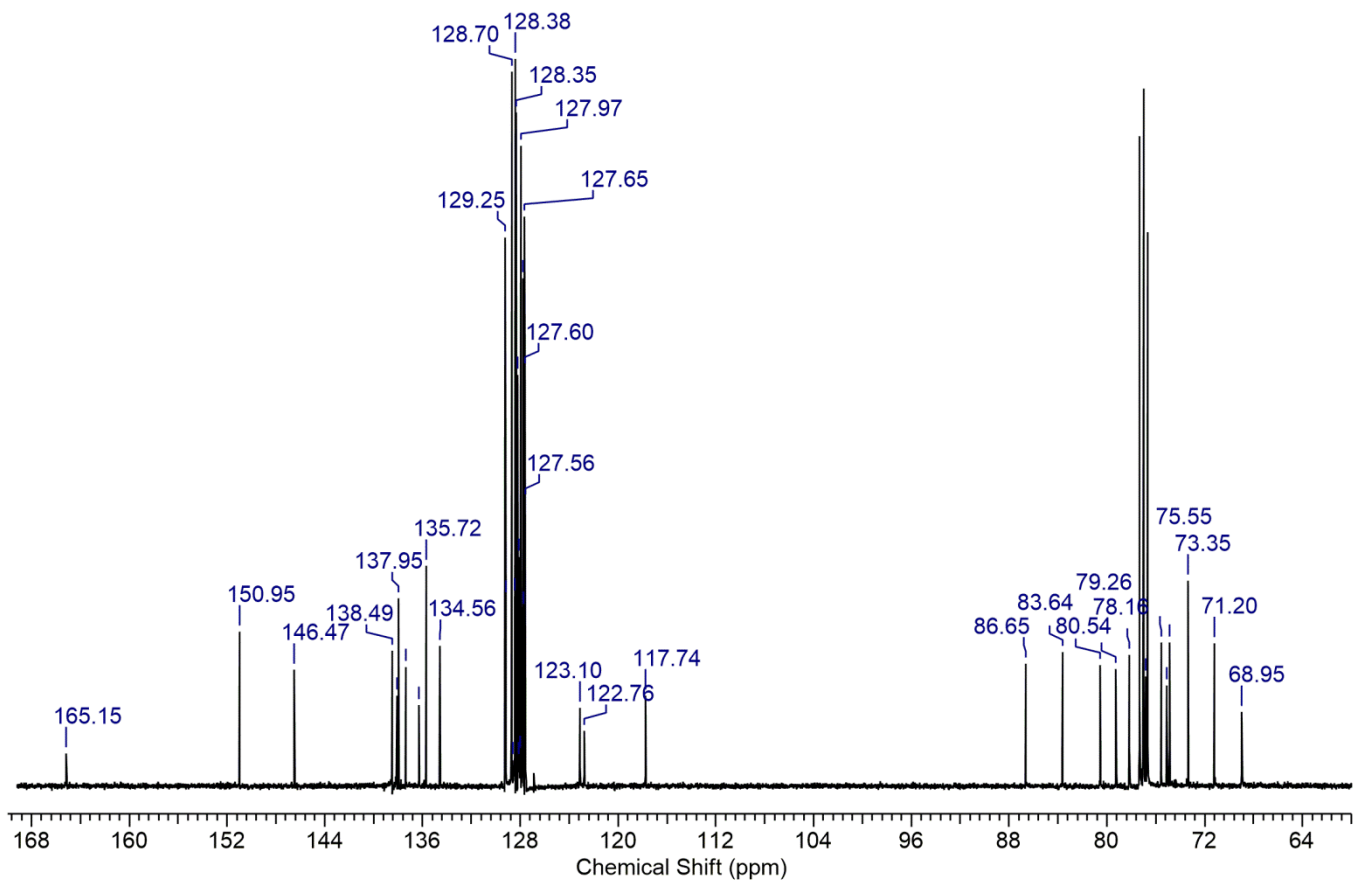


Figure 139 - Full ^{13}C spectrum (CDCl_3) of **4-19**.

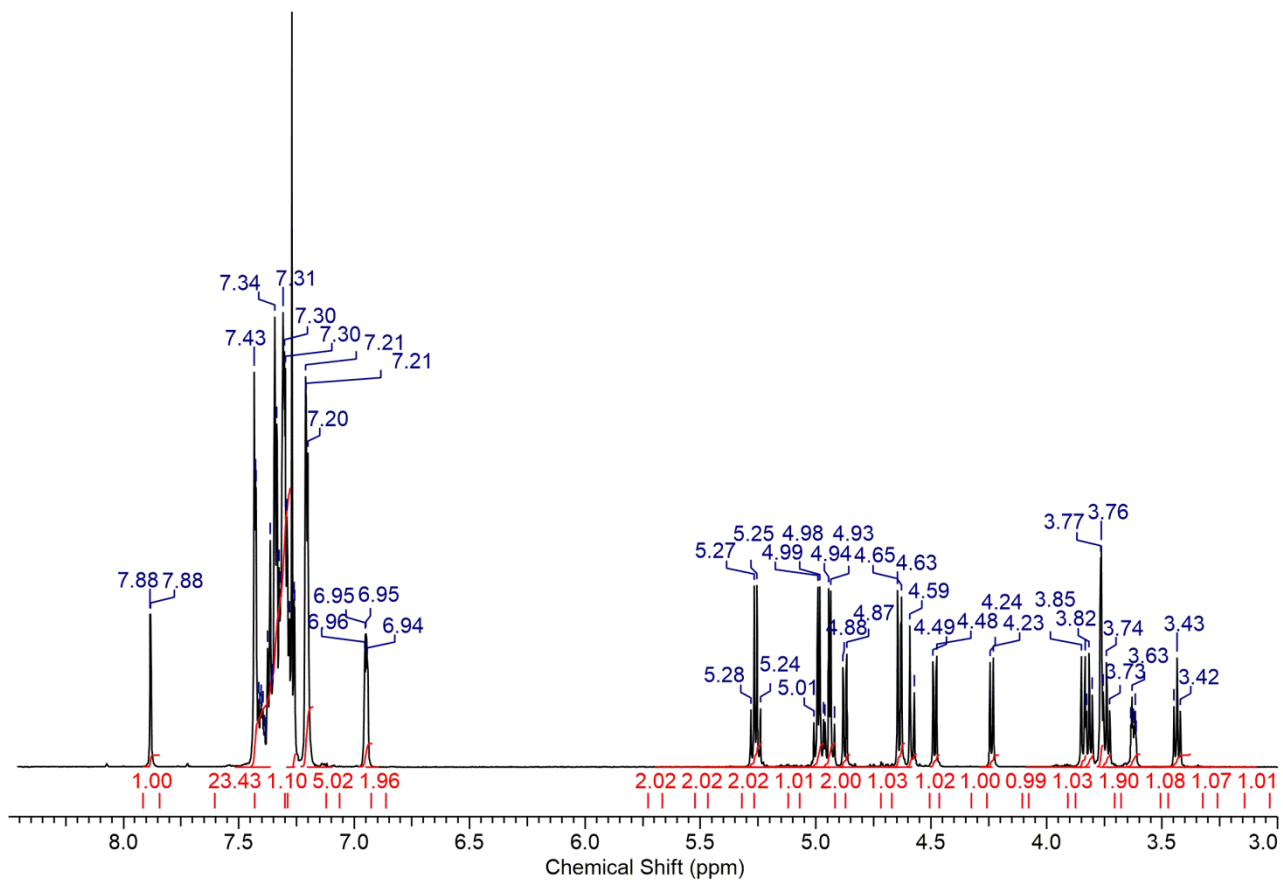


Figure 140 - Full ^1H spectrum (CDCl_3) of **4-19**.

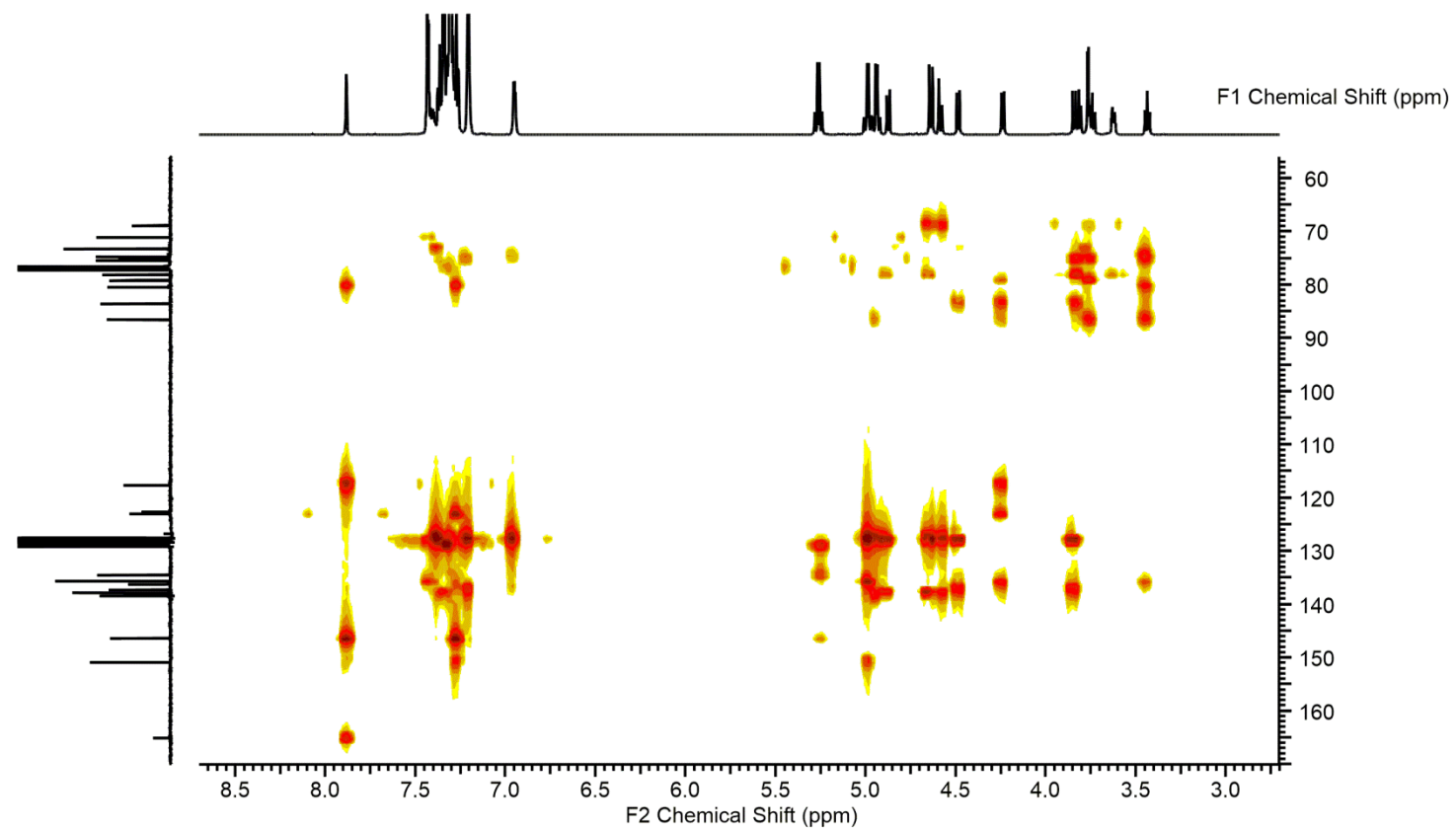


Figure 141 - Full HMBC spectrum (CDCl₃) of **4-19**.

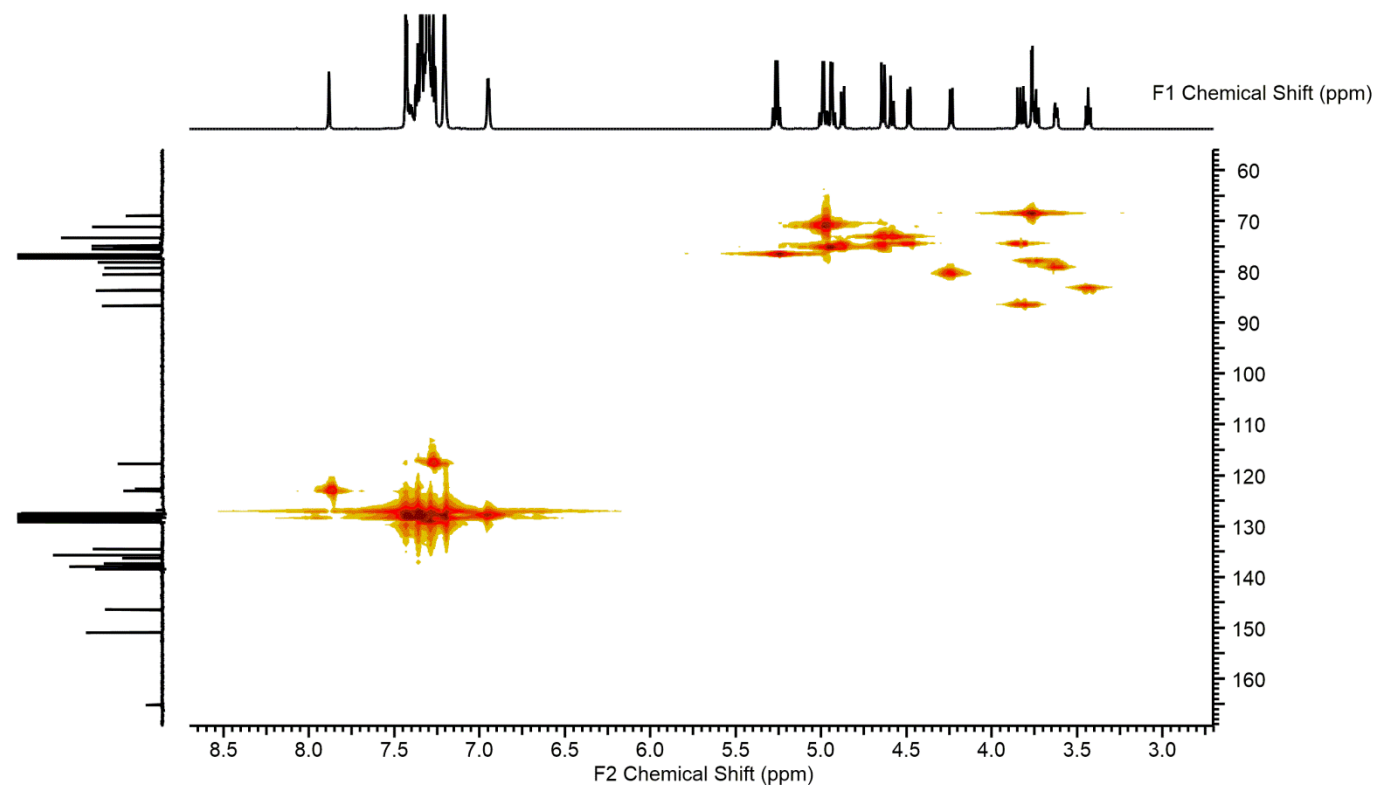


Figure 142 - Full HMQC spectrum (CDCl₃) of **4-19**.

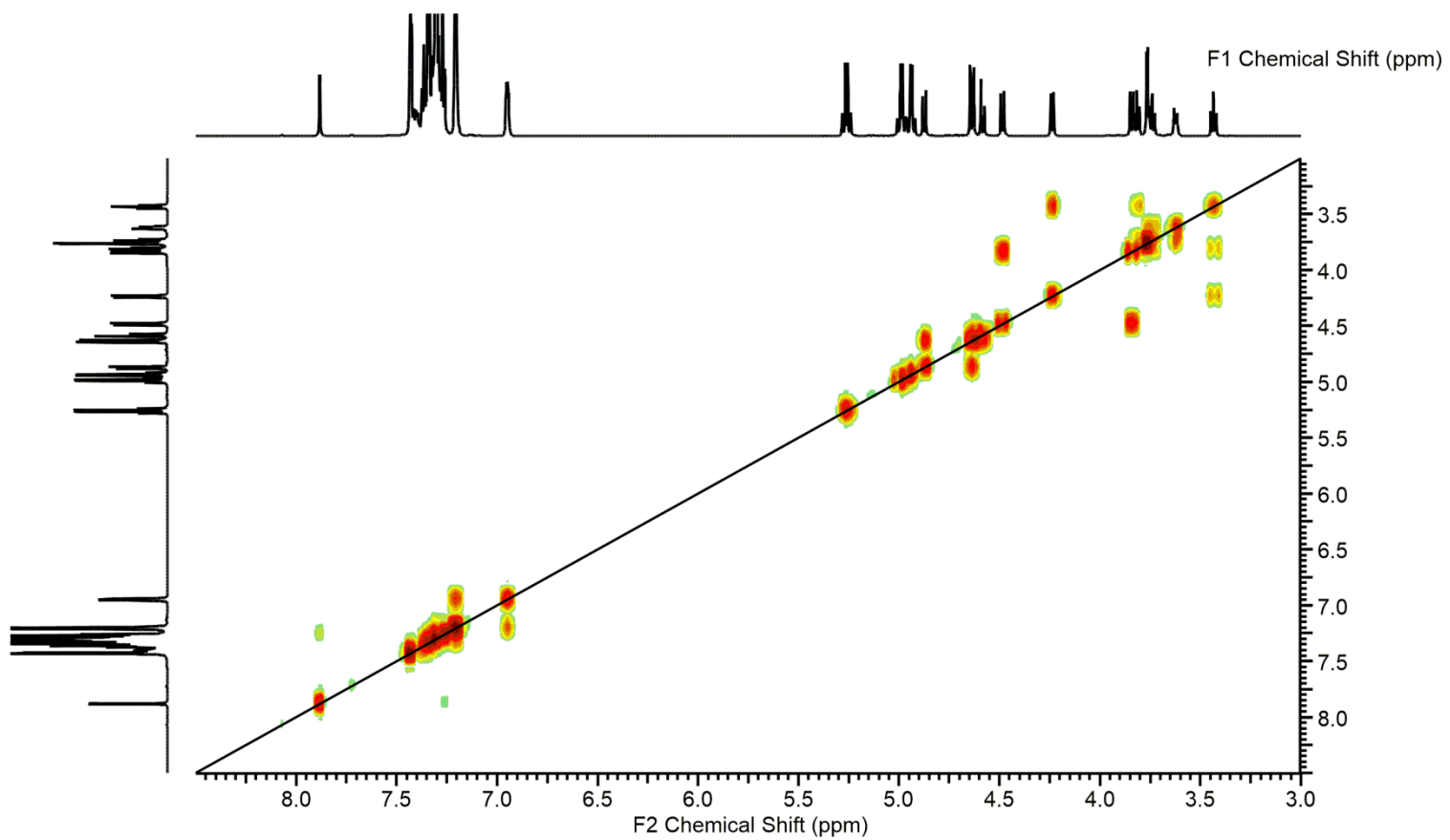


Figure 143 - Full COSY spectrum (CDCl_3) of **4-19**.

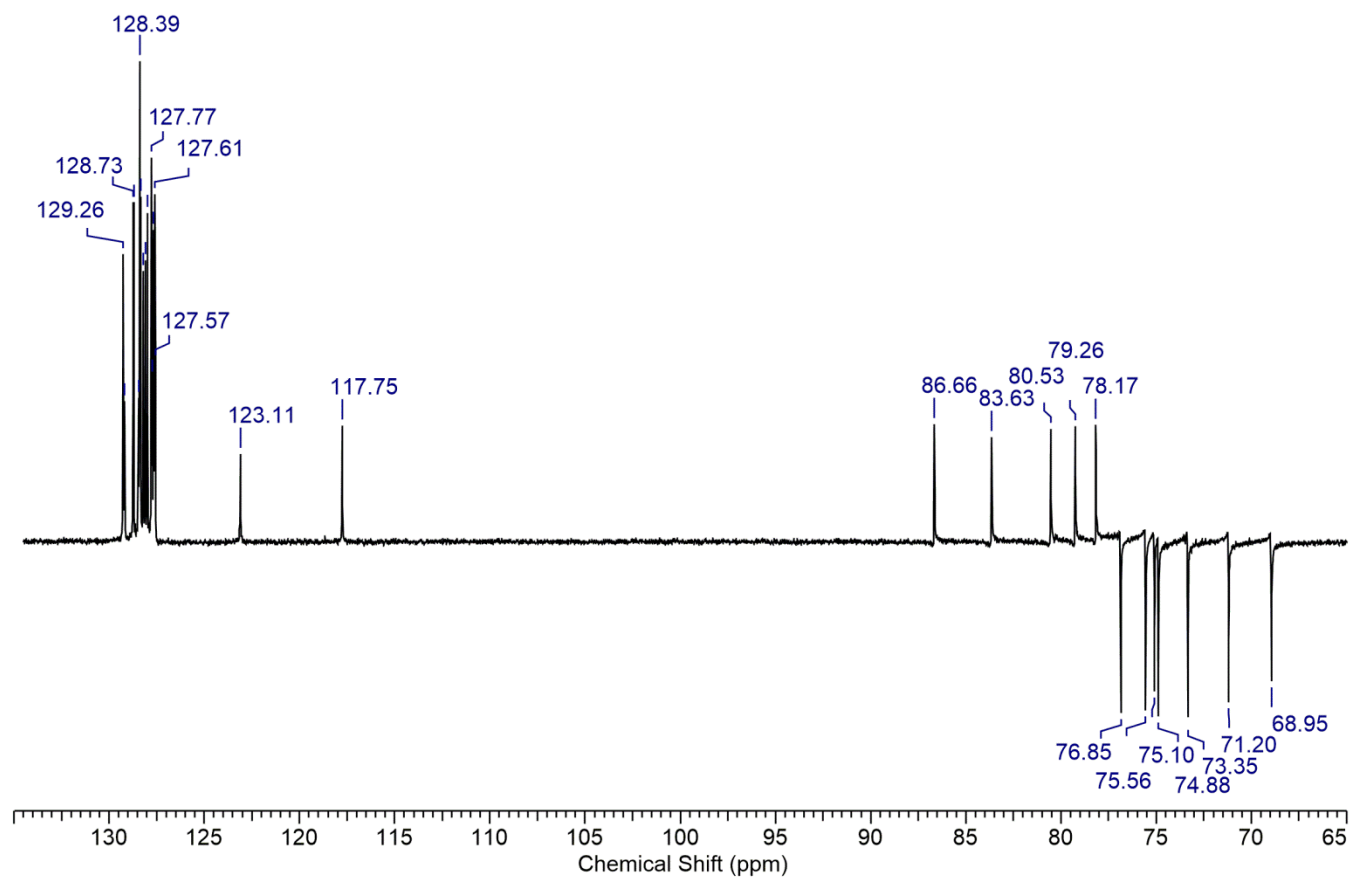


Figure 144 - Full DEPT spectrum (CDCl₃) of **4-19**.

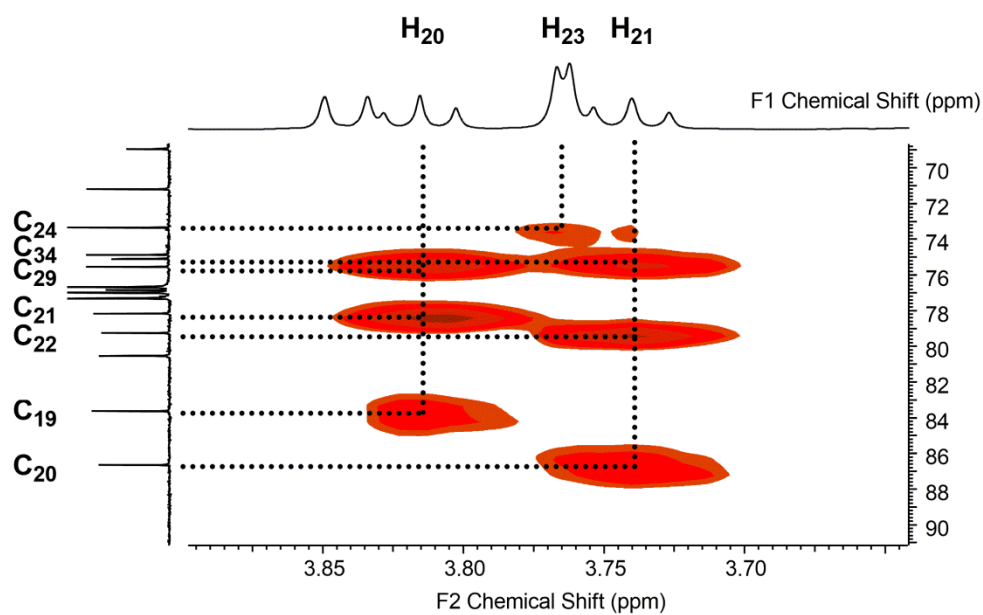


Figure 145 - HMBC spectrum (CDCl₃) of **4-19**.

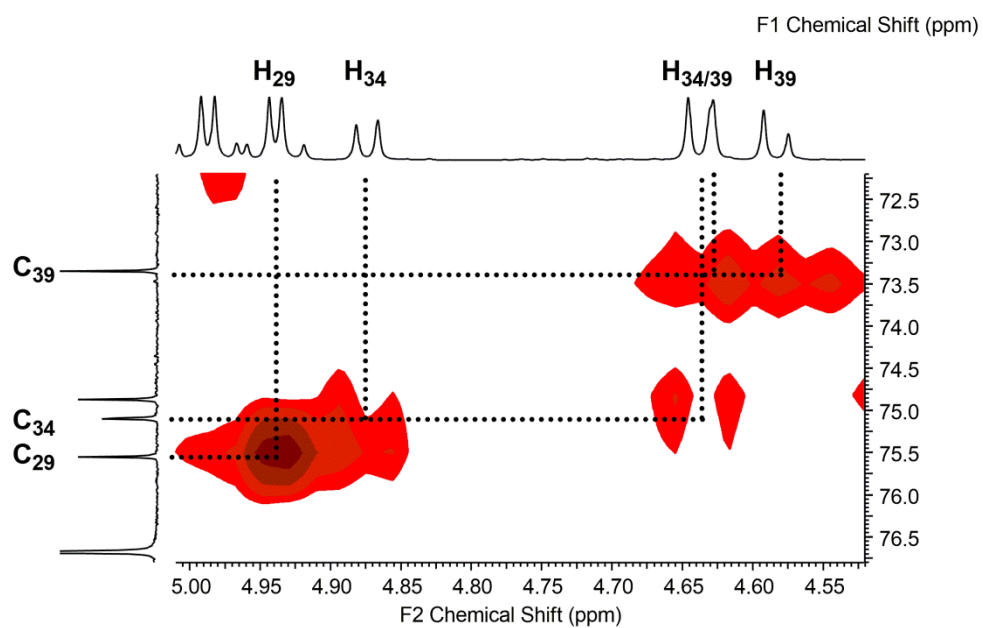


Figure 146 - HMQC spectrum (CDCl₃) of **4-19**.

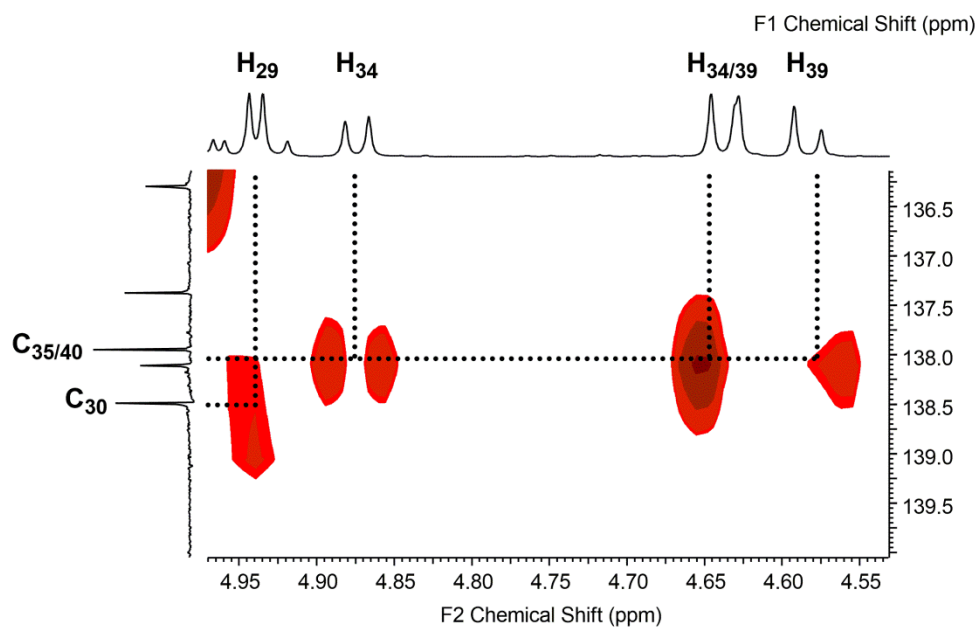


Figure 147 - HMBC spectrum (CDCl₃) of **4-19**.

Appendix V. Supporting spectra for compound 4-25

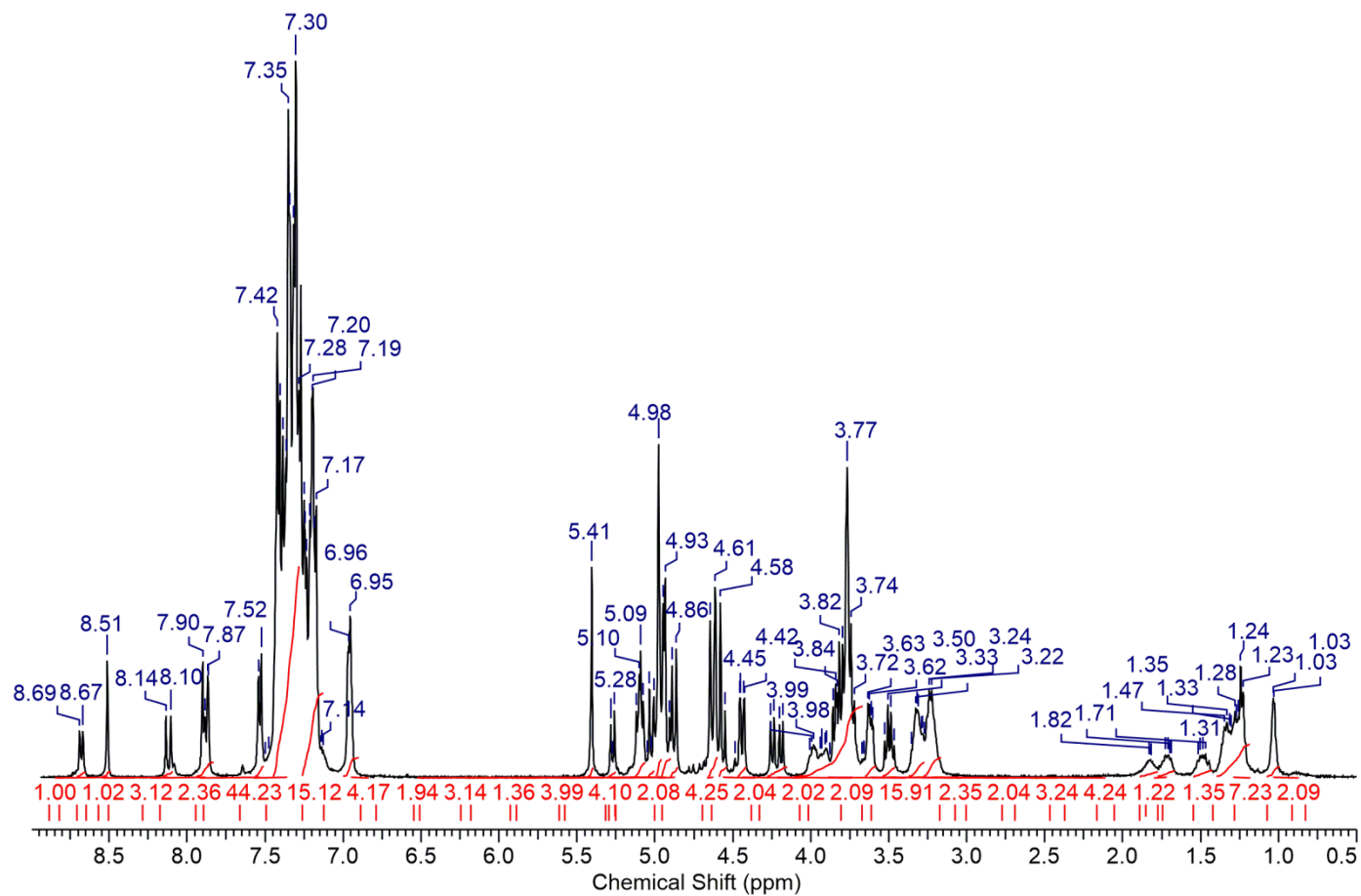


Figure 148 - Full ^1H spectrum (CDCl_3) of **4-25**.

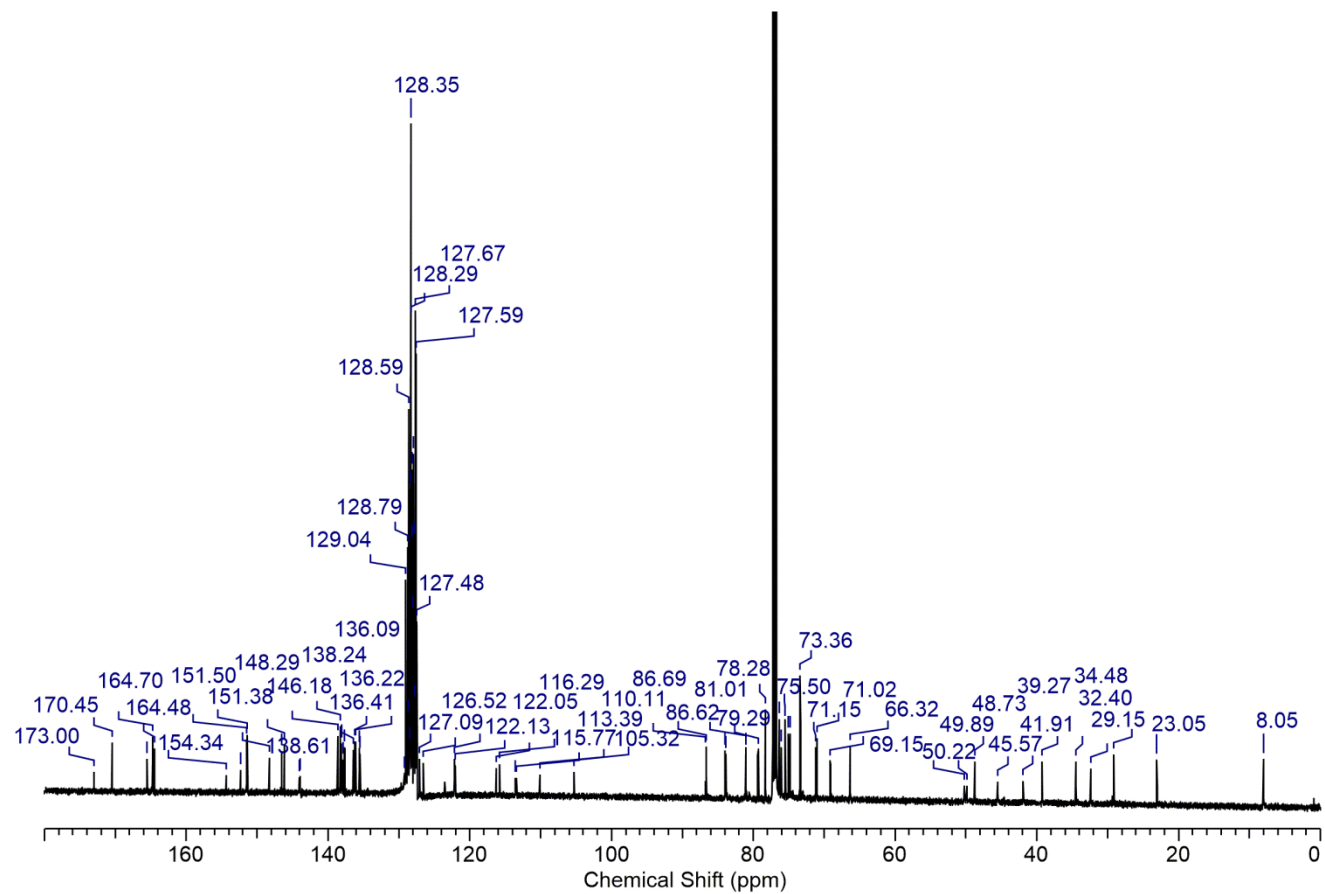


Figure 149 - Full ^{13}C spectrum (CDCl_3) of **4-25**.

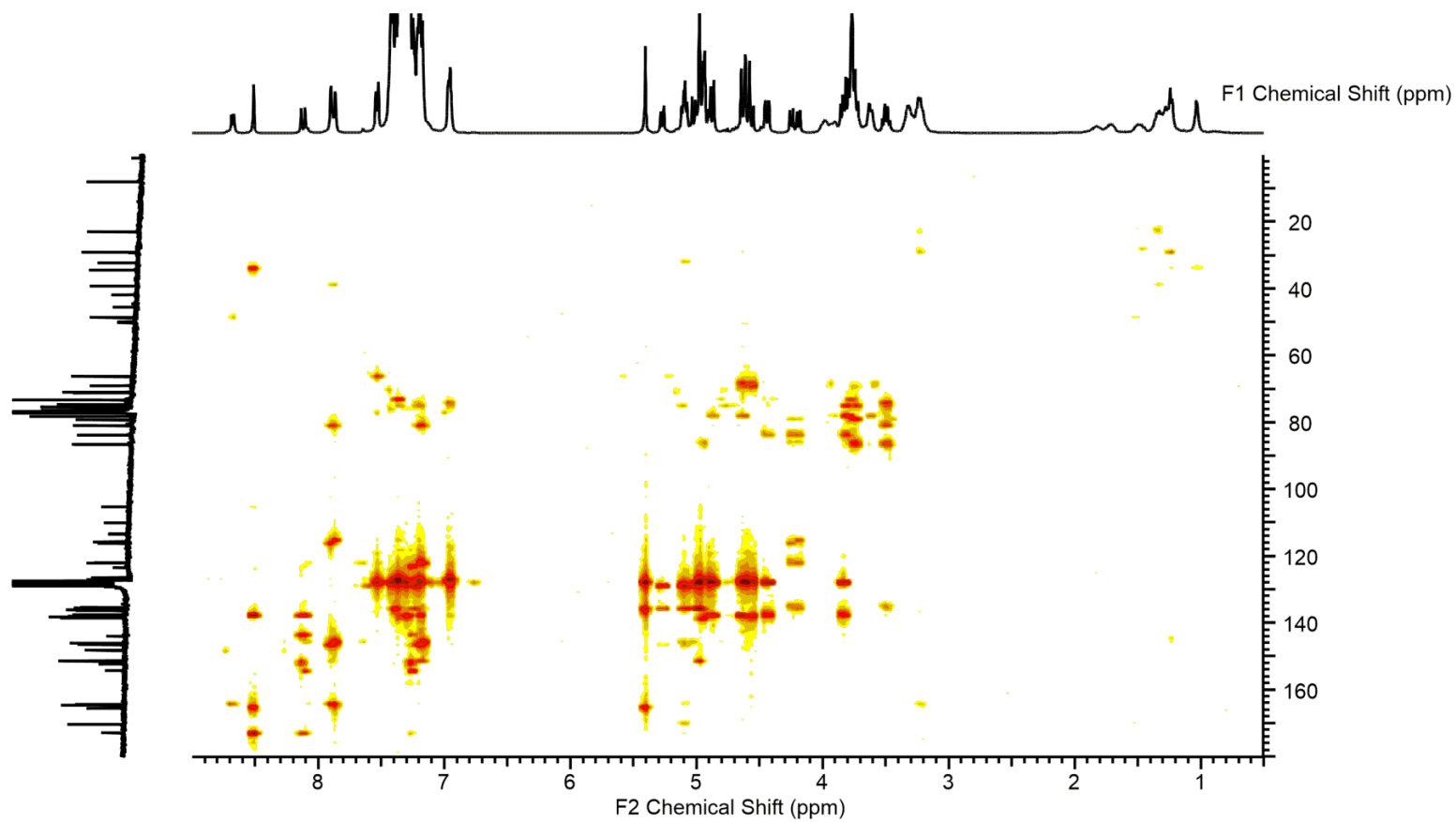


Figure 150 - Full HMBC spectrum (CDCl₃) of **4-25**.

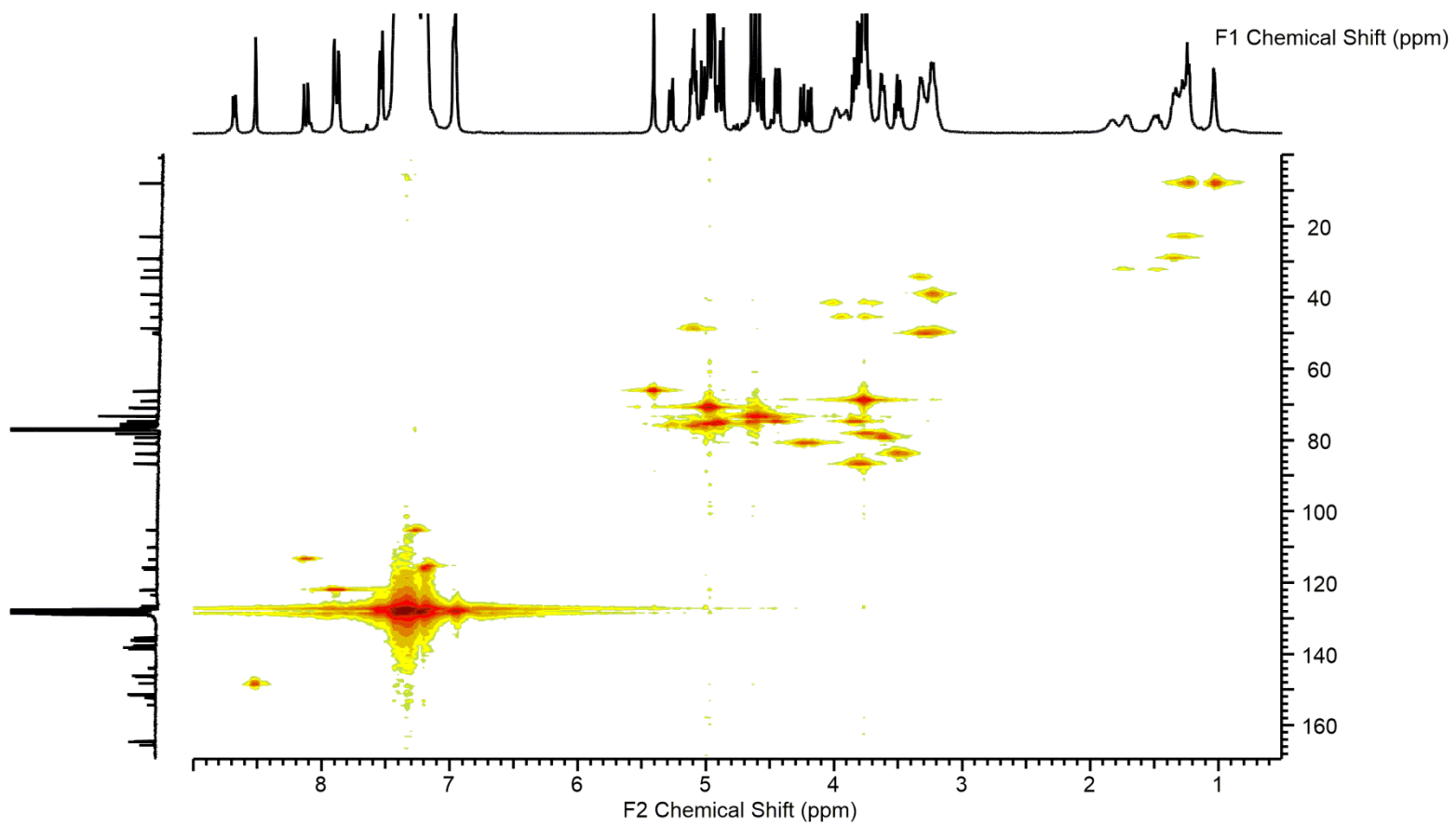


Figure 151 - Full HMQC spectrum (CDCl₃) of **4-25**.

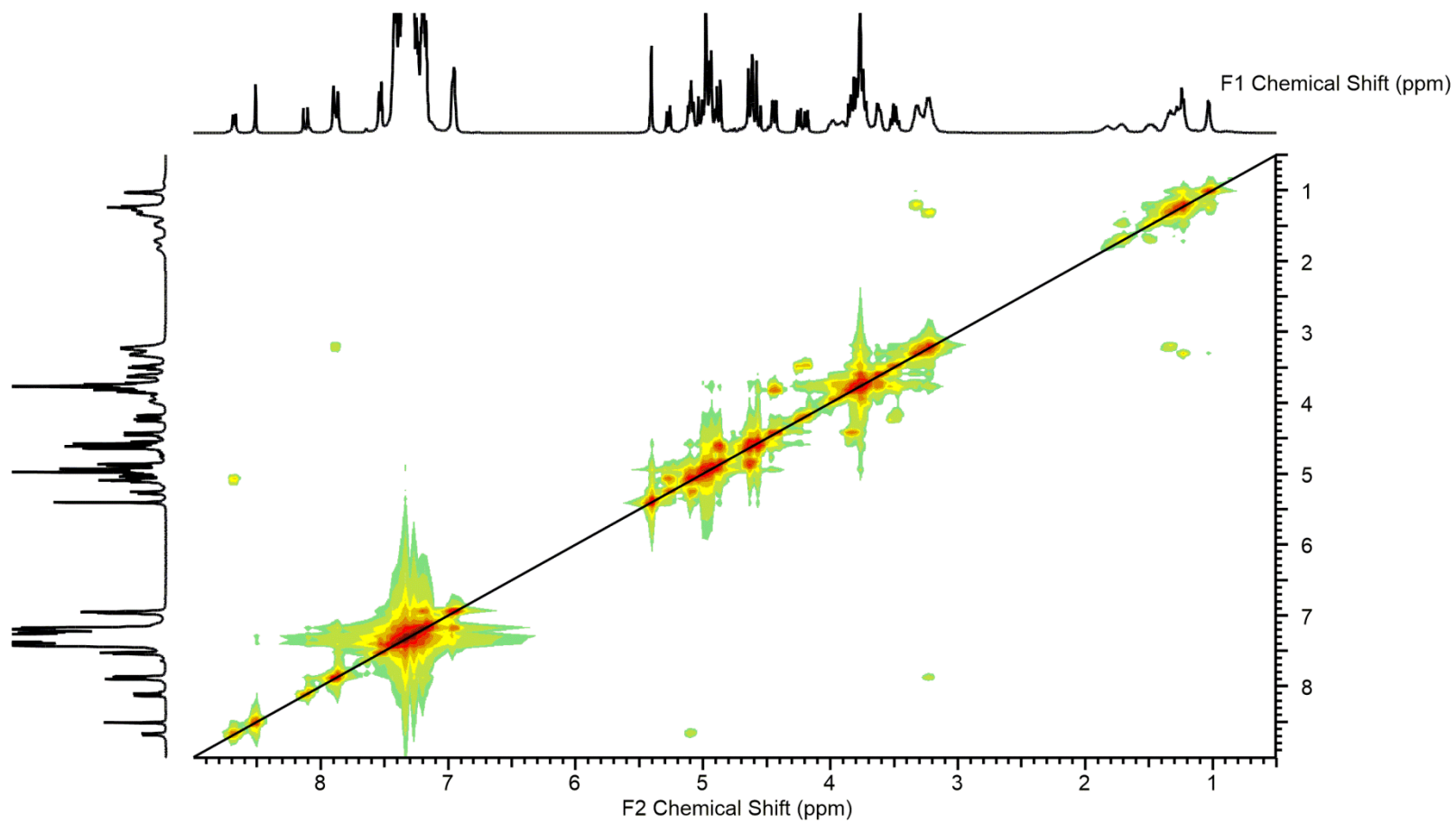


Figure 152 - Full COSY spectrum (CDCl₃) of **4-25**.

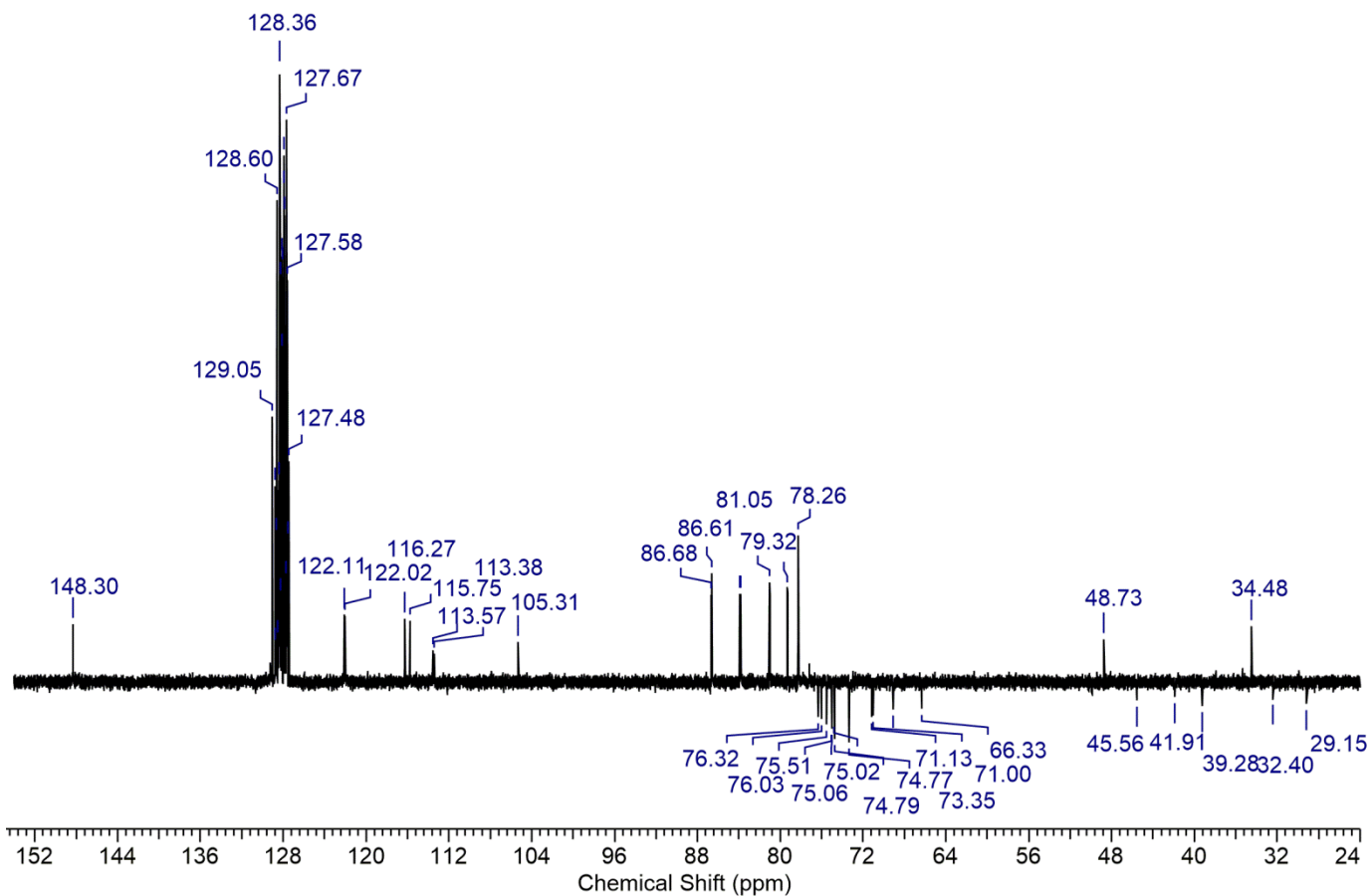


Figure 153 - Full DEPT spectrum (CDCl_3) of **4-25**.

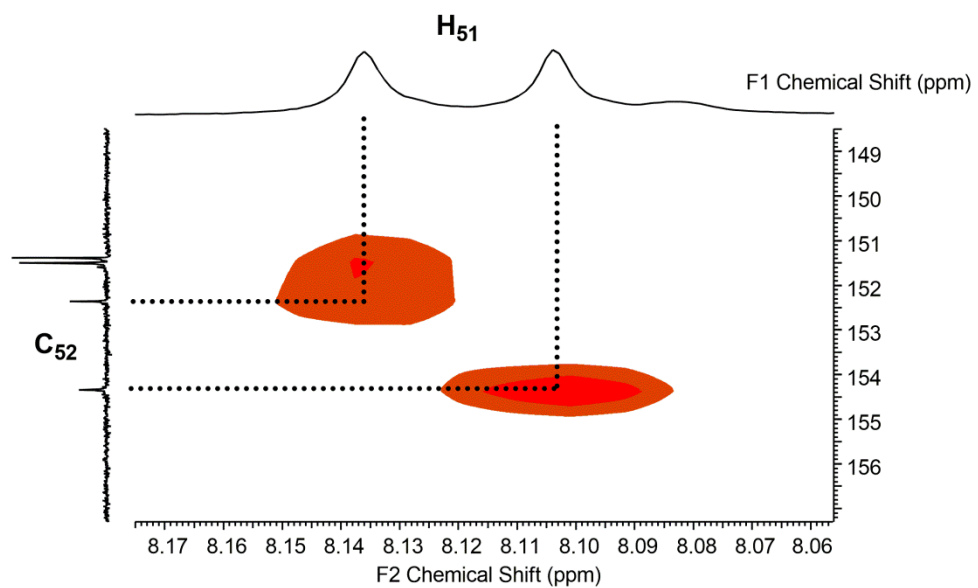


Figure 154 - HMBC spectrum (CDCl₃) of 4-25.

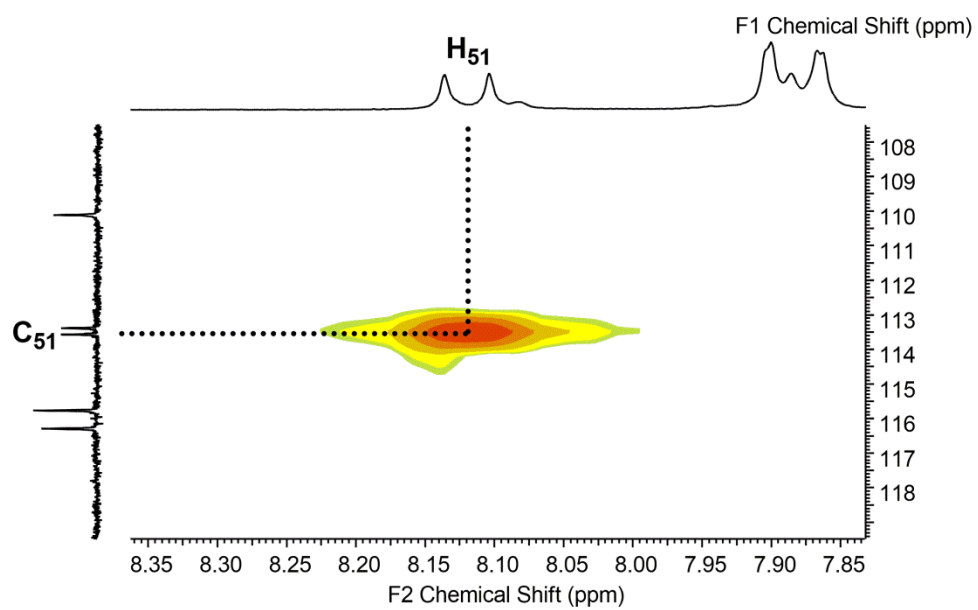


Figure 155 - HMQC spectrum (CDCl₃) of 4-25.

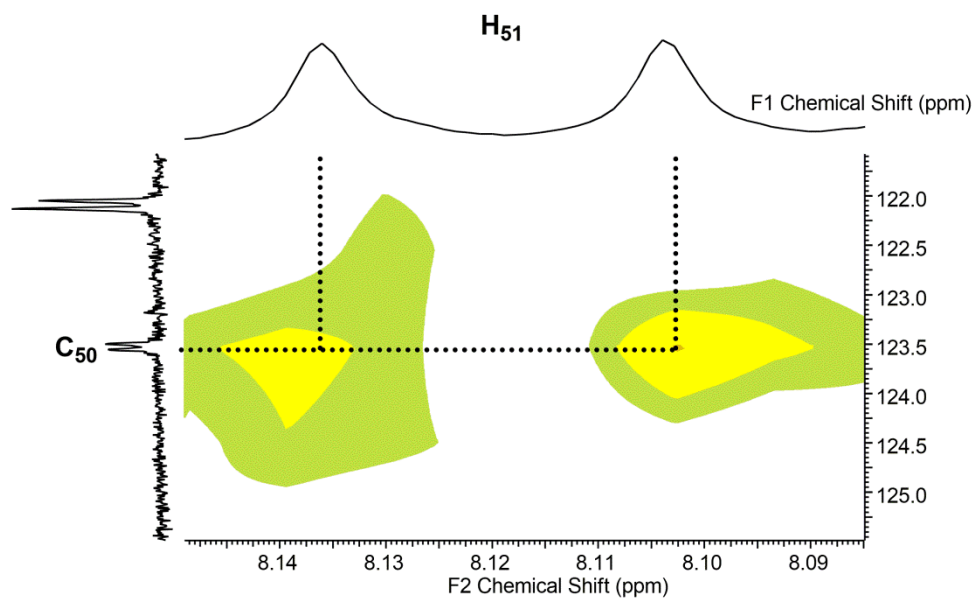


Figure 156 - HMBC spectrum (CDCl₃) of 4-25.

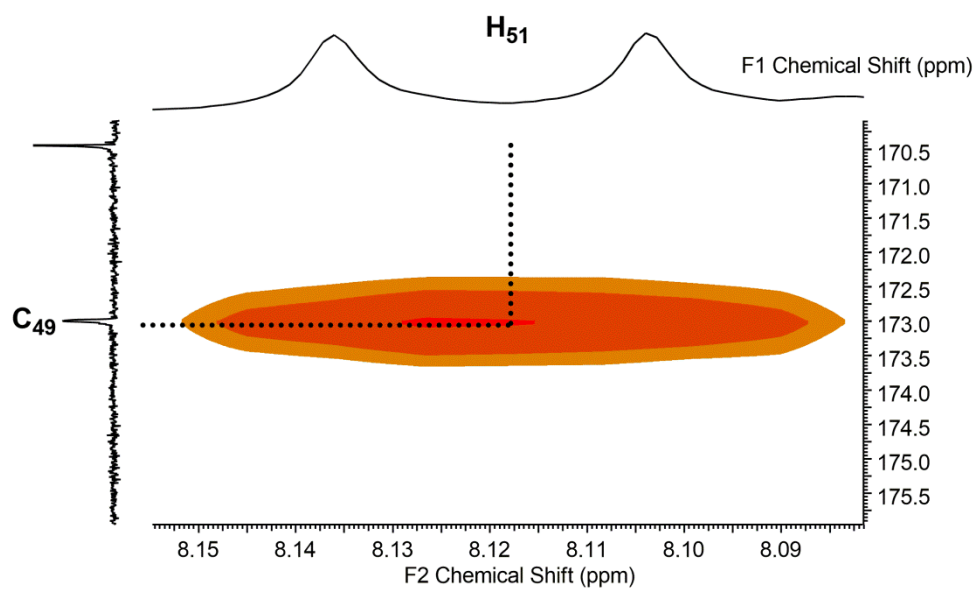


Figure 157 - HMBC spectrum (CDCl₃) of 4-25.

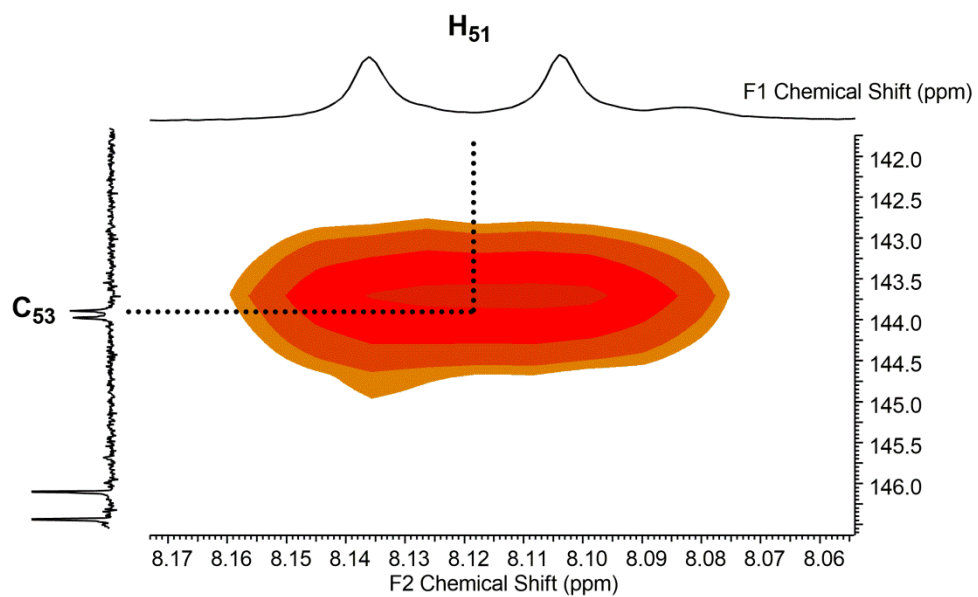


Figure 158 - HMBC spectrum (CDCl₃) of 4-25.

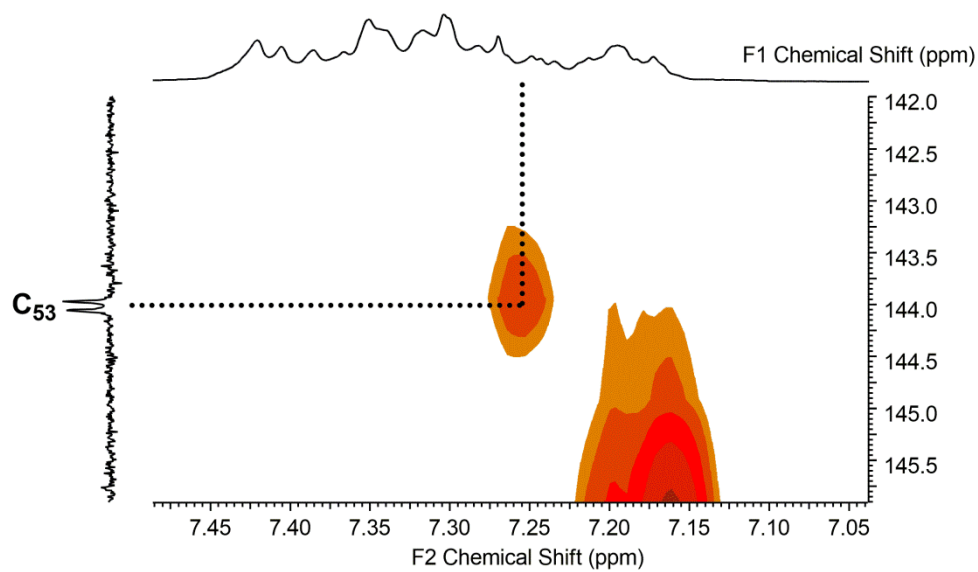


Figure 159 - HMBC spectrum (CDCl₃) of 4-25.

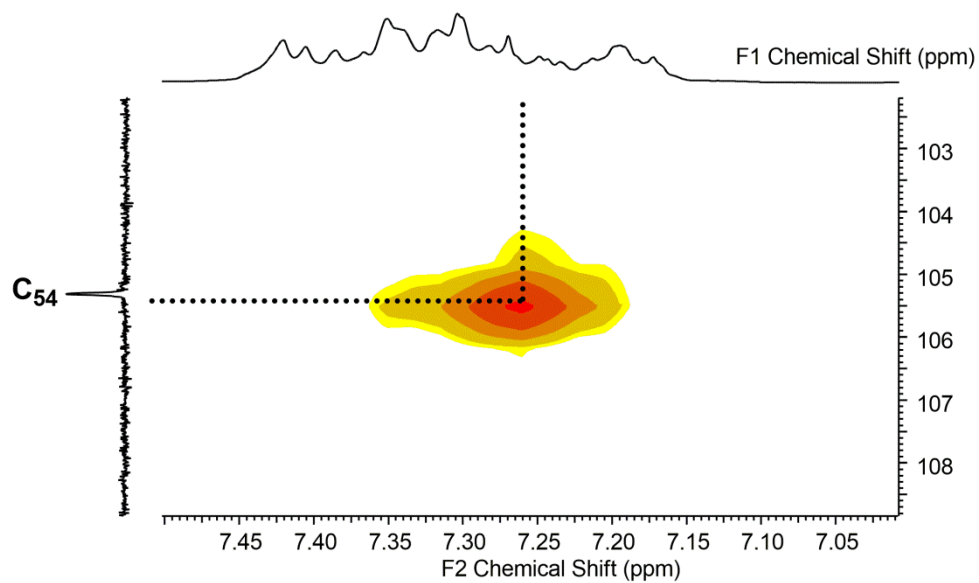


Figure 160 - HMQC spectrum (CDCl₃) of **4-25**.

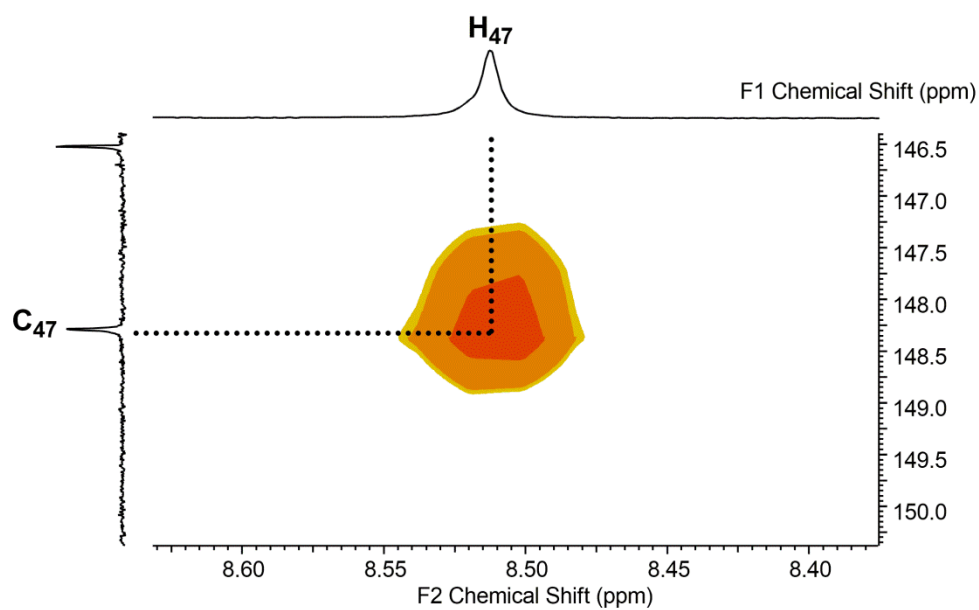


Figure 161 - HMQC spectrum (CDCl₃) of **4-25**.

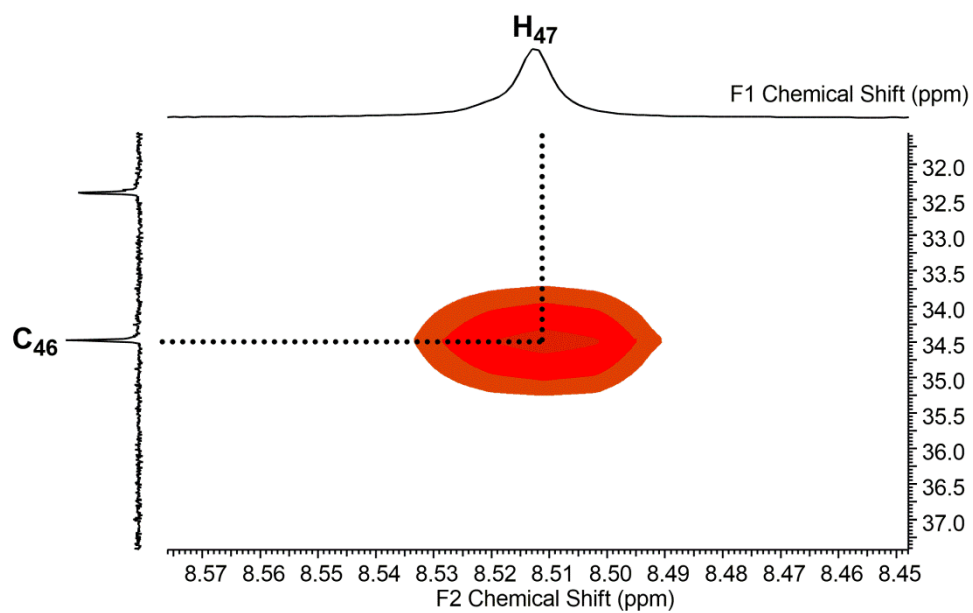


Figure 162 - HMBC spectrum (CDCl₃) of 4-25.

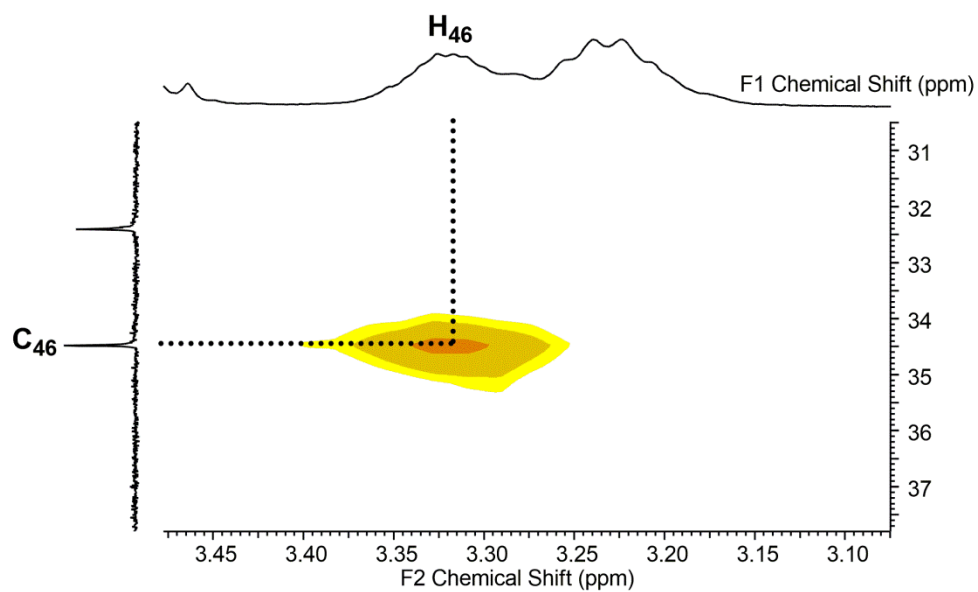


Figure 163 - HMQC spectrum (CDCl₃) of 4-25.

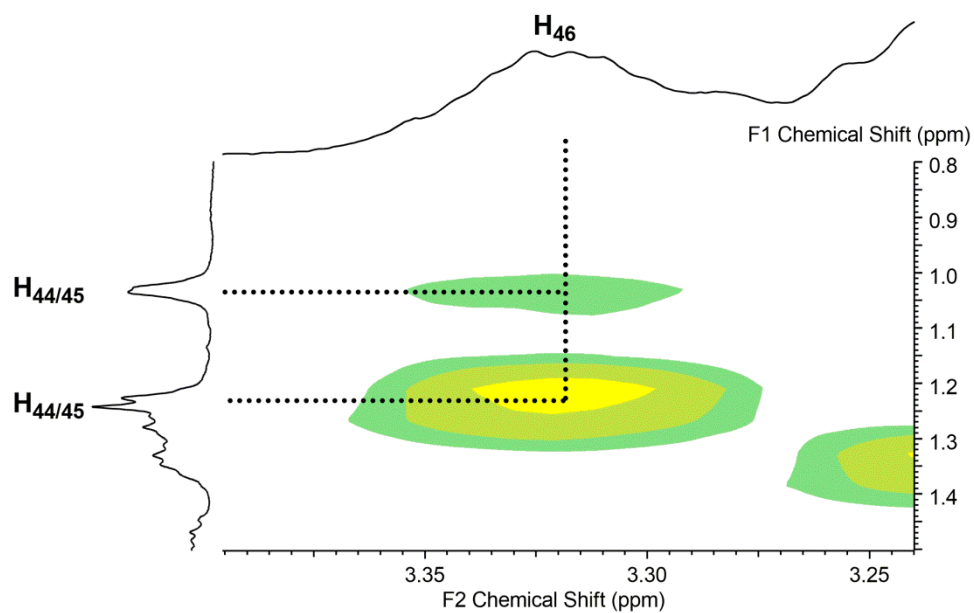


Figure 164 - COSY spectrum (CDCl_3) of **4-25**.

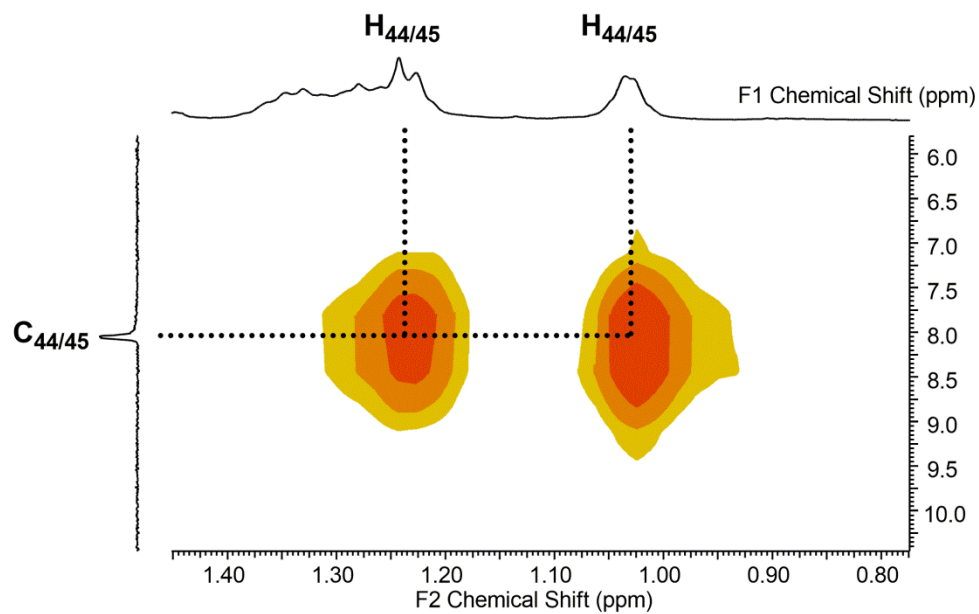


Figure 165 - HMQC spectrum (CDCl_3) of **4-25**.

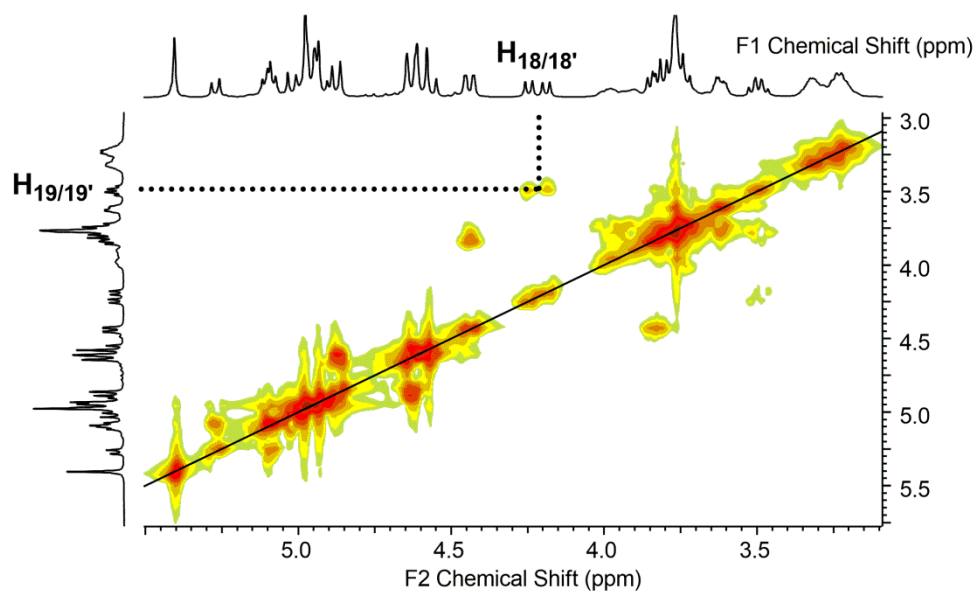


Figure 166 - COSY spectrum (CDCl₃) of **4-25**.

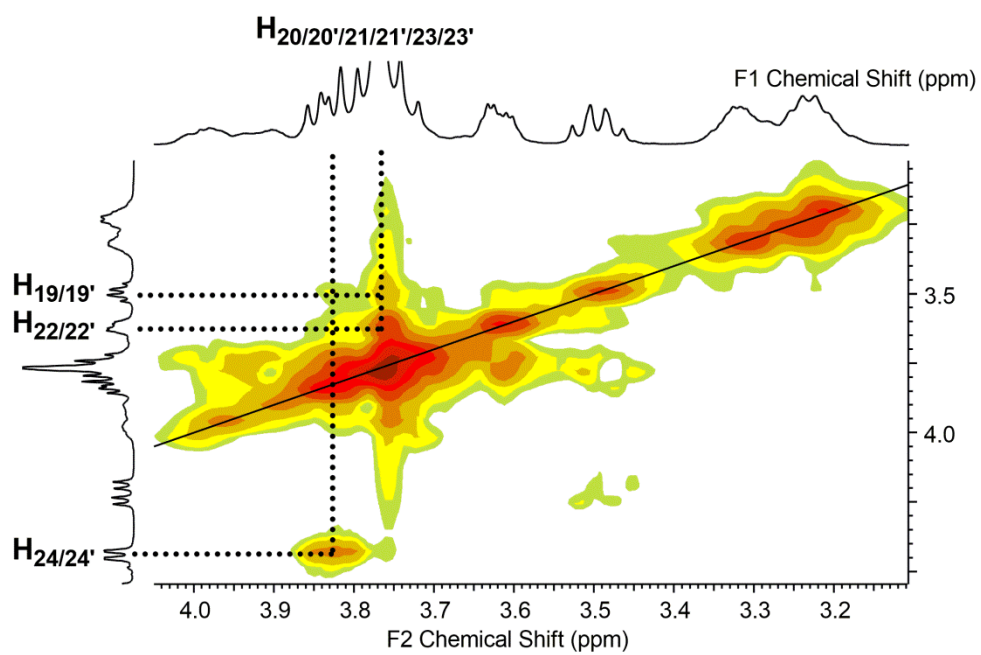


Figure 167 - COSY spectrum (CDCl₃) of **4-25**.

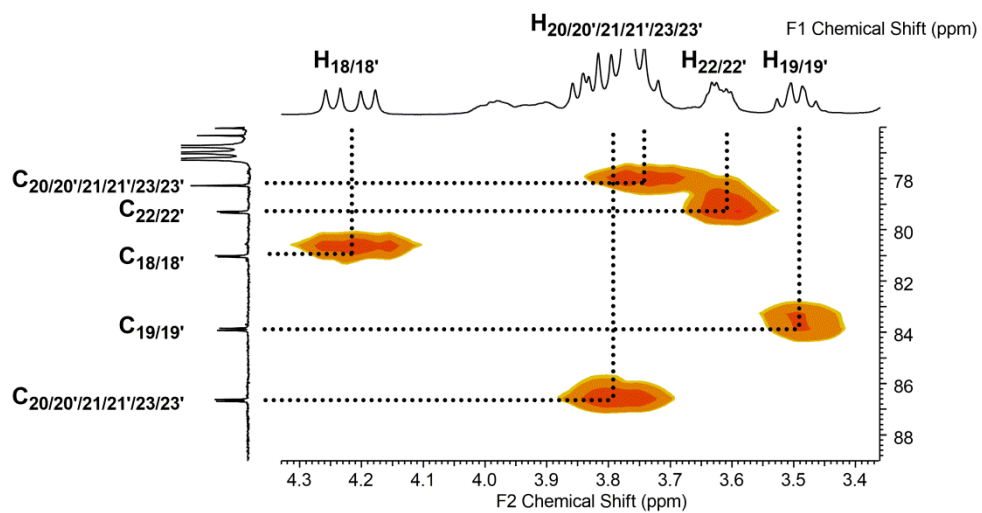


Figure 168 - HMBC spectrum (CDCl₃) of **4-25**.

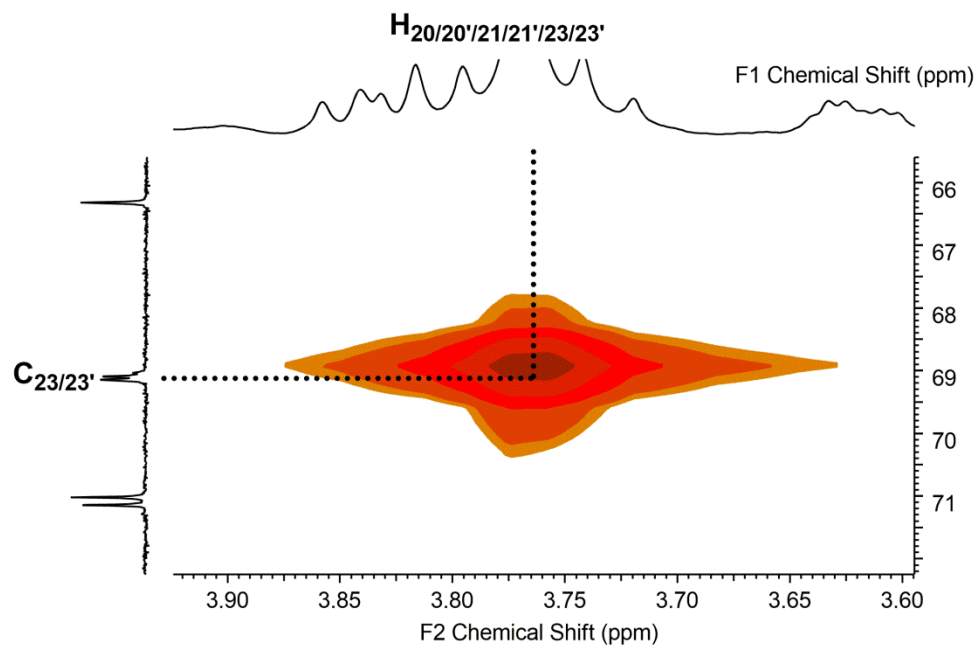


Figure 169 - HMBC spectrum (CDCl₃) of **4-25**.

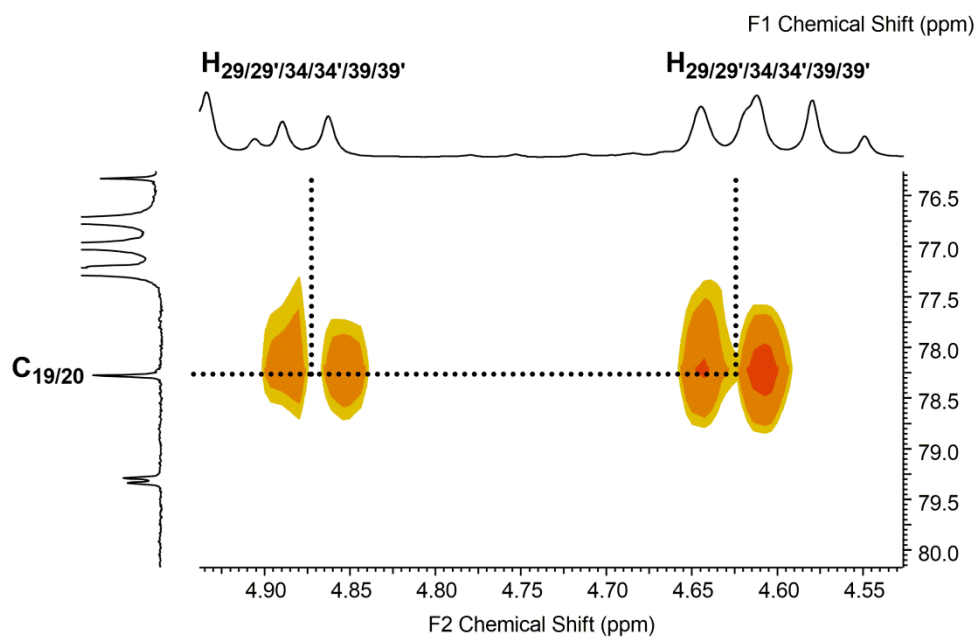


Figure 170 - HMBC spectrum (CDCl₃) of **4-25**.

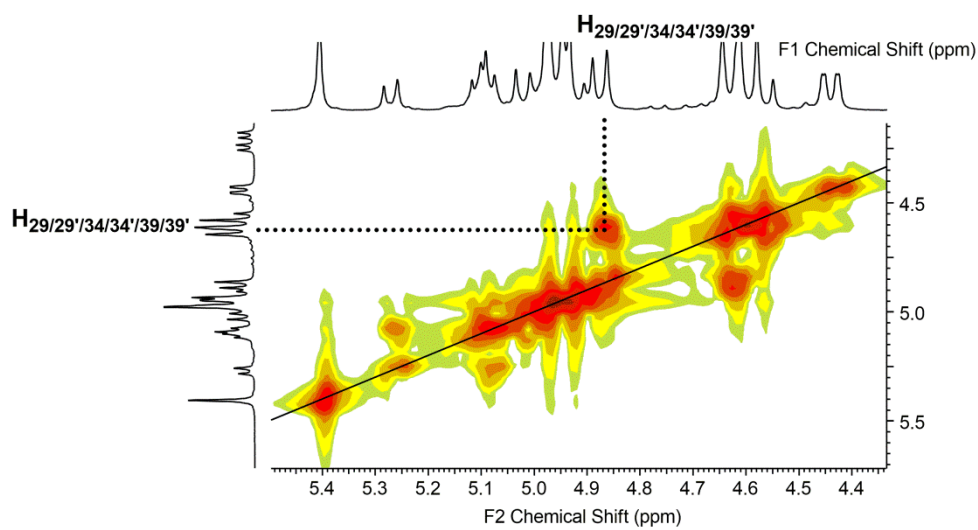


Figure 171 - COSY spectrum (CDCl₃) of **4-25**.

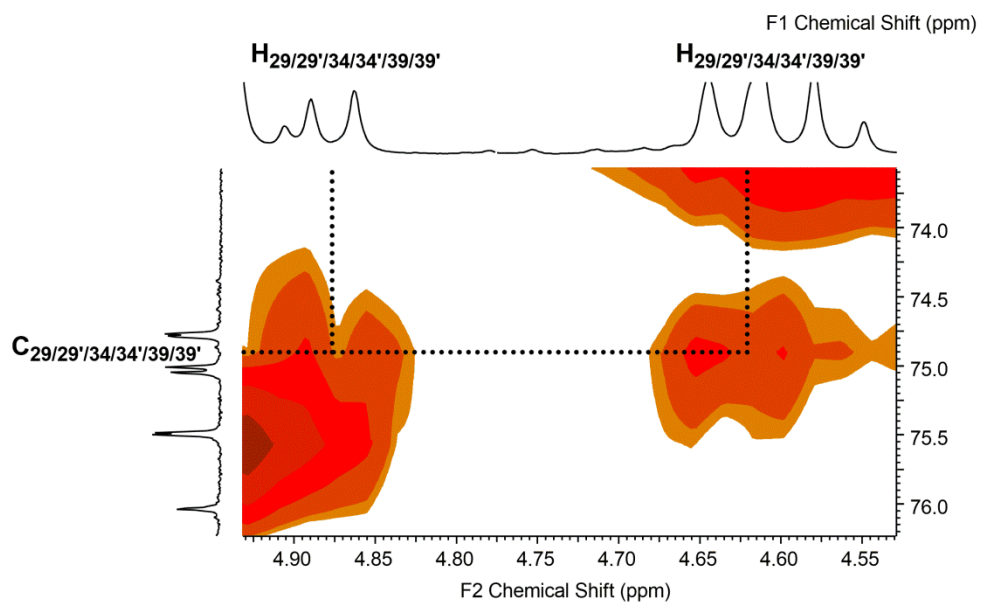


Figure 172 - HMQC spectrum (CDCl_3) of **4-25**.

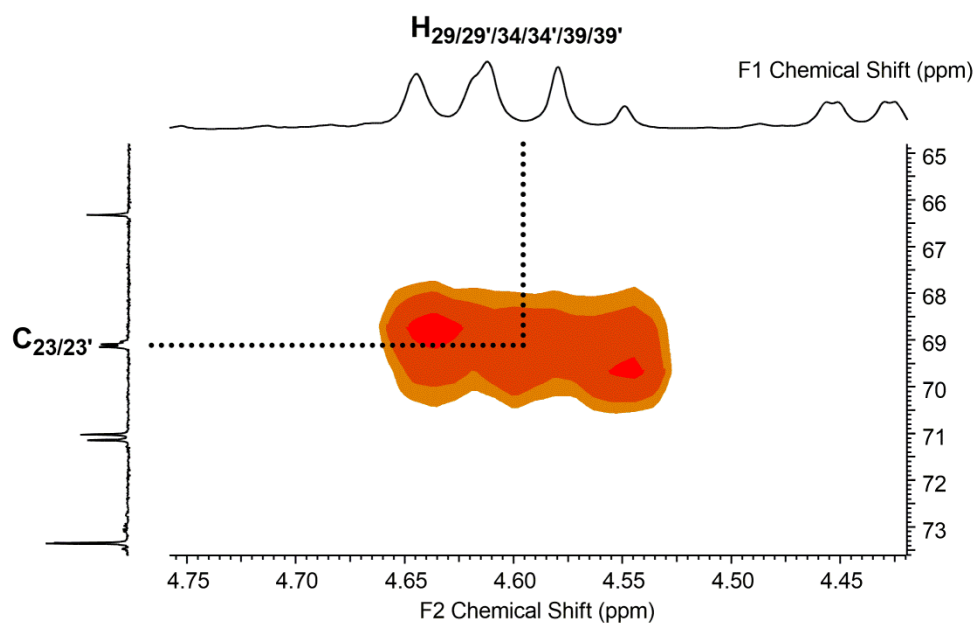


Figure 173 - HMBC spectrum (CDCl_3) of **4-25**.

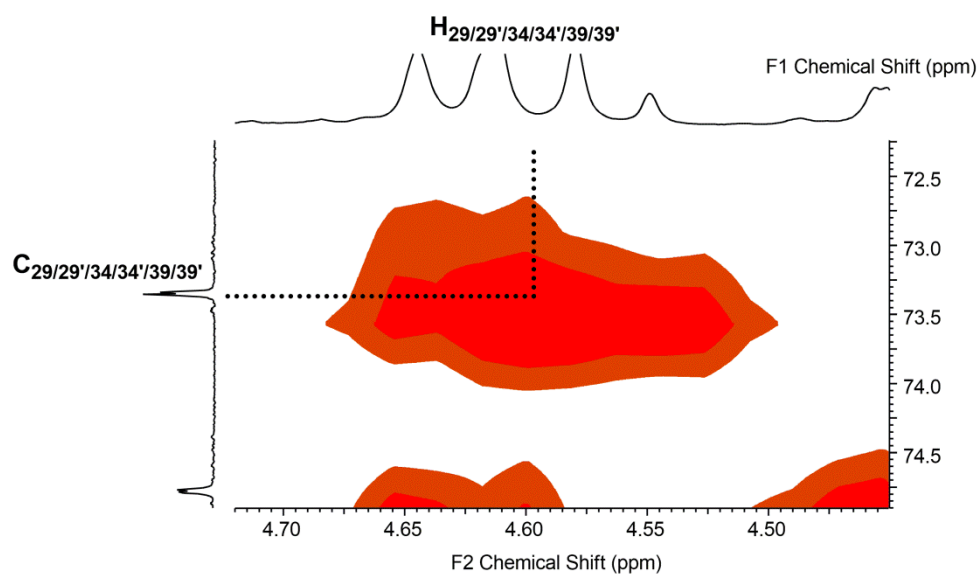


Figure 174 - HMQC spectrum (CDCl₃) of **4-25**.

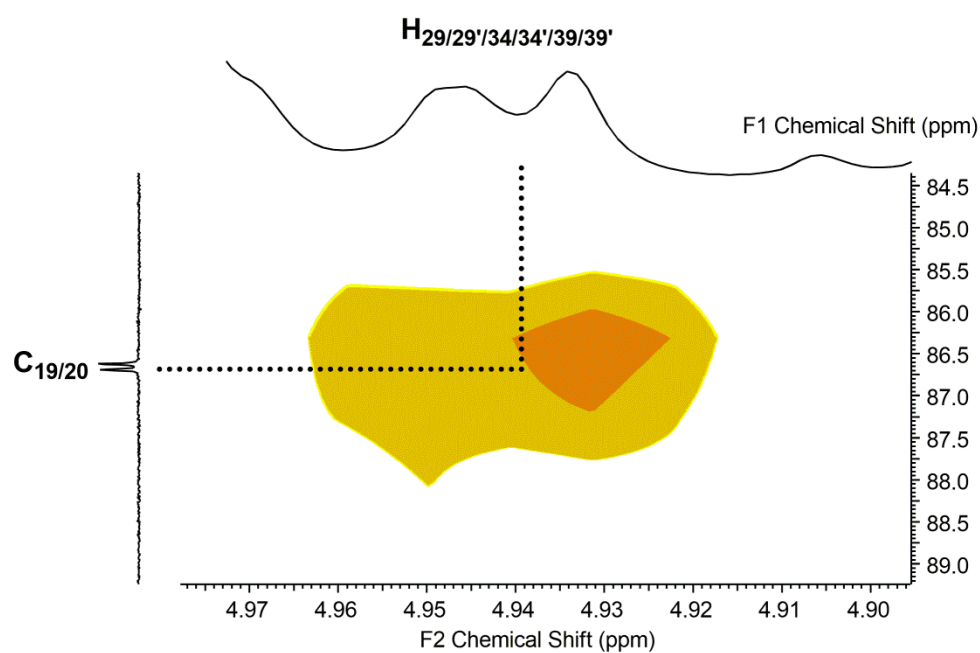


Figure 175 - HMBC spectrum (CDCl₃) of **4-25**.

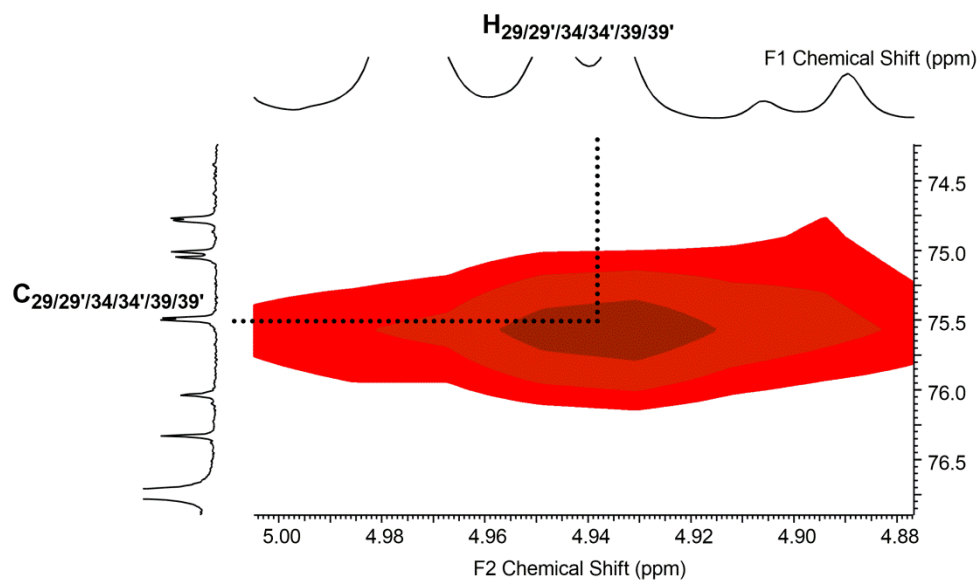


Figure 176 - HMBC spectrum (CDCl₃) of **4-25**.

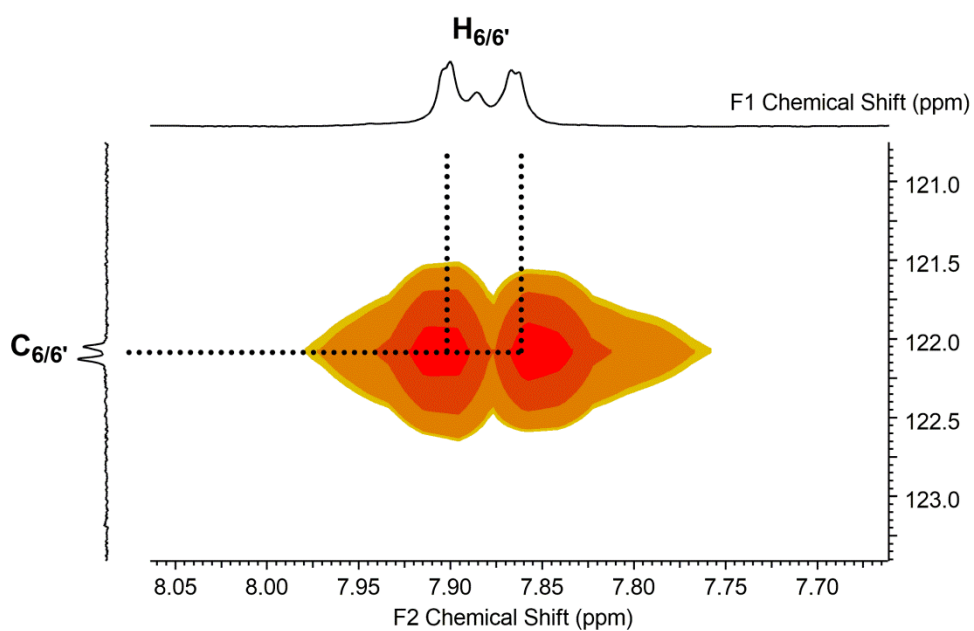


Figure 177 - HMBC spectrum (CDCl₃) of **4-25**.

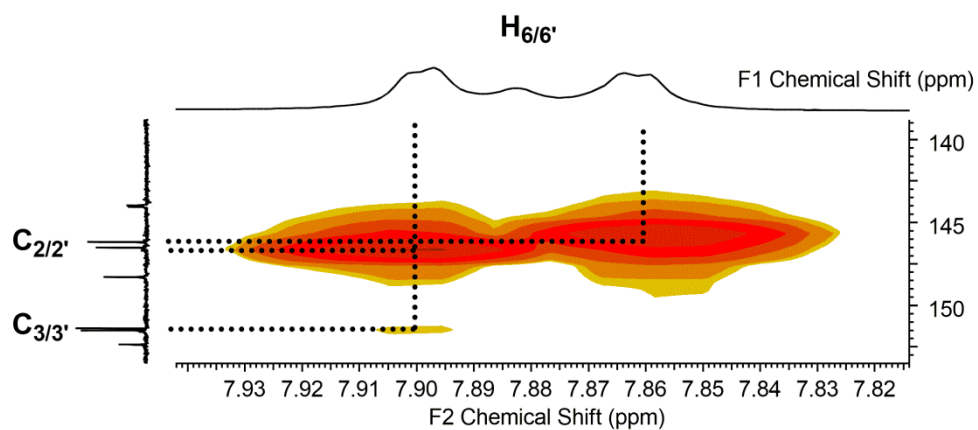


Figure 178 - HMBC spectrum (CDCl₃) of **4-25**.

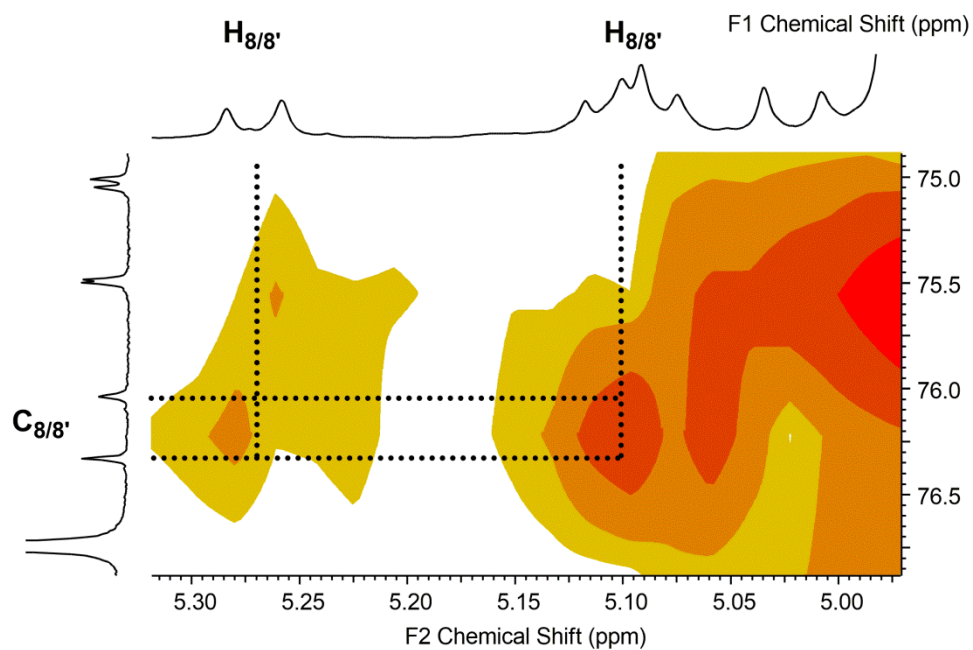


Figure 179 - HMQC spectrum (CDCl₃) of **4-25**.

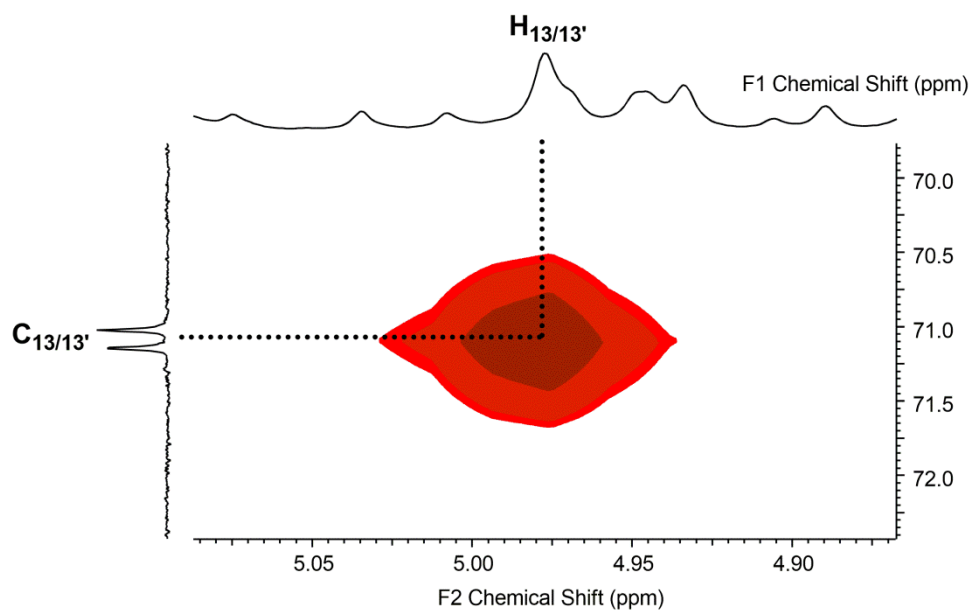


Figure 180 - HMQC spectrum (CDCl_3) of **4-25**.

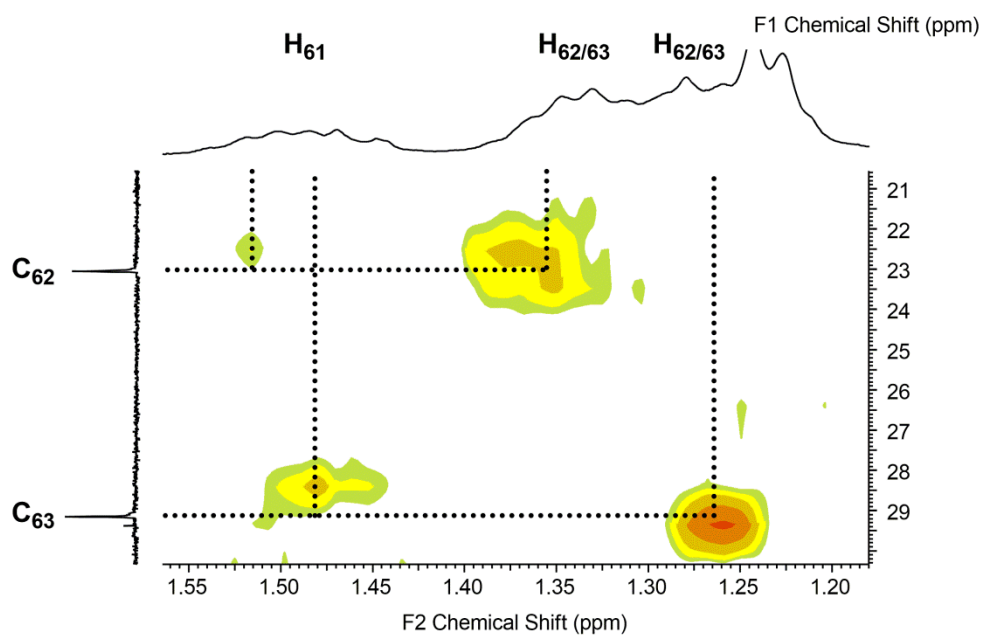


Figure 181 - HMBC spectrum (CDCl_3) of **4-25**.

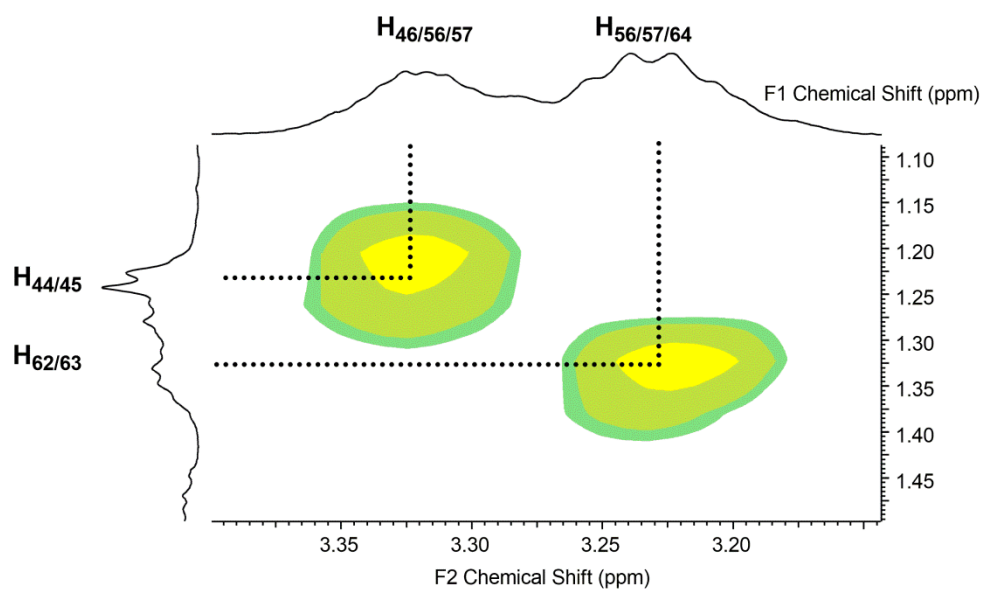


Figure 182 - COSY spectrum (CDCl_3) of **4-25**.

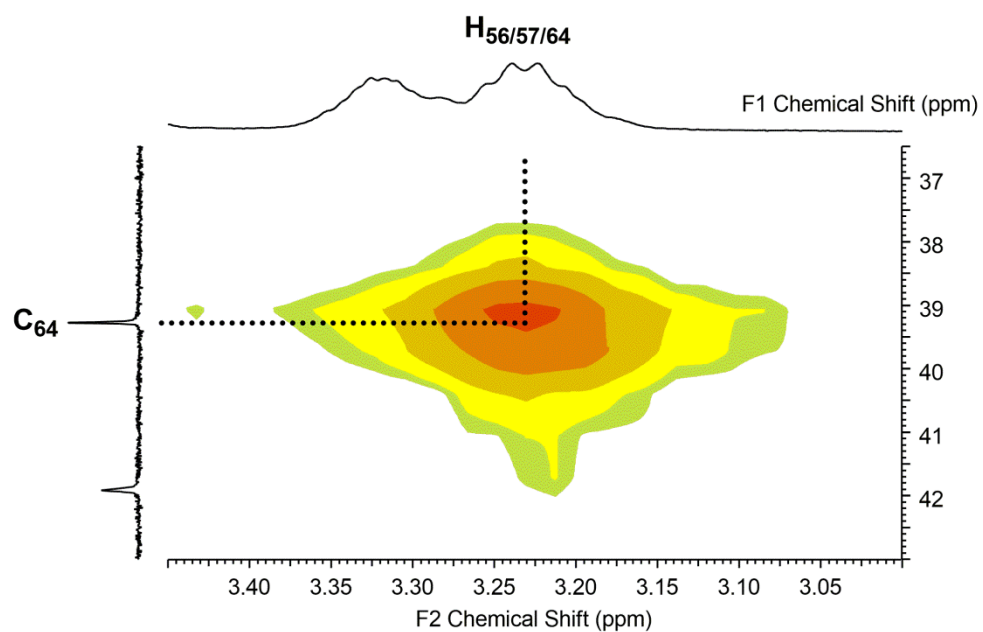


Figure 183 - HMQC spectrum (CDCl_3) of **4-25**.

Abbreviations

°	degrees
°C	degrees Celcius
μ (prefix)	micro
¹³ C	carbon
¹⁹ F	fluorine
¹ H	proton
Å	Angstrom
ABC	ATP-binding cassette
Ar	aromatic
atm	atmosphere
aq	aqueous
<i>B. subtilis</i>	<i>Bacillus subtilis</i>
BnBr	benzyl bromide
Boc	<i>tert</i> -butyloxycarbonyl
Boc ₂ O	di- <i>tert</i> -butyl dicarbonate
Ca(OH) ₂	calcium hydroxide
CBz	carboxybenzyl
CD ₃ OD	deuterated methanol
CDCl ₃	deuterated chloroform
CDI	1,1'-carbonyldiimidazole
CH ₂ Cl ₂	dichlormethane
CHCl ₃	chloroform
CO ₂	carbon dioxide
COMT	catechol <i>O</i> -methyl transferase
Cs ₂ CO ₃	caesium carbonate
d ₆ -DMSO	deuterated dimethyl sulfoxide
DCC	dicyclohexylcarbodiimide
DDQ	dichlorodicyanoquinone
DEPT	Distortionless Enhancement by Polarisation Transfer

DIPEA	<i>N-N'</i> -diisopropylethylamine
DMF	<i>N-N</i> -dimethylformamide
DMSO	dimethyl sulfoxide
DNA	deoxyribonucleic acid
DSC	<i>N-N'</i> -disuccinimidyl carbonate
<i>E. coli</i>	<i>Escherichia coli</i>
EDC	1-ethyl-3-(3-dimethylaminopropyl)carbodiimide
ESI	electrospray ionisation
Et ₃ N	triethylamine
EtOAc	ethyl acetate
EtOH	ethanol
Fmoc	fluorenylmethyloxycarbonyl
g	gram
h	hour
H ₂	hydrogen
H ₂ O	water
H ₂ SO ₄	sulfuric acid
HATU	1-[Bis(dimethylamino)methylene]-1 <i>H</i> -1,2,3-triazolo[4,5- <i>b</i>]pyridinium 3-oxid hexafluorophosphate
HCl	hydrochloric acid
HMBC	Heteronuclear Multiple-Bond Correlation
HMQC	Heteronuclear Multiple-Quantum Correlation
HOBt	hydroxybenzotriazole
HPLC	high performance liquid chromatography
HRMS	high resolution mass spectrometry
HSQC	Heteronuclear Single Quantum Correlation
K	Kelvin
K ₂ CO ₃	potassium carbonate
L	litre
LB	lysogeny broth
LC	liquid chromatography
M	Molar
m	metre

m (prefix)	milli
m/z	mass/charge
MDR	multi-drug resistant
MeOH	methanol
MIC	minimum inhibitory concentration
MS	mass spectrometry
n (prefix)	nano
NaHCO ₃	sodium hydrogen carbonate
NaOH	sodium hydroxide
Ni(COD) ₂	bis(1,5-cyclooctadiene)nickel(0)
nm	nanometer
NMR	nuclear magnetic resonance
OD ₆₅₀	optical density at 650 nm
<i>P. aeruginosa</i>	<i>Pseudomonas aeruginosa</i>
<i>P. putida</i>	<i>Pseudomonas putida</i>
ppm	parts per million
Qnr	quinolone resistance proteins
RPM	revolutions per minute
s	second
<i>S. aureus</i>	<i>Staphylococcus aureus</i>
<i>S. pneumoniae</i>	<i>Staphylococcus pneumoniae</i>
t	time
TBAH	tetrabutylammonium hydroxide
TBAI	tetrabutylammonium iodide
^t Bu-Terpy	4,4',4''-tert-butyl-2,2':6',2''-terpyridine
TFA	trifluoroacetic acid
THF	tetrahydrofuran
UV/Vis	ultra-violet-visible
wt.	weight
λ_{\max}	wavelength of maximum absorbance

References

1. J. H. Powers, *Clin. Microbiol. Infec.*, 2004, **10**, 23-31.
2. A. R. M. Coates, G. Halls and Y. Hu, *Brit. J. Pharmacol.*, 2011, **163**, 184-194.
3. L. A. Mitscher, *J. Nat. Prod.*, 2008, **71**, 497-509.
4. M. F. Chellat, L. Raguž and R. Riedl, *Angew. Chem. Int. Ed. Engl.*, 2016, **55**, 6600-6626.
5. J. M. Roosenberg, Y. M. Lin, Y. Lu and M. J. Miller, *Curr. Med. Chem.*, 2000, **7**, 159-197.
6. M. G. P. Page, *Ann. N. Y. Acad. Sci.*, 2013, **1277**, 115-126.
7. G. L. A. Mislin and I. J. Schalk, *Metallomics*, 2014, **6**, 408-420.
8. K. Li, W.-H. Chen and S. D. Bruner, *Biometals*, 2016, **29**, 377-388.
9. G. Y. Leshner, M. D. Gruett, E. J. Froelich, R. P. Brundage and J. H. Bailey, *J. Med. Pharm. Chem.*, 1962, **5**, 1063-1065.
10. L. A. Mitscher, *Chem. Rev.*, 2005, **105**, 559-592.
11. A. Naeem, S. Badshah, M. Muska, N. Ahmad and K. Khan, *Molecules*, 2016, **21**, 268.
12. G. S. Tillotson, *J. Med. Microbiol.*, 1996, **44**, 320-324.
13. H. Koga, A. Itoh, S. Murayama, S. Suzue and T. Irikura, *J. Med. Chem.*, 1980, **23**, 1358-1363.
14. R. Wise, J. Andrews and L. Edwards, *Antimicrob. Agents Chemother.*, 1983, **23**, 559-564.
15. S. Heeb, M. P. Fletcher, S. R. Chhabra, S. P. Diggle, P. Williams and M. Cámara, *FEMS Microbiol. Rev.*, 2011, **35**, 247-274.
16. K. J. Aldred, R. J. Kerns and N. Osheroff, *Biochemistry*, 2014, **53**, 1565-1574.
17. A. M. Emmerson and A. M. Jones, *J. Antimicrob. Chemother.*, 2003, **51**, 13-20.
18. P. Ball, *J. Antimicrob. Chemother.*, 2000, **46**, 17-24.
19. S. J. Harnett, A. P. Fraise, J. M. Andrews, G. Jevons, N. P. Brenwald and R. Wise, *J. Antimicrob. Chemother.*, 2004, **53**, 783-792.

20. S. Lemaire, P. M. Tulkens and F. Van Bambeke, *Antimicrob. Agents Chemother.*, 2011, **55**, 649-658.
21. M. Bassetti, P. Della Siega, D. Pecori, C. Scarparo and E. Righi, *Expert. Opin. Investig. Drugs*, 2015, **24**, 433-442.
22. F. Van Bambeke, *Future Microbiol.*, 2015, **10**, 1111-1123.
23. I. Laponogov, M. K. Sohi, D. A. Veselkov, X. S. Pan, R. Sawhney, A. W. Thompson, K. E. McAuley, L. M. Fisher and M. R. Sanderson, *Nat. Struct. Mol. Biol.*, 2009, **16**, 667-669.
24. B. D. Bax, P. F. Chan, D. S. Eggleston, A. Fosberry, D. R. Gentry, F. Gorrec, I. Giordano, M. M. Hann, A. Hennessy, M. Hibbs, J. Z. Huang, E. Jones, J. Jones, K. K. Brown, C. J. Lewis, E. W. May, M. R. Saunders, O. Singh, C. E. Spitzfaden, C. Shen, A. Shillings, A. J. Theobald, A. Wohlkonig, N. D. Pearson and M. N. Gwynn, *Nature*, 2010, **466**, 935-943.
25. A. Mustaev, M. Malik, X. L. Zhao, N. Kurepina, G. Luan, L. M. Oppedard, H. Hiasa, K. R. Marks, R. J. Kerns, J. M. Berger and K. Drlica, *J. Biol. Chem.*, 2014, **289**, 12300-12312.
26. K. Drlica and X. L. Zhao, *Microbiol. Mol. Biol. Rev.*, 1997, **61**, 377-392.
27. J. Roca, *Trends Biochem. Sci.*, 1995, **20**, 156-160.
28. L. L. Shen, L. A. Mitscher, P. N. Sharma, T. O'donnell, D. W. Chu, C. S. Cooper, T. Rosen and A. G. Pernet, *Biochemistry*, 1989, **28**, 3886-3894.
29. J. E. Dewese, A. B. Burgin and N. Osheroff, *Nucleic Acids Res.*, 2008, **36**, 4883-4893.
30. C. G. Noble, F. M. Barnard and A. Maxwell, *Antimicrob. Agents Chemother.*, 2003, **47**, 854-862.
31. K. J. Aldred, S. A. McPherson, C. L. Turnbough, R. J. Kerns and N. Osheroff, *Nucleic Acids Res.*, 2013, **41**, 4628-4639.
32. J. M. Domagala, *J. Antimicrob. Chemother.*, 1994, **33**, 685-706.
33. E. P. Abraham and E. Chain, *Nature*, 1940, **146**, 837.
34. W. H. Organization, *Antimicrobial Resistance: Global Report on Surveillance*, 2014.

35. J. Davies and D. Davies, *Microbiol. Mol. Biol. Rev.*, 2010, **74**, 417-433.
36. H. K. Allen, J. Donato, H. H. Wang, K. A. Cloud-Hansen, J. Davies and J. Handelsman, *Nat. Rev. Microbiol.*, 2010, **8**, 251-259.
37. L. J. V. Piddock, *Nat. Rev. Microbiol.*, 2006, **4**, 629-636.
38. D. C. Hooper, *Drug Resist. Update*, 1999, **2**, 38-55.
39. S. B. Levy and B. Marshall, *Nat. Med.*, 2004, **10**, S122-S129.
40. D. C. Hooper and G. A. Jacoby, *Ann. N. Y. Acad. Sci.*, 2015, **1354**, 12-31.
41. A. Robicsek, J. Strahilevitz, G. A. Jacoby, M. Macielag, D. Abbanat, C. Hye Park, K. Bush and D. C. Hooper, *Nat. Med.*, 2006, **12**, 83-88.
42. N. Høiby, T. Bjarnsholt, M. Givskov, S. Molin and O. Ciofu, *Int. J. Antimicrob. Agents*, 2010, **35**, 322-332.
43. L. J. Piddock, *J. Antimicrob. Chemother.*, 1991, **27**, 399-403.
44. M. G. Head, J. R. Fitchett, M. K. Cooke, F. B. Wurie, R. Atun, A. C. Hayward, A. Holmes, A. P. Johnson and N. Woodford, *J. Antimicrob. Chemother.*, 2013, **69**, 548-554.
45. R. C. Hider and X. L. Kong, *Nat. Prod. Rep.*, 2010, **27**, 637-657.
46. G. Cairo, F. Bernuzzi and S. Recalcati, *Genes Nutr.*, 2006, **1**, 25-39.
47. J. B. Neilands, *Biol. Met.*, 1991, **4**, 1-6.
48. K. N. Raymond, E. A. Dertz and S. S. Kim, *Proc. Natl. Acad. Sci. U.S.A.*, 2003, **100**, 3584-3588.
49. J. B. Neilands, *J. Biol. Chem.*, 1995, **270**, 26723-26726.
50. M. Miethke and M. A. Marahiel, *Microbiol. Mol. Biol. Rev.*, 2007, **71**, 413-451.
51. M. Saha, S. Sarkar, B. Sarkar, B. K. Sharma, S. Bhattacharjee and P. Tribedi, *Environ. Sci. Pollut. R.*, 2015, **23**, 3984-3999.
52. J. B. Neilands, *J. Am. Chem. Soc.*, 1952, **74**, 4846-4847.
53. L. D. Loomis and K. N. Raymond, *Inorg. Chem.*, 1991, **30**, 906-911.
54. R. E. W. Hancock, K. Hantke and V. Braun, *Arch. Microbiol.*, 1977, **114**, 231-239.

55. W. W. Yue, S. Grizot and S. K. Buchanan, *J. Mol. Biol.*, 2003, **332**, 353-368.
56. I. Gautier-Luneau, C. Merle, D. Phanon, C. Lebrun, F. Biaso, G. Serratrice and J. L. Pierre, *Chem. Eur. J.*, 2005, **11**, 2207-2219.
57. C. J. Carrano, H. Drechsel, D. Kaiser, G. Jung, B. Matzanke, G. Winkelmann, N. Rochel and A. M. Albrecht-Gary, *Inorg. Chem.*, 1996, **35**, 6429-6436.
58. K. D. Krewulak and H. J. Vogel, *Biochim. Biophys. Acta*, 2008, **1778**, 1781-1804.
59. S. Hussein, K. Hantke and V. Braun, *Eur. J. Biochem.*, 1981, **117**, 431-437.
60. W. Wagegg and V. Braun, *J. Bacteriol.*, 1981, **145**, 156-163.
61. M. Ogierman and V. Braun, *J. Bacteriol.*, 2003, **185**, 1870-1885.
62. A. D. Ferguson, R. Chakraborty, B. S. Smith, L. Esser, D. van der Helm and J. Deisenhofer, *Science*, 2002, **295**, 1715-1719.
63. S. K. Buchanan, B. S. Smith, L. Venkatramani, D. Xia, L. Esser, M. Palnitkar, R. Chakraborty, D. van der Helm and J. Deisenhofer, *Nat. Struct. Biol.*, 1999, **6**, 56-63.
64. T. E. Letain and K. Postle, *Mol. Microbiol.*, 1997, **24**, 271-283.
65. B. C. H. Chu, R. S. Peacock and H. J. Vogel, *Biometals*, 2007, **20**, 467-483.
66. M. Miethke, O. Klotz, U. Linne, J. J. May, C. L. Beckering and M. A. Marahiel, *Mol. Microbiol.*, 2006, **61**, 1413-1427.
67. P. M. Proulx-Curry and N. D. Chasteen, *Coord. Chem. Rev.*, 1995, **144**, 347-368.
68. P. M. Harrison and P. Arosio, *Biochim. Biophys. Acta*, 1996, **1275**, 161-203.
69. T. H. Flo, K. D. Smith, S. Sato, D. J. Rodriguez, M. A. Holmes, R. K. Strong, S. Akira and A. Aderem, *Nature*, 2004, **432**, 917-921.
70. R. J. Abergel, M. C. Clifton, J. C. Pizarro, J. A. Warner, D. K. Shuh, R. K. Strong and K. N. Raymond, *J. Am. Chem. Soc.*, 2008, **130**, 11524-11534.
71. M. C. Clifton, C. Corrent and R. K. Strong, *Biometals*, 2009, **22**, 557-564.

72. A. K. Sia, B. E. Allred and K. N. Raymond, *Curr. Opin. Chem. Biol.*, 2013, **17**, 150-157.
73. B. E. Allred, C. Correnti, M. C. Clifton, R. K. Strong and K. N. Raymond, *ACS Chem. Biol.*, 2013, **8**, 1882-1887.
74. M. A. Holmes, W. Paulsene, X. Jide, C. Ratledge and R. K. Strong, *Structure*, 2005, **13**, 29-41.
75. R. J. Abergel, M. K. Wilson, J. E. L. Arceneaux, T. M. Hoette, R. K. Strong, B. R. Byers and K. N. Raymond, *Proc. Natl. Acad. Sci. U.S.A.*, 2006, **103**, 18499-18503.
76. R. J. Abergel, A. M. Zawadzka and K. N. Raymond, *J. Am. Chem. Soc.*, 2008, **130**, 2124-2125.
77. K. Hantke, G. Nicholson, W. Rabsch and G. Winkelmann, *Proc. Natl. Acad. Sci. U.S.A.*, 2003, **100**, 3677-3682.
78. B. Bister, D. Bischoff, G. J. Nicholson, M. Valdebenito, K. Schneider, G. Winkelmann, K. Hantke and R. D. Süssmuth, *Biometals*, 2004, **17**, 471-481.
79. M. Zhu, M. Valdebenito, G. Winkelmann and K. Hantke, *Microbiology*, 2005, **151**, 2363-2372.
80. V. Braun, A. Pramanik, T. Gwinner, M. Köberle and E. Bohn, *Biometals*, 2009, **22**, 3-13.
81. G. F. Gause, *Brit. Med. J.*, 1955, **2**, 1177-1179.
82. A. D. Ferguson, J. W. Coulton, K. Diederichs, W. Welte, V. Braun and H.-P. Fiedler, *Prot. Sci.*, 2000, **9**, 956-963.
83. H. Zähner, H. Diddens, W. Keller-Schierlein and H.-U. Nägeli, *Jpn. J. Antibiot.*, 1977, **30**, 201-206.
84. M. Ghosh and M. J. Miller, *Bioorg. Med. Chem.*, 1996, **4**, 43-48.
85. U. Möllmann, L. Heinisch, A. Bauernfeind, T. Köhler and D. Ankel-Fuchs, *Biometals*, 2009, **22**, 615-624.
86. N. Ohi, B. Aoki, T. Shinozaki, K. Moro, T. Noto, T. Nehashi, H. Okazaki and I. Matsunaga, *J. Antibiot.*, 1986, **39**, 230-241.
87. N. Ohi, B. Aoki, K. Moro, T. Kuroki, N. Sugimura, T. Noto, T. Nehashi, M. Matsumoto, H. Okazaki and I. Matsunaga, *J. Antibiot.*, 1986, **39**, 242-250.

88. H. Mochizuki, H. Yamada, Y. Oikawa, K. Murakami, J. Ishiguro, H. Kosuzume, N. Aizawa and E. Mochida, *Antimicrob. Agents Chemother.*, 1988, **32**, 1648-1654.
89. E. K. Dolence, A. A. Minnick, C. E. Lin, M. J. Miller and S. M. Payne, *J. Med. Chem.*, 1991, **34**, 968-978.
90. A. Ghosh and M. J. Miller, *J. Org. Chem.*, 1993, **58**, 7652-7659.
91. M. Ghosh and M. J. Miller, *J. Org. Chem.*, 1994, **59**, 1020-1026.
92. M. J. Miller, *Chem. Rev.*, 1989, **89**, 1563-1579.
93. A. Ghosh, M. Ghosh, C. Niu, F. Malouin, U. Möllmann and M. J. Miller, *Chem. Biol.*, 1996, **3**, 1011-1019.
94. T. Kline, M. Fromhold, T. E. McKennon, S. Cai, J. Treiberg, N. Ihle, D. Sherman, W. Schwan, M. J. Hickey, P. Warrener, P. R. Witte, L. L. Brody, L. Goltry, L. M. Barker, S. U. Anderson, S. K. Tanaka, R. M. Shawar, L. Y. Nguyen, M. Langhorne, A. Bigelow, L. Embuscado and E. Naeemi, *Bioorg. Med. Chem.*, 2000, **8**, 73-93.
95. T. A. Wencewicz and M. J. Miller, *J. Med. Chem.*, 2013, **56**, 4044-4052.
96. C. Ji, P. A. Miller and M. J. Miller, *J. Am. Chem. Soc.*, 2012, **134**, 9898-9901.
97. N. Oki, B. Aoki, T. Kuroki, M. Matsumoto, K. Kojima and T. Nehashi, *J. Antibiot.*, 1987, **40**, 22-28.
98. T. Zheng and E. M. Nolan, *J. Am. Chem. Soc.*, 2014, **136**, 9677-9691.
99. P. Chairatana, T. Zheng and E. M. Nolan, *Chem. Sci.*, 2015, **6**, 4458-4471.
100. M. R. Barbachyn and T. C. Tuominen, *J. Antibiot.*, 1990, **43**, 1199-1203.
101. M. J. Mitton-Fry, J. T. Arcari, M. F. Brown, J. M. Casavant, S. M. Finegan, M. E. Flanagan, H. Y. Gao, D. M. George, B. S. Gerstenberger, S. Han, J. R. Hardink, T. M. Harris, T. Hoang, M. D. Huband, R. Irvine, M. S. Lall, M. M. Lemmon, C. Li, J. Lin, S. P. McCurdy, J. P. Mueller, L. Mullins, M. Niosi, M. C. Noe, D. Pattavina, J. Penzien, M. S. Plummer, H. Risley, B. P. Schuff, V.

- Shanmugasundaram, J. T. Starr, J. M. Sun, J. Winton and J. A. Young, *Bioorg. Med. Chem. Lett.*, 2012, **22**, 5989-5994.
102. M. F. Brown, M. J. Mitton-Fry, J. T. Arcari, R. Barham, J. Casavant, B. S. Gerstenberger, S. Han, J. R. Hardink, T. M. Harris, T. Hoang, M. D. Huband, M. S. Lall, M. M. Lemmon, C. Li, J. Lin, S. P. McCurdy, E. McElroy, C. McPherson, E. S. Marr, J. P. Mueller, L. Mullins, A. A. Nikitenko, M. C. Noe, J. Penzien, M. S. Plummer, B. P. Schuff, V. Shanmugasundaram, J. T. Starr, J. Sun, A. Tomaras, J. A. Young and R. P. Zaniewski, *J. Med. Chem.*, 2013, **56**, 5541-5552.
103. A. P. Tomaras, J. L. Crandon, C. J. McPherson and D. P. Nicolau, *Antimicrob. Agents Chemother.*, 2015, **59**, 2439-2442.
104. K. E. Murphy-Benenato, P. R. Bhagunde, A. Chen, H. E. Davis, T. F. Durand-Réville, D. E. Ehmman, V. Galullo, J. J. Harris, H. Hatoum-Mokdad, H. Jahic, A. Kim, M. R. Manjunatha, E. L. Manyak, J. Mueller, S. Patey, O. Quiroga, M. Rooney, L. Sha, A. B. Shapiro, M. Sylvester, B. Tan, A. S. Tsai, M. Uria-Nickelsen, Y. Wu, M. Zambrowski and S. X. Zhao, *J. Med. Chem.*, 2015, **58**, 2195-2205.
105. A. Kim, A. Kutschke, D. E. Ehmman, S. A. Patey, J. L. Crandon, E. Gorseth, A. A. Miller, R. E. McLaughlin, C. M. Blinn, A. Chen, A. S. Nayar, B. Dangel, A. S. Tsai, M. T. Rooney, K. E. Murphy-Benenato, A. E. Eakin and D. P. Nicolau, *Antimicrob. Agents Chemother.*, 2015, **59**, 7743-7752.
106. K. E. Murphy-Benenato, B. Dangel, H. E. Davis, T. F. Durand-Réville, A. D. Ferguson, N. Gao, H. Jahić, J. P. Mueller, E. L. Manyak, O. Quiroga, M. Rooney, L. Sha, M. Sylvester, F. Wu, M. Zambrowski and S. X. Zhao, *ACS Med. Chem. Lett.*, 2015, **6**, 537-542.
107. M. G. P. Page, C. Dantier and E. Desarbre, *Antimicrob. Agents Chemother.*, 2010, **54**, 2291-2302.
108. T. Mima, B. H. Kvitko, D. A. Rholl, M. G. P. Page, E. Desarbre and H. P. Schweizer, *Int. J. Anitmicrob. Agents*, 2011, **38**, 157-159.
109. T. A. Russo, M. G. P. Page, J. M. Beanan, R. Olson, A. M. Hujer, K. M. Hujer, M. Jacobs, S. Bajaksouzian, A. Endimiani and R. A. Bonomo, *J. Antimicrob. Chemother.*, 2011, **66**, 867-873.

110. N. Kohira, J. West, A. Ito, T. Ito-Horiyama, R. Nakamura, T. Sato, S. Rittenhouse, M. Tsuji and Y. Yamano, *Antimicrob. Agents Chemother.*, 2015, **60**, 729-734.
111. N. Kohira, J. West, A. Ito, T. Ito-Horiyama, R. Nakamura, T. Sato, S. Rittenhouse, M. Tsuji and Y. Yamano, *Antimicrob. Agents Chemother.*, 2016, **60**, 729-734.
112. T. Ito-Horiyama, Y. Ishii, A. Ito, T. Sato, R. Nakamura, N. Fukuhara, M. Tsuji, Y. Yamano, K. Yamaguchi and K. Tateda, *Antimicrob. Agents Chemother.*, 2016, **60**, 4384-4386.
113. M. Amélia Santos, *Coord. Chem. Rev.*, 2002, **228**, 187-203.
114. <https://clinicaltrials.gov/ct2/show/NCT02714595>, (accessed 19/09/2016).
115. C. Hennard, Q. C. Truong, J. F. Desnottes, J. M. Paris, N. J. Moreau and M. A. Abdallah, *J. Med. Chem.*, 2001, **44**, 2139-2151.
116. F. Rivault, C. Liébert, A. Burger, F. Hoegy, M. A. Abdallah, I. J. Schalk and G. L. A. Mislin, *Bioorg. Med. Chem. Lett.*, 2007, **17**, 640-644.
117. S. Noël, V. Gasser, B. Pesset, F. Hoegy, D. Rognan, I. J. Schalk and G. L. A. Mislin, *Org. Biomol. Chem.*, 2011, **9**, 8288-8300.
118. C. Ji and M. J. Miller, *Bioorg. Med. Chem.*, 2012, **20**, 3828-3836.
119. C. Ji and M. J. Miller, *Biometals*, 2015, **28**, 541-551.
120. T. Zheng and E. M. Nolan, *Bioorg. Med. Chem. Lett.*, 2015, **25**, 4987-4991.
121. S. R. Md-Saleh, E. C. Chilvers, K. G. Kerr, S. J. Milner, A. M. Snelling, J. P. Weber, G. H. Thomas, A. K. Duhme-Klair and A. Routledge, *Bioorg. Med. Chem. Lett.*, 2009, **19**, 1496-1498.
122. R. E. Juárez-Hernández, P. A. Miller and M. J. Miller, *ACS Med. Chem. Lett.*, 2012, **3**, 799-803.
123. T. F. Zheng, J. L. Bullock and E. M. Nolan, *J. Am. Chem. Soc.*, 2012, **134**, 18388-18400.
124. S. J. Milner, A. Seve, A. M. Snelling, G. H. Thomas, K. G. Kerr, A. Routledge and A. K. Duhme-Klair, *Org. Biomol. Chem.*, 2013, **11**, 3461-3468.

125. A. Souto, M. A. Montaos, M. Balado, C. R. Osorio, J. Rodríguez, M. L. Lemos and C. Jiménez, *Bioorg. Med. Chem.*, 2013, **21**, 295-302.
126. T. A. Wencewicz, T. E. Long, U. Möllmann and M. J. Miller, *Bioconjugate Chem.*, 2013, **24**, 473-486.
127. S. Fardeau, A. Dassonville-Klimpt, N. Audic, A. Sasaki, M. Pillon, E. Baudrin, C. Mullié and P. Sonnet, *Bioorg. Med. Chem.*, 2014, **22**, 4049-4060.
128. S. J. Milner, A. M. Snelling, K. G. Kerr, A. Abd-El-Aziz, G. H. Thomas, R. E. Hubbard, A. Routledge and A.-K. Duhme-Klair, *Bioorg. Med. Chem.*, 2014, **22**, 4499-4505.
129. M. Ghosh, L. J. Lambert, P. W. Huber and M. J. Miller, *Bioorg. Med. Chem. Lett.*, 1995, **5**, 2337-2340.
130. M. N. Levine and R. T. Raines, *Chem. Sci.*, 2012, **3**, 2412-2420.
131. I. Schröder, E. Johnson and S. de Vries, *FEMS Microbiol. Rev.*, 2003, **27**, 427-447.
132. J. Rautio, H. Kumpulainen, T. Heimbach, R. Oliyai, D. Oh, T. Järvinen and J. Savolainen, *Nat. Rev. Drug. Discov.*, 2008, **7**, 255-270.
133. A. L. Simplício, J. M. Clancy and J. F. Gilmer, *Molecules*, 2008, **13**, 519-547.
134. P. M. Potter and R. M. Wadkins, *Curr. Med. Chem.*, 2006, **13**, 1045-1054.
135. J. Arpigny and K. Jaeger, *Biochem. J.*, 1999, **343**, 177-183.
136. O. Vandenabeele-Trambouze, L. Garrelly, L. Mion, L. Boiteau and A. Commeyras, *Adv. Environ. Res.*, 2001, **6**, 67-80.
137. I. Christenson, *Acta Chem. Scand.*, 1964, **18**, 904-922.
138. P. Adams and F. A. Baron, *Chem. Rev.*, 1965, **65**, 567-602.
139. D. Ben-Ishai and A. Berger, *J. Org. Chem.*, 1952, **17**, 1564-1570.
140. T. Greene and P. Wuts, *Protective Groups In Organic Synthesis*, John Wiley & Sons, Canada, Second edn., 1991.
141. L. A. Carpino and G. Y. Han, *J. Org. Chem.*, 1972, **37**, 3404-3409.
142. Y.-h. Yang, H. Aloysius, D. Inoyama, Y. Chen and L.-q. Hu, *Acta Pharmaceut. Sin. B*, 2011, **1**, 143-159.
143. H. Devalapally, R. S. Navath, V. Yenamandra, R. R. Akkinapally and R. K. Devarakonda, *Arch. Pharm. Res.*, 2007, **30**, 723-732.

144. T. Chauvin, P. Durand, M. Bernier, H. Meudal, B. T. Doan, F. Noury, B. Badet, J. C. Beloeil and E. Tóth, *Angew. Chem. Int. Ed. Engl.*, 2008, **47**, 4370-4372.
145. K. C. Cundy, R. Branch, T. Chernov-Rogan, T. Dias, T. Estrada, K. Hold, K. Koller, X. Liu, A. Mann, M. Panuwat, S. P. Raillard, S. Upadhyay, Q. Q. Wu, J.-N. Xiang, H. Yan, N. Zerangue, C. X. Zhou, R. W. Barrett and M. A. Gallop, *J. Pharmacol. Ex. Ther.*, 2004, **311**, 315-323.
146. P. Tobin, S. Clarke, J. P. Seale, S. Lee, M. Solomon, S. Aulds, M. Crawford, J. Gallagher, T. Eyers and L. Rivory, *Br. J. Clin. Pharmacol.*, 2006, **62**, 122-129.
147. S. P. Sanghani, S. K. Quinney, T. B. Fredenburg, W. I. Davis, D. J. Murry and W. F. Bosron, *Drug Metab. Dispos.*, 2004, **32**, 505-511.
148. J. Alexander, R. A. Fromtling, J. A. Bland, B. A. Pelak and E. C. Gilfillan, *J. Med. Chem.*, 1991, **34**, 78-81.
149. J. Alexander, R. Cargill, S. R. Michelson and H. Schwam, *J. Med. Chem.*, 1988, **31**, 318-322.
150. D. Chaturvedi, *Tetrahedron*, 2012, **68**, 15-45.
151. D. Chaturvedi, N. Mishra and V. Mishra, *Current Organic Synthesis*, 2007, **4**, 308-320.
152. H. Babad and A. G. Zeiler, *Chem. Rev.*, 1973, **73**, 75-91.
153. L. Pasquato, G. Modena, L. Cotarca, P. Delogu and S. Mantovani, *J. Org. Chem.*, 2000, **65**, 8224-8228.
154. K. Takeda, K. Tsuboyama, M. Hoshino, M. Kishino and H. Ogura, *Synthesis*, 1987, **1987**, 557-560.
155. D. D'Addona and C. G. Bochet, *Tetrahedron Lett.*, 2001, **42**, 5227-5229.
156. A. K. Ghosh, T. T. Duong, S. P. McKee and W. J. Thompson, *Tetrahedron Lett.*, 1992, **33**, 2781-2784.
157. H. M. Li, C. Y. Chen and J. B. Padros, *Synlett*, 2011, 1454-1458.
158. M. Aresta, C. Berloco and E. Quaranta, *Tetrahedron*, 1995, **51**, 8073-8088.
159. K. Takeda, Y. Akagi, A. Saiki, T. Tsukahara and H. Ogura, *Tetrahedron Lett.*, 1983, **24**, 4569-4572.

160. K. J. Butcher, *Synlett*, 1994, **1994**, 825-826.
161. A. Inesi, V. Mucciante and L. Rossi, *J. Org. Chem.*, 1998, **63**, 1337-1338.
162. R. N. Salvatore, S. I. Shin, A. S. Nagle and K. W. Jung, *J. Org. Chem.*, 2001, **66**, 1035-1037.
163. R. M. Moriarty, C. J. Chany, R. K. Vaid, O. Prakash and S. M. Tuladhar, *J. Org. Chem.*, 1993, **58**, 2478-2482.
164. K. Hirota, H. Kitagawa, M. Shimamura and S. Ohmori, *Chem. Lett.*, 1980, -, 191-194.
165. H. Y. Guo, S. A. Naser, G. Ghobrial and O. Phanstiel, *J. Med. Chem.*, 2002, **45**, 2056-2063.
166. D. L. Ross and C. M. Riley, *Int. J. Pharm.*, 1990, **63**, 237-250.
167. D. R. Lide, *CRC Handbook of Chemistry & Physics 73rd Edition*, Taylor & Francis, 1992.
168. H. K. Hall, *J. Am. Chem. Soc.*, 1957, **79**, 5441-5444.
169. E.-I. Rööm, A. Kütt, I. Kaljurand, I. Koppel, I. Leito, I. A. Koppel, M. Mishima, K. Goto and Y. Miyahara, *Chemistry – A European Journal*, 2007, **13**, 7631-7643.
170. Patent US2011/105514 A1, 2011.
171. C. De Cola, A. Manicardi, R. Corradini, I. Izzo and F. De Riccardis, *Tetrahedron*, 2012, **68**, 499-506.
172. M. Balci, *Basic 1H-and 13C-NMR spectroscopy*, Elsevier, 2005.
173. J. Stothers, *Carbon-13 NMR Spectroscopy: Organic Chemistry, A Series of Monographs*, Elsevier, 1972.
174. C. F. Riber, A. A. Smith and A. N. Zelikin, *Adv. Healthc. Mater.*, 2015, **4**, 1887-1890.
175. A. Satyam, *Bioorg. Med. Chem. Lett.*, 2008, **18**, 3196-3199.
176. L. R. Jones, E. A. Goun, R. Shinde, J. B. Rothbard, C. H. Contag and P. A. Wender, *J. Am. Chem. Soc.*, 2006, **128**, 6526-6527.
177. W. A. Henne, D. D. Doorneweerd, A. R. Hilgenbrink, S. A. Kularatne and P. S. Low, *Bioorg. Med. Chem. Lett.*, 2006, **16**, 5350-5355.
178. K. V. S. Nemmani, S. V. Mali, N. Borhade, A. R. Pathan, M. Karwa, V. Pamidiboina, S. P. Senthilkumar, M. Gund, A. K. Jain, N. K.

- Mangu, N. P. Dubash, D. C. Desai, S. Sharma and A. Satyam, *Bioorg. Med. Chem. Lett.*, 2009, **19**, 5297-5301.
179. A. K. Jain, M. G. Gund, D. C. Desai, N. Borhade, S. P. Senthilkumar, M. Dhiman, N. K. Mangu, S. V. Mali, N. P. Dubash, S. Halder and A. Satyam, *Bioorganic Chem.*, 2013, **49**, 40-48.
180. H. S. Kim, W. Y. Song and H. J. Kim, *Org. Biomol. Chem.*, 2015, **13**, 73-76.
181. D. Ritz and J. Beckwith, *Annu. Rev. Microbiol.*, 2001, **55**, 21-48.
182. L. E. S. Netto, M. A. de Oliveira, C. A. Tairum and J. F. D. Neto, *Free Radic. Res.*, 2016, **50**, 206-245.
183. S. B. Wall, J.-Y. Oh, A. R. Diers and A. Landar, *Front. Physiol.*, 2012, **3**, 369.
184. R. Singh and G. M. Whitesides, *Techniques in Protein Chemistry*, 1995, **6**, 259-266.
185. S. G. Tadj, B. S. Tolbert, R. Basavappa and B. L. Miller, *J. Am. Chem. Soc.*, 2004, **126**, 10508-10509.
186. P. C. Jocelyn, in *Methods in Enzymology*, Academic Press, 1987, vol. Volume 143, pp. 246-256.
187. J. C. A. Bardwell, K. McGovern and J. Beckwith, *Cell*, 1991, **67**, 581-589.
188. J. W. Hastings, *Gene*, 1996, **173**, 5-11.
189. D. Witt, *Synthesis*, 2008, **2008**, 2491-2509.
190. M. Musiejuk and D. Witt, *Org. Prep. Proc. Int.*, 2015, **47**, 95-131.
191. S. Hitomi, K. Sei-ichi and N. Akira, *Bull. Chem. Soc. Jpn.*, 1992, **65**, 626-627.
192. J. K. Vandavasi, W.-P. Hu, C.-Y. Chen and J.-J. Wang, *Tetrahedron*, 2011, **67**, 8895-8901.
193. N. Jayasuriya and S. L. Regen, *Tetrahedron Lett.*, 1992, **33**, 451-452.
194. R. El Aissi, J.-M. Chezal, S. Tarrit, O. Chavignon and E. Moreau, *Eur. J. Med. Chem.*, 2015, **101**, 668-680.
195. E. Brzezinska and A. L. Ternay, *J. Org. Chem.*, 1994, **59**, 8239-8244.

196. B. M. R. Liénard, R. Hüting, P. Lassaux, M. Galleni, J.-M. Frère and C. J. Schofield, *J. Med. Chem.*, 2008, **51**, 684-688.
197. H. T. He, R. N. Gürsoy, L. Kupczyk-Subotkowska, J. Tian, T. Williams and T. J. Siahhan, *J. Pharm. Sci.*, 2006, **95**, 2222-2234.
198. M. Lovrić, I. Capanec, M. Litvić, A. Bartolinčić and V. Vinković, *Croat. Chem. Acta*, 2007, **80**, 109-115.
199. P. C. Sharma and S. Jain, *Acta Pol. Pharm.*, 2008, **65**, 551-556.
200. M. A. Fischbach, H. Lin, D. R. Liu and C. T. Walsh, *Nat. Chem. Biol.*, 2006, **2**, 132-138.
201. M. A. Fischbach, H. Lin, D. R. Liu and C. T. Walsh, *Proc. Natl. Acad. Sci. U.S.A.*, 2005, **102**, 571-576.
202. D. Foshag, C. Campbell and P. D. Pawelek, *Biochim. Biophys. Acta*, 2014, **1844**, 1619-1630.
203. G. Vassiliadis, J. Peduzzi, S. Zirah, X. Thomas, S. Rebuffat and D. Destoumieux-Garzón, *Antimicrob. Agents Chemother.*, 2007, **51**, 3546-3553.
204. D. J. Raines, O. Moroz, E. V. Blagova, J. P. Turkenburg, K. S. Wilson and A. K. Duhme-Klair, *Proc. Natl. Acad. Sci. U.S.A.*, 2016, **113**, 5850-5855.
205. M.-L. V. Crouch, M. Castor, J. E. Karlinsey, T. Kalhorn and F. C. Fang, *Mol. Microbiol.*, 2008, **67**, 971-983.
206. S. I. Müller, M. Valdebenito and K. Hantke, *Biometals*, 2009, **22**, 691-695.
207. H. G. Gong and M. R. Gagné, *J. Am. Chem. Soc.*, 2008, **130**, 12177-12183.
208. X. L. Yu, Y. J. Dai, T. Yang, M. R. Gagné and H. G. Gong, *Tetrahedron*, 2011, **67**, 144-151.
209. T. Bililign, B. R. Griffith and J. S. Thorson, *Nat. Prod. Rep.*, 2005, **22**, 742-760.
210. K. Lalitha, K. Muthusamy, Y. S. Prasad, P. K. Vemula and S. Nagarajan, *Carbohydr. Res.*, 2015, **402**, 158-171.
211. C. Jaramillo and S. Knapp, *Synthesis*, 1994, 1-20.
212. L. Kalvoda, J. Farkaš and F. Šorm, *Tetrahedron Lett.*, 1970, **11**, 2297-2300.

213. C. D. Hurd and W. A. Bonner, *J. Am. Chem. Soc.*, 1945, **67**, 1664-1668.
214. Y. Du, R. J. Linhardt and I. R. Vlahov, *Tetrahedron*, 1998, **54**, 9913-9959.
215. C. D. Hurd and W. A. Bonner, *J. Am. Chem. Soc.*, 1945, **67**, 1972-1977.
216. H. Böshagen, W. Geiger and B. Junge, *Angew. Chem. Int. Ed. Engl.*, 1981, **20**, 806-807.
217. D. Lednicer and J. C. Babcock, *J. Org. Chem.*, 1962, **27**, 2541-2544.
218. J. Panigot and W. Curley, *J. Carbohydr. Chem.*, 1994, **13**, 293-302.
219. G. A. Kraus and M. T. Molina, *J. Org. Chem.*, 1988, **53**, 752-753.
220. S. Czernecki and G. Ville, *J. Org. Chem.*, 1989, **54**, 610-612.
221. D. Y. W. Lee, W.-Y. Zhang and V. V. R. Karnati, *Tetrahedron Lett.*, 2003, **44**, 6857-6859.
222. S. Hainke, I. Singh, J. Hemmings and O. Seitz, *J. Org. Chem.*, 2007, **72**, 8811-8819.
223. K. W. Wellington and S. A. Benner, *Nucleos. Nucleot. Nucl.*, 2006, **25**, 1309-1333.
224. D. Y. Lee and M. He, *Curr. Top. Med. Chem.*, 2005, **5**, 1333-1350.
225. P. Merino, T. Tejero, E. Marca, F. Gomollón-Bel, I. Delso and R. Matute, *Heterocycles*, 2012, **86**, 791-820.
226. L. Nicolas, P. Angibaud, I. Stansfield, P. Bonnet, L. Meerpoel, S. Reymond and J. Cossy, *Angew. Chem. Int. Ed. Engl.*, 2012, **51**, 11101-11104.
227. J. Štambaský, M. Hocek and P. Kočovský, *Chem. Rev.*, 2009, **109**, 6729-6764.
228. A. H. F. Lee and E. T. Kool, *J. Org. Chem.*, 2005, **70**, 132-140.
229. J. C. Y. Cheng, U. Hacksell and G. D. Daves, *J. Org. Chem.*, 1986, **51**, 3093-3098.
230. Y. Bai, L. M. H. Kim, H. Liao and X.-W. Liu, *J. Org. Chem.*, 2013, **78**, 8821-8825.
231. S. Sakamaki, E. Kawanishi, S. Nomura and T. Ishikawa, *Tetrahedron*, 2012, **68**, 5744-5753.

232. R. W. Friesen and C. F. Sturino, *J. Org. Chem.*, 1990, **55**, 2572-2574.
233. R. W. Friesen, R. W. Loo and C. F. Sturino, *Can. J. Chem.*, 1994, **72**, 1262-1272.
234. E.-i. Negishi and S. Baba, *J. Chem. Soc., Chem. Commun.*, 1976, -, 596b-597b.
235. X. Chen, K. M. Engle, D.-H. Wang and J.-Q. Yu, *Angew. Chem. Int. Ed. Engl.*, 2009, **48**, 5094-5115.
236. M. M. Heravi, E. Hashemi and N. Nazari, *Mol. Divers.*, 2014, **18**, 441-472.
237. K. C. Nicolaou, P. G. Bulger and D. Sarlah, *Angew. Chem. Int. Ed. Engl.*, 2005, **44**, 4442-4489.
238. G. Lessene, *Aus. J. Chem.*, 2004, **57**, 107-107.
239. M. Ousmer, V. Boucard, N. Lubin-Germain, J. Uziel and J. Augé, *Eur. J. Org. Chem.*, 2006, **2006**, 1216-1221.
240. B. G. Davis and A. J. Fairbanks, *Carbohydrate Chemistry*, Oxford University Press, 2002.
241. G. D. Jones, J. L. Martin, C. McFarland, O. R. Allen, R. E. Hall, A. D. Haley, R. J. Brandon, T. Konovalova, P. J. Desrochers, P. Pulay and D. A. Vicic, *J. Am. Chem. Soc.*, 2006, **128**, 13175-13183.
242. V. B. Phapale, E. Buñuel, M. García-Iglesias and D. J. Cárdenas, *Angew. Chem. Int. Ed. Engl.*, 2007, **46**, 8790-8795.
243. H. Abe, S. Shuto and A. Matsuda, *J. Am. Chem. Soc.*, 2001, **123**, 11870-11882.
244. S. Lemaire, I. N. Houpis, T. Xiao, J. Li, E. Digard, C. Gozlan, R. Liu, A. Gavryushin, C. Diène, Y. Wang, V. Farina and P. Knochel, *Org. Lett.*, 2012, **14**, 1480-1483.
245. I. Zuravka, R. Roesmann, A. Susic, R. Göttlich and B. Gatto, *Bioorg. Med. Chem.*, 2015, **23**, 1241-1250.
246. K. Lippur, T. Tiirik, M. Kudrjashova, I. Järving, M. Lopp and T. Kanger, *Tetrahedron*, 2012, **68**, 9550-9555.
247. J. Sunkel and H. Staude, *Ber. Bunsenge. Ph. Chem.*, 1968, **72**, 567-573.
248. R. Aydın and U. Özer, *Chem. Pharm. Bull.*, 2004, **52**, 33-37.

249. S. P. Santoso, A. E. Angkawijaya, S. Ismadji, A. Ayucitra, F. E. Soetaredjo, T. N. P. Lan and Y.-H. Ju, *J. Solution Chem.*, 2016, **45**, 518-533.
250. T. Benković, D. Kontrec, V. Tomišić, A. Budimir and N. Galić, *J. Solution Chem.*, 2016, **45**, 1227-1245.
251. G. Vériot, J.-P. Dutasta, G. Matouzenko and A. Collet, *Tetrahedron*, 1995, **51**, 389-400.
252. E. W. Yue, J. M. Gerdes and C. A. Mathis, *J. Org. Chem.*, 1991, **56**, 5451-5456.
253. R. Francke, G. Schnakenburg and S. R. Waldvogel, *Eur. J. Org. Chem.*, 2010, -, 2357-2362.
254. A. V. Joshua, S. K. Sharma and D. N. Abrams, *Synth. Commun.*, 2008, **38**, 434-440.
255. A. K. Duhme, Z. Dauter, R. C. Hider and S. Pohl, *Inorg. Chem.*, 1996, **35**, 3059-3061.
256. W. A. Bubb, *Concept Magnetic Res.*, 2003, **19A**, 1-19.
257. C. Montalbetti and V. Falque, *Tetrahedron*, 2005, **61**, 10827-10852.
258. S. R. Md-Saleh, University of York, 2009.
259. S. A. C. Carabineiro, T. Thavorn-Amornsri, M. F. R. Pereira and J. L. Figueiredo, *Water Res.*, 2011, **45**, 4583-4591.
260. P. Klüfers and T. Kunte, *Chem. Eur. J.*, 2003, **9**, 2013-2018.
261. T. Allscher, X. Kästele, G. Kettenbach, P. Klüfers and T. Kunte, *Chem. Asian J.*, 2007, **2**, 1037-1045.
262. Y. Arendt, O. Labisch and P. Klüfers, *Carbohydr. Res.*, 2009, **344**, 1213-1224.
263. K. Gilg, T. Mayer, N. Ghaschghaie and P. Klüfers, *Dalton Trans.*, 2009, -, 7934-7945.
264. C. M. Cirtiu, A. F. Dunlop-Briere and A. Moores, *Green Chem.*, 2011, **13**, 288-291.
265. E. A. Nouh, M. Roy and S. Sarkar, *Mater. Express*, 2012, **2**, 275-284.
266. S. C. Andrews, A. K. Robinson and F. Rodríguez-Quiñones, *FEMS Microbiol. Rev.*, 2003, **27**, 215-237.
267. L. Ma and S. M. Payne, *J. Bacteriol.*, 2012, **194**, 6748-6757.

268. U. Holzgrabe and S. K. Branch, *Magn. Reson. Chem.*, 1994, **32**, 192-196.
269. K. Pearce and L. Creamer, *Aus. J. Chem.*, 1975, **28**, 2409-2415.
270. M. T. Rubino, D. Maggi, A. Laghezza, F. Loiodice and P. Tortorella, *Arch. Pharm. Chem. Life Sci.*, 2011, **344**, 557-563.
271. S. A. Telang and C. K. Bradsher, *J. Org. Chem.*, 1965, **30**, 752-754.
272. T. Baba, T. Ara, M. Hasegawa, Y. Takai, Y. Okumura, M. Baba, K. A. Datsenko, M. Tomita, B. L. Wanner and H. Mori, *Mol. Syst. Biol.*, 2006, **2**, 1-11.